The Thesis Committee for Kylie Anne Wright
Certifies that this is the approved version of the following thesis:

Correlating Cu-Fe Sulfides and Au Mineralization in the Ertsberg-Grasberg District of Papua, Indonesia using Volumetric Analysis and Trace Element Geochemistry

APPROVED BY
SUPERVISING COMMITTEE:

James R. Kyle, Supervisor

Richard A. Ketcham, Co-Supervisor

Nathaniel R. Miller

Correlating Cu-Fe Sulfides and Au Mineralization in the Ertsberg-Grasberg District of Papua, Indonesia using Volumetric Analysis and Trace Element Geochemistry

by

Kylie Anne Wright, B.A.

Thesis

Presented to the Faculty of the Graduate School of

The University of Texas at Austin

in Partial Fulfillment

of the Requirements

for the Degree of

Master of Science in Geological Sciences

The University of Texas at Austin
August, 2017

Dedication

To my animals, friends, and family.

Also to future Kylie, who will be glad she finished this degree.

Acknowledgements

I would like to thank many people for their help and encouragement along the way. First and foremost, my advisors Dr. Kyle and Dr. Ketcham have been invaluable sources of insight, direction, and motivation during this project, and I cannot thank them both enough for being wonderful advisors and people. It's extremely gratifying to work for people who are enthusiastic about their work, but who are also genuinely kind and supportive. I have learned a great deal from both of you.

This project would not have been completed without funding and support from PT Freeport Indonesia. Additional funding from the Society of Economic Geologists and the Jackson School of Geosciences is very much appreciated.

Dr. Miller has provided expertise and advice that have undoubtedly made this project and all things LA-ICP-MS in it, more focused, thoughtful, and in general, much better, and for that I am very grateful.

Immeasurable thanks are due for the entire UTCT staff and lab group. Jessie Maisano, Matt Colbert, Dave Edey, Romy Hanna, Gary Zuker, and Scott Eckley are some of the hardest working people at the University of Texas. They're also some of the kindest and most helpful people I've met during my graduate career. Thank you for providing motivation and technical advice when I needed it, copious snacks when I wanted them, and an intellectual haven always.

To Simone Runyon, Matt Steele-MacInnis, and Pilar Lecumberri-Sanchez: you provided me with insight and direction in the areas I understood the least, when I needed it most. Thank you for your help, and good luck in all of your exciting new endeavors.

Thank you to Daniel Young and Raeann Garcia for operating all of the many pieces of equipment in this building that I couldn't. You're help has been wonderful to have, and I wish you the best of luck in graduate school and the rest of college.

To my wonderful friends that I made during graduate school: you are one charming and smart group of people. Thank you for always being funny and engaging, I hope you know how rare that is. To my friends far away, thank you for your support, humor, and always being patient sounding boards when I needed it. Matt, Nate, and Mackenzie, thank you for your hard-won guidance and advice, you'll never know how much I appreciate all of it. I'm sure we'll stay in touch, and I wish the best for all of you.

At no point during these two years could I have done any of this without my family. Thank you so much Mom, Dad, Jesse, Zach, Anna, and Jason. You have been the most fiercely supportive and encouraging group of people to have around me as I strive towards my goals and find my way in my career. Thank you for your patience and love, even when I have not deserved it. Mostly, thank you for being some of the most intelligent, ambitious, funny, and driven people I have ever met. You each make me a better person.

Abstract

Correlating Cu-Fe Sulfides and Au Mineralization in the Ertsberg-Grasberg District of Papua, Indonesia using Volumetric Analysis and Trace Element Geochemistry

Kylie Anne Wright, M.S. Geo. Sci.
The University of Texas at Austin, 2017

Supervisors: James R. Kyle
Richard A. Ketcham

The Ertsberg-Grasberg District in Papua, Indonesia, hosts two of the world's largest intrusion-related Cu-Au deposits: the Ertsberg Intrusive System, a hybrid porphyry-skarn deposit, and the Grasberg Igneous Complex, a high-grade porphyry deposit. Cu mineralization within the Grasberg porphyry and Ertsberg skarn systems consists primarily of bornite and chalcopyrite, whereas native gold occurs as inclusions within, or along boundaries of these minerals. Experimental studies by other researchers have shown that at hydrothermal ore-forming temperatures (~300-700°C) and elevated sulfur activity, bornite and chalcopyrite can host 1000s ppm Au within the sulfide lattice or as nano-inclusions. Upon retrograde cooling of the hydrothermal system, the capacity of the Cu-Fe sulfides to host Au significantly decreases to ~10 ppm, suggesting that the Au becomes unstable within the Cu-Fe sulfide matrix and may passively migrate out of the sulfides and coalesce to form native gold grains. These data suggest that Cu-Fe sulfides could exert a

strong control on the gold contents of porphyry deposits. However, the traditional model for native gold deposition in large hydrothermal systems relies primarily on fluid pulses, and does not consider gold contributions from the exsolution of previously precipitated gold within Cu-Fe sulfides.

To assess the role of Au-bearing Cu-Fe sulfides in the concentration of native gold in this setting, High Resolution X-ray Computed Tomography was used to measure the native gold grains' shapes, textures, and occurrence modes, and map the extent of contiguous Cu-sulfides. HRXCT data were used to 3D modified Voronoi regions within the Cu-sulfides, as an estimate of diffusional domains that may have provided gold to the Au-grains during cooling. The modified Voronoi volumes are defined for each Au-grain as the set of points within the Cu-sulfide network that are closer to that Au-grain than any other, when measured along a path through the Cu-sulfide. HRXCT data for 11 Ertsberg-Grasberg District ore samples were processed with two different threshold criteria, which produced 16 linear correlation values between modified Voronoi volumes and gold grain volumes. Of these 16 correlation coefficients, none show statistically significant correlations. Because of the paucity of gold grains within our samples, calculated drainage regions commonly extended to the physical edge of the core samples, rendering their actual volumes ambiguous and the correlations associated with them un-interpretable. In cases where numerous gold grains were identified, correlation values were not statistically significant. In general, however, this analysis was impaired by the necessity of interpreting whether all grains in a sample were created by a single event and mechanism.

Complementary Laser Ablation Inductively Coupled Plasma Mass Spectrometry (LA-ICP-MS) was used to assess and compare trace element variation within the Cu-Fe sulfides in the district and to constrain spatial variation of Au within Cu-Fe sulfides that contain native gold grains. LA-ICP-MS data show a strong positive correlation between Bi and Ag, and a moderate, positive correlation between Bi and Au, throughout the data. Au occurrences are scattered rather than uniform, where Au concentrations appear in patches throughout the sulfides. This may imply that the majority of non-visible gold exists in Au nanoparticles, rather than solid solution with the Cu-Fe sulfides. Spot analyses and 2D maps indicate the presence of an "enrichment halo" of elevated Au contents in Cu-Fe sulfides surrounding the gold grains. This "enrichment halo" can be interpreted as evidence in support of a hybrid Ostwald-type ripening process that coarsens gold inclusions in chalcopyrite at high-temperatures in porphyry-skarn systems.

Table of Contents

List of Tables

List of Figures

Chapter 1: Introduction

1.1 Introduction and Geological Framework

Porphyry-skarn Cu-Au deposits are found in many regions, and the majority of economic recovery comes from very large, relatively low-grade deposits (Cooke, et al., 2005). The study area of this thesis, the Ertsberg-Grasberg District (EGD) is located in the Central Range of Papua, Indonesia, and contains world class porphyry and skarn deposits (Figures 1.1 and 1.2). PT Freeport Indonesia (PTFI), a subsidiary of Freeport McMoRan, is the majority stake holder and operator of the major Cu-Au district, which contains some of the world's largest known proven and probable copper and gold reserves (FCX, 2015). The USGS estimates that over 60% of copper on the global market has been sourced from porphyry deposits and associated skarns (Johnson, et al., 2014). Understanding the genetic connection between gold and copper mineralization in large ore deposits has been an enduring research focus. This study expands upon the current mineralization model for porphyry and skarn systems, where the majority of gold mineralization is derived from precipitation out of hydrothermal fluids. This research explores the potential for pre-existing Cu-Fe sulfide minerals to host, and then exsolve large volumes of gold that could yield a population of gold grains in the deposit derived from a second mineralization mechanism.

The EGD deposits are related to several late Cenozoic intrusions of quartz monzonite to diorite composition, known as the Grasberg Igneous Complex (GIC), and the Ertsberg Intrusive Complex (EIC) (MacDonald & Arnold, 1994; Leys, et al., 2012). The potassium-rich magmas were emplaced (3.5–2.6 Ma) into a Tertiary and Jurassic-Cretaceous sedimentary sequence and formed the porphyry and hybrid porphyry-skarn deposits around 3 Ma. Three intrusions define the GIC: the Dalam, the Main Grasberg Intrusion (MGI) which lies concentrically within the Dalam, and the Kali Dike which crosscuts both the Dalam and MGI (Figure 1.3) (Leys, et al., 2012). The

Grasberg Open Pit is currently the only operational mine for the Grasberg porphyry, but mining is in a planned transition to a block cave operation (Figure 1.4) (FCX, 2015). The EIC consists of a large quartz monzodiorite intrusion into the New Guinea Limestone and Kembelangan siliciclastic sequences. The orebodies in this part of the district are vertically stacked, with mining currently occurring in the Deep Ore Zone (DOZ) and Deep Mill Level Zone (DMLZ) underground mines. Operations are currently suspended in the Big Gossan underground mine, which lies in between the open pit mine and the DOZ/DMLZ mines (FCX, 2015). Copper mineralization in the EGD primarily consists of bornite and chalcopyrite, with covellite, digenite, and chalcocite present in lesser amounts. Using a cutoff of 0.1% Cu, Leys et al. (2012), calculated that the two GIC-related deposits contain 7.5 billion tonnes of ore at 0.70% Cu and 0.64 g/ton Au, and the four EIC-related deposits contain 3.6 billion tonnes of ore at 0.60% Cu and 0.44 g/ton Au.

Like most porphyry and skarn systems, the formation of these deposits is linked to circulation of magmatically derived hydrothermal fluids, which, during interactions with the host rocks, formed the Cu and Au mineralization (Cloos, 2001; Sillitoe, 2010). However, some of the Au mineralization may be derived from an alternate process, involving cooling induced exsolution from within previously mineralized Cu-sulfides (Frank, et al., 2011). Previous studies by Kesler et al. (2002) and Fraley and Frank (2014) indicate that the primary copper sulfides, bornite and chalcopyrite, in porphyry and skarn deposits like those in the EGD can host elevated gold contents in their matrices at high-temperatures, but were likely already saturated with gold at much lower temperatures. This could potentially indicate that the maximum amount of gold within a porphyry deposit (or porphyry-related skarn) could be limited by the volume of copper sulfides present and the amount of gold that will go into solid solution with those Cu-Fe sulfides at high temperatures (Kesler, et al., 2002; Fraley & Frank, 2014). Building on the body of knowledge on the source of

gold in ores using quantitative geochemical and imaging techniques can help further clarify the nature of these important ore systems.

1.2 Mining History, Tectonic Setting, and Regional Geology

The Ertsberg district was discovered in 1936 by geologist J. J. Dozy with the Royal Dutch Shell Company when he noticed exposed mineralization within the Central Range (Dozy, 1939). In the 1960s Forbes Wilson and the Freeport Sulfur Company returned to the region to assess the deposit and eventually begin development (Wilson, 1981). A contract of work was signed with the Indonesian government in 1967, granting Freeport mining rights for a 100 km^2 area, and mining started in 1968. The Grasberg porphyry deposit was not discovered until 20 years later in 1988 (Van Nort, et al., 1991). The combination of the giant porphyry and skarn deposits truly make this a world class Cu-Au district.

The island of New Guinea was formed by the subduction of the north edge of the Australian continent beneath the Melanesian fore-arc (Figure 1.5). This compressional tectonic environment drove kilometer-scale folding and reverse and thrust faulting in the EGD. Although syn-collisional magmatism was likely present, the high Au/Mo signature in the EGD suggests that the hydrothermal systems that formed the ore deposits in the district were derived from a post-collisional ancient lithospheric mantle source (Cloos, et al., 2005; Leys, et al., 2012).

The island of New Guinea and the surrounding islands of Indonesia host some of the largest Cu-Au porphyry deposits in the world, including Grasberg, Batu Hijau, Ok Tedi, Panguna, and Dizon, among others (Arif & Baker, 2004). The EGD is located within the Irian Fold and Thrust Belt of the Central Range, adjacent to Puncak Jaya, the highest peak on the island at 4884 m above sea level (Leys, et al., 2012). Pliocene magmas intruded Cenozoic carbonates, mid- to late-

Cretaceous limestones, and Jurassic-Cretaceous siliciclastic sequences, which comprise the wall-rocks of the EGD (Leys, et al., 2012). The relatively young age of these deposits means that they have not been overprinted by later deformation or thermal events which can obscure key relationships in older porphyry-skarn systems. Therefore, EGD mineralization can be used as a minimally adulterated example within the spectrum of global porphyry-skarn systems.

1.3 THE ERTSBERG-GRASBERG DISTRICT

1.3.1 Stratigraphy

The predominant surface exposures in the EGD are the upper Kembelangan Group and the New Guinea Group (Leys, et al., 2012). The Kembelangan Group is comprised of a series of four siliciclastic formations (from mid-Jurassic to late Cretaceous, respectively): the Kopai Formation, the Woniwogi Sandstone, the Piniya Mudstone, and the Ekmai Formation (Figure 1.6). The Kopai formation is the basal unit in the Kembelangan, and is a mid-Jurassic to early Cretaceous sandstone that is variable upwards and includes: a ~200m thick cross-bedded sandstone, a ~30-40m crinoidal grainstone, a ~250m laminated mudstone, and an upper ~500m calcareous sandstone. The Woniwogi is a Cretaceous quartz sandstone. The Piniya Mudstone is a sequence of late Cretaceous, carbonaceous mudstone to siltstone with interbedded quartz arenite (Quarles van Ufford, 1996). The late Cretaceous Ekmai Formation can be separated into a basal ~600m thick sandstone section, followed by a 100m thick calcareous mudstone-limestone section, capped with a 3-5 m thick shale (Leys, et al., 2012).

The Cenozoic New Guinea Limestone Group overlies the Kembelangan Group and is separated into four formations (Figure 1.6). The Paleocene Waripi Formation is characterized by dolostone, mudstone, and calcareous quartz arenite with local gypsum-bearing beds. The Eocene

Faumai Formation lies above the Waripi, and is a foraminiferal, granular, micritic limestone and dolostone. Above this lies the early Oligocene Sirga Formation, a ~30m thick, fine-grained, fossiliferous sandstone. The Kais Formation is a >1000m thick Oligocene to mid-Miocene foraminiferal limestone with thin coal interbeds in the upper portion (Quarles van Ufford, 1996; Quarles van Ufford & Cloos, 2005).

1.3.2 Structure

The Central Range of New Guinea is a ~1300km long orogenic belt with kilometer-scale folds and thrust faults that formed during late Cenozoic orogenesis. The Australian plate entered the north-dipping subduction zone, where it was pulled under the Pacific plate; at about 12 Ma, the leading edge of the continental margin of the Australian plate entered the trench. Collisional tectonism began around the mid-Miocene (~8 Ma). Lithospheric delamination and the detachment of the subducted portion of the Australian plate, is postulated to have been complete by about 4 Ma. This tectonic sequence allowed for magma generation due to decompression melting, when the asthenosphere moved into the gap left from crustal delamination (Figure 1.7) (Sapiie & Cloos, 2004; Cloos, et al., 2005; Leys, et al., 2012).

Regional shortening and deformation between 12 and 4 Ma occurred after the edge of the Australian plate stalled within the subduction zone, effectively jamming it. This jamming and subsequent 10s of km shortening generated folds, where Mesozoic-Cenozoic strata are deformed into chevron folds, open synclines and tight anticlines. The Yellow Valley Syncline, is one of the most prominent folds in the district into which the Grasberg Igneous Complex was emplaced. Some NE-striking strike-slip tear faults occur within the EGD, which have been interpreted to provide local structural controls on mineralization. After 4 Ma, regional left-lateral strike-slip motion dominated and generated fault zones within the district that generally trend NW around

300°; this activity continued until approximately 2 Ma. Strike-slip faulting coincides with igneous activity in the district, and structures formed between these faults provided a structural control on hydrothermal activity (Sapiie & Cloos, 2004; Baline, 2007; Leys, et al., 2012; Ledvina, 2017).

1.3.3 Magmatism

Within the New Guinea highlands, igneous and volcanic deposits of generally intermediate composition are widely dispersed, and appear to represent shallowly emplaced magma. The igneous rocks were produced during two major magmatic events within the strike-slip deformation regime: one event between 4.4 and 3.5 Ma and another between 3.5 and 2.6 Ma. The igneous activity was geochemically distinct during these periods. There are two major igneous intrusions in the region, the EIC and the GIC (McMahon, 1994a) (Leys, et al., 2012). Recent zircon U/Pb ages from Wafforn (2017) for relevant intrusions in the district indicate a maximum duration of EGD magmatism of less than 1 million years (Wafforn, 2017). EIC ages range from 3.2 ± 0.2 Ma to 2.8 ± 0.1 Ma, and GIC ages range from 3.5 ± 0.1 Ma to 3.1 ± 0.1 Ma. Thermochronology supports previous interpretations that the igneous phases, including both plutons and volcanics, represent shallowly emplaced magma with a local maar volcano (Wafforn, 2017).

The majority of the magmatic activity in the EIC can be characterized as porphyritic stocks and sills. The source of magmatism has been proposed as either subduction-related magmatism due to water-fluxed melting of the asthenosphere, or decompression melting and asthenospheric upwelling after slab break off (McMahon, 1994a; McMahon, 1994b; McDowell, et al., 1996; Cloos, et al., 2005). Intrusions throughout the district display high Au/Mo ratios, which can be indicative of a lithospheric mantle melt source, rather than direct water-fluxed asthenospheric melt (Cloos, et al., 2005) (Leys, et al., 2012). The mafic assemblage of the EIC predominantly consists

of titanite and clinopyroxene, with some associated porphyritic dikes and sills also containing hornblende and biotite (McMahon, 1994a).

The GIC can be separated into three distinct concentrically placed intrusive phases, of decreasing age: the Dalam Diatreme, the Main Grasberg Intrusion (MGI), and the Kali Dike (Figure 1.3). These phases are mostly porphyritic, with major mineral assemblages of plagioclase, biotite, and hornblende. Although similar, the GIC is chemically distinct from the EIC as it is generally more crystal and silica rich (McMahon, 1999; Cloos, 2001). The Dalam diatreme, the oldest igneous intrusion of the GIC, consists of the Dalam Diorite (3.48 ± 0.05 Ma), the Dalam Andesite, the Dalam Fragmental, and the Dalam Volcanic (3.6 to 3.3 Ma). The next intrusion is the MGI (3.22 ± 0.04 Ma), which contains the quartz stockwork and the main stage Cu-Au mineralization. The early and late Kali dikes, 3.2 ± 0.04 and 3.09 ± 0.05 Ma, respectively, were the final intrusive phase and cross cut the MGI and Dalam (Wafforn, 2017).

1.3.4 Orebodies

EGD mineralization mostly occurs within potassic-altered intrusive rocks or prograde skarns. Primary Cu ore minerals in the district are chalcopyrite and bornite, with chalcopyrite being more abundant overall, but bornite increases with depth. Molybdenite is relatively uncommon but occurs throughout the district in all orebodies. Most of the gold in the district occurs as free inclusions of native gold or electrum in both chalcopyrite and bornite, and occasionally with digenite (Rubin, 1996; Rubin & Kyle, 1997; Leys, et al., 2012).

GIC mineralization occurs in a silicified stockwork in the interior of the concentrically nested igneous phases. The highest-grade Cu-Au mineralization occurs within this quartz-magnetite stockwork, though Cu mineralization overprints the stockwork as evidenced by

crosscutting sulfide veinlets within this region. Phyllic alteration occurs in the MGI and extends to the Dalam phases, where alteration transitions to propylitic. The Kucing Liar skarn, which occurs between 3000 and 2500m elevation, is the only skarn-hosted ore zone associated with the GIC (Leys, et al., 2012). The Kucing Liar skarn is not currently in production (FCX, 2015).

Ertsberg orebodies are closely spatially associated with the previously discussed intrusions, and are either wallrock-hosted skarns or the diorite-hosted porphyry deposit, the Ertsberg Stockwork Zone. Seven separate skarn orebodies have been identified within the Ertsberg system (not including the Grasberg associated Kucing Liar), though four of these represent a continuous ore system that has been delineated based on engineering constraints. The Ertsberg East Skarn System (EESS) is a series of stacked skarn orebodies adjacent to the Ertsberg stockwork. In order of increasing depth they are: the Gunung Bijih Timur (GBT), the Intermediate Ore Zone (IOZ), the Deep Ore Zone (DOZ), and the Deep Mill Level Zone (DMLZ). The Big Gossan skarn lies west of the Ertsberg diorite, and contains the highest Cu-Au grades in the district. The Dom skarn crops out at 4200 m on a peak southeast of the EESS (Figure 1.8).

Au mineralization within the district typically occurs, in close association with the primary Cu-Fe sulfide minerals, chalcopyrite and bornite (Rubin & Kyle, 1997; Kyle, et al., 2008). Au can occur as grains of either native gold or electrum. The majority of the Au mineralization in the region is associated with chalcopyrite and bornite. Au mineralization appears preferentially associated with bornite when it is present (Rubin & Kyle, 1997; Kyle, et al., 2008). Au occurrences outside of the Grasberg porphyry and the EESS (e.g., Big Gossan; Dom) are diverse and occur with pyrrhotite, sphalerite, and galena, among others (Rubin & Kyle, 1997; Prendergast, et al., 2005).

1.4 Model for Porphyry and Skarn Deposit Formation

Traditional models for ore deposit formation invoke the circulation of high temperature fluids, magmatically or otherwise derived, that have elevated metal contents or efficiently strip metals during interactions with wall and host rocks. These fluids circulate through host rocks, and physicochemical conditions promote the precipitation of ore minerals in economic quantities.

Many of the world's porphyry deposits are formed at plate boundaries, typically subduction zones, where decompression or water-assisted melting can readily occur and provide the necessary parent magma of the porphyry deposit. According to Cloos (2001) and Sillitoe (2010) porphyry deposits are formed by the injection of metal-rich, S- and Cl- saturated magmas into cool wallrock (Figure 1.8). These intrusions are derived from deep crustal, batholithic magma chambers that provide a heat and metal source to the smaller crustal intrusion, which provides a pathway for magma ascent, cooling, and degassing. The temperature disparity between the cool country rock and magma forms thermal gradients which induce cooling and crystallization within the intrusion. As crystallization proceeds and the magma becomes more fluid saturated, it will rise to shallower depths within the crust (~2-5 km) where the decrease in pressure will allow metal-rich vapor bubbles within the magma to charge a cupola at top of the intrusion. The fluid contained within this cupola interacts with the shallow country rock and forms the large scale hydrothermal systems responsible for the formation of porphyry and associated skarn and epithermal deposits (Cloos, 2001; Sillitoe, 2010).

Frequently found in association with plutons and shallow geothermal systems, skarns form during contact and regional metamorphism of carbonate rocks (Figure 1.8) (Einaudi & Burt, 1982; Meinert, 1992; Sillitoe, 2010). However, skarns can form from a variety of metamorphic and metasomatic processes, and in many different geologic settings including lower crustal depths and

on the seafloor (Einaudi & Burt, 1982). The primary characterization of a skarn, given the variety of occurrences, is the mineralogy of the deposit, which includes a range of calc-silicates, commonly dominated by pyroxene and garnet. When a hydrothermal system containing base and precious metals is responsible for skarn formation and precipitation of economically important minerals, a 'skarn deposit' is formed (Einaudi & Burt, 1982; Meinert, 1992; Meinert, et al., 2005).

Although the initial source of the gold in these economic deposits is still debated, the entrainment of gold at economic concentrations, within porphyry and skarn systems does occur, evidently. The physicochemical constraints on gold precipitation within hydrothermal systems are known to be primarily temperature and sulfur fugacity of the hydrothermal fluid, but also include pressure, oxygen fugacity, and other metal contents of the fluid (e.g., Fe, Cl) (Zhu, et al., 2011). However, the mechanisms of gold precipitation in large ore deposits remain elusive. Evidence suggests that at high temperatures gold can be contained at very high concentrations in the matrices of copper-iron sulfides, though as temperature decreases, it becomes unstable within these minerals (Kesler, et al., 2002; Fraley & Frank, 2014). Though much of the gold undoubtedly comes from the traditional deposit model and is precipitated directly from the saturated hydrothermal fluid, the portion of gold contained within these Cu-Fe sulfides remains largely unaccounted for in many models. Where does this gold go? Does it form grains of native gold along the boundaries of the sulfides that hosted the gold at elevated temperatures? Are the volumes of the native gold grains and the Cu-Fe sulfides that provided the gold to those grains correlated in any way (i.e. do larger gold grains come from larger Cu-Fe sulfide volumes)?

1.5 Goals of This Study

During economically challenging periods, cost-cutting and efficiency measures within the mining industry encourage a renewed level of importance to understanding ore minerals and

mineralization in fine detail. Trace element data can elucidate the mechanisms of ore formation and has been used to underscore vector-based approaches in mineral exploration (e.g., arsenic association with Carlin type gold deposits (Zhu, et al., 2011)). There is potential for using trace elements to provide understanding of small scale vectors and spatial geochemical variation in mineralized samples. These trace element "vector studies" could provide us with a detailed comparison of the geochemistry of primary copper minerals in different locations within porphyry and skarn deposits. Is there a trace element signature that distinguishes bornite in a skarn deposit versus bornite in a porphyry deposit? Does chalcopyrite that hosts native gold contain a specific trace element suite compared to chalcopyrite that apparently lacks associated native gold? We can also broaden the understanding of native gold occurrences within Cu-Au porphyry and skarn deposits by assessing the trace elements within native gold grains. Is there a way to fingerprint native gold sourced from gold contained within Cu-Fe sulfides versus gold that has precipitated directly from a hydrothermal fluid?

To answer these questions, we are using Laser Ablation-Inductively Coupled Plasma-Mass Spectrometry (LA-ICP-MS) and High-Resolution X-ray Computed Tomography (HRXCT). This study includes an evaluation and comparison of the trace element contents of the primary Cu-Fe sulfides, bornite and chalcopyrite, within the EGD. It also includes data on the trace element contents of native gold grains within the Grasberg porphyry deposit. To ascertain the potential volume of Cu-Fe sulfide that could have provided gold to a native gold grain, we used HRXCT to model 3D diffusional regions within sulfide networks of core samples. These diffusional regions, known as Modified Voronoi regions, are discussed in depth in Chapter 3 of this report.

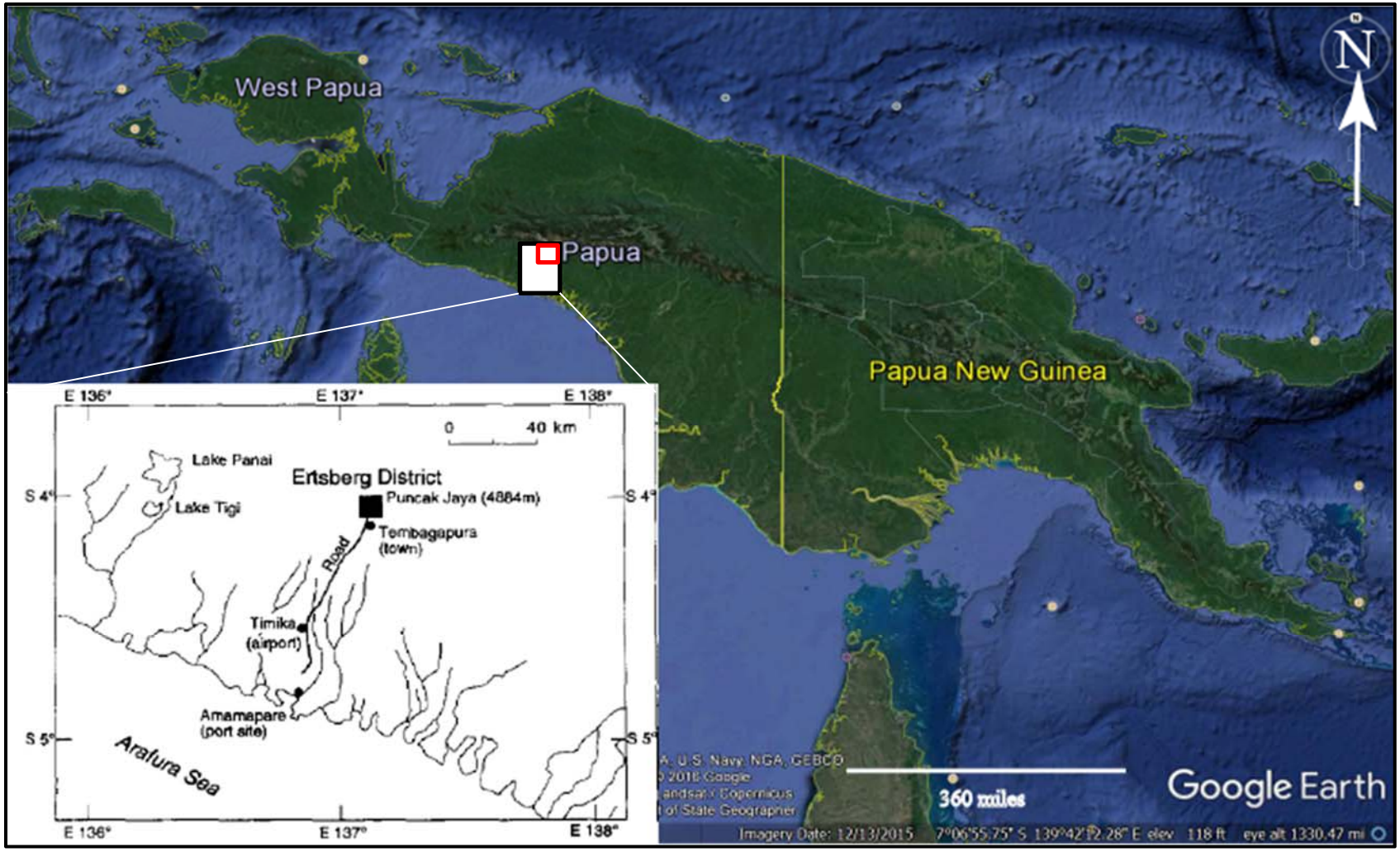

Figure 1.1 Location of Ertsberg Grasberg District

Contract of Work Area (white box). District (red box) in Papua, Indonesia. Inset map modified from Mertig et al. (1994).

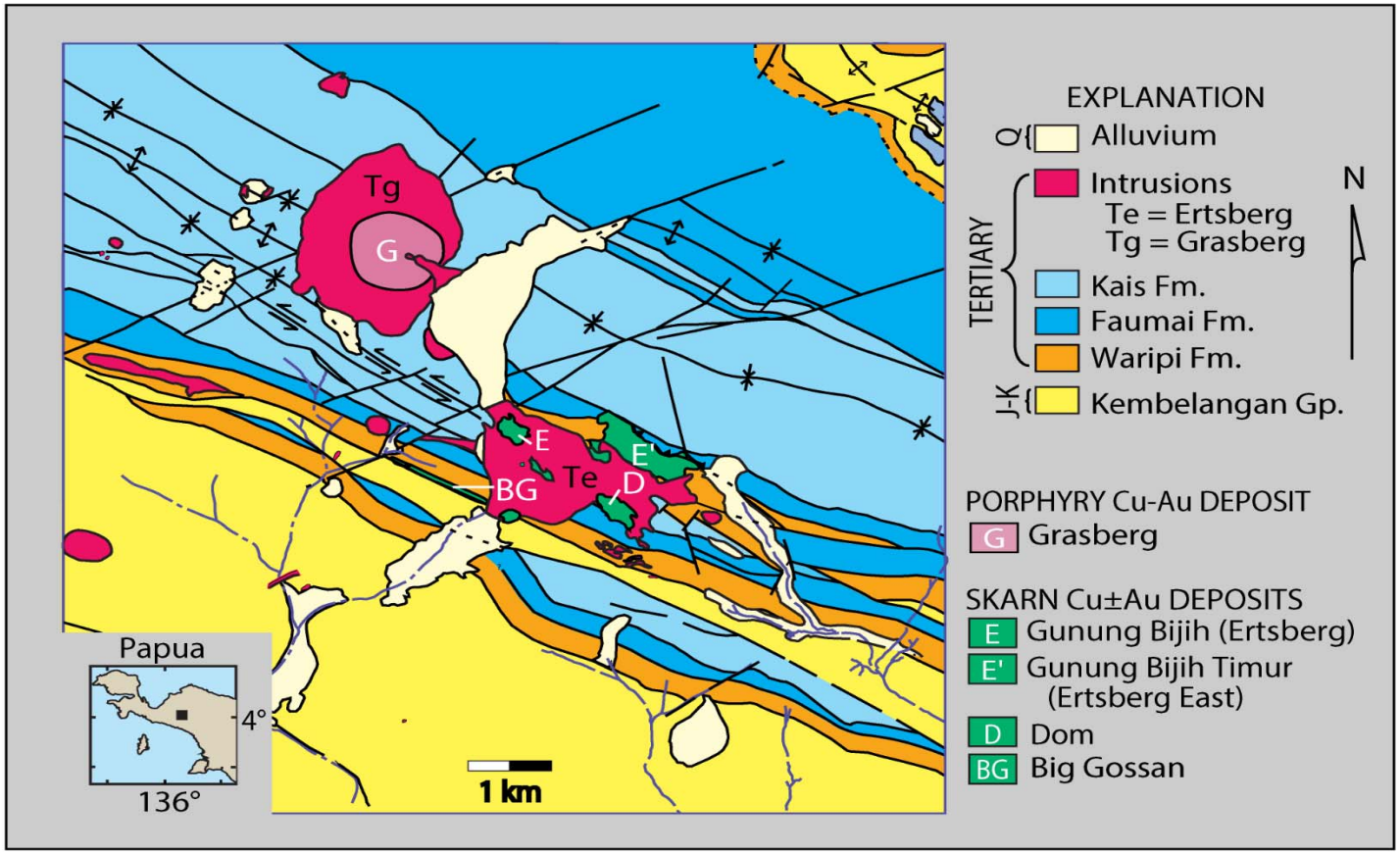

Figure 1.2 Generalized Geologic Map of Ertsberg-Grasberg District

GIC and EIC intermediate porphyry intrusions in pink and ore deposits in light pink and green.

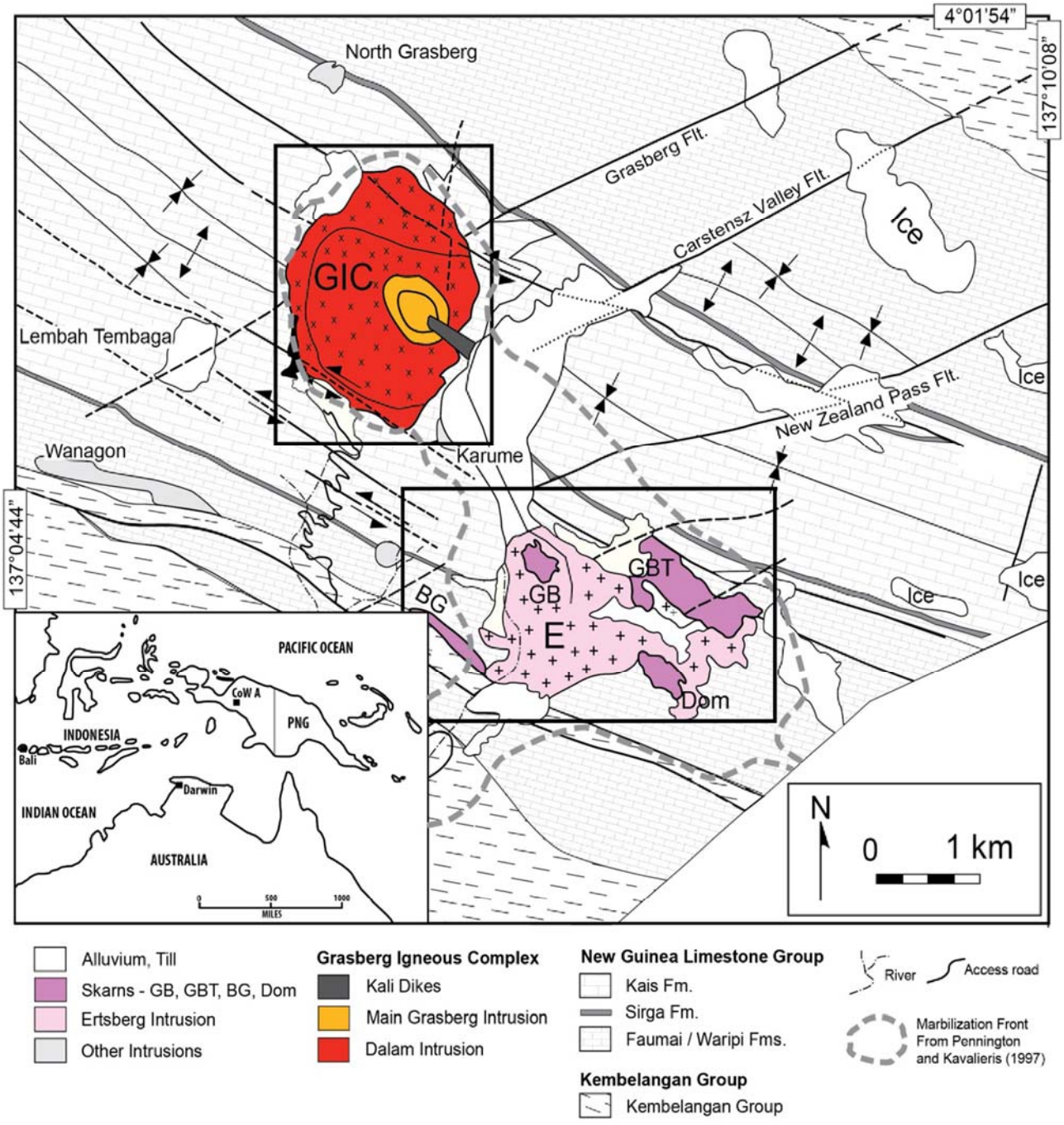

Figure 1.3 Ertsberg-Grasberg District Igneous Phases and Orebodies

GIC= Grasberg Igneous Intrusion; E= Ertsberg Intrusion; GB= Gunung Bijih; GBT= Gunung Bijih Timur; BG= Big Gossan. Modified from Wafforn (2017).

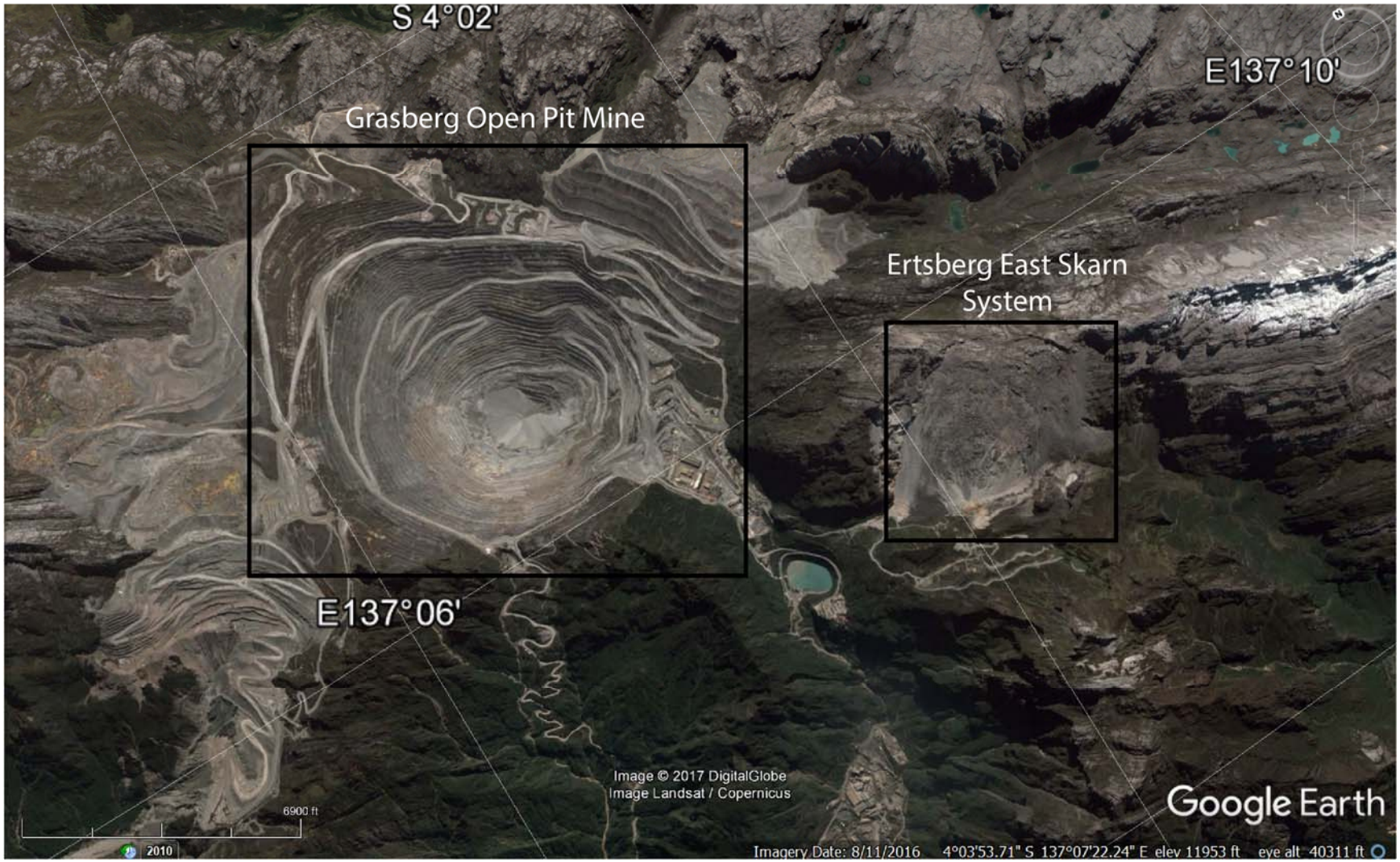

Figure 1.4 Grasberg Open Pit Mine

Satellite image of Grasberg open pit mine, and surface expression of Ertsberg East Skarn block cave mine.

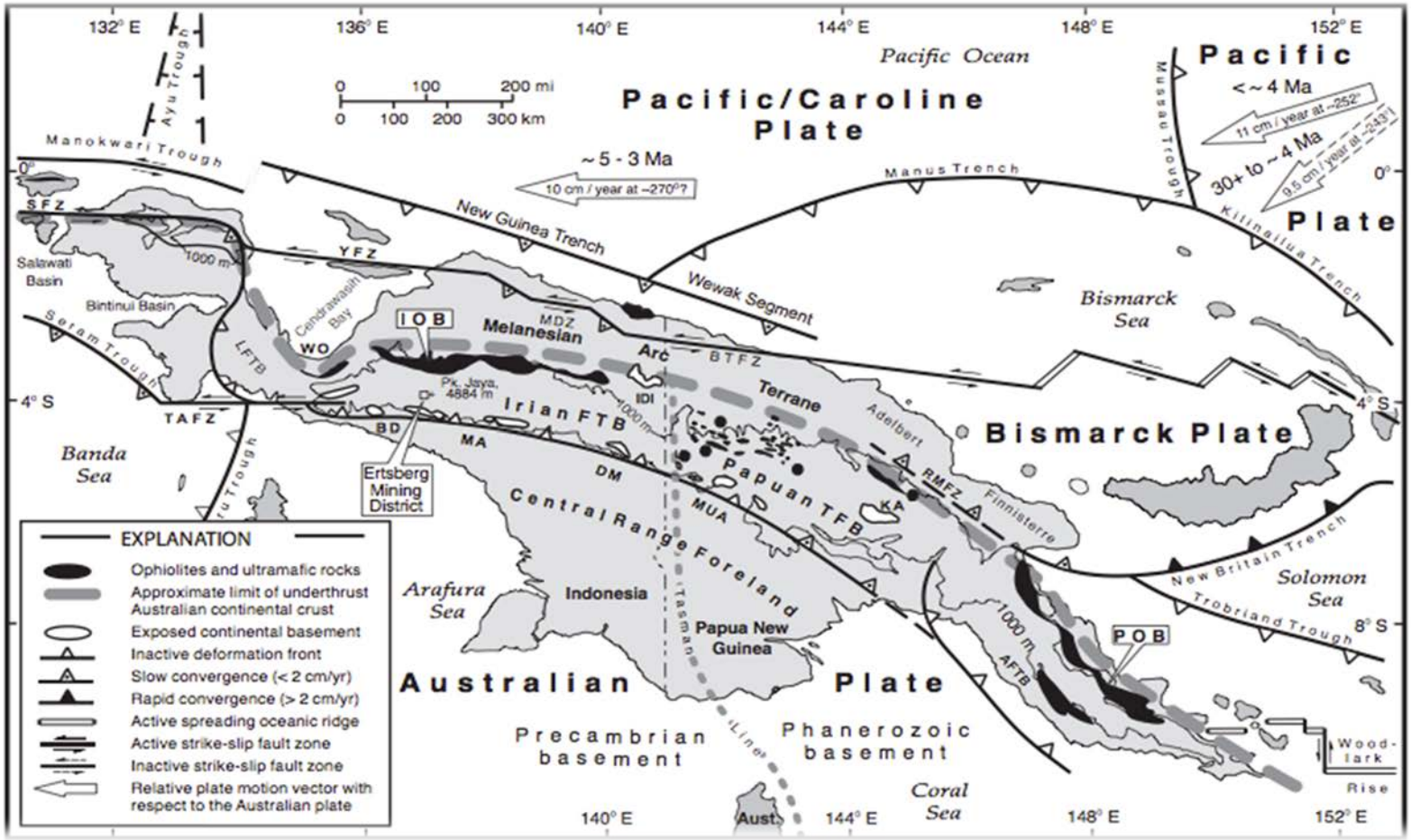

Figure 1.5 Tectonic Map of New Guinea

From Cloos et al. (2005).

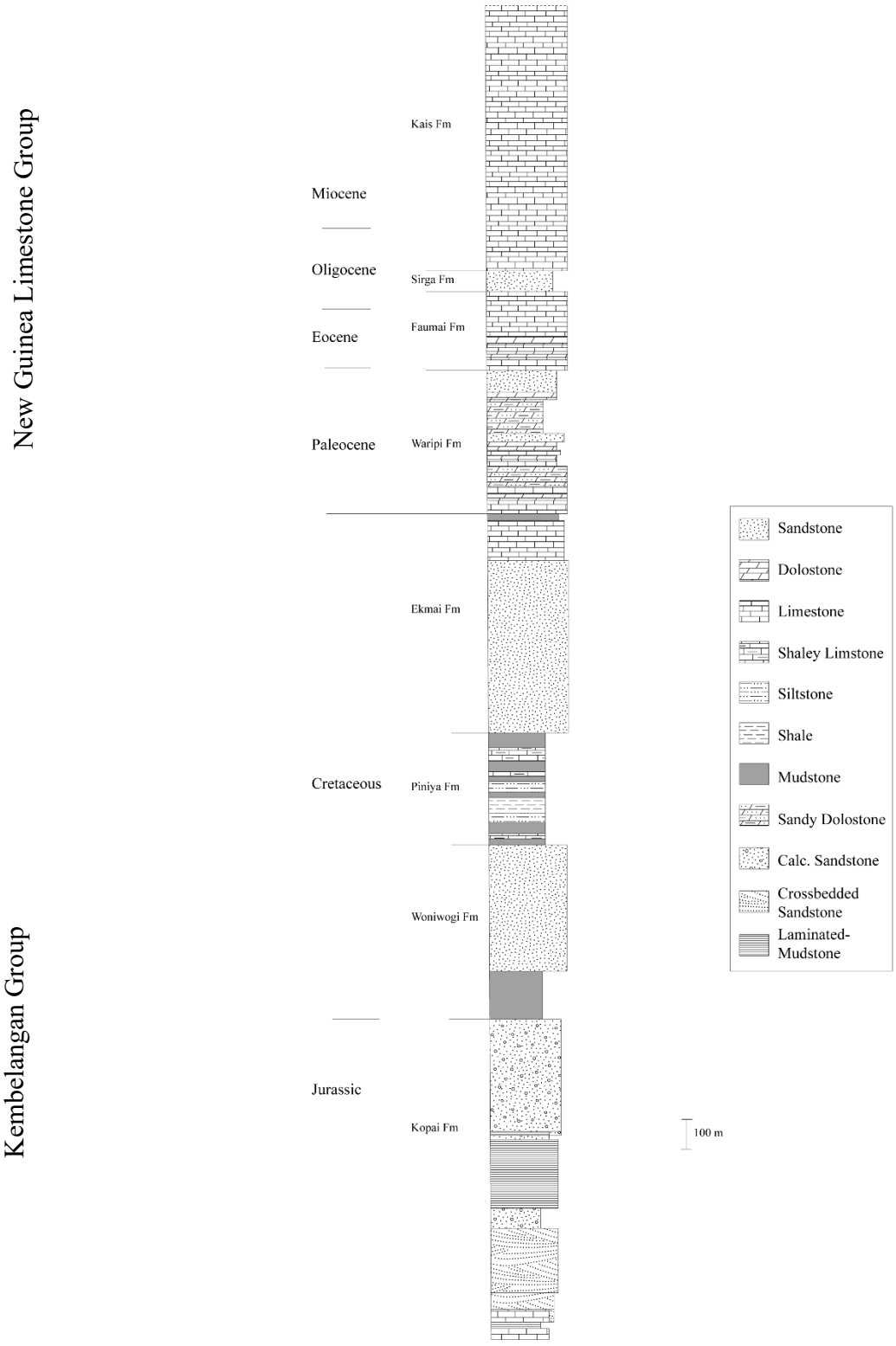

Figure 1.6 Kembelangan and New Guinea Group Stratigraphic Column

Modified from Gandler (2006); after Quarles van Ufford (1996).

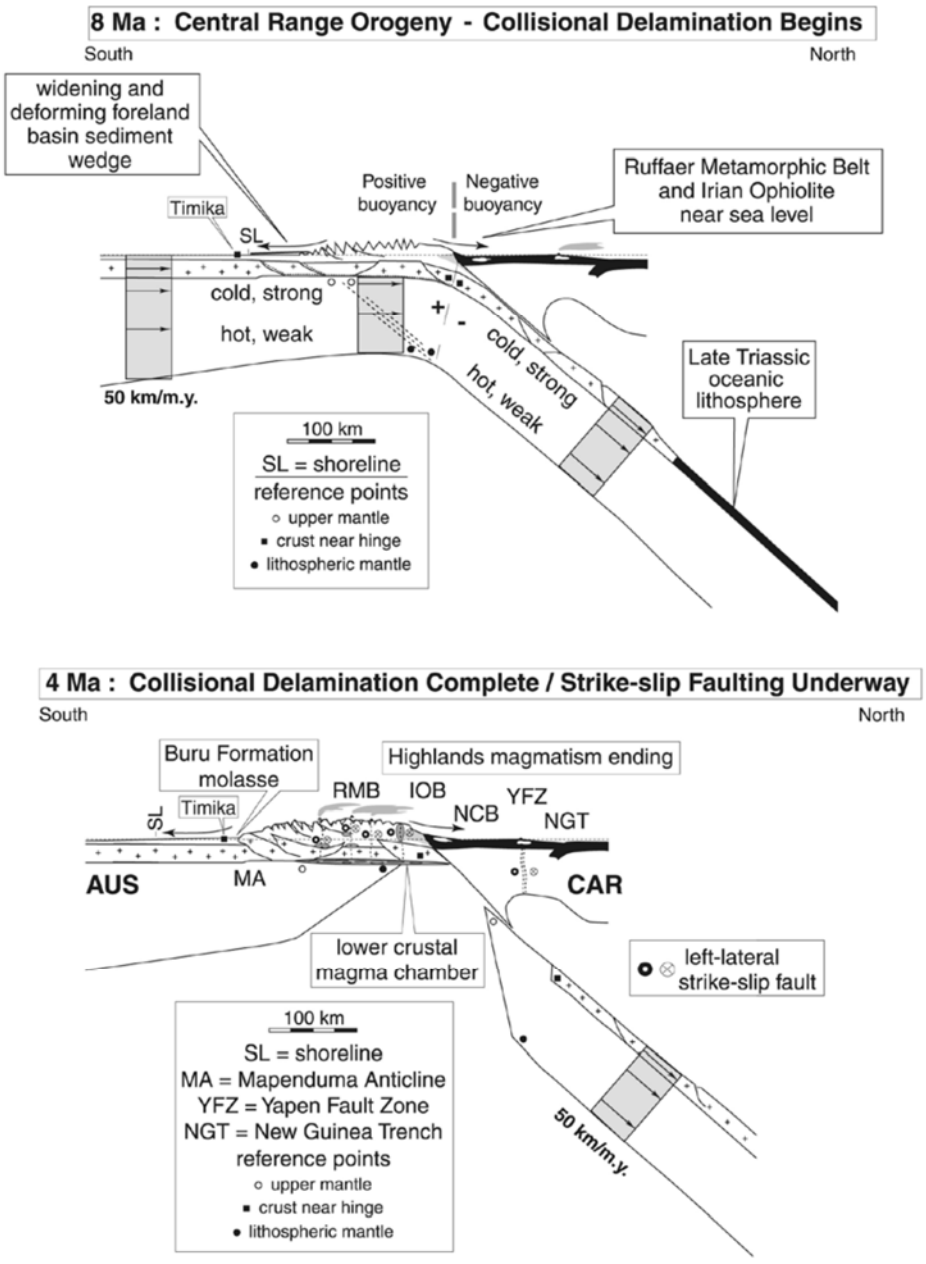

Figure 1.7 Collisional Delamination of Australian Plate

(Top) Lithospheric cross section of Central Range Orogeny at 8 Ma. Slab delamination is initiated when the Australian plate lithosphere stalls within the subduction trench, and the negative buoyancy of the lithosphere is translated updip to the cold, upper part of the plate where breakoff is induced in the region of high bending. (Bottom) Lithospheric cross section of complete collisional delamination at 4 Ma. From Cloos et al. (2005).

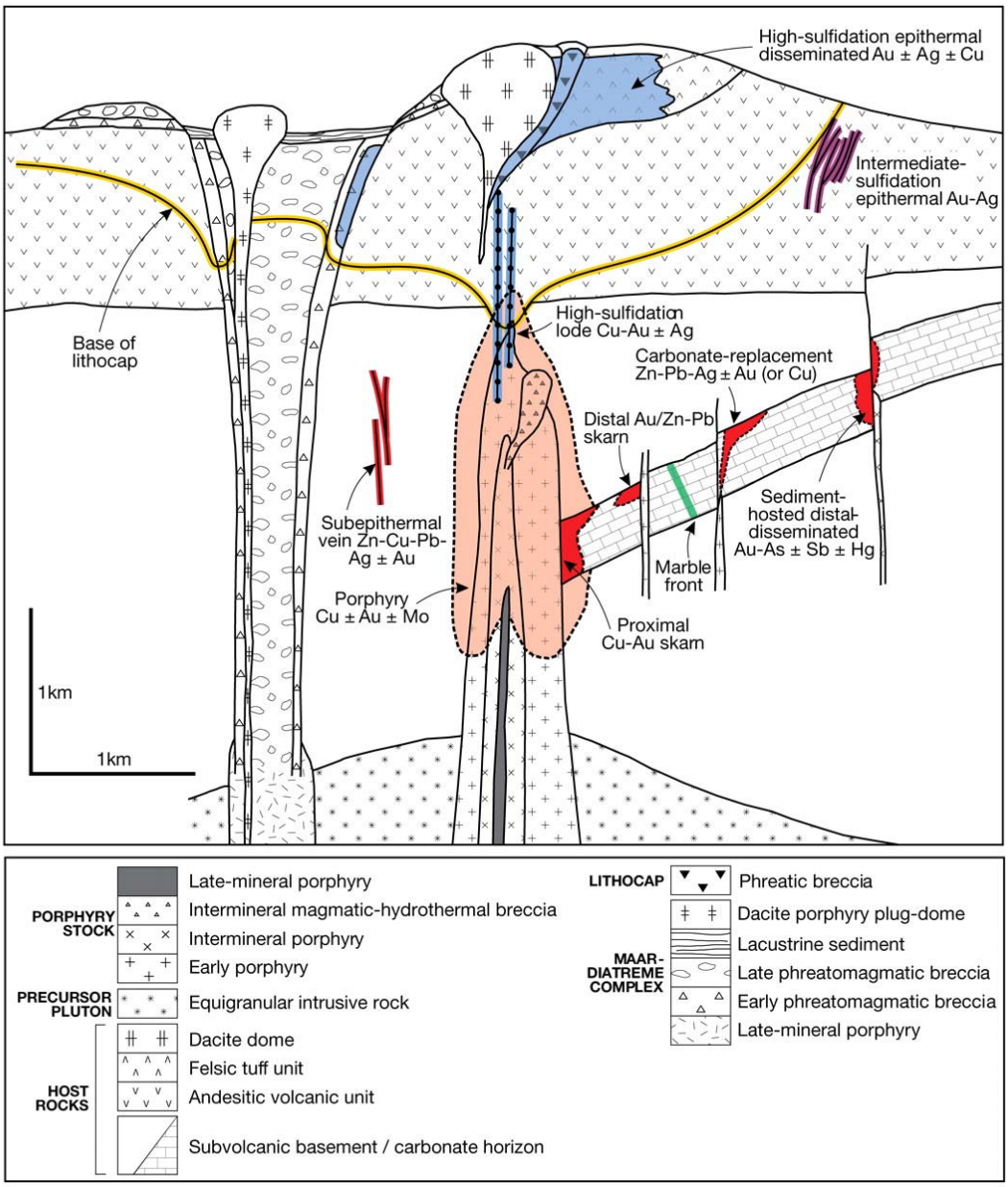

Figure 1.8 Porphyry and Skarn Deposit Model

Model of porphyry Cu system with a central porphyry intrusion and stock (Cu±Au±Mo) in orange. Associated host rocks, distal, and proximal deposit types are included. The EGD system includes multiple porphyry Cu-Au deposits (e.g., Grasberg, Ertsberg) and numerous proximal Cu-Au skarn deposits (e.g., Ertsberg, Kucing Liar) From Sillitoe (2010).

Chapter 2: Connecting Gold and Copper Iron Sulfides in Porphyry and Skarn Deposits

2.1 INTRODUCTION

Understanding the controls and intricacies of ore deposit formation is an enduring and important area of study. Correlating the mineralization mechanisms and occurrences between major economic mineral phases (e.g., Cu-Fe sulfides and gold) within a deposit can provide valuable information for metallurgical processing and reserve estimations (Norman, et al., 2003; Cook, et al., 2011). Numerous previous studies have noted the common occurrence of native gold grains along the boundaries of bornite and chalcopyrite crystals in porphyry-skarn systems (Figure 2.1) (Rubin & Kyle, 1997; Kyle & Ketcham, 2003; Arif & Baker, 2004). This close and consistent occurrence of gold with Cu-Fe sulfides at the microscopic scale mirrors the macroscopic trends of mineralization in the district. The EGD has a 1:1 Cu to Au ratio, where 1% Cu corresponds to 1 g/t Au (Cooke, et al., 2005). The highest grades of copper (2-5%) and gold (2-5 ppm) mineralization spatially coincide (Figure 2.2) (Leys, et al., 2012). This overlap in high grade gold and copper, when coupled with the proximal occurrence of gold grains along Cu-Fe sulfide boundaries, suggests that there is some intimate connection between copper and gold mineralization within the district.

To achieve economic concentrations, a specific set of conditions must be maintained over an interval of time long enough to yield a high economic mineral to host rock ratio. This set of conditions includes high-temperature fluids that are highly enriched in economic metals, which then circulate through a volume of reactive host rock small enough to concentrate mineralization, but large enough to produce a deposit which can be mined economically. As noted in the previous chapter, porphyry and skarn mineralization

models rely primarily on the precipitation of economic minerals directly from the circulating hydrothermal fluids, when those fluids come into contact with reactive country rock at low pressure and temperature (John, et al., 2010).

Experimental studies, e.g., Fraley and Frank (2014), Kesler et al. (2002), Kesler (2004), and Simon et al. (2000), indicate that at elevated, hydrothermal ore-forming temperatures, gold solubility in the Cu-Fe-S system is very high (Table 2.1). However, during cooling of the hydrothermal system, gold solubility in bornite and chalcopyrite decreases dramatically from 1000s ppm Au, to 10s ppm Au. The gold that was contained within the bornite and chalcopyrite at high temperatures becomes unstable at low temperatures, and may exit the sulfide matrix. Therefore, during retrograde cooling of an ore system with Cu-Fe sulfides and gold, there is a mass of 'free' native gold which has been exsolved, and must *go somewhere* (Kesler, et al., 2002; Kesler, 2004; Fraley & Frank, 2014). Many of the studies that noted the occurrence of gold grains along the boundaries of bornite and chalcopyrite suggested that these grains may be formed from the exsolved or purged gold from within the sulfide minerals (Rubin & Kyle, 1997; Arif & Baker, 2004; Kyle, et al., 2008). This would mean that along with gold precipitated directly out of hydrothermal fluids, we must also consider this potential new mechanism by which native gold grains were created or increased in size. Elucidating and seeking evidence of this model for gold mineralization is the central goal of this thesis.

2.2 GOLD FROM WITHIN: CU-FE-S MODEL

Research is scarce on the occurrence and distribution of gold in Cu-Fe sulfides at high temperatures, and there is currently no consensus on how the gold is contained within the sulfides (future atomic-scale studies of the sulfide lattice are needed to expand on this area). Previous studies on gold in pyrite (FeS) and arsenopyrite (FeAsS) show that gold

can be contained in sulfides in large quantities as metallic nano-inclusions or incorporated directly into the sulfide lattice structure (Cook & Chryssoulis, 1990; Tomkins & Mavrogenes, 2001; Reich, et al., 2005). Although gold behaves differently in the Fe-S system and the Cu-Fe-S system, Tomkins and Mavrogenes (2001) indicate that gold is able to move in and out of sulfide lattices by diffusional processes. Based on this, and the lack of any other reasonable mechanism, we propose that gold movement in the Cu-Fe-S system is also controlled by diffusion (Tomkins & Mavrogenes, 2001).

A diffusional growth mechanism can potentially be discerned from textural clues. Carlson (1991) showed that during nucleation and growth of garnet porphyroblasts during regional metamorphism, diffusional competition for nutrients between garnet crystals affected the textural features in the samples, specifically crystal size and spacing. Carlson (1991) suggested that a diffusion-controlled crystal growth process (i.e. gold grains on the edge of sulfides), should yield a correlation between the size (i.e. volume) of a crystal, and the size of the diffusional area it scavenged for nutrients (Carlson, 1991). If local depletion of nutrients around a growing crystal also inhibits nucleation of new crytals, the region around a crystal may be interpreted as the diffusional domain captured by that crystal. If nutrient scavenging continued unchecked until all the desired nutrients were incorporated by the crystals, the entire matrix would be depleted. To retain only locally depleted zones surrounding crystals, diffusion would need to be stopped prior to reaction completion, potentially by a decrease in temperature. Correlations between crystal volumes and domain areas were relatively low in Carlson (1991), in part because the diffusional growth model is strongly affected by garnet nucleation time, such that garnets which nucleated earlier had a longer period of time to gather nutrients compared to other crystals that nucleated later, resulting in a larger diffusional domain for earlier garnets. Carlson and Denison (1992) indicate that the scatter in volumetric correlations between Voronoi polyhedra and

garnet crystals is also due to inhomogeneity in the initial distribution of nutrients within the matrix, and that Voronoi polyhedral are only rough approximations of actual diffusional domains.

For the purposes of this study, we postulate that gold grains along the boundaries of bornite or chalcopyrite crystals could be getting all or the majority of their mass from gold that was exsolved from the sulfides. If the gold was mostly contained in the sulfides as structurally bound atomic gold, we expect that there must be a minimum volume of Cu-Fe-S capable of hosting the amount of gold present in a boundary gold grain (Figure 2.3). Based on the research referenced in the preceding paragraph and our assumptions here, we posit that there could be a correlation between the volume of Cu-Fe sulfide and the volume of associated native gold. Specifically, there should be a correlation between the volume of a specific diffusional drainage region within the Cu-Fe sulfide that provided gold to a specific native gold grain along the sulfide grain network. We would expect a positive correlation where a large gold grain is associated with a large diffusional drainage region of Cu-Fe sulfide. To assess this potential relationship, we used High Resolution X-ray Computed Tomography. We might also expect to see that isolated Cu-Fe sulfide crystals with no boundary gold grains have markedly higher gold contents because the gold did not exsolve to form boundary grains.

Gold diffusion though copper sulfides has not been extensively modeled or researched, and the specific evidence of this behavior is somewhat ambiguous. However, we expect that removing 100s to 1000s of ppm of gold from within a Cu-Fe sulfide lattice would leave a geochemical fingerprint within both the sulfide crystals (bornite and chalcopyrite) and the gold grains. Characteristic gold proxy elements, like As, are not abundant in the EGD, thus the exact manifestation of this geochemical fingerprint is not

well constrained. Carlson and Denison (1992) state that if crystallization is governed by a diffusion-controlled nucleation-and-growth mechanism, there should be a correlation between crystal size and the relative isolation of that crystal within the matrix. However, if this is not the governing mechanism, for example, if nucleation is controlled by other constraints, like heat flow, we would not expect the size of the crystal to be related to the diffusional regions (Figure 2.4) (Carlson, 1991; Carlson & Denison, 1992). If gold grain growth is primarily controlled by diffusion, then a nutrient depleted zone may be present in Cu-Fe sulfides that donated gold to a growing gold grain, and we could potentially find evidence of this using trace element geochemical analyses. LA-ICP-MS was used in this study to analyze EGD porphyry and skarn Cu-Fe sulfide samples.

2.3 HYPOTHESES

Following the preceding discussion, this study aims to explore the hypothesis of diffusional draining in the Cu-Fe-S-Au system by analyzing potential textural and geochemical clues.

2.3.1 HRXCT

We will determine the presence or absence and nature of the correlation between the volume of Cu-Fe sulfide "diffusional drainage regions" and gold grain volumes. HRXCT analyses can provide data on many more gold grains than traditional 2D petrography, which will improve counting statistics for textural analyses. However, HRXCT analyses are limited by our assumptions of homogeneous distribution of gold throughout the sulfides, that all gold in gold grains came from the Cu-Fe sulfides, and that all gold grains will be unambiguously within the resolution limit of the HRXCT data. Another limitation we encounter is that, due to trade-offs between sample size, data

resolution, and gold grain abundance, modified Voronoi polyhedral are rarely completely defined within the physical core sample, and their true volumes are thus ambiguous.

2.3.2 LA-ICP-MS

We will examine the trace element geochemical data for the differences in geochemistry between porphyry/skarn Cu-Fe sulfides with and without gold grains, if any differences exist. We will also determine the presence or absence of a region of gold depletion immediately surrounding gold grains. LA-ICP-MS is sensitive enough to determine concentrations down to ppb and ppt levels, but there is no systematic way to fully explain the nuanced variations of trace elements in Cu-Fe sulfides, which could restrict our understanding.

2.4 SAMPLES IN THIS STUDY

Samples in this study are from both the porphyry and skarn deposits in the EGD and were selected based on three characteristics. First, the available thousands of EGD core samples were screened based on assay values for gold, and samples with elevated gold values were preferentially selected from core data. Assayed cores are typically 3-meter intervals of longitudinally split core, such that high or low assay values do not equate directly to the presence of gold in a typically ≤ 10 cm half-core piece. Although high gold values were important during sample selection, the morphology of the copper sulfide network within the samples was deemed more critical during sample screening. Specifically, copper sulfide networks with apparently isolated and poorly interconnected copper sulfide networks were chosen. Potentially, choosing samples with this morphology could yield more confident analyses of the volume of a copper sulfide network (Figure 2.5).

Using these criteria, a representative suite of 23 core and hand samples of porphyry and skarn ores were selected for detailed analysis (Appendix A). Digital radiographs (DR) of each sample were taken to determine the presence of gold grains within the samples (Appendix A). Digital radiography has proven to be a useful, fast, and inexpensive means of determining the presence of gold grains in samples prior to completing a full HRXCT scan (Kyle, et al., 2008). DRs are similar to medical X-rays, and are made by passing X-rays through one side of a sample at a single angle. This generates a 2D grayscale image, where darker objects in the image typically correspond to more dense phases in the sample (Figure 2.6). DRs are discussed in more detail in Kyle et al. (2008). DRs are affected by sample thickness, where thicker and more complex samples appear darker in DRs and are more difficult to interpret. Because of this imaging limitation, some DRs in this sample feasibility study were unsuitable and the presence of gold grains could not be ascertained.

Based on DR images and other criteria, we narrowed the sample suite to 11 samples that either obviously contained potential gold grains, or had specific copper sulfide network morphologies (i.e. very isolated sulfide grains near potential gold grains) (Table 2.2). All Grasberg samples are from Tgm, the monzodioritic main Grasberg intrusion; Ertsberg samples are from Te, the Ertsberg diorite intrusion, and Tw, the Waripi skarn (Leys, et al., 2012). Within the Tgm, samples are located between 734,495-734,676 E, 9,551,340 – 9,551,450 N, and elevations of 3,063-3,821m (Figure 2.7a). Within the Ertsberg system, samples occur between 737,188-734,567 E, 9,548,910 - 9,549,411 N, and elevations of 2,535 – 2,976m (Figure 2.7b). After HRXCT scanning and image processing, the 11 samples were cut into billets and sectioned for LA-ICP-MS work. Twenty-two thick sections were made for LA-ICP-MS analyses (Appendix A).

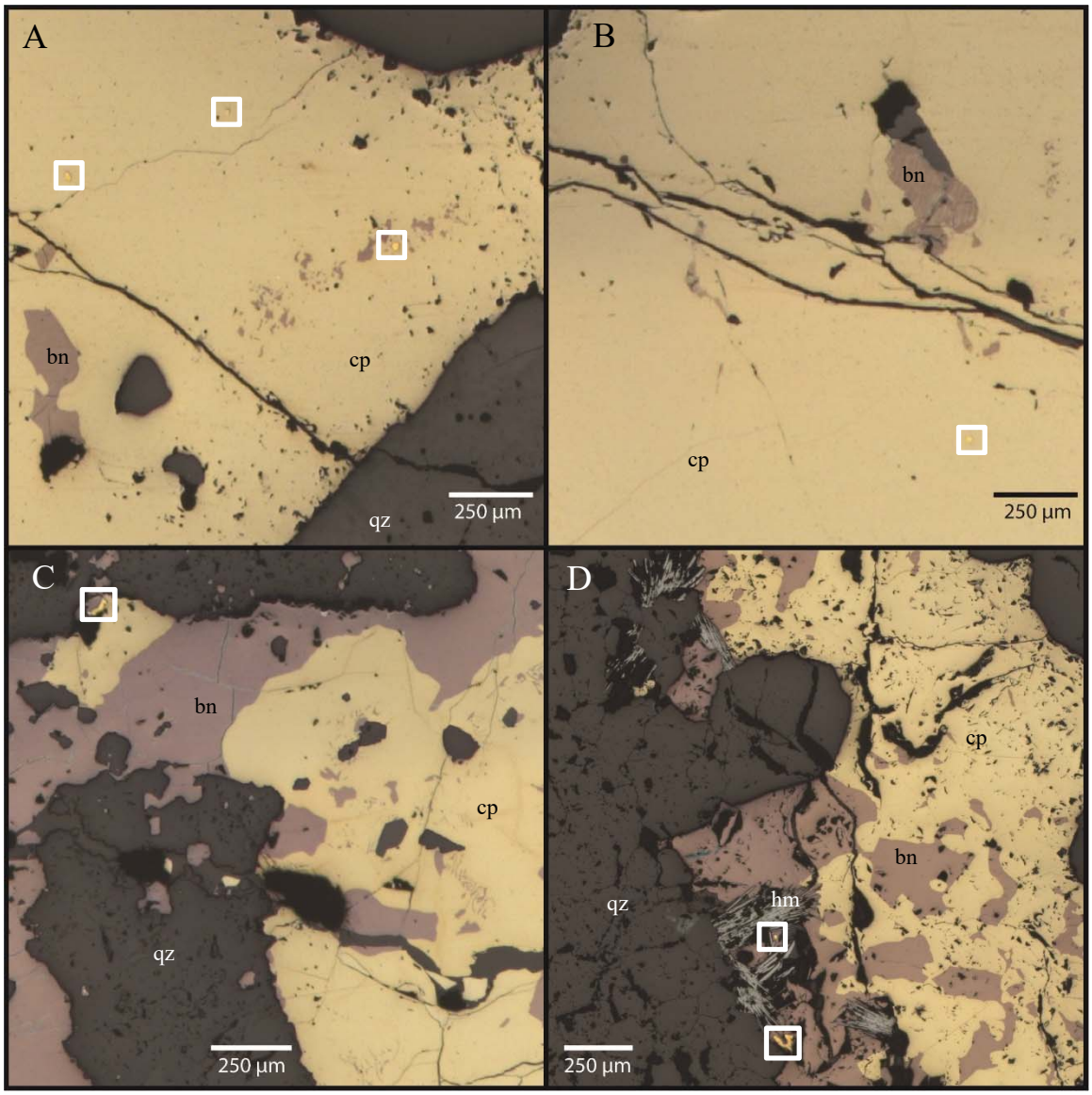

Figure 2.1 Occurrence of Microscopic Gold Grains Near Cu-Fe Sulfide

(A, B) Gold in chalcopyrite vein of porphyry stockwork sample GRS37-170-742.2. (C) Gold in bornite/chalcopyrite in high grade breccia sample AH90-4C-F. (D) Gold in bornite on edge of chalcopyrite/bornite vein with hematite from porphyry sample GRS37-170-714.2.

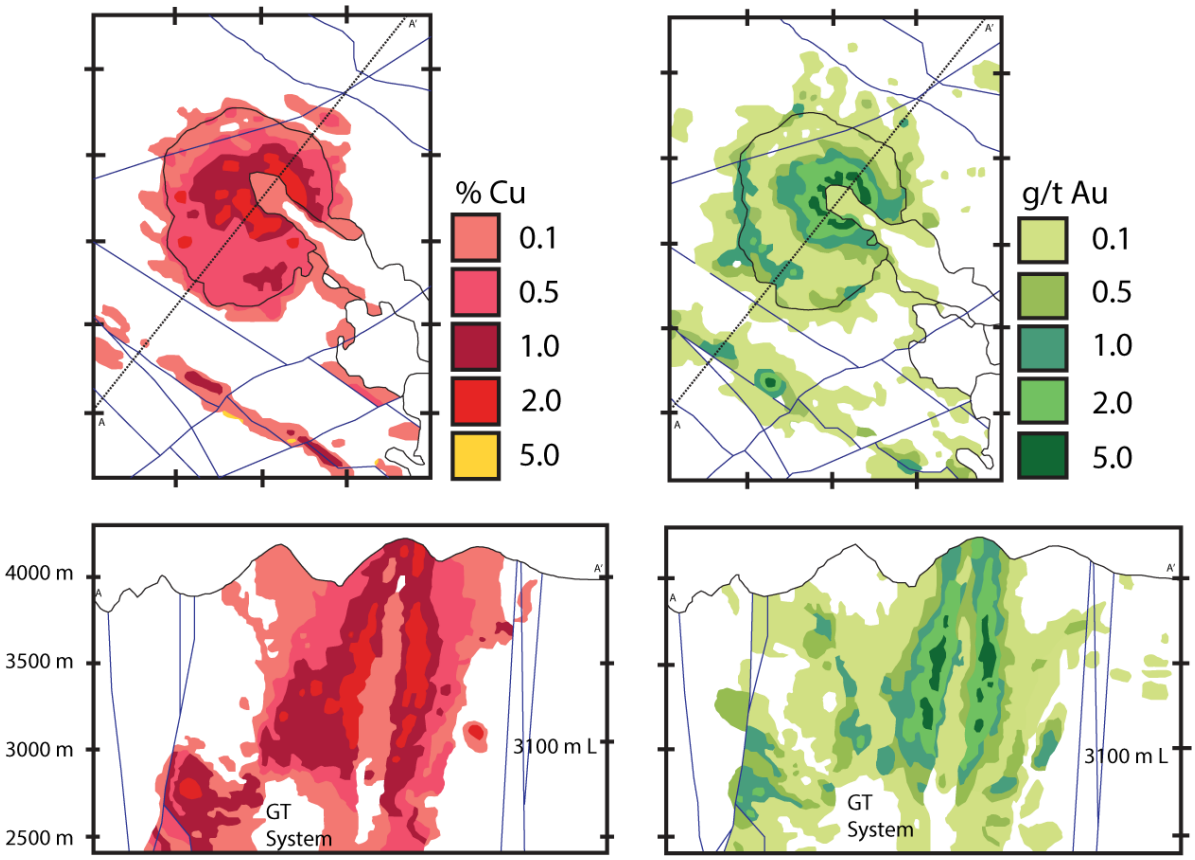

Figure 2.2 Cu and Au Mineralization Grades in GIC

Plan view (top) of 3100 level, and cross-sectional view (bottom) of Cu (%) and Au (g/t) mineralization grades within the Grasberg porphyry deposit. The highest grades of copper and gold mineralization coincide spatially at a deposit scale, indicating that Cu and Au likely share some mineralization controls. Modified from Leys et al. (2012).

Table 2.1 Au solubility in Cu-Fe-S system

Solubility of Au (ppm) in Cu-Fe-S System					
Temperatures (°C)		400°	500°	600°	700°
Simon et al. (2000)	bn	13-80	235-364	1280-8200	1350*
	cp	2-4	5-16	100-125	1100 ± 200
Kesler et al. (2002)	bn	10	–	<1000	>1000
	cp	1	–	<1000	>1000
Fraley and Frank (2014)	bn	–	1000 ± 300	1500 ± 300	1800 ± 300
	cp	–	300 ± 100	800 ± 200	1100 ± 300

Gold is very soluble in Cu-Fe sulfide minerals at high temperatures, but quickly becomes unstable within bornite and chalcopyrite as temperatures decrease (Fraley & Frank, 2014) (Kesler, et al., 2002) (Simon, et al., 2000).

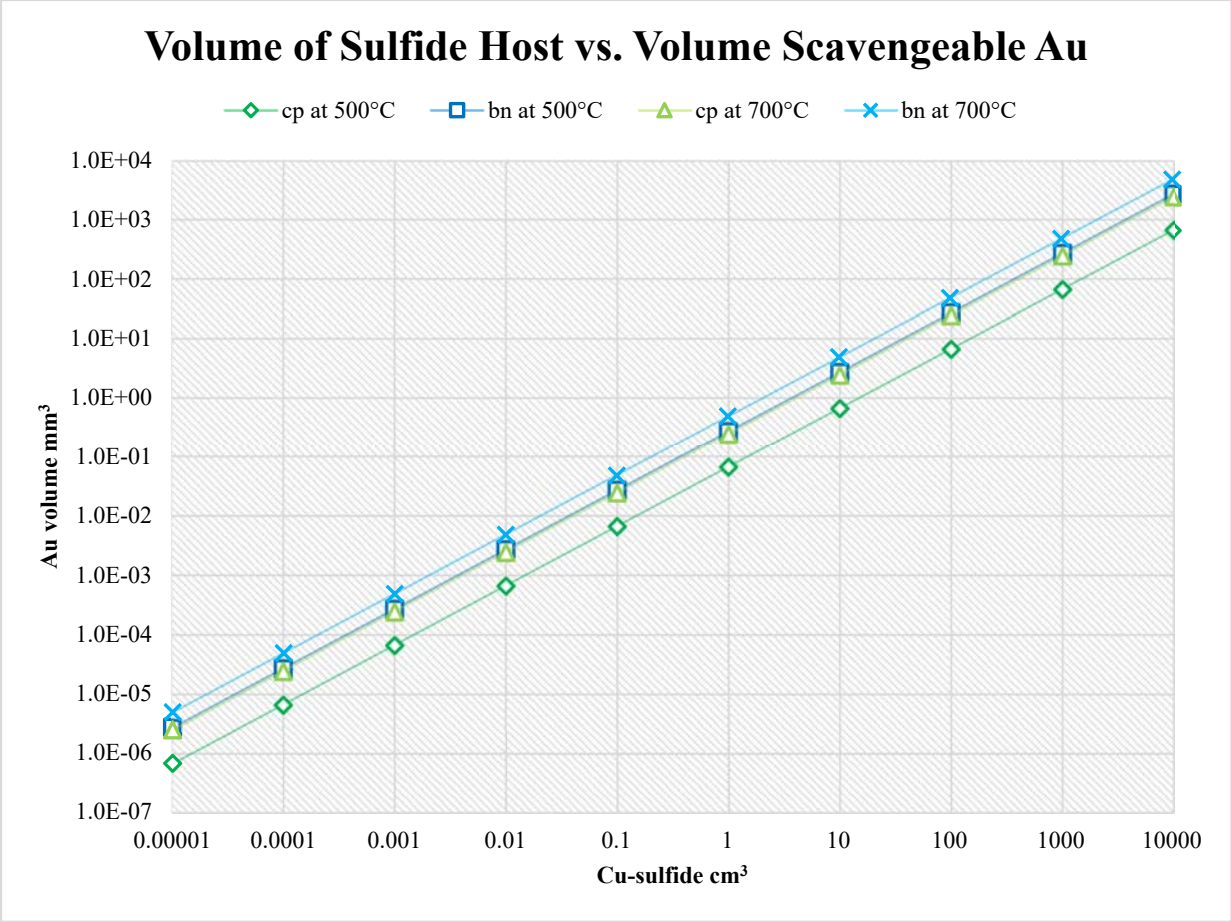

Figure 2.3 Potential Exsolved Au Volume from Cu-Fe Sulfide Volume

Based on experimental studies by Fraley and Frank (2014), this graph shows the specific volume of gold that could be scavenged from a volume of copper sulfide. This data was calculated based on a simple volumetric transform where D=m/V where d= mineral density, m=mass, and v=volume. A specific volume of sulfide was multiplied by the density of either bornite or chalcopyrite, which was then multiplied by the volume of gold that can be held in that mineral at a specific temperature based on Fraley and Frank (2014) (e.g., chalcopyrite can host 300 µg/g of Au in its matrices at 500 °C). The resultant mass of gold was multiplied by the density of gold (19 g/cm^3) to extract a volume of gold that could be scavenged from the original volume of copper sulfide.

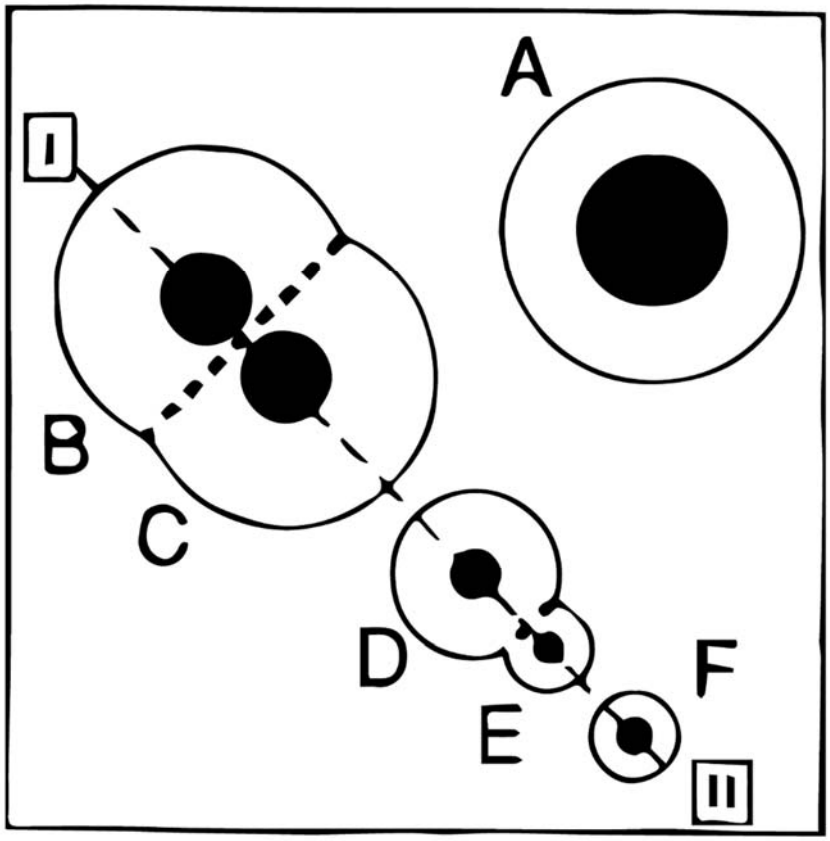

Figure 2.4 Model of Diffusional Depletion

Diffusional depletion of matrix material by garnet nucleation and growth. Crystal A is isolated. Crystal B and C nucleated and grew in close proximity, so their depletion areas overlap. Rather than garnet, this model can be applied to gold grain nucleation and growth near Cu-Fe sulfides. If the sulfides contained gold, which was then exsolved and drawn together to form a gold grain, that gold grain might have an area of gold depletion surrounding it similar to these regions. From Carlson (1991).

Figure 2.5 Half-Core Sample with Cu-Fe Sulfide Crystals

Cu-Fe sulfide crystals appear to be at least superficially isolated such that they might produce isolated diffusional drainage regions during HRXCT scanning and processing.

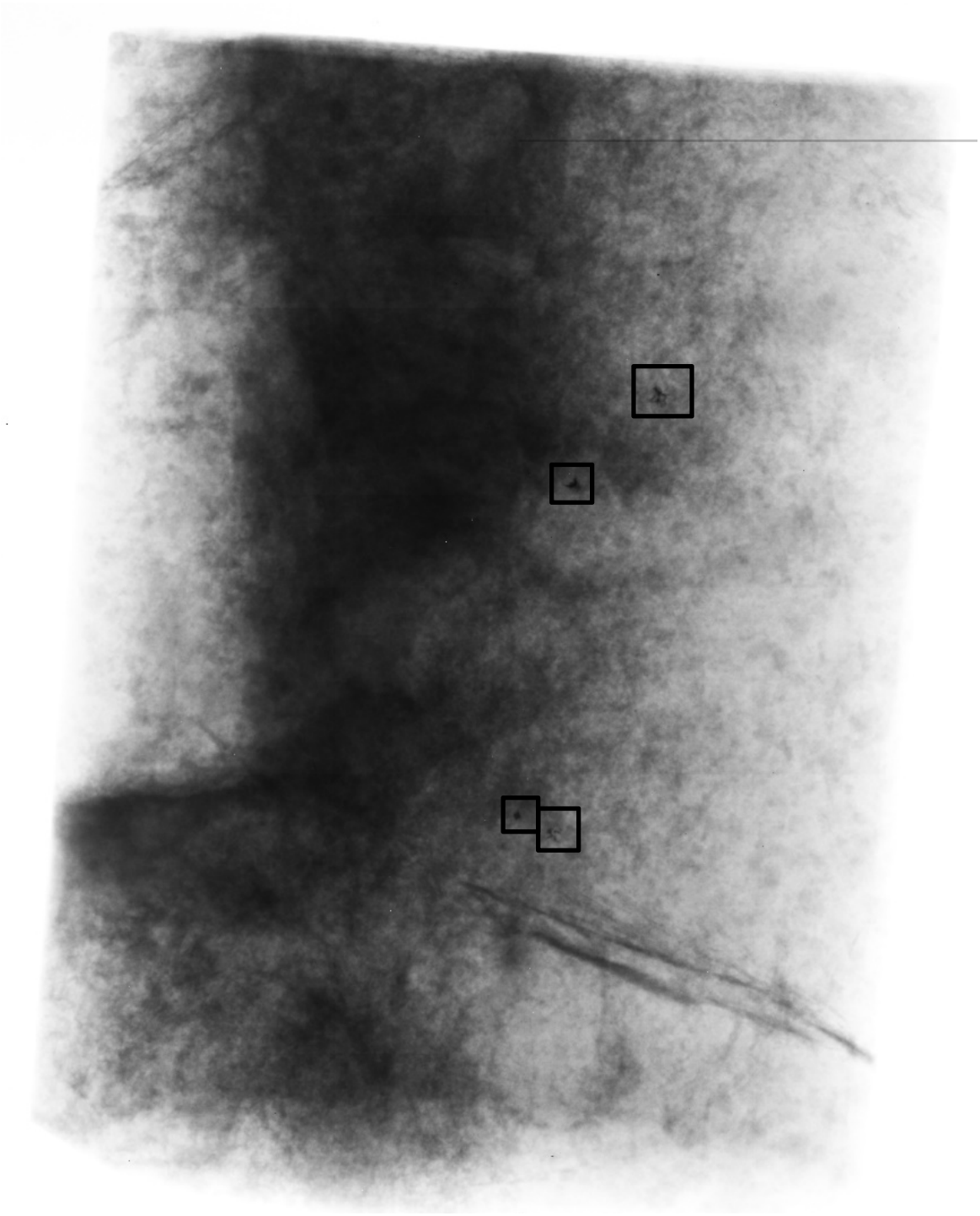

Figure 2.6 Digital Radiograph of AH90-4C-C

Gold grains (black boxes) are visible as black splotches within the gray Cu-Fe sulfide network of AH90-4C-C Grasberg stockwork breccia sample.

Table 2.2 Locations and descriptions of samples used in this study

Sample	Easting (m)	Northing (m)	Elev (m)	Unit	Description
GRS97-9	734,583	9,551,354	3,821	Tgm	qz+cp (±bn) stockwork +Au (6 mm core from Kyle et al. 2008)
GRS14-OP1	734,670	9,551,450	3,325	Tgm	bn+qz+an hand sample from open pit
GRS37-170-714.2-5	734,676	9,551,365	3,092	Tgm	qz+cp+bn matrix +bn/cp +Au veinlet
GRS37-170-645.9	734,674	9,551,361	3,158	Tgm	qz+cp veinlets (±bn±dg)
GRS37-170-742.2	734,677	9,551,366	3,063	Tgm	qz+cp "sawtooth vein" (±mt±bn) +Au+Pd-Te
GRS37-184-7.8A+B	734,495	9,551,361	3,797	Tgm	qz+cp+hm+mt veinlet +Au
AH90-4C-C	734,620	9,551,340	3,820	Tgm	qz+or+bn+cp (±mt±bt) +Au altered breccia
AH90-4C-F	734,620	9,551,340	3,820	Tgm	qz+or+bn+cp (±mt±bt±dg±cc) +Au altered breccia
TE01-16-566	737,188	9,549,411	2,535	Te	diorite qz+bt+mt +qz+bn+an vein
TE14-01-754.3	737,567	9,548,910	2,793	Te	diorite qz+bt+mt with +qz+cp+mo vein
DOZ-90-29	737,199	9,549,011	2,976	Tw	qz+an+bn vein

All were scanned at UTCT and sectioned for LA-ICP-MS work. Abbreviations used throughout: an= anhydrite, Au= native gold, bt= biotite, bn= bornite, cp= chalcopyrite, cc= chalcocite, dg=digenite, hm= hematite (specular), mt= magnetite, mo= molybdenite, or= orthoclase, Pd-Te= unidentified palladium telluride phase (vasilite?), qz= quartz, Tgm= Main Grasberg, Te= Ertsberg Intrusion, Tw= Waripi Formation.

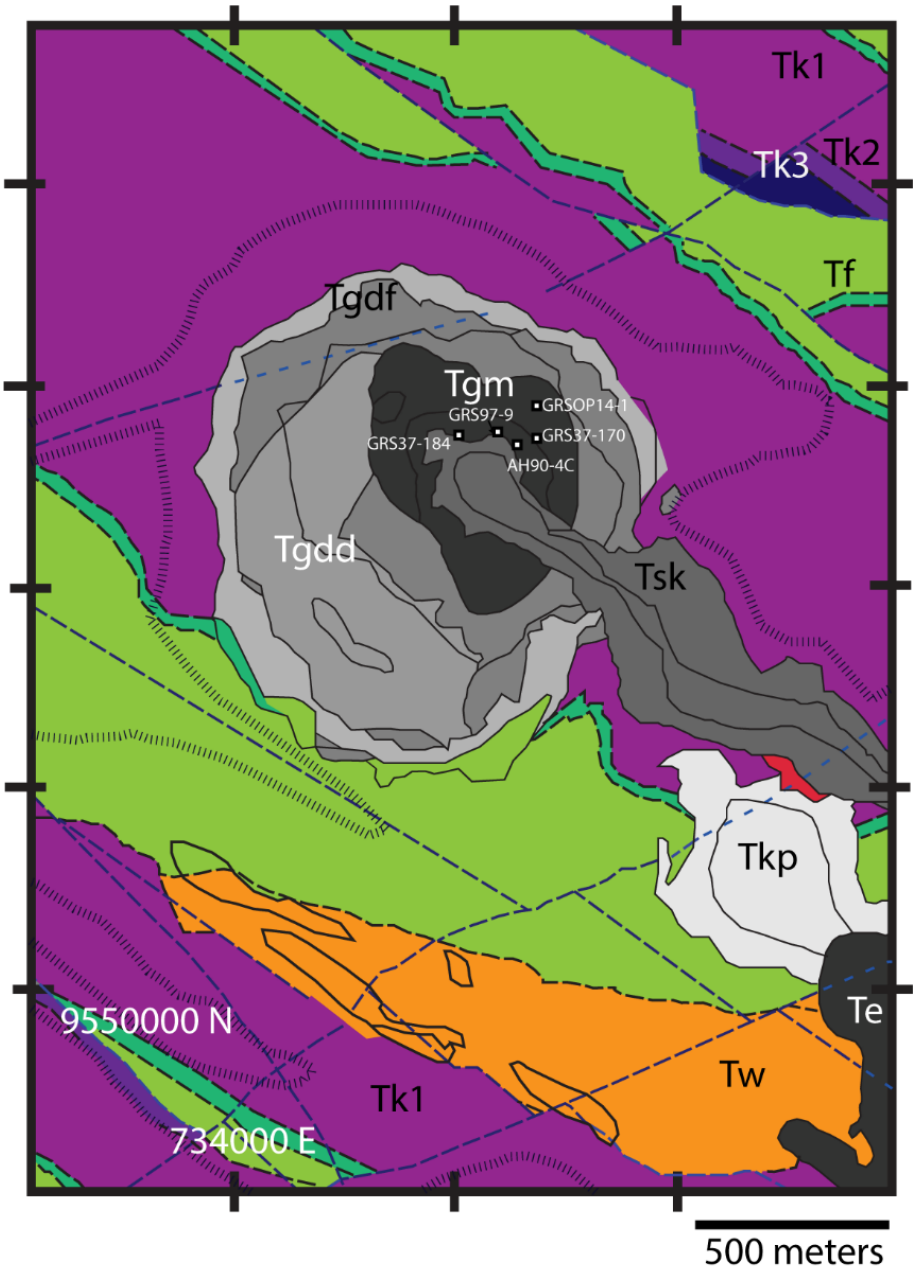

Figure 2.7a Grasberg Igneous Complex with Sample HRXCT Sample Locations

3100 level plan map of Grasberg Igneous Complex. Tk1, Tk2, Tk3= Kais Fm.; Tf= Faumai Fm.; Tw= Waripi Fm.; Tkp= Karume porphyry; Te= Ertsberg Diorite; Tsk= South Kali Dike; Tgm= Main Grasberg Intrusion; Tgdd= Dalam Diorite Intrusion; Tgdf= Dalam fragmental and volcanic; red= misc. intrusions. Modified from Leys et al., (2012).

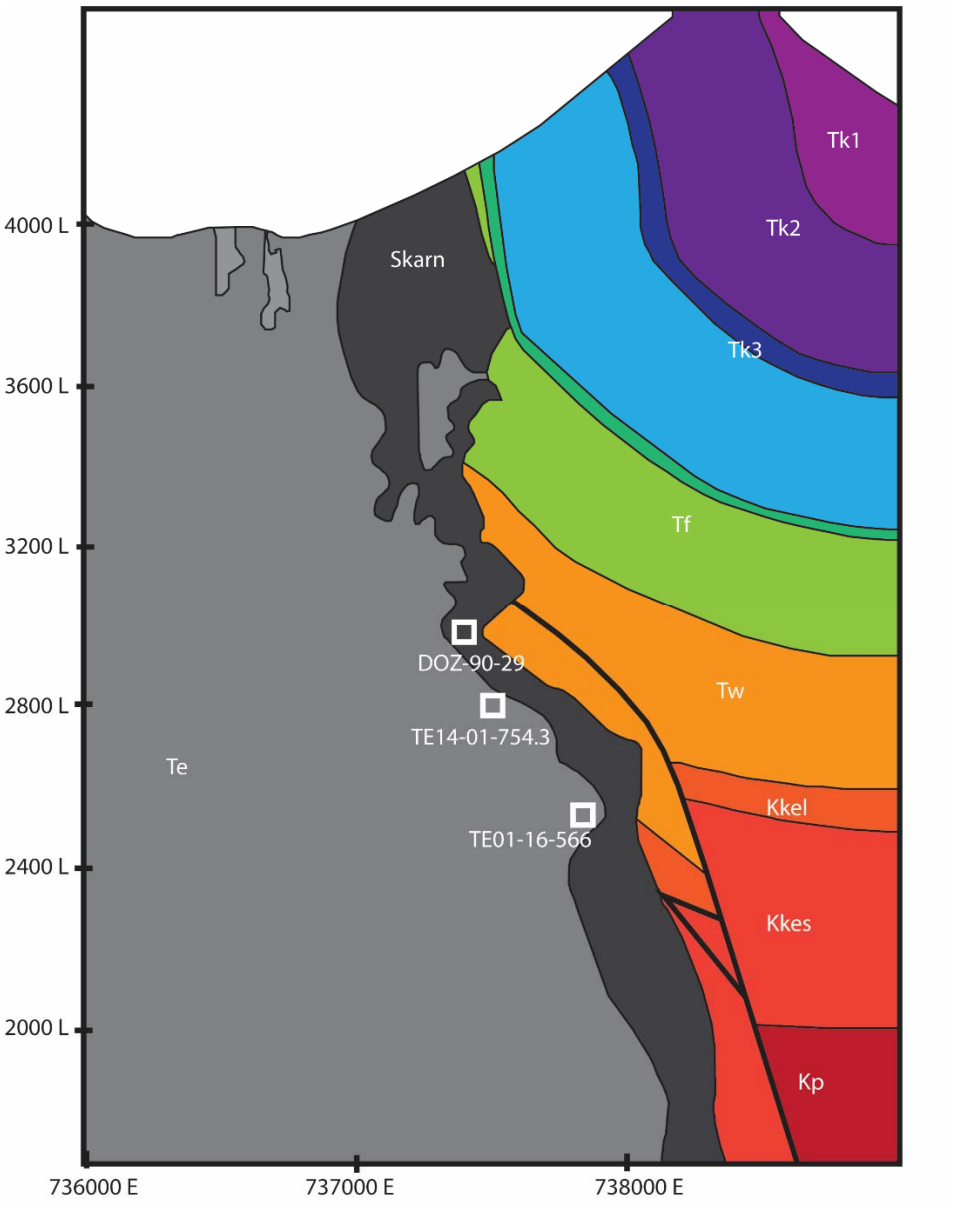

Figure 2.7b Ertsberg Intrusive Complex Cross-Section with Sample Locations

Cross-section of Ertsberg Intrusive Complex. Tk1, Tk2, Tk3= Kais Fm.; Tf= Faumai Fm.; Tw= Waripi Fm.; Kkel= Ekmai Fm. Limestone; Kkes= Ekmai Fm. Sandstone; Kp= Piniya Formation; Te=Ertsberg Diorite. Samples are plotted at the correct elevation but are schematically shown with respect to the pluton-skarn contact, and may be offset from their absolute easting and northing. Modified from Ledvina (2017) and Leys et al. (2012).

Chapter 3: High-Resolution X-ray Computed Tomography: 3D Petrography of Gold and Modified Voronoi Volumetric Modeling

3.1 Introduction

High-resolution X-ray computed tomography (HRXCT) is a nondestructive 3D imaging technique that permits in-situ analyses of the dimensions, spatial orientations, and relationships of minerals in a rock sample. According to Ketcham and Carlson (2001), HRXCT is similar to medical CAT (computed axial tomography) scanning, but because the imaged samples are inanimate, HRXCT can employ much higher energy X-rays for longer durations. When coupled with more finely spaced detectors and smaller X-ray focal spots, this allows for very high-resolution imaging of geologic samples (Ketcham & Carlson, 2001; Kyle & Ketcham, 2015). The basic elements for a HRXCT imaging set up include an X-ray source, a sample to be imaged, and a detector or array of detectors, and a motion system that allows the sample to be imaged over a range of angular orientations (Figure 3.1).

HRXCT imaging generates 2D images, called 'slices,' which represent a thickness of the sample that has been averaged down into a 2D plane. To generate tomographic volumes for image processing and analyses, 2D digital radiographs are captured at a number of angles as the sample rotates through 360 degrees. Two-dimensional digital slices are then reconstructed normal to the axis of rotation and, when placed into a stack, form the third dimension that allows for volumetric analyses (Ketcham & Carlson, 2001; Kyle & Ketcham, 2015; UTCT, 2016a). HRXCT volumes are comprised of 'voxels' or volume

elements, which are pixels with the third dimension (Ketcham & Carlson, 2001; Ketcham, 2005; Mote, 2004).

A key aspect of HRXCT is that X-rays traveling through different minerals in a sample are differentially attenuated based on the minerals' densities and compositions (Ketcham & Carlson, 2001; Ketcham, 2005; Kyle & Ketcham, 2015; UTCT, 2016a). HRXCT images are a manifestation of this X-ray attenuation, and minerals are represented by a range of grayscale values (referred to as 'CT numbers') (Figure 3.2). For an 8bit image, there are 256 potential grayscales, typically mapped from black (0) to white (255). X-ray attenuation is determined by the X-ray energy being used and the density and electron number of the phase being imaged, and when using a polychromatic X-ray beam, the size and geometry of the object. Dense minerals with high atomic numbers are more attenuating and are thus represented by the brightest grayscales in an HRXCT image (Figure 3.3).

Mineral phases with dramatically different densities or compositions are easily differentiated in HRXCT. The average density range for most Cu-Fe sulfide minerals in the EGD is 4.2 – 5.2 g/cm^3, while the average density of gold in the district is 19.0 g/cm^3 (Rubin & Kyle, 1997). Gold is therefore highly attenuating and appears very bright in images, in excellent contrast to most other mineral phases in metallic ore samples (Kyle, et al., 2008). When samples contain numerous, distinct, and isolated mineral grains within an homogeneous matrix, it is easy to separate one phase from another based on their grayscale values in the HRXCT data. However, common mineral intergrowths of voluminous phases, like bornite and chalcopyrite, which have similar attenuation, make it

difficult to separate all metallic phases during processing (Figure 3.4) (Kyle, et al., 2008). Bornite, a hypogene mineral phase in many porphyry deposits, is frequently overprinted as the hydrothermal system develops, leading to these intergrowths of common Cu-Fe sulfide minerals (Arif & Baker, 2004). In porphyry sample GRS37-184-7.8A+B, chalcopyrite veins were commonly intergrown with hematite (± magnetite) blades, which are very visible in reflected light, but are almost imperceptible in an HRXCT slice due to their small size. In the interpretation of the HRXCT data for this sample, hematite was included in the Cu-Fe sulfide phase as it was impossible to effectively separate the blades from the chalcopyrite vein. Many samples also contained minor copper sulfides like digenite, chalcocite, and covellite as individual, small grains or as alteration phases within the major Cu-Fe sulfide phases. Because hematite, chalcopyrite, bornite, chalcocite, covellite, and digenite all partition gold very differently or not at all, the lumping of all of these phases as one "copper sulfide" phase during HRXCT data analysis could potentially result in some inaccuracies.

As noted above, HRXCT provides an excellent tool for the analysis of gold-bearing ores (Kyle & Ketcham, 2003; Kyle, et al., 2008; Kyle & Ketcham, 2015). Gold in HRXCT data stands out in high contrast to most phases encountered in EGD ores, especially against typical rock forming minerals like quartz and anhydrite (Figure 3.3) (Kyle, et al., 2008). Because of this, individual gold grains can typically be separated from surrounding minerals, and their dimensions and occurrence modes can be assessed using a program such as Blob3D (Ketcham, 2005; Kyle & Ketcham, 2015). Blob3D extracts quantitative measurements from HRXCT volumes and provides a unique way to measure the in-situ

sizes, shapes, and relationships between ore minerals (Ketcham, 2005). Numerous previous studies have used HRXCT imaging for gold ore processing, and more detailed descriptions of the development of HRXCT ore applications can be found in these publications (Kyle & Ketcham, 2003; Mote, et al., 2005; Kyle, et al., 2008; Kyle & Ketcham, 2015).

Based on the information presented in Chapter 2, correlating the volumes of Cu-Fe sulfides and adjacent native gold grains could provide supporting evidence for the new mineralization model we are proposing. Blob3D was used in this study to:

Perform 3D petrological assessments of gold grains including occurrence modes (e.g., contacting minerals, location with reference to sulfide minerals, presence of other gold grains, etc.)

Extract quantitative measurements of gold grains (e.g., volume, shape, grayscale value)

Extract quantitative measurements of Cu-Fe sulfide networks (e.g., volume).

3.2 Methods: Imaging, Partial Volume Effects, and Modified Voronoi Modeling

3.2.1 HRXCT Methods

Full scans were acquired of 11 samples at the University of Texas High-Resolution X-ray Computed Tomography Facility (UTCT). Details on scanning procedure development and use are provided on the UTCT website (UTCT, 2016a), in Ketcham and Carlson (2001), Kyle et al. (2008), and in Kyle and Ketcham (2015). Ten samples were scanned on the NSI scanner and one sample was scanned on the Zeiss (formerly Xradia) microXCT 400 scanner. The NSI scanner utilizes two X-ray sources: a 225 kV FeinFocus

FXE225 microfocal source, and a 450 kV GE Titan source. A PerkinElmer XRD 1621 series flat panel detector is used for the NSI scanner (Kyle & Ketcham, 2015). Scanning parameters for all scans in this study can be found in Table 3.1.

Three-dimensional measurements of samples were extracted using Blob3D, a specialized program written at UTCT (Ketcham, 2005). To extract these 3D measurements, voxels must be assigned to the different mineral phases in a sample. This is done by defining a grayscale threshold in Blob3D for the mineral phase of interest. This process always begins with defining the HRXCT number threshold for the brightest phase present in a sample (e.g., gold). The threshold is defined as a range of CT numbers between 0 and 255 (in 8-bit data), ideally so that all voxels of a particular phase are included within the threshold, and no other phases are included. This portion of image processing is referred to as 'segmentation.' HRXCT segmentation threshold data for these samples can be found in Table 3.2.

Occasionally, mineral phases were challenging to segment from one another for various reasons. Mineral intergrowths of bornite and chalcopyrite were particularly common and were very challenging to segment from one another because of their similar grayscales (Figure 3.4). Because of this, bornite and chalcopyrite were grouped as one 'Cu-Sulfide' phase during HRXCT image processing. In some cases, isolated gold grains result in 'starburst' artifacts, where bright streaks emanate from the gold and extend into surrounding phases, locally altering their grayscales (Figure 3.5) (UTCT, 2016a). In some cases, beam hardening artifacts occurred in reconstructed images. Beam hardening is caused by an increase in mean X-ray energy as the beam passes through a sample, as low-energy X-rays are preferentially attenuated. This can cause the centers of highly attenuating minerals to appear darker than the edges, and can cause the CT number for a specific

mineral to change based on its location in the sample (Kyle, et al., 2008; Kyle & Ketcham, 2015). In sample TE01-16-566, severe beam hardening artifacts occurred around a large barite vein on one end of the sample. These artifacts significantly altered the grayscales of the surrounding phases and prevented accurate segmentation of phases throughout the scan volume which ultimately led to its exclusion from our HRXCT analysis.

Once identified, segmented mineral phases are then 'separated' into individual 'blobs,' which are a contiguous set of voxels that usually define an individual crystal (e.g., one gold grain is one blob). In this study, all blobs were separated using the 'Process all blobs as single objects' option, which does not require further inspection of the blobs. However, Blob3D offers a manual separation option where each blob can be individually inspected and modified (e.g., a single blob that is actually two separate crystals can be separated into its component crystals) (Mote, 2004; Ketcham, 2005). Once all mineral phases in the entire sample are represented by blobs, Blob3D can extract quantitative information on each blob.

Extracting accurate information on very small volume mineral crystals can pose another challenge in HRXCT processing. Each voxel in a volume represents the average CT number of all of the materials contained in that voxel. Thus, if there is a small gold grain that only extends halfway through a voxel, and the rest of the voxel contains quartz, the CT number of that voxel will represent the average of the properties of quartz and gold. This is termed the 'partial-volume effect (PVE),' and is primarily limited based on imaging resolution, such that a smaller voxel size is less likely to contain multiple materials and have an averaged CT number. PVE can significantly alter the calculated volume for a thresholded mineral. Another feature of limited resolution is that the boundaries of each

mineral are blurred, such that the properties of each voxel are affected by the surrounding voxels.

To mitigate PVE and blurring issues, corrections were applied during measurement extraction, in which the ideal end-member grayscale value for the phase of interest was compared to a calculated local-background grayscale (Table 3.2) (Kyle & Ketcham, 2015; UTCT, 2016b). As mentioned above, PVE can greatly affect the volume extracted for a specific blob (Figure 3.6). Because this study is primarily concerned with comparing the volumes of gold grains with volumes of Cu-Fe sulfides, having an accurate measurement is of utmost importance. The correction above can provide more accurate data on gold grain volumes, and thus, we compared the PVE volume measurements to the Cu-Fe sulfide volume measurements. PVE end-member values are determined during the segmentation and separation phase of Blob3D processing. We estimated end-member PVE values for gold grains as the maximum grayscale value of gold in that sample. The max-grayscale was extracted from separated Blob3D data for gold and plugged back into the PVE function of Blob3D for each sample. The local background grayscale was auto-calculated by Blob3D.

3.2.2 Modified Voronoi Methods

The same methods as above were used to calculate the total volumes of the Cu-Fe sulfide networks in our samples. The threshold value for Cu-Fe sulfides in each sample can be found in Table 3.2. To define the Cu-Fe sulfide volumes that could represent regions of diffusional drainage, the total Cu-Fe sulfide network volumes had to be separated into individual regions corresponding to a particular gold grain. To do this, we applied Voronoi analyses. Voronoi analyses are used to partition regions in a plane or volume based on the distance to previously defined seed points of interest. This results in a partitioned plane (or

volume) where each seed point has a corresponding region closer to it than any other seed point (Figure 3.7) (Aurenhammer, 1991).

For this study, we modified Voronoi analyses to only include the 3D Cu-Fe sulfide network in our samples, and all other matrix material is excluded. Furthermore, path lengths were calculated only through contiguous sulfide, corresponding to the assumption that diffusion of gold would only be through the sulfide, and not through the silicate matrix. The resultant isolated regions represent potential volumetric diffusional drainage regions as in Carlson (1991), and are referred to in this study as 'modified Voronoi regions' or 'diffusional drainage regions.' This modified Voronoi analysis was included as a new processing feature in Blob3D as written by R. Ketcham from 2016-2017. The Blob3D method uses each gold grain defined in the sample volume as a seed point, and then dilates outward stepwise until unique modified Voronoi regions encounter one another. Using this method each gold grain has its own corresponding volume of Cu-Fe sulfide from which it could have drawn gold during cooling and exsolution (Figure 3.8).

Using ImageJ, original 16-bit scan data were converted to 8-bit data. The 8-bit slice volumes for all samples were then binned by 2 on x, y, and z, to make the volumes were small enough to process in Blob3D in a reasonable amount of time (Rasband, 1997-2016). This doubled the voxel size for each volume, which results in a tomographic volume with one eighth the data size. Processing times on volumes that were not down-sampled were on the order of approximately five days to one week. Slice volumes for each sample were processed in Blob3D where 'gold' and 'cu-sulfide' were the primary components identified for most volumes. If other mineral phases were present (e.g., magnetite, molybdenite), they were segmented and separated as well, though no data were extracted for these phases.

Small objects in the CT data that appeared only somewhat brighter than sulfide were ambiguous, due to PVE effects: they could be small but blurred gold grains, or slightly larger instances of some other phase denser than sulfide but less dense than gold. Each sample was thus processed with a 'strict' and 'generous' threshold. The 'strict' threshold generally restricted the grayscale values of the gold grains to CT numbers above approximately 200. The 'generous' threshold attempted to include all grains brighter than the sulfide as potential gold grains, and thus spanned a broader range of CT numbers. The 'generous' threshold was tailored to each specific sample volume, thus the lower bound of grayscale range varied dramatically. Volumetric and grayscale statistics measurements were extracted for each sample for both thresholds. The maximum grayscale for gold was retrieved from grayscale statistics output and was used as the "Component Gray Level" to correct for the partial volume effect; the local background gray calculated by Blob3D was used as the "Background Gray Level." Modified Voronoi analyses were run for each sample where the 'gold' component was directed to grow into the 'cu-sulfide' component. PVE corrected volumes of gold grains and Modified Voronoi region volumes were compared graphically to determine the correlation between them.

3.3 RESULTS

HRXCT data for each sample were processed using Blob3D in numerous ways to determine the effects different processing schemes (e.g., 'generous' CT number threshold range versus 'strict' range of CT values). Results here include data for these various iterations of image processing.

3.3.1 3D Visualizations of Ore Samples

Using Avizo Lite 9.1.1 (FEI, 2016), the HRXCT scan data were rendered into 3D videos which are archived at UTCT. These images represent some of the most detailed 3D views of Cu-Fe sulfide networks within ore samples to date (Figure 3.9). Sulfides are rendered as semi-transparent, and each separate color represents an individual Modified Voronoi region. Native gold grains are colored in gold. In some cases, gold grains that correspond with a diffusional drainage region cannot be seen either because they are too small or because they are behind too great a thickness of Cu-Fe sulfide. Individual modified Voronoi regions were segmented using the threshold tool in Avizo 9.1.1. Isosurfaces were generated for each region because the volume render function in Avizo could not effectively colorize and display each Voronoi region distinctively as there were too many regions and the colors were not distinct enough to distinguish between regions. In some cases, modified Voronoi regions were too numerous and could not be separated using the segment tool in Avizo because only a limited number of regions can be segmented at a time in Avizo.

3.3.2 Gold Particles

HRXCT was used to perform 3D petrography on the gold in these samples to note any distinctive patterns in their occurrence mode, size, shape, or CT numbers. Depending on the segmentation and separation criteria used during image processing, this study presents data on dozens of gold grains. Twenty-seven of the grains separated during image processing are thought to be gold with a great degree of certainty based on their extremely high CT numbers, and in some cases visual confirmation of gold in thick sections made from scanned core samples. CT numbers for gold grains with a high degree of confidence range from 180 to 255. Numerous other grains (n=1022) could also be gold, however some

aspect of their character (e.g., low CT number, unusual morphology, anomalous mineral association, etc.) makes this less likely. Some gold grains which were very small and not highly attenuating have been confirmed in polished section to be gold, suggesting that there is still a degree of ambiguity when separating small gold grains from other bright phases using HRXCT.

3.3.2.1 Sizes

It is very unusual to observe native gold grains in EGD samples, and frequently the grains that are visible are anomalously large, thus characterizations of these grains are likely not representative of the majority of gold grains within the deposits (Kyle, et al., 2008) (Rubin & Kyle, 1997). Gold grains from the EGD have been characterized using CT, but the present study offers grain characterizations from recent high-resolution scans on a range of samples from both the porphyry and skarn deposits. Volumes will be reported as PVE-corrected volumes, so that any overestimations of grain size are somewhat mitigated by PVE calculations.

For only the high confidence gold grains, the average grain PVE corrected volume is 2.149×10^{-3} mm^3. Of the brightest gold grains, the largest grain separated was 1.34×10^{-2} mm^3. Some larger grains were separated in sample GRS14-OP1, although the veracity of these "gold" grains is uncertain. If all potential gold grains are considered, the average grain volume is 5.22×10^{-3} mm^3, an order of magnitude smaller than for the exclusively high confidence grains. Grain size distributions indicate that when including every gold grain, approximately 80% fall below 5.0×10^{-4} mm^3 (Figures 3.10 and 3.11). If even half of those grains are actually gold, studies on exclusively high confidence gold grains may not be representative of typical mine run products. The average gold grain volume for grains separated near bornite is 1.5×10^{-3} mm^3. The average volume of potential gold grains near

chalcopyrite is $4.75x10^{-4}$ mm^3, an order of magnitude smaller than grains near bornite. Gathering evidence on gold grain size from additional porphyry and skarn samples may further clarify the exact size distribution of gold in the EGD ore deposits.

3.3.2.2 Shapes

Native gold typically occurs in an anhedral or subhedral habit as granular or as platy "sheets" (Stefanova, et al., 2015). Arif and Baker (2004) determined grain shapes for native gold in the nearby Batu Hijau porphyry deposit to be dominantly well-rounded to sub-rounded. We can approximate the typical habit of EGD native gold grains using Blob3D estimations of grain shapes. Grains in this suite of EGD samples typically occur as rounded to sub-rounded, elongate granules. Aspect ratios and best fit ellipsoid radii for grains were extracted using Blob3D, which can be used to approximate shapes. Best fit ellipsoid radii for native gold grains separated in our porphyry and skarn samples were plotted on a Sneed and Folk (1958) ternary diagram using Tri-plot software to characterize gold grain shape (Figure 3.12) (Sneed & Folk, 1958; Graham & Midgley, 2000; Lindgren, et al., 2015). Of all of the gold grains separated in Blob3D 56.9% were elongate or rod-shaped grains, 27.3% were platy or disc-shaped, and 15.8% were compact or spherical grains. Those ratios stay approximately the same for porphyry grains and skarn grains. The aspect ratio of best fit ellipsoid for all segmented native gold grains has a mean of 1.85 ± 0.66. The higher the aspect ratio, the more irregular, less "compact," the grain shape. If gold grains become less "compact" as they increase in size, or vice versa, there should be a positive correlation between grain size and aspect ratio. There is only a moderate, positive correlation between grain size and aspect ratio in our data (Figure 3.13). Grains seen in polished sections in chalcopyrite appear smaller, more rounded, and less angular, while gold near bornite appears less regular in shape. However, the aspect ratios of bornite-gold and chalcopyrite-

gold appear very similar in the HRXCT data (Figure 3.14). There is no apparent correlation between a particular shape and an increase in modified Voronoi volume correlation, suggesting that these flat gold grains are not produced through a unique mineralization mechanism.

3.3.2.3 Compositional Variation based on CT Number

In most cases HRXCT has excellent resolution, but the blurring effect that occurs (3.2.1 HRXCT Methods) when dealing with micrometer scale objects can be challenging to overcome when characterizing bright phases. Samples TE14-01-754.3 and GRS37-170-742.2 exemplify the previously mentioned limitations encountered in this study regarding confident separation of small volume gold grains (3.2.1.) Within TE14-01-754.3 there are numerous small, dull grains that could potentially be gold grains, but are more likely grains of another mineral (Figure 3.15). GRS37-170-742.2 has numerous small, dull grains which appear very similar to the grains in TE14-01-754.3 (Figure 3.16). However, thick sections through this porphyry sample have verified the presence of very small (~1 μms) gold grains. Petrography and supporting SEM EDS of GRS37-170-742.2 also show the presence of small, gold-colored grains which are morphologically similar to gold, but are instead a Pd-Te phase (Figure 3.17).

3.3.2.4 Occurrences

In our samples, the morphologies and occurrences of the native gold grains associated with chalcopyrite or bornite differ greatly. Gold was observed in both CT and in thick section in the following instances. Gold grains were seen primarily as inclusions within chalcopyrite, while grains associated with bornite were typically found on crystal boundaries of chalcopyrite-bornite intergrowths. Native gold seen as inclusions in

chalcopyrite appears as symmetrical, spherical, ~1 μms grains. Morphologies of gold grains associated with bornite were varied, although grains typically appeared larger and less symmetrical (Figure 3.18).

In GRS14-OP1, gold was not seen in thick section, but a bright phase was separated during CT image processing that could be gold. This bright phase was seen painting or draping around adjacent grains within the sample (Figure 3.19). This morphology could be similar to platy or sheet-like gold, or this phase could be a separate mineral phase. Gold grains occurred near Cu-Fe sulfide phases 99% of the time; of these, 91% occurred near chalcopyrite while 8% occurred near bornite. Thirty-eight percent of grains occurred on the edges of Cu-Fe sulfide minerals, while 53% occurred as inclusions within bornite or chalcopyrite. Only 9% of grains were found in matrix material.

3.3.3 Volume Correlations

Modified Voronoi volumes were compared to PVE-corrected gold grain volumes to determine the degree of correlation between the volumes. Correlations presented here are Pearson bivariate correlation coefficients (r), with values between +1 and -1, where +1 indicates a very strong, positive correlation between x and y variables, and -1 indicates a very strong, negative correlation between variables. A value of or near zero indicates no apparent correlation. Critical values are for a 95% confidence interval, from a two-tailed t-test of Pearson correlation. PVE gold grain volumes used in these correlations were either from a broad range of CT values (inclusive of grains which are potentially not gold) referred to as “generous”, and a narrow range of CT values (includes only grains that are the most highly attenuating and are very likely to be gold, and excludes most small grains) referred to as “strict”. For some samples including only the brightest grains limits the population of gold to zero or one grain(s); no correlation is possible in these instances.

Results are shown in Table 3.3 for both separations on all samples, where minimum and maximum volumes for both grains and Voronoi regions, correlation coefficients, and grain counts are presented.

The hypothesized positive correlation is not present in the majority of samples (Table 3.3). The highest correlation coefficients were determined for strict separations of four porphyry stockwork samples. These high correlations were returned on samples with very few gold grains, such that the modified Voronoi regions extended to the physical edge of the core sample, making their actual volumes ambiguous. In 11 of the 20 separations, the largest gold grains are associated with some of the smallest diffusional drainage regions. However, these regions could have been prematurely truncated and are, in fact, much larger. None of the calculated correlation coefficients were statistically significant based on their critical values. Correlations between all generous and all strict grains are 0.07 and 0.04, respectively. Based on the estimates of the volume of gold that could be extracted from bornite and chalcopyrite at 500° and 700° C, gold volumes commonly are much less than expected for each modified Voronoi region.

3.3.3.1 Porphyry Samples

Volume correlations were calculated for eight porphyry samples (Figures 3.20 to 3.27). Generous separations of porphyry samples resulted in consistently low correlation coefficients, although the lowest correlations were found for samples with the most gold grains separated. Strict separations returned very high correlation coefficients, but they did not exceed the critical values. This is likely due to the paucity of high confidence gold grains (n=24).

3.3.3.2 Skarn Samples

Three skarn samples were scanned; volume correlations were calculated for two of these, and HRXCT data for the third were deemed unusable because of imaging artifacts (Figures 3.28 and 3.29). Calculations on strict separations in skarn samples returned no correlation as there were too few high confidence gold grains. Generous separations returned low, negative correlations between diffusional drainage regions and gold grain volume. TE14-01-754.3 had over 400 "gold grains" in this separation, 36% of which returned modified Voronoi region volumes of zero. These grains were not included in modified Voronoi calculations. This sample contains both extremes, large gold grains coupled with very small diffusional drainage regions, and small gold grains with large modified Voronoi regions (Figure 3.29). Gold grains in the generous separation of DOZ-90-29 had small volumes (average: 1.17×10^{-4} mm^3), but modified Voronoi regions were large (average: 75.52 mm^3).

3.4 DISCUSSION

Petrologic information from HRXCT scans agrees well with previously published data on EGD gold (Rubin, 1996; Baline, 2007). Gold grains almost ubiquitously occur near Cu-Fe sulfide minerals, either as inclusions or along grain boundaries. However, gold grains in this study are more commonly found associated with chalcopyrite than bornite, as was found in previous studies (Kesler, et al., 2002; Arif & Baker, 2004; Kyle, et al., 2008; Fraley & Frank, 2014). Numerous grains found as inclusions in a chalcopyrite vein do occur near a bornite intergrowth within the vein, suggesting that bornite's ability to host significant gold contents still controls gold grain occurrence even when chalcopyrite is the dominant mineral. Grains of a palladium-telluride mineral in sample GRS37-170-742.2, that appear physically very similar to gold, occur in close proximity to gold grains within

a chalcopyrite vein that also hosts numerous gold inclusions. This other type of "fool's gold" could be responsible for the "high-Pd" gold found in Rubin (1996).

We plotted the maximum grayscale against the non-PVE corrected volumes for samples with numerous small, dull grains to elucidate the presence of multiple grain populations. Different minerals will have separate trends based on their differences in attenuation, and these populations can be identified. In GRS37-170-742.2, grains appear to be following two trends, indicating that at least five grains could belong to a separate mineral phase (e.g., Pd-Te mineral) (Figure 3.30). Removing these grains from the modified Voronoi calculations increases the correlation coefficient from 0.031 to 0.114, although the result is still not statistically significant. GRS37-184-7.8A+B and TE14-01-754.3 also contained numerous small, difficult to identify grains, but identifying the trends of different mineral phases was more challenging in these instances. TE14-01-754.3 shows at least one other clear trend other than gold, but multiple additional trends may also be present, indicating numerous other mineral phases (Figure 3.31). Removing these grains from the modified Voronoi calculations changes the correlation coefficient from -0.086 to -0.072. The correlation decreased slightly, and still shows the negative correlation between grain size and modified Voronoi region. Reyes et al. (2017) utilized HRXCT coupled with SEM-Energy Dispersive X-ray Spectroscopy to confidently determine the phases present in HRXCT scans by serial sectioning their samples and characterizing each phase using the SEM. This method could have utility in future studies, but since some of the appeal of HRXCT is bound in its non-destructive nature, this is not a panacea (Reyes, et al., 2017).

Kyle et al. (2008) provided HRXCT data on a sample of Grasberg stockwork ore, GRS97-9. This sample is an approximately 6mm-diameter core with a quartz matrix and abundant chalcopyrite. This 2008 study determined the presence of 56 gold grains within

the sample based on 2006 scan data (Kyle, et al., 2008). Newer (2016) HRXCT scans of this same core indicate that some of the previously reported smaller gold grains may in fact be non-gold phases. During segmentation and separation of this core, the number of extracted gold grains varied from 3 to 42 gold grains, depending on the grayscale threshold used. Five alternate segmentations/separations were completed on the 2016 scan data for GRS97-9 in an attempt to replicate the data from 2006 (Table 3.4); none were fully successful. This could indicate that there are more bright phases than just gold in this sample, and that a less bright phase was misinterpreted as gold in 2006, or that there is a divergence in gold grain morphology which resulted in a similar divergence in grayscale (e.g., platy, thin gold grains may have a lower maximum CT number). This difference is likely due to an increase in resolution and sharpness of the scanning instrument in the intervening decade. This could result in more accurate calculations for the volumes of larger, brighter grains, and reveal that smaller, duller grains previously thought to be gold were potentially a different mineral phase altogether.

Threshold #4 grain data and 2006 data are compared in the following discussion, as the grains defined in threshold #4 are most similar to the 2006 data. Separate populations of grains can be seen when maximum grayscale is plotted against grain volume for threshold range #4 (Figure 3.32). These separate populations of grains may be gold of varying fineness or composition, or could be other highly attenuating mineral phases. All gold grains extracted from the 2016 scan are found in close association with chalcopyrite, as was asserted in the 2008 study. Comparing the PVE corrected volumes of 2016 gold grains (n=42) with the 2006 gold grains (n=56), a divergence in grain volume becomes apparent (Figure 3.33). The primary differences between the grains in each scan appear at the maximum and minimum volumes. The smallest volume grains that were included in the 2006 separation were left out of the 2016 separation. The volumes of the largest grains

determined in the 2016 separation are markedly larger than the largest grains defined in 2006, which is likely due to the different end-member CT values used during data processing in 2006 versus 2016. End-member PVE values used in 2006 were likely slightly higher, resulting in smaller calculated grain volumes. Higher resolution in 2016 scans potentially reduced overall noise, such that a higher number of voxels averaged together yielded a more accurate PVE end-member grayscale than 2006 scans. Alternatively, the methods used to estimate PVE end-member grayscales for gold could have been different in 2006 and 2016. Grain volume can also be affected by the exact segmentation and separation thresholding, expanding, and separating is done. There is excellent agreement of grain volumes from 7.82 $x10^{-7}$ mm^3 to 3.19 $x10^{-6}$ mm^3 (range 0.2% to 33%, mean 10%, n= 20). Beyond this range, there is significant (max= 52%; min= 10%; mean= 30%) divergence in grain volume. This comparison suggests that resolution improvement for HRXCT scanning has had a marked effect on the measurements of both large and small grains.

Kyle et al. (2008) completed a "ground-truth" study on the Blob3D calculated PVE volume of a gold grain, and the actual volume of the same gold grain after being separated from the sample by acid digestion. The measured volume of the individual, separated gold grain (0.0284 mm^3) was essentially identical to the Blob3D calculated PVE volume (0.0279 mm^3), which indicates an overall high-level of confidence in Blob3D volume estimations. This study also that gold grains frequently had a complex grain morphology, and specifically noted the intricate shape of the acid-separated gold grain (Kyle, et al., 2008). Some grains were reported to have a complex "dumbbell shape," where two small grains appeared to have either grown together or been separated together and interpreted by Blob3D as one grain (Kyle, 2017). Based on our "diffusional collection of gold" model, this could indicate that gold grains form near other, pre-existing gold grains, which can act

as “proto-grains” or “seed grains” from which a larger gold grain could be formed. Some indication of this could be found by zonation within gold grains, which is a necessary area of future study.

Correlation coefficients for modified Voronoi region and gold grain volumes were consistently low. The poor correlations could be due to the assumptions of the model not accurately accounting for the complexity of the physical system. For example, gold grains separated in this study were treated as though they were derived from a single mechanism (diffusional collection of gold), during a single event or time period. The ore system likely underwent numerous nucleation events for both copper and gold ores, where gold grains were generated by a number of different mechanisms including both precipitation of ore minerals from hydrothermal fluids and diffusion of gold from within pre-existing copper sulfides. Therefore, individual gold grains could be derived from multiple processes working in concert (e.g., a “seed” gold grain precipitated directly out of hydrothermal solution, then gold from within Cu-Fe sulfides added to the original grain). The Carlson (1991) model of diffusion controlled growth assumes that nucleation is suppressed in nutrient-depleted areas. However, if nucleation and growth are not prevented in previously scoured areas, we would not expect a correlation between diffusional drainage regions and crystal sizes. In this case, gold atoms could be sourced from areas far afield of the grain, and could be moving within diffusion-prone pathways, like grain boundaries or fractures. In conjunction with this, if Au mobility is based on the presence of “excess Au” diffusing out of Cu-Fe sulfides, rates of cooling could have a dramatic effect on the ability of Au to exsolve from sulfides and then move an appreciable distance.

The modified Voronoi regions assumed a uniform distribution of gold throughout both major Cu-Fe sulfides, and that gold would diffuse equally well through both minerals.

Because intergrowths of these minerals were common in our samples, chalcopyrite and bornite were treated as one Cu-Fe-S mineral phase for Voronoi calculations. Chalcopyrite has been shown to hold significantly smaller volumes (*see* Table 2.1; ~100s ppm Au at elevated temperatures) of gold within its matrices at high-temperatures compared to bornite (Fraley & Frank, 2014). Bornite is more capable of exsolving the volume of gold necessary to form an entire gold grain, and characterizing chalcopyrite identically in Voronoi analyses does not accurately represent the behavior of either mineral in the ore system. Our correlation values only provide a minimum estimate of the correlation between Cu-Fe sulfides and boundary gold grains, suggesting that there is, especially in high grade porphyry samples, some correlation between the volume of copper sulfide minerals and the volume of gold present in a sample.

Using only the largest, brightest, and least ambiguous gold grains typically resulted in fewer total grains identified in a sample. This resulted in fewer modified Voronoi regions calculated for that core, which made the regions more likely to intersect the physical edge of the core sample. When modified Voronoi regions intersected the edge of the physical core sample, their volumes are prematurely truncated as there is no way to know the exact extent of the Cu-Fe sulfide network, thus their volumes are ambiguous. For volumetric correlations between modified Voronoi regions and gold grains, high confidence in gold grains was typically coupled with low confidence in diffusional drainage volume. The majority, at least ~95%, of modified Voronoi regions calculated intersected the edge of the core sample, rendering a significant portion of the volumetric correlation coefficients dubious. Future modifications of this analysis should consider these assumptions when exploring the connection between gold grains and Cu-Fe sulfides. Sample selection proved to be a significantly constraining factor of this study. A perfect sample for modified Voronoi analyses would have an isolated Cu-Fe sulfide network of one phase (bn or cp)

and numerous, easily identifiable gold grains within or around it. Even though this sample would have been beneficial to the study of the volumetric correlation between gold grains and Cu-Fe sulfides, it likely would not be representative of the ore system on a deposit scale.

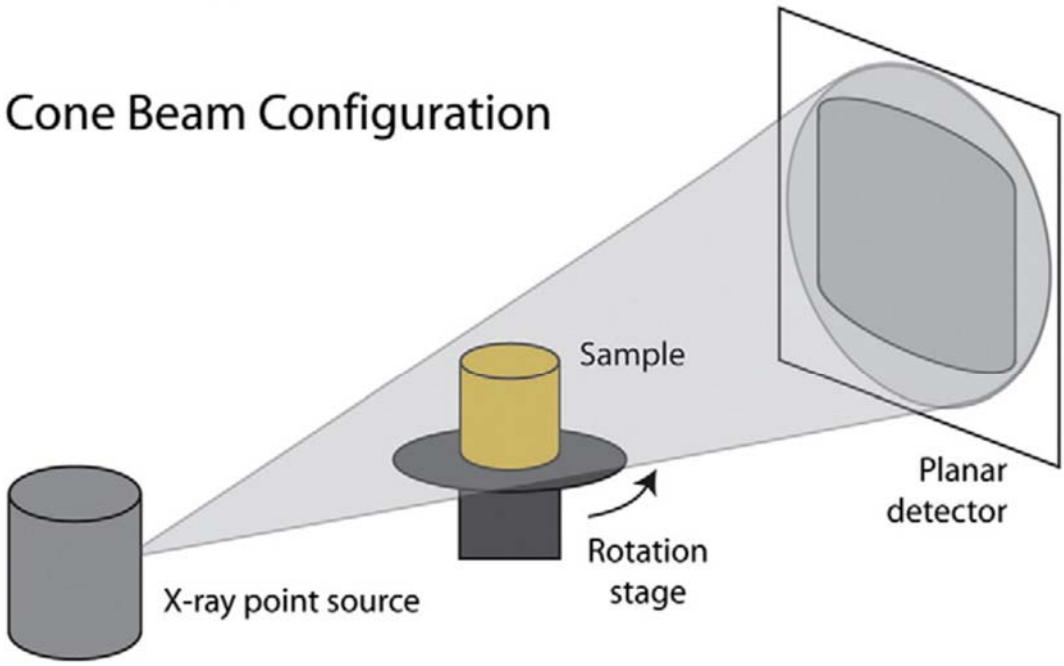

Figure 3.1 X-ray Tomography Imaging Set-up

Schematic of image acquisition with cone-beam set up. From Kyle and Ketcham (2015).

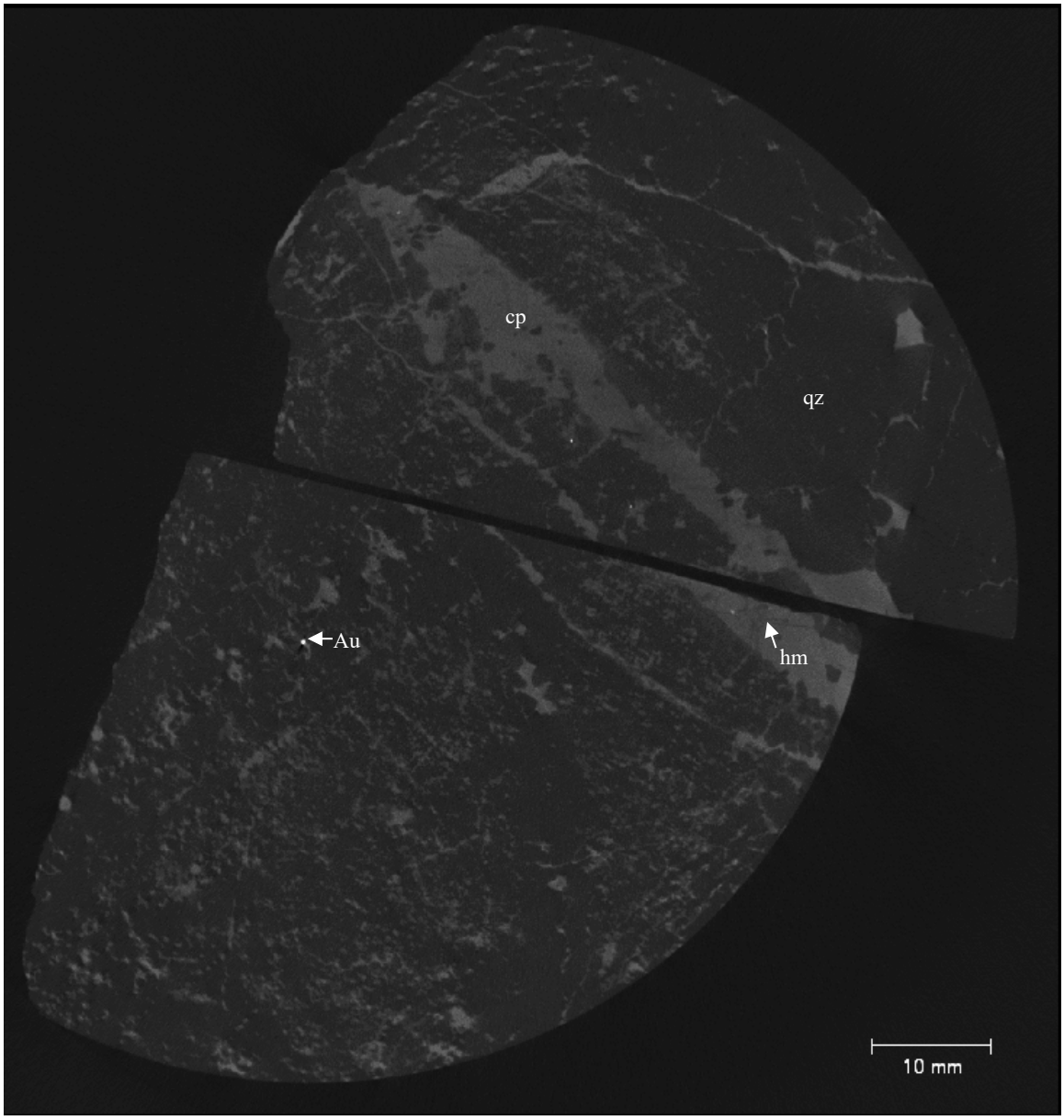

Figure 3.2 Example HRXCT Slice

Porphyry sample GRS37-184-7.8A+B with quartz matrix, chalcopyrite, specular hematite (thin, slightly darker blades within cp vein), and gold.

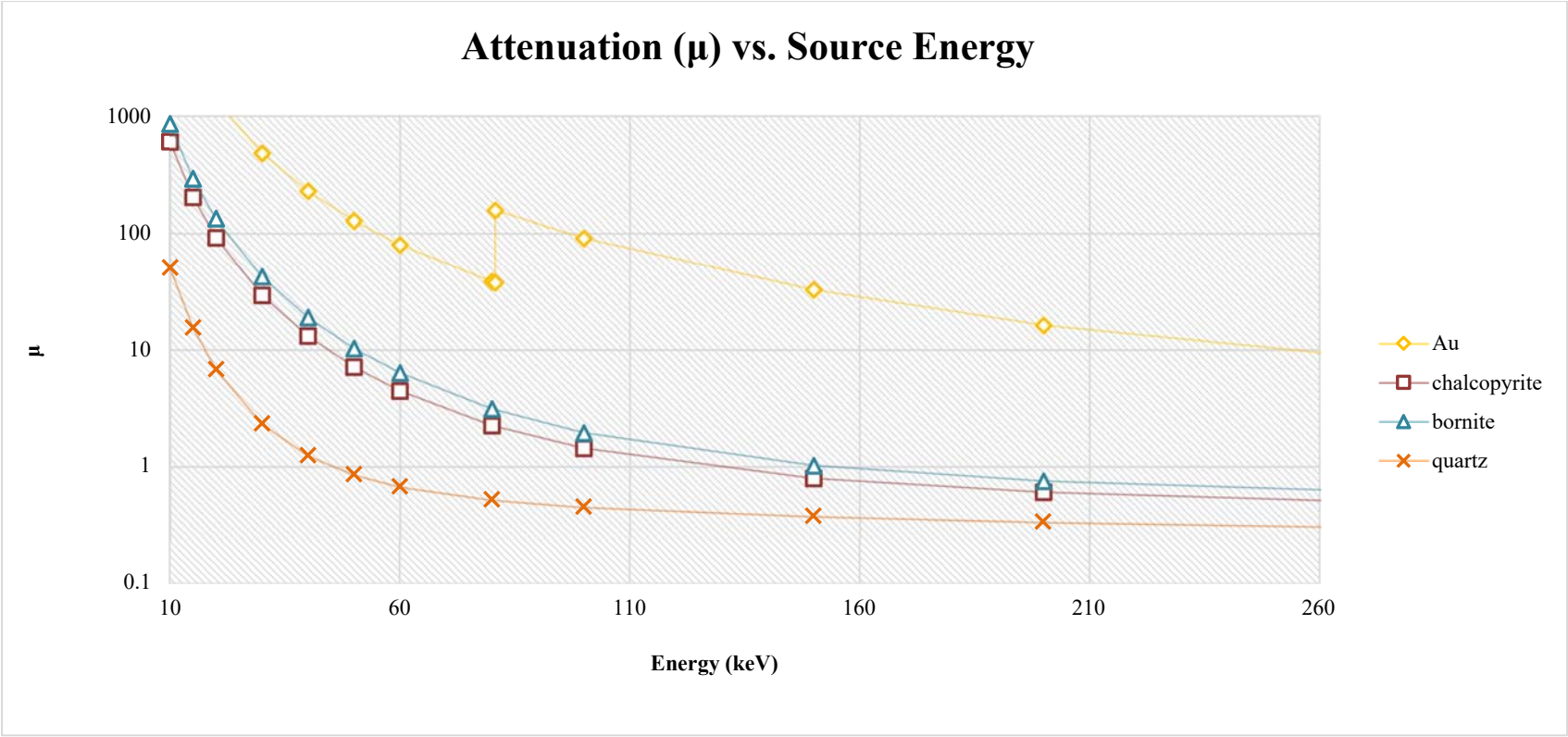

Figure 3.3. Linear Attenuation Coefficients as a Function of X-ray Energy

Linear attenuation coefficients of main matrix material (quartz), copper ore minerals (chalcopyrite and bornite), and gold as a function of X-ray energy. Chalcopyrite and bornite have very similar attenuation, and appear very similar in CT slices. Gold has a much higher linear attenuation coefficient, and appears very bright in CT slices. Spike along the gold curve is an absorption edge, where inner shell electrons are ejected from an atom of gold.

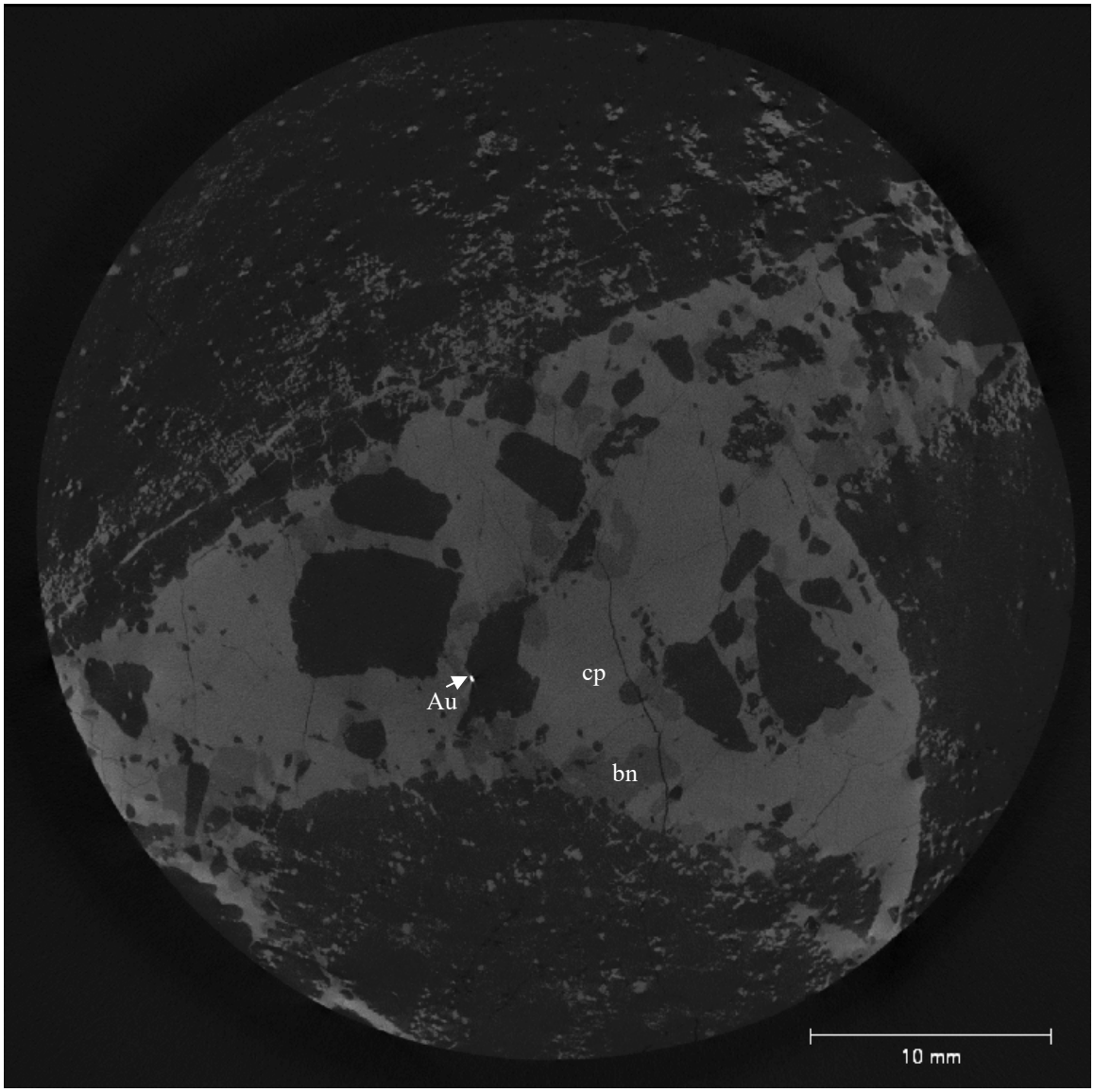

Figure 3.4 HRXCT Slice of Cu-Fe-S Minerals

Porphyry sample AH90-4C-F with quartz matrix and a large Cu-Fe sulfide vein running through the center of the core. The similar grayscales of bornite and chalcopyrite are visible in the vein intergrowths.

Table 3.1 Scanning Parameters

Sample			Scanning Parameters[1]			
Sample ID	**Description**	**Size**	**X-ray (KeV)**	**X-ray Intensity (mA)**	**Slice Spacing (µm)**	**Total Slices**
AH90-4C-C	qz+bn+cp Grasberg stockwork	12 mm diameter core	200	0.12	9.63	1729
AH90-4C-F	qz+Bn+cp Grasberg stockwork	22 mm diameter core	200	0.12	11.7	1127
GRS97-9[2]	qz+cp Grasberg stockwork	6 mm diameter core	120	0.083	6.33	1176
GRS14-OP1	bn+an Open pit hand sample	50 mm	220	0.20	48.1	1797
GRS37-170-645.9[3]	qz+cp MGI core	35 mm diameter core	190	0.21	23.8	4424
GRS37-170-742.2A[3]	qz+cp vein MGI core	35 mm diameter core	190	0.21	23.8	4424
GRS37-184-7.8A+B[4]	cp+hm+mt+qz Grasberg	30 mm diameter core	200	0.21	26.7	2923
GRS37-170-714.2-5	qz+cp vein MGI core	46 mm diameter core	200	0.12	26.2	1806
TE01-16-566	bn+cp+an+qz+ ba+py Ertsberg diorite	62 mm diameter core	200	0.14	45.7	1888
TE14-01-754.3	qz+cp+mo+an+ba Ertsberg diorite vein	45 mm diameter core	200	0.21	26.7	3040
DOZ-90K-29[5]	bn+qz+an Deep Ore Zone hand sample core	22 mm	210	0.30	12.7	3536

[1]Scanned on NSI

[2]Scanned on Zeiss (formerly Xradia) micro-CT scanner

[3]Scanned at the same time and then separated during image processing into individual volumes

[4]Two sides of one broken core sample scanned together

[5]DOZ-90K-29 unleveled so that peak CT number/brightness fell below the max for a 16bit image

Table 3.2 HRXCT Thresholding Ranges for Ore Samples

		AH90-4C-C	AH90-4C-F	GRS37-170-714.2-5	GRS37-170-645.9	GRS37-170-742.2	GRS37-184-7.8A+B	GRS14-OP1	GRS97-9	DOZ-90K-29	TE14-01-754.3
Narrow CT Threshold: Strict	**Gold**	210-255 (±31-255 0/3)	175-255 (±49-255 0/3)	200-255 (±40-255 0/3)	–	165-255 (±55-255 0/3)	200-255 (±40-255 0/2)	195-255 (±45-255 0/3)	190-255 (±35-255 0/4)	200-255 (±50-255 0/2)	195-255 (±45-255 0/3)
	Cu-Fe-Sulfide	14-255 (±13-255 0/1)	15-255 (±12-255 0/1)	15-255 (±13-255 0/2)	–	24-255 (±23-255 0/1)	125-255 (±45-255 0/2)	27-255	15-255 (±11-255 0/2)	20-255	22-255 (±20-255 0/1)
	Other$_1$	85-255 (±30-255 0/3)	60-255 (±25-255 0/1)	125-255 (±45-255 0/2)	–	42-255 (±34-255 0/2)	40-255 (±30-255 0/2)	99-255(±45-255 0/3)	80-255 (±30-255 0/2)	45-255	75-255 (±45-255 0/2)
	Other$_2$	–	–	–	–	–	–	–	–	–	37-255 (±20-255 0/1)
Broad CT Threshold: Generous	**Gold**	130-255 (±28-255 0/3)	84-255 (±25-255 0/3)	125-255 (±45-255 0/2)	50-255 (±35-255 0/2)	42-255 (±34-255 0/2)	40-255 (±30-255 0/2)	99-255(±45-255 0/3)	100-255 (±20-255 0/2)	90-255 (±45-255 0/2)	75-255 (±45-255 0/3_
	Cu-Fe-Sulfide	14-255 (±13-255 0/1)	15-255 (±12-255 0/1)	15-255 (±13-255 0/2)	26-255 (±25-255 0/1)	24-255 (±23-255 0/1)	15-255 (± 14-255 0/1)	27-255	15-255 (±11-255 0/2)	20-255	22-255 (±20-255 0/1)
	Other$_1$	85-255 (±30-255 0/3)	–	–	–	–	–	–	50-255 (±30-255 0/2)	–	37-255 (±25-255 0/1)
End-member Au CT Values for PVE calc.		248	235	248	128	240	243	216	216	231	244

Thresholding values used in Blob3D "segment" feature as a "general threshold." CT numbers are for 8bit grayscale HRXCT slices with values of 0-255, where 255 is white and 0 is black. Parenthetical values indicate the expand/contract range used in conjunction with the general threshold range. "0/X" numbers represent the number of voxels contracted/expanded from the general threshold range.

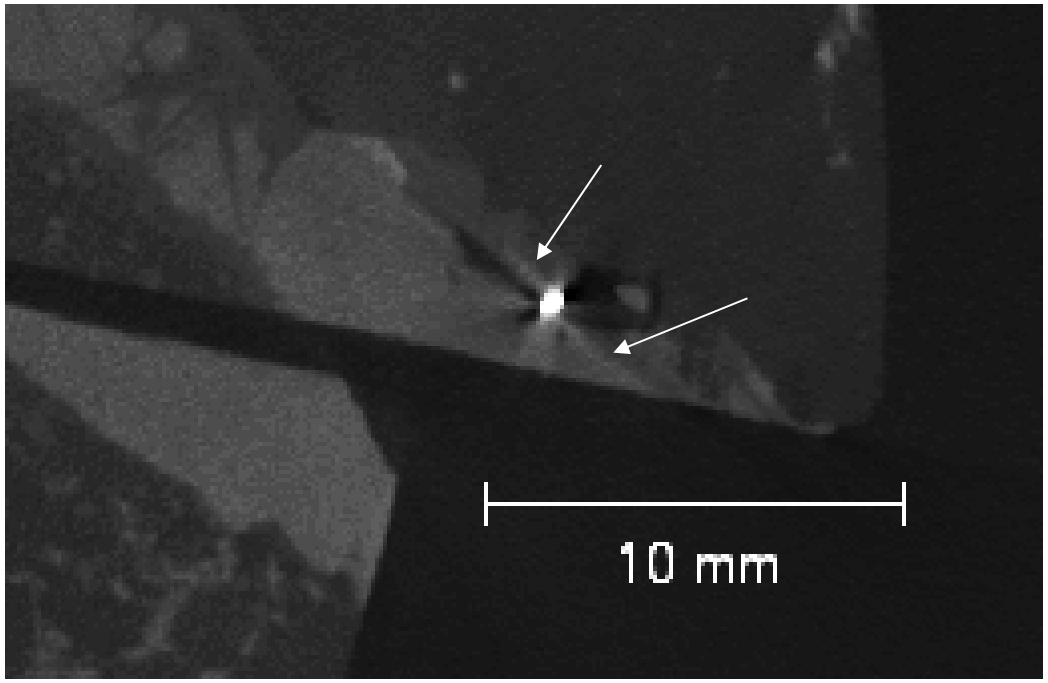

Figure 3.5 Starburst Artifact near Gold Grain

Porphyry sample GRS37-184-7.8A+B with gold grain in chalcopyrite vein. Bright streaks (arrows) on either side of gold grain are “starburst” artifacts which artificially brighten surrounding voxels.

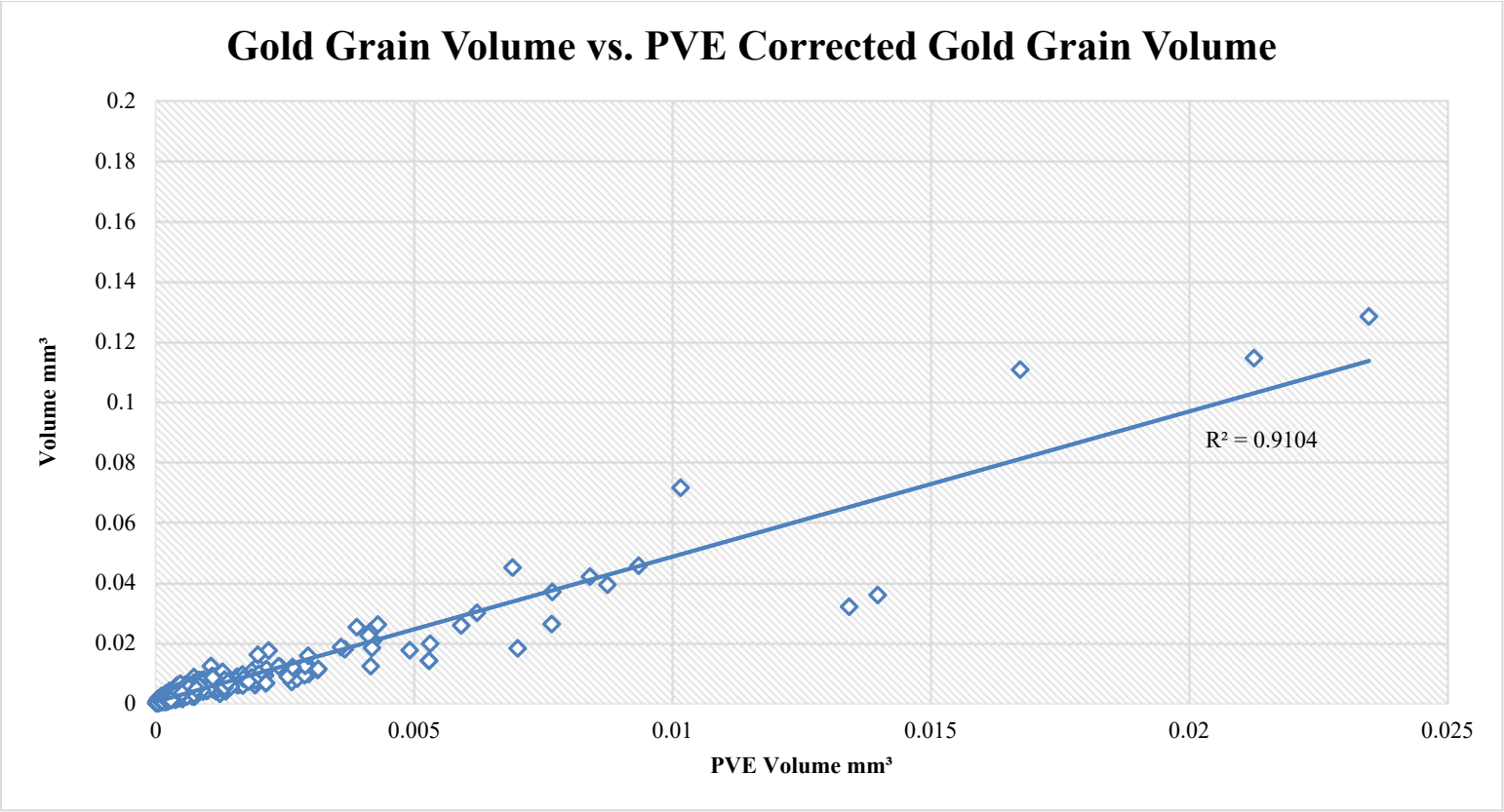

Figure 3.6 Partial Volume Error Corrected Gold Grain Volumes vs. Uncorrected Volumes

PVE volumes are much smaller than uncorrected volumes, but the correlation between the two volumes (r = 0.95) is excellent, indicating that although the PVE correction significantly alters grain volume, it does so consistently.

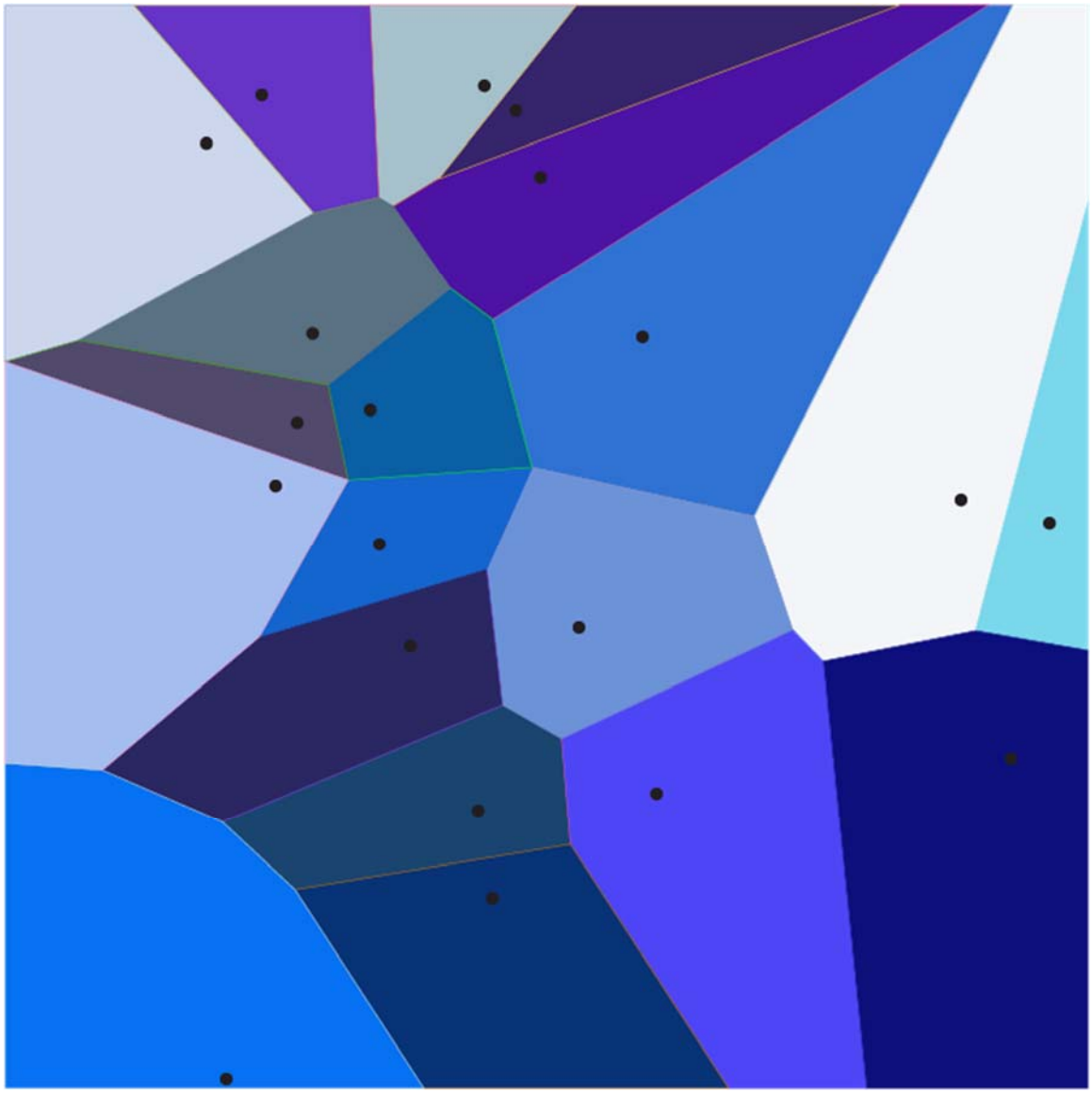

Figure 3.7 Plane Partitioned into Voronoi Regions

Voronoi analyses partition planes or volumes into unique regions (blue shades) based on closeness to an interior seed point (black dots). The regions are the set of points in the plane or volume closer to the interior seed point than any other seed point. Lines represent points that are equidistant from two seed points. Junctions are points which are equidistant from three seed points.

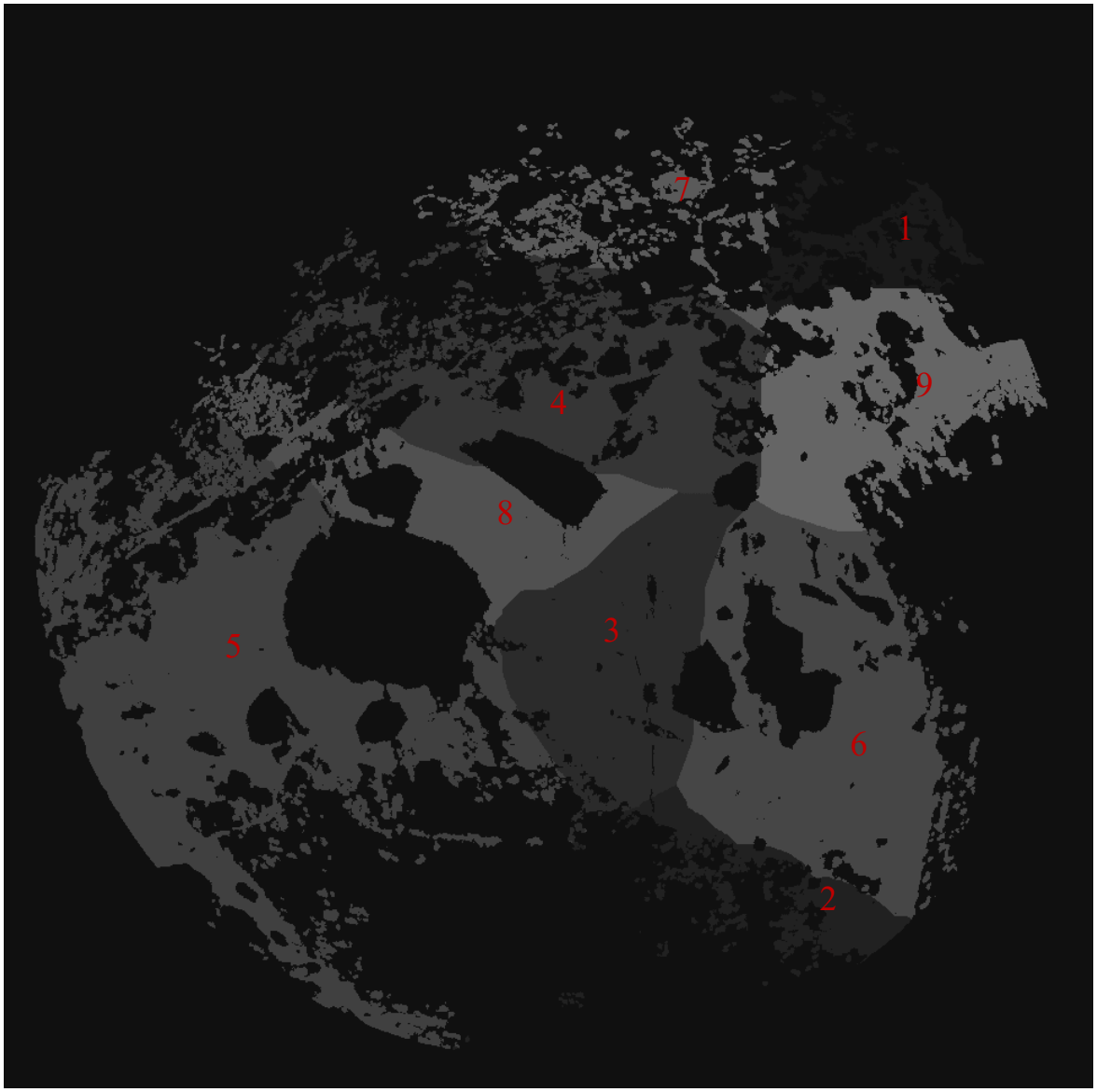

Figure 3.8 HRXCT Slice of Cu-Fe Sulfides Partitioned into Modified Voronoi Regions

Each modified Voronoi region is represented as a distinct grayscale. Red numbers identify the modified Voronoi regions where “1” is the darkest grayscale, and “9” is the lightest grayscale.

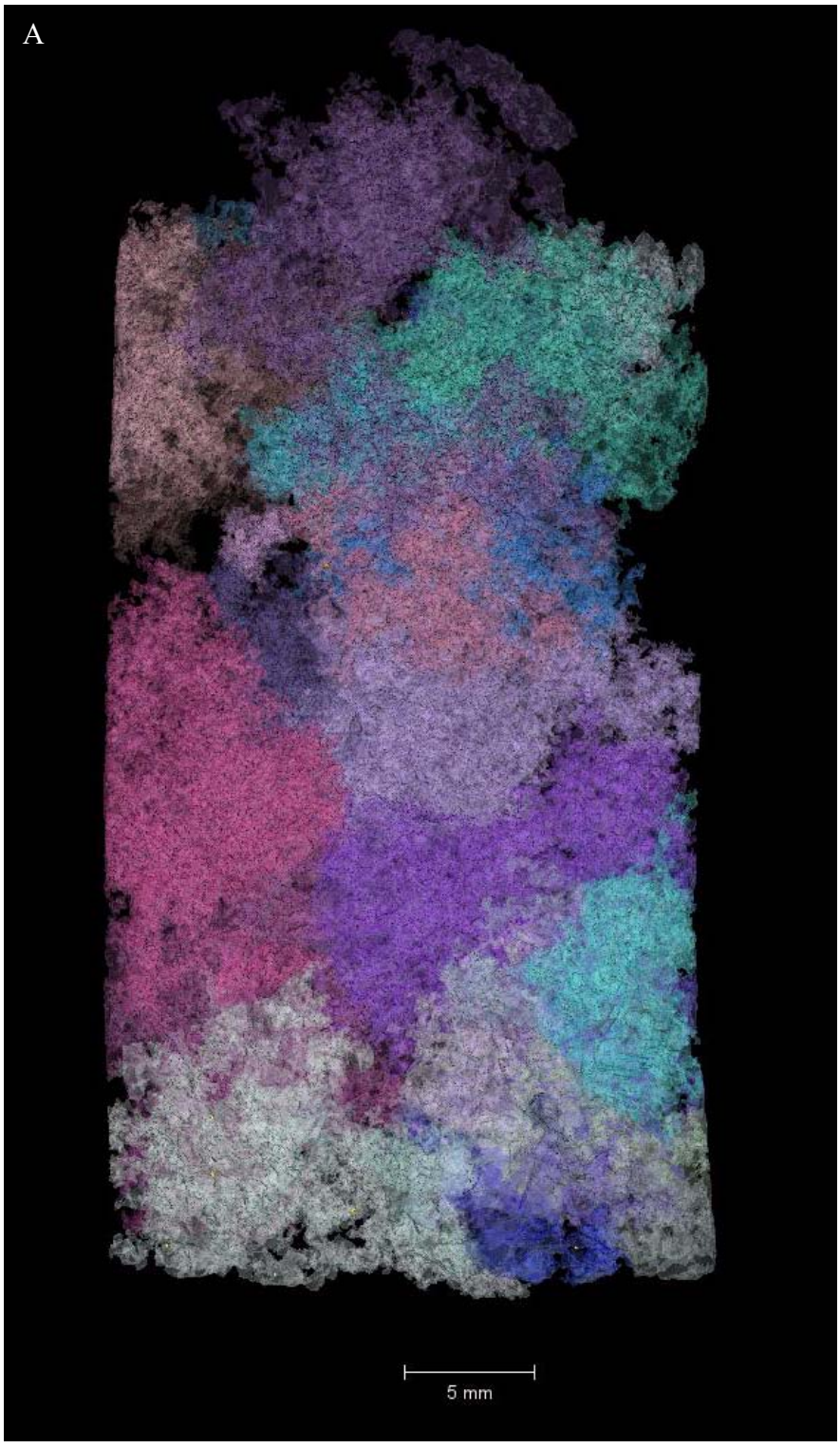
A
5 mm

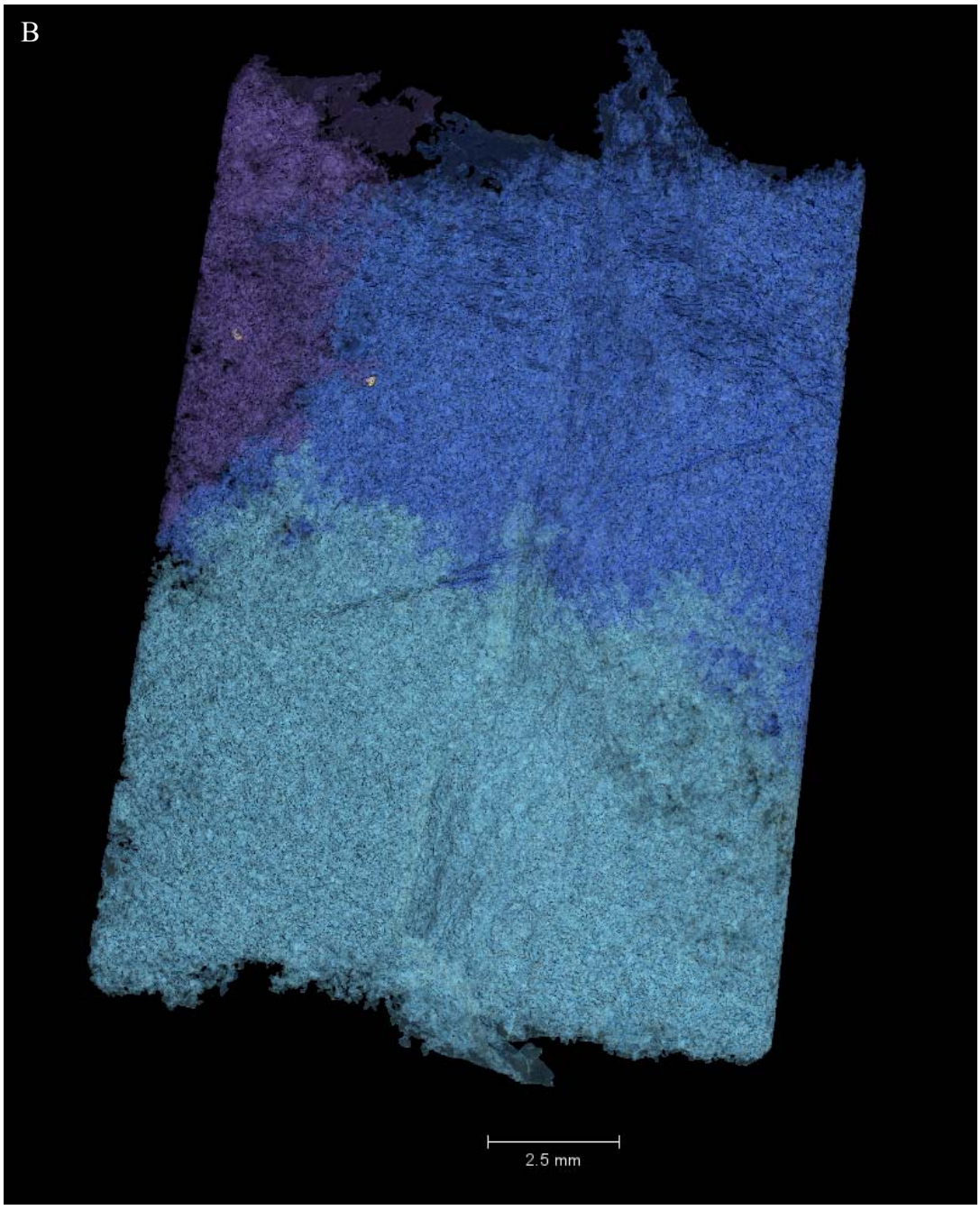
B
2.5 mm

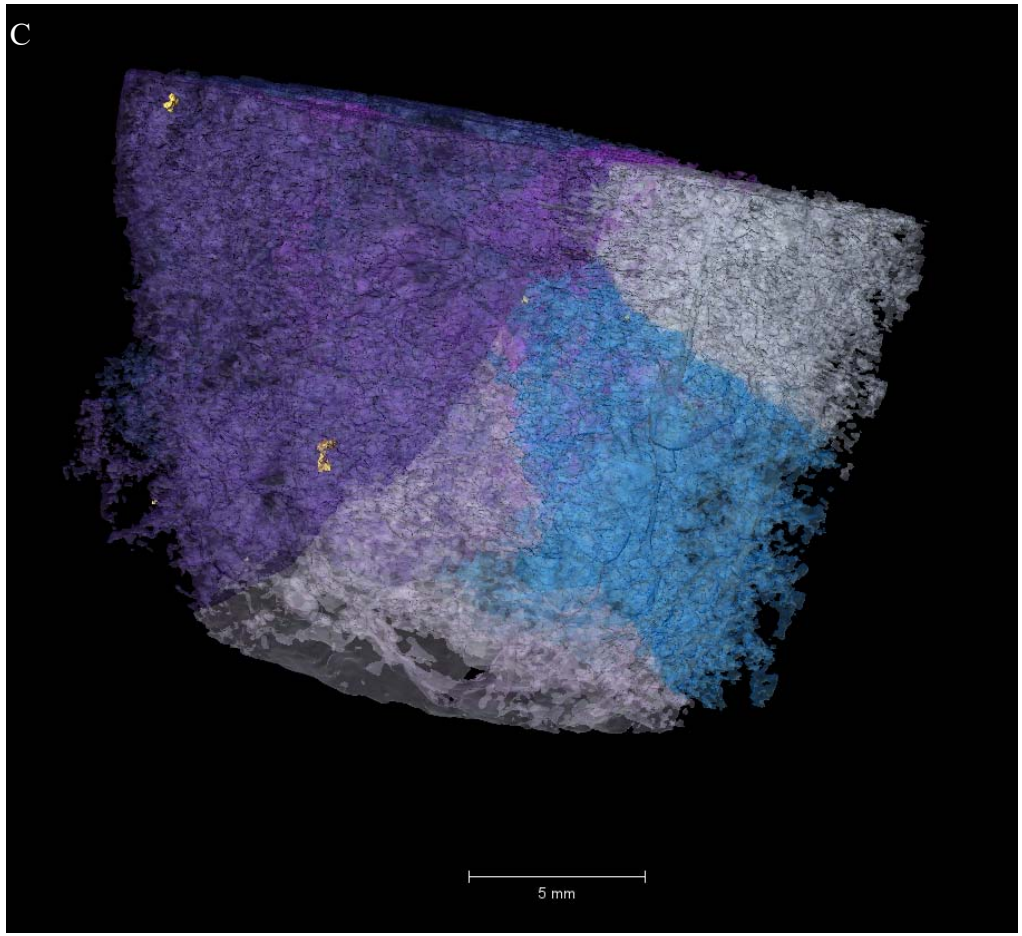

Figure 3.9 3D Visualizations of Gold Grains and Modified Voronoi Regions in Cu-Fe sulfide Networks

Skarn sample DOZ-90-29 (a), and porphyry samples AH90-4C-C (b) and AH90-4C-F (c). Each colored region represents a unique modified Voronoi regions that corresponds to a particular gold grain (rendered in yellow).

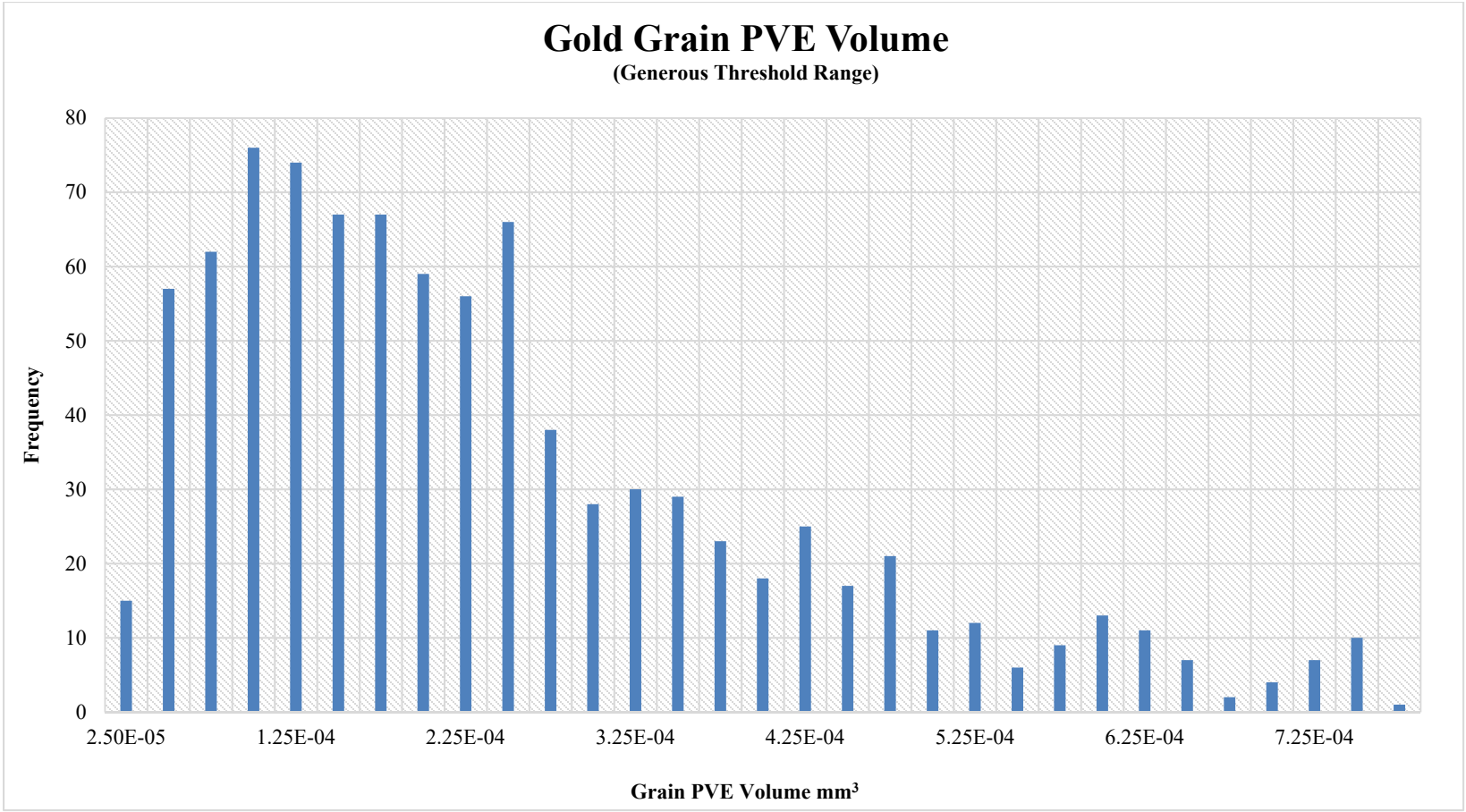

Figure 3.10 Distribution of Grain Size for Gold Grains with Small Volumes

Grain volumes for gold grains smaller than 7.75×10^{-4} mm^3; the majority of gold grains separated are included in this size distribution (n=921).

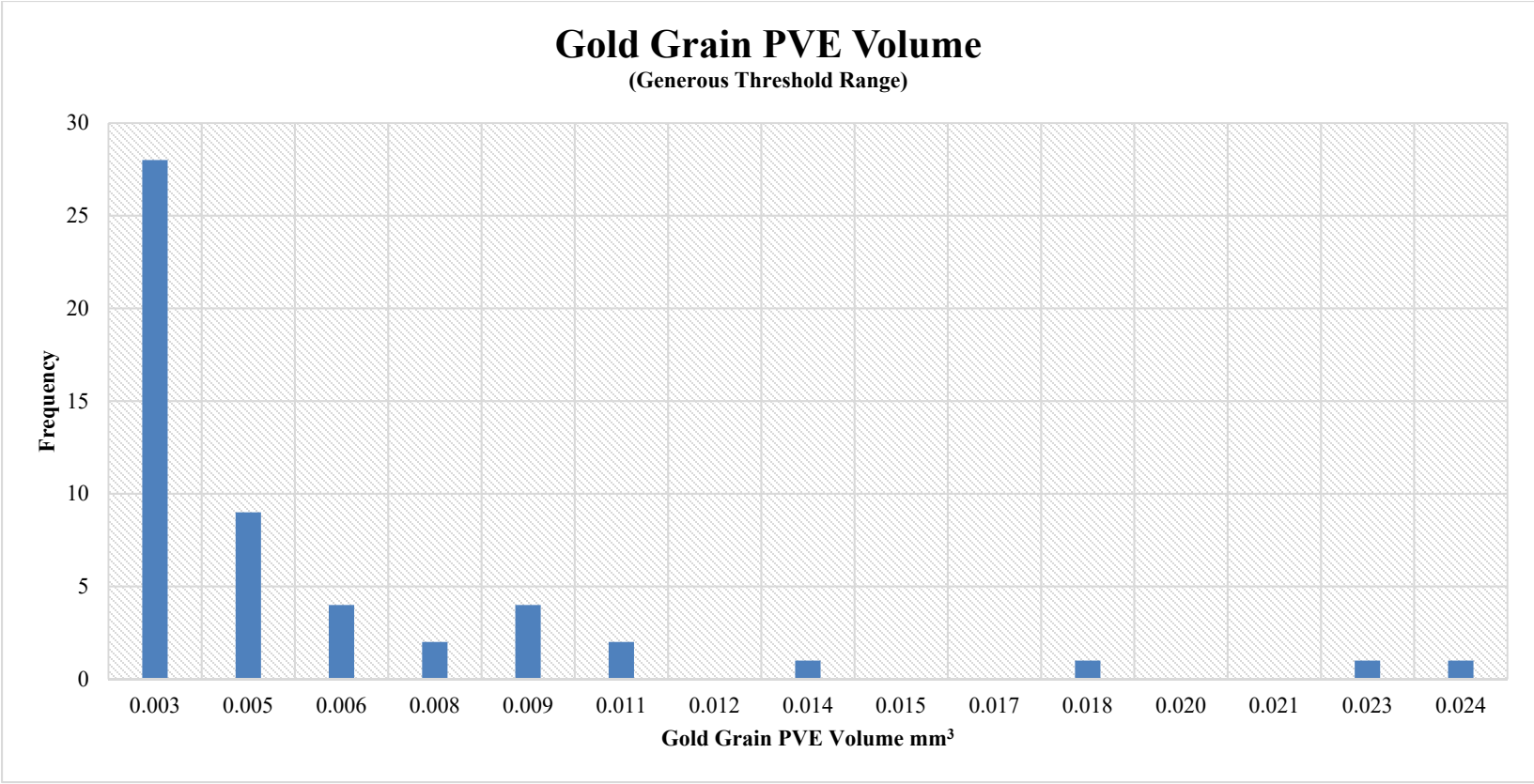

Figure 3.11 Distribution of Grain Size for Gold Grains with Large Volumes

Grain volumes for gold grains larger than 2.0×10^{-3} mm^3 (n=128).

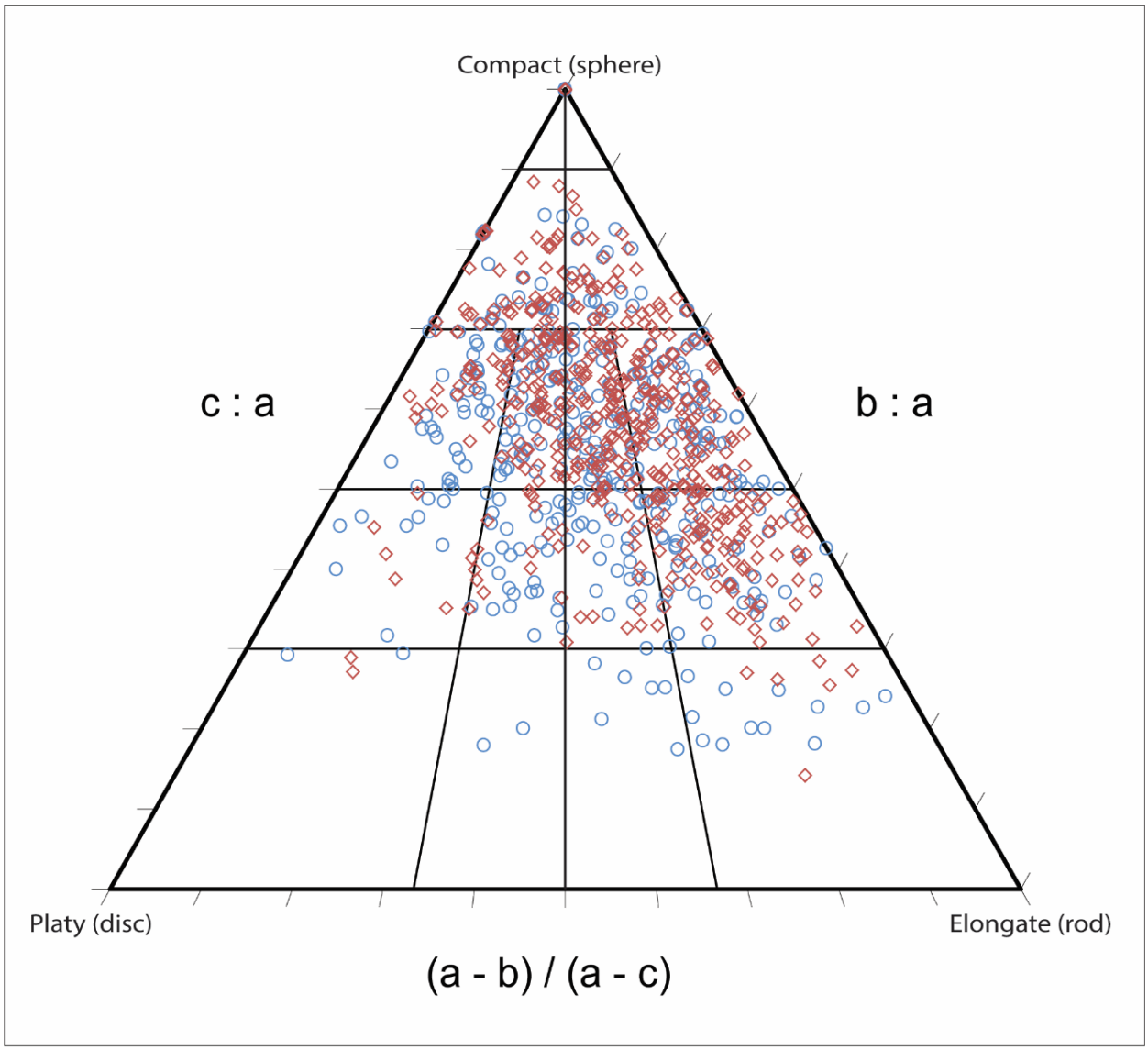

Figure 3.12 Ternary Diagram of Native Gold Grain Shape

HRXCT data for skarn grains (blue) and porphyry grains (red) plotted on a Sneed and Folk (1958) ternary diagram (Appendix B). The best fit ellipsoid axis lengths of each grain were used to plot each gold grain shape within the diagram; the apices represent the grain shapes indicated. Skarn grains (n=437) were 12.36% compact, 33.64% platy, and 54% elongate. Porphyry grains (n=632) were 18.2% compact, 22.94% platy, and 58.86% elongate.

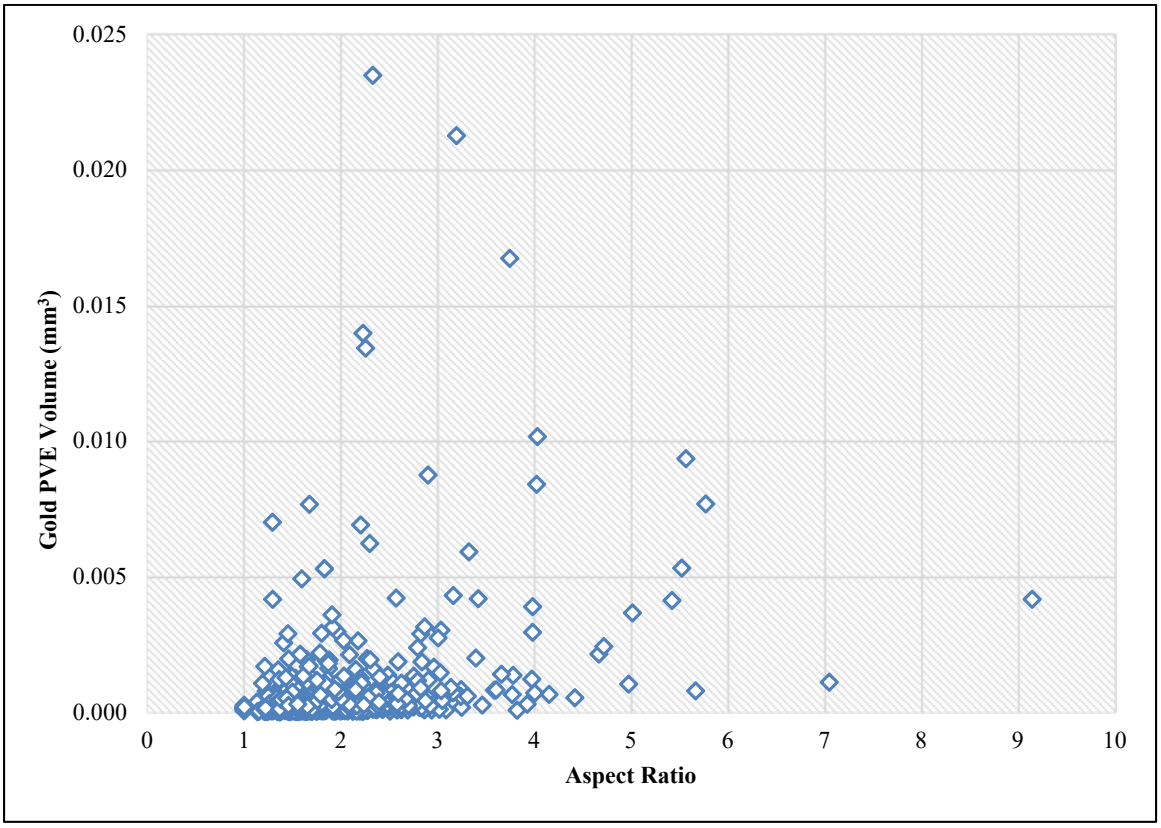

Figure 3.13 Aspect Ratio vs. PVE Volume for All Gold Grains

All gold grains separated in HRXCT data are included. Pearson correlation between gold grain volume and aspect ratio is 0.34.

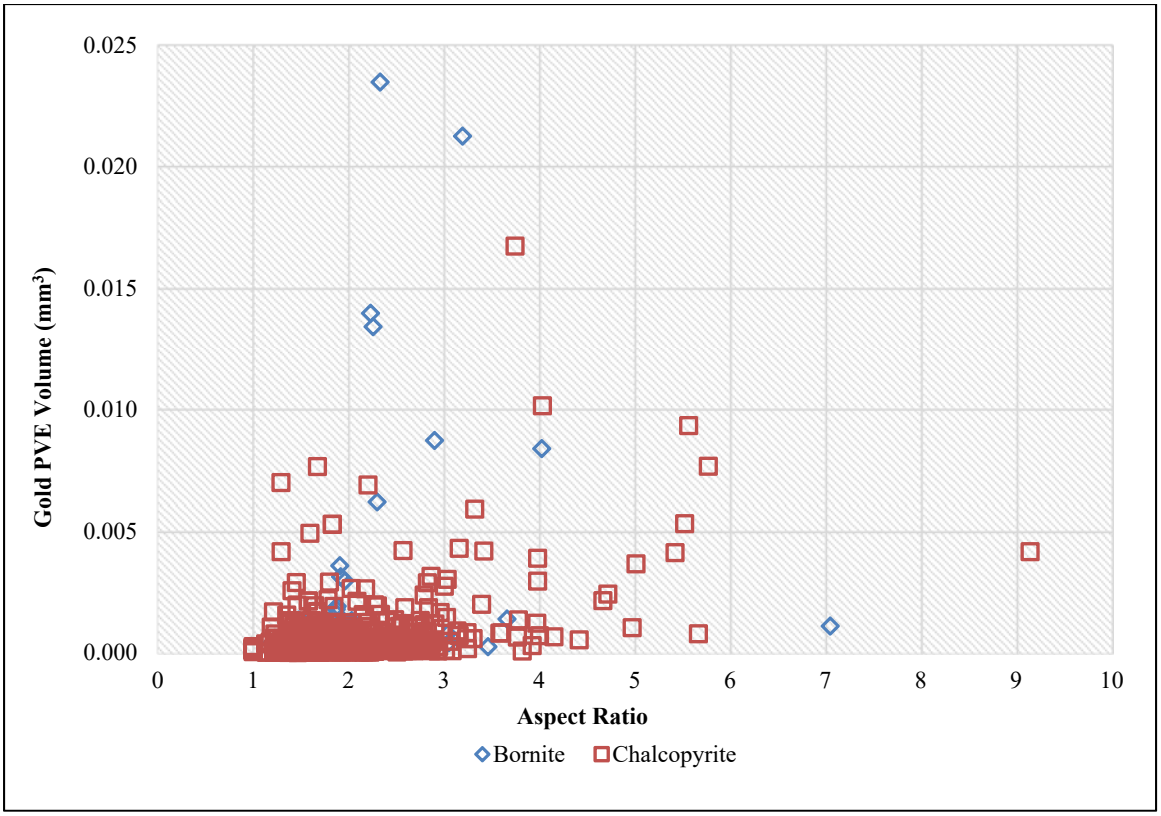

Figure 3.14 PVE Volume vs. Aspect Ratio for Bornite and Chalcopyrite Associated Gold

Aspect ratios of gold grains associated with either bornite (blue) or chalcopyrite (red)or both. Grains associated (on the edge of) both bornite and chalcopyrite were plotted twice, once for bornite and once for chalcopyrite.

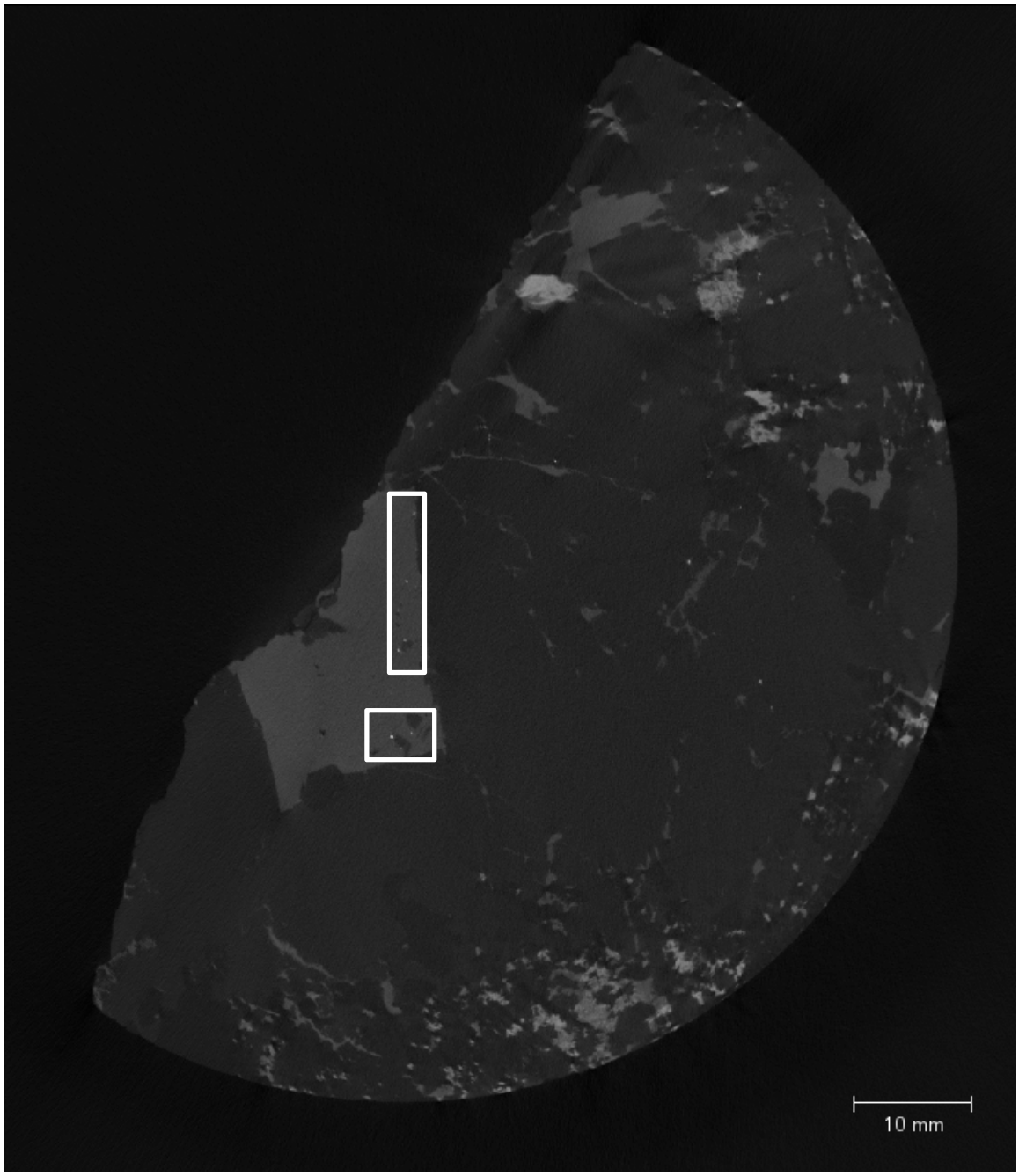

Figure 3.15 Sample TE14-01-754.3 with Small Grains

Skarn sample TE14-01-754.3 with numerous small grains (white boxes) that could be gold, although reflected light microscopy and digital radiography do not support this.

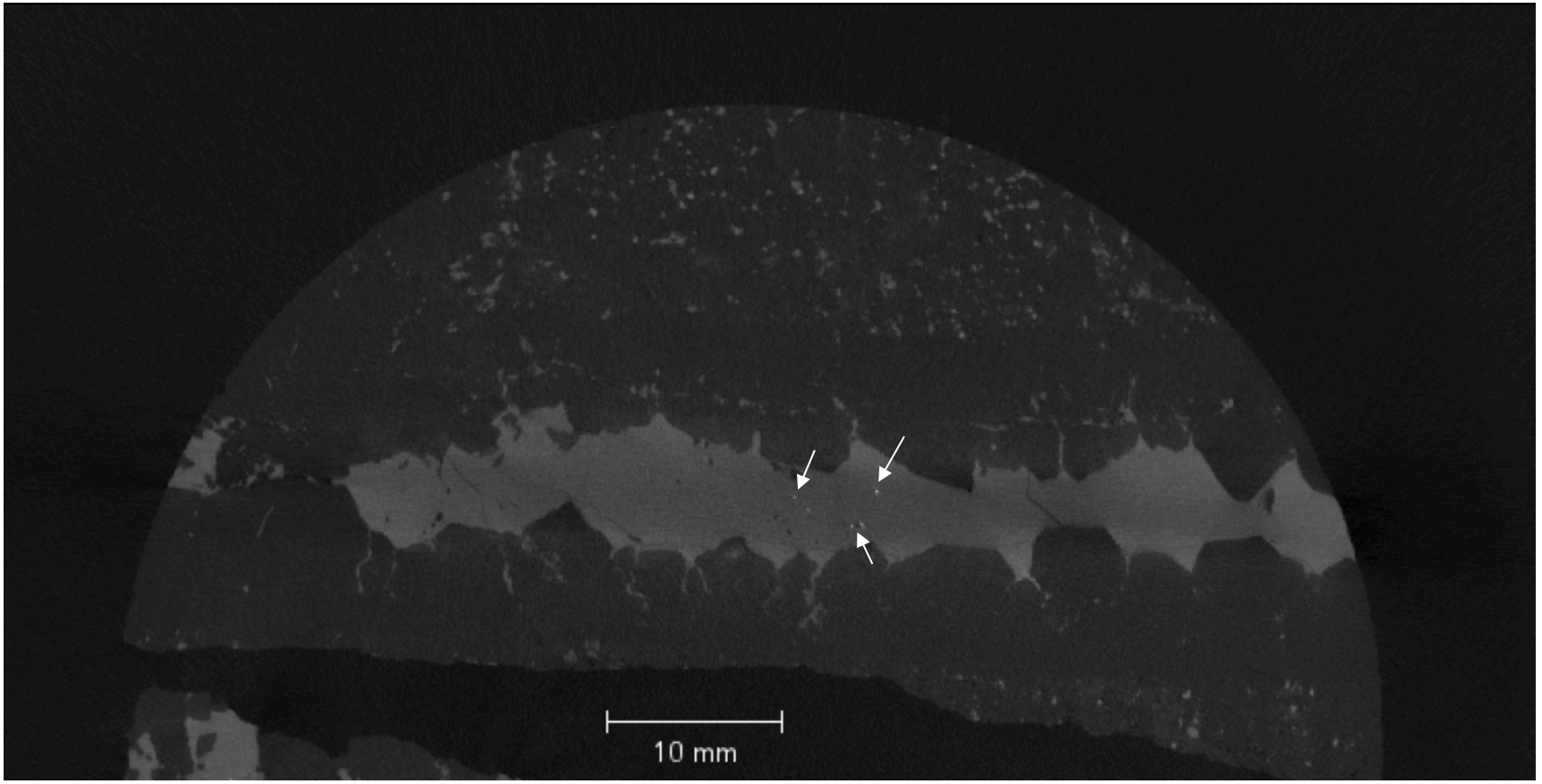

Figure 3.16 Sample GRS37-170-742.2 with Small Grains

Porphyry sample with small dull grains that are very likely gold grains based on reflected light microscopy of GRS37-170-742.2 thick sections with very small gold grains that occur in the same locations as bright grains in HRXCT slices.

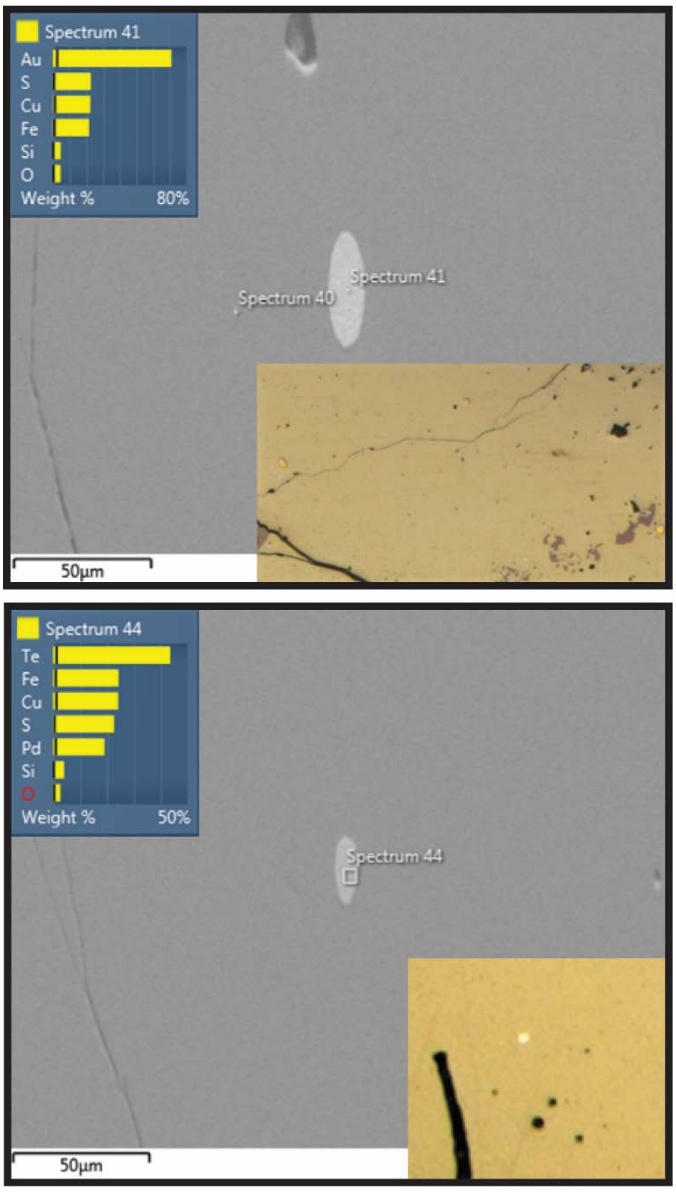

Figure 3.17 SEM Secondary Electron Images, EDS Data, and Reflected Light Images for Gold and Pd-Te Grains

GRS37-170-742.2 gold grain (top) and Pd-Te grain (bottom) have very similar morphologies and colors, but have markedly different geochemical constituents.

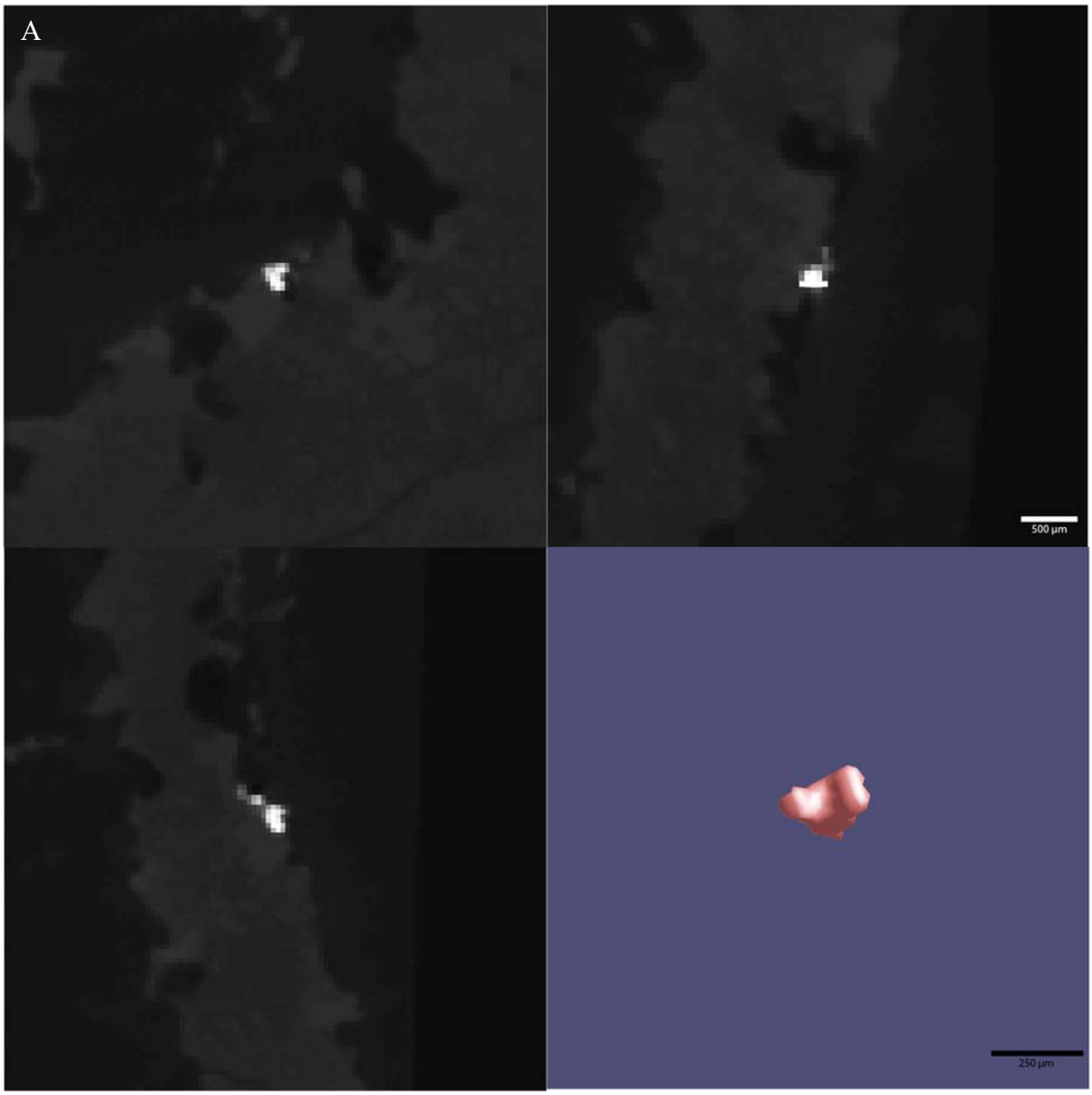
A
500 µm
250 µm

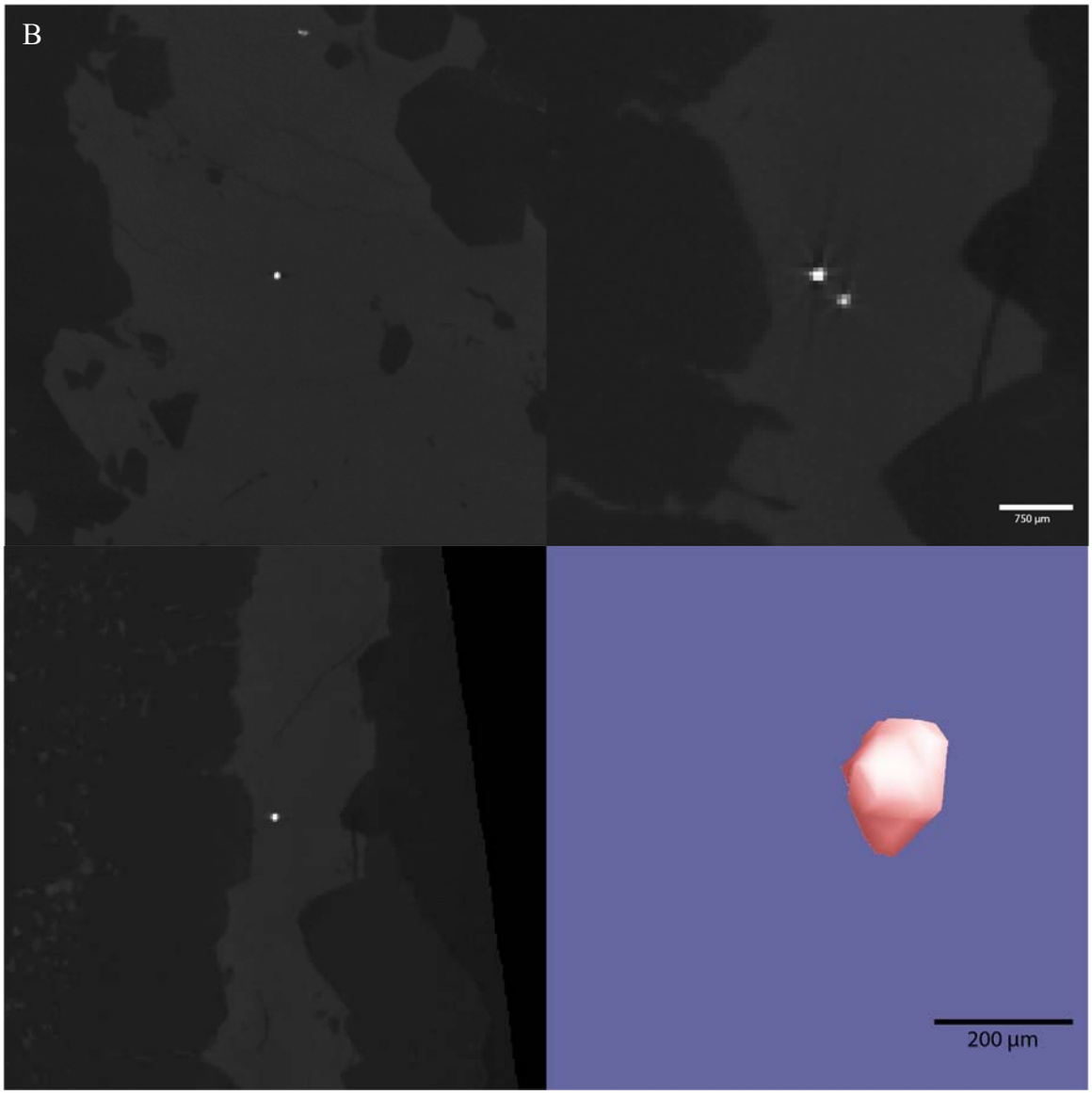

Figure 3.18 Gold Grain Morphologies in Bornite and Chalcopyrite

AH90-4C-C (a) gold grain in bornite is “wishbone” shaped. GRS37-170-742.2 (b) gold inclusion in chalcopyrite appears compact.

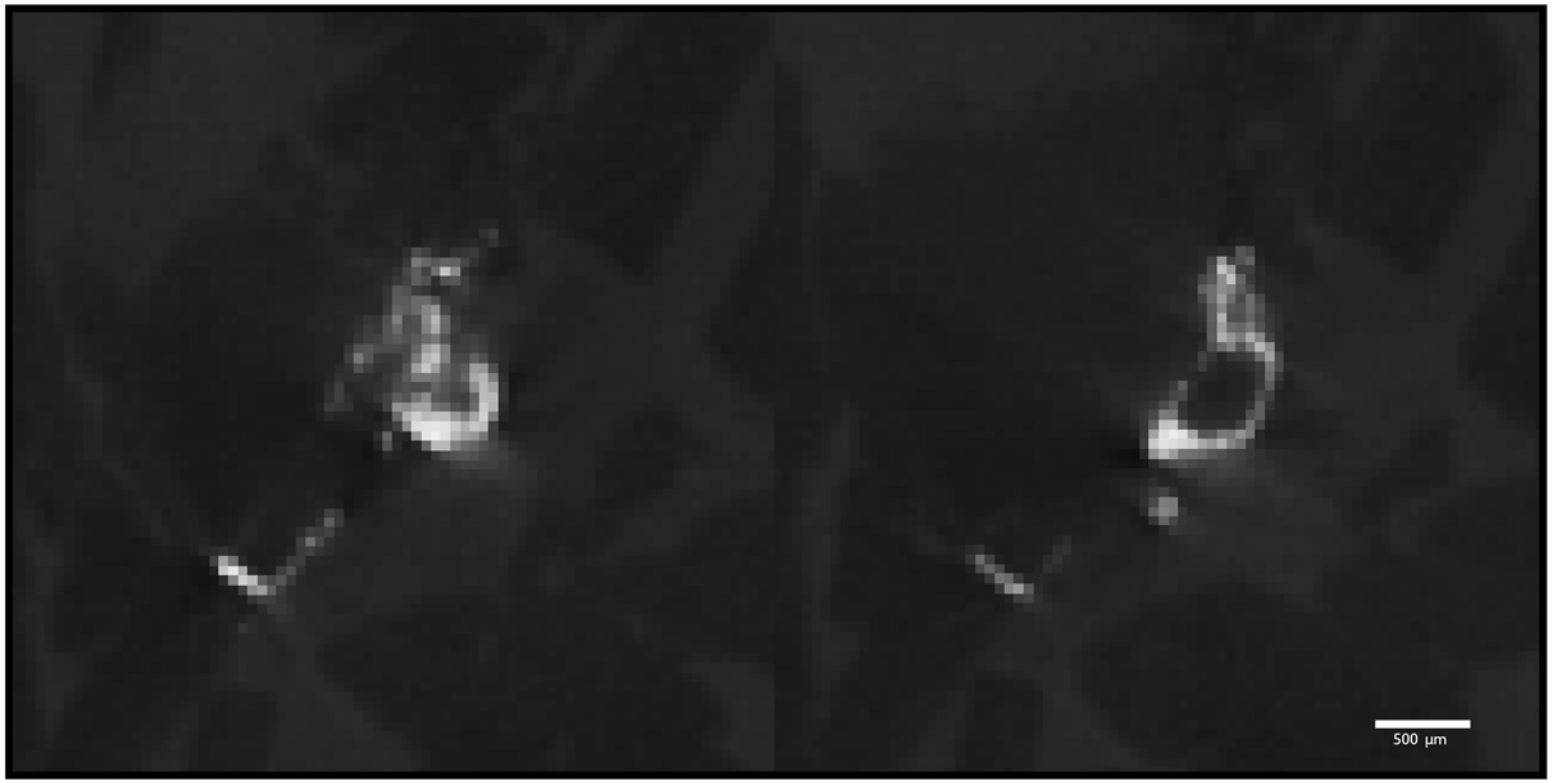

Figure 3.19 Gold Grain Morphology in GRS14-OP1

Bright grains in this porphyry sample are frequently found occurring in a “moly-coating” morphology where the bright grains drape over a proximal crystal and highlight the crystal boundaries. This is a very unusual habit and is not found in any other samples.

Table 3.3 Modified Voronoi and Gold Grain Volumetric Data and Correlations

Strict CT Threshold	AH90-4C-C	AH90-4C-F	GRS37-170-714.2-5	GRS37-170-645.9	GRS37-170-742.2	GRS37-184-7.8A+B	GRS14-OP1	GRS97-9	DOZ-90K-29	TE14-01-754.3
# Gold Grains	3	6	3	–	4	4	1	3	1	2
Min Gold Grain PVE Volume (mm^3)	$6.15x10^{-5}$	$1.64x10^{-4}$	$2.88x10^{-3}$	–	$7.02\ x10^{-4}$	$1.32x10^{-3}$	$1.79x10^{-4}$	$2.97x10^{-5}$	$3.84x10^{-4}$	$2.13x10^{-3}$
Max Gold Grain Volume (mm^3)	$1.35x10^{-3}$	$1.24x10^{-3}$	$1.40x10^{-2}$	–	$3.02\ x10^{-3}$	$7.0x10^{-3}$	–	$4.31x10^{-5}$	–	$5.29x10^{-3}$
Min Voronoi Volume (mm^3)	11.81	85.24	10.70	–	0.60	1675.3	2206.3	3.17	2491.9	$1.04x10^{-2}$
Max Voronoi Volume (mm^3)	281.46	591.09	792.93	–	463.14	7055.7	–	7.12	–	1.74
R^2	0.60	0.37	0.64	–	0.813	0.57	–	0.13	–	1
R	0.78	-0.61	0.80		-0.90	-0.75	–	0.36	–	1
DF (n-1)	2	5	2	–	3	3	–	2	–	1
Critical Value of r (for two tailed t-test at 95% confidence)	0.95	0.878	0.95	–	0.878	0.878	–	0.95	–	0.997
Figures	3.20	3.21	3.22	–	3.24	3.25	3.26	3.27	3.28	3.29

Generous CT Threshold	AH90-4C-C	AH90-4C-F	GRS37-170-714.2-5	GRS37-170-645.9	GRS37-170-742.2	GRS37-184-7.8A+B	GRS14-OP1	GRS97-9	DOZ-90K-29	TE14-01-754.3
# Gold Grains	6	14	8	216	96	234	27	14	33	401
Min Gold Grain PVE	$5.30x10^{-5}$	$3.95x10^{-5}$	$3.01x10^{-4}$	$5.43x10^{-5}$	$2.23x10^{-5}$	$4.01x10^{-5}$	$1.16x10^{-4}$	$6.53x10^{-6}$	$3.07x10^{-5}$	$8.79x10^{-5}$

Table 3.3 (continued)

Volume (mm^3)										
Max Gold Grain Volume (mm^3)	$1.23x10^{-3}$	$4.20x10^{-3}$	$3.14x10^{-2}$	$1.96x10^{-3}$	$1.67x10^{-2}$	$7.66x10^{-3}$	$2.35x10^{-2}$	$4.48x10^{-5}$	$7.94x10^{-4}$	$1.02x10^{-2}$
Min Voronoi Volume (mm^3)	0.11	35.88	3.32	$4.31x10^{-3}$	$1.25x10^{-2}$	$9.14x10^{-3}$	$1.13x10^{-2}$	0.41	$2.36x10^{-3}$	0
Max Voronoi Volume (mm^3)	200.06	264.07	413.98	581.41	207.69	538.47	404.69	4.41	273.15	136.90
R^2	0.08	0.03	0.18	0.00	0.00	0.00	0.07	0.11	0.05	0.01
R	-0.28	0.18	0.43	-0.02	0.03	0.04	0.26	0.33	-0.22	-0.09
DF (n-1)	5	13	7	215	95	233	26	13	32	400
Critical Value of r (for two tailed t-test at 95% confidence)	0.878	0.533	0.754	0.139	0.207	0.139	0.388	0.950	0.361	0.098
Figures	3.20	3.21	3.22	3.23	3.24	3.25	3.26	3.27	3.28	3.29

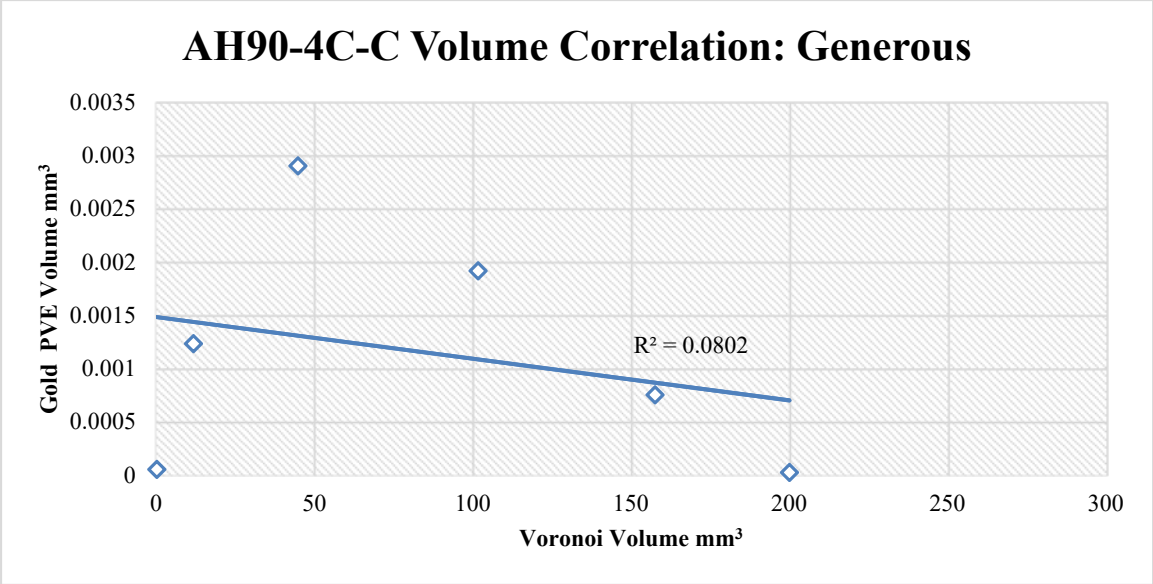

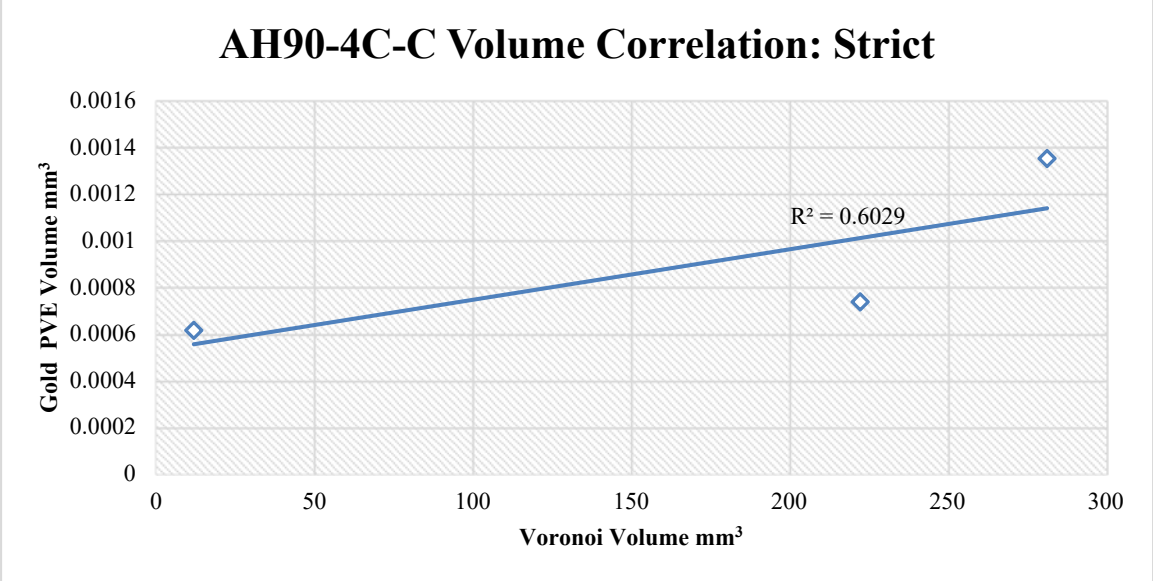

Figure 3.20 AH90-4C-C Volume Correlations

Porphyry sample AH90-4C-C generous (a, top) and strict (b, bottom) volume correlations between gold grain PVE volumes and modified Voronoi volumes in Cu-Fe sulfide network. Best fit linear trendline (blue) and goodness of fit value (R^2) are included.

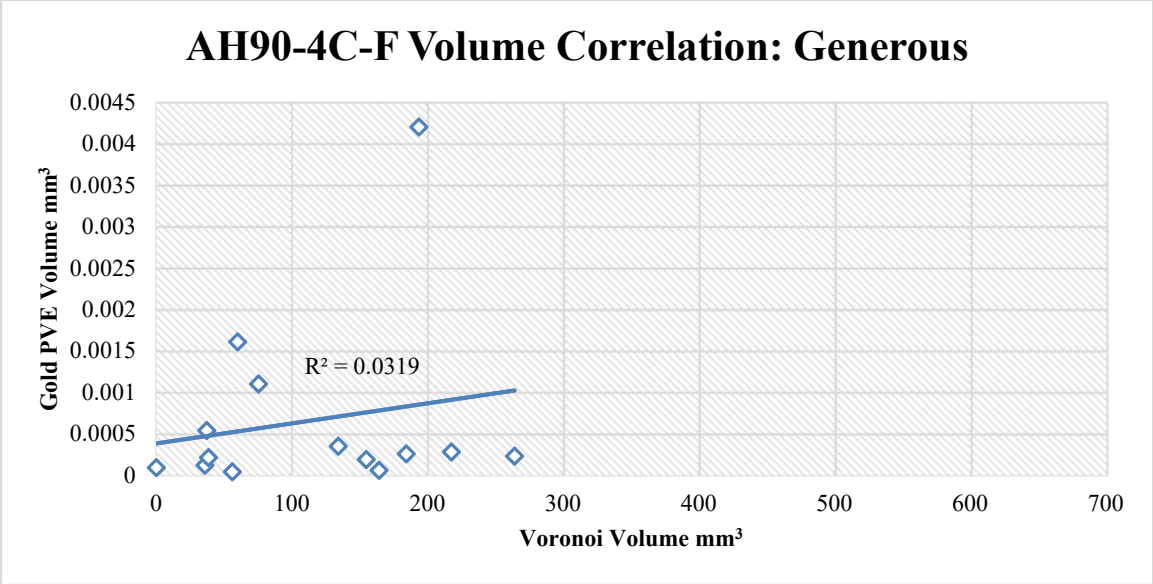

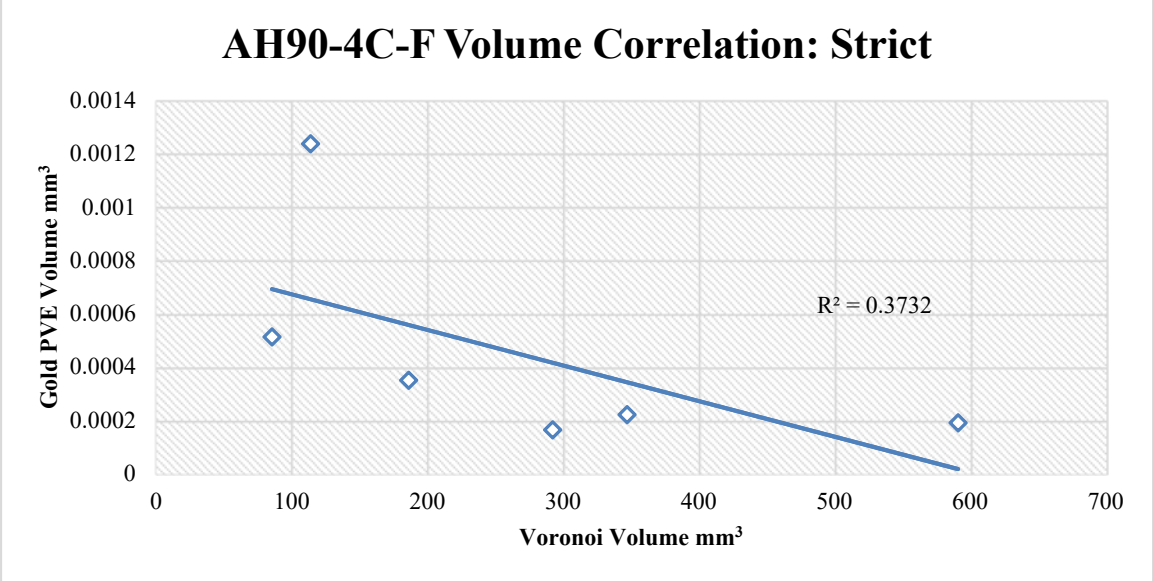

Figure 3.21 AH90-4C-F Volume Correlations

Porphyry sample AH90-4C-F generous (a, top) and strict (b, bottom) volume correlations between gold grain PVE volumes and modified Voronoi volumes in Cu-Fe sulfide network. Best fit linear trendline (blue) and goodness of fit value (R^2) are included.

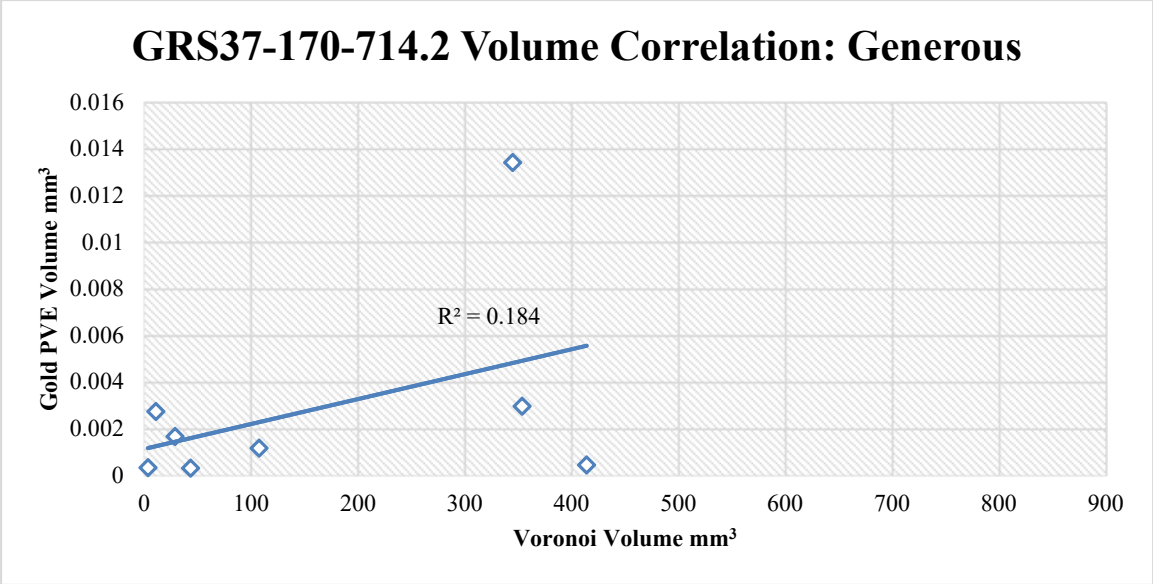

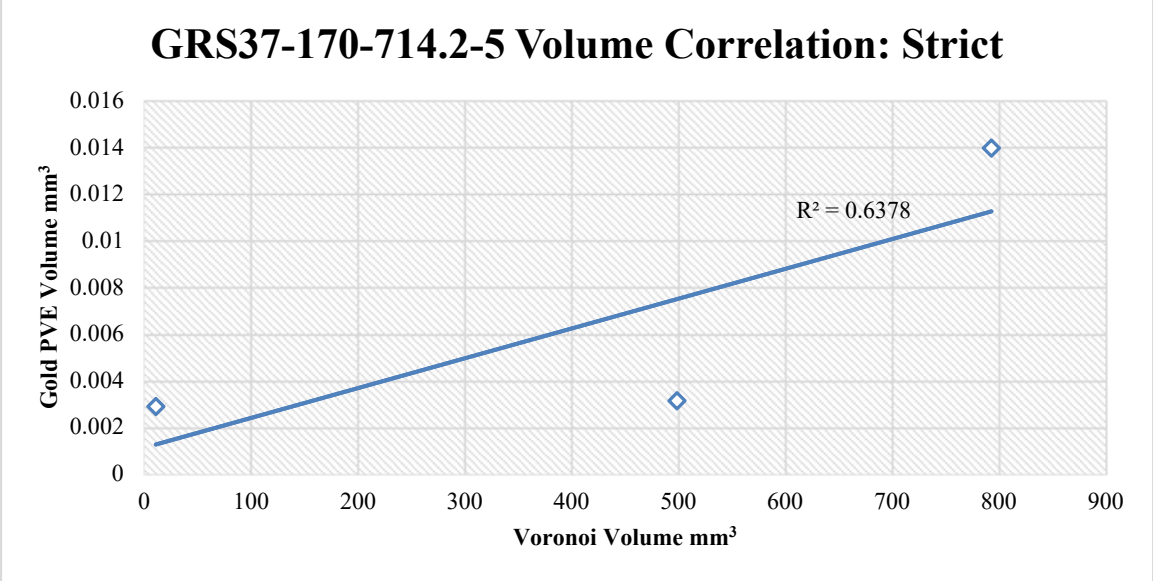

Figure 3.22 GRS37-170-714.2-5 Volume Correlations

Porphyry sample GRS37-170-714.2-5 generous (a, top) and strict (b, bottom) volume correlations between gold grain PVE volumes and modified Voronoi volumes in Cu-Fe sulfide network. Best fit linear trendline (blue) and goodness of fit value (R^2) are included.

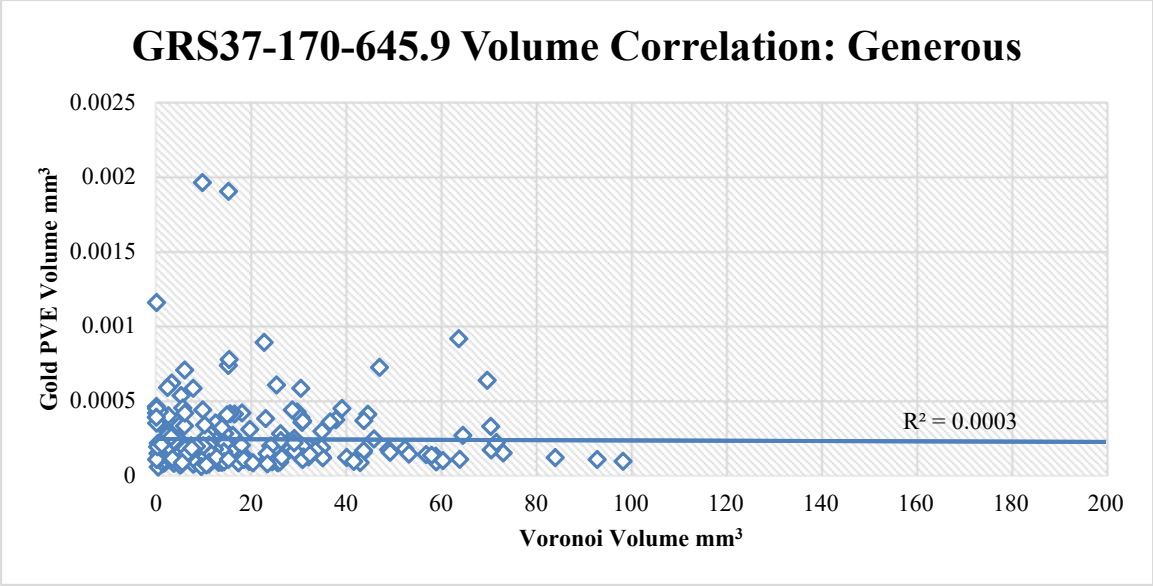

Figure 3.23 GRS37-170-645.9 Volume Correlation

Porphyry sample GRS37-170-645.9 generous volume correlation between gold grain PVE volumes and modified Voronoi volumes in Cu-Fe sulfide network. A strict correlation is not included as gold CT values were all very low, and no grains would have been included. Best fit linear trendline (blue) and goodness of fit value (R^2) are included.

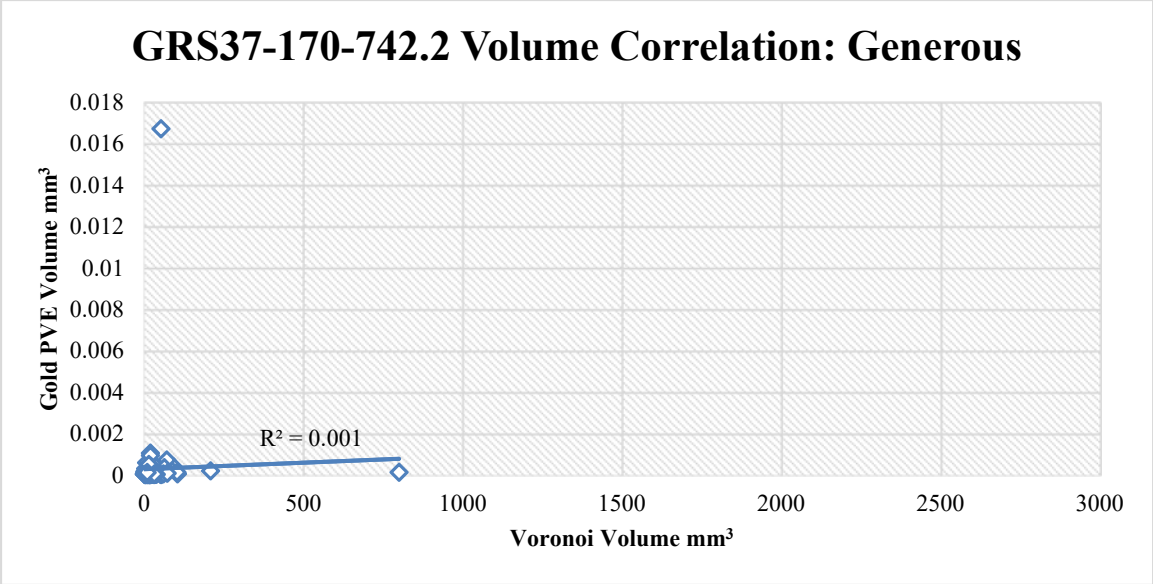

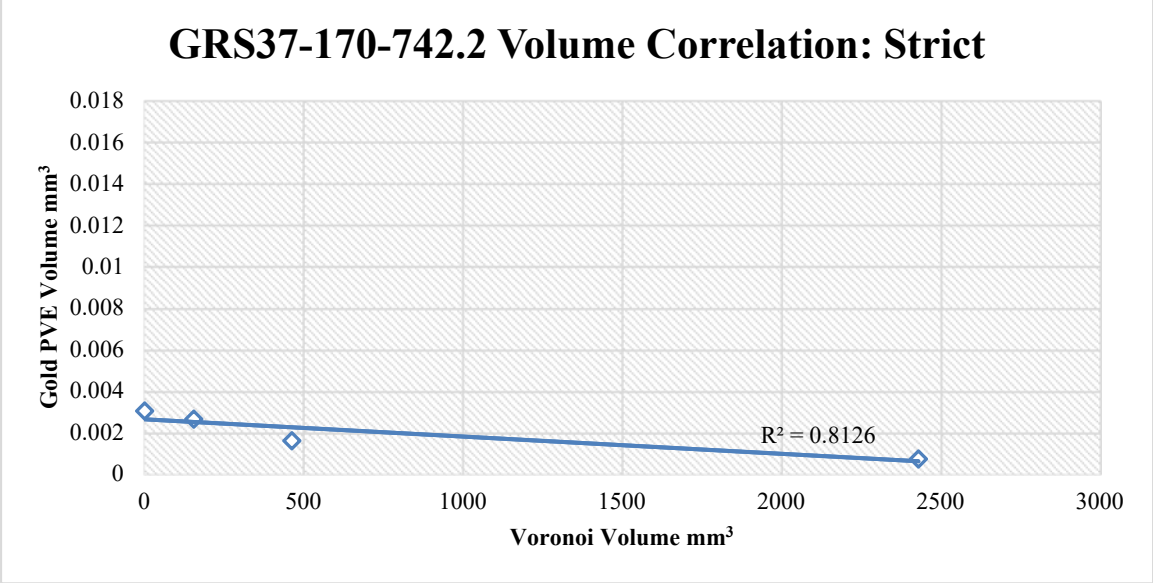

Figure 3.24 GRS37-170-742.2 Volume Correlations

Porphyry sample GRS37-170-742.2 generous (a, top) and strict (b, bottom) volume correlations between gold grain PVE volumes and modified Voronoi volumes in Cu-Fe sulfide network. Best fit linear trendline (blue) and goodness of fit value (R^2) are included.

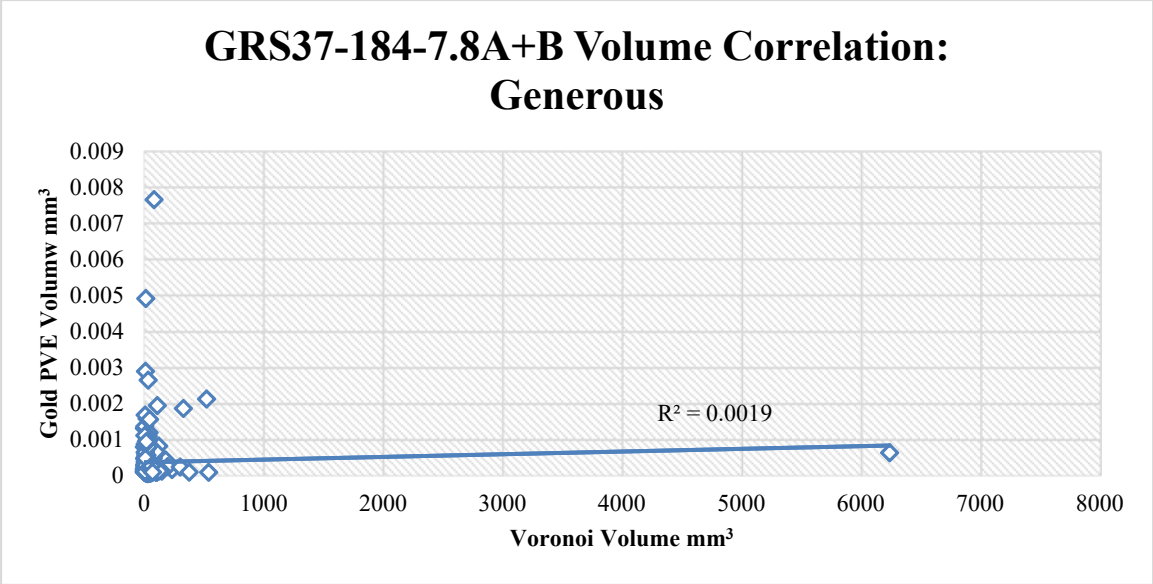

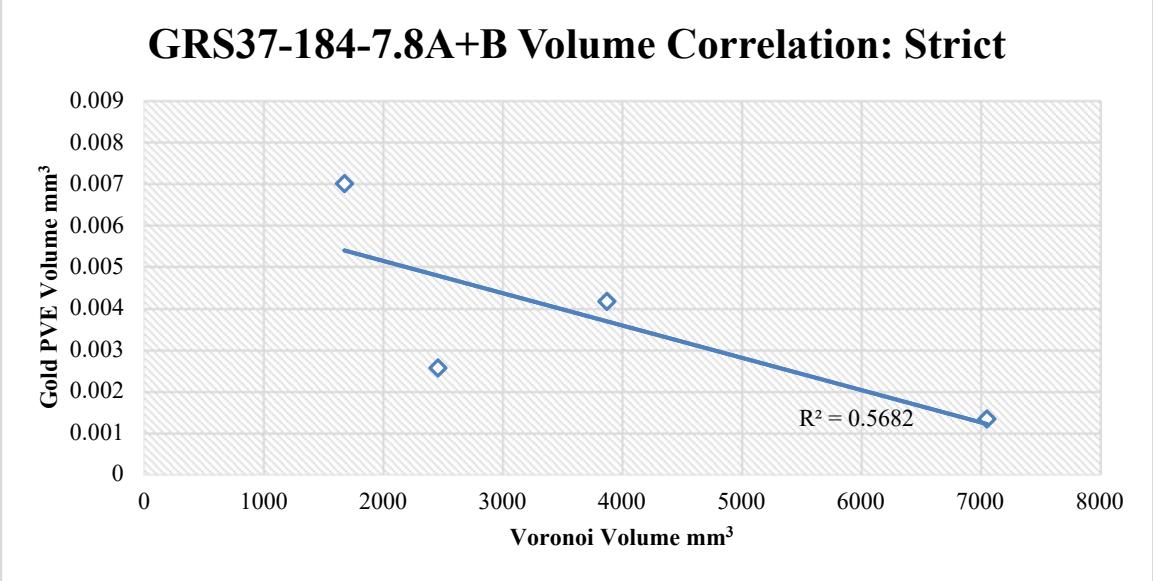

Figure 3.25 GRS37-184-7.8A+B Volume Correlations

Porphyry sample GRS37-184-7.8A+B generous (a, top) and strict (b, bottom) volume correlations between gold grain PVE volumes and modified Voronoi volumes in Cu-Fe sulfide network. Best fit linear trendline (blue) and goodness of fit value (R^2) are included.

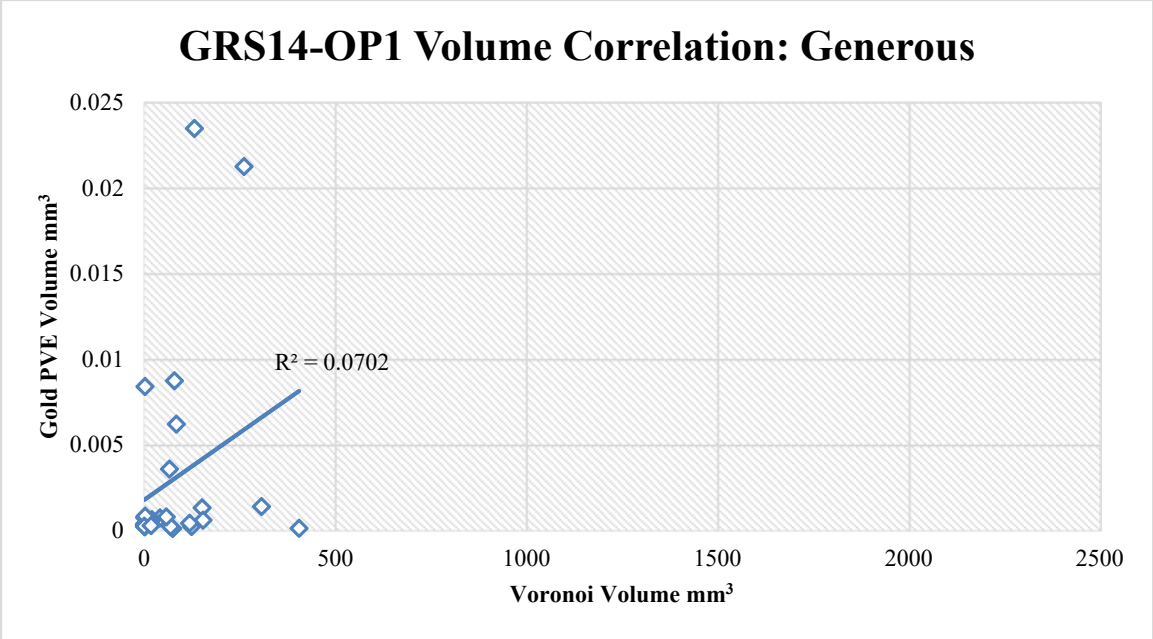

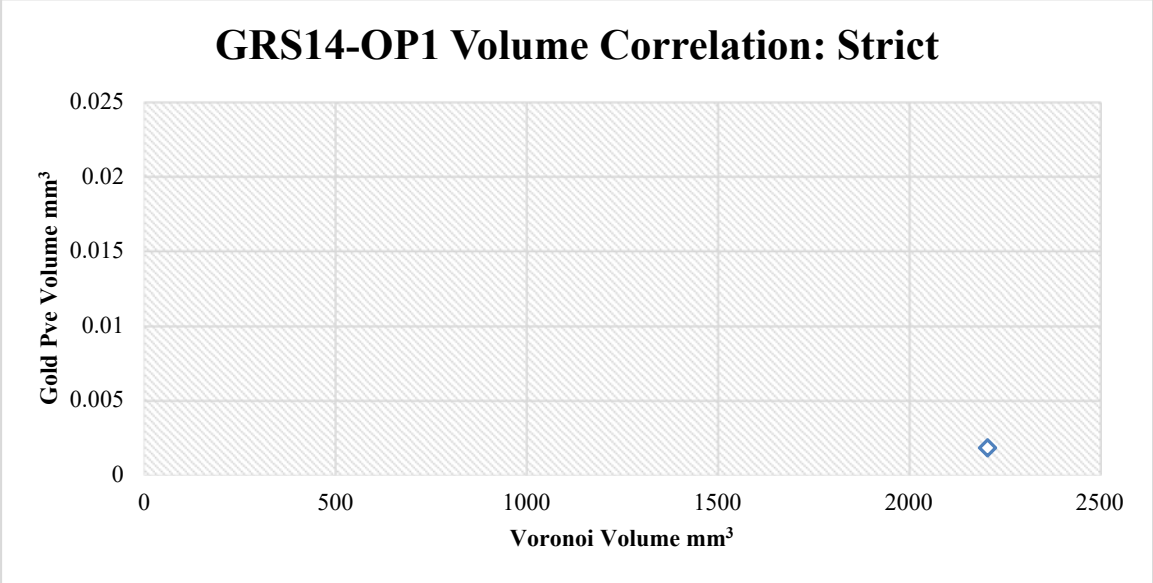

Figure 3.26 GRS14-OP1 Volume Correlations

Porphyry sample GRS14-OP1 generous (a, top) and strict (b, bottom) volume correlations between gold grain PVE volumes and modified Voronoi volumes in Cu-Fe sulfide network. Best fit linear trendline (blue) and goodness of fit value (R^2) are included.

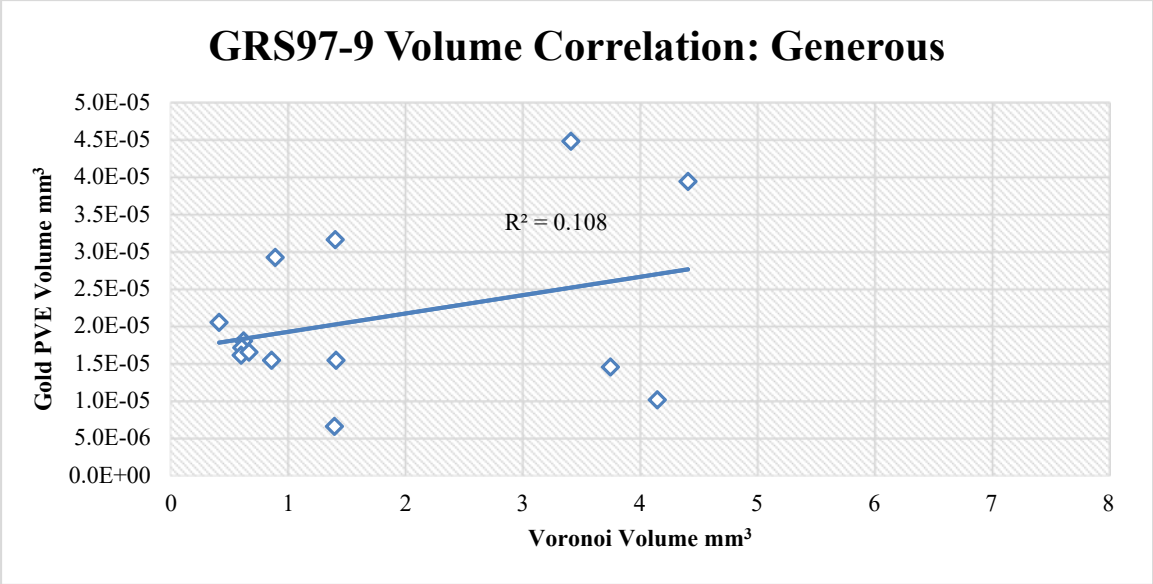

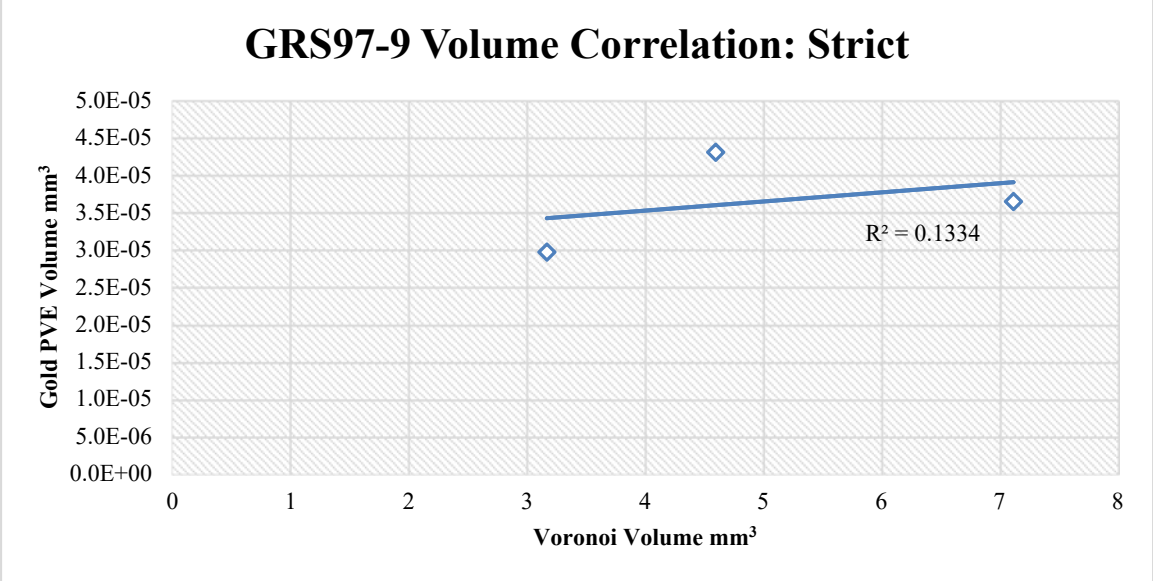

Figure 3.27 GRS97-9 Volume Correlations

Porphyry sample GRS97-9 generous (a, top) and strict (b, bottom) volume correlations between gold grain PVE volumes and modified Voronoi volumes in Cu-Fe sulfide network. Best fit linear trendline (blue) and goodness of fit value (R^2) are included.

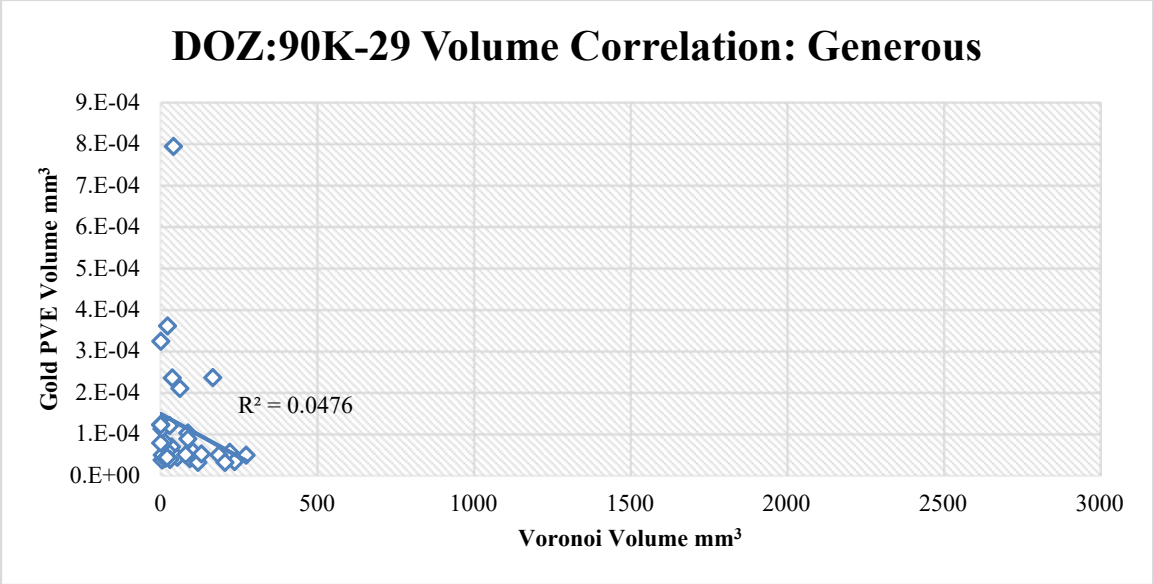

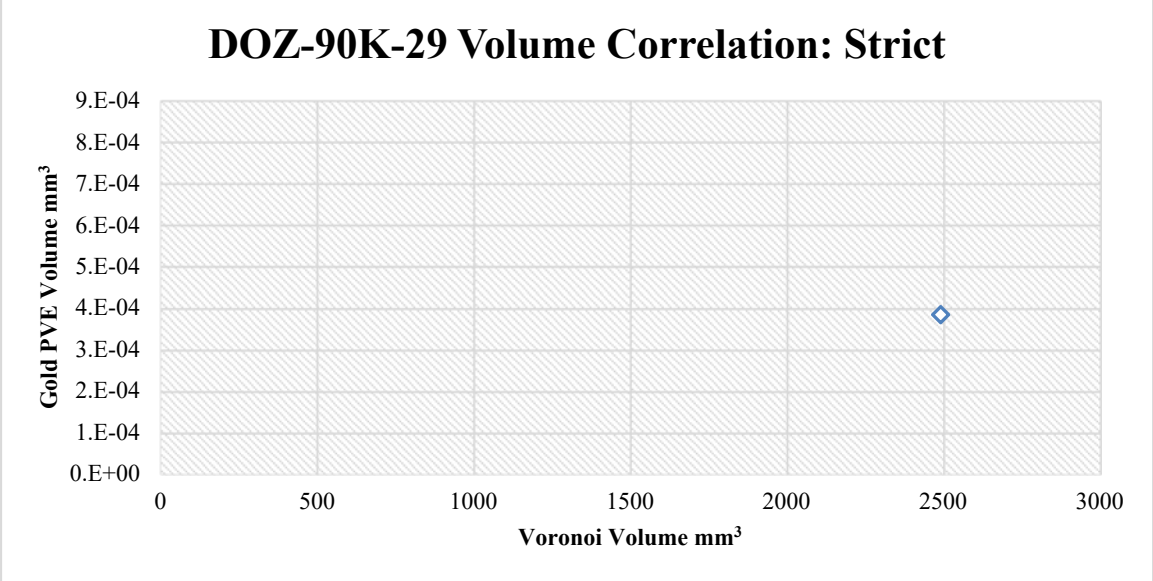

Figure 3.28 DOZ-90-29 Volume Correlations

Skarn sample DOZ-90-29 generous (a, top) and strict (b, bottom) volume correlations between gold grain PVE volumes and modified Voronoi volumes in Cu-Fe sulfide network. Best fit linear trendline (blue) and goodness of fit value (R^2) are included.

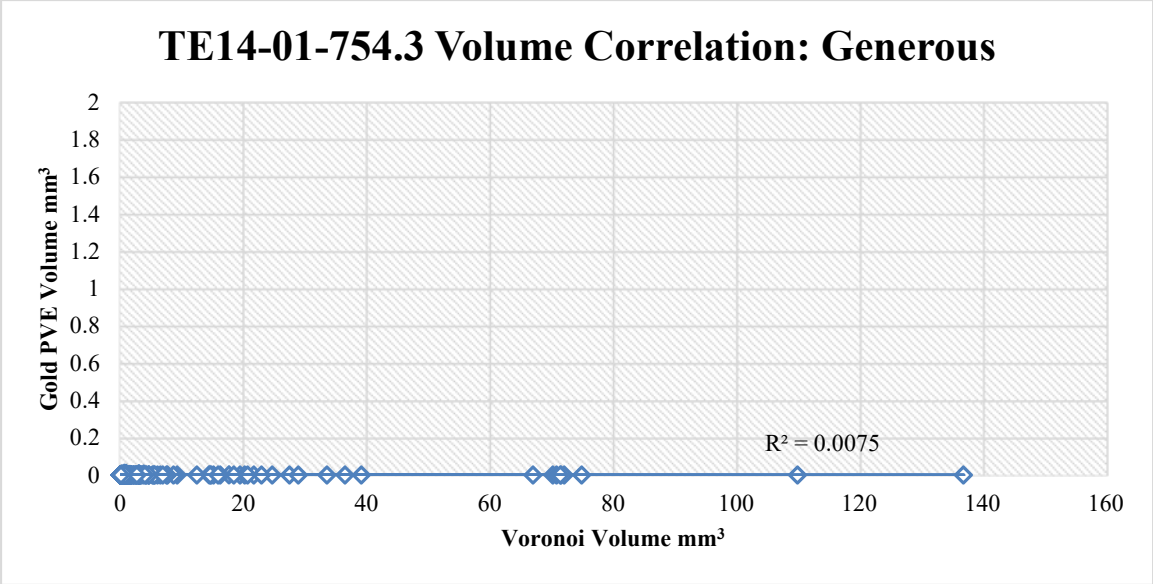

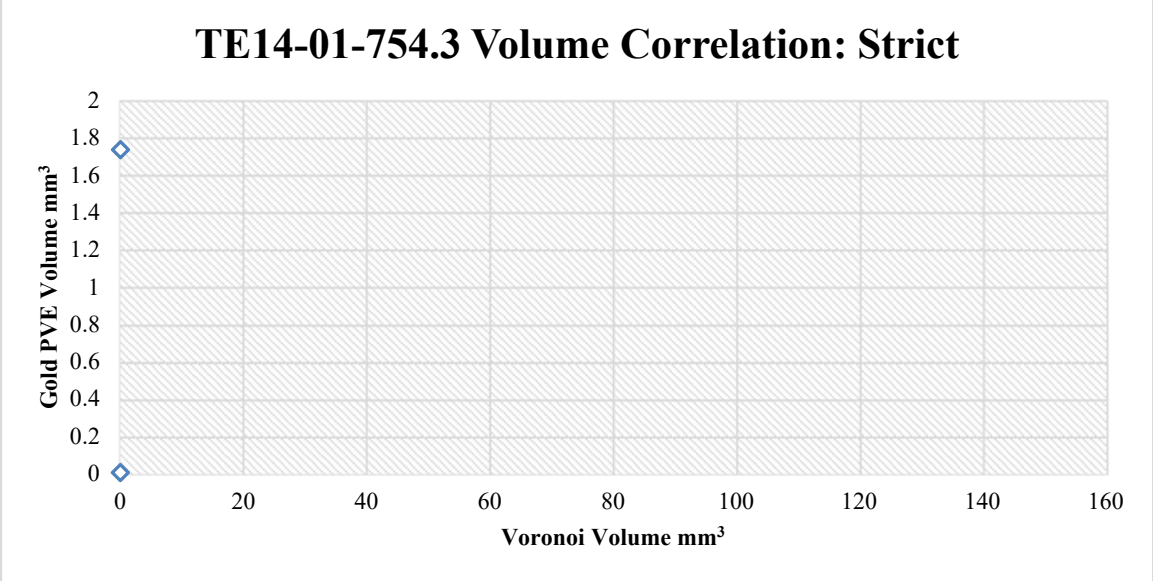

Figure 3.29 TE14-01-754.3 Volume Correlations

Skarn sample TE14-01-754.3 generous (a, top) and strict (b, bottom) volume correlations between gold grain PVE volumes and modified Voronoi volumes in Cu-Fe sulfide network. Best fit linear trendline (blue) and goodness of fit value (R^2) are included.

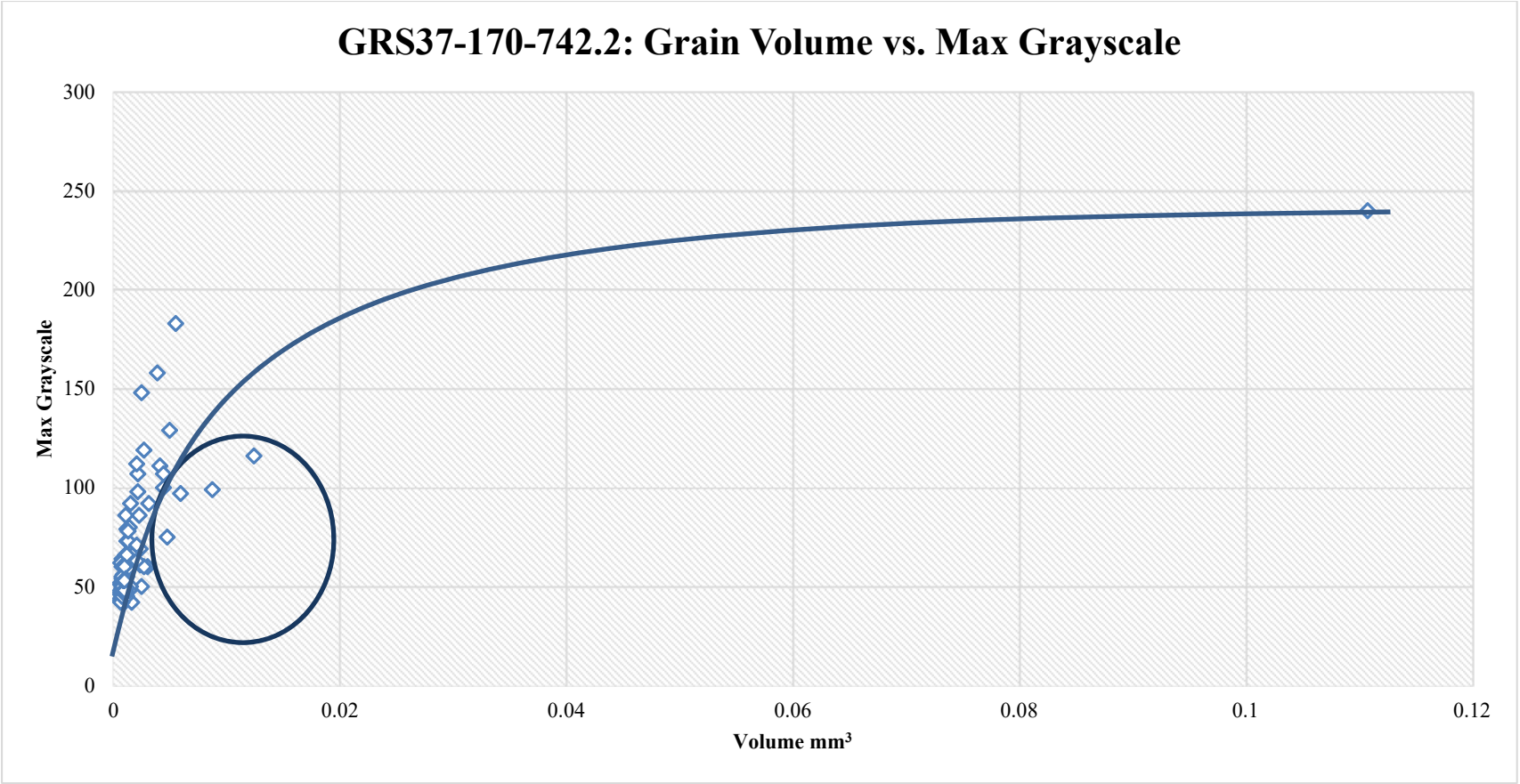

Figure 3.30 Porphyry Sample with Different Populations Among Grains

Grains within circle are candidates for mineral phases other than gold. Grains proximal to or above the curve are considered to be gold.

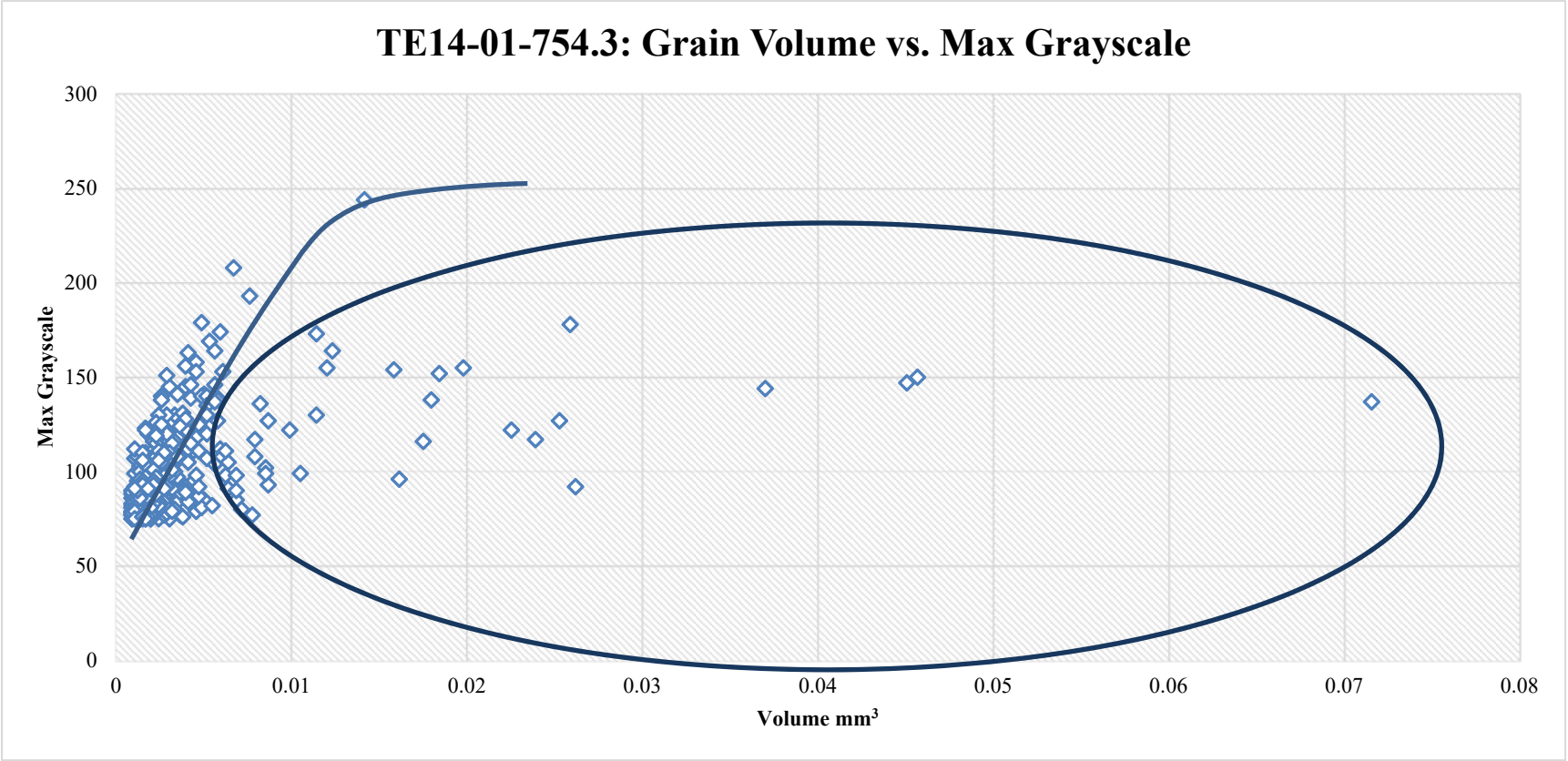

Figure 3.31 Skarn Sample with Different Populations Among Grains

Grains within circle are very likely not gold grains. Grains along curve are more likely to be gold.

Table 3.4. Blob3D Segmentation and Separation Specifications for GRS97-9 2016 Scan

	Au CT Threshold Range	Grains	Use	Total PVE Grain Vol. ($mm^{3)}$
#1	190-255	3	Mod. Voronoi	1.09×10^{-4}
#2	100-255	13	Mod. Voronoi	2.95×10^{-4}
#3	35-255	41	Compare 2016 to 2006	3.95×10^{-4}
#4	30-255	42	Compare 2016 to 2006	3.96×10^{-4}
#5	25-255	673	Compare 2016 to 2006	7.95×10^{-4}

Threshold range is given as an 8bit grayscale value between 0 and 255.

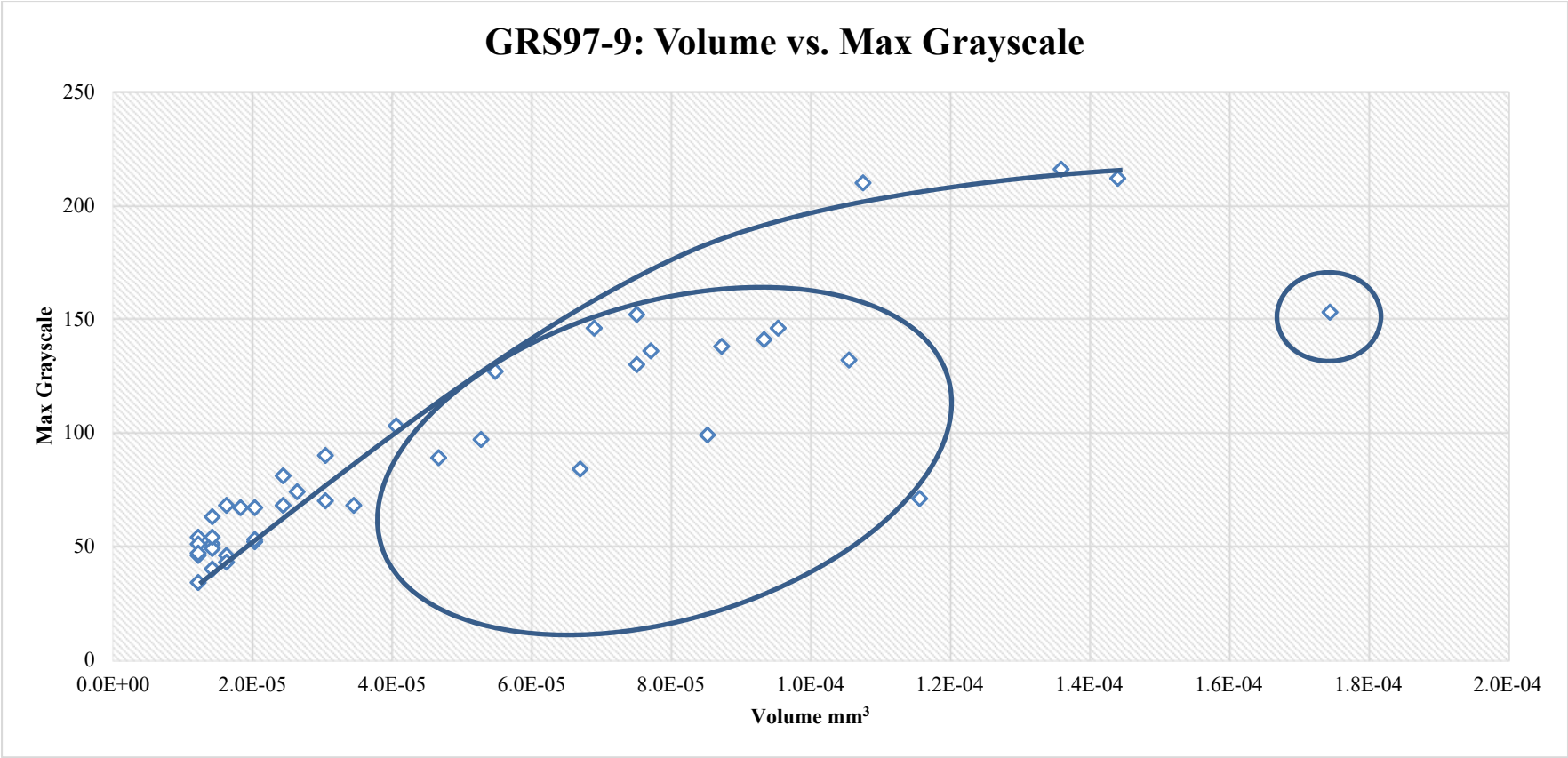

Figure 3.32 Grain Populations in GRS97-9 (2016)

Volume (mm^3) vs. maximum grayscale for GRS97-9 indicates the presence of unique grain populations among the separated gold volumes. Each point represents a single grain, and grains within the circles are potential candidates for bright mineral phases that are not gold. Grains that fall along the curve are likely to be gold.

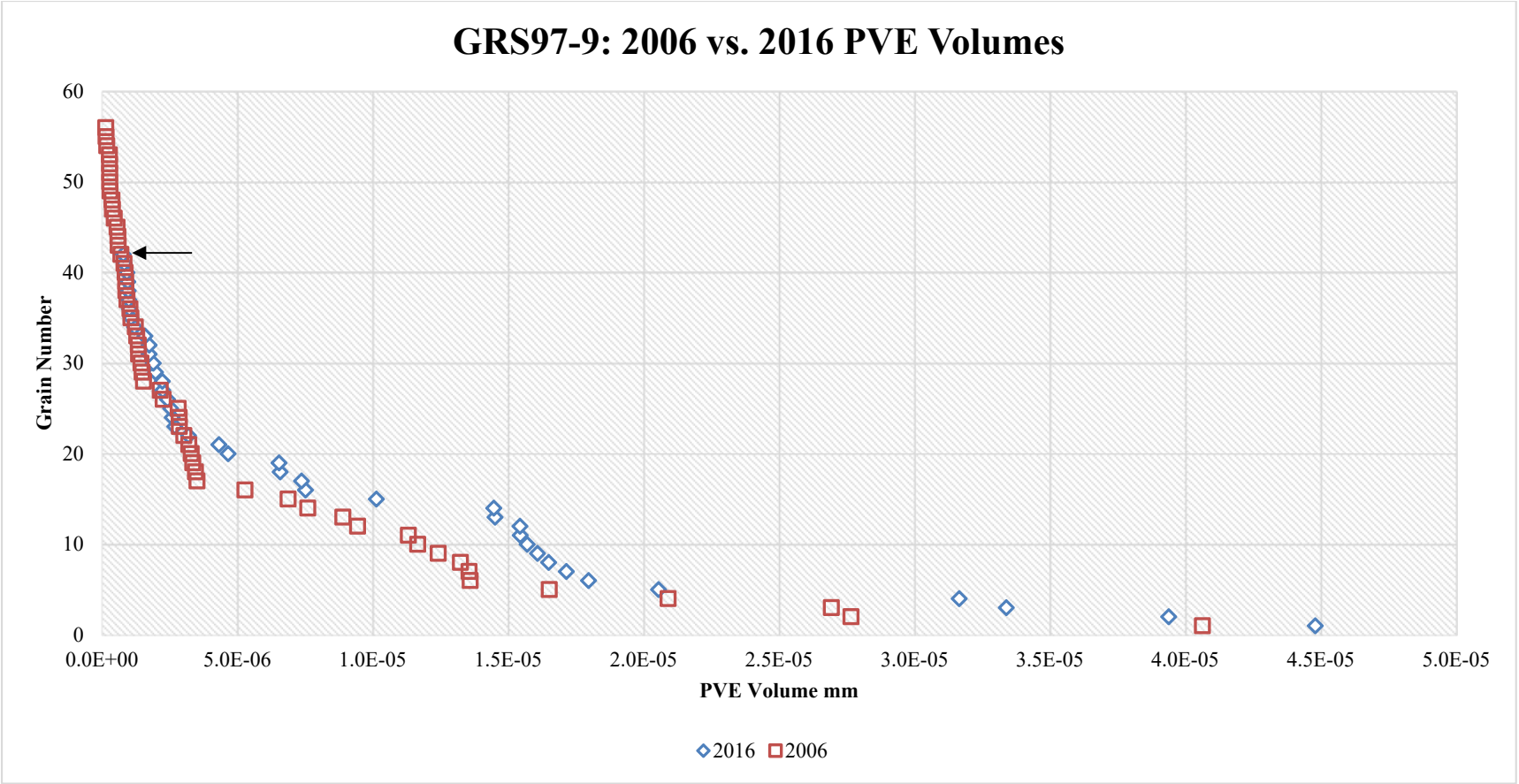

Figure 3.33 GRS97-9 2006 vs. 2016 PVE Volumes

PVE volume data for each grain in the 2006 separation and 2016 separation. The black arrow marks the smallest volume grain included in the 2016 separation. Divergence in grain volume occurs for volumes above $3.21 \times 10^{-6} mm^3$.

Chapter 4: LA-ICP-MS Trace Element Geochemistry

4.1 Introduction

Understanding the depositional relationships between gold and Cu-Fe sulfides, mechanisms that control gold abundance and deposition, and associated trace elements can constrain how world class porphyry skarn deposits form (Simon, et al., 2000; Norman, et al., 2003; Cook, et al., 2011). Trace element concentrations, variations, and occurrences in common ore mineral phases (e.g., Fe sulfides, Fe oxides, and Cu-Fe sulfides) are determined by redox and hydrothermal conditions, post-depositional weathering, and metal sources. Additionally, knowledge of trace elements in sulfide ores informs metallurgical processing procedures (Kyle, et al., 2011).

Two primary mechanisms have been proposed to explain the occurrence of native gold grains along sulfide boundaries: (1) direct precipitation of gold grains from gold-rich hydrothermal fluids, and (2) exsolution from nano-inclusions or lattice-bound Au within Cu-Fe sulfides (Kesler, et al., 2002; Sillitoe, 2010; Fraley & Frank, 2014). This study sought evidence of the second mechanism. Gold deposits are frequently associated with enrichments in other metals, (e.g., Ag, As, Hg, and Sb); thus, such elements have been used as pathfinders for gold (Robert, et al., 1997). Based on this exploration technique, we hypothesize that gold exsolution from cooling Cu-Fe sulfides could leave a metal-depleted zone, similar to that proposed by Carlson (1991), where gold and/or pathfinder metals are depleted around the gold grain (Carlson, 1991; Carlson & Denison, 1992; Robert, et al., 1997; Kesler, et al., 2002). Because the EGD is geologically recent and has

not been extensively overprinted or reworked, gold remobilization within the deposit is unlikely, and primary elemental distributions associated with gold mineralization should be preserved (Kesler, et al., 2002; Leys, et al., 2012).

Electron Microprobe analyses on EGD skarn samples (± porphyry samples) have previously assessed trace elements in EGD Cu-Fe sulfides (Rubin and Kyle, 1997). This study documents the trace element concentrations of bornite and chalcopyrite, from porphyry and skarn systems of the EGD. More than 300 laser spots were analyzed, 41 in bornite and 327 in chalcopyrite. The higher percentage of chalcopyrite analyses corresponds to the higher volume of chalcopyrite within our sample suite.

4.2 LA-ICP-MS AND ORE MINERALS: PREVIOUS STUDIES

LA-ICP-MS is a sensitive mass spectrometry technique (with ppb to ppt detection limits) that has been used to determine the elemental compositions of pyrite, arsenian pyrite, magnetite, and other ore minerals (Watling & Herbert, 1994; Watling, et al., 1995; Carew, et al., 2006). LA-ICP-MS studies have also investigated compositions of fluid and melt inclusions within ore samples (Audétat, et al., 1998; Günther, et al., 1998; Heinrich, et al., 2003; Halter, et al., 2005). Trace element compositions in Cu-Fe sulfides, namely bornite and chalcopyrite, however, are little studied (Arif & Baker, 2004; Cook, et al., 2011).

Cu-Fe sulfide analysis using LA-ICP-MS can be challenging, partially because sulfur has a high first ionization potential and tends to readily adsorb on to instrument surfaces and produce memory effects during analyses (Rees, 1978; Danyushevsky, et al.,

2011). LA-ICP-MS data accuracy and precision can be limited by sensitivity drift, elemental fractionation, interferences, and in many cases, the lack of suitable, matrix-matched reference materials with a representative suite of elements for standardization and calibration (Danyushevsky, et al., 2011; Cook, et al., 2016). Natural sulfide sources for reference materials have not emerged because their compositions are widely variable (Danyushevsky, et al., 2011). Most commercial standards (e.g., the NIST 600 series), are glass (silicate)-matrix standards with chalcophile element concentrations that are too low for instrument calibration. USGS synthetic basalt glasses (GS series) can be used for sulfide standardization, as they contain reasonably high Fe contents for the internal standard element, but important elements are often missing or occur in limited concentrations compared to levels in sulfides (Jochum, et al., 2005; Sylvester, et al., 2005). Our experiments using the USGS basalt glass series (GSC, GSD, and GSE) and the synthetic polymetal sulfide (MASS-1) generally resulted in poor recoveries on secondary standards. Because few well-characterized sulfide standards are in production (e.g., USGS MASS-1 is not distributed anymore), formulation of in-house sulfide standards has become increasingly common. In this regard, we used University of Tasmania CODES standard STDGL3 #36 (CODES-1, henceforth) as the primary reference material, with the GS glasses as secondary reference standards. CODES-1 is a lithium borate glass doped with a large suite of chalcophile elements difficult to find, or at low concentrations, in other standards (Table 4.1) (Danyushevsky, et al., 2011).

Gold may reside within sulfide phases as nano-inclusions or lattice-bound matrix atoms (Reich, et al., 2005; Cook, et al., 2011). Because elemental quantification by LA-

ICP-MS is phase specific, any gold inclusion sampled by the laser will increase the apparent gold concentration of the target phase. Cook *et al.* (2011) suggested that LA-ICP-MS gold measurements within a sulfide matrix might be artificially increased by the presence of regularly placed, nano-scale gold inclusions. According to Cook et al. (2011), gold inclusions may be identified as sporadic Au spikes during the down-hole dwell interval. However, if these Au inclusions are evenly dispersed, ablated material from the inclusions will be averaged with ablated matrix material. This issue can be alleviated by decreasing the spot size of the laser such that fewer inclusions will be intercepted. Performing pre-ablation SEM Back-scatter Electron Detector (BSE) imaging can reveal previously unseen inclusions or zonation within the target spots or areas. However, as these inclusions could be < few μm, it can still be nearly impossible to pre-determine their locations and avoid them.

4.3 Methods: Experiment Design and Sulfide Standardization

4.3.1 Samples

Core samples were assembled from the EGD samples available at the University of Texas at Austin (Chapter 2.4). Polished (n = 20) sections were prepared from regions of the skarn (n = 3) and porphyry (n = 6) core samples that contained gold, according to computed tomography. Due to the small size of gold grains and difficulty of precisely cutting to match CT slices, only three sections revealed gold grains on the polished surface. Eleven polished sections were analyzed with LA-ICP-MS. More samples were primarily chalcopyrite (n = 7) than bornite (n = 1), which is reflected in the polished

sections and the number of laser spots placed in each mineral. Three sections had appreciable volumes of both bornite and chalcopyrite (AH90-4C-C/F and GRS37-170-714.2-5). Although most samples contained small (~ 1 μms) bornite intergrowths, these were usually not large enough to place a laser spot in. Photomicrographs were taken of all polished sections in reflected light to assist with laser spot placement. Reflected light images (and SEM BSE images, if available) are used to determine the mineral phases and boundaries within the polished section and prevent spot placement over mineral inclusions. For the benefit of follow-up studies using the same material, digital radiographs of billets and sections were captured to determine the presence of gold grains that could not be seen on the surface (Appendix B). Most billets contained dark grains that were thought to be gold, and the sections could be polished to expose these grains for future studies.

4.3.2 Spot Analyses in Cu-Fe Sulfides

LA-ICP-MS analyses were carried out on a New Wave Research UP193-FX 193 nm fast excimer laser system (4-6ns pulse width) coupled to an Agilent 7500ce ICP-MS (operated in no-gas mode) in the Jackson School of Geosciences, University of Texas at Austin. For each analytical session, samples (6-8) and standards were loaded at the same time in the large format ablation cell, precluding the need to open the sample drawer until all analyses were completed (Figure 4.1). Instrument tune up was performed by monitoring analyte intensities during a line scan on GSD-1G (65 μm spot scanning 5 μm/s with a laser fluence of 2.35 J/cm^2) until RSD% ((Std. Dev./Mean Result) *100) and oxide

production were within acceptable ranges (Table 4.2) (2D map tune line: GSD-1G line 75 µm spot, 5 µm/s, fluence of ~1.35 J/cm^2.) Optimal instrument parameters were determined from spot tests in Cu-Fe sulfide while modulating laser energy density and then repetition rate. Prior to analyses, sample spots were pre-ablated with a 75 µm spot, 2 s dwell, and 2 s intersite pause. Samples were analyzed using 65 µm spots, arranged as individual spots, grids of 6 spots (spaced 130 µm apart), or lines of spots (spaced 65 µm apart); He and Ar flows of 700 mL/min, and 900 mL/min; repetition rate of 6 Hz; and fluence of 0.92 J/cm^2. The quadrupole time-resolved method involved measurement of 22 analytes, refined (reduced by 6 analytes) from analytes used in Boyle (1979) and Cook et al. (2011): ^{34}S, ^{51}V, ^{52}Cr, ^{53}Cr, ^{55}Mn, ^{57}Fe, ^{60}Ni, ^{65}Cu, ^{66}Zn, ^{75}As, ^{77}Se, ^{95}Mo, ^{105}Pd, ^{107}Ag, ^{115}In, ^{118}Sn, ^{121}Sb, ^{125}Te, ^{182}W, ^{197}Au, ^{208}Pb, and ^{209}Bi. Sample spot analyses were bracketed hourly by my standard measurement (CODES-1, GSC-1G, GSD-1G, and GSE-1G) in duplicate or triplicate. Analyte intensities were converted to elemental concentrations (ppm) using Iolite software with CODES-1 (STDGL3#36) as the primary reference material for calibration and ^{57}Fe as the internal standard element. Stoichiometric Cu, Fe, and S concentrations for bornite and chalcopyrite were assumed for data reduction. Although 22 analytes were monitored, only 15 are reported, not including ^{34}S, ^{51}V, ^{52}Cr, ^{53}Cr, ^{57}Fe, ^{65}Cu, ^{105}Pd, and ^{182}W.

Bornite and chalcopyrite grains were analyzed in areas near (within ~5 µm) and far away (~10s- 100s µm) from gold grains, as targeted using reflected light micrographs and computed tomography. Spots targeted within the matrix of isolated Cu-Fe sulfide grains were labeled “matrix,” whereas spots targeting veins or veinlets were labeled as

"veins." Three spots were placed near (100 – 800 μm away) a visible gold grain, in porphyry sample AH90-4C-F, to determine if the presence of a gold grain altered the trace element contents of nearby bornite/chalcopyrite. To test for possible chemical gradients within the sulfide matrix near gold grains, we established lines of spots radiating outward from gold grain centers, or spot grids adjacent to gold grains (Figure 4.2). Gold grains analyzed were in sample GRS37-170-742.2 in a chalcopyrite vein. Four gold grains were identified: three spaced ~0.5 – 1 mm apart, near the edge of the vein with minor bornite intergrowths, and one grain ~300 μm from a microfracture within the chalcopyrite vein (Figure 4.2). Line-of-spot traverses were analyzed going away from the gold grain.

4.3.3 Maps of Cu-Fe Sulfides and Gold Grains

To better assess spatial variations among analytes within Cu-Fe sulfides, we analyzed contiguous line scans over ~1 mm x 1 mm target areas in order to generate 2D chemical maps. Target areas (n = 3) included bornite, chalcopyrite, and gold grains in sample GRS37-170-742.2, and AH90-4C-F (Figure 4.3). To determine optimal instrument parameters, test lines were scanned at varied laser fluences and repetition rates. Lines were pre-ablated with rasters at 100 μm/s, ~0.49 J/cm^2, 10 Hz, with a 100 μm spot size. Samples were analyzed with 25 x 25 μm "square" aperture mask, scanning at 100 μm/s. Adjacent lines were scanned in the same direction to cover the entire target area. Ablation was carried out with He at 850 mL/min, Ar at 700 mL/min, 20 Hz, fluence ~1.4 J/cm^2. Each pixel in the 2D maps accounts for ~1.17 data points, based on the product of the sampling period and the scan rate. The quadrupole time-resolved method involved measurement of 16 analytes: ^{55}Mn, ^{57}Fe, ^{60}Ni, ^{66}Zn, ^{75}As, ^{77}Se, ^{95}Mo, ^{105}Pd, ^{107}Ag, ^{115}In, ^{118}Sn, ^{121}Sb, ^{125}Te, ^{197}Au, ^{208}Pb, and ^{209}Bi. Analyses were bracketed hourly by CODES and GSE-1G, run in

duplicate. Data reduction and 2D map generation was completed offline using Iolite software (Paton, et al., 2011).

4.4 RESULTS

Average analyte recoveries on external standards are in Table 4.3. GSC, GSD, and GSE recoveries were within 10% for Mn, Ni, Cu, Mo, In, Sb, W, and Pb, 15% for Ag, Au, and Bi. Recoveries were typically high for Zn, As, Se, and Sn. Standard error, LOD, and signal to noise data for analytes in unknowns and standards are included in Appendix C. Analyses of sulfide matrix material immediately around gold grains were limited to gold in chalcopyrite. Only one bornite polished section had an exposed gold grain. The grain was situated on the edge of the sulfide vein, between multiple mineral phases, making it difficult to analyze as the laser would have to sample multiple phases. We assume that consistent analyte intensities during dwell intervals reflect homogeneous distributions within the matrix of the host phase, whereas episodic peaks in depth profiles may indicate the presence of nano-inclusions (Cook, et al., 2011). Spikes in Zn and Au analyses, suggest that some spots could have sampled sphalerite and gold inclusions (Figure 4.4).

4.4.1 Gold Contents in Cu-Fe Sulfides

Gold concentrations in sulfide matrix samples were <1 ppm, in general (Tables 4.4 and 4.5). The mean gold concentration in porphyry samples is difficult to assess, as some spots have very high gold concentrations and may represent inclusions. Assuming these spots are not inclusions, mean Au is 41.1 ppm Au in porphyry samples, but without these spots mean Au is 0.96 ppm. Gold depth profiles for lines 44 and 48 have obvious peaks within them, suggesting that the spot is sampling a gold inclusion (Figure 4.2, Figure 4.4). Average gold contents for all skarn samples is 0.28 ppm. TE01-16-566 had the most gold

measurements (n = 20), even though HRXCT data indicated it had few gold grains. Maximum gold concentrations occur in discrete regions of Cu-Fe sulfide minerals, with veins (n =129) generally enriched over matrix (n = 21).

Linear traverses of spots (260-325 µm in length, spot size 65 µm, spaced 65 µm apart) were arranged around gold grains within the GRS37-170-742.2 chalcopyrite vein to assess elemental variation (Figure 4.2). In lines # 44, 48, 53, approaching each of three proximal gold grains, gold concentrations ranged from 0.1 to 3770 ppm (3770 ppm measured closest to gold grain) (in Appendix C; Figure 4.2A). All concentrations slightly decreased (from >1 ppm to <1 ppm) in spots further away from the gold grains, except one spot (650 ppm) may have sampled a gold inclusion below the surface (Line# 48 in Figure 4.2A). This decrease could indicate a concentration gradient, where gold is enriched in the sulfide closest to the gold grain. These measurements may also be sampling any ablated material that has resettled on the surface, rather than a real concentration gradient. All but one spot (10.9 ppm) in lines # 39, 40, 41, radially surrounding a single gold grain, were below the detection limit. (Appendix C; Figure 4.2B).

Grids of spots placed in Cu-Fe sulfide near three gold grains (~400 µm away, Grid 42; ~600 µm away, Grid #43; Figure 4.2) ranged from 0.02 to 0.43 ppm, with no clear enrichment pattern. The overall trend realized from these various transect, grid, and line-of-spot analyses is that the Cu-Fe sulfide matrix could be enriched in gold near gold grains, suggesting an enrichment halo (Figure 4.5). However, pre-ablation of spots near gold grains could have deposited a portion of the ablation plume onto the mineral surface. This could result in an apparent, but inaccurate, increase in gold concentration around the grain. Grids of spots in GRS37-170-742.2 proximal (~100 µm) to a Pd-Te grain ~300 µm from a ~50 µm wide microfracture, have measurable gold concentrations (n = 8, range: 0.024 –

0.33 ppm). Analyses ~100 μm away from another Pd-Te grain (~100 μm from a 2 μm wide microfracture) had no measurable gold concentrations.

4.4.2 Trace Element Contents

Data and elemental correlations are reported in Tables 4.6 – 4.15. ^{65}Cu data are not reported, as Cu values are so high in both chalcopyrite and bornite, that even with a generous washout time, measurements never reached original background levels once analyses began. Signal-to-noise ratios for analytes, standard error, and limit of detection (LOD) data are contained in Appendix C.

4.4.2.1 Bornite

Bornite analyses consisted of 18 spots from skarn samples and 23 from porphyry samples (Table 4.6 and 4.7; Appendix C). Spots proximal to a gold grain (~100 μms) in bornite in AH90-4C-F have no measurable gold contents. A number of elemental correlations show moderate positive correlations, and some show strong positive correlations: Ni and Te (r = 0.80), Ag and Bi (r = 0.67), Sn and Bi (r = 0.71), and Au and Bi (r = 0.67) (Figure 4.6 and Table 4.7). Data points that are anomalously high compared to general local measurements have been interpreted to be inclusions and elemental correlation matrices do not include these data points. Bornite appears generally enriched in Ag, Bi, and Te, over chalcopyrite.

Skarn

The trace element contents of skarn bornite deviate from porphyry bornite for Zn, Ag, Sn, Pb, and Bi (Table 4.6). All skarn bornite analyses are from sample DOZ-90-29, which contains almost exclusively bornite with minor digenite and chalcocite, and rare, small chalcopyrite inclusions. Though there is a notable deviation to 600 ppm in one spot,

Ag typically ranges from ~50 ppm to 185 ppm. Within DOZ-09-29, Ag and Te correlate very well (r = 0.96) (Table 4.11B). Te ranges from 54.2 ppm to 366 ppm. Ag and Bi correlate over all skarn samples, but not in DOZ-90-29 (r = -0.20) (Table 4.11B). Bi has a narrow range, from 112.2 ppm to 131.4 ppm in DOZ-90-29. Although gold correlates with Bi across all skarn samples, DOZ-90-29 alone does not show a strong correlation between Au and Bi. Au ranges from 0.01ppm to 0.09 ppm.

Porphyry

Porphyry bornite samples are AH90-4C-C and AH90-4C-F. Single spots were also placed in bornite within the matrix of GRS37-170-742.2 and GRS37-184-7.8. Matrix-bound bornite (GRS37-184-7.8 and GRS37-170-742.2) is anomalously enriched in Bi (mean = 1355 ppm), Au (22.42 ppm), Te (131.7 ppm), Sn (47.5 ppm), Ag (368 ppm), and Se (634 ppm). Porphyry samples (AH90-4C-C/F) have Ag concentrations from 225.6 ppm to 451.7 ppm.

4.4.2.2 Chalcopyrite

Chalcopyrite analyses consisted of 287 spots in porphyry (n = 203) and skarn (n = 84) samples, in matrix (n = 17) and vein (n= 270) chalcopyrite (Table 4.8 and 4.9; Appendix C). Element-pair correlations show positive correlations between Sn and Se (r=0.48), Au and Bi (r= 0.44), Ag and Bi (r= 0.55) (Figure 4.7). Ni and As display a slightly stronger correlation (r=0.63) (Table 4.9). Chalcopyrite is typically depleted in Ni, As, and Mo, and enriched in In and Zn. Spots proximal to a gold grain (~100 μms) in chalcopyrite in AH90-4C-F have gold concentrations that range from 0.02 ppm to 0.08 ppm. Average Ag and Bi are generally higher in skarn (Bi = 22.2 ppm, Ag = 31.2 ppm) than porphyry (Bi = 2.1, Ag = 5.5) chalcopyrite.

Skarn

Se has a broad range of concentrations in skarn samples, from 70 ppm to 988 ppm. The highest and lowest Se values were recorded in skarn chalcopyrite. The lowest Sn concentration was measured in a skarn sample (0.42 ppm), but typically the range was from ~20 ppm to ~50 ppm. Ni and As range from 0.01 ppm to 84.7 ppm, and 0.25 ppm to 26 ppm, respectively. Gold was low, ranging from 0.08 ppm to 1.43 ppm. Zn is elevated in skarn chalcopyrite samples (mean = 781.5 ppm).

Porphyry

Zn concentrations are lower in porphyry chalcopyrite (mean = 427.9 ppm). Bi and Ag concentrations are lower in porphyry chalcopyrite, and range from 0.02 ppm to 281 ppm and 0.55 ppm to 274 ppm, respectively. Gold concentrations were inconsistent, ranging from 0.05 ppm to 3770 ppm. Ni and As do not correlate well in porphyry chalcopyrite samples, and have inconsistent concentrations, where most measurements were below the minimum detection limit.

4.4.2.3 Transect Across Vein

Mn, Zn, Ag, Sb, Au, Pb, and Bi measurements vary systematically along the transect across the chalcopyrite vein in sample GRS37-170-742.2, potentially demonstrating some chemical zonation in the chalcopyrite (Figures 4.8 and 4.9). At 1.1mm across the transect all of these elements increase markedly, indicating the ablation of an inclusion high in these components, followed by a dramatic drop in these elements immediately after the inclusion, potentially indicating a halo of elemental depletion immediately around the inclusion (Figure 4.9). In (~3 ppm), Sn (~40 ppm), Te (~10 ppm),

and Se (~540 ppm) have consistent concentrations across the transect. Gold concentrations are sporadic at ~0.1 ppm levels in patches along the transect.

4.4.3 2D Maps

Average analyte recoveries are found in Table 4.3. GSE recoveries were within 10% for Mn, Ni, Cu, Mo, Ag, In, Sb, Pb, and Bi, and within 15% for Au. Recoveries for As, Se, and Sn were high. Standard error, LOD, and signal to noise data for the secondary standard are included in Appendix C. The LA-ICP-MS trace element maps in Figures 4.10 A, B, C, and D reveal unexpected patterns in bornite and chalcopyrite. Elemental maps in GRS37-170-742.2 show a potential halo (~10s μm) of high to low Au measurements surrounding individual Au grains (Figures 4.10 C and D). Figures 4.10 A and B are maps of the same area in AH90-4C-F, however Figure 4.10A is standardized based on Fe in chalcopyrite (30.418 wt. % Fe), thus only chalcopyrite areas have accurate concentrations. Figure 4.10B is standardized based on Fe in bornite (11.17 wt % Fe).

Figure 4.10A: Veinlets with envelopes of chalcocite and covellite are not markedly enriched or depleted in any of the maps. Compared to bornite, chalcopyrite in these maps is trace element depleted, and only seems to be enriched in In, Se, and Sn.

Figure 4.10B: Veinlets in bornite with chalcocite/covellite envelopes have elevated Ag, Au, In, Pb, and Zn concentrations. Au is almost entirely restricted within the veins and small “enrichment haloes” around the veins. Bornite contains elevated concentrations of Ag, Bi, Pb, Se, and Te. Quartz along the lower edge of the map appears enriched in Bi, In, Mn, Ni, Pb, Se, Sn, and Zn.

Figure 4.10C: Veins/fracture surfaces in the upper right corner are enriched in Ag, Bi, Fe, Mn, Ni, and Pb. In comparison, Se, Sn, Te, and Zn are evenly distributed throughout the

map, and fractures are depleted. Ag and Bi concentrations are elevated near fractures and small bornite intergrowths. Ag is also slightly elevated near the gold grain; no other elements show marked variation near the gold grain. Ag, Bi, Fe, Pb, Sb, and Zn indicate some zonation in the chalcopyrite matrix that is not visible in reflected light. The zoning is most obvious as similar variations in Ag and Pb concentrations, indicating a potential correlation between the two.

Figure 4.10D: Veins/fracture surfaces are enriched in Ag, Bi, Fe, Mn, Ni, and Pb. Decreasing gold concentrations away from three gold grains define apparent haloes. The gold grains are also enriched in Ag. Bornite is enriched in Ag, Bi, Fe, Pb, Se, Sn, and Te. The chalcopyrite shows similar zonation to Figure 4.10B in Ag, Bi, Pb, Sb, and Zn. However, the zoning is most apparent in Ag, Pb and Zn in these maps. At least one of the major zones seems to be bound on either side by a small fracture and a band of bornite intergrowths.

4.5 DISCUSSION

This study presents new and minor element data for bornite and chalcopyrite that can improve understanding of Cu-Au mineralization in the EGD. Although gold in association with the Cu-Fe-S system has been previously studied (e.g., Reich et al., 2005; Cook et al., 2011; Reich et al., 2013) associated trace element distributions have received far less attention.

4.5.1 Gold

EGD bornite appears to have low to negligible gold concentrations. Gold occurrences were erratic within Cu-Fe sulfides and concentrations were typically under 1 ppm. This suggests that either, all of the gold that could potentially have been held by the

Cu-Fe sulfides analyzed was exsolved during cooling, or that little gold went into solid solution to begin with. Cu-Fe sulfide samples analyzed in this study also may not be representative of the most gold enriched sulfides in the EGD. The noted patchiness of gold enrichment could indicate that gold concentrates within Cu-Fe sulfides, either as groups of nano-inclusions, or as lattice bound gold. Gold nanoparticles have been observed in pyrite (Reich et al., 2013), but have not been imaged in bornite or chalcopyrite. Structurally bound gold atoms have not been imaged within sulfides (e.g., with Tunneling Electron Microscopy). Because Cu-Fe sulfides are such poor hosts for Au at low temperatures, even low degrees of gold enrichment may indicate that gold not lost to exsolution during cooling, could still diffuse and collect within the sulfide lattice. Such a process may account for the small gold inclusions (~10s μm) seen in GRS37-170-742.2. Further studies of gold diffusion and solubility within the Cu-Fe-S system are needed to confirm this mechanism.

LA-ICP-MS analyses (spots, traverses, 2D imaging) support that gold (and silver) enrichment haloes may occur within the Cu-Fe sulfide matrix surrounding gold grains (Figures 4.5, 4.10 and Table 4.5). These enrichment haloes could represent sampling of previously ablated and redeposited material around the gold grains. However, three observations lead us to conclude that these are genuine features: (1) their presence over consistent length scales (~10 μms) around each analyzed gold grain, (2) their absence in almost every other elemental map (except Ag, which has been previously noted by Cook et al. (2011) to be incorporated into Au nanoparticles), and (3) laser spot analyses that also show measurable gold contents surrounding the gold grains. These features are inconsistent with the simple diffusion-limited model proposed by Carlson (1991, 1992), which concluded that garnet porphyroblast growth would result in a nutrient depleted area surrounding the grain. Our data are inconsistent with additional aspects of the Carlson (1991, 1992) model, where porphyroblast clustering stifles the growth of the inner-most

crystals. Au nanoparticles surrounding a larger, central particle would be more likely to grow than the insulated larger particle, as the surrounding nanoparticles are still able to scavenge nutrients from the matrix. We propose that a hybrid mechanism, including both gradient driven diffusion and Ostwald-type ripening operating over different length-scales, could promote gold migration, nanoparticle concentration, and μm-scale grain formation within Cu-Fe sulfides in the EGD.

Ostwald ripening is a phenomenon driven by surface energy minimization of an inhomogeneous structure over time, where small particles dissolve and redeposit onto larger particles (Ostwald, 1896). Reich et al. (2006) showed that at high-temperatures, Au nanoparticles in arsenian pyrite become unstable, unless Ostwald ripening coarsens the largest nanoparticles at the expense of smaller nanoparticles (Figure 4.11). At high-temperatures, when chalcopyrite and bornite can host high gold concentrations (incorporated in solid solution or as nanoparticles), gold should be able to easily diffuse through the sulfide lattice as atoms, clusters of atoms, or nanoparticles (e.g., ~4nm particles in Reich et al. (2013)) (Fraley & Frank, 2014). Through diffusion, gold becomes heterogeneously distributed throughout the sulfide matrix, occurring primarily in clusters of nanoparticles (or atom clusters, as the exact mode of incorporation of Au into Cu-Fe sulfides has not been observed). To minimize surface energy, Ostwald-type ripening redistributes gold from small nanoparticles to larger nanoparticles. Ostwald ripening and diffusion could have occurred until the temperature dropped too low in the EGD system to sustain these processes. Diffusion allows for gold transport throughout the sulfide matrix, encouraging the growth of an enrichment halo, while Ostwald-type ripening allows for the redistribution of gold onto the largest gold grain. From the elemental maps in Figure 4.10, gold appears enriched along quartz-Cu-Fe sulfide crystal boundaries and in veins and veinlets. These relationships suggest that grain boundaries and microfractures within

samples operated as pathways for concentrated gold movement once it had diffused from the sulfides or fluids.

There are sparse data within this study on gold in bornite due to the paucity of bornite within our sample suite, as previously noted. The available data offer conservative estimates that bornite has comparable mean Au contents (~0.1 ppm) to chalcopyrite (~0.14 ppm). This is an unexpected finding, as previous ore studies have concluded bornite contains higher structurally-bound Au contents (Arif and Baker, 2004), and is a better host for Au at high-temperatures (Fraley and Frank, 2014). However, Cook et al. (2011) showed that cool bornite was a poor host for Au. This could indicate that bornite is an excellent host for Au at high temperatures, but as it cools, Au becomes increasingly unstable within the sulfide lattice, and bornite becomes very efficient at exsolving it. This could reconcile the similarity of gold contents in bornite and chalcopyrite analyses, while still accounting for the potential of bornite to host significantly higher gold contents at elevated temperatures.

4.5.2 Trace Element Comparisons to Published Data

Analyses on polished sections of Cu-Fe sulfide mineral grains indicate that EGD skarn and porphyry samples have markedly different trace element assemblages. Average trace element concentrations for Mn, Ni, Zn, As, Mo, and Te are higher in skarn samples (for all samples and all minerals) (Table 4.11 and Appendix C), whereas porphyry samples are higher in Se, In, Sn, Sb, Au, Pb, and Bi (Table 4.13). No clear differentiation is apparent in Se, Mo, In, Sn, Sb, and Pb between deposit types. Elevated Ni contents in skarn samples derive largely from analyses within matrix chalcopyrite in TE14-01-754.3, which have Ni values one to two orders of magnitude greater than any other spots. Skarn samples were showed the greatest range of trace element concentrations, with maximum values for Mn,

Ni, As, Se, Ag, In, Sb, Te, and Pb and minimum values for Ni, Se, Mo, In, Sn, Te, and Pb. Porphyry samples appear to have a more consistent trace element suite in this study. Overall, correlations between trace element pairs are difficult to interpret because of the potential effects of micro- (or nano-) inclusion sampling, which can induce local excursions in the data and mask average matrix concentrations of bornite and chalcopyrite. To allay this issue, we have removed 12 anomalous data points. These deletions are based on the time-resolved depth profiles presented in Figure 4.2, the line-of-spots transect in Figure 4.8, or appear to be anomalously high compared to the general local signal for an analyte. Data were removed (n=12 total) for Mn (n=1), Ni (n=1), Zn (n=3), Ag (n=2), Au (n=2), Pb (n=1), and Bi (n=2).

4.5.2.1 Element Pair Relationships (Bi:Ag, Ag:In, Ni:As, Au:Ag, Au:Te, Bi:Au)

Exploration geochemistry makes use of pathfinder elements that tend to correlate with elements of economic interest (e.g., As and Au) to find valuable ore deposits. Because element pairs can vary between deposit types and locations, there is value in defining the strongest pathfinders in the EGD. We note that Bi is strongly positively correlated with Ag (r= 0.86) as also noted by Cook et al. (2011) (Figure 4.12 and Table 4.15). Bi also shows a moderate positive correlation with Au across the entire dataset (r= 0.54) (Figure 4.12). Ag and In have a moderate, inverse correlation (r= -0.58), which is expected based on preferential Ag enrichment in bornite samples, and preferential In enrichment in chalcopyrite samples (Figure 4.12; Tables 4.7 and 4.9; Figure 4.10A and B). Ni and As have an unexpectedly strong positive correlation (r= 0.63), considering their erratic and low concentrations in the dataset. As is a useful gold tracer in many deposits, (e.g., Carlin). If Ni and As are positively correlated, there could be some utility in exploring Ni anomalies for gold (Appendix C; Figure 4.12) (Cline, 2001).

For chalcopyrite samples, we find a positive correlation between Au and Ag (and Te) that has also been documented by Arif and Baker (2004), Reich et al. (2013), and Cook et al. (2011). Cook et al. (2011) suggest that sub-microscopic inclusions of Au-Ag tellurides may account for this correlation. We also found telluride grains (~10 μm) enriched in Pd (±Au) in our chalcopyrite samples (Figure 3.17). Rubin (1996) and Rubin and Kyle (1997), reported a high Pd gold phase in some EGD samples. Our samples also have Pd grains, although they appear to be Pd-(±Au) tellurides, rather than high Pd gold grains. Gibbins (2006) recorded gold mineralization in Ertsberg stockwork samples as micron to sub-micron Au- and Ag-telluride grains in biotite-anhydrite-bornite (±chalcopyrite) veinlets. These grains appear morphologically similar to the telluride blebs recorded in our samples: small and elliptical (Gibbins, 2006). Grains in Gibbins (2006) have a wider range of mineral occurrences (e.g., edge of zircon, edge of bornite, inclusion in chalcopyrite) than our telluride grains, which were found exclusively within chalcopyrite veins. Deditius et al. (2011) noted the presence of nanoparticles with a Pb-Te-Sb-Au-Ag-Bi-S geochemical signature in pyrite, which could be similar to the Pd-Te grains we see in EGD samples (Deditius, et al., 2011).

4.5.2.2 Trace Element Spatial Variation in Chalcopyrite

Elemental maps of Cu-Fe sulfides reveal geochemical variations. Ag, Bi, Pb, Sb, and Zn are enriched, and potentially zoned within a large (~3mm) chalcopyrite vein in sample GRS37-170-742.2. In Figure 4.9D, Zn zonation in chalcopyrite appears to correlate with areas bounded by fluid inclusions or bornite intergrowths. This could indicate that at high-temperatures, when bornite is the dominant Cu-Fe sulfide phase, Zn is not incorporated into the sulfides. However, as temperatures decrease and chalcopyrite becomes the dominant phase, Zn becomes more soluble within the sulfides and is

incorporated within the chalcopyrite. Because skarn mineralization is generally thought to occur at lower temperatures than porphyry mineralization, this theory is supported by the higher Zn contents in our skarn sulfides. Zn data indicate two potential sphalerite inclusions (10200 ppm and 62900 ppm). Zn is also consistently higher in skarn samples (mean= 712.74 ppm; range:1.54 - 3900 ppm) rather than porphyry samples (mean= 135.14 ppm; range:1.31-1,620 ppm), which corresponds well with Zn-rich fluid inclusions in the skarn system (Ledvina, 2017). Ag and Bi are positively correlated in our data. The evidence of similar spatial variation between Bi and Ag within the chalcopyrite supports this.

Table 4.1 STDGL3#36 Certified Composition

Element	Composition (ppm)	Precision 1σ, %	Accuracy 1σ, %	Element	Composition (ppm)	Precision 1σ, %	Accuracy 1σ, %	Element	Composition (ppm)	Precision 1σ, %	Accuracy 1σ, %
Na	53342	0.7	<1.0	**Co**	74	1.3	<1.2	**Sr**	28	2.0	<3.1
Mg	59	2.8	<0.9	**Ni**	247	1.6	<0.6	**Zr**	43	2.1	<0.8
Al	118	1.7	<1.5	**Cu**	367	2.1	<0.8	**Mo**	167	1.8	<2.9
S	12148	2.0	<2.0	**Zn**	5795	1.0	<2.0	**Ag**	99	2.7	<0.5
Ti	255	3.3	<1.7	**Ge**	172	1.5	<3.0	**Cd**	517	2.0	<2.1
Mn	214	1.1	<1.0	**As**	349	1.4	<3.8	**In**	101	1.3	<4.0
Fe	17380	1.5	<1.0	**Se**	3297	3.7	<4.0	**Sn**	150	1.4	<0.4

Element	Composition (ppm)	Precision 1σ, %	Accuracy 1σ, %	Element	Composition (ppm)	Precision 1σ, %	Accuracy 1σ, %
Sb	91	1.5	<4.4	**Pt**	14.8	3.7	<5.0
Te	1236	2.1	<0.5	**Au**	18.1	4.1	<5.0
Gd	80	2.3	<3.3	**Tl**	158	2.2	<3.0
Hf	36	2.4	<2.4	**Pb**	59	1.6	<2.3
Ta	16.2	2.2	<1.3	**Bi**	18.8	1.8	<1.9
W	78	1.7	<3.0	**Th**	13.7	2.0	<1.7
Re	15.2	2.5	<4.2	**U**	13.8	1.9	<0.9

From L. Danyushevsky and I. Belousov, CODES, University of Tasmania, Jan. 2017; based on Danyushevsky (2011).

Table 4.2 Counts for Monitored Isotopes in Standard During Instrument Tune

Spot Analyses			2D Maps		
m/z	**Mean (counts)**	**RSD%**	**m/z**	**Mean (counts)**	**RSD%**
7	4396.6	3.01	**7**	2537.3	4.04
43	9582.4	2.56	**43**	5133.5	3.88
89	6197.0	3.05	**89**	3058.1	4.18
141	9537.3	2.30	**141**	5220.1	3.59
232	5137.7	2.85	**232**	2716.8	4.75
248/232	0.430%	19.97	**248/232**	0.366%	27.95
238/232	120.281%	3.22	**238/232**	115.646%	5.92

Table 4.3 GeoREM Preferred Values and Average Analyte Recoveries for Secondary Reference Materials

A	Mn (ppm)	Ni (ppm)	Cu (ppm)	Zn (ppm)	As (ppm)	Se (ppm)	Mo (ppm)	Ag (ppm)	In (ppm)	Sn (ppm)	Sb (ppm)	W (ppm)	Au (ppm)	Pb (ppm)	Bi (ppm)
GSC-1G	176	21	16	12.7	3.2	0.2	4.6	4.1	4.5	5.3	5.3	4.5	6	14	3.4
GSD-1G	220	58	42	54	27	2	39	23	38	29	43	43	4	50	35
GSE-1G	590	440	380	460	260	20	390	200	370	280	450	430	7	378	320

B	Mn	Ni	Cu	Zn	As	Se	Mo	Ag	In	Sn	Sb	W	Au	Pb	Bi
GSC-1G	1.05	1.04	0.95	0.95	1.61	-4.97	0.95	1.05	0.99	1.02	1.01	0.95	0.87	0.97	1.13
GSD-1G	1.00	1.07	1.06	1.21	1.36	2.48	1.00	1.09	1.06	1.45	1.08	0.94	1.04	0.98	1.03
GSE-1G	0.98	1.03	1.03	1.20	1.34	1.89	0.98	1.12	1.06	1.46	1.02	0.92	1.02	0.98	1.08
GSE-1G (Maps)	1.00	1.00	1.06	–	1.36	4.32	0.94	1.03	1.03	1.38	0.98	–	0.79	0.96	1.08

(a) GeoREM preferred values; (b) average analyte recoveries during spot and 2D map analyses (Max Planck Institute).

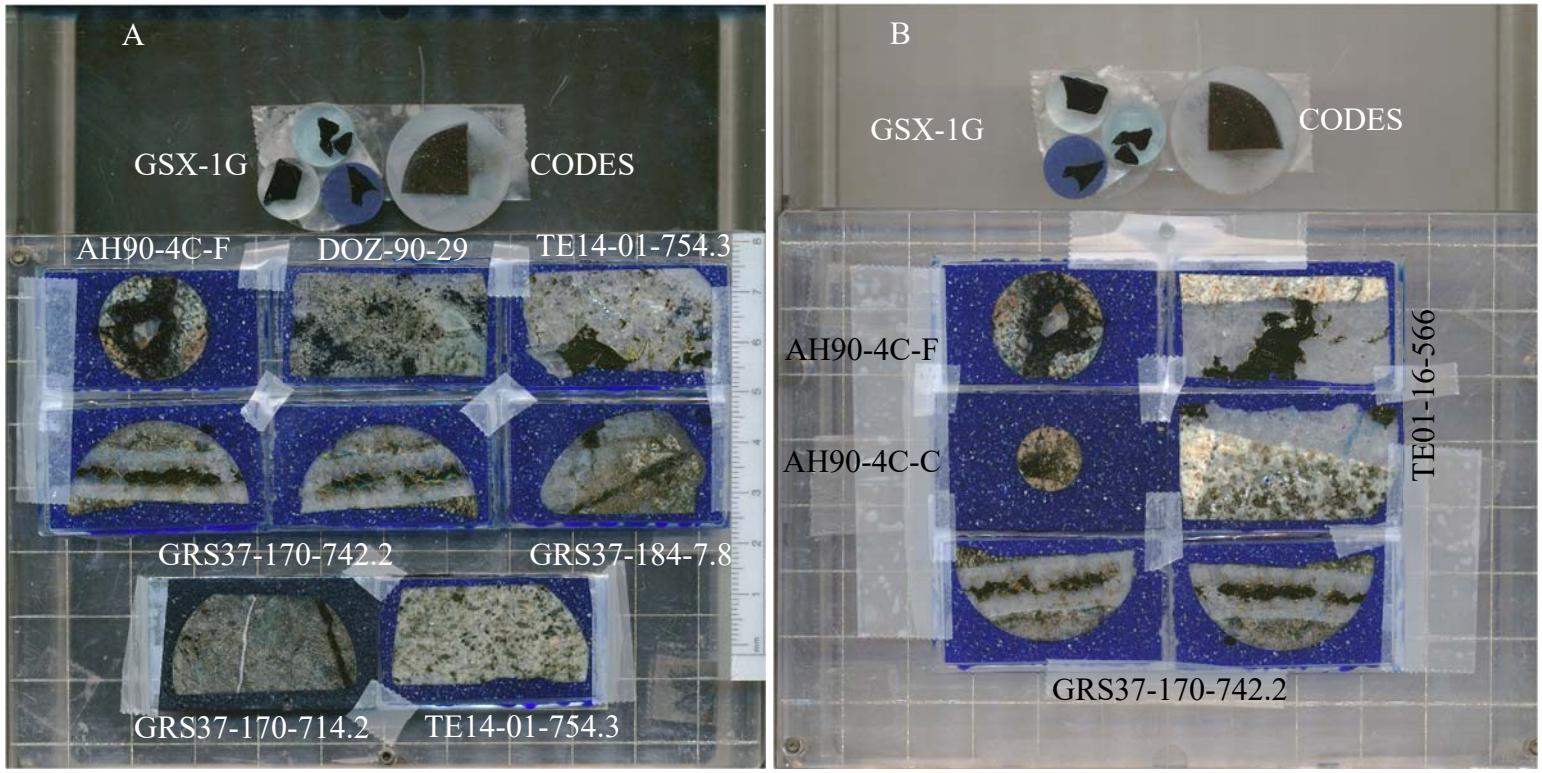

Figure 4.1 LA-ICP-MS Sample Drawer with Polished Sections and Standards

Sample sections for analytical days in (a) April 2017 and (b) May/June 2017. “GSX” standards from light to dark blue are GSC, GSD, and GSE.

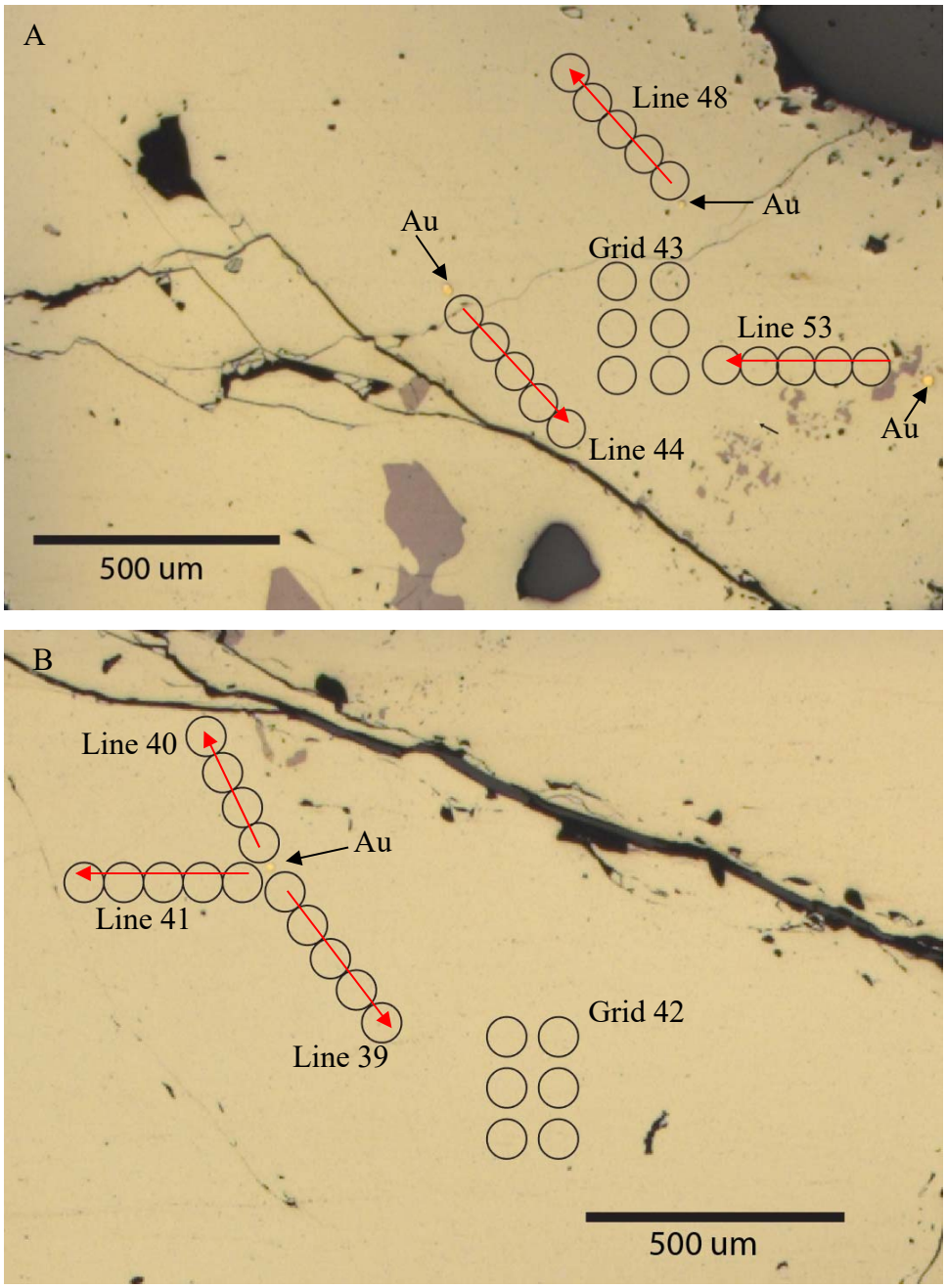

Figure 4.2 Spots Near Gold in Chalcopyrite in GRS37-170-742.2

Reflected light micrograph of (a) three gold grains near bornite intergrowth; (b) single gold grain near fracture. Spot diameters are 65 µm; red arrows indicate analysis direction.

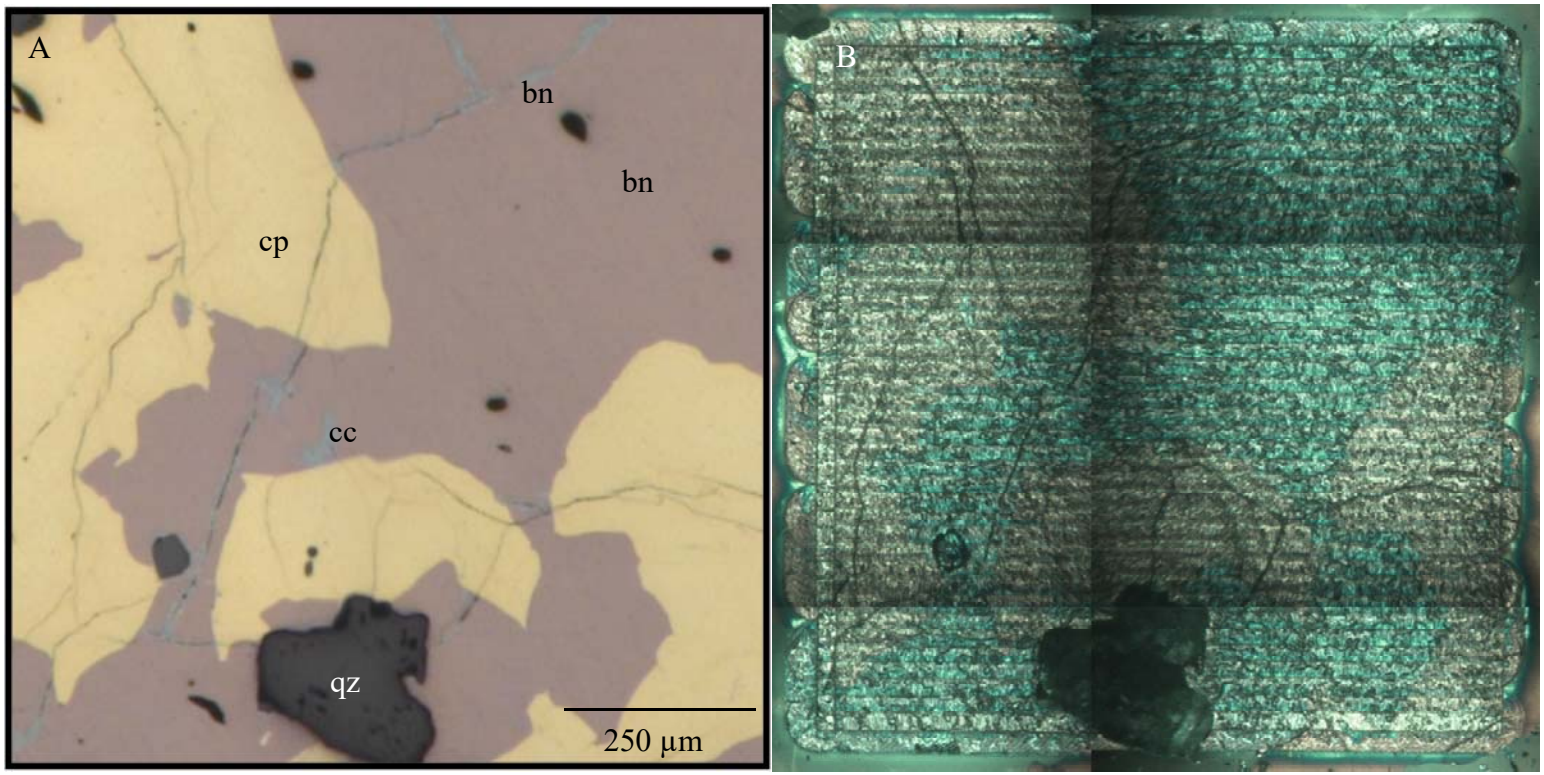
A
bn
bn
cp
cc
qz
250 µm
B

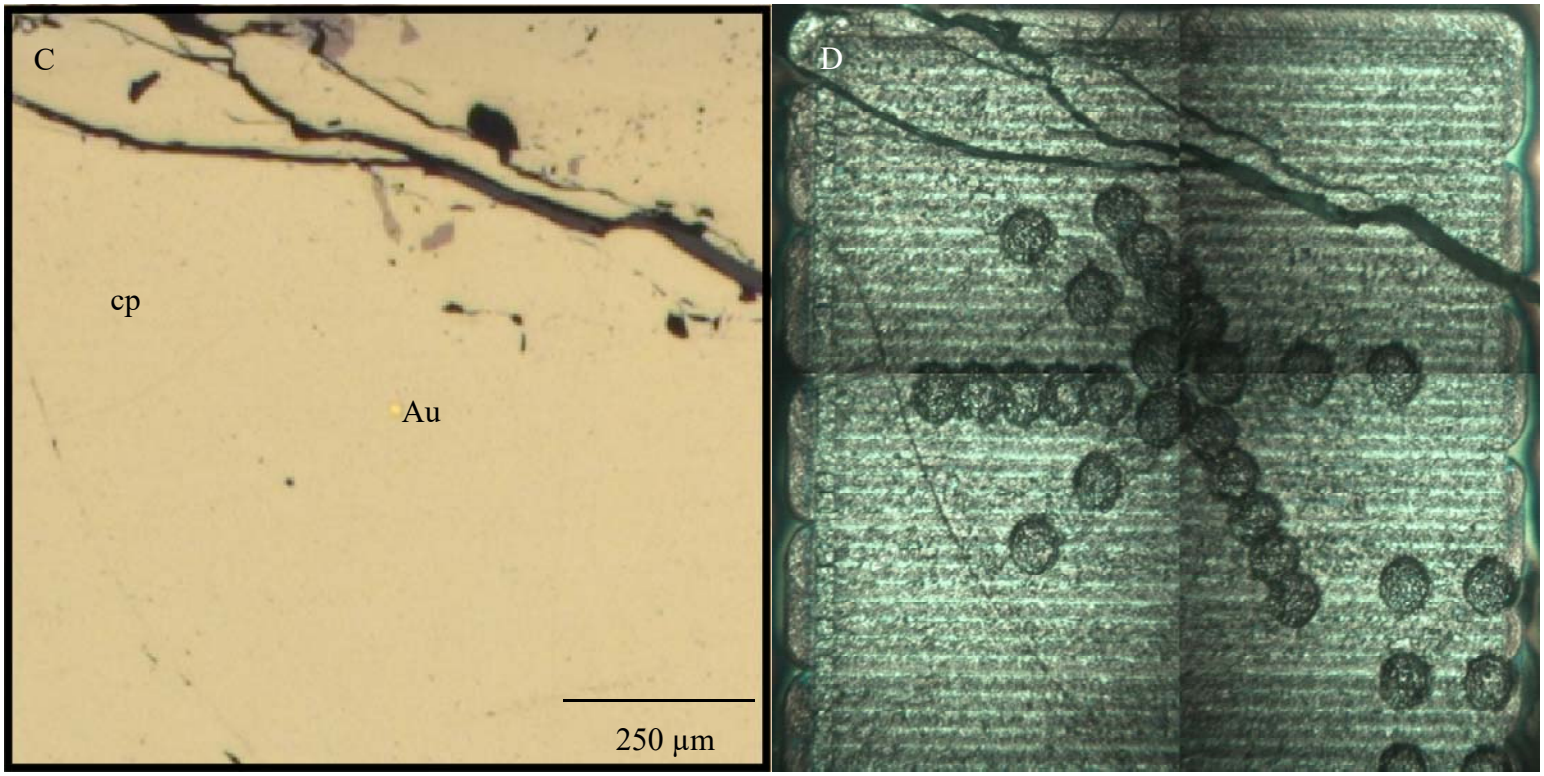
C
cp
Au
250 µm
D

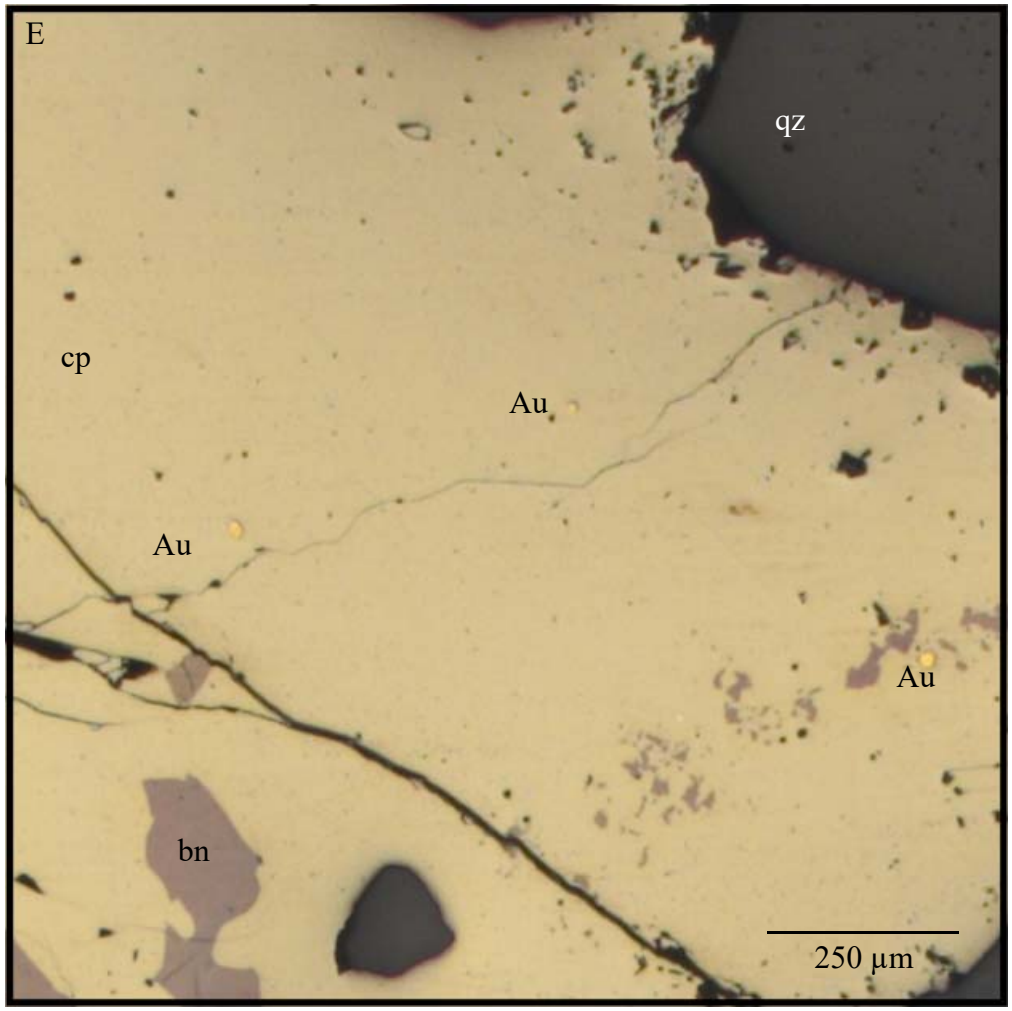
E
qz
cp
Au
Au
Au
bn
250 µm

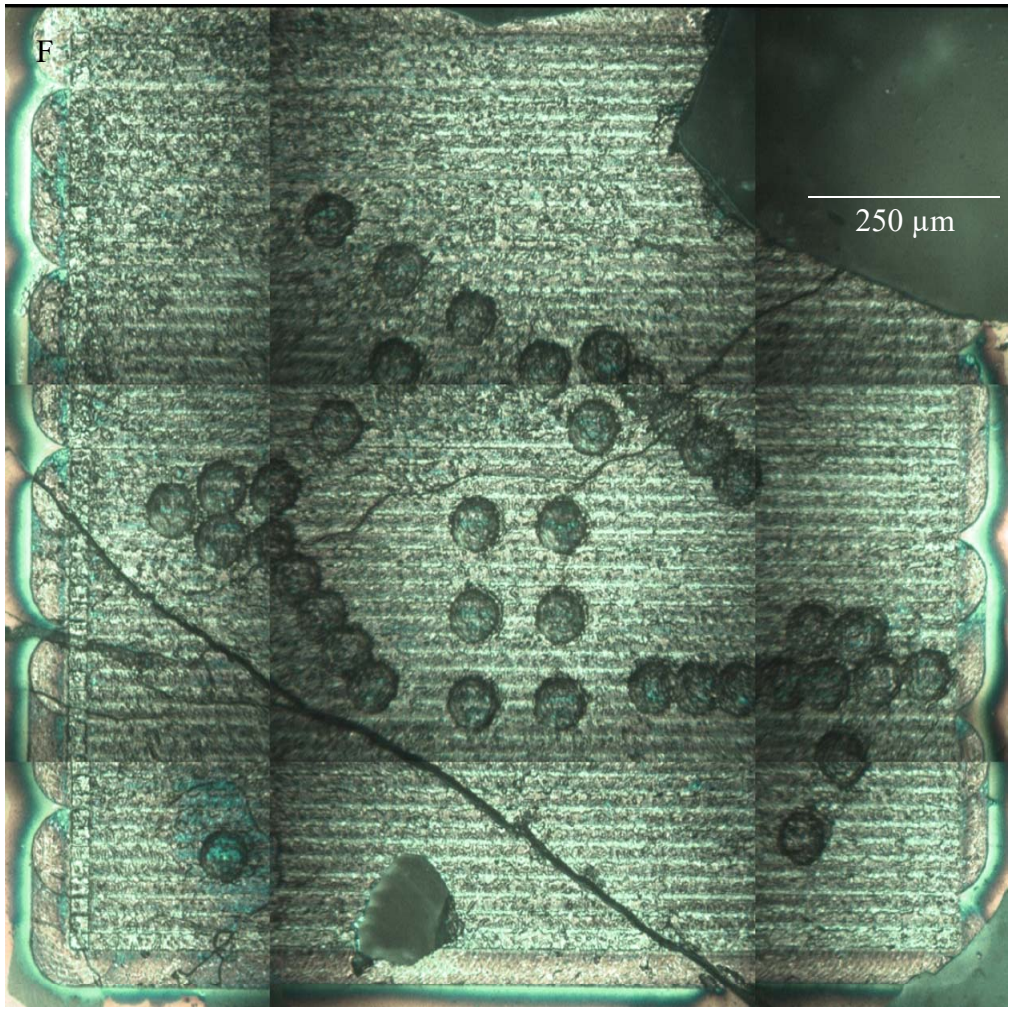

Figure 4.3 2D Map Areas

All 2D maps completed using adjacent scan lines, run in the same direction, with no offset between the 25 x 25 μm "square" aperture. Composite figures represent areas targeted for 2D elemental maps pre- and post-ablation. Elemental maps of these areas were used to assess spatial variation of trace elements. (a) AH90-4C-F map area of chalcopyrite and bornite intergrowth (1 x 1 mm). (b) post-ablation area. (c) GRS37-170-742.2 map area of single gold grain and fracture in chalcopyrite (1 x 1 mm). (d) post-ablation area. (e) GRS37-170-742.2 map area of three gold grains, fracture, and bornite in chalcopyrite and quartz (1.3 x 1.3 mm). (f) post-ablation area.

A

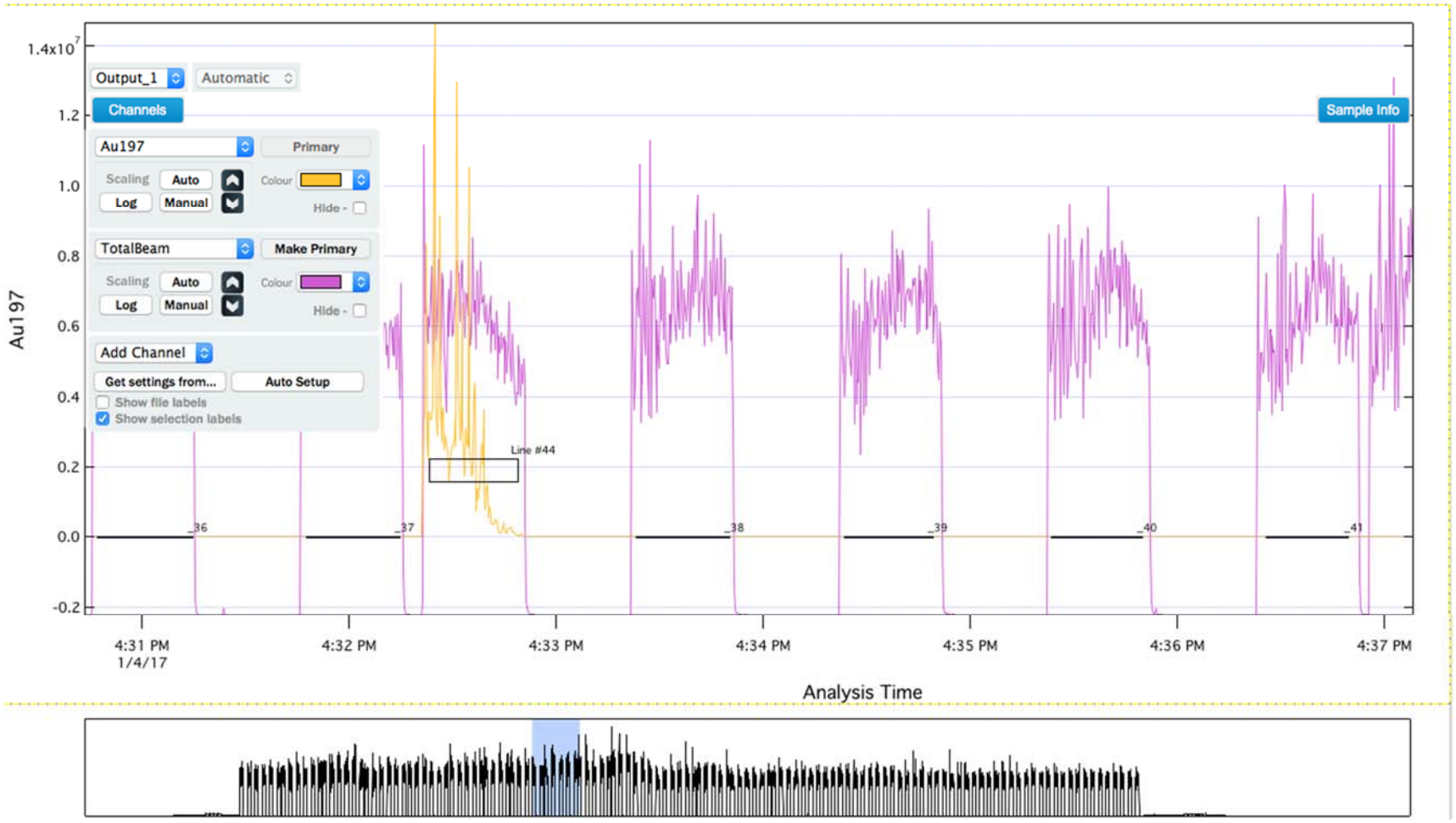
1.4x10^7
1.2
1.0
0.8
0.6
0.4
0.2
0.0
-0.2
Au197
Output_1
Automatic
Channels
Au197
Primary
Scaling
Auto
Log
Manual
Colour
Hide
TotalBeam
Make Primary
Add Channel
Get settings from...
Auto Setup
Show file labels
Show selection labels
Sample Info
Line #44
_36
_37
_38
_39
_40
_41
4:31 PM
1/4/17
4:32 PM
4:33 PM
4:34 PM
4:35 PM
4:36 PM
4:37 PM
Analysis Time

B

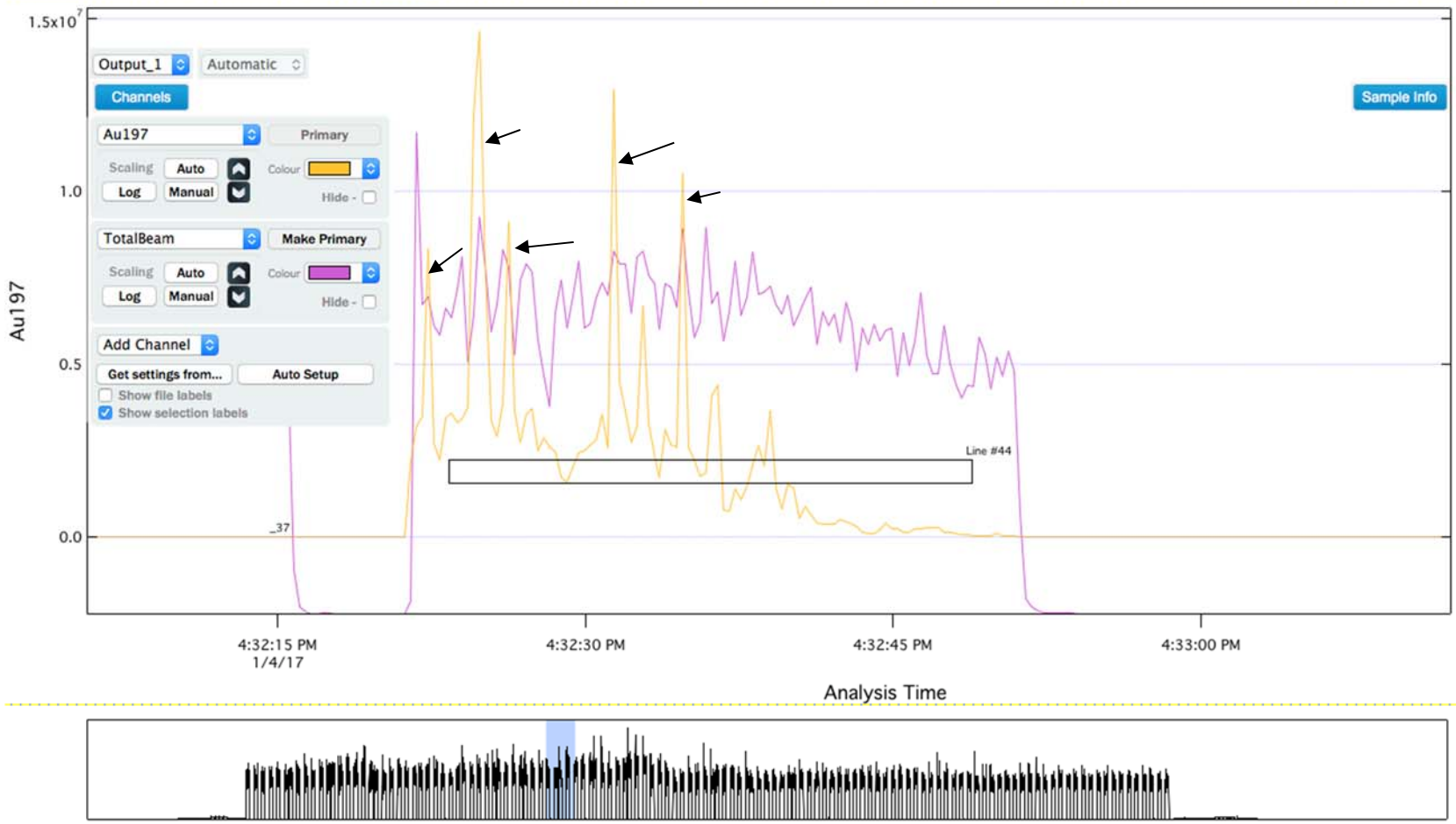
1.5x10^7
Output_1
Automatic
Channels
Sample Info
Au197
Primary
Scaling
Auto
Log
Manual
Colour
Hide -
TotalBeam
Make Primary
Add Channel
Get settings from...
Auto Setup
Show file labels
Show selection labels
Au197
1.0
0.5
0.0
Line #44
_37
4:32:15 PM
1/4/17
4:32:30 PM
4:32:45 PM
4:33:00 PM
Analysis Time

C

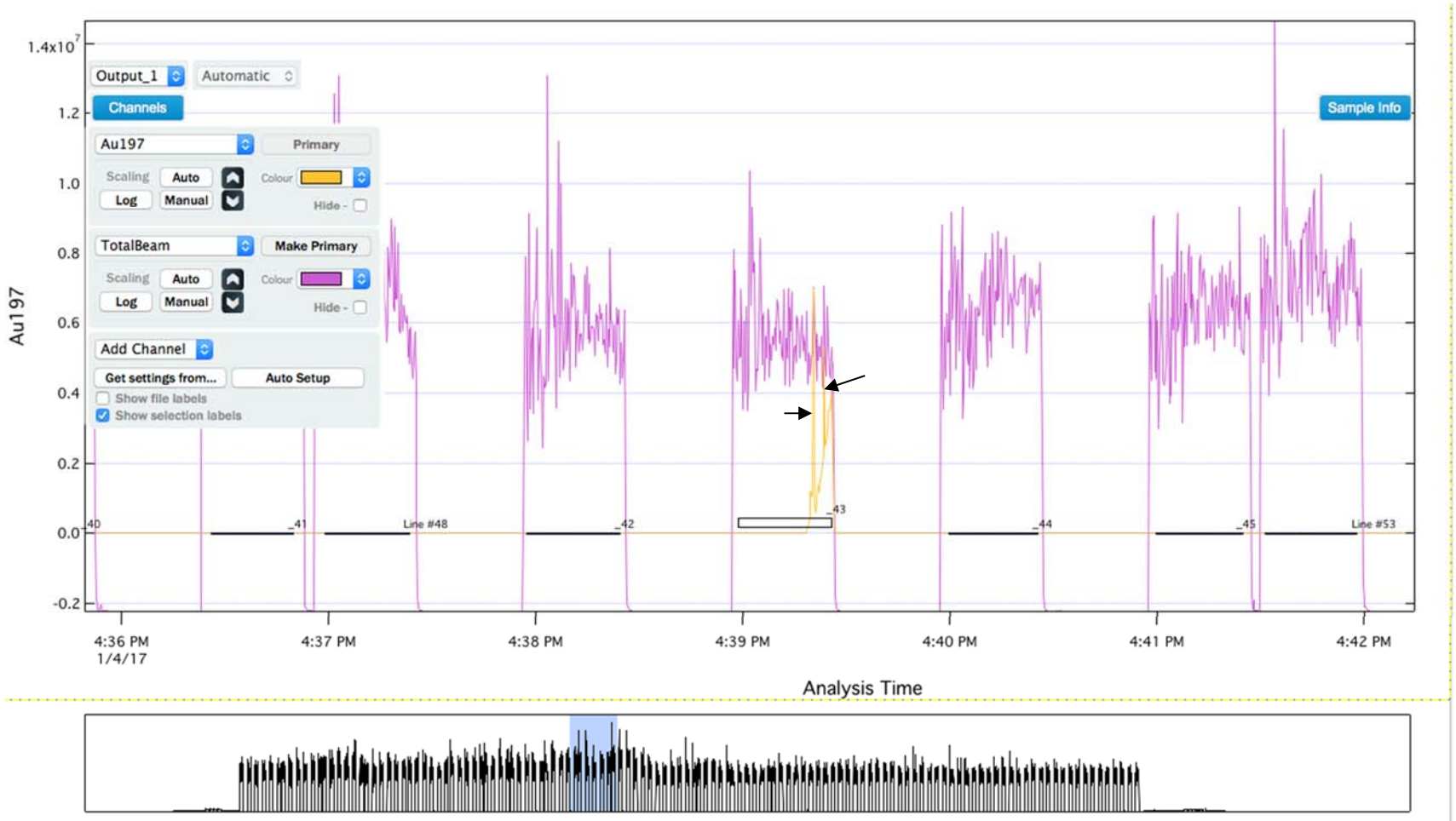
1.4x10^7
1.2
1.0
0.8
0.6
0.4
0.2
0.0
-0.2
Au197
Output_1
Automatic
Channels
Sample Info
Au197
Primary
Scaling
Auto
Log
Manual
Colour
Hide
TotalBeam
Make Primary
Add Channel
Get settings from...
Auto Setup
Show file labels
Show selection labels
_40
_41
Line #48
_42
_43
_44
_45
Line #53
4:36 PM
1/4/17
4:37 PM
4:38 PM
4:39 PM
4:40 PM
4:41 PM
4:42 PM
Analysis Time

D

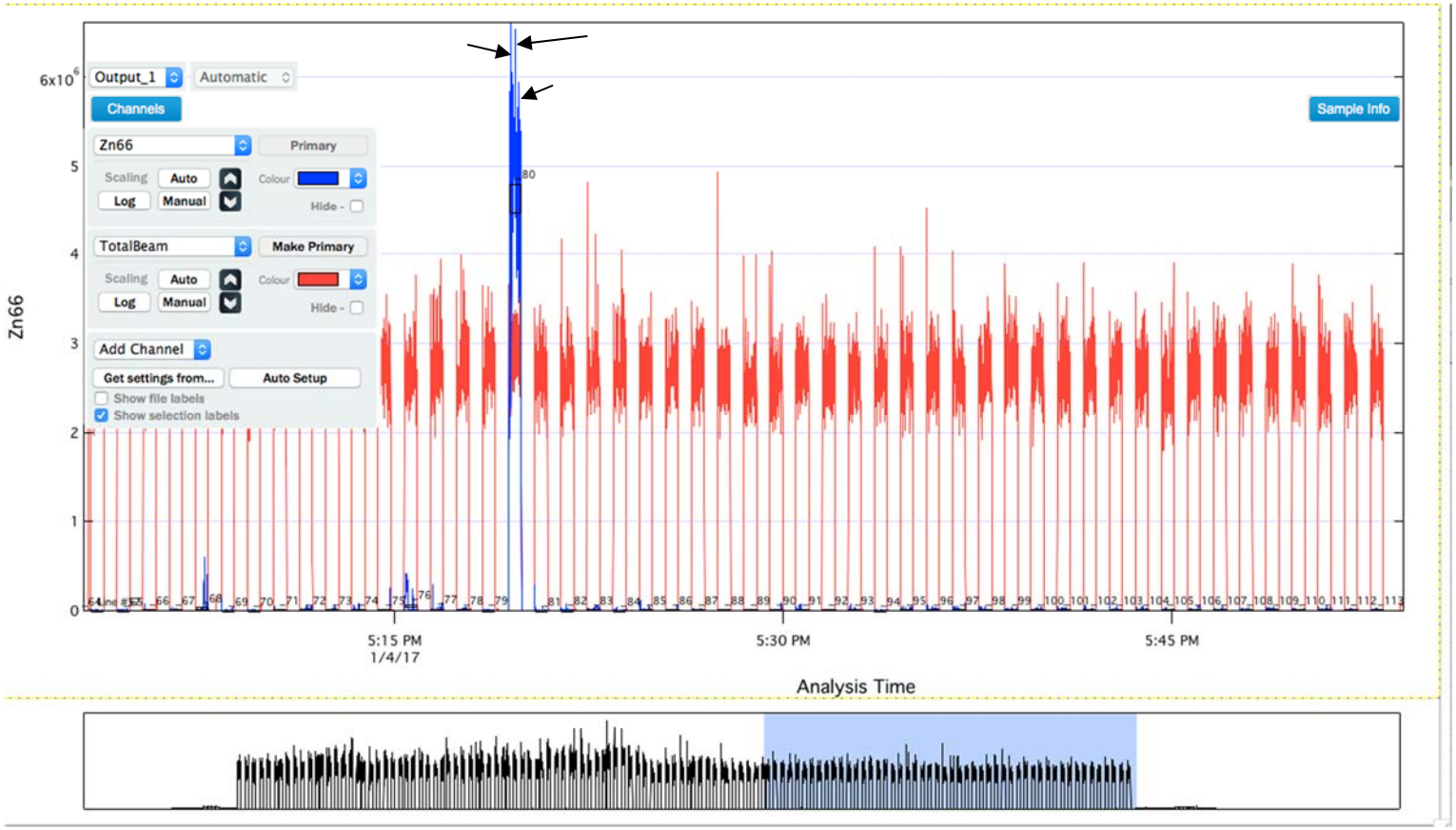

Figure 4.4 Time-Resolved Depth Profiles for LA-ICP-MS Spot Analyses

Time-resolved LA-ICP-MS depth profiles of (a, b, c) Au (gold) vs. Total Beam (pink), and (d) Zn (blue) vs. Total beam (red) for porphyry chalcopyrite sample GRS37-170-742.2. Black arrows point to peaks within depth-profiles. (a, b) Line 44, spot 1 (3770 ppm Au). (b) Line 48, spot 3 (650 ppm Au). (d) Line(-of-spots) 57, spot 17 across (62,900 ppm Zn).

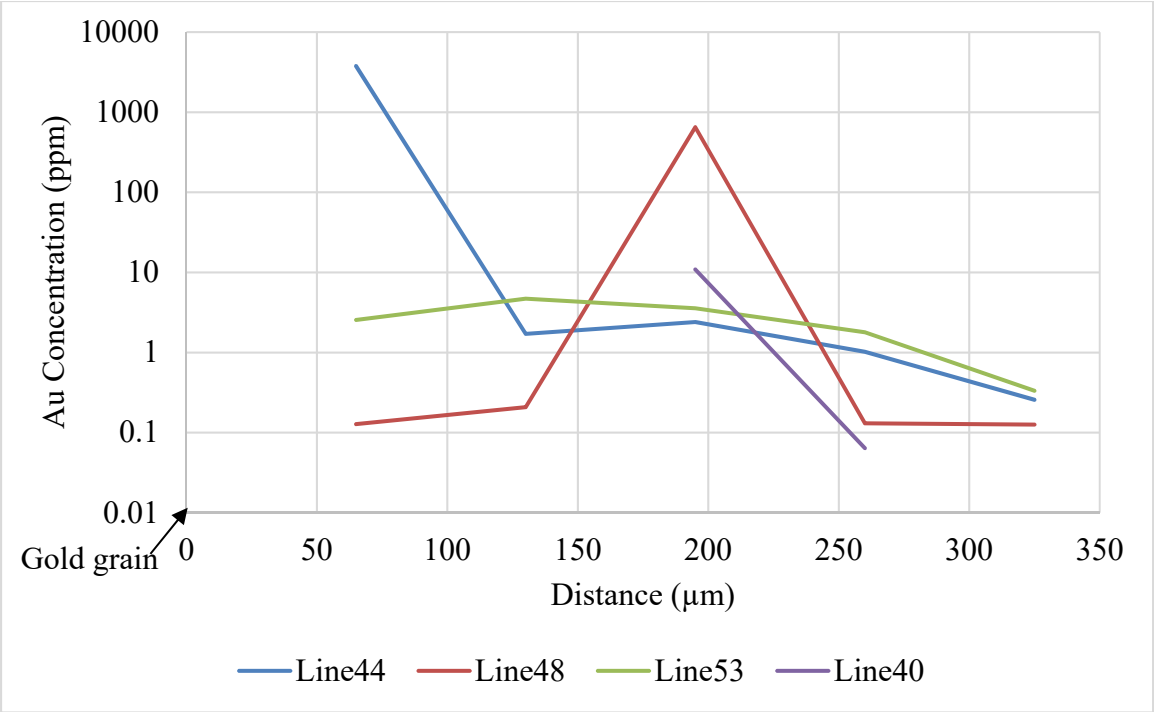

Figure 4.5 Spot Transects Proximal to Gold Grains in GRS37-170-742.2A-2

Distance is plotted based on spot size (65µm); the first data point is plotted according to the end of the first spot, or 65 µm. The peak in Line 48 could represent ablation of a small gold inclusion. Line 40 only recorded two measurements above the minimum detection limit for Au.

Table 4.4 Composite Gold Concentrations in Porphyry and Skarn Samples

Sample	Mean (ppm)	Max (ppm)	Min (ppm)	Std. Dev. (ppm)	Mean (LOD)
AH90-4C-F	0.188	0.600	0.022	0.232	0.024
AH90-4C-C	1.371	8.800	0.018	3.278	0.015
GRS37-170-714.2	0.229	0.480	0.050	0.198	0.033
GRS37-184-7.8 (cp)	0.230	1.500	0.030	0.350	0.010
GRS37-184-7.8 (bn)	42.30	–	–	–	0.02
GRS37-170-742.2A-2	117.367	3770.000	0.021	617.583	0.133
GRS37-170-742.2A-2*	1.110	10.900	0.021	2.031	0.136
GRS37-170-742.2A-3	0.159	0.540	0.024	0.119	0.016
DOZ-90-29	0.061	0.090	0.031	0.042	0.030
TE01-16-566C	0.270	0.760	0.028	0.218	0.015
TE01-16-566A	0.202	0.349	0.062	0.078	0.014
TE14-01-754.3	0.491	1.430	0.058	0.503	0.034

[1]GRS37-170-742.2A-2* statistics after removal of two spots thought to contain gold inclusions (n=2).

[2]GRS37-170-742.2A-2 and A-3 are different polished sections from the same core sample.

[3]TE16-566A and C are different polished sections from the same core sample.

[4]GRS37-184-7.8 includes 1 spot analysis of Au in bornite, which has been included separately as it was markedly higher than measurements in chalcopyrite. Au measurements in chalcopyrite are included in their own row.

Skarn samples are shown in blue.

LOD = limit of detection; mean LOD is the average detection limit across all gold measurements.

Table 4.5 Gold Concentrations in Cu-Fe Sulfide Phases for Porphyry and Skarn Samples.

Sample & Deposit	Phase	Association	Au (ppm)	Au (2σ std error)	Au (LOD)
AH90-4C-F porphyry	bn	vein	0.062	0.028	0.025
	bn	matrix	0.330	0.340	0.015
	cp	vein	0.083	0.040	0.008
	cp	vein	0.032	0.013	0.009
	cp	vein	0.022	0.011	0.010
	cp	vein	0.600	0.110	0.007
AH90-4C-C porphyry	cp	vein	0.060	0.019	0.017
	cp	vein	0.018	0.011	0.010
	cp	vein	0.063	0.023	0.015
	cp	vein	0.128	0.030	0.014
	bn	vein	8.800	4.100	0.018
	bn	vein	0.312	0.042	0.015
	bn	vein	0.215	0.045	0.010
GRS37-170-714.2 porphyry	cp	vein	0.083	0.035	0.024
	cp	vein	0.057	0.029	0.044
	cp	vein	0.480	0.120	0.033
	cp	vein	0.196	0.059	0.053
	cp	matrix	0.062	0.034	0.023
	cp	vein	0.050	0.027	0.033
	cp	vein	0.442	0.095	0.037
	cp	vein	0.460	0.110	–
GRS37-184-7.8A-B porphyry	cp	vein	0.050	0.030	0.036
	cp	vein	0.249	0.066	0.035
	cp	vein	0.420	0.130	0.032
	cp	vein	0.101	0.040	0.022
	cp	vein	0.067	0.035	0.030
	cp	vein	0.169	0.061	0.024
	cp	vein	0.140	0.048	0.040
	cp	vein	1.500	0.550	0.026
	cp	vein	0.067	0.035	0.044
	bn	matrix	42.300	4.100	0.019
	cp	vein	0.157	0.071	0.052
	cp	vein	0.056	0.032	0.033
	cp	vein	0.112	0.057	0.039
	cp	vein	0.250	0.077	0.032
	cp	vein	0.232	0.076	0.035
GRS37-170-742.2A-2 porphyry	cp	vein	0.236	0.092	0.051
	cp	vein	0.096	0.058	0.034
	bn	matrix	2.540	0.300	0.020
	cp	vein	0.530	0.130	0.043
	cp	vein	0.272	0.079	0.043
	cp	vein	0.350	0.100	0.038
	cp	vein	0.410	0.170	0.083
	cp	vein	0.360	0.110	7.300
	cp	vein	0.400	0.100	0.041
	cp	vein	0.320	0.120	0.052
	cp	vein	0.078	0.037	0.023
	cp	vein	0.047	0.034	0.023
	cp	vein	*0.431*	0.065	0.019
	cp	vein	*0.077*	0.030	0.020

Table 4.5 (continued)

	cp	vein	*0.333*	0.068	0.010
	cp	vein	*0.380*	0.093	0.010
	cp	vein	*0.074*	0.026	0.010
	cp	vein	*0.021*	0.013	0.010
	cp	vein	*0.380*	0.100	–
	cp	vein	*0.049*	0.038	0.013
	cp	vein	*2.690*	0.880	0.017
	cp	vein	*10.900*	5.100	–
	cp	vein	*0.064*	0.067	0.010
	cp	vein	*3770.000*	700.000	0.028
	cp	vein	*1.710*	0.600	0.026
	cp	vein	*2.400*	0.630	0.010
	cp	vein	*1.020*	0.310	0.014
	cp	vein	*0.257*	0.086	0.019
	cp	vein	*0.128*	0.066	0.013
	cp	vein	*0.208*	0.082	0.015
	cp	vein	*650.000*	320.000	0.017
GRS37-170-742.2A-2 porphyry	cp	vein	*0.131*	0.065	0.019
	cp	vein	*0.126*	0.059	0.019
	cp	vein	*2.550*	0.460	–
	cp	vein	*4.700*	0.720	–
	cp	vein	*3.570*	0.510	0.016
	cp	vein	*1.790*	0.900	–
	cp	vein	0.333	0.096	0.010
GRS37-170-742.2A-3 porphyry	cp	vein	0.026	0.015	0.021
	cp	vein	0.053	0.021	0.018
	cp	vein	0.024	0.015	0.013
	cp	vein	0.036	0.018	0.020
	cp	vein	0.034	0.017	0.018
	cp	vein	0.028	0.016	0.021
	cp	vein	0.036	0.017	0.014
	cp	vein	0.330	0.110	0.011
	cp	vein	0.027	0.016	0.024
	cp	vein	0.047	0.021	0.021
	cp	vein	0.194	0.050	–
	cp	vein	0.219	0.049	0.012
	cp	vein	0.141	0.046	–
	cp	vein	0.235	0.099	0.022
	cp	vein	0.540	0.140	0.012
	cp	vein	0.245	0.063	0.016
	cp	vein	0.188	0.048	0.012
	cp	vein	0.296	0.074	0.013
	cp	vein	0.131	0.039	0.022
	cp	vein	0.031	0.025	0.012
	cp	vein	0.067	0.035	0.016
	cp	vein	0.299	0.072	0.017
	cp	vein	0.336	0.071	0.016
	cp	vein	0.257	0.059	0.016
	cp	vein	0.192	0.088	0.011
	cp	vein	0.104	0.056	0.011
	cp	vein	0.234	0.058	0.011
	cp	vein	0.212	0.054	0.026
	cp	vein	0.149	0.042	0.015

Table 4.5 (continued)

	cp	vein	0.049	0.022	0.011
	cp	vein	0.180	0.049	0.017
	cp	vein	0.140	0.046	0.011
	cp	vein	0.191	0.049	0.011
	cp	vein	0.283	0.084	0.011
	cp	vein	0.132	0.043	0.027
	cp	vein	0.049	0.024	0.026
DOZ-90-29 skarn	bn	vein	0.031	0.021	0.026
	bn	vein	0.090	0.037	0.035
TE01-16-566C skarn	cp	vein	0.067	0.023	0.017
	cp	vein	0.028	0.016	0.007
	cp	vein	0.760	0.370	0.014
	cp	vein	0.367	0.061	–
	cp	vein	0.213	0.042	0.028
	cp	vein	0.183	0.038	–
	cp	vein	0.421	0.073	–
	cp	vein	0.341	0.057	0.018
	cp	vein	0.254	0.048	0.015
	cp	vein	0.069	0.022	0.010
TE01-16-566A skarn	cp	vein	0.132	0.039	0.008
	cp	vein	0.062	0.021	0.012
	cp	vein	0.197	0.034	0.017
	cp	vein	0.189	0.043	0.013
	cp	vein	0.257	0.045	0.019
	cp	vein	0.349	0.054	0.019
	cp	vein	0.256	0.047	0.010
	cp	vein	0.226	0.043	0.010
	cp	vein	0.185	0.040	0.015
	cp	vein	0.162	0.036	–
TE14-01-754.3 skarn	cp	vein	0.124	0.067	0.054
	cp	matrix	0.530	0.150	0.050
	cp	matrix	0.252	0.034	0.012
	cp	matrix	0.058	0.033	0.038
	cp	matrix	0.549	0.086	0.013
	cp	matrix	1.430	0.270	0.030

*Italicized values are from lines of spots and grids of spots proximal to gold grains.

Table 4.6 Elemental Concentrations in Bornite Samples

Sample	Mn (ppm)	Ni (ppm)	Zn (ppm)	As (ppm)	Se (ppm)	Ag (ppm)	In (ppm)	Sn (ppm)	Sb (ppm)	Te (ppm)	Au (ppm)	Pb (ppm)	Bi (ppm)	
AH90-4C-F (19)	0.10	0.05	49.26	0.17	367.37	247.58	0.88	6.18	0.15	19.17	0.02	52.76	428.00	**Mean**
	0.54	0.30	111.00	0.81	618.00	283.00	1.34	7.88	0.37	20.90	0.33	176.50	476.00	**Max**
	<mdl	<mdl	1.31	<mdl	319.00	225.60	0.12	<mdl	<mdl	16.10	<mdl	14.90	364.00	**Min**
AH90-4C-C (3)	0.43	0.26	101.13	0.58	443.00	451.67	0.60	9.27	0.07	48.57	3.11	107.33	392.87	**Mean**
	0.48	0.40	136.00	0.72	452.00	<mdl	0.65	10.23	0.10	53.40	8.80	194.00	398.00	**Max**
	0.39	0.18	74.80	0.50	432.00	<mdl	0.50	8.41	<mdl	41.50	0.22	63.30	389.50	**Min**
	–	–	–	–	–	–	–	–	–	–	0.26	–	–	**No Incl.**
DOZ-90-29 (18) (skarn)	0.15	0.66	26.25	0.54	499.83	150.06	0.25	1.70	0.09	129.12	0.01	781.61	121.87	**Mean**
	2.39	2.37	276.00	1.26	740.00	600.00	0.42	2.46	0.19	366.00	0.09	2250.00	131.40	**Max**
	<mdl	<mdl	1.54	<mdl	399.00	51.30	0.18	0.66	<mdl	54.20	<mdl	47.90	112.20	**Min**
	–	–	10.92	–	–	116.72	–	–	–	–	–	299.38	–	**No Incl.**
GRS37-170-742.2A-2 (1)	<mdl	0.39	19.70	0.59	557.00	425.00	0.05	15.90	0.05	109.00	42.30	4.17	1464.00	
GRS37-184-7.8 (1)	<mdl	0.24	151.00	0.70	711.00	311.00	0.08	79.00	0.54	154.30	2.54	102.30	1246.00	

*Number in brackets = number of spot analyses. Skarn samples are shown in blue.

Table 4.7 Correlation Matrix for Elements in Bornite Samples

bn	*Mn (ppm)*	*Ni (ppm)*	*Zn (ppm)*	*As (ppm)*	*Se (ppm)*	*Mo (ppm)*	*Ag (ppm)*	*In (ppm)*	*Sn (ppm)*	*Sb (ppm)*	*Te (ppm)*	*Au (ppm)*	*Pb (ppm)*	*Bi (ppm)*
Mn (ppm)	1.00													
Ni (ppm)	0.17	1.00												
Zn (ppm)	-0.10	-0.34	1.00											
As (ppm)	-0.03	0.01	-0.15	1.00										
Se (ppm)	-0.03	0.18	-0.06	0.52	1.00									
Mo (ppm)	0.11	-0.14	-0.16	0.07	-0.07	1.00								
Ag (ppm)	0.12	-0.43	0.55	-0.11	-0.25	0.10	1.00							
In (ppm)	-0.12	-0.47	0.61	-0.51	-0.47	0.06	0.43	1.00						
Sn (ppm)	-0.06	-0.14	0.50	0.05	0.28	-0.01	0.37	0.20	1.00					
Sb (ppm)	-0.07	-0.10	0.55	-0.33	0.02	-0.17	0.11	0.58	0.66	1.00				
Te (ppm)	0.02	0.80	-0.32	0.39	0.55	-0.16	-0.50	-0.61	0.04	-0.07	1.00			
Au (ppm)	-0.03	0.00	0.03	0.11	0.18	-0.04	0.40	-0.09	0.18	-0.11	0.07	1.00		
Pb (ppm)	0.19	0.35	-0.39	0.07	0.36	-0.11	-0.51	-0.47	-0.21	-0.14	0.41	-0.12	1.00	
Bi (ppm)	-0.09	-0.31	0.44	-0.11	0.01	0.05	0.67	0.38	0.71	0.42	-0.26	0.67	-0.45	1.00

(Ni vs. Te n=23; Zn vs. Ag n=42; Zn vs. In n=42; Zn vs. Sn n=41; Zn vs. Sb n=35; As vs. Se n=21; As vs. In n=21; Se vs. Te n=42; Ag vs. Te n=42; Ag vs. Pb n=42; Ag vs. Bi n=42; In vs. Sb n=35; In vs. Te n=42; Sn vs. Sb n=35; Sn vs. Bi n=41; Au vs. Bi n=10)

Table 4.8 Elemental Concentrations in Chalcopyrite Samples

Sample	Mn (ppm)	Ni (ppm)	Zn (ppm)	As (ppm)	Se (ppm)	Mo (ppm)	Ag (ppm)	In (ppm)	Sn (ppm)	Sb (ppm)	Te (ppm)	Au (ppm)	Pb (ppm)	Bi (ppm)	
AH90-4C-F (17)	0.44	0.19	220.20	0.26	344.71	0.01	6.17	4.45	12.48	0.06	4.19	0.05	8.38	1.89	**Mean**
	1.44	0.46	506.00	1.12	451.00	0.11	70.80	4.97	16.12	0.19	7.60	0.60	46.50	24.90	**Max**
	<mdl	<mdl	25.10	<mdl	205.00	<mdl	0.63	3.76	6.00	<mdl	<mdl	<mdl	<mdl	<mdl	**Min**
AH90-4C-C (6)	1.09	0.02	363.50	0.84	406.83	<mdl	6.57	4.42	15.37	<mdl	4.34	0.04	18.26	0.12	**Mean**
	1.99	0.10	520.00	0.90	508.00	<mdl	17.40	4.59	16.29	<mdl	6.50	0.13	47.10	0.21	**Max**
	0.32	<mdl	136.00	0.71	234.00	<mdl	3.79	4.20	13.91	<mdl	2.91	<mdl	0.27	0.04	**Min**
GRS37-184-7.8 (19)	2.39	0.18	668.68	0.82	254.63	0.01	1.36	6.00	36.73	0.13	10.43	0.19	354.24	1.33	**Mean**
	<mdl	0.57	10700.00	1.43	378.00	0.10	3.57	7.01	43.10	0.27	42.00	1.50	925.00	2.86	**Max**
	<mdl	<mdl	14.80	<mdl	210.00	<mdl	0.14	5.45	31.10	<mdl	<mdl	<mdl	1.34	0.17	**Min**
	–	0.12	105.52	–	–	–	–	–	–	–	–	–	–	–	**No Incl.**
GRS37-170-714.2 (18)	0.60	0.13	127.57	0.60	315.78	0.14	4.88	3.27	15.54	0.21	8.80	0.10	226.62	0.09	**Mean**
	1.42	0.46	460.00	1.15	394.00	2.30	8.72	3.46	20.31	0.54	24.20	0.48	709.00	0.56	**Max**
	<mdl	<mdl	12.60	<mdl	234.00	<mdl	2.27	3.05	5.72	<mdl	3.50	<mdl	2.13	<mdl	**Min**
GRS37-170-742.2A-2 (75)	7.44	0.14	128.49	0.47	604.84	0.04	11.42	3.13	43.19	0.24	10.86	59.43	214.34	9.09	**Mean**
	481.00	6.04	1620.00	1.45	947.00	0.97	274.00	3.73	57.30	1.02	57.00	3770.00	1500.00	281.00	**Max**
	<mdl	<mdl	14.10	<mdl	303.00	<mdl	0.55	2.33	6.73	<mdl	0.00	<mdl	0.61	<mdl	**Min**
	1.03	0.06	–	–	–	–	7.73	–	–	–	–	0.50	–	–	**No Incl.**
GRS37-170-742.2A-3 (68)	1.07	<mdl	1059.33	<mdl	545.28	0.04	2.54	3.11	41.87	0.21	8.94	0.10	232.98	0.42	**Mean**
	7.30	0.09	62900.00	<mdl	707.00	0.66	10.10	4.00	46.70	0.82	19.50	0.54	840.00	3.17	**Max**
	<mdl	<mdl	35.80	<mdl	384.00	<mdl	0.44	2.91	36.70	<mdl	4.30	<mdl	0.90	0.02	**Min**
	–	–	134.33	–	–	–	–	–	–	–	–	–	–	–	**No Incl.**
TE14-01-754.3 (38)	118.65	8.31	1191.97	2.48	636.63	0.07	6.24	2.70	24.36	0.22	35.67	0.08	70.65	48.42	**Mean**
	2700.00	84.70	3900.00	24.90	988.00	1.23	68.10	6.99	35.80	1.06	750.00	1.43	1100.00	970.00	**Max**
	<mdl	<mdl	7.74	<mdl	<mdl	<mdl	<mdl	0.03	0.21	<mdl	<mdl	<mdl	<mdl	<mdl	**Min**
	–	–	–	–	–	–	–	–	–	–	–	–	41.70	10.55	**No Incl.**
TE01-16-566C (27)	3.22	0.01	629.17	2.03	187.76	0.04	29.97	2.92	23.21	0.06	11.11	0.10	17.86	3.88	**Mean**
	14.48	0.10	2360.00	26.00	302.00	0.71	109.80	7.01	52.00	0.19	24.10	0.76	109.50	14.80	**Max**
	0.31	<mdl	4.68	<mdl	70.00	<mdl	3.55	0.65	0.42	<mdl	3.70	<mdl	0.07	0.27	**Min**
TE01-16-566A (19)	7.09	<mdl	523.41	0.25	266.45	0.02	57.41	2.21	26.45	0.08	15.62	0.14	27.69	14.30	**Mean**
	15.13	<mdl	1057.00	0.99	333.00	0.39	90.10	2.93	37.00	0.16	24.50	0.35	81.40	22.30	**Max**
	0.33	<mdl	7.82	<mdl	210.00	<mdl	6.09	1.76	5.89	<mdl	3.17	<mdl	1.93	1.34	**Min**

*Number in brackets = number of spot analyses. Skarn samples are shown in blue.

Table 4.9 Correlation Matrix for Elements in Chalcopyrite Samples

cp	*Mn (ppm)*	*Ni (ppm)*	*Zn (ppm)*	*As (ppm)*	*Se (ppm)*	*Mo (ppm)*	*Ag (ppm)*	*In (ppm)*	*Sn (ppm)*	*Sb (ppm)*	*Te (ppm)*	*Au (ppm)*	*Pb (ppm)*	*Bi (ppm)*
Mn (ppm)	1.00													
Ni (ppm)	0.34	1.00												
Zn (ppm)	-0.01	-0.06	1.00											
As (ppm)	0.17	0.63	-0.04	1.00										
Se (ppm)	-0.16	-0.22	0.13	-0.14	1.00									
Mo (ppm)	0.13	0.19	-0.10	0.15	-0.16	1.00								
Ag (ppm)	0.16	0.00	0.11	0.09	-0.28	-0.02	1.00							
In (ppm)	-0.21	-0.37	-0.15	-0.19	-0.12	-0.16	-0.24	1.00						
Sn (ppm)	-0.09	-0.30	-0.12	-0.29	0.48	-0.12	-0.10	0.05	1.00					
Sb (ppm)	0.09	-0.04	0.03	-0.01	0.22	0.01	0.06	-0.03	0.20	1.00				
Te (ppm)	0.04	0.28	0.02	0.25	0.08	-0.03	0.08	-0.13	-0.04	0.08	1.00			
Au (ppm)	0.09	0.02	-0.08	0.03	0.04	-0.03	0.22	-0.03	0.11	0.32	0.06	1.00		
Pb (ppm)	-0.04	-0.08	-0.11	-0.06	0.07	-0.06	-0.17	0.22	0.35	0.17	-0.03	0.00	1.00	
Bi (ppm)	0.30	0.15	0.01	0.13	0.01	-0.02	0.55	-0.13	0.06	0.31	0.11	0.44	-0.03	1.00

(As vs. Ni n=43; Sn vs. Se n=285; Bi vs. Au n=161)

Table 4.10 Elemental Concentrations in Skarn Samples

Sample	Mn (ppm)	Ni (ppm)	Zn (ppm)	As (ppm)	Se (ppm)	Mo (ppm)	Ag (ppm)	In (ppm)	Sn (ppm)	Sb (ppm)	Te (ppm)	Au (ppm)	Pb (ppm)	Bi (ppm)	
DOZ-90-29 (18)	0.15	0.67	26.25	0.54	499.83	<mdl	150.06	0.25	1.70	0.09	129.12	0.01	781.61	121.87	**Mean**
	2.39	2.37	276.00	1.26	740.00	0.01	600.00	0.42	2.46	0.19	366.00	0.09	2250.00	131.40	**Max**
	<mdl	<mdl	1.54	<mdl	399.00	<mdl	51.30	0.18	0.66	<mdl	54.20	<mdl	47.90	112.20	**Min**
	–	–	10.92	–	–	–	116.72	–	–	–	–	–	–	–	**No Incl.**
TE01-16-566C (27)	3.22	0.01	629.17	2.03	187.76	0.04	29.97	2.92	23.21	0.06	11.11	0.10	17.86	3.88	**Mean**
	14.48	0.10	2360.00	26.00	302.00	0.71	109.80	7.01	52.00	0.19	24.10	0.76	109.50	14.80	**Max**
	0.31	<mdl	4.68	<mdl	70.00	<mdl	3.55	0.65	0.42	<mdl	3.70	<mdl	0.07	0.27	**Min**
TE01-16-566A (19)	7.09	<mdl	523.41	0.25	266.45	0.02	57.41	2.21	26.45	0.08	15.62	0.14	27.69	14.30	**Mean**
	15.13	<mdl	0.70	0.99	333.00	0.39	90.10	2.93	37.00	0.16	24.50	0.35	81.40	22.30	**Max**
	0.33	<mdl	7.82	<mdl	210.00	<mdl	6.09	1.76	5.89	<mdl	3.17	<mdl	1.93	1.34	**Min**
TE14-01-754.3 (65)	118.65	8.31	1191.97	2.48	636.63	0.07	6.24	2.70	24.36	0.22	35.67	0.08	70.65	48.42	**Mean**
	2700.00	84.70	3900.00	24.90	988.00	1.23	68.10	6.99	35.80	1.06	750.00	1.43	1100.00	970.00	**Max**
	<mdl	<mdl	7.74	<mdl	<mdl	<mdl	<mdl	0.03	0.21	<mdl	<mdl	<mdl	<mdl	<mdl	**Min**
	–	–	–	–	–	–	–	–	–	–	–	–	41.70	10.55	**No Incl.**

*Number in brackets = number of spot analyses.

Table 4.11 Correlation Matrices for Elements in Skarn Samples

A. All Samples

skarn	*Mn (ppm)*	*Ni (ppm)*	*Zn (ppm)*	*As (ppm)*	*Se (ppm)*	*Mo (ppm)*	*Ag (ppm)*	*In (ppm)*	*Sn (ppm)*	*Sb (ppm)*	*Te (ppm)*	*Au (ppm)*	*Pb (ppm)*	*Bi (ppm)*
Mn (ppm)	1.00													
Ni (ppm)	0.33	1.00												
Zn (ppm)	-0.08	-0.17	1.00											
As (ppm)	0.15	0.62	-0.16	1.00										
Se (ppm)	-0.18	-0.24	0.32	-0.11	1.00									
Mo (ppm)	0.24	0.37	-0.18	0.28	-0.29	1.00								
Ag (ppm)	0.01	-0.14	-0.38	-0.09	-0.16	-0.12	1.00							
In (ppm)	-0.15	-0.33	0.30	-0.12	0.05	-0.19	-0.52	1.00						
Sn (ppm)	0.00	-0.31	0.49	-0.24	0.23	-0.27	-0.42	0.49	1.00					
Sb (ppm)	0.21	0.00	0.29	0.07	0.14	-0.06	-0.13	0.18	0.11	1.00				
Te (ppm)	-0.02	0.19	-0.22	0.15	0.17	-0.09	0.28	-0.36	-0.30	0.06	1.00			
Au (ppm)	0.71	0.32	-0.06	0.42	-0.26	0.14	0.12	-0.06	0.16	0.15	0.05	1.00		
Pb (ppm)	-0.04	-0.06	-0.22	-0.07	0.11	-0.08	0.53	-0.44	-0.48	0.03	0.30	-0.11	1.00	
Bi (ppm)	0.18	0.03	-0.38	0.01	0.08	-0.11	0.76	-0.67	-0.61	-0.03	0.43	0.06	0.70	1.00

B. DOZ-90-29

	Mn (ppm)	***Ni (ppm)***	***Zn (ppm)***	***As (ppm)***	***Se (ppm)***	***Mo (ppm)***	***Ag (ppm)***	***In (ppm)***	***Sn (ppm)***	***Sb (ppm)***	***Te (ppm)***	***Au (ppm)***	***Pb (ppm)***	***Bi (ppm)***
Mn (ppm)	1.00													
Ni (ppm)	0.22	1.00												
Zn (ppm)	-0.09	-0.23	1.00											
As (ppm)	-0.32	-0.35	-0.12	1.00										
Se (ppm)	-0.14	-0.19	0.47	0.22	1.00									
Mo (ppm)	-0.05	-0.04	-0.18	-0.15	-0.37	1.00								
Ag (ppm)	-0.03	0.66	-0.04	0.20	0.20	-0.19	1.00							
In (ppm)	0.10	-0.27	0.82	-0.26	0.49	-0.10	-0.31	1.00						
Sn (ppm)	0.03	-0.05	-0.43	-0.27	-0.64	0.43	-0.39	-0.24	1.00					
Sb (ppm)	0.53	0.32	0.00	-0.23	0.20	-0.14	0.01	0.37	-0.05	1.00				
Te (ppm)	0.02	0.74	-0.11	0.09	0.15	-0.21	0.96	-0.32	-0.24	0.08	1.00			
Au (ppm)	-0.08	-0.03	-0.11	0.25	0.60	-0.15	0.27	0.04	0.01	0.15	0.37	1.00		
Pb (ppm)	0.25	-0.03	-0.07	-0.33	0.14	0.19	-0.19	0.12	0.40	0.27	-0.12	0.36	1.00	
Bi (ppm)	-0.41	-0.49	0.04	0.28	0.07	0.13	-0.20	0.02	0.51	-0.14	-0.16	0.36	0.30	1.00

C. TE14-01-754.3

	Mn (ppm)	***Ni (ppm)***	***Zn (ppm)***	***As (ppm)***	***Se (ppm)***	***Mo (ppm)***	***Ag (ppm)***	***In (ppm)***	***Sn (ppm)***	***Sb (ppm)***	***Te (ppm)***	***Au (ppm)***	***Pb (ppm)***	***Bi (ppm)***
Mn (ppm)	1.00													
Ni (ppm)	0.28	1.00												
Zn (ppm)	-0.22	-0.40	1.00											
As (ppm)	0.18	0.86	-0.29	1.00										
Se (ppm)	-0.45	-0.65	0.29	-0.37	1.00									
Mo (ppm)	0.25	0.41	-0.31	-0.07	-0.62	1.00								
Ag (ppm)	0.83	0.17	-0.12	0.23	-0.44	-0.06	1.00							
In (ppm)	-0.36	-0.72	0.31	-0.46	0.35	-0.56	0.09	1.00						
Sn (ppm)	-0.12	-0.75	0.33	-0.48	0.87	-0.61	-0.14	0.37	1.00					
Sb (ppm)	0.15	-0.14	0.11	-0.02	-0.19	-0.18	0.39	0.32	-0.03	1.00				
Te (ppm)	-0.01	0.24	-0.16	0.32	0.04	-0.07	0.09	-0.14	-0.08	0.09	1.00			
Au (ppm)	0.89	0.42	-0.25	0.47	-0.42	0.00	0.91	-0.23	-0.17	0.17	0.17	1.00		
Pb (ppm)	0.05	0.51	0.06	0.60	-0.27	-0.06	0.18	-0.19	-0.36	0.23	0.22	0.29	1.00	
Bi (ppm)	0.08	0.26	-0.17	0.33	0.00	-0.06	0.17	-0.16	-0.08	0.11	0.98	0.27	0.34	1.00

D. TE01-16-566

	Mn (ppm)	***Ni (ppm)***	***Zn (ppm)***	***As (ppm)***	***Se (ppm)***	***Mo (ppm)***	***Ag (ppm)***	***In (ppm)***	***Sn (ppm)***	***Sb (ppm)***	***Te (ppm)***	***Au (ppm)***	***Pb (ppm)***	***Bi (ppm)***
Mn (ppm)	1.00													
Ni (ppm)	-0.09	1.00												
Zn (ppm)	0.45	-0.22	1.00											
As (ppm)	-0.13	0.99	-0.28	1.00										
Se (ppm)	0.45	-0.05	0.06	-0.02	1.00									
Mo (ppm)	-0.13	0.87	-0.26	0.88	0.09	1.00								
Ag (ppm)	0.56	-0.01	0.07	0.01	0.77	0.06	1.00							
In (ppm)	-0.49	-0.03	-0.34	-0.01	-0.25	0.06	-0.27	1.00						
Sn (ppm)	0.63	-0.32	0.49	-0.37	0.18	-0.30	0.32	-0.10	1.00					
Sb (ppm)	0.48	0.20	0.58	0.13	0.21	0.15	0.30	-0.51	0.41	1.00				
Te (ppm)	0.87	-0.17	0.40	-0.19	0.59	-0.15	0.68	-0.47	0.60	0.41	1.00			
Au (ppm)	0.65	0.41	0.22	0.39	0.57	0.47	0.53	-0.25	0.36	0.35	0.63	1.00		
Pb (ppm)	-0.14	0.23	-0.35	0.30	0.63	0.36	0.58	0.12	-0.17	-0.08	0.10	0.28	1.00	
Bi (ppm)	0.73	0.15	0.15	0.13	0.63	0.17	0.74	-0.45	0.42	0.58	0.71	0.58	0.25	1.00

Table 4.12 Elemental Concentrations in Porphyry Samples

Sample	Mn (ppm)	Ni (ppm)	Zn (ppm)	As (ppm)	Se (ppm)	Mo (ppm)	Ag (ppm)	In (ppm)	Sn (ppm)	Sb (ppm)	Te (ppm)	Au (ppm)	Pb (ppm)	Bi (ppm)	
AH90-4C-F (36)	0.26	0.11	129.98	0.21	356.67	0.01	133.58	2.57	9.16	0.11	12.09	0.03	31.80	226.78	**Mean**
	1.44	0.46	506.00	1.12	618.00	0.11	261.00	4.97	16.12	0.37	20.90	0.60	176.50	476.00	**Max**
	<mdl	<mdl	1.31	<mdl	205.00	<mdl	0.63	0.12	<mdl	<mdl	<mdl	<mdl	<mdl	<mdl	**Min**
AH90-4C-C (9)	0.87	0.10	276.04	0.75	418.89	<mdl	154.93	3.14	13.34	0.02	19.08	1.07	47.95	131.03	**Mean**
	1.99	0.40	520.00	0.90	508.00	<mdl	472.00	4.59	16.29	0.10	53.40	8.80	194.00	398.00	**Max**
	0.32	<mdl	74.80	0.50	234.00	<mdl	3.79	0.50	8.41	<mdl	2.91	<mdl	0.27	0.04	**Min**
GRS37-184-7.8 (20)	2.27	0.19	636.23	0.81	269.75	0.01	22.55	5.72	35.69	0.12	15.36	2.30	336.74	74.46	**Mean**
	5.83	0.57	10700.00	1.43	557.00	0.10	425.00	7.01	43.10	0.27	109.00	42.30	925.00	1464.00	**Max**
	<mdl	<mdl	14.80	<mdl	210.00	<mdl	0.14	0.33	15.90	<mdl	<mdl	<mdl	1.34	0.17	**Min**
	–	0.14	101.23	–	–	–	–	–	–	–	–	–	–	–	**No Incl**
GRS37-170-714.2 (18)	0.60	0.13	127.57	0.60	315.78	0.14	4.88	3.27	15.54	0.21	8.80	0.10	226.62	0.09	**Mean**
	1.42	0.46	460.00	1.15	394.00	0.14	1.60	3.46	20.31	0.54	24.20	0.48	709.00	0.56	**Max**
	<mdl	<mdl	12.60	<mdl	234.00	<mdl	0.20	3.05	5.72	<mdl	3.50	<mdl	2.13	<mdl	**Min**
GRS37-170-742.2A-2 (76)	7.34	0.14	128.78	0.47	606.24	0.04	15.36	3.10	43.66	0.24	12.75	58.68	212.87	25.36	**Mean**
	481.00	6.04	1620.00	1.45	947.00	0.97	311.00	3.73	79.00	1.02	154.30	3770.00	1500.00	1246.00	**Max**
	<mdl	<mdl	14.10	<mdl	303.00	<mdl	0.55	0.64	6.73	<mdl	<mdl	<mdl	0.61	<mdl	**Min**
	1.01	0.07	–	–	–	–	11.72	–	–	–	–	12.75	–	–	**No Incl**
GRS37-170-742.2A-3 (68)	1.07	<mdl	1059.33	<mdl	545.28	0.04	2.54	3.11	41.87	0.21	8.94	0.10	232.98	0.42	**Mean**
	7.30	0.09	62900.00	<mdl	707.00	0.66	10.10	4.00	46.70	0.82	19.50	0.54	840.00	3.17	**Max**
	<mdl	<mdl	35.80	<mdl	384.00	<mdl	0.44	2.91	36.70	<mdl	4.30	<mdl	0.90	0.02	**Min**
	–	–	134.33	–	–	–	–	–	–	–	–	–	–	–	**No Incl**

*Number in brackets = number of spot analyses.

Table 4.13 Correlation Matrices for Elements in Porphyry Samples

A. All Samples

porphyry	*Mn (ppm)*	*Ni (ppm)*	*Zn (ppm)*	*As (ppm)*	*Se (ppm)*	*Mo (ppm)*	*Ag (ppm)*	*In (ppm)*	*Sn (ppm)*	*Sb (ppm)*	*Te (ppm)*	*Au (ppm)*	*Pb (ppm)*	*Bi (ppm)*
Mn (ppm)	1.00													
Ni (ppm)	0.11	1.00												
Zn (ppm)	0.64	0.21	1.00											
As (ppm)	0.05	0.27	0.02	1.00										
Se (ppm)	-0.04	-0.17	-0.06	-0.15	1.00									
Mo (ppm)	-0.03	-0.08	-0.06	0.02	-0.05	1.00								
Ag (ppm)	-0.17	0.12	-0.17	-0.02	-0.16	-0.06	1.00							
In (ppm)	0.25	0.12	0.17	0.27	-0.30	-0.01	-0.68	1.00						
Sn (ppm)	0.20	-0.20	0.00	-0.07	0.57	0.03	-0.47	0.22	1.00					
Sb (ppm)	0.01	-0.02	-0.07	-0.05	0.27	0.06	-0.04	-0.09	0.25	1.00				
Te (ppm)	-0.03	0.21	-0.05	0.05	0.10	-0.06	0.60	-0.38	0.04	0.14	1.00			
Au (ppm)	-0.05	0.15	-0.07	0.03	0.06	-0.02	0.34	-0.18	-0.05	0.05	0.53	1.00		
Pb (ppm)	0.58	0.07	0.29	0.11	0.03	-0.05	-0.20	0.22	0.33	0.10	0.00	-0.06	1.00	
Bi (ppm)	-0.16	0.13	-0.15	-0.03	-0.09	-0.06	0.88	-0.62	-0.34	0.02	0.77	0.55	-0.19	1.00

B. AH90-4C-F

	Mn (ppm)	***Ni (ppm)***	***Zn (ppm)***	***As (ppm)***	***Se (ppm)***	***Mo (ppm)***	***Ag (ppm)***	***In (ppm)***	***Sn (ppm)***	***Sb (ppm)***	***Te (ppm)***	***Au (ppm)***	***Pb (ppm)***	***Bi (ppm)***
Mn (ppm)	1.00													
Ni (ppm)	0.26	1.00												
Zn (ppm)	0.40	0.47	1.00											
As (ppm)	0.42	-0.36	-0.32	1.00										
Se (ppm)	0.00	-0.27	-0.07	0.17	1.00									
Mo (ppm)	-0.11	0.18	-0.07	-0.01	-0.01	1.00								
Ag (ppm)	-0.47	-0.44	-0.63	-0.07	0.18	-0.07	1.00							
In (ppm)	0.47	0.42	0.68	0.02	-0.17	0.08	-0.98	1.00						
Sn (ppm)	0.36	0.43	0.76	-0.20	-0.07	0.09	-0.81	0.88	1.00					
Sb (ppm)	-0.49	-0.24	-0.12	-0.43	-0.11	-0.19	0.44	-0.35	-0.15	1.00				
Te (ppm)	-0.44	-0.34	-0.60	-0.14	0.16	-0.03	0.97	-0.97	-0.78	0.44	1.00			
Au (ppm)	0.17	0.02	-0.06	0.37	-0.04	0.03	-0.06	0.06	-0.08	-0.14	-0.11	1.00		
Pb (ppm)	-0.07	-0.28	-0.38	0.16	0.28	-0.04	0.62	-0.61	-0.42	0.23	0.63	0.01	1.00	
Bi (ppm)	-0.52	-0.41	-0.62	-0.16	0.15	-0.09	0.99	-0.97	-0.79	0.50	0.97	-0.10	0.60	1.00

C. AH90-4C-C

	Mn (ppm)	***Ni (ppm)***	***Zn (ppm)***	***As (ppm)***	***Se (ppm)***	***Mo (ppm)***	***Ag (ppm)***	***In (ppm)***	***Sn (ppm)***	***Sb (ppm)***	***Te (ppm)***	***Au (ppm)***	***Pb (ppm)***	***Bi (ppm)***
Mn (ppm)	1.00													
Ni (ppm)	-0.41	1.00												
Zn (ppm)	0.62	-0.70	1.00											
As (ppm)	0.29	-0.82	0.70	1.00										
Se (ppm)	-0.08	0.26	-0.57	-0.24	1.00									
Mo (ppm)	-0.23	0.23	-0.31	-0.08	0.13	1.00								
Ag (ppm)	-0.52	0.89	-0.78	-0.83	0.20	0.52	1.00							
In (ppm)	0.52	-0.88	0.81	0.84	-0.23	-0.49	-0.99	1.00						
Sn (ppm)	0.63	-0.77	0.85	0.75	-0.23	-0.58	-0.96	0.97	1.00					
Sb (ppm)	-0.41	0.80	-0.65	-0.89	0.12	-0.19	0.73	-0.76	-0.66	1.00				
Te (ppm)	-0.49	0.92	-0.78	-0.88	0.18	0.38	0.99	-0.99	-0.93	0.83	1.00			
Au (ppm)	-0.25	0.26	-0.34	-0.11	0.14	1.00	0.55	-0.52	-0.61	-0.16	0.41	1.00		
Pb (ppm)	-0.18	0.53	-0.50	-0.43	0.32	0.90	0.74	-0.73	-0.74	0.15	0.65	0.91	1.00	

D. GRS37-184-7.8

	Mn (ppm)	***Ni (ppm)***	***Zn (ppm)***	***As (ppm)***	***Se (ppm)***	***Mo (ppm)***	***Ag (ppm)***	***In (ppm)***	***Sn (ppm)***	***Sb (ppm)***	***Te (ppm)***	***Au (ppm)***	***Pb (ppm)***	***Bi (ppm)***
Mn (ppm)	1.00													
Ni (ppm)	-0.09	1.00												
Zn (ppm)	0.16	-0.23	1.00											
As (ppm)	-0.07	-0.16	-0.09	1.00										
Se (ppm)	-0.37	0.44	-0.04	0.02	1.00									
Mo (ppm)	0.50	-0.22	-0.11	-0.25	-0.19	1.00								
Ag (ppm)	-0.24	0.24	-0.06	-0.13	0.84	-0.13	1.00							
In (ppm)	0.15	-0.26	0.23	0.15	-0.79	0.04	-0.97	1.00						
Sn (ppm)	0.41	-0.17	0.06	0.18	-0.59	0.17	-0.86	0.81	1.00					
Sb (ppm)	-0.15	-0.20	0.17	-0.06	-0.16	-0.08	-0.20	0.32	0.04	1.00				
Te (ppm)	-0.19	0.32	-0.07	-0.01	0.88	-0.13	0.92	-0.92	-0.77	-0.14	1.00			
Au (ppm)	-0.25	0.25	-0.06	-0.12	0.85	-0.14	1.00	-0.97	-0.86	-0.21	0.93	1.00		
Pb (ppm)	0.04	-0.06	0.31	-0.15	-0.34	0.08	-0.22	0.29	-0.08	0.25	-0.32	-0.23	1.00	
Bi (ppm)	-0.24	0.24	-0.06	-0.13	0.84	-0.13	1.00	-0.97	-0.86	-0.21	0.92	1.00	-0.22	1.00

E. GRS37-170-714.2

	Mn (ppm)	***Ni (ppm)***	***Zn (ppm)***	***As (ppm)***	***Se (ppm)***	***Mo (ppm)***	***Ag (ppm)***	***In (ppm)***	***Sn (ppm)***	***Sb (ppm)***	***Te (ppm)***	***Au (ppm)***	***Pb (ppm)***	***Bi (ppm)***
Mn (ppm)	1.00													
Ni (ppm)	0.26	1.00												
Zn (ppm)	0.32	0.32	1.00											
As (ppm)	-0.26	-0.07	0.21	1.00										
Se (ppm)	0.18	0.14	0.27	0.19	1.00									
Mo (ppm)	-0.18	-0.20	-0.26	0.07	-0.17	1.00								
Ag (ppm)	0.41	0.09	0.52	0.11	0.01	-0.33	1.00							
In (ppm)	-0.07	-0.30	0.29	0.25	0.14	-0.12	0.30	1.00						
Sn (ppm)	0.01	-0.29	-0.09	-0.10	-0.75	0.17	-0.08	0.22	1.00					
Sb (ppm)	-0.28	0.13	0.46	0.23	0.11	-0.11	0.48	0.39	-0.15	1.00				
Te (ppm)	0.73	-0.27	0.17	-0.02	0.02	-0.20	0.42	0.32	0.31	-0.34	1.00			
Au (ppm)	0.67	-0.28	0.19	-0.06	-0.26	-0.12	0.39	0.17	0.48	-0.41	0.92	1.00		
Pb (ppm)	0.84	-0.09	0.22	-0.03	0.22	-0.21	0.38	0.14	0.10	-0.30	0.85	0.76	1.00	
Bi (ppm)	0.00	0.32	0.18	0.09	0.51	-0.13	0.39	-0.12	-0.81	0.27	-0.18	-0.32	-0.13	1.00

F. GRS37-170-742.2

	Mn (ppm)	***Ni (ppm)***	***Zn (ppm)***	***As (ppm)***	***Se (ppm)***	***Mo (ppm)***	***Ag (ppm)***	***In (ppm)***	***Sn (ppm)***	***Sb (ppm)***	***Te (ppm)***	***Au (ppm)***	***Pb (ppm)***	***Bi (ppm)***
Mn (ppm)	1.00													
Ni (ppm)	0.98	1.00												
Zn (ppm)	0.01	-0.01	1.00											
As (ppm)	0.13	0.23	-0.05	1.00										
Se (ppm)	-0.26	-0.21	-0.05	0.26	1.00									
Mo (ppm)	0.00	-0.02	-0.03	0.02	-0.15	1.00								
Ag (ppm)	-0.02	0.00	-0.01	0.01	0.13	-0.05	1.00							
In (ppm)	-0.22	-0.21	0.27	0.00	-0.02	0.03	-0.51	1.00						
Sn (ppm)	-0.35	-0.34	0.02	-0.01	0.06	0.08	0.30	0.15	1.00					
Sb (ppm)	-0.02	0.02	0.06	0.06	0.16	0.08	0.35	-0.08	0.05	1.00				
Te (ppm)	-0.02	0.03	-0.02	0.05	0.17	-0.05	0.71	-0.57	0.39	0.23	1.00			
Au (ppm)	-0.01	-0.01	-0.01	-0.06	-0.04	-0.03	0.62	-0.03	-0.03	0.15	-0.03	1.00		
Pb (ppm)	-0.06	-0.03	0.27	0.08	-0.07	-0.04	-0.07	0.25	0.24	0.02	0.06	-0.06	1.00	
Bi (ppm)	-0.01	0.02	-0.01	0.06	0.17	-0.04	0.76	-0.70	0.39	0.24	0.92	-0.01	-0.05	1.00

Table 4.14 Elemental Concentrations in All Samples

Sample	# Spots	Cu-Mineral	Deposit	Mn (ppm)	Ni (ppm)	Zn (ppm)	As (ppm)	Se (ppm)	Mo (ppm)	Ag (ppm)
AH90-4C-F	36	bn/cp	porphyry	0.45	<mdl	129.98	0.78	356.67	<mdl	133.58
AH90-4C-C	9	bn/cp	porphyry	0.87	0.26	276.04	0.58	418.89	<mdl	154.93
GRS37-170-714.2	18	cp	porphyry	0.76	<mdl	127.57	0.92	315.78	0.82	4.88
GRS37-184-7.8	20	cp	porphyry	2.41	<mdl	636.23	1.05	269.75	0.10	22.55
GRS37-170-742.2A-2	76	cp	porphyry	7.86	<mdl	128.78	1.19	606.24	0.26	15.36
GRS37-170-742.2A-3	68	cp	porphyry	1.08	<mdl	1059.33	<mdl	545.28	0.24	2.54
DOZ-90-29	18	bn	skarn	<mdl	0.85	26.25	0.91	499.83	0.01	150.06
TE01-16-566C	27	cp	skarn	3.22	0.09	629.17	16.87	187.76	0.53	29.97
TE01-16-566A	19	cp	skarn	155.46	39.05	1191.97	3.30	636.68	0.46	6.78
TE14-01-754.3	38	cp	skarn	155.46	39.05	1191.97	3.30	636.68	0.46	6.78
	# Spots	**Cu-Mineral**	**Deposit**	**In (ppm)**	**Sn (ppm)**	**Sb (ppm)**	**Te (ppm)**	**Au (ppm)**	**Pb (ppm)**	**Bi (ppm)**
AH90-4C-F	36	bn/cp	porphyry	2.57	9.33	0.17	13.44	0.17	31.84	313.99
AH90-4C-C	9	bn/cp	porphyry	3.14	13.34	0.10	21.10	1.37	47.95	196.52
GRS37-170-714.2	18	cp	porphyry	3.27	15.54	0.22	8.80	0.20	226.62	0.30
GRS37-184-7.8	20	cp	porphyry	5.72	35.69	0.17	17.92	2.87	336.74	74.46
GRS37-170-742.2A-2	76	cp	porphyry	3.10	43.66	0.27	13.16	127.11	212.87	32.12
GRS37-170-742.2A-3	68	cp	porphyry	3.11	41.87	0.23	8.94	0.18	232.98	0.51
DOZ-90-29	18	bn	skarn	0.25	1.70	0.10	129.12	<mdl	781.61	121.87
TE01-16-566C	27	cp	skarn	2.92	23.21	0.12	11.11	0.29	17.86	3.88
TE01-16-566A	19	cp	skarn	2.70	24.36	0.32	46.82	0.58	72.56	52.57
TE14-01-754.3	38	cp	skarn	2.70	24.36	0.32	46.82	0.58	72.56	52.57

Skarn samples are shown in blue.

Table 4.15 Correlation Matrix for Elements in All Samples

all	*Mn (ppm)*	*Ni (ppm)*	*Zn (ppm)*	*As (ppm)*	*Se (ppm)*	*Mo (ppm)*	*Ag (ppm)*	*In (ppm)*	*Sn (ppm)*	*Sb (ppm)*	*Te (ppm)*	*Au (ppm)*	*Pb (ppm)*	*Bi (ppm)*
Mn (ppm)	1.00													
Ni (ppm)	0.34	1.00												
Zn (ppm)	0.00	-0.05	1.00											
As (ppm)	0.18	0.63	-0.03	1.00										
Se (ppm)	-0.16	-0.21	0.13	-0.13	1.00									
Mo (ppm)	0.13	0.20	-0.08	0.15	-0.15	1.00								
Ag (ppm)	0.01	-0.04	-0.12	-0.02	-0.14	-0.07	1.00							
In (ppm)	-0.13	-0.25	0.02	-0.11	-0.06	-0.07	-0.58	1.00						
Sn (ppm)	-0.05	-0.22	0.01	-0.20	0.42	-0.05	-0.44	0.40	1.00					
Sb (ppm)	0.09	-0.03	0.05	-0.01	0.22	0.02	-0.06	0.06	0.25	1.00				
Te (ppm)	0.02	0.22	-0.06	0.19	0.10	-0.05	0.23	-0.35	-0.22	0.02	1.00			
Au (ppm)	0.02	0.00	-0.05	0.01	0.04	-0.02	0.32	-0.11	-0.01	0.06	0.10	1.00		
Pb (ppm)	-0.04	-0.06	-0.13	-0.05	0.09	-0.06	0.01	-0.08	0.02	0.07	0.20	-0.04	1.00	
Bi (ppm)	0.02	-0.01	-0.13	-0.02	-0.03	-0.06	0.86	-0.48	-0.28	0.02	0.22	0.54	-0.02	1.00

A

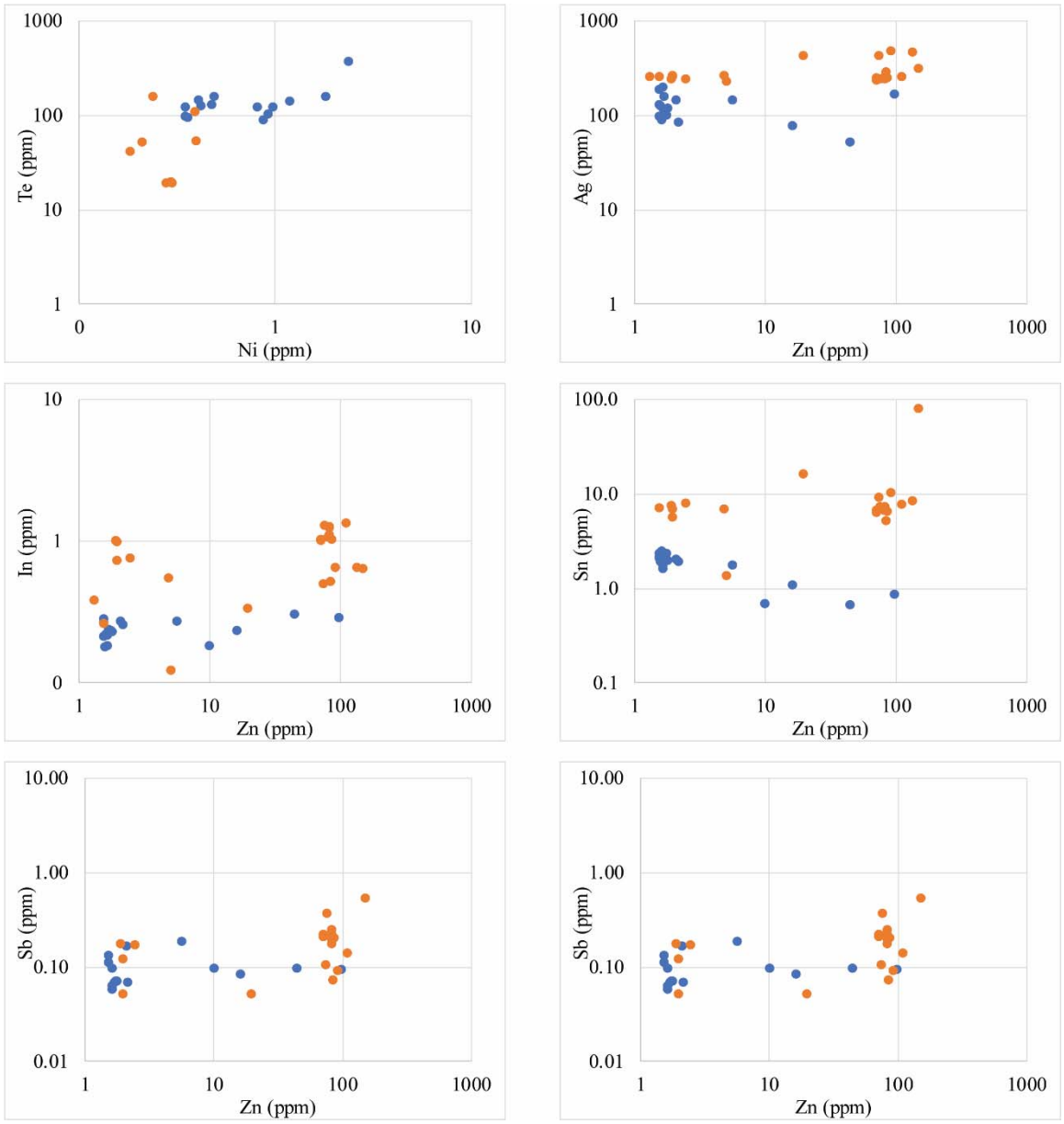
1000
100
10
1
Te (ppm)
0
1
10
Ni (ppm)
1000
100
10
1
Ag (ppm)
1
10
100
1000
Zn (ppm)
10
1
0
In (ppm)
1
10
100
1000
Zn (ppm)
100.0
10.0
1.0
0.1
Sn (ppm)
1
10
100
1000
Zn (ppm)
10.00
1.00
0.10
0.01
Sb (ppm)
1
10
100
1000
Zn (ppm)
10.00
1.00
0.10
0.01
Sb (ppm)
1
10
100
1000
Zn (ppm)

B

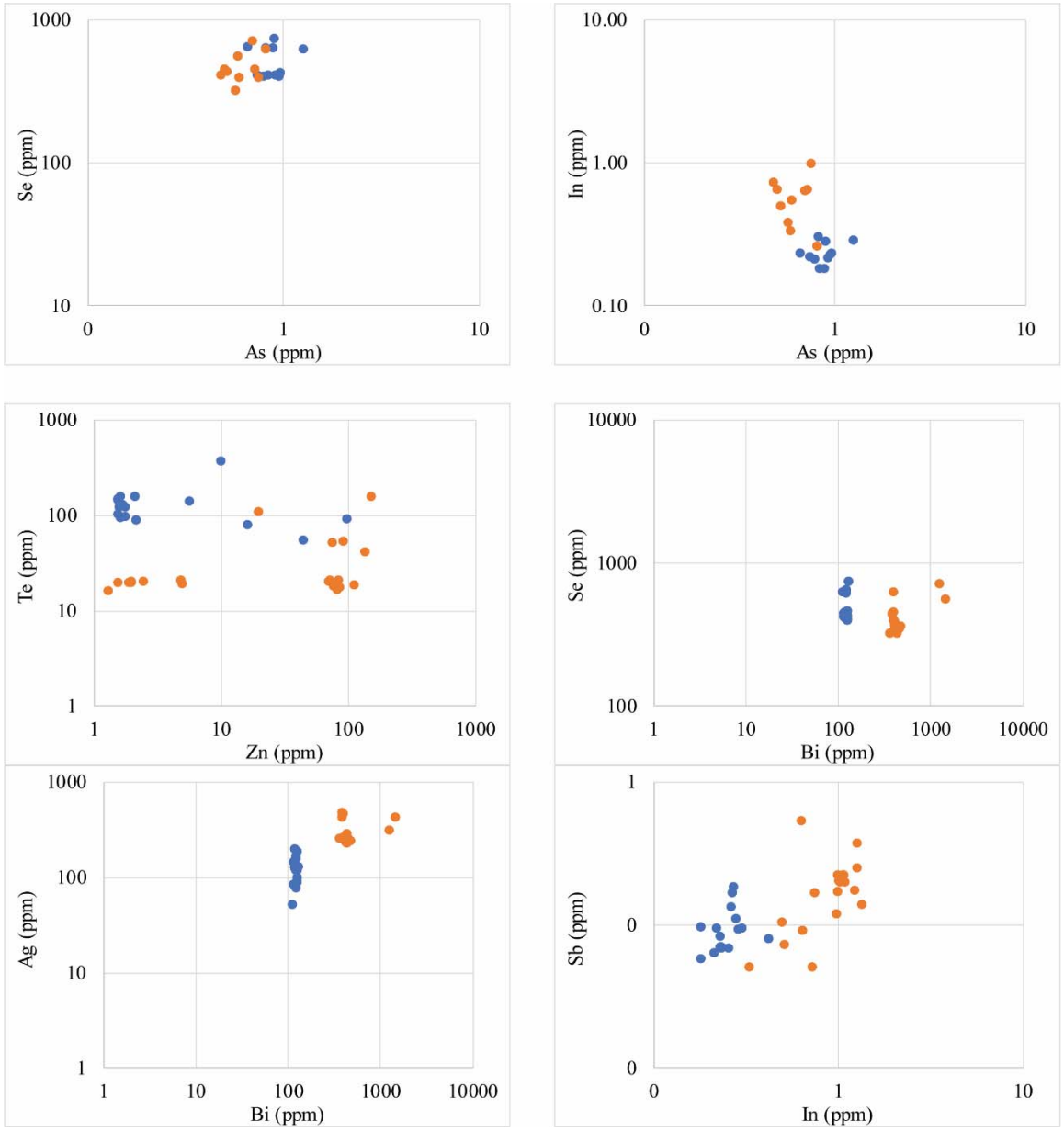
1000
100
10
Se (ppm)
0
1
10
As (ppm)
10.00
1.00
0.10
In (ppm)
0
1
10
As (ppm)
1000
100
10
1
Te (ppm)
1
10
100
1000
Zn (ppm)
10000
1000
100
Se (ppm)
1
10
100
1000
10000
Bi (ppm)
1000
100
10
1
Ag (ppm)
1
10
100
1000
10000
Bi (ppm)
1
0
0
Sb (ppm)
0
1
10
In (ppm)

C

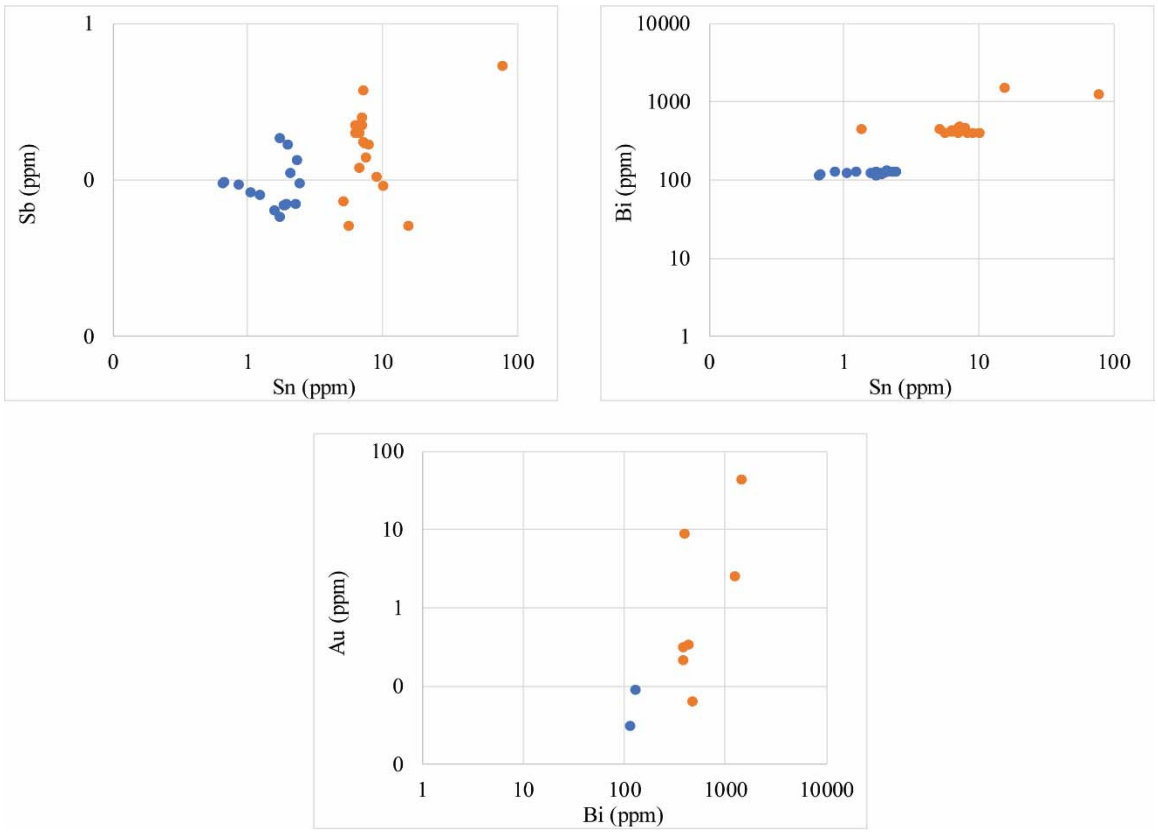

Figure 4.6 Trace Element-Pair Relationships in Bornite

Log-log plots of selected elemental correlations where r>±0.5 for trace elements in bornite samples. Orange= porphyry. Blue= skarn. Elemental comparisons were based on similar plots in previous studies and on correlation matrices generated for this data which indicated potential correlations (Cook, et al., 2011; Reich, et al., 2013).

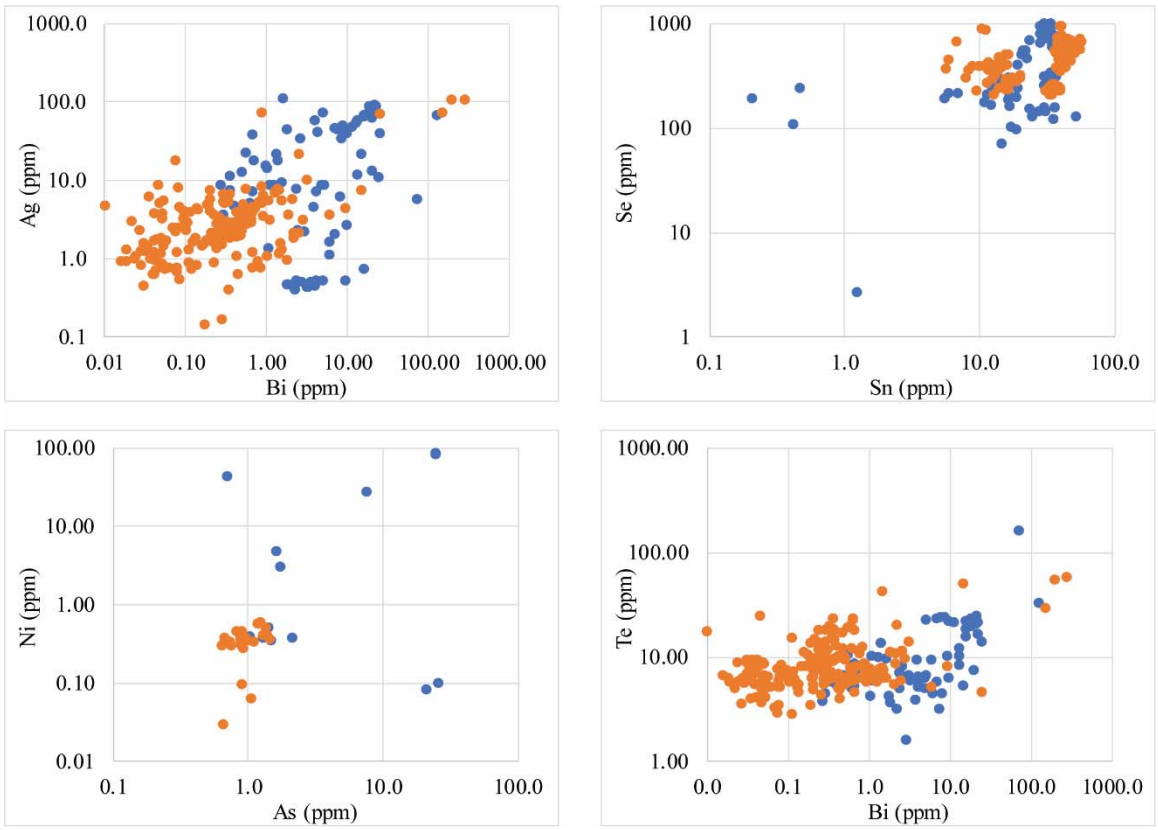

Figure 4.7 Trace Element-Pair Relationships in Chalcopyrite

Log-log plots of selected elemental correlations for trace elements in chalcopyrite samples. Orange= porphyry. Blue= skarn. Elemental comparisons were based on similar plots in previous studies and on correlation matrices generated for this data which indicated potential correlations (Cook, et al., 2011; Reich, et al., 2013).

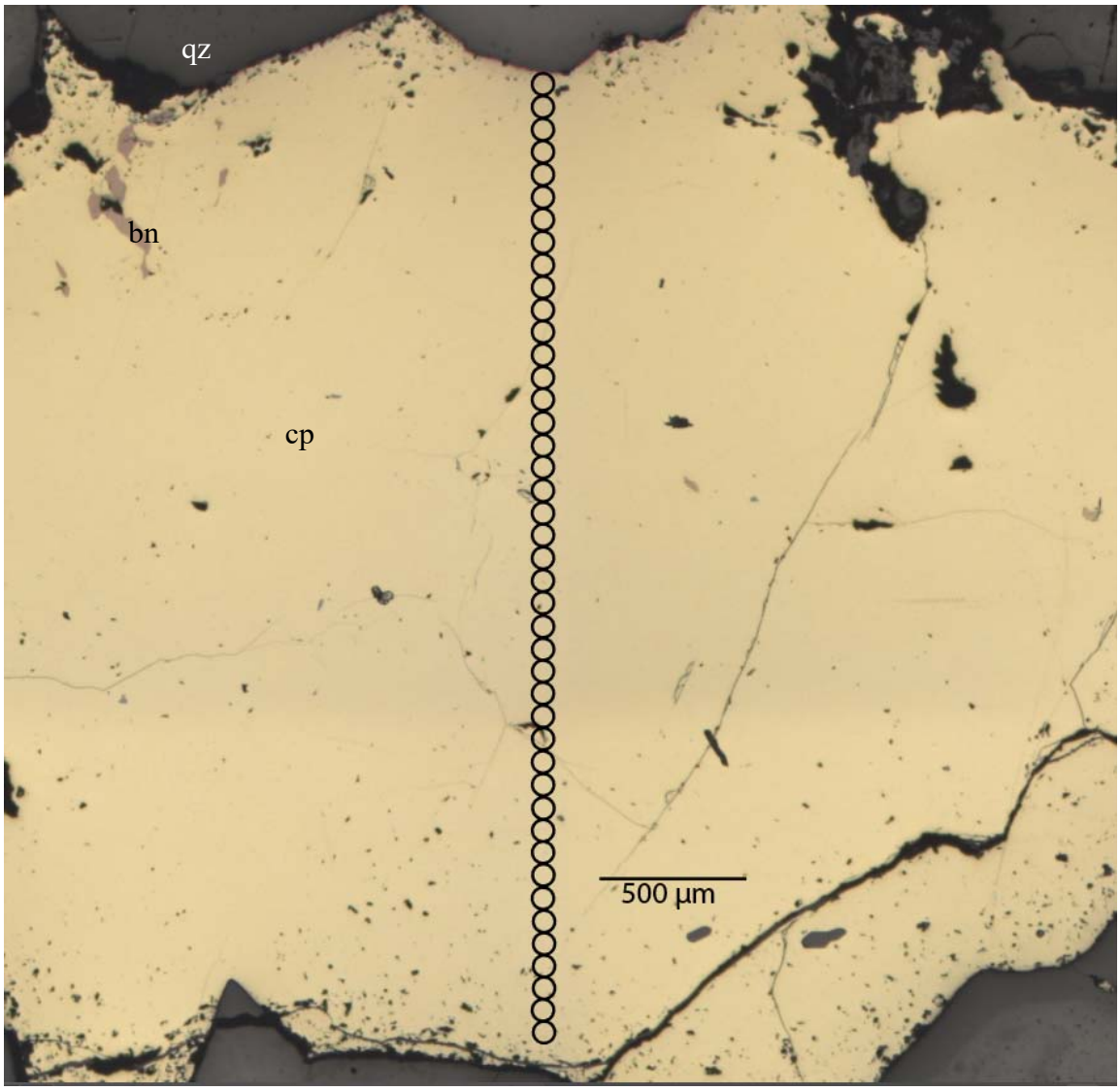

Figure 4.8 Line-of-Spots Across Chalcopyrite Vein in GRS37-170-742.2

Spots are 65 µm. Total transect length is 3650 µm.

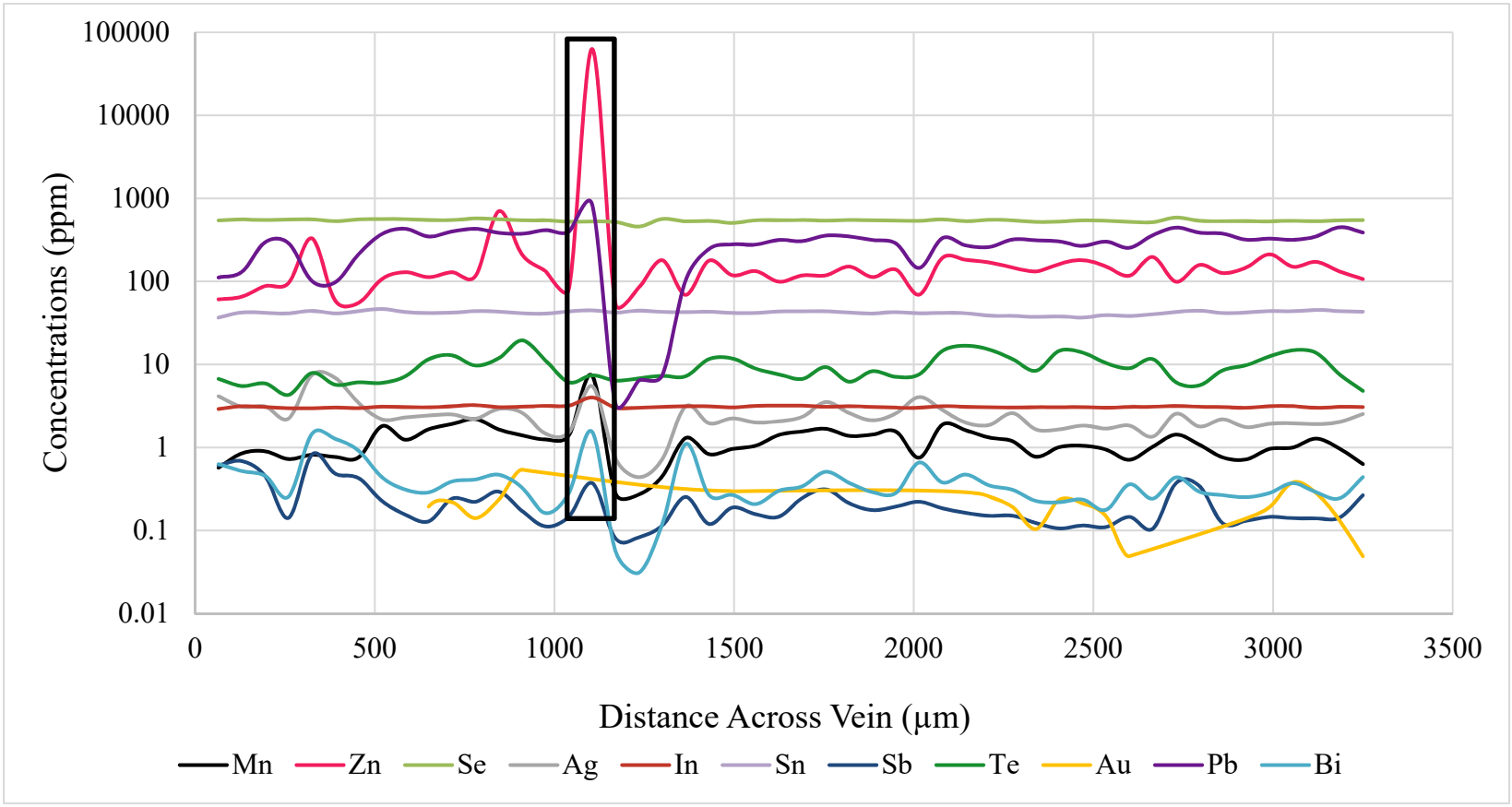

Figure 4.9 Trace Element Variation Across Chalcopyrite Vein Transect in GRS37-170-742.2

Semi-log plot of trace element concentrations. Unusually high Zn, Bi, Pb, Ag, and Mn indicate the ablation of a sphalerite inclusion (black box).

A

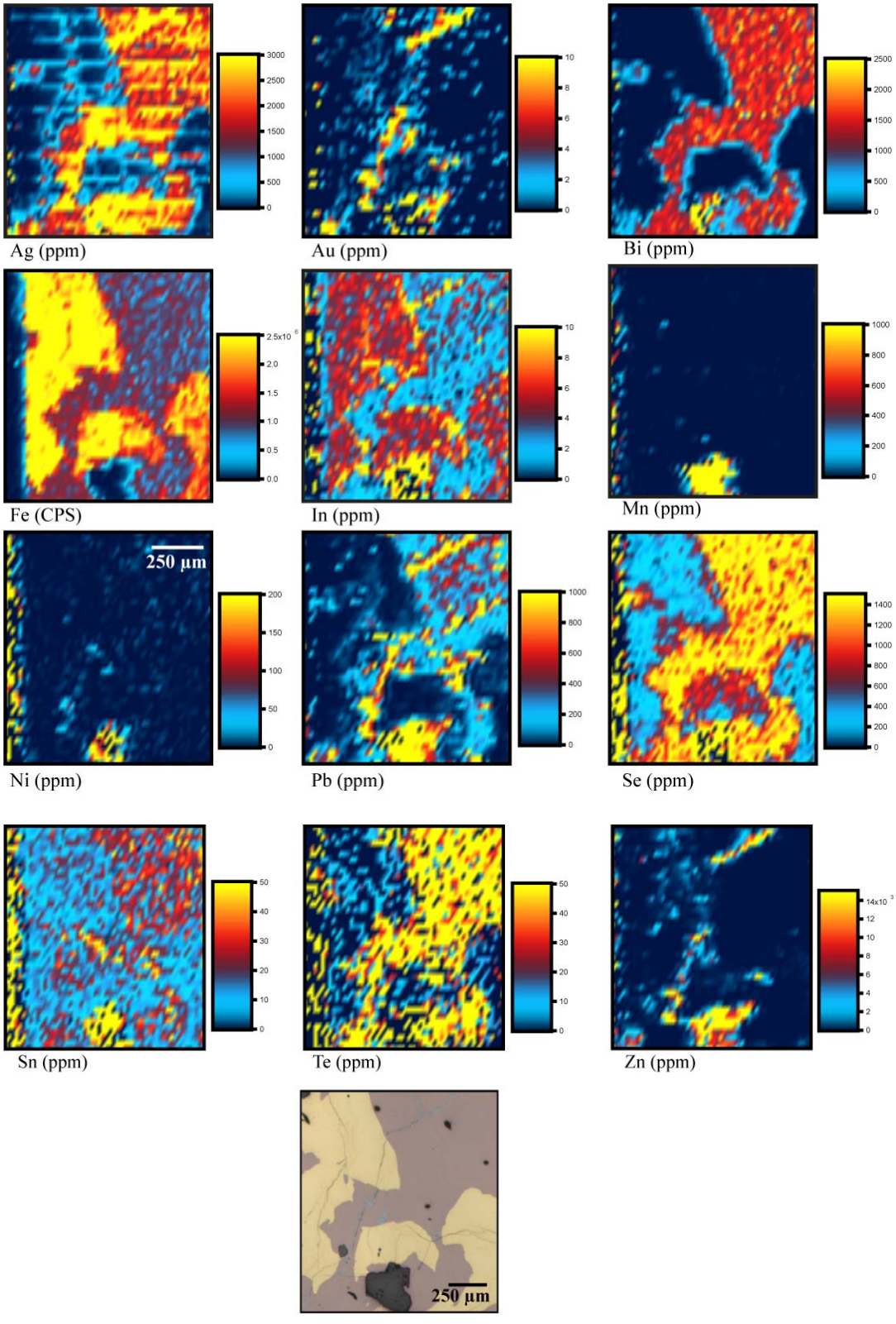
Ag (ppm)
Au (ppm)
Bi (ppm)
Fe (CPS)
In (ppm)
Mn (ppm)
250 µm
Ni (ppm)
Pb (ppm)
Se (ppm)
Sn (ppm)
Te (ppm)
Zn (ppm)
250 µm

B

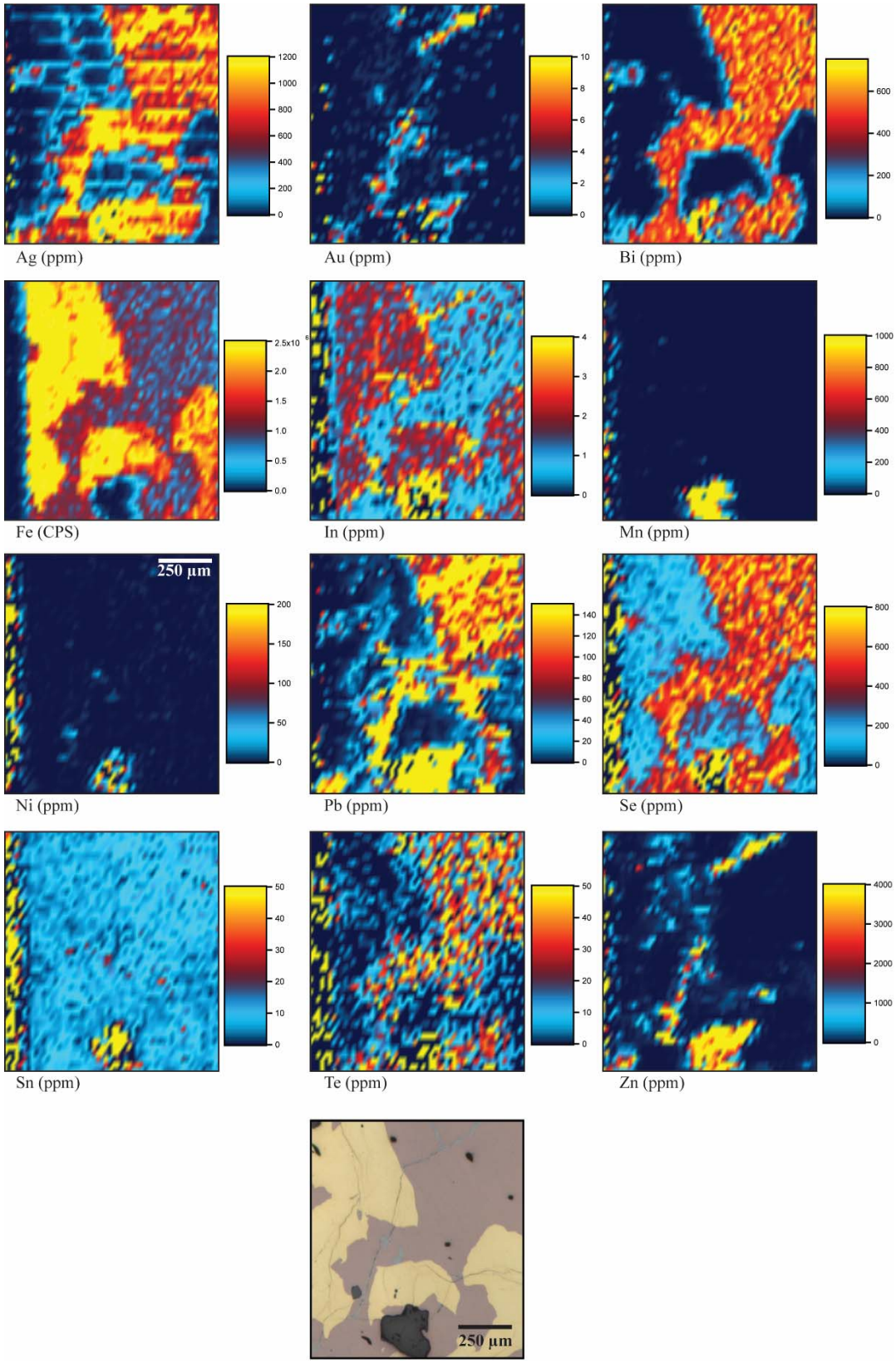
Ag (ppm)
Au (ppm)
Bi (ppm)
Fe (CPS)
In (ppm)
Mn (ppm)
Ni (ppm)
Pb (ppm)
Se (ppm)
Sn (ppm)
Te (ppm)
Zn (ppm)
250 µm
250 µm

C

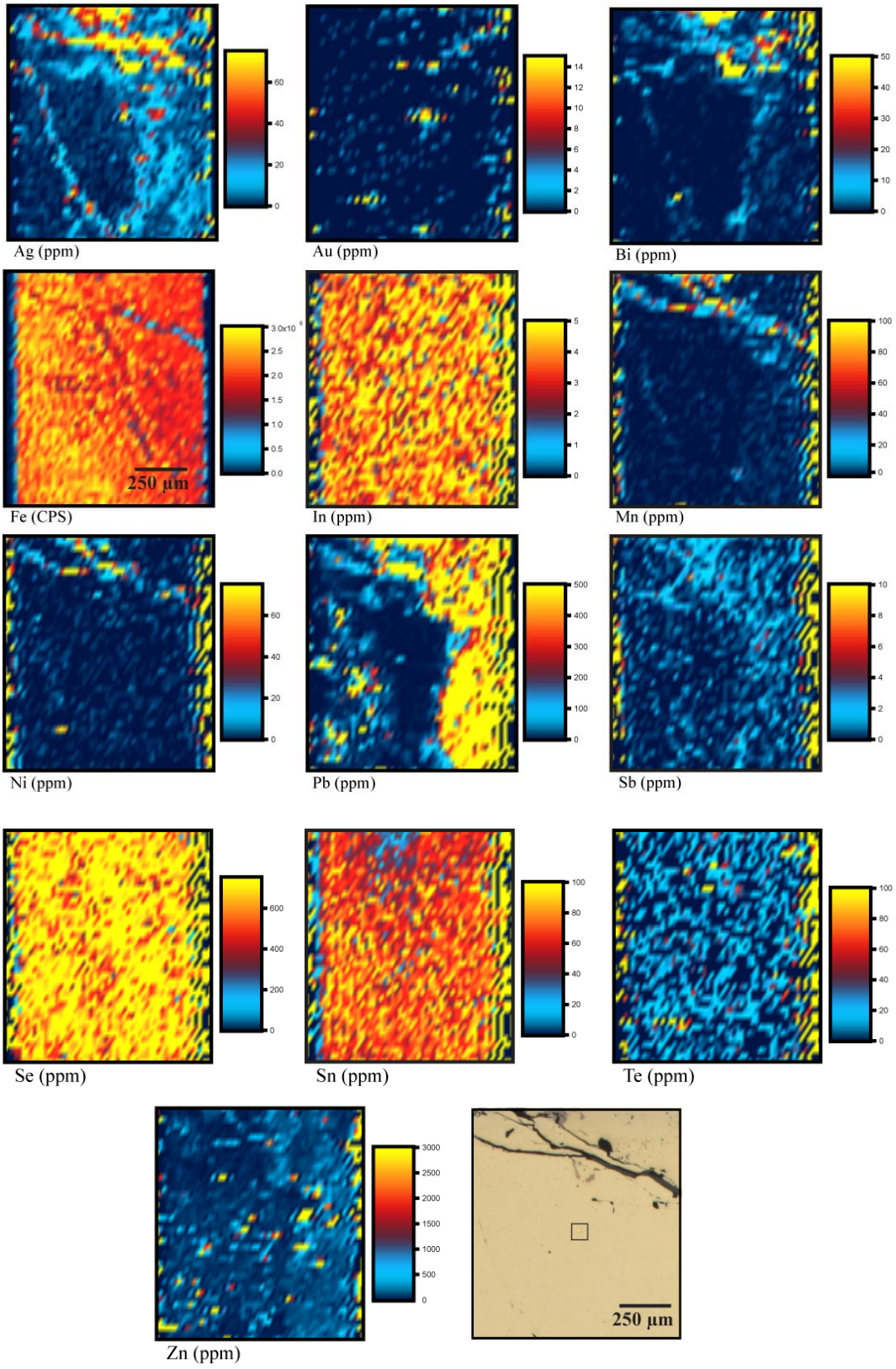
Ag (ppm)
Au (ppm)
Bi (ppm)
Fe (CPS)
250 µm
In (ppm)
Mn (ppm)
Ni (ppm)
Pb (ppm)
Sb (ppm)
Se (ppm)
Sn (ppm)
Te (ppm)
Zn (ppm)
250 µm

D

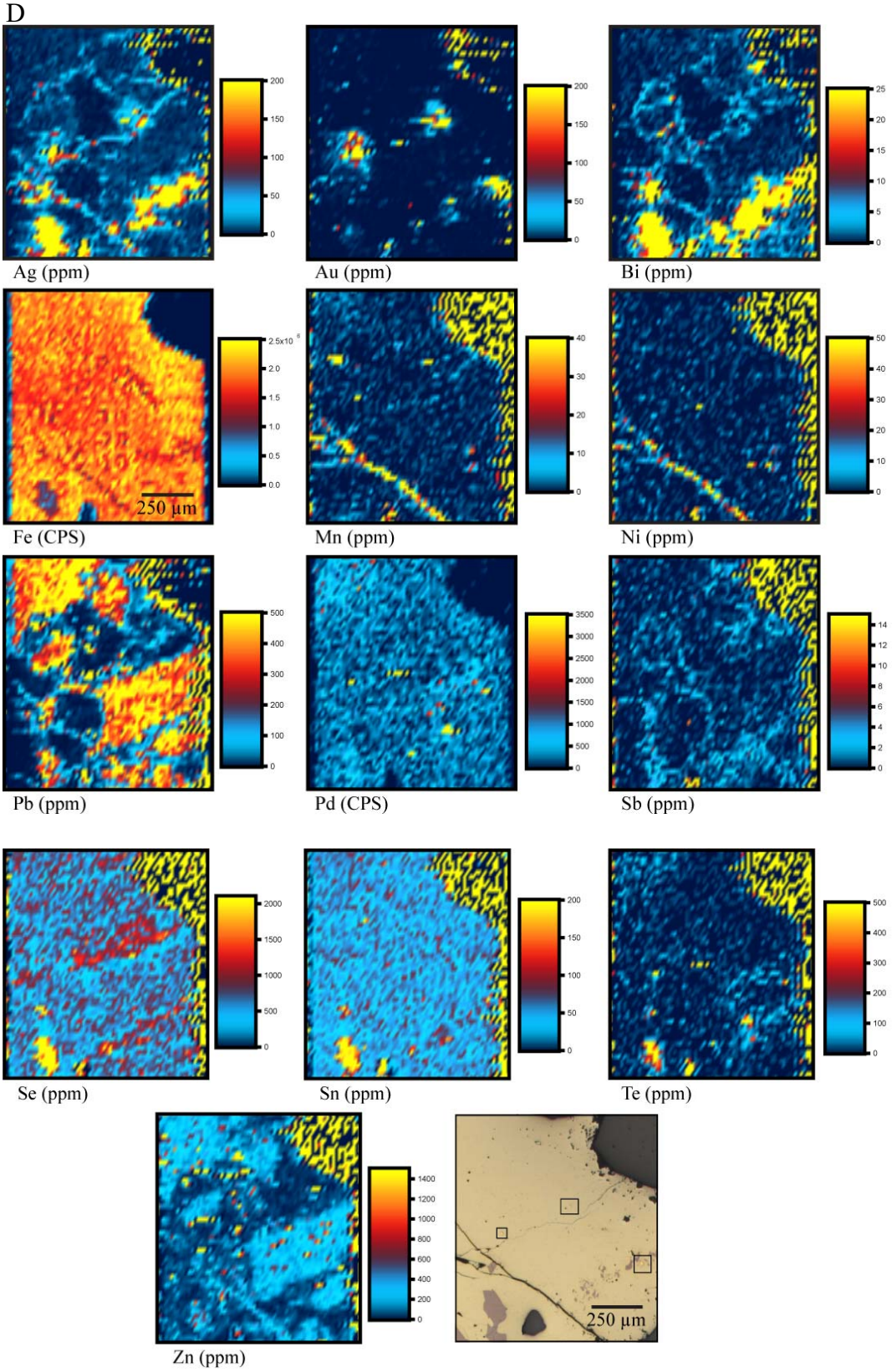
Ag (ppm)
Au (ppm)
Bi (ppm)
Fe (CPS)
250 µm
Mn (ppm)
Ni (ppm)
Pb (ppm)
Pd (CPS)
Sb (ppm)
Se (ppm)
Sn (ppm)
Te (ppm)
Zn (ppm)
250 µm

Figure 4.10 Trace Elemental Maps of Gold Grains and Cu-Fe Sulfides

LA-ICP-MS trace element maps of (a) chalcopyrite-standardized data and (b) bornite standardized data, such that chalcopyrite crystals within the chalcopyrite standardized data show accurate elemental concentrations, but chalcopyrite regions within bornite standardized data do not show accurate data. (c) Raster of single gold grain and (d) three gold grains in GRS37-170-742.2 chalcopyrite vein. In general, warmer colors indicate higher concentrations and cooler colors indicate lower concentrations.

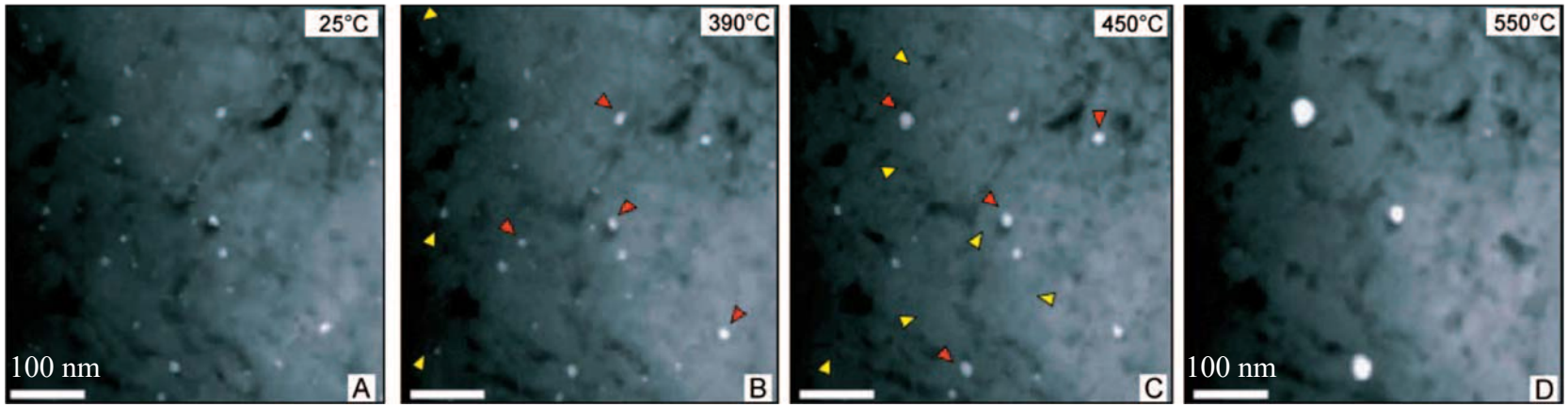

Figure 4.11 Ostwald Ripening of Au Nanoparticles in Arsenian Pyrite

High-angle annular dark field scanning transmission electron microscopy (HAADF-STEM) images of Carlin-type arsenian pyrite with Au nanoparticles. (a) 25°C starting size and shape of Au nanoparticles (b) 390°C shows smallest nanoparticles dissolving and larger particles growing in size (c) 450°C smaller particles are still decreasing in size, while larger particles are growing at the expense of the smaller particles (d) 550°C where only 3 large (>20 nm) Au nanoparticles remain. Red arrows show coarsening particles. Yellow arrows show diminishing particles. From Reich et al. (2006).

Table 4.16 Trace Element Concentrations (Mean) in Vein and Matrix Chalcopyrite

Cp Type	Mn (ppm)	Ni (ppm)	Zn (ppm)	As (ppm)	Se (ppm)	Mo (ppm)	Ag (ppm)	In (ppm)	Sn (ppm)	Sb (ppm)	Te (ppm)	Au (ppm)	Pb (ppm)	Bi (ppm)
Vein	3.63	0.08	639.92	0.58	485.33	0.04	12.05	3.34	34.29	0.17	12.22	16.58	159.14	8.40
Matrix	261.92	18.54	120.29	4.11	267.70	0.16	10.13	2.50	9.79	0.23	30.92	0.17	217.96	42.18

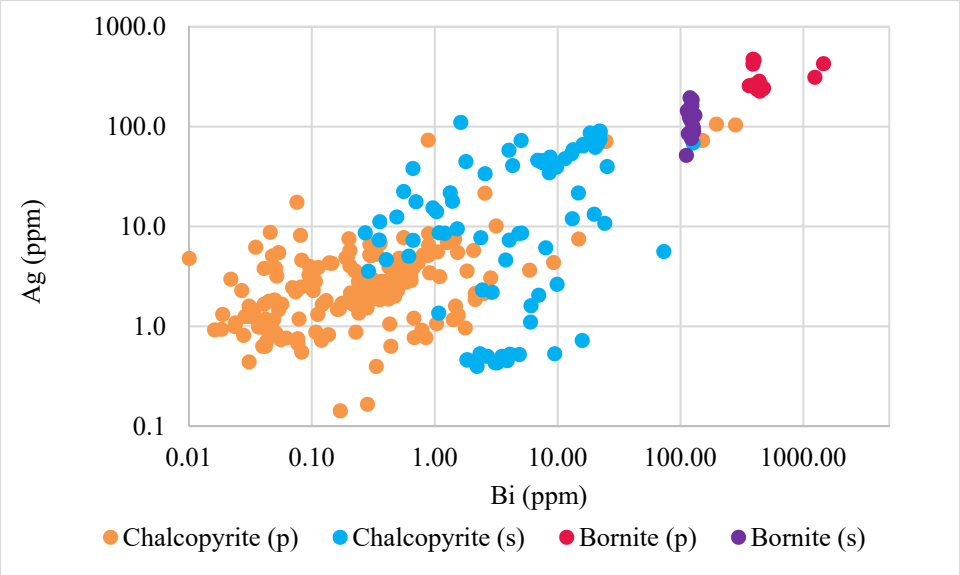
1000.0
100.0
10.0
1.0
0.1
Ag (ppm)
0.01
0.10
1.00
10.00
100.00
1000.00
Bi (ppm)
Chalcopyrite (p)
Chalcopyrite (s)
Bornite (p)
Bornite (s)

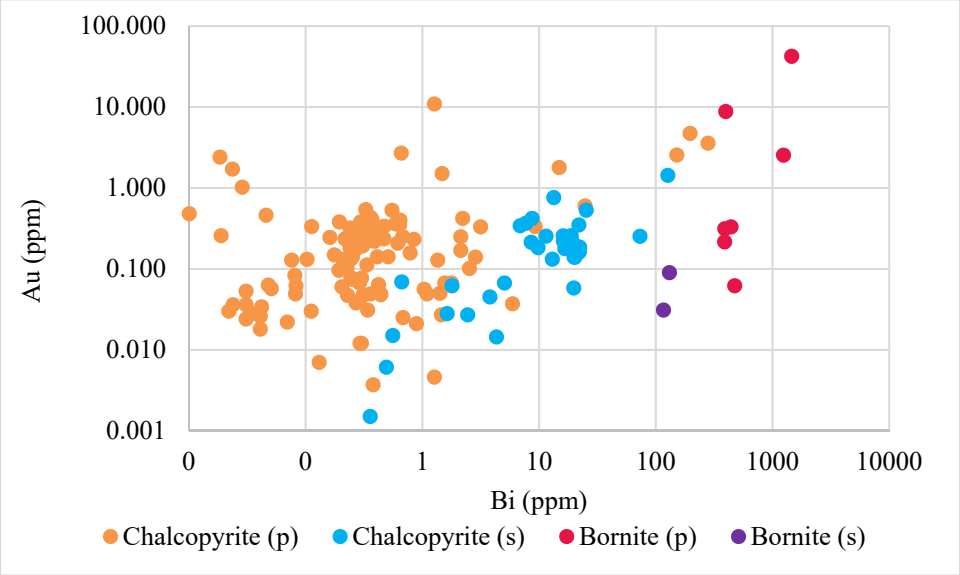
100.000
10.000
1.000
0.100
0.010
0.001
Au (ppm)
0
0
1
10
100
1000
10000
Bi (ppm)
Chalcopyrite (p)
Chalcopyrite (s)
Bornite (p)
Bornite (s)

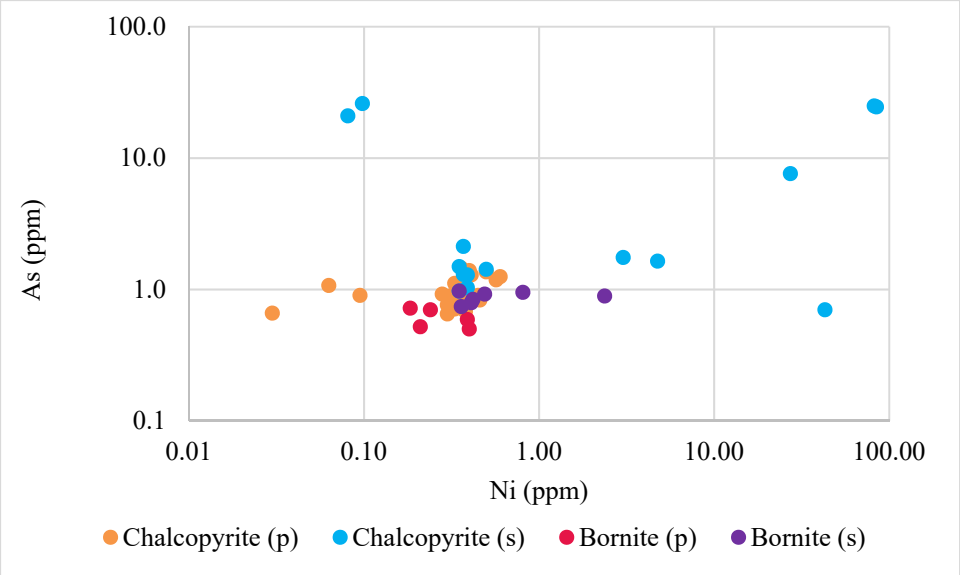

Figure 4.12 Trace Elemental Correlations for All Data

Log-log elemental correlations for element pairs where r>0.5 (Table 4.15). “S” and “p” represent skarn and porphyry samples. Each point represents a single spot measurement (Appendix C).

Chapter 5: Conclusions

5.1 Introduction

The main conclusions of this study are:

1. The EGD samples analyzed for this study did not provide evidence for a volumetric correlation between gold grains and potential "drainage regions" as postulated. Our data do not support, but also do not preclude the possibility that enlargement of gold grains occurs via diffusion from dispersed gold in a volume of high-temperature Cu-Fe sulfides.

2. There is evidence of a possible gold enrichment halo surrounding gold grains in chalcopyrite veins. This suggests that a hybrid mechanism of gold diffusion in concert with Ostwald ripening could be operating within the Cu-Fe sulfides at high-temperature to form μm-scale gold grains with gold enrichment haloes in the surrounding sulfide.

3. Bi and Ag are preferentially partitioned into bornite over chalcopyrite. However, Bi and Ag (and Au) display a positive correlation throughout Cu-Fe sulfide and deposit types. Bi could potentially be used as a tracer of precious metals, Au and Ag, in porphyry-skarn systems.

5.2 Volumetric Correlations

We found no correlation between the volume of a specific gold grain and its associated modified Voronoi volume. Carlson (1991, 1992) studies suggest that we might see a positive correlation between modified Voronoi diffusional drainage regions of Cu-Fe sulfide and gold grain volumes. However, none of the measured correlations exceed the

critical values of a two-tailed t-test at a 95% confidence interval. In many cases, statistically insignificant correlations were likely due to the paucity of high-confidence gold grains in our samples. Because of the limited number of gold grains, many modified Voronoi regions intersected the physical edge of the core sample, and were artificially truncated, making the actual volume of the region ambiguous. Thus, correlations between gold grains and these volumes would not be accurate.

The complexity of the physical ore system was difficult to represent within the HRXCT volumetric analyses, which led to various limitations in the model's applicability. One such limitation is that the modified Voronoi analyses assumed all of the gold in an individual gold grain came from within the diffusional drainage area calculated by the modified Voronoi method. However, native gold grains could have been formed in part by different mechanisms, where the seed of the grain was precipitated directly out of hydrothermal fluids, and then exsolved gold from the sulfides accumulated on the existing seed grain. Under these conditions, the total volume of the grain would not represent the volume of gold exsolved from the Cu-Fe sulfides. Although the analyses assumed homogeneity, gold was probably distributed heterogeneously through the sulfide network. If gold was heterogeneously distributed, portions of Cu-Fe sulfide would have more gold to exsolve to form grains.

Carlson (1991, 1992) posited that nutrient transport is the rate-limiting factor for crystal growth, which would result in the nutrient depleted region around a crystal (although the rate-limiting process could instead be the grain-boundary reaction which would result in potentially different textures). Because there are no specific constraints on gold movement within a Cu-Fe sulfide, gold could potentially exsolve from the sulfides, and move, instead of to the closest gold grain, along the easiest pathway (e.g., grain

boundaries, microfractures, etc.). This could result in gold accumulation on a grain that was not necessarily the closest grain to the Cu-Fe sulfide region which originally exsolved the gold, thus there would be no correlation between their volumes. Our data neither support nor preclude the presence of any correlation between gold grain volume and drainage region volume, and we can neither confirm nor refute that an appreciable volume of gold could be exsolved from Cu-Fe sulfides during cooling, and form gold grains on crystal boundaries.

5.3 "ENRICHMENT HALO"

Understanding gold grain formation dynamics could assist in understanding the processes which lead to gold enrichment within certain hydrothermal systems. LA-ICP-MS data in this study indicate the possible presence of an "enrichment halo" surrounding gold inclusions within chalcopyrite (Figures 4.4, 4.10C, D). These "enrichment haloes" are defined as an area within the chalcopyrite (from grain-adjacent to ~500 μm from the gold grain) that contains elevated gold contents (~0.1 to 1 or 10 ppms) compared to the surrounding Cu-Fe sulfide (~0.01 to 0.1 ppms) (Table 4.2). Carlson (1991, 1992) found that nutrient diffusion through the surrounding matrix was the limiting process during garnet porphyroblast growth, resulting in a nutrient depleted halo around the porphyroblast. Based on this, our study hypothesized that gold exsolution from Cu-Fe sulfides would yield an area of gold depletion within the sulfide matrix surrounding gold grains, where most of lattice-bound gold had been scavenged. Our data have some inconsistencies with this model, where instead of proximal nutrient depletion, line-of-spot scans and 2D maps show proximal gold enrichment. We postulate that gold grain growth could be due to a hybrid mechanism.

Ostwald ripening is driven by surface energy minimization, where in a solid solution, small particles dissolve and redeposit onto larger particles (Ostwald, 1896). Reich et al. (2006) suggest that "melting" or dissolution of smaller gold nanoparticles in arsenian pyrite at high-temperatures allows for the coarsening of other, larger gold particles through Ostwald ripening (Figure 4.11). Based on the presence of "enrichment haloes" around gold grains, we propose that gold inclusions in EGD chalcopyrite could be formed by the gradual coarsening of large gold nanoparticles at the expense of smaller nanoparticles. Gradient-driven diffusion may be responsible for gold diffusion through the Cu-Fe sulfide matrix, either as Au atoms or nanoparticles, which could yield the observed "patchiness" of gold concentrations within our Cu-Fe sulfides. If Au nanoparticles occur in a cluster, Ostwald ripening could redistribute the gold from small nanoparticles to larger nanoparticles, to reduce surface energy. In turn, diffusion of gold within the sulfide matrix may continue to supply gold to the small Au nanoparticles that are losing gold to the larger, central Au particle.

Although this hypothesis suggests that there could be an area around the gold grain that is enriched in gold, it does not prevent the possibility of there still being an area further-afield of the gold grain which is depleted in gold. Our analyses covered mere millimeters around the gold grains, which may not have been a large enough area to determine the presence of an enriched zone, a depleted zone, and a potential "normal" zone of gold within Cu-Fe sulfides. Future studies could be done to determine the presence of gold nanoparticles within chalcopyrite and further this conclusion.

5.4 Bi as a Precious Metal Tracer

Chalcophile elements As, Sb, and Bi have long been used as "pathfinder" elements for gold-rich deposits (Boyle, 1979). Of those elements, Bi has frequently been considered

slightly less universal in its applications as a tracer element for exploration purposes, as it is typically less abundant in hypogene deposits, typically occurring in the <5 ppm range (Boyle, 1979). However, Cook et al. (2011) data show highly elevated (100s -1000s ppm) Bi contents across a range of deposit types including metamorphic vein systems and magmatic-hydrothermal systems (e.g., porphyry, skarn, and epithermal). Their study concluded that bornite was an excellent host for Ag and Bi, regardless of the presence of discrete Ag or Bi mineral phases, suggesting that Ag and Bi are structurally bound within the bornite.

Our data indicate a similar affinity of bornite for Bi (mean ~315 ppm, n= 40 spots) and Ag (mean ~272 ppm, n=40) (not including single analyses in GRS37-184-7.8 and GRS37-170-742.2) (Table 4.3). We also did not record the presence of discrete Ag or Bi mineral inclusions within our samples, based on the lack of any anomalously high measurements within the majority of the Cu-Fe sulfide data (except for matrix analyses in GRS37-184 and 170, which warrants further analysis). EGD chalcopyrite samples in our study also contain Bi and Ag, but at significantly lower amounts (Bi: mean ~ 5 ppm, n=278; Ag: mean~ 14 ppm, n=283) (Table 4.5). However, the entire dataset, including both bornite and chalcopyrite measurements, displays a strong, positive correlation between Ag and Bi (r= 0.86). Although not noted by Cook et al. (2011) in their samples, our data display a moderate but consistent, positive correlation between Bi and Au (r= 0.54) (Tables 4.3, 4.5, 4.9, and 4.12). The data do not indicate any remarkable, positive correlations between Au and As or Sb, suggesting that Bi may serve as a viable and perhaps preferable trace element for precious metals exploration in porphyry-skarn systems.

Appendix A: Samples

Assay values available for this sample suite for Cu, Au, and Ag were provided by PT Freeport Indonesia. Assays used in this study were performed on sampled retrieved from diamond drill core. Assay intervals were 3m.

Sample	From (m)	To (m)	Elevation	Cu (wt %)	Au (ppm)	Ag (ppm)
GRS37-170-645.9	645	648	3158	3.04	8.25	4.10
GRS37-170-714.2	714	717	3092	3.00	4.10	10.40
GRS37-170-742.2	741	744	3063	3.52	5.67	13.10
GRS37-184-7.8	6	9	3797	3.19	6.57	5.50
TE01-16-566	565	568	2353	0.45	0.45	2.30
TE14-01-754.3	752	754.9	2793	1.25	1.02	1.25

GRS14-OP1

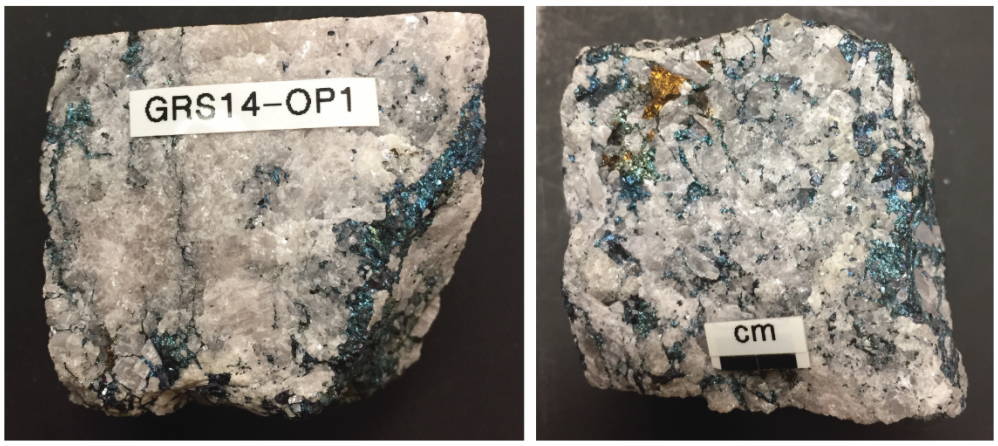

GRS97-9

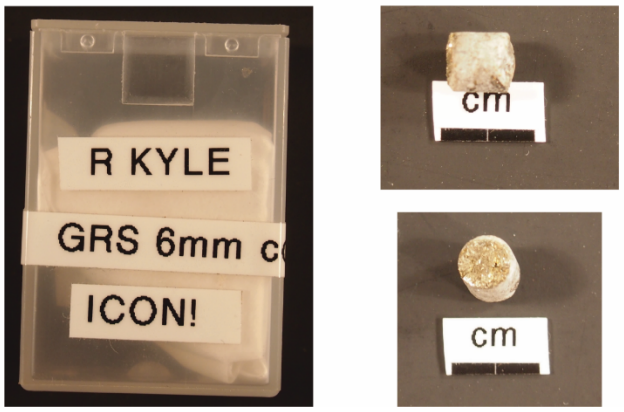

AH90-4

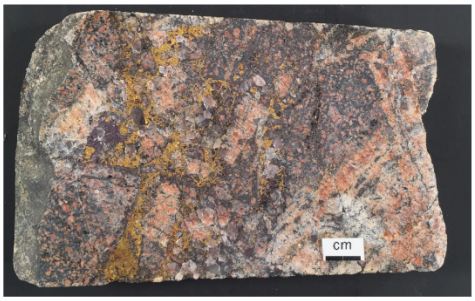
cm

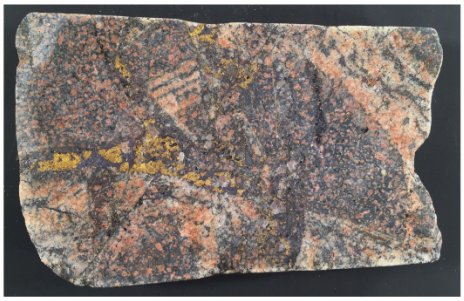

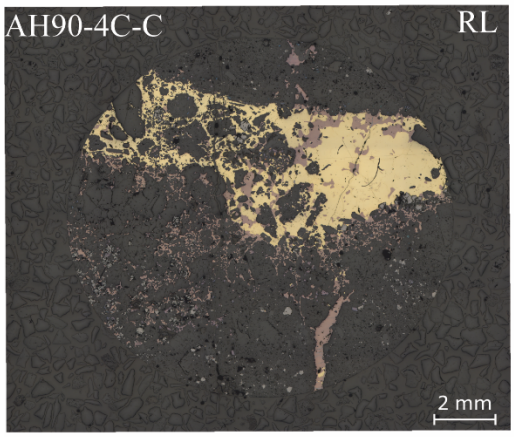
AH90-4C-C
RL
2 mm

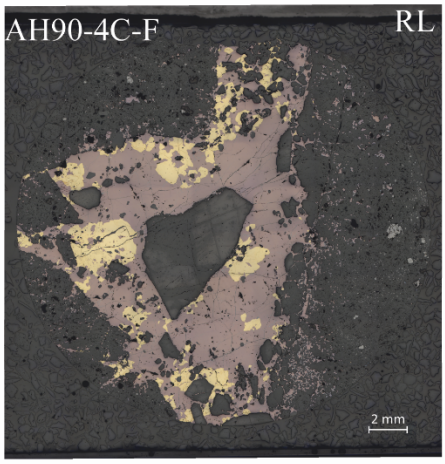
AH90-4C-F
RL
2 mm

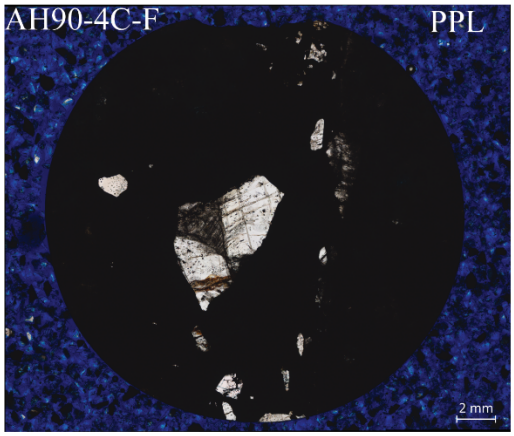
AH90-4C-F
PPL
2 mm

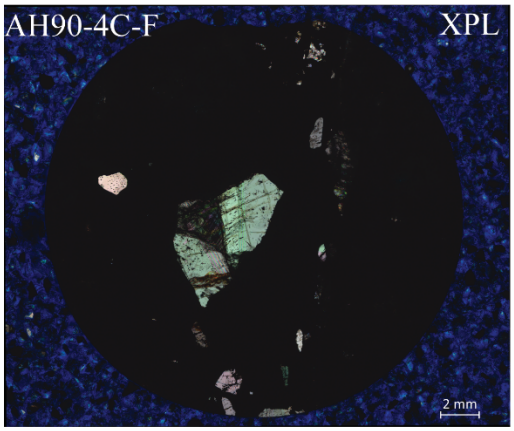
AH90-4C-F
XPL
2 mm

GRS37-170-645.9

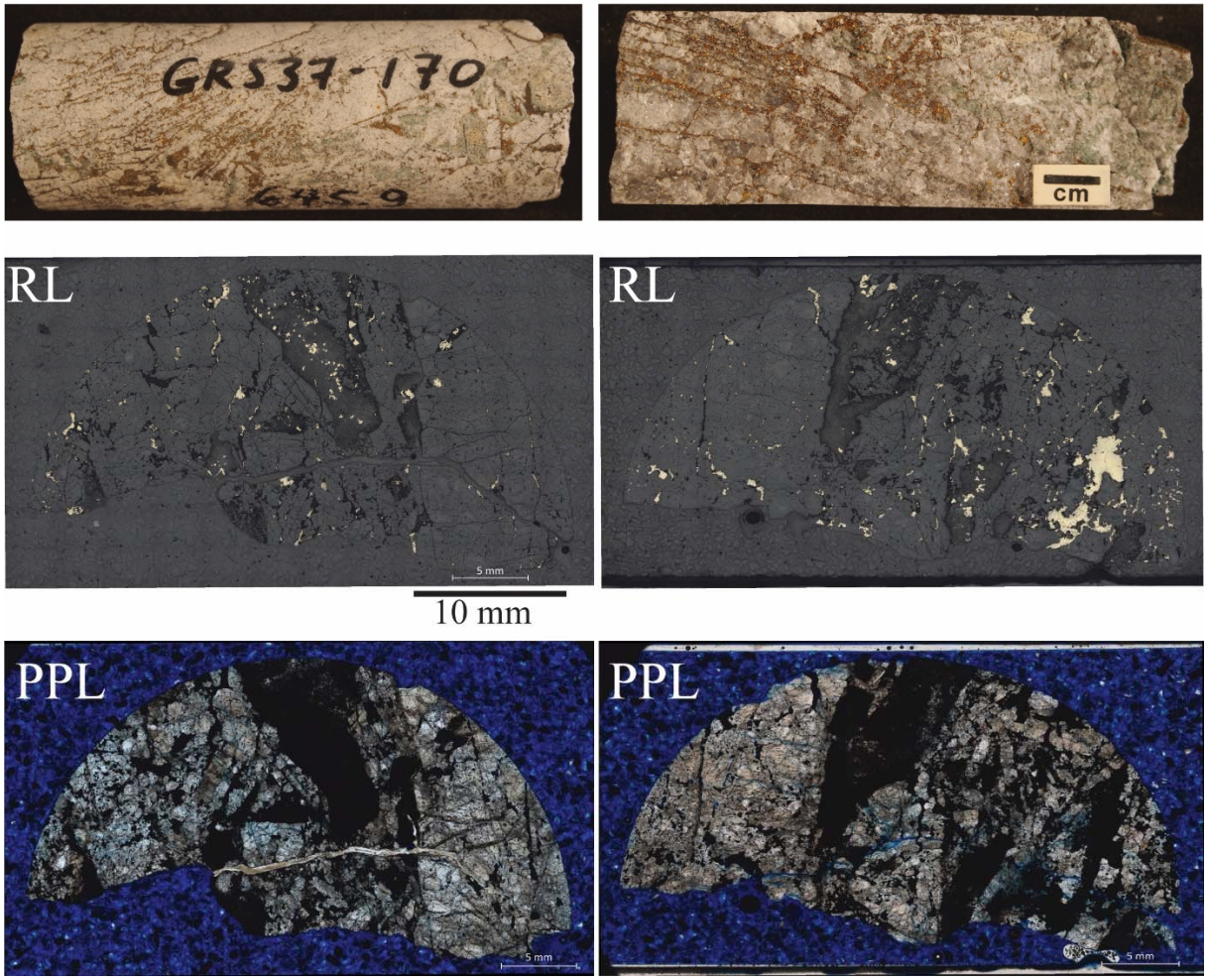

GRS37-170-714.2

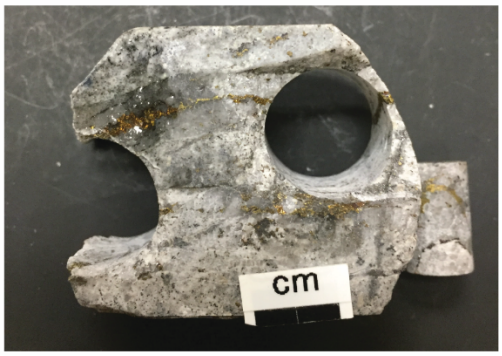

Section A

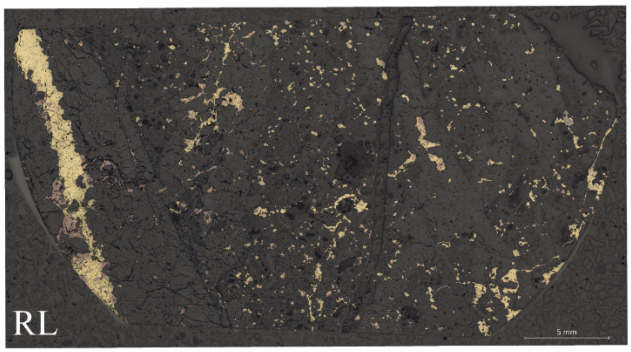

10 mm

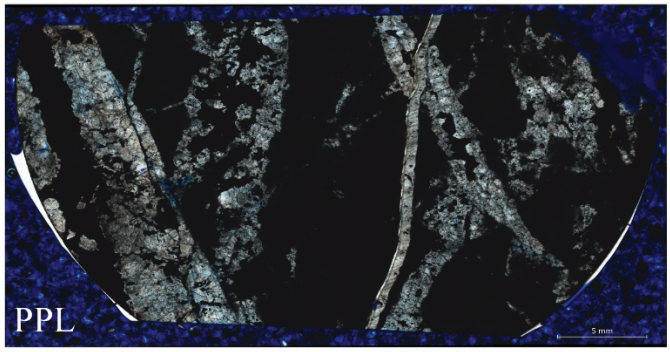

Section B

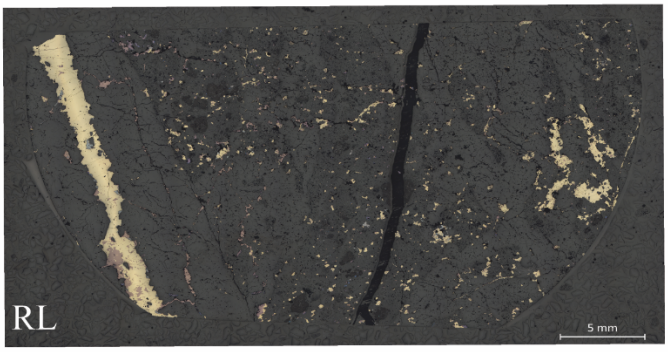

GRS37-170-742.2

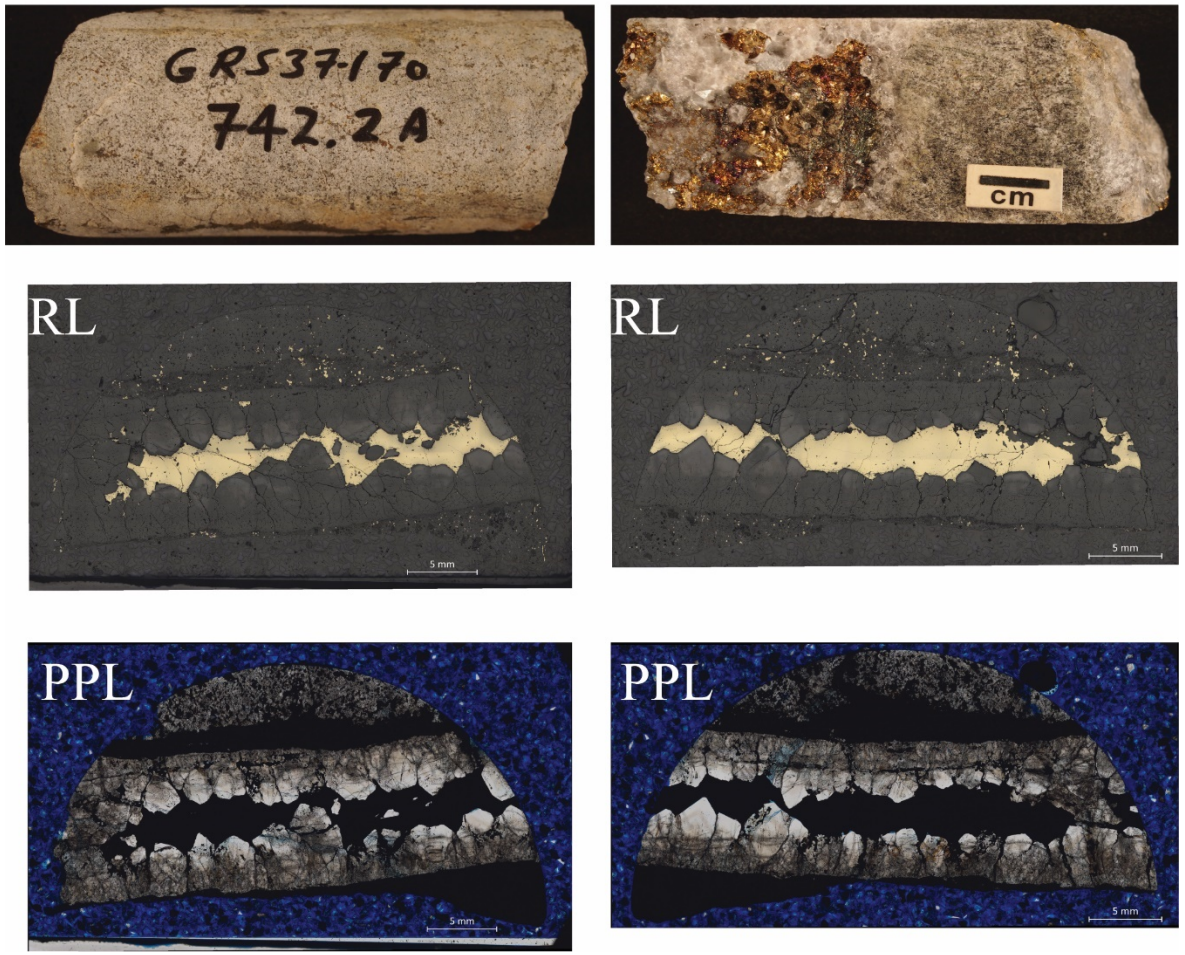

GRS37-184-7.8A+B

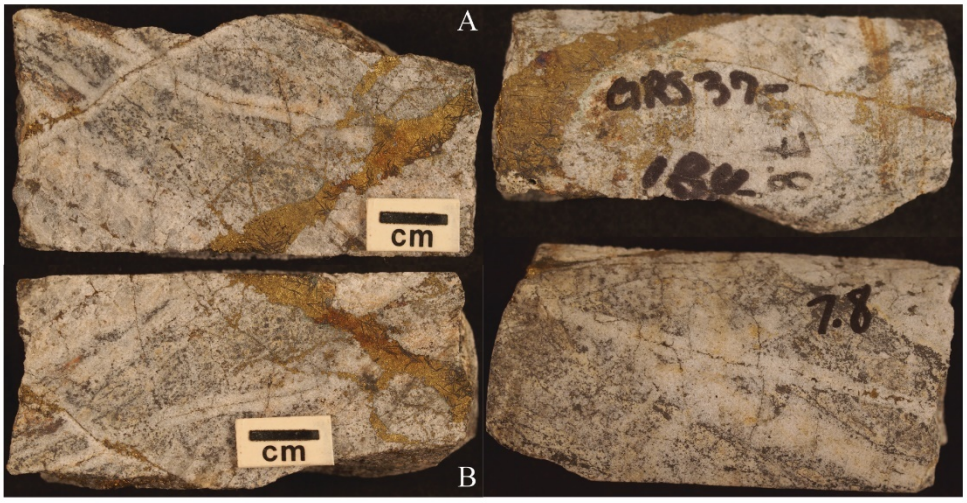

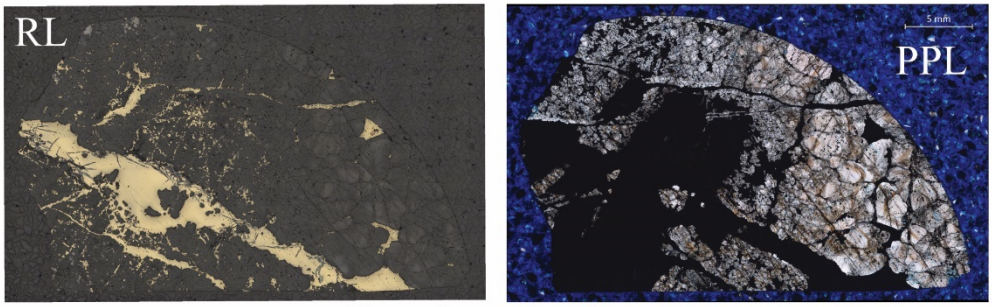

Section A-A

10 mm

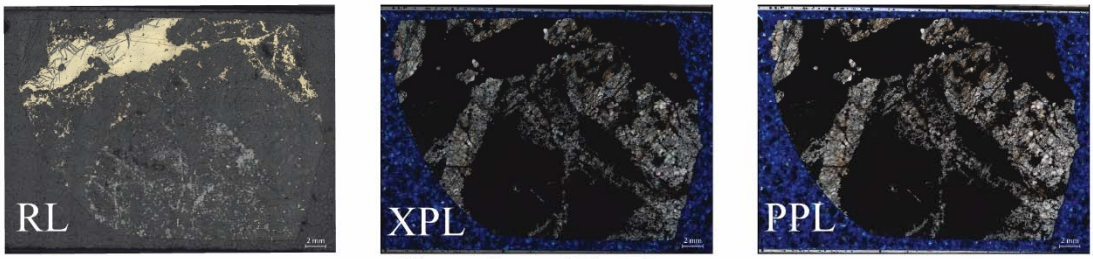

Section B-B

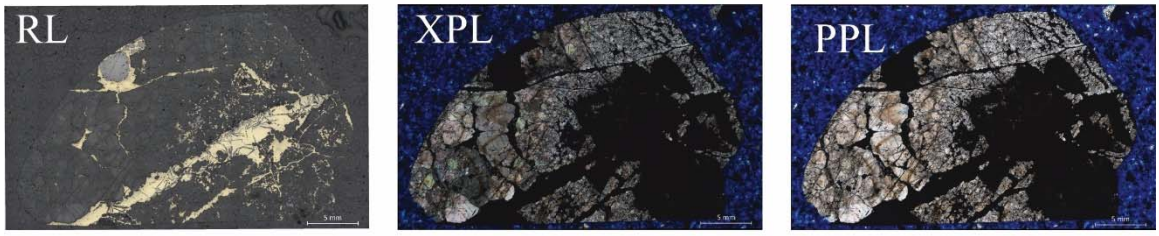

Section A-B

DOZ-90-29

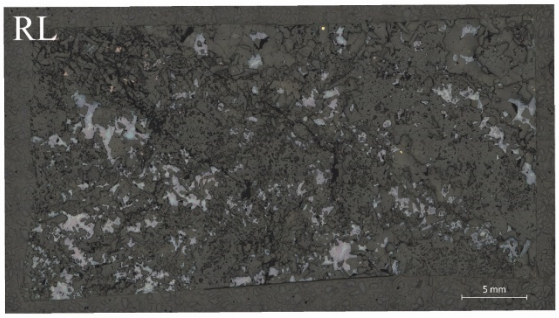

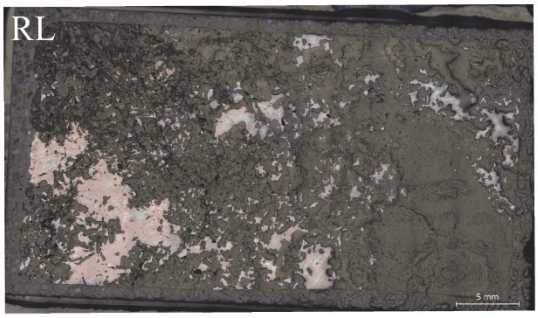

10 mm

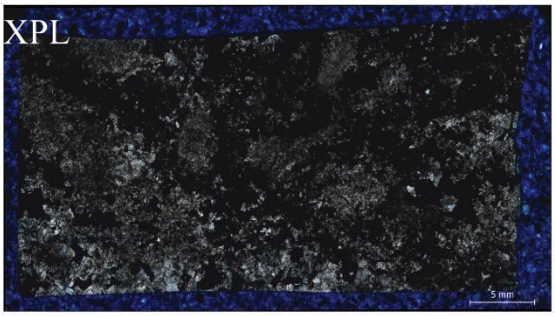

TE14-01-754.3

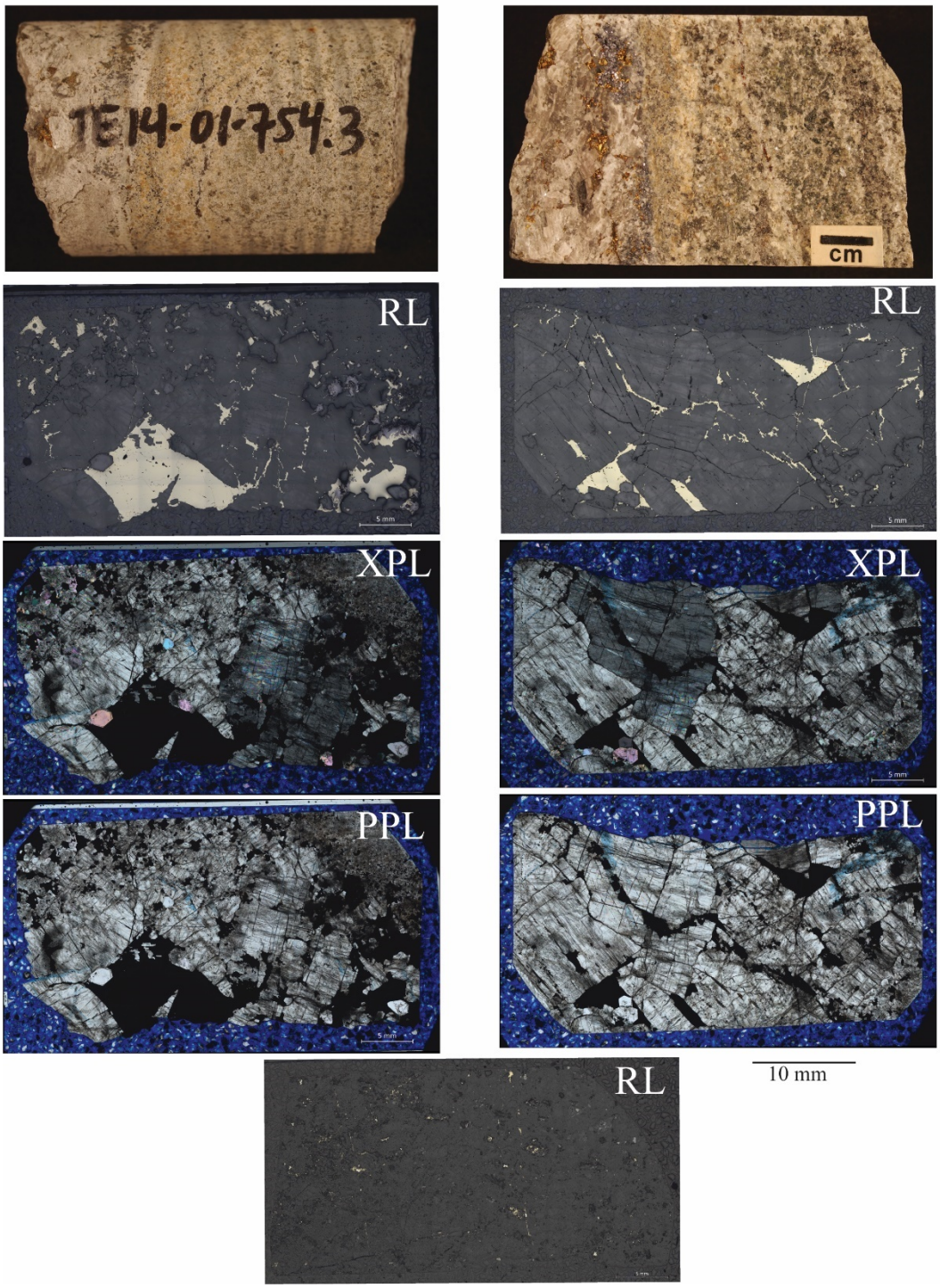

TE01-16-566

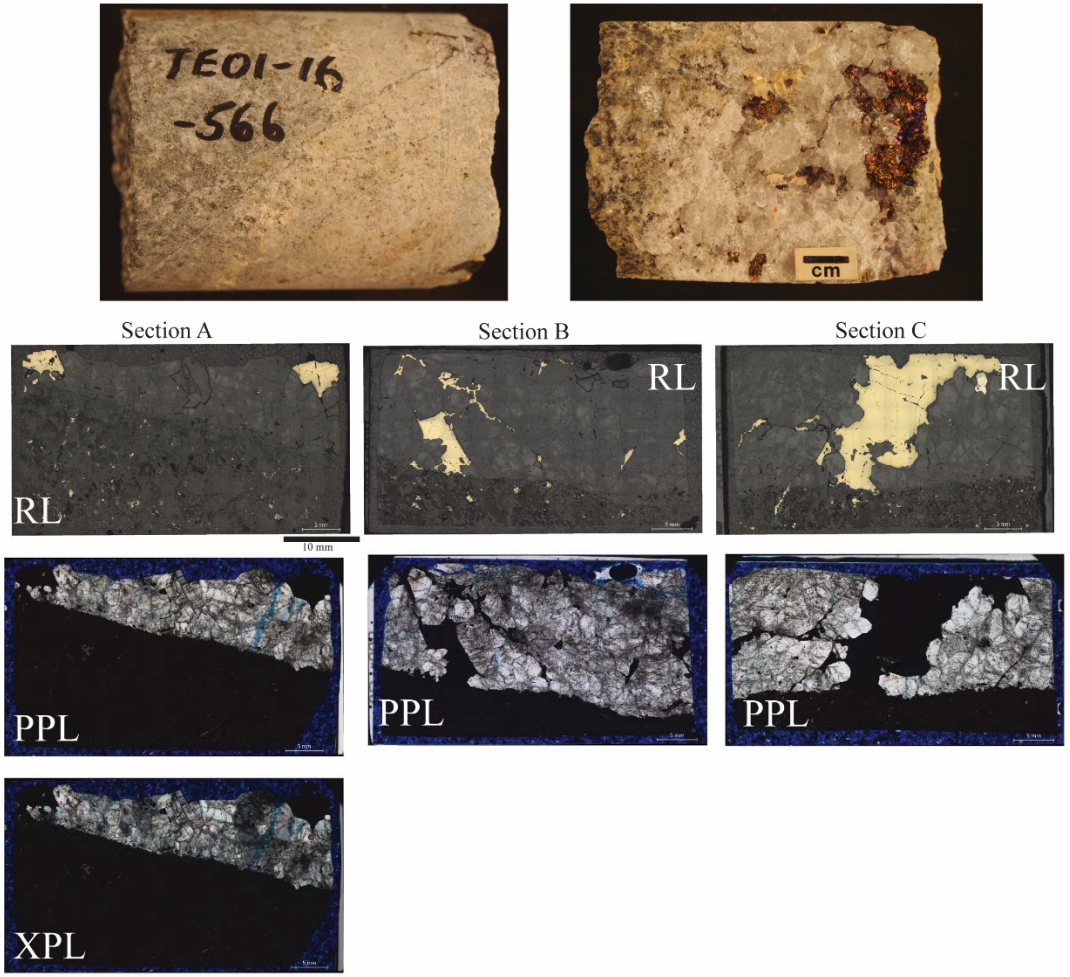
TE01-16
-566
cm
Section A
Section B
Section C
RL
RL
RL
10 mm
PPL
PPL
PPL
XPL

Appendix B: HRXCT Data

	Unique #	Sample	PVE (mm^3)	Volume (mm^3)	Voronoi (mm^3)	Max GS	Local Bkg GS	Type of Seg/Sep	Cu-Fe-S	Location	Aspect Ratio	Rad1	Rad2	Rad3
1	146602133	AH90-4C-C	0.0014	0.0040	281.46	245	30.24	strict	bn	edge	1.48	0.130	0.104	0.088
2	265714908	AH90-4C-C	0.0007	0.0022	222.43	248	20.79	strict	bn	edge	1.44	0.101	0.087	0.070
3	278653010	AH90-4C-C	0.0006	0.0029	11.81	235	35.42	strict	bn	edge	2.14	0.163	0.078	0.076
4	45010752	AH90-4C-C	0.0001	0.0002	0.11	187	16.97	generous	cp	edge	1.39	0.046	0.043	0.033
5	113597340	AH90-4C-C	0.0029	0.0126	44.70	209	21.50	generous	cp	edge	1.80	0.234	0.165	0.130
6	124356805	AH90-4C-C	0.0000	0.0002	200.06	130	17.10	generous	cp	edge	1.24	0.038	0.035	0.031
7	145709034	AH90-4C-C	0.0019	0.0061	101.66	245	18.60	generous	bn	edge	1.88	0.188	0.139	0.100
8	265714908	AH90-4C-C	0.0008	0.0024	157.59	248	19.44	generous	bn	edge	1.37	0.102	0.087	0.074
9	277761909	AH90-4C-C	0.0012	0.0056	11.69	235	21.24	generous	bn	edge	1.53	0.150	0.135	0.098
10	11983687	AH90-4C-F	0.0012	0.0032	113.67	235	28.84	strict	both	edge	2.04	0.161	0.125	0.079
11	126349638	AH90-4C-F	0.0002	0.0004	292.21	208	29.15	strict	bn	edge	2.06	0.078	0.050	0.038
12	133792535	AH90-4C-F	0.0002	0.0005	591.09	199	23.82	strict	bn	edge	1.87	0.071	0.053	0.038
13	140303625	AH90-4C-F	0.0002	0.0005	347.03	224	26.75	strict	cp	edge	1.76	0.075	0.044	0.042
14	300134088	AH90-4C-F	0.0004	0.0013	185.97	193	37.37	strict	both	edge	2.36	0.103	0.083	0.044
15	307596397	AH90-4C-F	0.0005	0.0014	85.24	224	30.86	strict	both	edge	2.51	0.110	0.088	0.044
16	11051503	AH90-4C-F	0.0016	0.0061	59.92	235	17.31	generous	bn	edge	1.87	0.182	0.149	0.097
17	40280097	AH90-4C-F	0.0000	0.0003	56.03	89	17.86	generous	bn	edge	1.54	0.056	0.045	0.036
18	126349637	AH90-4C-F	0.0011	0.0057	75.40	208	17.02	generous	bn	edge	7.05	0.361	0.111	0.051
19	130346533	AH90-4C-F	0.0001	0.0003	164.24	137	16.71	generous	bn	edge	1.37	0.051	0.045	0.037
20	132860351	AH90-4C-F	0.0002	0.0009	264.08	199	16.18	generous	bn	edge	1.89	0.085	0.059	0.045
21	140302658	AH90-4C-F	0.0003	0.0011	217.55	224	15.89	generous	cp	edge	1.56	0.085	0.068	0.054
22	190786478	AH90-4C-F	0.0003	0.0025	134.10	128	18.95	generous	both	edge	1.72	0.136	0.097	0.079
23	199538241	AH90-4C-F	0.0001	0.0008	35.88	137	16.12	generous	bn	edge	1.65	0.076	0.065	0.046
24	287066083	AH90-4C-F	0.0042	0.0208	193.60	224	19.14	generous	cp	edge	2.57	0.393	0.241	0.152
25	429749663	AH90-4C-F	0.0005	0.0025	37.11	235	16.78	generous	bn	edge	2.39	0.164	0.073	0.069
26	443681265	AH90-4C-F	0.0003	0.0021	184.22	104	17.68	generous	bn	edge	3.46	0.144	0.127	0.042
27	456163846	AH90-4C-F	0.0002	0.0008	38.36	184	16.26	generous	bn	edge	2.24	0.104	0.052	0.047
28	456623456	AH90-4C-F	0.0002	0.0012	154.75	135	18.33	generous	bn	edge	1.75	0.101	0.065	0.058
29	506446590	AH90-4C-F	0.0001	0.0004	0.01	186	14.83	generous	bn	edge	1.31	0.054	0.047	0.041
30	109220025	DOZ-90K-29	0.0000	0.0003	4.55	88	33.03	generous	bn	edge	1.35	0.046	0.043	0.034
31	163745408	DOZ-90K-29	0.0001	0.0004	35.08	94	33.04	generous	bn	edge	1.38	0.056	0.050	0.041
32	190286063	DOZ-90K-29	0.0001	0.0003	29.09	94	32.03	generous	bn	edge	1.30	0.050	0.043	0.038
33	191523010	DOZ-90K-29	0.0000	0.0003	53.14	85	32.68	generous	bn	edge	1.38	0.052	0.042	0.038
34	204489145	DOZ-90K-29	0.0000	0.0003	5.14	99	30.59	generous	bn	edge	1.36	0.051	0.042	0.037
35	208175102	DOZ-90K-29	0.0000	0.0003	93.72	82	33.54	generous	bn	edge	2.07	0.065	0.043	0.031
36	327458605	DOZ-90K-29	0.0000	0.0002	119.32	82	32.28	generous	bn	edge	1.38	0.045	0.040	0.033
37	383233973	DOZ-90K-29	0.0001	0.0007	87.35	94	33.68	generous	bn	edge	2.35	0.089	0.057	0.038
38	432929849	DOZ-90K-29	0.0001	0.0004	102.14	94	30.91	generous	bn	edge	1.36	0.054	0.047	0.040
39	437310125	DOZ-90K-29	0.0002	0.0010	61.31	161	29.56	generous	bn	edge	2.60	0.128	0.053	0.049

40	522485714	DOZ-90K-29	0.0001	0.0007	87.30	96	33.86	generous	bn	edge	1.66	0.077	0.051	0.046
41	584740186	DOZ-90K-29	0.0001	0.0004	103.00	86	34.94	generous	bn	edge	2.24	0.076	0.044	0.034
42	598534955	DOZ-90K-29	0.0008	0.0032	41.10	231	33.45	generous	bn	edge	2.05	0.139	0.099	0.068
43	598541597	DOZ-90K-29	0.0003	0.0014	0.58	143	29.88	generous	bn	edge	1.94	0.098	0.081	0.050
44	712947894	DOZ-90K-29	0.0001	0.0004	220.88	91	31.58	generous	bn	edge	1.49	0.056	0.047	0.037
45	757554563	DOZ-90K-29	0.0002	0.0016	166.88	97	34.90	generous	bn	edge	2.15	0.099	0.095	0.046
46	912221158	DOZ-90K-29	0.0000	0.0004	186.50	83	32.64	generous	bn	edge	1.42	0.053	0.049	0.038
47	1.109E+09	DOZ-90K-29	0.0001	0.0005	11.22	108	30.87	generous	bn	edge	1.46	0.059	0.049	0.040
48	1.166E+09	DOZ-90K-29	0.0000	0.0003	273.15	92	31.82	generous	bn	edge	1.49	0.054	0.046	0.036
49	1.185E+09	DOZ-90K-29	0.0000	0.0004	79.93	89	36.20	generous	bn	edge	1.49	0.056	0.049	0.038
50	1.2E+09	DOZ-90K-29	0.0000	0.0002	236.16	84	33.63	generous	bn	edge	1.64	0.048	0.032	0.029
51	1.247E+09	DOZ-90K-29	0.0000	0.0002	30.05	92	30.91	generous	bn	edge	1.28	0.043	0.042	0.034
52	1.259E+09	DOZ-90K-29	0.0000	0.0003	14.46	89	31.61	generous	bn	edge	1.65	0.051	0.042	0.031
53	1.265E+09	DOZ-90K-29	0.0000	0.0003	20.85	85	30.23	generous	bn	edge	1.58	0.053	0.044	0.034
54	1.269E+09	DOZ-90K-29	0.0000	0.0002	205.53	84	32.87	generous	bn	edge	1.20	0.043	0.038	0.035
55	1.286E+09	DOZ-90K-29	0.0001	0.0004	0.45	106	28.17	generous	bn	matrix	1.47	0.056	0.051	0.038
56	1.322E+09	DOZ-90K-29	0.0002	0.0009	37.34	174	29.32	generous	bn	edge	1.39	0.074	0.060	0.053
57	1.362E+09	DOZ-90K-29	0.0001	0.0006	4.28	118	32.97	generous	bn	matrix	1.75	0.077	0.050	0.044
58	1.369E+09	DOZ-90K-29	0.0001	0.0006	28.82	130	30.78	generous	bn	edge	1.48	0.066	0.054	0.044
59	1.405E+09	DOZ-90K-29	0.0004	0.0016	22.11	158	31.79	generous	bn	edge	1.82	0.094	0.084	0.052
60	1.451E+09	DOZ-90K-29	0.0001	0.0003	130.54	94	32.26	generous	bn	edge	1.47	0.057	0.039	0.039
61	1.523E+09	DOZ-90K-29	0.0001	0.0005	0.13	151	29.71	generous	bn	matrix	1.32	0.057	0.051	0.043
62	1.537E+09	DOZ-90K-29	0.0001	0.0006	0.00	124	29.38	generous	bn	matrix	1.48	0.067	0.054	0.045
63	598534955	DOZ-90K-29	0.0004	0.0012	2491.92	231	42.67	strict	bn	edge	1.19	0.073	0.069	0.061
64	47940378	GRS37-170-645.9	0.0002	0.0012	581.41	75	29.26	generous	cp	inclusion	1.27	0.075	0.071	0.059
65	52475210	GRS37-170-645.9	0.0002	0.0011	17.06	66	30.68	generous	cp	inclusion	1.59	0.086	0.057	0.054
66	56517385	GRS37-170-645.9	0.0002	0.0013	17.07	72	29.39	generous	cp	inclusion	1.54	0.083	0.077	0.054
67	62483469	GRS37-170-645.9	0.0002	0.0011	8.16	75	30.38	generous	cp	inclusion	1.22	0.070	0.070	0.057
68	69572393	GRS37-170-645.9	0.0002	0.0010	52.38	76	29.81	generous	cp	inclusion	1.40	0.076	0.066	0.054
69	70163454	GRS37-170-645.9	0.0002	0.0013	16.24	71	30.16	generous	cp	inclusion	1.48	0.084	0.071	0.057
70	72300583	GRS37-170-645.9	0.0003	0.0018	16.08	70	30.53	generous	cp	inclusion	1.70	0.107	0.075	0.063
71	80327585	GRS37-170-645.9	0.0002	0.0009	32.13	70	30.21	generous	cp	inclusion	1.00	0.000	0.000	0.000
72	82117578	GRS37-170-645.9	0.0002	0.0010	11.43	75	30.00	generous	cp	inclusion	1.46	0.077	0.065	0.053
73	85532531	GRS37-170-645.9	0.0002	0.0013	3.40	69	29.73	generous	cp	inclusion	2.09	0.111	0.059	0.053
74	88946570	GRS37-170-645.9	0.0001	0.0006	5.41	53	30.30	generous	cp	inclusion	1.56	0.067	0.056	0.043
75	89942637	GRS37-170-645.9	0.0001	0.0008	58.84	61	30.09	generous	cp	inclusion	1.48	0.073	0.058	0.049
76	98324856	GRS37-170-645.9	0.0004	0.0016	9.76	96	29.51	generous	cp	inclusion	1.18	0.083	0.076	0.071
77	100439047	GRS37-170-645.9	0.0001	0.0009	53.21	57	29.67	generous	cp	edge	1.00	0.000	0.000	0.000
78	101091609	GRS37-170-645.9	0.0001	0.0006	24.39	52	29.05	generous	cp	inclusion	1.56	0.067	0.056	0.043
79	118820899	GRS37-170-645.9	0.0001	0.0010	0.57	62	29.65	generous	cp	inclusion	1.46	0.077	0.065	0.053
80	121379371	GRS37-170-645.9	0.0002	0.0017	2.15	55	29.84	generous	cp	inclusion	1.99	0.114	0.071	0.057
81	142693505	GRS37-170-645.9	0.0002	0.0016	2.59	66	29.86	generous	cp	inclusion	2.24	0.120	0.071	0.054
82	143552767	GRS37-170-645.9	0.0005	0.0029	5.23	89	30.19	generous	cp	inclusion	1.65	0.129	0.089	0.079

83	145198885	GRS37-170-645.9	0.0001	0.0009	40.06	50	29.92	generous	cp	inclusion	1.00	0.000	0.000	0.000
84	151966202	GRS37-170-645.9	0.0001	0.0010	73.08	68	29.76	generous	cp	inclusion	1.40	0.074	0.069	0.053
85	159690603	GRS37-170-645.9	0.0002	0.0014	45.83	82	28.84	generous	cp	edge	1.62	0.092	0.069	0.057
86	167430898	GRS37-170-645.9	0.0003	0.0026	3.01	67	30.18	generous	cp	inclusion	2.09	0.151	0.082	0.072
87	169145718	GRS37-170-645.9	0.0001	0.0006	1.02	52	30.52	generous	cp	inclusion	2.27	0.087	0.050	0.038
88	170013196	GRS37-170-645.9	0.0001	0.0008	1.63	50	29.77	generous	cp	inclusion	1.95	0.081	0.055	0.042
89	170850452	GRS37-170-645.9	0.0001	0.0006	8.04	55	30.10	generous	cp	inclusion	1.56	0.067	0.056	0.043
90	172549665	GRS37-170-645.9	0.0007	0.0039	15.15	83	29.21	generous	cp	inclusion	2.78	0.198	0.094	0.071
91	179389641	GRS37-170-645.9	0.0001	0.0008	0.62	55	28.82	generous	cp	inclusion	1.48	0.073	0.058	0.049
92	181115419	GRS37-170-645.9	0.0001	0.0009	2.71	56	28.46	generous	cp	inclusion	1.00	0.000	0.000	0.000
93	181947186	GRS37-170-645.9	0.0002	0.0010	1.49	60	29.23	generous	cp	inclusion	1.78	0.085	0.060	0.048
94	181956372	GRS37-170-645.9	0.0001	0.0010	5.63	61	29.93	generous	cp	inclusion	1.59	0.082	0.072	0.052
95	182804606	GRS37-170-645.9	0.0002	0.0011	5.72	61	27.71	generous	cp	inclusion	1.59	0.086	0.057	0.054
96	187087942	GRS37-170-645.9	0.0002	0.0012	4.06	57	28.47	generous	cp	inclusion	1.64	0.090	0.060	0.055
97	224840847	GRS37-170-645.9	0.0001	0.0011	6.53	55	29.93	generous	cp	inclusion	1.55	0.081	0.074	0.052
98	227538017	GRS37-170-645.9	0.0002	0.0016	10.48	74	30.27	generous	cp	inclusion	1.29	0.084	0.076	0.065
99	230709639	GRS37-170-645.9	0.0002	0.0015	30.85	56	30.11	generous	cp	inclusion	1.89	0.115	0.074	0.061
100	236559191	GRS37-170-645.9	0.0001	0.0011	30.98	62	29.83	generous	cp	inclusion	2.34	0.108	0.057	0.046
101	246158659	GRS37-170-645.9	0.0001	0.0006	25.54	57	30.60	generous	cp	inclusion	1.70	0.075	0.055	0.044
102	248511324	GRS37-170-645.9	0.0004	0.0018	2.26	82	29.75	generous	cp	inclusion	1.61	0.099	0.076	0.062
103	250217889	GRS37-170-645.9	0.0001	0.0010	10.33	54	29.88	generous	cp	inclusion	2.57	0.107	0.061	0.041
104	267897851	GRS37-170-645.9	0.0001	0.0010	56.80	69	29.39	generous	cp	inclusion	1.46	0.077	0.065	0.053
105	273625209	GRS37-170-645.9	0.0002	0.0018	4.20	74	30.78	generous	cp	inclusion	1.47	0.093	0.080	0.063
106	274900441	GRS37-170-645.9	0.0003	0.0015	70.42	82	29.71	generous	cp	inclusion	1.41	0.082	0.082	0.058
107	281221731	GRS37-170-645.9	0.0002	0.0010	43.56	65	29.92	generous	cp	inclusion	1.40	0.076	0.063	0.054
108	281257549	GRS37-170-645.9	0.0002	0.0017	12.65	65	30.31	generous	cp	inclusion	2.16	0.121	0.071	0.056
109	284296979	GRS37-170-645.9	0.0001	0.0008	58.95	60	29.29	generous	cp	inclusion	1.54	0.077	0.056	0.050
110	287048184	GRS37-170-645.9	0.0002	0.0011	5.75	71	29.33	generous	cp	inclusion	1.47	0.079	0.066	0.054
111	293863413	GRS37-170-645.9	0.0002	0.0013	7.34	68	29.90	generous	cp	inclusion	1.52	0.088	0.064	0.058
112	293863425	GRS37-170-645.9	0.0001	0.0008	4.22	57	29.64	generous	cp	inclusion	1.48	0.073	0.058	0.049
113	304698766	GRS37-170-645.9	0.0002	0.0012	70.55	68	29.19	generous	cp	inclusion	1.27	0.075	0.071	0.059
114	306031524	GRS37-170-645.9	0.0001	0.0009	6.06	56	30.25	generous	cp	inclusion	1.59	0.077	0.059	0.049
115	307515058	GRS37-170-645.9	0.0003	0.0012	14.41	81	29.22	generous	cp	inclusion	1.45	0.086	0.059	0.059
116	318243668	GRS37-170-645.9	0.0001	0.0011	57.98	55	30.21	generous	cp	inclusion	1.55	0.080	0.074	0.052
117	319313929	GRS37-170-645.9	0.0002	0.0013	14.43	70	29.72	generous	cp	inclusion	1.45	0.083	0.071	0.057
118	320894772	GRS37-170-645.9	0.0002	0.0011	43.66	73	29.96	generous	cp	inclusion	1.24	0.074	0.068	0.059
119	321128960	GRS37-170-645.9	0.0001	0.0009	6.33	55	29.92	generous	cp	inclusion	1.00	0.000	0.000	0.000
120	328148942	GRS37-170-645.9	0.0005	0.0024	5.56	84	29.59	generous	cp	inclusion	1.33	0.098	0.085	0.074
121	328889762	GRS37-170-645.9	0.0001	0.0010	30.27	54	29.31	generous	cp	inclusion	1.50	0.081	0.058	0.054
122	331652853	GRS37-170-645.9	0.0001	0.0009	9.24	66	30.26	generous	cp	inclusion	1.44	0.070	0.068	0.049
123	334933820	GRS37-170-645.9	0.0004	0.0018	18.02	91	29.50	generous	cp	inclusion	1.22	0.089	0.075	0.073
124	338740670	GRS37-170-645.9	0.0001	0.0008	84.01	51	29.50	generous	cp	inclusion	1.22	0.061	0.061	0.050
125	345016256	GRS37-170-645.9	0.0001	0.0010	17.59	60	29.40	generous	cp	inclusion	1.31	0.072	0.067	0.055

126	348425691	GRS37-170-645.9	0.0001	0.0006	8.72	57	30.10	generous	cp	inclusion	1.56	0.067	0.056	0.043
127	349278526	GRS37-170-645.9	0.0001	0.0008	13.11	54	29.41	generous	cp	inclusion	1.47	0.073	0.058	0.049
128	372240434	GRS37-170-645.9	0.0001	0.0006	2.57	56	29.35	generous	cp	inclusion	1.56	0.067	0.056	0.043
129	377598768	GRS37-170-645.9	0.0001	0.0011	34.84	59	28.79	generous	cp	inclusion	1.70	0.091	0.059	0.054
130	407153752	GRS37-170-645.9	0.0004	0.0016	16.43	96	28.54	generous	cp	inclusion	1.58	0.098	0.076	0.062
131	413123505	GRS37-170-645.9	0.0004	0.0019	30.67	90	27.97	generous	cp	inclusion	1.41	0.099	0.076	0.070
132	413191503	GRS37-170-645.9	0.0002	0.0010	2.32	71	29.69	generous	cp	inclusion	1.49	0.081	0.058	0.054
133	421428818	GRS37-170-645.9	0.0001	0.0006	42.93	60	30.35	generous	cp	inclusion	1.70	0.075	0.055	0.044
134	429124391	GRS37-170-645.9	0.0003	0.0028	12.45	67	30.28	generous	cp	inclusion	1.89	0.138	0.100	0.073
135	430821776	GRS37-170-645.9	0.0004	0.0037	2.53	56	30.43	generous	cp	inclusion	2.31	0.185	0.100	0.080
136	433384833	GRS37-170-645.9	0.0003	0.0018	4.79	91	30.16	generous	cp	inclusion	1.51	0.099	0.080	0.065
137	438551258	GRS37-170-645.9	0.0001	0.0006	41.58	52	28.43	generous	cp	edge	2.05	0.086	0.052	0.042
138	453944362	GRS37-170-645.9	0.0001	0.0008	63.91	61	30.00	generous	cp	inclusion	1.91	0.087	0.051	0.045
139	467495925	GRS37-170-645.9	0.0006	0.0035	25.31	78	30.03	generous	cp	inclusion	1.92	0.140	0.098	0.073
140	472657723	GRS37-170-645.9	0.0002	0.0013	34.80	64	29.33	generous	cp	inclusion	1.69	0.092	0.075	0.054
141	487989337	GRS37-170-645.9	0.0002	0.0016	17.45	55	30.62	generous	cp	inclusion	1.85	0.108	0.084	0.058
142	489286265	GRS37-170-645.9	0.0006	0.0024	7.75	101	27.87	generous	cp	inclusion	1.67	0.117	0.078	0.070
143	490895667	GRS37-170-645.9	0.0004	0.0027	29.65	74	29.57	generous	cp	inclusion	2.34	0.145	0.081	0.062
144	491759489	GRS37-170-645.9	0.0001	0.0011	0.34	62	29.79	generous	cp	inclusion	1.90	0.091	0.068	0.048
145	495168023	GRS37-170-645.9	0.0003	0.0025	2.41	55	28.98	generous	cp	inclusion	3.93	0.211	0.071	0.054
146	510184681	GRS37-170-645.9	0.0001	0.0009	18.50	56	29.29	generous	cp	inclusion	1.38	0.076	0.055	0.055
147	510986126	GRS37-170-645.9	0.0001	0.0006	5.28	50	29.80	generous	cp	inclusion	1.70	0.075	0.055	0.044
148	520370843	GRS37-170-645.9	0.0003	0.0015	5.91	98	29.33	generous	cp	inclusion	1.36	0.085	0.076	0.063
149	523356144	GRS37-170-645.9	0.0003	0.0015	10.53	60	29.71	generous	cp	inclusion	1.99	0.103	0.074	0.052
150	531541747	GRS37-170-645.9	0.0002	0.0015	71.60	63	29.14	generous	cp	inclusion	1.66	0.097	0.080	0.059
151	538295698	GRS37-170-645.9	0.0008	0.0044	15.34	90	29.51	generous	cp	inclusion	1.23	0.135	0.127	0.110
152	542898407	GRS37-170-645.9	0.0001	0.0008	13.12	52	29.68	generous	cp	inclusion	1.63	0.080	0.058	0.049
153	547697898	GRS37-170-645.9	0.0002	0.0012	6.52	71	29.72	generous	cp	inclusion	1.65	0.087	0.072	0.052
154	549788133	GRS37-170-645.9	0.0003	0.0016	26.14	73	29.83	generous	cp	inclusion	1.63	0.101	0.071	0.062
155	551955586	GRS37-170-645.9	0.0006	0.0028	3.22	128	29.88	generous	cp	inclusion	1.50	0.115	0.087	0.077
156	551989564	GRS37-170-645.9	0.0003	0.0020	13.81	68	30.29	generous	cp	inclusion	2.14	0.127	0.084	0.059
157	552219781	GRS37-170-645.9	0.0002	0.0012	17.19	64	29.45	generous	cp	inclusion	1.55	0.086	0.064	0.056
158	553927263	GRS37-170-645.9	0.0001	0.0006	13.75	51	29.38	generous	cp	inclusion	2.05	0.086	0.052	0.042
159	560701278	GRS37-170-645.9	0.0003	0.0016	34.86	71	29.78	generous	cp	inclusion	1.60	0.090	0.082	0.056
160	566006405	GRS37-170-645.9	0.0001	0.0012	11.06	57	29.48	generous	cp	inclusion	1.68	0.092	0.068	0.055
161	576941653	GRS37-170-645.9	0.0004	0.0018	30.45	79	29.46	generous	cp	inclusion	1.55	0.100	0.080	0.064
162	577791717	GRS37-170-645.9	0.0002	0.0017	25.07	62	29.90	generous	cp	inclusion	2.01	0.123	0.077	0.061
163	578405000	GRS37-170-645.9	0.0002	0.0011	16.04	65	29.57	generous	cp	inclusion	1.52	0.082	0.070	0.054
164	578510656	GRS37-170-645.9	0.0002	0.0014	48.92	59	29.03	generous	cp	edge	1.33	0.085	0.069	0.063
165	580298571	GRS37-170-645.9	0.0001	0.0008	11.49	56	30.05	generous	cp	inclusion	1.48	0.073	0.058	0.049
166	590233247	GRS37-170-645.9	0.0002	0.0016	0.90	59	31.20	generous	cp	inclusion	1.53	0.106	0.085	0.068
167	590237839	GRS37-170-645.9	0.0001	0.0006	0.39	50	31.40	generous	cp	inclusion	1.61	0.079	0.054	0.049
168	591242989	GRS37-170-645.9	0.0002	0.0013	17.93	72	30.00	generous	cp	inclusion	1.73	0.096	0.068	0.055

169	591941647	GRS37-170-645.9	0.0003	0.0025	2.33	64	30.71	generous	cp	inclusion	2.03	0.137	0.088	0.067
170	595911051	GRS37-170-645.9	0.0002	0.0014	28.32	56	30.16	generous	cp	inclusion	1.39	0.084	0.078	0.061
171	598122489	GRS37-170-645.9	0.0002	0.0015	29.06	75	30.59	generous	cp	inclusion	1.77	0.111	0.077	0.062
172	601477774	GRS37-170-645.9	0.0001	0.0009	23.50	62	30.54	generous	cp	inclusion	1.77	0.084	0.060	0.048
173	602342519	GRS37-170-645.9	0.0001	0.0009	7.95	71	30.76	generous	cp	inclusion	1.39	0.075	0.059	0.054
174	605812577	GRS37-170-645.9	0.0001	0.0008	6.12	53	30.30	generous	cp	inclusion	2.33	0.094	0.060	0.040
175	611248237	GRS37-170-645.9	0.0001	0.0008	60.36	57	30.09	generous	cp	inclusion	1.95	0.081	0.055	0.042
176	616927731	GRS37-170-645.9	0.0002	0.0011	29.07	70	29.36	generous	cp	inclusion	1.53	0.078	0.072	0.051
177	638912856	GRS37-170-645.9	0.0001	0.0009	17.56	58	30.52	generous	cp	inclusion	1.55	0.079	0.064	0.051
178	640723439	GRS37-170-645.9	0.0007	0.0036	47.00	101	30.06	generous	cp	inclusion	2.12	0.171	0.091	0.080
179	650855113	GRS37-170-645.9	0.0001	0.0006	3.66	53	30.40	generous	cp	inclusion	1.56	0.067	0.056	0.043
180	666984503	GRS37-170-645.9	0.0001	0.0010	14.36	52	29.73	generous	cp	inclusion	1.46	0.080	0.056	0.055
181	682488699	GRS37-170-645.9	0.0004	0.0020	44.55	88	29.10	generous	cp	inclusion	1.32	0.096	0.080	0.073
182	684170473	GRS37-170-645.9	0.0001	0.0010	32.07	60	29.96	generous	cp	inclusion	1.31	0.072	0.067	0.055
183	696155027	GRS37-170-645.9	0.0001	0.0008	35.04	59	31.05	generous	cp	inclusion	1.48	0.073	0.058	0.049
184	696887315	GRS37-170-645.9	0.0002	0.0010	9.88	53	29.69	generous	cp	inclusion	1.46	0.080	0.056	0.055
185	697741057	GRS37-170-645.9	0.0001	0.0006	5.00	51	30.30	generous	cp	inclusion	3.82	0.117	0.046	0.030
186	699441192	GRS37-170-645.9	0.0001	0.0006	9.40	55	30.00	generous	cp	inclusion	1.70	0.075	0.055	0.044
187	701243264	GRS37-170-645.9	0.0001	0.0006	26.00	59	29.30	generous	cp	inclusion	1.56	0.067	0.056	0.043
188	708907935	GRS37-170-645.9	0.0001	0.0010	12.75	57	29.08	generous	cp	inclusion	1.46	0.080	0.056	0.055
189	713085521	GRS37-170-645.9	0.0001	0.0008	30.80	57	30.35	generous	cp	inclusion	2.22	0.093	0.054	0.042
190	737007806	GRS37-170-645.9	0.0001	0.0011	11.95	53	29.93	generous	cp	inclusion	1.55	0.086	0.075	0.056
191	761845331	GRS37-170-645.9	0.0004	0.0025	37.80	66	29.92	generous	cp	inclusion	1.62	0.107	0.105	0.066
192	764803807	GRS37-170-645.9	0.0001	0.0010	92.86	54	29.81	generous	cp	inclusion	2.01	0.096	0.058	0.048
193	767098803	GRS37-170-645.9	0.0004	0.0016	30.83	96	28.79	generous	cp	inclusion	1.33	0.087	0.073	0.066
194	779879233	GRS37-170-645.9	0.0004	0.0018	28.63	108	28.92	generous	cp	inclusion	1.33	0.095	0.079	0.071
195	788931538	GRS37-170-645.9	0.0001	0.0008	7.77	51	29.60	generous	cp	inclusion	2.69	0.105	0.060	0.039
196	796827553	GRS37-170-645.9	0.0004	0.0014	43.70	81	30.09	generous	cp	inclusion	1.72	0.095	0.073	0.055
197	800978433	GRS37-170-645.9	0.0002	0.0017	26.22	56	28.68	generous	cp	inclusion	1.84	0.107	0.070	0.058
198	802663161	GRS37-170-645.9	0.0002	0.0011	14.21	64	28.96	generous	cp	inclusion	1.42	0.076	0.072	0.054
199	805243723	GRS37-170-645.9	0.0003	0.0022	10.17	71	29.29	generous	cp	inclusion	1.58	0.104	0.085	0.066
200	813759924	GRS37-170-645.9	0.0001	0.0006	11.05	55	29.10	generous	cp	inclusion	1.37	0.066	0.059	0.048
201	823912778	GRS37-170-645.9	0.0007	0.0032	5.97	92	29.43	generous	cp	inclusion	1.60	0.116	0.110	0.072
202	827527246	GRS37-170-645.9	0.0009	0.0041	63.68	116	29.29	generous	cp	inclusion	1.81	0.154	0.095	0.085
203	832626741	GRS37-170-645.9	0.0006	0.0030	69.69	113	29.75	generous	cp	inclusion	1.77	0.134	0.081	0.076
204	844385092	GRS37-170-645.9	0.0002	0.0015	12.25	61	30.06	generous	cp	inclusion	1.77	0.108	0.067	0.061
205	858403995	GRS37-170-645.9	0.0001	0.0008	98.31	52	29.95	generous	cp	inclusion	1.22	0.061	0.061	0.050
206	881122844	GRS37-170-645.9	0.0001	0.0006	8.52	51	28.50	generous	cp	inclusion	1.56	0.067	0.056	0.043
207	899928995	GRS37-170-645.9	0.0002	0.0013	11.35	57	29.69	generous	cp	inclusion	1.76	0.102	0.069	0.058
208	900780731	GRS37-170-645.9	0.0002	0.0017	29.02	50	29.97	generous	cp	inclusion	1.65	0.096	0.078	0.059
209	959663130	GRS37-170-645.9	0.0001	0.0008	12.94	58	29.45	generous	cp	inclusion	1.95	0.081	0.055	0.042
210	960564574	GRS37-170-645.9	0.0002	0.0011	10.54	66	28.63	generous	cp	inclusion	1.44	0.082	0.069	0.057
211	968977163	GRS37-170-645.9	0.0019	0.0078	15.21	126	30.29	generous	cp	inclusion	1.85	0.178	0.128	0.096

212	996400494	GRS37-170-645.9	0.0001	0.0008	26.43	53	29.22	generous	cp	inclusion	1.94	0.091	0.052	0.047
213	1.009E+09	GRS37-170-645.9	0.0004	0.0022	36.60	76	29.57	generous	cp	inclusion	1.23	0.095	0.083	0.077
214	1.012E+09	GRS37-170-645.9	0.0003	0.0015	19.67	84	30.34	generous	cp	inclusion	1.79	0.100	0.073	0.056
215	1.013E+09	GRS37-170-645.9	0.0002	0.0014	11.08	71	29.94	generous	cp	inclusion	1.47	0.085	0.074	0.057
216	1.021E+09	GRS37-170-645.9	0.0002	0.0016	2.68	58	30.03	generous	cp	inclusion	1.81	0.101	0.080	0.056
217	1.022E+09	GRS37-170-645.9	0.0006	0.0037	2.36	65	29.82	generous	cp	inclusion	1.67	0.121	0.117	0.073
218	1.029E+09	GRS37-170-645.9	0.0001	0.0010	10.31	62	30.38	generous	cp	inclusion	1.49	0.082	0.061	0.055
219	1.035E+09	GRS37-170-645.9	0.0001	0.0009	19.55	52	30.04	generous	cp	inclusion	1.99	0.086	0.061	0.043
220	1.055E+09	GRS37-170-645.9	0.0004	0.0026	23.01	67	29.81	generous	cp	inclusion	1.68	0.121	0.085	0.072
221	1.08E+09	GRS37-170-645.9	0.0001	0.0011	11.58	60	30.15	generous	cp	inclusion	1.55	0.083	0.062	0.054
222	1.09E+09	GRS37-170-645.9	0.0003	0.0020	64.57	70	29.12	generous	cp	inclusion	1.59	0.097	0.091	0.061
223	1.118E+09	GRS37-170-645.9	0.0002	0.0013	24.08	56	29.66	generous	cp	inclusion	1.92	0.102	0.061	0.053
224	1.123E+09	GRS37-170-645.9	0.0001	0.0009	17.27	52	30.71	generous	cp	inclusion	1.46	0.076	0.068	0.052
225	1.167E+09	GRS37-170-645.9	0.0004	0.0022	5.99	96	30.05	generous	cp	inclusion	1.23	0.091	0.084	0.074
226	1.193E+09	GRS37-170-645.9	0.0002	0.0010	9.86	61	27.27	generous	cp	inclusion	1.46	0.080	0.056	0.055
227	1.245E+09	GRS37-170-645.9	0.0005	0.0022	0.00	69	25.38	generous	cp	inclusion	1.61	0.109	0.077	0.068
228	1.245E+09	GRS37-170-645.9	0.0004	0.0019	0.02	71	26.46	generous	cp	inclusion	1.47	0.101	0.075	0.068
229	1.247E+09	GRS37-170-645.9	0.0012	0.0049	0.01	83	25.34	generous	cp	edge	1.70	0.137	0.111	0.081
230	1.25E+09	GRS37-170-645.9	0.0001	0.0009	18.44	50	30.54	generous	cp	inclusion	1.00	0.000	0.000	0.000
231	1.25E+09	GRS37-170-645.9	0.0009	0.0043	22.71	116	30.32	generous	cp	inclusion	1.62	0.145	0.109	0.090
232	1.253E+09	GRS37-170-645.9	0.0002	0.0015	4.56	67	29.61	generous	cp	inclusion	2.14	0.117	0.073	0.055
233	1.256E+09	GRS37-170-645.9	0.0001	0.0006	1.16	61	30.00	generous	cp	inclusion	1.37	0.066	0.059	0.048
234	1.262E+09	GRS37-170-645.9	0.0002	0.0016	4.26	67	29.37	generous	cp	inclusion	1.44	0.092	0.076	0.064
235	1.267E+09	GRS37-170-645.9	0.0002	0.0016	3.11	63	30.83	generous	cp	inclusion	1.84	0.104	0.075	0.056
236	1.272E+09	GRS37-170-645.9	0.0001	0.0008	14.24	55	29.86	generous	cp	inclusion	1.22	0.061	0.061	0.050
237	1.287E+09	GRS37-170-645.9	0.0001	0.0006	11.12	58	30.50	generous	cp	inclusion	1.56	0.067	0.056	0.043
238	1.29E+09	GRS37-170-645.9	0.0004	0.0025	0.63	72	29.68	generous	cp	inclusion	1.32	0.103	0.089	0.079
239	1.314E+09	GRS37-170-645.9	0.0002	0.0022	0.40	52	29.67	generous	cp	inclusion	1.90	0.111	0.090	0.058
240	1.319E+09	GRS37-170-645.9	0.0001	0.0008	20.34	55	31.04	generous	cp	inclusion	2.28	0.104	0.055	0.046
241	1.324E+09	GRS37-170-645.9	0.0004	0.0023	0.01	73	26.37	generous	cp	inclusion	1.84	0.109	0.091	0.060
242	1.353E+09	GRS37-170-645.9	0.0003	0.0028	0.06	50	28.18	generous	cp	inclusion	1.62	0.117	0.094	0.072
243	1.356E+09	GRS37-170-645.9	0.0001	0.0008	0.17	53	29.45	generous	cp	inclusion	1.22	0.061	0.061	0.050
244	1.425E+09	GRS37-170-645.9	0.0004	0.0020	0.00	68	25.49	generous	cp	inclusion	1.42	0.101	0.076	0.071
245	1.426E+09	GRS37-170-645.9	0.0001	0.0010	3.33	65	30.08	generous	cp	inclusion	1.50	0.081	0.058	0.054
246	1.446E+09	GRS37-170-645.9	0.0001	0.0008	1.69	51	29.86	generous	cp	inclusion	1.22	0.061	0.061	0.050
247	1.461E+09	GRS37-170-645.9	0.0002	0.0013	3.71	55	30.03	generous	cp	inclusion	2.04	0.104	0.067	0.051
248	1.462E+09	GRS37-170-645.9	0.0001	0.0010	0.57	53	29.04	generous	cp	inclusion	1.81	0.088	0.064	0.048
249	1.54E+09	GRS37-170-645.9	0.0002	0.0013	4.72	61	30.19	generous	cp	inclusion	1.78	0.097	0.074	0.054
250	1.541E+09	GRS37-170-645.9	0.0004	0.0024	15.53	75	29.43	generous	cp	inclusion	1.46	0.104	0.084	0.071
251	1.573E+09	GRS37-170-645.9	0.0002	0.0017	0.61	63	30.74	generous	cp	inclusion	1.51	0.090	0.082	0.059
252	1.573E+09	GRS37-170-645.9	0.0002	0.0015	33.49	54	30.31	generous	cp	inclusion	1.93	0.106	0.070	0.055
253	1.577E+09	GRS37-170-645.9	0.0002	0.0012	8.45	59	30.83	generous	cp	inclusion	1.87	0.100	0.063	0.054
254	1.601E+09	GRS37-170-645.9	0.0006	0.0036	30.44	83	31.27	generous	cp	inclusion	1.69	0.132	0.098	0.078

255	1.62E+09	GRS37-170-645.9	0.0001	0.0011	12.69	53	30.43	generous	cp	inclusion	1.53	0.086	0.057	0.056
256	1.634E+09	GRS37-170-645.9	0.0002	0.0011	49.24	52	29.61	generous	cp	inclusion	1.53	0.086	0.057	0.056
257	1.636E+09	GRS37-170-645.9	0.0002	0.0014	3.04	80	29.87	generous	cp	inclusion	1.29	0.079	0.079	0.061
258	1.652E+09	GRS37-170-645.9	0.0001	0.0006	9.48	51	30.72	generous	cp	inclusion	1.22	0.061	0.061	0.050
259	1.652E+09	GRS37-170-645.9	0.0002	0.0016	5.68	63	30.05	generous	cp	inclusion	2.59	0.137	0.064	0.053
260	1.662E+09	GRS37-170-645.9	0.0002	0.0013	4.59	75	30.30	generous	cp	inclusion	1.52	0.088	0.064	0.058
261	1.665E+09	GRS37-170-645.9	0.0001	0.0008	0.06	50	27.55	generous	cp	inclusion	1.95	0.081	0.055	0.042
262	1.666E+09	GRS37-170-645.9	0.0001	0.0010	32.33	60	30.12	generous	cp	inclusion	1.49	0.081	0.058	0.054
263	1.668E+09	GRS37-170-645.9	0.0020	0.0124	9.70	90	30.36	generous	cp	inclusion	1.46	0.217	0.169	0.149
264	1.673E+09	GRS37-170-645.9	0.0002	0.0017	2.79	55	31.60	generous	cp	inclusion	2.75	0.133	0.091	0.048
265	1.684E+09	GRS37-170-645.9	0.0001	0.0009	5.98	64	30.59	generous	cp	inclusion	2.85	0.089	0.072	0.031
266	1.688E+09	GRS37-170-645.9	0.0002	0.0012	7.47	67	29.18	generous	cp	inclusion	1.40	0.081	0.066	0.058
267	1.691E+09	GRS37-170-645.9	0.0001	0.0010	3.05	55	30.15	generous	cp	inclusion	1.50	0.081	0.058	0.054
268	1.71E+09	GRS37-170-645.9	0.0001	0.0011	3.40	58	30.48	generous	cp	inclusion	1.55	0.084	0.064	0.054
269	1.71E+09	GRS37-170-645.9	0.0001	0.0006	10.53	50	30.05	generous	cp	inclusion	1.70	0.075	0.054	0.044
270	1.724E+09	GRS37-170-645.9	0.0001	0.0006	5.44	54	30.29	generous	cp	inclusion	1.85	0.074	0.062	0.040
271	1.732E+09	GRS37-170-645.9	0.0002	0.0010	0.27	68	30.77	generous	cp	inclusion	1.46	0.080	0.056	0.055
272	1.754E+09	GRS37-170-645.9	0.0004	0.0023	14.88	81	29.69	generous	cp	inclusion	2.26	0.135	0.078	0.060
273	1.765E+09	GRS37-170-645.9	0.0001	0.0009	15.18	50	29.71	generous	cp	inclusion	1.59	0.077	0.059	0.049
274	1.786E+09	GRS37-170-645.9	0.0001	0.0013	23.32	62	29.53	generous	cp	inclusion	1.79	0.101	0.060	0.056
275	1.788E+09	GRS37-170-645.9	0.0002	0.0015	1.12	61	29.63	generous	cp	inclusion	2.42	0.132	0.065	0.055
276	1.792E+09	GRS37-170-645.9	0.0001	0.0012	23.37	51	31.87	generous	cp	inclusion	1.69	0.102	0.066	0.060
277	1.809E+09	GRS37-170-645.9	0.0004	0.0024	39.07	77	31.04	generous	cp	inclusion	1.69	0.123	0.082	0.072
278	1.853E+09	GRS37-170-645.9	0.0002	0.0014	3.64	68	30.21	generous	cp	inclusion	1.65	0.093	0.070	0.056
279	1.855E+09	GRS37-170-645.9	0.0003	0.0019	3.12	62	30.66	generous	cp	inclusion	1.53	0.106	0.082	0.069
280	83384057	GRS37-170-742.2	0.0001	0.0024	799.53	61	30.02	generous	cp	inclusion	2.24	0.144	0.093	0.064
281	84246058	GRS37-170-742.2	0.0000	0.0010	2.84	49	29.73	generous	cp	inclusion	1.50	0.081	0.058	0.054
282	126810963	GRS37-170-742.2	0.0000	0.0006	6.32	52	30.35	generous	cp	inclusion	1.37	0.066	0.059	0.048
283	244596865	GRS37-170-742.2	0.0001	0.0012	1.56	56	30.67	generous	cp	inclusion	1.64	0.090	0.060	0.055
284	258242005	GRS37-170-742.2	0.0001	0.0012	6.81	55	31.07	generous	cp	inclusion	1.30	0.079	0.070	0.061
285	265643786	GRS37-170-742.2	0.0001	0.0011	8.92	66	30.57	generous	cp	inclusion	2.01	0.098	0.059	0.049
286	269895044	GRS37-170-742.2	0.0000	0.0006	2.33	48	30.00	generous	cp	inclusion	1.37	0.066	0.059	0.048
287	311695243	GRS37-170-742.2	0.0000	0.0009	4.48	48	29.92	generous	cp	inclusion	1.00	0.000	0.000	0.000
288	356705723	GRS37-170-742.2	0.0000	0.0008	31.76	44	30.14	generous	cp	inclusion	1.22	0.061	0.061	0.050
289	384790092	GRS37-170-742.2	0.0000	0.0008	17.62	54	29.32	generous	cp	inclusion	1.22	0.061	0.061	0.050
290	389401218	GRS37-170-742.2	0.0000	0.0006	8.98	51	30.00	generous	cp	inclusion	1.70	0.075	0.055	0.044
291	393300847	GRS37-170-742.2	0.0002	0.0031	35.47	92	30.88	generous	cp	inclusion	1.85	0.140	0.087	0.076
292	420319499	GRS37-170-742.2	0.0000	0.0010	2.27	42	28.85	generous	cp	inclusion	1.46	0.080	0.056	0.055
293	421168654	GRS37-170-742.2	0.0001	0.0025	10.32	50	30.13	generous	cp	inclusion	2.43	0.160	0.072	0.066
294	437663191	GRS37-170-742.2	0.0006	0.0039	27.59	158	27.98	generous	cp	inclusion	1.60	0.132	0.095	0.082
295	442441393	GRS37-170-742.2	0.0000	0.0008	20.72	44	30.55	generous	cp	inclusion	1.48	0.073	0.058	0.049
296	452172151	GRS37-170-742.2	0.0000	0.0008	17.07	52	30.70	generous	cp	inclusion	1.80	0.079	0.060	0.044
297	452930462	GRS37-170-742.2	0.0001	0.0014	32.64	59	30.91	generous	cp	inclusion	1.48	0.093	0.066	0.063

298	486385160	GRS37-170-742.2	0.0000	0.0008	27.67	42	29.00	generous	cp	inclusion	1.22	0.061	0.061	0.050
299	504407364	GRS37-170-742.2	0.0001	0.0011	12.36	46	29.64	generous	cp	inclusion	1.59	0.086	0.057	0.054
300	508545657	GRS37-170-742.2	0.0000	0.0016	32.60	42	31.05	generous	cp	inclusion	1.64	0.107	0.081	0.065
301	525779312	GRS37-170-742.2	0.0001	0.0011	11.79	48	28.79	generous	cp	inclusion	1.59	0.086	0.057	0.054
302	529733119	GRS37-170-742.2	0.0000	0.0006	16.56	46	29.40	generous	cp	inclusion	1.70	0.075	0.054	0.044
303	549575670	GRS37-170-742.2	0.0000	0.0006	53.76	43	29.45	generous	cp	inclusion	1.56	0.067	0.056	0.043
304	550434955	GRS37-170-742.2	0.0006	0.0050	7.03	129	29.70	generous	cp	inclusion	1.22	0.124	0.114	0.102
305	552271884	GRS37-170-742.2	0.0000	0.0008	4.60	43	29.55	generous	cp	inclusion	1.48	0.073	0.058	0.049
306	555551888	GRS37-170-742.2	0.0000	0.0008	11.08	45	30.22	generous	cp	inclusion	2.23	0.094	0.054	0.042
307	556432240	GRS37-170-742.2	0.0000	0.0009	24.86	56	30.13	generous	cp	inclusion	1.64	0.080	0.057	0.049
308	594101424	GRS37-170-742.2	0.0000	0.0008	21.92	47	29.09	generous	cp	inclusion	1.92	0.087	0.051	0.045
309	595069929	GRS37-170-742.2	0.0002	0.0030	33.94	60	29.05	generous	cp	inclusion	1.80	0.127	0.099	0.070
310	599323970	GRS37-170-742.2	0.0000	0.0010	4.61	45	29.96	generous	cp	inclusion	1.66	0.082	0.065	0.049
311	606007925	GRS37-170-742.2	0.0001	0.0011	7.70	47	29.93	generous	cp	inclusion	1.55	0.081	0.074	0.052
312	612960856	GRS37-170-742.2	0.0000	0.0009	9.15	47	30.04	generous	cp	inclusion	2.20	0.105	0.055	0.048
313	618563354	GRS37-170-742.2	0.0001	0.0012	47.53	79	29.37	generous	cp	inclusion	1.59	0.087	0.073	0.055
314	621494576	GRS37-170-742.2	0.0000	0.0009	9.39	55	29.48	generous	cp	inclusion	1.68	0.080	0.061	0.048
315	623898812	GRS37-170-742.2	0.0000	0.0009	7.16	53	29.21	generous	cp	inclusion	1.44	0.078	0.066	0.054
316	633440505	GRS37-170-742.2	0.0000	0.0006	13.45	43	29.00	generous	cp	inclusion	1.56	0.067	0.056	0.043
317	633453350	GRS37-170-742.2	0.0002	0.0022	48.22	98	28.12	generous	cp	inclusion	1.57	0.114	0.079	0.073
318	638387612	GRS37-170-742.2	0.0003	0.0027	4.04	119	28.33	generous	cp	inclusion	1.60	0.116	0.084	0.072
319	647540043	GRS37-170-742.2	0.0001	0.0011	7.58	66	28.39	generous	cp	inclusion	1.59	0.086	0.057	0.054
320	652886508	GRS37-170-742.2	0.0000	0.0006	2.81	44	29.52	generous	cp	inclusion	2.12	0.093	0.053	0.044
321	654603168	GRS37-170-742.2	0.0000	0.0008	9.30	49	28.41	generous	cp	inclusion	1.48	0.073	0.058	0.049
322	678394948	GRS37-170-742.2	0.0001	0.0012	29.09	64	27.57	generous	cp	inclusion	1.57	0.084	0.075	0.054
323	678444531	GRS37-170-742.2	0.0001	0.0014	4.35	80	28.03	generous	cp	inclusion	1.98	0.103	0.070	0.052
324	686939690	GRS37-170-742.2	0.0000	0.0008	5.86	44	28.63	generous	cp	inclusion	2.51	0.104	0.055	0.042
325	687688790	GRS37-170-742.2	0.0001	0.0008	29.65	64	27.77	generous	cp	inclusion	1.48	0.073	0.058	0.049
326	691267148	GRS37-170-742.2	0.0000	0.0008	2.75	51	27.62	generous	cp	inclusion	1.46	0.071	0.061	0.049
327	691408576	GRS37-170-742.2	0.0000	0.0006	0.01	62	26.00	generous	cp	matrix	1.56	0.067	0.056	0.043
328	693828366	GRS37-170-742.2	0.0000	0.0008	14.30	48	27.86	generous	cp	inclusion	1.82	0.076	0.062	0.042
329	704036536	GRS37-170-742.2	0.0002	0.0027	2.29	60	28.00	generous	cp	inclusion	2.50	0.164	0.083	0.065
330	704863647	GRS37-170-742.2	0.0001	0.0008	4.36	46	27.73	generous	cp	inclusion	1.22	0.061	0.061	0.050
331	708050023	GRS37-170-742.2	0.0001	0.0011	36.44	61	28.42	generous	cp	inclusion	1.22	0.070	0.070	0.057
332	710613069	GRS37-170-742.2	0.0002	0.0022	10.18	107	28.74	generous	cp	inclusion	1.34	0.096	0.081	0.072
333	713415746	GRS37-170-742.2	0.0002	0.0020	1.23	68	27.39	generous	cp	inclusion	1.33	0.095	0.080	0.071
334	714963477	GRS37-170-742.2	0.0001	0.0011	6.99	86	28.50	generous	cp	inclusion	1.54	0.089	0.059	0.058
335	720230978	GRS37-170-742.2	0.0001	0.0015	1.71	50	27.64	generous	cp	inclusion	2.24	0.120	0.063	0.053
336	729007025	GRS37-170-742.2	0.0004	0.0044	90.18	100	30.03	generous	cp	inclusion	1.89	0.148	0.107	0.078
337	729716636	GRS37-170-742.2	0.0002	0.0024	19.83	69	29.76	generous	cp	inclusion	2.36	0.144	0.078	0.061
338	730559371	GRS37-170-742.2	0.0001	0.0012	12.26	73	28.00	generous	cp	inclusion	1.55	0.086	0.064	0.056
339	731163418	GRS37-170-742.2	0.0001	0.0008	13.01	60	28.96	generous	cp	inclusion	1.84	0.084	0.061	0.046
340	731994229	GRS37-170-742.2	0.0000	0.0006	6.66	47	27.50	generous	cp	inclusion	1.56	0.067	0.056	0.043

341	737971304	GRS37-170-742.2	0.0000	0.0012	11.92	45	29.16	generous	cp	inclusion	1.66	0.091	0.073	0.055
342	738239366	GRS37-170-742.2	0.0004	0.0025	60.88	148	25.57	generous	cp	inclusion	1.29	0.102	0.085	0.079
343	742355702	GRS37-170-742.2	0.0000	0.0008	9.86	55	28.82	generous	cp	inclusion	1.22	0.061	0.061	0.050
344	750872878	GRS37-170-742.2	0.0001	0.0014	7.03	48	28.69	generous	cp	inclusion	1.73	0.105	0.073	0.060
345	750876554	GRS37-170-742.2	0.0011	0.0124	19.15	116	28.35	generous	cp	inclusion	2.50	0.319	0.181	0.112
346	756003582	GRS37-170-742.2	0.0001	0.0012	6.96	66	28.14	generous	cp	inclusion	1.37	0.078	0.071	0.057
347	758824684	GRS37-170-742.2	0.0003	0.0020	78.73	112	26.29	generous	cp	edge	1.38	0.100	0.076	0.072
348	782433722	GRS37-170-742.2	0.0000	0.0008	29.30	42	28.95	generous	cp	inclusion	1.22	0.061	0.061	0.050
349	786582173	GRS37-170-742.2	0.0001	0.0015	21.27	92	28.69	generous	cp	inclusion	1.50	0.089	0.072	0.059
350	801909082	GRS37-170-742.2	0.0001	0.0013	14.94	73	28.78	generous	cp	inclusion	1.62	0.094	0.058	0.058
351	801932006	GRS37-170-742.2	0.0000	0.0006	17.59	42	28.95	generous	cp	inclusion	1.93	0.079	0.049	0.041
352	820835536	GRS37-170-742.2	0.0001	0.0013	42.16	78	28.83	generous	cp	inclusion	1.39	0.079	0.076	0.056
353	857428799	GRS37-170-742.2	0.0000	0.0008	51.78	45	29.32	generous	cp	inclusion	1.22	0.061	0.061	0.050
354	879871131	GRS37-170-742.2	0.0002	0.0023	207.69	86	27.26	generous	cp	edge	1.89	0.111	0.088	0.059
355	922097354	GRS37-170-742.2	0.0001	0.0013	17.58	59	29.37	generous	cp	inclusion	1.38	0.078	0.076	0.057
356	928189177	GRS37-170-742.2	0.0004	0.0059	35.36	97	29.46	generous	cp	inclusion	2.30	0.209	0.106	0.091
357	929118185	GRS37-170-742.2	0.0001	0.0011	103.99	48	29.75	generous	cp	inclusion	1.59	0.086	0.057	0.054
358	929897568	GRS37-170-742.2	0.0009	0.0055	18.70	183	28.73	generous	cp	inclusion	1.38	0.133	0.125	0.096
359	946854914	GRS37-170-742.2	0.0000	0.0008	5.83	49	28.14	generous	cp	edge	1.95	0.081	0.055	0.042
360	949432646	GRS37-170-742.2	0.0004	0.0041	20.53	111	28.06	generous	cp	inclusion	1.45	0.121	0.109	0.083
361	1.035E+09	GRS37-170-742.2	0.0007	0.0087	70.18	99	30.03	generous	cp	inclusion	1.64	0.173	0.149	0.105
362	1.04E+09	GRS37-170-742.2	0.0004	0.0047	62.40	75	29.54	generous	cp	inclusion	2.18	0.179	0.088	0.082
363	1.118E+09	GRS37-170-742.2	0.0000	0.0009	50.67	47	29.38	generous	cp	inclusion	2.04	0.097	0.054	0.048
364	1.125E+09	GRS37-170-742.2	0.0000	0.0011	31.93	47	29.90	generous	cp	inclusion	2.18	0.110	0.055	0.050
365	1.129E+09	GRS37-170-742.2	0.0001	0.0020	102.19	63	26.78	generous	cp	edge	2.06	0.133	0.093	0.064
366	1.162E+09	GRS37-170-742.2	0.0001	0.0008	59.59	50	25.09	generous	cp	inclusion	1.95	0.081	0.055	0.042
367	1.232E+09	GRS37-170-742.2	0.0167	0.1108	51.88	240	27.17	generous	cp	inclusion	3.75	0.767	0.666	0.208
368	1.234E+09	GRS37-170-742.2	0.0001	0.0010	71.48	60	28.65	generous	cp	inclusion	1.46	0.080	0.056	0.055
369	1.252E+09	GRS37-170-742.2	0.0001	0.0009	0.02	48	26.13	generous	cp	edge	1.69	0.080	0.058	0.047
370	1.253E+09	GRS37-170-742.2	0.0005	0.0044	13.76	107	27.59	generous	cp	inclusion	2.35	0.184	0.103	0.078
371	1.307E+09	GRS37-170-742.2	0.0000	0.0011	2.02	54	29.80	generous	cp	matrix	1.53	0.078	0.072	0.051
372	1.33E+09	GRS37-170-742.2	0.0000	0.0010	8.67	48	29.08	generous	cp	inclusion	1.46	0.080	0.056	0.055
373	1.384E+09	GRS37-170-742.2	0.0000	0.0009	37.36	53	31.32	generous	cp	inclusion	2.00	0.086	0.061	0.043
374	1.569E+09	GRS37-170-742.2	0.0001	0.0010	30.88	53	29.54	generous	cp	inclusion	1.46	0.080	0.056	0.055
375	1.582E+09	GRS37-170-742.2	0.0001	0.0020	9.01	71	30.38	generous	cp	inclusion	1.57	0.112	0.077	0.071
376	929898486	GRS37-170-742.2	0.0007	0.0023	2430.40	183	36.60	strict	cp	inclusion	1.38	0.101	0.083	0.073
377	1.235E+09	GRS37-170-742.2	0.0016	0.0060	463.14	181	38.72	strict	cp	edge	2.33	0.204	0.141	0.087
378	1.243E+09	GRS37-170-742.2	0.0030	0.0112	0.60	204	40.53	strict	cp	edge	3.03	0.291	0.170	0.096
379	1.247E+09	GRS37-170-742.2	0.0026	0.0071	155.13	240	37.39	strict	cp	edge	2.18	0.196	0.113	0.090
380	92046503	GRS37-170-714.2-5	0.0017	0.0065	28.67	154	24.36	generous	cp	matrix	2.96	0.234	0.112	0.079
381	106138261	GRS37-170-714.2-5	0.0030	0.0098	353.54	229	26.90	generous	bn	edge	1.96	0.203	0.160	0.104
382	108570357	GRS37-170-714.2-5	0.0012	0.0040	107.35	171	28.67	generous	bn	edge	1.99	0.162	0.092	0.081
383	139221109	GRS37-170-714.2-5	0.0027	0.0082	10.73	222	24.98	generous	cp	edge	3.01	0.252	0.108	0.084

384	166018676	GRS37-170-714.2-5	0.0134	0.0321	344.83	248	27.79	generous	bn	edge	2.26	0.304	0.225	0.135
385	171428871	GRS37-170-714.2-5	0.0003	0.0013	43.25	132	21.19	generous	cp	edge	1.50	0.089	0.063	0.059
386	223812017	GRS37-170-714.2-5	0.0004	0.0016	413.98	150	29.90	generous	cp	edge	1.56	0.089	0.083	0.057
387	259171602	GRS37-170-714.2-5	0.0003	0.0013	3.32	146	22.88	generous	cp	edge	1.84	0.097	0.068	0.053
388	106138261	GRS37-170-714.2-5	0.0031	0.0111	498.54	229	26.02	strict	bn	edge	1.92	0.221	0.155	0.116
389	138876193	GRS37-170-714.2-5	0.0029	0.0094	10.70	222	22.92	strict	cp	edge	2.83	0.252	0.116	0.089
390	166018676	GRS37-170-714.2-5	0.0140	0.0360	792.93	248	24.73	strict	bn	edge	2.23	0.314	0.228	0.141
391	412157135	GRS37-184-7.8A+B	0.0042	0.0123	3872.73	242	27.46	strict	cp	edge	1.29	0.169	0.146	0.130
392	566507832	GRS37-184-7.8A+B	0.0070	0.0183	1675.25	243	27.49	strict	cp	inclusion	1.29	0.189	0.181	0.146
393	837124888	GRS37-184-7.8A+B	0.0026	0.0088	2458.29	224	27.20	strict	cp	inclusion	1.41	0.155	0.135	0.110
394	970407027	GRS37-184-7.8A+B	0.0013	0.0050	7055.65	206	26.58	strict	cp	edge	1.39	0.124	0.119	0.089
395	12679979	GRS37-184-7.8A+B	0.0006	0.0049	6240.73	82	20.95	generous	cp	edge	1.81	0.150	0.105	0.083
396	25590258	GRS37-184-7.8A+B	0.0013	0.0059	0.19	149	16.94	generous	cp	edge	1.50	0.138	0.121	0.092
397	32238522	GRS37-184-7.8A+B	0.0001	0.0009	44.23	54	20.15	generous	cp	edge	1.70	0.084	0.061	0.049
398	88677766	GRS37-184-7.8A+B	0.0001	0.0009	2.29	52	20.15	generous	cp	matrix	1.23	0.069	0.062	0.056
399	98007419	GRS37-184-7.8A+B	0.0001	0.0012	105.83	44	23.17	generous	cp	edge	2.17	0.099	0.064	0.046
400	138098821	GRS37-184-7.8A+B	0.0003	0.0021	3.04	106	19.36	generous	cp	edge	1.73	0.108	0.081	0.062
401	145577811	GRS37-184-7.8A+B	0.0004	0.0021	5.82	84	21.31	generous	cp	edge	2.06	0.131	0.065	0.064
402	162667842	GRS37-184-7.8A+B	0.0001	0.0009	19.29	52	19.25	generous	cp	edge	1.94	0.089	0.055	0.046
403	162812708	GRS37-184-7.8A+B	0.0001	0.0009	0.07	69	19.83	generous	cp	edge	1.21	0.069	0.069	0.057
404	163356781	GRS37-184-7.8A+B	0.0001	0.0009	1.22	59	20.85	generous	cp	edge	1.77	0.084	0.062	0.048
405	187178037	GRS37-184-7.8A+B	0.0001	0.0012	28.27	55	18.17	generous	cp	edge	1.59	0.086	0.066	0.055
406	188122937	GRS37-184-7.8A+B	0.0001	0.0011	25.42	65	19.24	generous	cp	edge	1.45	0.080	0.069	0.055
407	191478929	GRS37-184-7.8A+B	0.0001	0.0009	14.07	51	19.50	generous	cp	edge	1.37	0.074	0.066	0.054
408	201120794	GRS37-184-7.8A+B	0.0002	0.0014	50.68	69	19.69	generous	cp	edge	1.46	0.090	0.063	0.061
409	218833965	GRS37-184-7.8A+B	0.0003	0.0018	210.36	82	19.71	generous	cp	edge	1.82	0.115	0.074	0.063
410	220284053	GRS37-184-7.8A+B	0.0002	0.0018	64.03	79	21.00	generous	cp	inclusion	1.57	0.100	0.076	0.064
411	220955625	GRS37-184-7.8A+B	0.0002	0.0017	1.82	64	19.30	generous	cp	edge	1.64	0.101	0.067	0.061
412	224123002	GRS37-184-7.8A+B	0.0001	0.0009	17.97	45	19.50	generous	cp	edge	1.56	0.075	0.062	0.048
413	226072969	GRS37-184-7.8A+B	0.0004	0.0034	43.77	77	21.58	generous	cp	edge	1.94	0.137	0.104	0.071
414	235516153	GRS37-184-7.8A+B	0.0004	0.0034	178.09	100	19.38	generous	cp	edge	1.80	0.129	0.107	0.072
415	236104721	GRS37-184-7.8A+B	0.0005	0.0035	73.64	114	19.16	generous	cp	edge	1.29	0.112	0.091	0.087
416	239825344	GRS37-184-7.8A+B	0.0001	0.0012	0.49	64	18.58	generous	cp	edge	1.00	0.065	0.065	0.065
417	242127263	GRS37-184-7.8A+B	0.0002	0.0017	231.90	63	23.00	generous	cp	edge	2.37	0.113	0.084	0.048
418	242178917	GRS37-184-7.8A+B	0.0002	0.0018	31.14	52	20.00	generous	cp	edge	2.22	0.126	0.079	0.057
419	246225122	GRS37-184-7.8A+B	0.0005	0.0044	16.75	80	20.50	generous	cp	edge	1.62	0.139	0.099	0.086
420	248376793	GRS37-184-7.8A+B	0.0001	0.0011	538.47	46	19.59	generous	cp	edge	1.22	0.068	0.068	0.056
421	250080993	GRS37-184-7.8A+B	0.0001	0.0009	21.29	53	18.45	generous	cp	edge	1.56	0.075	0.062	0.048
422	250101349	GRS37-184-7.8A+B	0.0001	0.0009	44.48	47	18.65	generous	cp	matrix	1.56	0.075	0.062	0.048
423	250564168	GRS37-184-7.8A+B	0.0002	0.0017	8.54	86	20.04	generous	cp	edge	1.40	0.090	0.074	0.064
424	250805491	GRS37-184-7.8A+B	0.0003	0.0021	28.79	81	20.21	generous	cp	edge	1.61	0.102	0.085	0.063
425	253665290	GRS37-184-7.8A+B	0.0002	0.0015	122.16	72	22.04	generous	cp	inclusion	1.53	0.090	0.080	0.059
426	254926339	GRS37-184-7.8A+B	0.0006	0.0035	29.26	134	18.02	generous	cp	edge	1.39	0.117	0.091	0.084

427	255729697	GRS37-184-7.8A+B	0.0008	0.0041	0.06	129	18.96	generous	cp	edge	1.38	0.118	0.106	0.085
428	257050222	GRS37-184-7.8A+B	0.0003	0.0023	11.96	77	20.89	generous	cp	edge	1.71	0.106	0.090	0.062
429	258778456	GRS37-184-7.8A+B	0.0001	0.0011	24.89	47	21.91	generous	cp	edge	1.91	0.097	0.057	0.051
430	270297517	GRS37-184-7.8A+B	0.0001	0.0011	10.81	61	20.27	generous	cp	edge	1.82	0.086	0.070	0.047
431	277480807	GRS37-184-7.8A+B	0.0002	0.0015	22.76	82	18.71	generous	cp	edge	1.59	0.097	0.064	0.061
432	277488251	GRS37-184-7.8A+B	0.0014	0.0081	3.57	118	20.05	generous	cp	edge	2.48	0.227	0.115	0.091
433	279740521	GRS37-184-7.8A+B	0.0003	0.0020	25.40	85	20.30	generous	cp	edge	1.57	0.105	0.086	0.067
434	281093560	GRS37-184-7.8A+B	0.0003	0.0029	32.26	101	20.76	generous	cp	edge	1.43	0.101	0.100	0.071
435	288336571	GRS37-184-7.8A+B	0.0001	0.0009	0.06	60	19.65	generous	cp	edge	1.56	0.075	0.062	0.048
436	301341821	GRS37-184-7.8A+B	0.0002	0.0015	0.78	80	20.85	generous	cp	edge	1.47	0.089	0.074	0.060
437	302013381	GRS37-184-7.8A+B	0.0010	0.0059	25.61	138	18.83	generous	cp	edge	1.61	0.154	0.110	0.095
438	304959615	GRS37-184-7.8A+B	0.0005	0.0053	64.92	74	21.94	generous	cp	edge	2.91	0.223	0.104	0.077
439	305523490	GRS37-184-7.8A+B	0.0001	0.0015	102.54	53	19.57	generous	cp	edge	1.59	0.097	0.064	0.061
440	312147832	GRS37-184-7.8A+B	0.0001	0.0015	57.00	62	22.86	generous	cp	edge	1.99	0.109	0.068	0.055
441	318404630	GRS37-184-7.8A+B	0.0012	0.0085	39.55	109	21.77	generous	cp	edge	2.90	0.269	0.131	0.093
442	336696386	GRS37-184-7.8A+B	0.0002	0.0018	32.43	56	21.18	generous	cp	edge	2.81	0.151	0.064	0.054
443	339278843	GRS37-184-7.8A+B	0.0001	0.0009	46.76	58	22.20	generous	cp	edge	1.37	0.074	0.066	0.054
444	348084326	GRS37-184-7.8A+B	0.0002	0.0027	28.95	61	21.16	generous	cp	inclusion	2.69	0.176	0.072	0.065
445	357314986	GRS37-184-7.8A+B	0.0019	0.0081	108.60	176	19.22	generous	cp	edge	1.65	0.163	0.127	0.099
446	358059794	GRS37-184-7.8A+B	0.0003	0.0034	13.08	84	21.55	generous	cp	edge	1.70	0.122	0.117	0.072
447	358239685	GRS37-184-7.8A+B	0.0004	0.0038	18.39	64	18.79	generous	cp	edge	2.50	0.158	0.117	0.063
448	366919865	GRS37-184-7.8A+B	0.0001	0.0012	47.08	67	21.88	generous	cp	edge	1.38	0.086	0.062	0.062
449	368288683	GRS37-184-7.8A+B	0.0002	0.0023	28.62	56	20.03	generous	cp	edge	2.02	0.119	0.084	0.059
450	370303327	GRS37-184-7.8A+B	0.0001	0.0015	31.59	64	22.26	generous	cp	inclusion	1.80	0.105	0.073	0.058
451	380488381	GRS37-184-7.8A+B	0.0011	0.0091	27.22	102	21.93	generous	cp	edge	2.54	0.237	0.128	0.093
452	382682707	GRS37-184-7.8A+B	0.0003	0.0024	32.27	95	20.49	generous	cp	edge	1.87	0.118	0.084	0.063
453	395141718	GRS37-184-7.8A+B	0.0001	0.0012	4.90	65	20.96	generous	cp	edge	1.31	0.082	0.070	0.062
454	397056784	GRS37-184-7.8A+B	0.0002	0.0034	16.78	53	22.70	generous	cp	inclusion	1.65	0.125	0.119	0.076
455	401331959	GRS37-184-7.8A+B	0.0001	0.0011	99.31	47	22.13	generous	cp	edge	2.94	0.109	0.070	0.037
456	403778962	GRS37-184-7.8A+B	0.0004	0.0030	19.24	99	20.07	generous	cp	edge	2.12	0.153	0.086	0.072
457	405650336	GRS37-184-7.8A+B	0.0001	0.0009	3.86	69	21.95	generous	cp	edge	1.56	0.075	0.062	0.048
458	406656320	GRS37-184-7.8A+B	0.0004	0.0027	30.76	88	20.63	generous	cp	edge	1.48	0.108	0.094	0.073
459	408803468	GRS37-184-7.8A+B	0.0001	0.0009	14.10	49	21.15	generous	cp	edge	1.56	0.075	0.062	0.048
460	410022377	GRS37-184-7.8A+B	0.0001	0.0009	11.68	52	22.15	generous	cp	edge	1.70	0.084	0.061	0.049
461	410707203	GRS37-184-7.8A+B	0.0001	0.0009	6.36	47	21.20	generous	cp	inclusion	1.56	0.075	0.062	0.048
462	410931781	GRS37-184-7.8A+B	0.0001	0.0011	95.48	46	18.68	generous	cp	edge	1.22	0.068	0.068	0.056
463	412156306	GRS37-184-7.8A+B	0.0049	0.0177	11.59	242	20.89	generous	cp	edge	1.60	0.211	0.181	0.132
464	412264600	GRS37-184-7.8A+B	0.0001	0.0012	56.34	68	19.29	generous	cp	edge	1.38	0.086	0.062	0.062
465	419391753	GRS37-184-7.8A+B	0.0001	0.0017	4.96	48	22.44	generous	cp	edge	2.20	0.129	0.061	0.058
466	420880557	GRS37-184-7.8A+B	0.0002	0.0017	41.50	79	20.00	generous	cp	edge	1.64	0.100	0.067	0.061
467	421554614	GRS37-184-7.8A+B	0.0001	0.0011	4.98	45	21.73	generous	cp	edge	1.22	0.068	0.068	0.056
468	423145271	GRS37-184-7.8A+B	0.0001	0.0012	30.98	59	19.96	generous	cp	edge	1.35	0.084	0.063	0.062
469	423879978	GRS37-184-7.8A+B	0.0005	0.0041	75.05	81	23.00	generous	cp	inclusion	1.98	0.153	0.095	0.077

470	432834685	GRS37-184-7.8A+B	0.0008	0.0041	120.67	135	18.10	generous	cp	edge	1.78	0.142	0.096	0.080
471	436742705	GRS37-184-7.8A+B	0.0002	0.0023	12.70	54	21.19	generous	cp	edge	2.03	0.123	0.083	0.060
472	437430786	GRS37-184-7.8A+B	0.0002	0.0034	9.08	45	22.06	generous	cp	edge	1.94	0.149	0.097	0.077
473	438864135	GRS37-184-7.8A+B	0.0001	0.0021	5.15	44	21.94	generous	cp	inclusion	1.92	0.119	0.086	0.062
474	447294158	GRS37-184-7.8A+B	0.0002	0.0012	0.01	73	19.00	generous	cp	edge	1.38	0.086	0.062	0.062
475	447653011	GRS37-184-7.8A+B	0.0001	0.0009	14.96	43	23.71	generous	cp	inclusion	2.27	0.098	0.056	0.043
476	449960090	GRS37-184-7.8A+B	0.0002	0.0012	2.19	64	19.54	generous	cp	edge	1.00	0.065	0.065	0.065
477	460626089	GRS37-184-7.8A+B	0.0001	0.0011	28.63	49	19.78	generous	cp	edge	2.37	0.102	0.062	0.043
478	460635200	GRS37-184-7.8A+B	0.0001	0.0015	6.47	50	18.64	generous	cp	edge	1.58	0.093	0.070	0.059
479	465066050	GRS37-184-7.8A+B	0.0003	0.0023	11.74	69	19.97	generous	cp	edge	1.54	0.101	0.089	0.065
480	465574895	GRS37-184-7.8A+B	0.0007	0.0034	96.82	149	19.07	generous	cp	edge	1.45	0.119	0.094	0.082
481	471345199	GRS37-184-7.8A+B	0.0001	0.0017	8.99	49	21.00	generous	cp	inclusion	1.30	0.089	0.078	0.068
482	472743412	GRS37-184-7.8A+B	0.0002	0.0014	66.45	91	19.35	generous	cp	edge	1.78	0.095	0.067	0.054
483	474968696	GRS37-184-7.8A+B	0.0001	0.0014	46.41	65	21.08	generous	cp	inclusion	1.67	0.090	0.075	0.054
484	477821347	GRS37-184-7.8A+B	0.0004	0.0056	27.25	56	21.71	generous	cp	inclusion	2.86	0.184	0.143	0.064
485	480033911	GRS37-184-7.8A+B	0.0005	0.0046	8.62	80	21.88	generous	cp	edge	1.94	0.151	0.114	0.078
486	480762603	GRS37-184-7.8A+B	0.0005	0.0032	2.59	140	21.12	generous	cp	edge	1.39	0.108	0.097	0.078
487	482859270	GRS37-184-7.8A+B	0.0001	0.0009	51.49	41	22.35	generous	cp	inclusion	1.56	0.075	0.062	0.048
488	489409921	GRS37-184-7.8A+B	0.0001	0.0012	3.56	45	21.24	generous	cp	edge	1.99	0.097	0.069	0.049
489	492347811	GRS37-184-7.8A+B	0.0016	0.0088	22.28	145	20.39	generous	cp	edge	2.15	0.218	0.120	0.101
490	493718257	GRS37-184-7.8A+B	0.0001	0.0009	7.32	53	18.95	generous	cp	edge	1.70	0.084	0.061	0.049
491	493818422	GRS37-184-7.8A+B	0.0002	0.0012	16.03	69	22.71	generous	cp	edge	2.17	0.099	0.064	0.046
492	496589936	GRS37-184-7.8A+B	0.0001	0.0011	13.49	42	23.60	generous	cp	edge	2.01	0.099	0.078	0.049
493	496713214	GRS37-184-7.8A+B	0.0001	0.0012	48.60	53	22.57	generous	cp	inclusion	1.56	0.086	0.071	0.055
494	498037362	GRS37-184-7.8A+B	0.0002	0.0021	2.52	52	21.83	generous	cp	edge	1.78	0.109	0.088	0.061
495	498839709	GRS37-184-7.8A+B	0.0007	0.0046	23.78	143	19.94	generous	cp	edge	1.65	0.140	0.099	0.085
496	500400508	GRS37-184-7.8A+B	0.0002	0.0021	45.26	59	22.91	generous	cp	inclusion	1.66	0.104	0.086	0.062
497	500947938	GRS37-184-7.8A+B	0.0001	0.0018	16.28	44	22.18	generous	cp	edge	2.44	0.133	0.077	0.054
498	505972540	GRS37-184-7.8A+B	0.0002	0.0020	16.55	78	21.68	generous	cp	inclusion	1.83	0.116	0.073	0.064
499	506106624	GRS37-184-7.8A+B	0.0003	0.0021	11.10	94	20.30	generous	cp	inclusion	1.40	0.101	0.076	0.073
500	508177617	GRS37-184-7.8A+B	0.0002	0.0017	17.28	82	20.78	generous	cp	inclusion	1.45	0.097	0.067	0.067
501	511917883	GRS37-184-7.8A+B	0.0001	0.0011	10.93	65	20.56	generous	cp	inclusion	1.00	0.067	0.067	0.067
502	516261823	GRS37-184-7.8A+B	0.0004	0.0029	16.21	115	19.78	generous	cp	inclusion	1.13	0.096	0.093	0.084
503	518953051	GRS37-184-7.8A+B	0.0001	0.0014	3.58	47	22.72	generous	cp	inclusion	1.65	0.089	0.073	0.054
504	519101161	GRS37-184-7.8A+B	0.0003	0.0041	26.71	54	22.08	generous	cp	inclusion	2.95	0.184	0.120	0.062
505	519137647	GRS37-184-7.8A+B	0.0003	0.0020	4.85	71	18.88	generous	cp	edge	1.66	0.113	0.072	0.068
506	521975344	GRS37-184-7.8A+B	0.0005	0.0037	7.10	117	21.31	generous	cp	inclusion	1.62	0.134	0.088	0.083
507	522563338	GRS37-184-7.8A+B	0.0002	0.0020	2.38	59	20.86	generous	cp	inclusion	3.25	0.146	0.095	0.045
508	525520288	GRS37-184-7.8A+B	0.0001	0.0009	14.86	43	22.40	generous	cp	edge	1.56	0.075	0.062	0.048
509	525586474	GRS37-184-7.8A+B	0.0002	0.0030	4.58	55	21.18	generous	cp	inclusion	2.26	0.151	0.084	0.067
510	526854322	GRS37-184-7.8A+B	0.0001	0.0020	19.84	51	21.71	generous	cp	edge	2.21	0.112	0.105	0.051
511	526927112	GRS37-184-7.8A+B	0.0001	0.0014	33.25	46	21.58	generous	cp	inclusion	2.01	0.105	0.062	0.052
512	528334843	GRS37-184-7.8A+B	0.0001	0.0014	4.86	43	22.75	generous	cp	inclusion	2.58	0.105	0.093	0.041

513	529047777	GRS37-184-7.8A+B	0.0008	0.0078	42.27	106	21.34	generous	cp	inclusion	3.24	0.254	0.112	0.078
514	529899834	GRS37-184-7.8A+B	0.0003	0.0034	20.31	69	21.90	generous	cp	edge	2.50	0.170	0.094	0.068
515	530528372	GRS37-184-7.8A+B	0.0003	0.0024	5.97	91	19.78	generous	cp	edge	1.62	0.107	0.089	0.066
516	531345606	GRS37-184-7.8A+B	0.0004	0.0029	8.30	101	22.58	generous	cp	edge	1.41	0.112	0.088	0.079
517	533310175	GRS37-184-7.8A+B	0.0002	0.0023	20.82	57	20.95	generous	cp	matrix	1.67	0.102	0.096	0.061
518	534958315	GRS37-184-7.8A+B	0.0001	0.0012	9.48	44	20.92	generous	cp	inclusion	1.99	0.097	0.069	0.049
519	536973067	GRS37-184-7.8A+B	0.0001	0.0021	31.99	41	22.06	generous	cp	inclusion	2.02	0.112	0.102	0.055
520	546548580	GRS37-184-7.8A+B	0.0001	0.0014	14.72	54	18.96	generous	cp	edge	1.46	0.089	0.063	0.061
521	549357472	GRS37-184-7.8A+B	0.0001	0.0015	12.21	54	21.00	generous	cp	edge	1.59	0.097	0.064	0.061
522	549378785	GRS37-184-7.8A+B	0.0001	0.0020	38.88	41	22.69	generous	cp	inclusion	2.04	0.128	0.082	0.063
523	553529514	GRS37-184-7.8A+B	0.0001	0.0009	63.81	41	18.80	generous	cp	edge	1.56	0.075	0.062	0.048
524	554508572	GRS37-184-7.8A+B	0.0011	0.0053	32.03	166	21.07	generous	cp	inclusion	1.43	0.136	0.108	0.095
525	555113238	GRS37-184-7.8A+B	0.0001	0.0017	0.48	52	21.50	generous	cp	edge	1.72	0.099	0.079	0.057
526	563607181	GRS37-184-7.8A+B	0.0001	0.0011	17.35	43	23.18	generous	cp	edge	1.22	0.068	0.068	0.056
527	566507003	GRS37-184-7.8A+B	0.0077	0.0263	81.17	243	22.86	generous	cp	inclusion	1.67	0.249	0.200	0.149
528	577795186	GRS37-184-7.8A+B	0.0019	0.0107	326.98	101	19.75	generous	cp	edge	2.59	0.212	0.168	0.082
529	583282444	GRS37-184-7.8A+B	0.0001	0.0009	39.70	40	23.19	generous	cp	inclusion	2.07	0.093	0.060	0.045
530	599820275	GRS37-184-7.8A+B	0.0001	0.0011	10.17	50	22.64	generous	cp	edge	3.09	0.134	0.061	0.043
531	600697961	GRS37-184-7.8A+B	0.0006	0.0035	14.18	113	21.56	generous	cp	edge	1.35	0.112	0.098	0.083
532	601974876	GRS37-184-7.8A+B	0.0001	0.0014	27.45	43	22.50	generous	cp	edge	2.14	0.111	0.076	0.052
533	601988096	GRS37-184-7.8A+B	0.0001	0.0011	27.08	62	21.91	generous	cp	inclusion	1.80	0.088	0.068	0.049
534	607707493	GRS37-184-7.8A+B	0.0001	0.0012	24.15	46	22.63	generous	cp	edge	1.00	0.065	0.065	0.065
535	608420885	GRS37-184-7.8A+B	0.0001	0.0011	12.65	57	17.73	generous	cp	edge	1.22	0.068	0.068	0.056
536	608444434	GRS37-184-7.8A+B	0.0002	0.0024	46.83	74	20.46	generous	cp	edge	1.88	0.116	0.088	0.062
537	619144543	GRS37-184-7.8A+B	0.0002	0.0024	195.01	73	21.06	generous	cp	edge	1.69	0.123	0.078	0.073
538	619331566	GRS37-184-7.8A+B	0.0001	0.0021	53.48	46	21.97	generous	cp	inclusion	2.00	0.130	0.081	0.065
539	621481194	GRS37-184-7.8A+B	0.0002	0.0021	23.70	76	22.19	generous	cp	inclusion	1.52	0.104	0.078	0.069
540	623736778	GRS37-184-7.8A+B	0.0001	0.0009	21.60	47	21.90	generous	cp	inclusion	1.56	0.075	0.062	0.048
541	624323921	GRS37-184-7.8A+B	0.0003	0.0034	24.53	71	20.93	generous	cp	edge	2.65	0.186	0.097	0.070
542	627884523	GRS37-184-7.8A+B	0.0001	0.0014	56.69	48	22.74	generous	cp	inclusion	2.05	0.114	0.060	0.055
543	633111121	GRS37-184-7.8A+B	0.0001	0.0012	10.14	62	21.56	generous	cp	edge	1.92	0.101	0.067	0.053
544	633719778	GRS37-184-7.8A+B	0.0004	0.0032	13.49	99	22.93	generous	cp	inclusion	1.49	0.112	0.097	0.075
545	637393757	GRS37-184-7.8A+B	0.0001	0.0011	40.38	50	22.68	generous	cp	inclusion	1.82	0.086	0.070	0.047
546	638047161	GRS37-184-7.8A+B	0.0010	0.0067	22.49	122	22.86	generous	cp	inclusion	1.96	0.181	0.110	0.092
547	640284496	GRS37-184-7.8A+B	0.0001	0.0009	8.94	54	22.57	generous	cp	inclusion	2.06	0.092	0.065	0.044
548	671855522	GRS37-184-7.8A+B	0.0001	0.0011	22.74	53	22.38	generous	cp	edge	1.46	0.080	0.069	0.055
549	674824143	GRS37-184-7.8A+B	0.0002	0.0018	8.57	62	21.90	generous	cp	edge	1.62	0.094	0.087	0.058
550	676253337	GRS37-184-7.8A+B	0.0001	0.0014	30.20	42	22.92	generous	cp	inclusion	2.62	0.122	0.062	0.047
551	681461709	GRS37-184-7.8A+B	0.0002	0.0018	8.47	59	21.65	generous	cp	edge	1.73	0.107	0.070	0.062
552	682149008	GRS37-184-7.8A+B	0.0011	0.0070	3.28	128	21.15	generous	cp	edge	2.69	0.215	0.108	0.080
553	690777227	GRS37-184-7.8A+B	0.0006	0.0049	22.15	82	20.38	generous	cp	inclusion	2.64	0.196	0.100	0.074
554	690799740	GRS37-184-7.8A+B	0.0000	0.0009	26.62	41	23.70	generous	cp	inclusion	1.61	0.088	0.061	0.055
555	693670355	GRS37-184-7.8A+B	0.0001	0.0015	104.79	58	22.21	generous	cp	edge	2.01	0.112	0.068	0.056

556	695098830	GRS37-184-7.8A+B	0.0006	0.0061	13.01	68	21.99	generous	cp	inclusion	2.70	0.186	0.144	0.069
557	698018526	GRS37-184-7.8A+B	0.0002	0.0023	13.17	55	23.03	generous	cp	inclusion	1.89	0.142	0.080	0.075
558	699366551	GRS37-184-7.8A+B	0.0002	0.0024	53.22	74	22.03	generous	cp	inclusion	1.50	0.107	0.084	0.071
559	701649543	GRS37-184-7.8A+B	0.0002	0.0023	6.75	52	22.27	generous	cp	inclusion	2.02	0.132	0.079	0.066
560	702174477	GRS37-184-7.8A+B	0.0001	0.0009	9.72	41	21.40	generous	cp	edge	1.56	0.075	0.062	0.048
561	703839652	GRS37-184-7.8A+B	0.0002	0.0020	11.34	72	19.81	generous	cp	edge	1.47	0.094	0.085	0.064
562	705903246	GRS37-184-7.8A+B	0.0001	0.0017	17.11	52	22.78	generous	cp	edge	1.90	0.114	0.086	0.060
563	708840207	GRS37-184-7.8A+B	0.0001	0.0012	12.48	58	21.00	generous	cp	edge	1.00	0.065	0.065	0.065
564	711062740	GRS37-184-7.8A+B	0.0001	0.0012	6.90	50	20.75	generous	cp	edge	1.00	0.065	0.065	0.065
565	714594414	GRS37-184-7.8A+B	0.0001	0.0018	24.69	50	22.59	generous	cp	edge	1.92	0.115	0.068	0.060
566	715363668	GRS37-184-7.8A+B	0.0003	0.0032	13.99	65	20.81	generous	cp	edge	2.59	0.178	0.078	0.069
567	721129348	GRS37-184-7.8A+B	0.0001	0.0014	13.60	64	21.52	generous	cp	inclusion	1.40	0.083	0.078	0.059
568	721831553	GRS37-184-7.8A+B	0.0001	0.0011	18.25	45	21.68	generous	cp	inclusion	1.63	0.090	0.059	0.055
569	722426984	GRS37-184-7.8A+B	0.0003	0.0029	22.82	76	22.92	generous	cp	inclusion	1.45	0.110	0.095	0.075
570	723196183	GRS37-184-7.8A+B	0.0001	0.0009	30.02	42	21.10	generous	cp	inclusion	1.77	0.085	0.062	0.048
571	723271569	GRS37-184-7.8A+B	0.0002	0.0014	28.57	73	20.84	generous	cp	edge	1.65	0.089	0.073	0.054
572	727502085	GRS37-184-7.8A+B	0.0000	0.0009	25.62	45	23.10	generous	cp	edge	1.70	0.084	0.061	0.049
573	729073599	GRS37-184-7.8A+B	0.0002	0.0020	7.17	66	21.66	generous	cp	edge	1.77	0.113	0.073	0.064
574	732583804	GRS37-184-7.8A+B	0.0001	0.0012	16.85	46	22.83	generous	cp	inclusion	1.44	0.079	0.076	0.055
575	734872438	GRS37-184-7.8A+B	0.0003	0.0035	9.20	63	23.13	generous	cp	inclusion	1.62	0.134	0.102	0.083
576	737981989	GRS37-184-7.8A+B	0.0021	0.0093	520.59	145	19.76	generous	cp	edge	2.09	0.192	0.149	0.092
577	738304815	GRS37-184-7.8A+B	0.0006	0.0056	8.53	114	22.54	generous	cp	inclusion	2.55	0.212	0.104	0.083
578	742806810	GRS37-184-7.8A+B	0.0002	0.0017	7.15	64	21.97	generous	cp	inclusion	1.55	0.097	0.072	0.062
579	746379862	GRS37-184-7.8A+B	0.0002	0.0021	20.50	98	22.29	generous	cp	inclusion	1.27	0.093	0.080	0.074
580	749179553	GRS37-184-7.8A+B	0.0001	0.0012	21.59	42	23.46	generous	cp	inclusion	1.92	0.103	0.062	0.054
581	751413605	GRS37-184-7.8A+B	0.0005	0.0053	7.44	84	21.66	generous	cp	inclusion	2.49	0.181	0.112	0.072
582	752177077	GRS37-184-7.8A+B	0.0002	0.0017	7.19	67	21.23	generous	cp	edge	1.64	0.100	0.067	0.061
583	754929542	GRS37-184-7.8A+B	0.0002	0.0027	18.86	58	23.31	generous	cp	inclusion	2.40	0.152	0.087	0.063
584	755740983	GRS37-184-7.8A+B	0.0001	0.0011	25.36	49	23.36	generous	cp	inclusion	1.22	0.068	0.068	0.056
585	757278667	GRS37-184-7.8A+B	0.0001	0.0015	2.44	55	21.11	generous	cp	edge	2.01	0.110	0.066	0.055
586	757793744	GRS37-184-7.8A+B	0.0002	0.0018	17.76	77	23.03	generous	cp	inclusion	1.45	0.093	0.080	0.064
587	760065081	GRS37-184-7.8A+B	0.0002	0.0026	38.55	53	23.13	generous	cp	inclusion	1.44	0.111	0.083	0.077
588	765177383	GRS37-184-7.8A+B	0.0003	0.0030	9.80	89	20.65	generous	cp	inclusion	1.70	0.119	0.091	0.070
589	765878725	GRS37-184-7.8A+B	0.0006	0.0050	6.03	101	20.65	generous	cp	inclusion	1.44	0.131	0.112	0.091
590	767778251	GRS37-184-7.8A+B	0.0001	0.0011	45.00	44	21.41	generous	cp	edge	1.48	0.082	0.065	0.055
591	771541823	GRS37-184-7.8A+B	0.0002	0.0020	9.08	77	21.63	generous	cp	inclusion	1.47	0.094	0.085	0.064
592	771543477	GRS37-184-7.8A+B	0.0001	0.0012	13.66	53	22.58	generous	cp	inclusion	1.72	0.096	0.067	0.056
593	776024834	GRS37-184-7.8A+B	0.0001	0.0015	17.86	47	23.67	generous	cp	inclusion	2.24	0.131	0.060	0.059
594	779561409	GRS37-184-7.8A+B	0.0009	0.0062	29.12	108	22.03	generous	cp	inclusion	1.73	0.146	0.128	0.085
595	780227230	GRS37-184-7.8A+B	0.0001	0.0020	25.03	45	22.89	generous	cp	inclusion	2.42	0.122	0.099	0.050
596	781733434	GRS37-184-7.8A+B	0.0001	0.0018	32.68	63	22.66	generous	cp	inclusion	1.45	0.093	0.080	0.064
597	784478362	GRS37-184-7.8A+B	0.0002	0.0018	10.94	72	20.63	generous	cp	edge	2.12	0.122	0.067	0.058
598	792516328	GRS37-184-7.8A+B	0.0005	0.0047	8.91	80	22.23	generous	cp	edge	1.75	0.145	0.112	0.083

599	793191150	GRS37-184-7.8A+B	0.0001	0.0017	13.76	46	23.62	generous	cp	inclusion	3.02	0.144	0.073	0.048
600	795368129	GRS37-184-7.8A+B	0.0001	0.0014	13.43	59	21.64	generous	cp	inclusion	1.31	0.081	0.075	0.062
601	798975058	GRS37-184-7.8A+B	0.0001	0.0020	46.85	45	21.71	generous	cp	inclusion	2.01	0.122	0.086	0.061
602	799698796	GRS37-184-7.8A+B	0.0001	0.0017	17.51	55	21.60	generous	cp	inclusion	1.64	0.100	0.067	0.061
603	807538700	GRS37-184-7.8A+B	0.0002	0.0015	10.78	70	24.21	generous	cp	edge	1.59	0.097	0.064	0.061
604	814769275	GRS37-184-7.8A+B	0.0001	0.0015	15.11	47	24.64	generous	cp	inclusion	1.59	0.097	0.064	0.061
605	828453562	GRS37-184-7.8A+B	0.0017	0.0096	6.12	148	20.10	generous	cp	edge	1.66	0.175	0.132	0.105
606	834422960	GRS37-184-7.8A+B	0.0003	0.0030	24.51	84	22.68	generous	cp	edge	1.25	0.108	0.089	0.086
607	836403659	GRS37-184-7.8A+B	0.0029	0.0125	9.31	224	22.78	generous	cp	inclusion	1.45	0.177	0.150	0.122
608	837279710	GRS37-184-7.8A+B	0.0026	0.0120	31.31	184	20.86	generous	cp	inclusion	2.03	0.207	0.162	0.102
609	837731684	GRS37-184-7.8A+B	0.0001	0.0011	145.44	69	23.68	generous	cp	edge	1.48	0.082	0.065	0.055
610	840607092	GRS37-184-7.8A+B	0.0001	0.0009	36.14	49	20.50	generous	cp	edge	1.70	0.084	0.061	0.049
611	841429912	GRS37-184-7.8A+B	0.0008	0.0076	35.99	82	20.61	generous	cp	edge	3.59	0.307	0.112	0.088
612	843442181	GRS37-184-7.8A+B	0.0002	0.0030	300.00	59	22.42	generous	cp	edge	2.20	0.153	0.086	0.070
613	847946652	GRS37-184-7.8A+B	0.0001	0.0018	23.46	58	23.58	generous	cp	inclusion	2.11	0.117	0.071	0.056
614	855344452	GRS37-184-7.8A+B	0.0009	0.0050	6.89	146	22.43	generous	cp	inclusion	1.45	0.129	0.118	0.090
615	865825230	GRS37-184-7.8A+B	0.0003	0.0017	7.39	99	20.53	generous	cp	edge	1.83	0.111	0.066	0.061
616	868699372	GRS37-184-7.8A+B	0.0002	0.0017	82.66	73	20.61	generous	cp	edge	1.82	0.105	0.078	0.058
617	869758296	GRS37-184-7.8A+B	0.0001	0.0017	6.94	51	23.20	generous	cp	inclusion	1.95	0.110	0.082	0.057
618	870621138	GRS37-184-7.8A+B	0.0001	0.0011	101.87	56	20.77	generous	cp	edge	1.48	0.082	0.065	0.055
619	871922815	GRS37-184-7.8A+B	0.0001	0.0015	5.19	56	23.57	generous	cp	inclusion	2.38	0.133	0.061	0.056
620	884881717	GRS37-184-7.8A+B	0.0002	0.0020	46.35	61	23.24	generous	cp	inclusion	1.51	0.095	0.085	0.063
621	892831870	GRS37-184-7.8A+B	0.0002	0.0023	46.27	75	22.45	generous	cp	inclusion	1.43	0.101	0.088	0.070
622	901483301	GRS37-184-7.8A+B	0.0005	0.0065	9.41	62	23.26	generous	cp	edge	2.17	0.180	0.147	0.083
623	902076174	GRS37-184-7.8A+B	0.0001	0.0015	123.12	54	20.90	generous	cp	edge	2.44	0.129	0.067	0.053
624	907259764	GRS37-184-7.8A+B	0.0009	0.0079	15.70	124	22.33	generous	cp	inclusion	1.90	0.190	0.146	0.100
625	914460461	GRS37-184-7.8A+B	0.0003	0.0024	60.25	75	22.72	generous	cp	edge	2.18	0.133	0.084	0.061
626	968155737	GRS37-184-7.8A+B	0.0001	0.0009	67.86	52	19.14	generous	cp	edge	2.86	0.099	0.059	0.035
627	970407026	GRS37-184-7.8A+B	0.0016	0.0078	44.11	206	21.52	generous	cp	edge	1.35	0.145	0.130	0.107
628	994198523	GRS37-184-7.8A+B	0.0001	0.0011	374.57	61	21.57	generous	cp	edge	1.55	0.087	0.062	0.056
629	9358131	GRS97-9	0.0000	0.0001	0.62	146	22.75	generous	cp	inclusion	1.53	0.038	0.027	0.025
630	10560842	GRS97-9	0.0000	0.0000	1.39	103	18.80	generous	cp	edge	1.47	0.028	0.022	0.019
631	15375650	GRS97-9	0.0000	0.0001	3.75	130	20.46	generous	cp	edge	1.38	0.032	0.027	0.023
632	17742662	GRS97-9	0.0000	0.0001	0.60	141	21.13	generous	cp	edge	1.63	0.037	0.029	0.023
633	18229683	GRS97-9	0.0000	0.0001	0.89	153	22.30	generous	cp	edge	2.16	0.054	0.030	0.025
634	18814275	GRS97-9	0.0000	0.0001	1.41	152	18.86	generous	cp	edge	1.55	0.033	0.028	0.021
635	20059580	GRS97-9	0.0000	0.0001	0.41	132	18.81	generous	cp	edge	1.75	0.041	0.029	0.023
636	21057976	GRS97-9	0.0000	0.0001	0.60	138	22.13	generous	cp	edge	1.34	0.033	0.029	0.024
637	58236224	GRS97-9	0.0000	0.0001	0.85	146	16.76	generous	cp	edge	1.14	0.028	0.027	0.025
638	58814564	GRS97-9	0.0000	0.0001	3.41	212	18.16	generous	cp	edge	1.59	0.041	0.035	0.026
639	59294477	GRS97-9	0.0000	0.0001	1.40	210	17.46	generous	cp	matrix	1.25	0.033	0.031	0.027
640	109771899	GRS97-9	0.0000	0.0001	4.41	216	17.84	generous	cp	edge	1.58	0.042	0.031	0.026
641	111102071	GRS97-9	0.0000	0.0001	0.66	136	18.57	generous	cp	edge	1.37	0.031	0.029	0.023

642	129536701	GRS97-9	0.0000	0.0001	4.15	127	16.86	generous	cp	edge	1.37	0.029	0.022	0.022
643	58815076	GRS97-9	0.0000	0.0001	4.60	212	19.67	strict	cp	edge	1.64	0.041	0.032	0.025
644	59294477	GRS97-9	0.0000	0.0001	3.17	210	19.94	strict	cp	edge	1.15	0.031	0.028	0.027
645	110033531	GRS97-9	0.0000	0.0001	7.12	216	20.73	strict	cp	edge	1.52	0.039	0.029	0.025
646	1.012E+09	TE14-01-754.3	0.0021	0.0067	0.0104	208	27.65	strict	cp	matrix	1.58	0.156	0.114	0.099
647	1.047E+09	TE14-01-754.3	0.0053	0.0142	1.7379	244	27.81	strict	cp	edge	1.83	0.223	0.141	0.122
648	115812894	TE14-01-754.3	0.0002	0.0018	70.22	80	33.94	generous	cp	edge	2.65	0.141	0.071	0.053
649	116564459	TE14-01-754.3	0.0002	0.0017	0.15	77	31.83	generous	cp	edge	1.99	0.113	0.078	0.057
650	117322487	TE14-01-754.3	0.0005	0.0040	0.22	86	34.04	generous	cp	edge	2.43	0.157	0.124	0.065
651	125600191	TE14-01-754.3	0.0003	0.0015	1.13	107	29.74	generous	cp	edge/matrix	1.42	0.085	0.081	0.060
652	130060230	TE14-01-754.3	0.0006	0.0037	2.55	89	28.43	generous	cp	edge/matrix	3.24	0.191	0.095	0.059
653	136011243	TE14-01-754.3	0.0003	0.0017	33.54	97	25.21	generous	cp	edge/matrix	1.60	0.102	0.070	0.064
654	137496578	TE14-01-754.3	0.0039	0.0253	0.17	127	31.72	generous	cp	edge/matrix	3.98	0.596	0.200	0.136
655	138257839	TE14-01-754.3	0.0005	0.0027	9.21	108	27.43	generous	cp	edge/matrix	1.80	0.122	0.098	0.068
656	139019111	TE14-01-754.3	0.0031	0.0114	0.18	173	28.08	generous	cp	edge/matrix	2.87	0.229	0.173	0.080
657	144267921	TE14-01-754.3	0.0042	0.0239	0.12	117	29.30	generous	cp	edge/matrix	9.15	0.580	0.221	0.116
658	144280054	TE14-01-754.3	0.0002	0.0014	0.38	86	26.44	generous	cp	edge/matrix	1.65	0.089	0.073	0.054
659	144296234	TE14-01-754.3	0.0003	0.0014	3.03	103	28.04	generous	cp	edge/matrix	1.40	0.083	0.078	0.059
660	146538792	TE14-01-754.3	0.0053	0.0198	0.30	155	26.58	generous	cp	edge/matrix	5.52	0.481	0.152	0.087
661	148764360	TE14-01-754.3	0.0007	0.0035	0.01	118	24.71	generous	cp	edge/matrix	4.15	0.261	0.070	0.063
662	150294993	TE14-01-754.3	0.0003	0.0017	0.02	88	25.72	generous	cp	edge/matrix	1.71	0.099	0.079	0.058
663	150358912	TE14-01-754.3	0.0010	0.0059	17.62	112	29.19	generous	cp	edge/matrix	4.97	0.308	0.122	0.062
664	151077294	TE14-01-754.3	0.0003	0.0017	0.13	98	27.58	generous	cp	edge/matrix	2.72	0.127	0.073	0.047
665	152554535	TE14-01-754.3	0.0002	0.0011	0.57	92	28.83	generous	cp	edge/matrix	2.84	0.101	0.074	0.036
666	153292348	TE14-01-754.3	0.0006	0.0034	1.76	130	25.98	generous	cp	edge/matrix	1.80	0.136	0.093	0.076
667	153311762	TE14-01-754.3	0.0007	0.0030	0.22	145	25.60	generous	cp	edge/matrix	1.61	0.125	0.091	0.078
668	154047148	TE14-01-754.3	0.0011	0.0053	1.02	124	26.56	generous	cp	edge/matrix	2.72	0.181	0.134	0.067
669	156527514	TE14-01-754.3	0.0004	0.0021	0.01	101	26.58	generous	cp	edge/matrix	2.43	0.129	0.086	0.053
670	157056633	TE14-01-754.3	0.0002	0.0015	0.02	81	29.14	generous	cp	edge/matrix	2.36	0.112	0.085	0.047
671	158560570	TE14-01-754.3	0.0004	0.0018	1.40	120	25.93	generous	cp	edge/matrix	1.52	0.099	0.072	0.065
672	158664919	TE14-01-754.3	0.0005	0.0034	4.14	85	27.45	generous	cp	edge/matrix	2.35	0.140	0.109	0.060
673	160053990	TE14-01-754.3	0.0002	0.0009	0.07	83	28.00	generous	cp	edge/matrix	1.56	0.075	0.062	0.048
674	160223861	TE14-01-754.3	0.0002	0.0015	0.06	75	27.28	generous	cp	edge/matrix	2.45	0.125	0.068	0.051
675	161040944	TE14-01-754.3	0.0059	0.0259	3.78	178	29.16	generous	cp	edge/matrix	3.32	0.372	0.209	0.112
676	161723754	TE14-01-754.3	0.0007	0.0038	0.01	131	28.94	generous	cp	edge/matrix	2.52	0.172	0.092	0.068
677	162548920	TE14-01-754.3	0.0001	0.0009	0.66	83	28.70	generous	cp	edge/matrix	1.56	0.075	0.062	0.048
678	163161365	TE14-01-754.3	0.0005	0.0021	2.92	120	27.31	generous	cp	edge/matrix	1.96	0.115	0.084	0.059
679	163226883	TE14-01-754.3	0.0002	0.0012	0.14	79	29.52	generous	cp	edge/matrix	1.99	0.097	0.069	0.049
680	163974401	TE14-01-754.3	0.0004	0.0018	1.02	91	25.90	generous	cp	edge/matrix	1.54	0.093	0.086	0.060
681	163991392	TE14-01-754.3	0.0008	0.0043	0.34	139	28.57	generous	cp	edge/matrix	1.63	0.132	0.113	0.081
682	163998667	TE14-01-754.3	0.0002	0.0015	0.00	76	23.25	generous	cp	edge/matrix	1.59	0.097	0.064	0.061
683	164610279	TE14-01-754.3	0.0004	0.0024	0.61	97	26.68	generous	cp	edge/matrix	2.30	0.134	0.090	0.058
684	166209679	TE14-01-754.3	0.0009	0.0040	19.42	145	25.86	generous	cp	edge/matrix	1.98	0.144	0.100	0.073

685	166244463	TE14-01-754.3	0.0010	0.0043	0.41	146	27.46	generous	cp	edge/matrix	1.74	0.135	0.106	0.078
686	167040498	TE14-01-754.3	0.0003	0.0020	24.64	80	25.88	generous	cp	edge/matrix	2.10	0.114	0.087	0.054
687	167581755	TE14-01-754.3	0.0006	0.0024	1.68	124	27.89	generous	cp	edge/matrix	1.74	0.105	0.100	0.061
688	167723329	TE14-01-754.3	0.0012	0.0058	1.36	139	24.61	generous	cp	edge/matrix	2.20	0.157	0.153	0.071
689	168348697	TE14-01-754.3	0.0042	0.0184	0.74	152	30.13	generous	cp	edge/matrix	3.42	0.271	0.258	0.079
690	168502384	TE14-01-754.3	0.0021	0.0114	0.38	130	29.56	generous	cp	edge/matrix	4.67	0.350	0.164	0.075
691	169232115	TE14-01-754.3	0.0077	0.0370	2.99	144	28.77	generous	cp	edge/matrix	5.77	0.645	0.299	0.112
692	169241013	TE14-01-754.3	0.0020	0.0099	0.02	122	28.06	generous	cp	edge/matrix	3.40	0.248	0.204	0.073
693	170763541	TE14-01-754.3	0.0093	0.0457	0.93	150	28.53	generous	cp	edge/matrix	5.57	0.630	0.428	0.113
694	171358187	TE14-01-754.3	0.0008	0.0064	1.61	91	32.77	generous	cp	edge/matrix	3.61	0.256	0.155	0.072
695	171374362	TE14-01-754.3	0.0003	0.0020	0.85	84	28.06	generous	cp	edge/matrix	2.05	0.108	0.097	0.053
696	172167180	TE14-01-754.3	0.0006	0.0026	0.01	116	27.48	generous	cp	edge/matrix	2.06	0.122	0.099	0.059
697	172869402	TE14-01-754.3	0.0014	0.0085	2.81	102	30.64	generous	cp	edge/matrix	3.78	0.265	0.150	0.070
698	172965676	TE14-01-754.3	0.0041	0.0225	0.71	122	28.48	generous	cp	edge/matrix	5.42	0.507	0.224	0.094
699	173709956	TE14-01-754.3	0.0007	0.0044	1.39	111	29.20	generous	cp	edge/matrix	4.00	0.232	0.104	0.058
700	173728557	TE14-01-754.3	0.0007	0.0035	4.63	106	28.65	generous	cp	edge/matrix	1.96	0.127	0.112	0.065
701	174452622	TE14-01-754.3	0.0003	0.0030	0.17	75	33.87	generous	cp	edge/matrix	2.13	0.133	0.108	0.062
702	174504382	TE14-01-754.3	0.0003	0.0017	3.30	80	29.03	generous	cp	edge/matrix	2.05	0.109	0.079	0.053
703	174529435	TE14-01-754.3	0.0006	0.0030	0.36	100	27.48	generous	cp	edge/matrix	2.45	0.159	0.090	0.065
704	176025292	TE14-01-754.3	0.0001	0.0009	0.47	77	31.41	generous	cp	edge/matrix	2.00	0.100	0.054	0.050
705	176051981	TE14-01-754.3	0.0005	0.0034	8.61	89	27.89	generous	cp	edge/matrix	3.06	0.179	0.119	0.058
706	176793029	TE14-01-754.3	0.0004	0.0029	0.21	98	27.36	generous	cp	edge/matrix	1.88	0.121	0.101	0.064
707	176800309	TE14-01-754.3	0.0007	0.0041	0.32	121	28.50	generous	cp	edge/matrix	1.90	0.137	0.120	0.072
708	177379586	TE14-01-754.3	0.0029	0.0158	0.31	154	30.16	generous	cp	edge/matrix	3.98	0.332	0.176	0.083
709	177505791	TE14-01-754.3	0.0012	0.0059	0.02	107	27.78	generous	cp	edge/matrix	1.86	0.162	0.118	0.087
710	177519524	TE14-01-754.3	0.0003	0.0018	0.27	100	25.63	generous	cp	edge/matrix	1.75	0.097	0.090	0.056
711	177526813	TE14-01-754.3	0.0003	0.0018	15.12	88	29.63	generous	cp	edge/matrix	2.35	0.145	0.062	0.062
712	177538935	TE14-01-754.3	0.0002	0.0015	5.53	95	29.00	generous	cp	edge/matrix	1.95	0.106	0.076	0.054
713	178278366	TE14-01-754.3	0.0002	0.0012	0.35	85	26.72	generous	cp	edge/matrix	1.68	0.089	0.078	0.053
714	178287264	TE14-01-754.3	0.0019	0.0087	0.11	127	27.22	generous	cp	edge/matrix	2.84	0.212	0.165	0.075
715	178295351	TE14-01-754.3	0.0007	0.0044	0.62	95	29.78	generous	cp	edge/matrix	3.16	0.191	0.132	0.060
716	178311544	TE14-01-754.3	0.0002	0.0015	0.11	76	29.89	generous	cp	edge/matrix	1.68	0.091	0.082	0.054
717	178931247	TE14-01-754.3	0.0005	0.0035	0.38	84	26.75	generous	cp	edge/matrix	2.33	0.139	0.118	0.060
718	178981416	TE14-01-754.3	0.0012	0.0056	14.41	146	28.55	generous	cp	edge/matrix	3.97	0.247	0.127	0.062
719	179051763	TE14-01-754.3	0.0002	0.0021	0.19	79	33.53	generous	cp	edge/matrix	2.05	0.126	0.079	0.062
720	179795252	TE14-01-754.3	0.0008	0.0040	0.19	128	27.26	generous	cp	edge/matrix	2.27	0.160	0.098	0.071
721	180394737	TE14-01-754.3	0.0001	0.0011	21.67	76	27.33	generous	cp	edge/matrix	1.45	0.080	0.069	0.055
722	182013552	TE14-01-754.3	0.0006	0.0029	1.49	110	28.09	generous	cp	edge/matrix	2.20	0.133	0.095	0.060
723	182045900	TE14-01-754.3	0.0004	0.0024	2.22	86	28.33	generous	cp	edge/matrix	1.94	0.124	0.090	0.064
724	185042456	TE14-01-754.3	0.0005	0.0035	0.02	97	30.37	generous	cp	edge/matrix	4.42	0.264	0.076	0.060
725	185739009	TE14-01-754.3	0.0003	0.0018	0.41	102	24.84	generous	cp	edge/matrix	1.62	0.094	0.087	0.058
726	185769758	TE14-01-754.3	0.0002	0.0012	1.70	87	26.38	generous	cp	edge/matrix	1.59	0.086	0.066	0.055
727	188923201	TE14-01-754.3	0.0002	0.0017	4.19	81	33.52	generous	cp	edge/matrix	2.15	0.127	0.062	0.059

728	191036356	TE14-01-754.3	0.0024	0.0120	0.81	155	28.22	generous	cp	edge/matrix	4.72	0.338	0.191	0.072
729	191781450	TE14-01-754.3	0.0002	0.0009	0.97	90	31.95	generous	cp	edge/matrix	1.85	0.083	0.070	0.045
730	194032904	TE14-01-754.3	0.0037	0.0180	0.64	138	26.87	generous	cp	edge/matrix	5.01	0.424	0.274	0.085
731	197057759	TE14-01-754.3	0.0006	0.0029	1.47	113	27.76	generous	cp	edge/matrix	2.06	0.137	0.091	0.067
732	199394922	TE14-01-754.3	0.0006	0.0034	0.26	100	27.58	generous	cp	edge/matrix	2.19	0.139	0.099	0.064
733	202385815	TE14-01-754.3	0.0006	0.0040	1.28	92	28.82	generous	cp	edge/matrix	2.61	0.173	0.126	0.066
734	370309834	TE14-01-754.3	0.0004	0.0030	1.59	82	30.26	generous	cp	edge/matrix	1.77	0.117	0.108	0.066
735	371324301	TE14-01-754.3	0.0006	0.0029	0.17	122	26.02	generous	cp	edge/matrix	1.47	0.117	0.082	0.079
736	385485059	TE14-01-754.3	0.0002	0.0014	1.22	75	30.92	generous	cp	edge/matrix	1.46	0.089	0.063	0.061
737	388489687	TE14-01-754.3	0.0003	0.0020	0.90	87	28.41	generous	cp	edge/matrix	2.13	0.120	0.076	0.056
738	392852655	TE14-01-754.3	0.0008	0.0062	0.33	98	34.40	generous	cp	edge/matrix	2.11	0.176	0.129	0.083
739	395998840	TE14-01-754.3	0.0022	0.0175	0.48	116	35.76	generous	cp	edge/matrix	1.78	0.237	0.197	0.133
740	397359598	TE14-01-754.3	0.0002	0.0017	3.12	90	29.40	generous	cp	edge/matrix	1.85	0.100	0.081	0.054
741	399718630	TE14-01-754.3	0.0007	0.0069	3.07	85	34.32	generous	cp	edge/matrix	1.43	0.155	0.131	0.109
742	404182710	TE14-01-754.3	0.0005	0.0046	0.32	79	34.21	generous	cp	edge/matrix	1.88	0.148	0.108	0.079
743	404928613	TE14-01-754.3	0.0020	0.0161	0.04	96	34.18	generous	cp	edge/matrix	2.27	0.286	0.161	0.126
744	405687455	TE14-01-754.3	0.0008	0.0072	1.55	80	35.08	generous	cp	edge/matrix	1.39	0.148	0.139	0.107
745	406457614	TE14-01-754.3	0.0002	0.0021	0.02	79	30.46	generous	cp	edge/matrix	1.66	0.101	0.092	0.061
746	411656266	TE14-01-754.3	0.0001	0.0009	0.11	86	29.85	generous	cp	edge/matrix	1.70	0.084	0.061	0.049
747	412418347	TE14-01-754.3	0.0102	0.0716	0.65	137	34.41	generous	cp	edge/matrix	4.03	0.671	0.261	0.166
748	413189322	TE14-01-754.3	0.0013	0.0105	0.04	99	33.48	generous	cp	edge/matrix	2.40	0.218	0.168	0.091
749	416931766	TE14-01-754.3	0.0011	0.0087	0.46	93	33.74	generous	cp	edge/matrix	2.20	0.200	0.180	0.091
750	417688179	TE14-01-754.3	0.0004	0.0040	7.64	90	36.29	generous	cp	edge/matrix	1.76	0.137	0.104	0.078
751	420004010	TE14-01-754.3	0.0002	0.0020	1.53	81	32.67	generous	cp	edge/matrix	1.80	0.109	0.084	0.060
752	422903013	TE14-01-754.3	0.0001	0.0011	0.68	77	29.59	generous	cp	edge/matrix	1.47	0.082	0.065	0.055
753	427415617	TE14-01-754.3	0.0003	0.0017	0.14	102	29.55	generous	cp	edge/matrix	1.55	0.097	0.072	0.062
754	430495481	TE14-01-754.3	0.0069	0.0451	0.79	147	34.50	generous	cp	edge/matrix	2.20	0.400	0.238	0.181
755	449136075	TE14-01-754.3	0.0003	0.0024	39.13	100	36.28	generous	cp	edge/matrix	1.90	0.117	0.097	0.061
756	449920784	TE14-01-754.3	0.0003	0.0014	0.50	91	28.04	generous	cp	edge/matrix	1.46	0.089	0.063	0.061
757	450798968	TE14-01-754.3	0.0005	0.0026	0.92	104	30.22	generous	cp	edge/matrix	2.69	0.148	0.097	0.055
758	464314492	TE14-01-754.3	0.0006	0.0026	2.91	140	25.46	generous	cp	edge/matrix	1.61	0.105	0.096	0.065
759	465808720	TE14-01-754.3	0.0002	0.0014	0.01	88	30.38	generous	cp	edge/matrix	2.62	0.123	0.062	0.047
760	468050468	TE14-01-754.3	0.0003	0.0020	0.62	105	29.30	generous	cp	edge/matrix	1.38	0.093	0.083	0.068
761	470200831	TE14-01-754.3	0.0011	0.0050	1.05	141	28.19	generous	cp	edge/matrix	1.97	0.173	0.093	0.088
762	496475583	TE14-01-754.3	0.0002	0.0009	0.17	90	30.20	generous	cp	edge/matrix	1.56	0.075	0.062	0.048
763	500270581	TE14-01-754.3	0.0002	0.0011	0.52	107	29.62	generous	cp	edge/matrix	1.46	0.080	0.069	0.055
764	511487408	TE14-01-754.3	0.0002	0.0014	0.09	107	27.69	generous	cp	edge/matrix	1.50	0.090	0.065	0.060
765	519003832	TE14-01-754.3	0.0006	0.0026	0.08	138	26.18	generous	cp	edge/matrix	1.25	0.101	0.083	0.081
766	525009853	TE14-01-754.3	0.0003	0.0012	0.61	85	26.83	generous	cp	edge/matrix	1.00	0.065	0.065	0.065
767	533869899	TE14-01-754.3	0.0009	0.0078	5.22	77	30.83	generous	cp	edge/matrix	1.77	0.197	0.124	0.111
768	537768607	TE14-01-754.3	0.0002	0.0012	3.23	75	24.17	generous	cp	edge/matrix	1.00	0.065	0.065	0.065
769	564916451	TE14-01-754.3	0.0005	0.0023	2.11	113	28.41	generous	cp	edge/matrix	1.97	0.121	0.086	0.061
770	646628276	TE14-01-754.3	0.0003	0.0021	0.02	102	28.91	generous	cp	edge/matrix	1.57	0.102	0.085	0.065

771	669963929	TE14-01-754.3	0.0003	0.0021	0.27	83	28.89	generous	cp	edge/matrix	1.91	0.111	0.092	0.058
772	722020835	TE14-01-754.3	0.0002	0.0011	1.23	91	27.32	generous	cp	edge/matrix	1.48	0.082	0.065	0.055
773	725039441	TE14-01-754.3	0.0001	0.0009	0.81	75	34.90	generous	cp	edge/matrix	1.56	0.075	0.062	0.048
774	748159446	TE14-01-754.3	0.0002	0.0021	1.75	78	31.88	generous	cp	edge/matrix	1.37	0.100	0.079	0.073
775	768253442	TE14-01-754.3	0.0008	0.0029	0.04	151	25.55	generous	cp	edge/matrix	1.60	0.110	0.100	0.069
776	795955950	TE14-01-754.3	0.0002	0.0015	70.81	86	29.37	generous	cp	edge/matrix	1.84	0.098	0.075	0.053
777	799161553	TE14-01-754.3	0.0002	0.0014	5.34	83	27.23	generous	cp	edge/matrix	1.50	0.090	0.065	0.060
778	804932441	TE14-01-754.3	0.0006	0.0050	71.54	85	33.67	generous	cp	edge/matrix	1.72	0.147	0.113	0.086
779	837366340	TE14-01-754.3	0.0002	0.0015	2.48	76	33.10	generous	cp	edge/matrix	1.56	0.092	0.088	0.059
780	841099828	TE14-01-754.3	0.0005	0.0030	72.06	110	28.05	generous	cp	edge/matrix	1.83	0.128	0.094	0.070
781	843407507	TE14-01-754.3	0.0005	0.0041	2.06	112	37.07	generous	cp	edge/matrix	1.72	0.143	0.105	0.083
782	844266652	TE14-01-754.3	0.0006	0.0064	6.47	105	37.92	generous	cp	edge/matrix	1.80	0.180	0.112	0.100
783	844877770	TE14-01-754.3	0.0006	0.0037	67.01	108	32.96	generous	cp	inclusion	1.73	0.142	0.093	0.082
784	847204815	TE14-01-754.3	0.0005	0.0024	2.63	127	27.25	generous	cp	edge/matrix	1.91	0.125	0.087	0.066
785	851018569	TE14-01-754.3	0.0003	0.0015	3.10	98	28.63	generous	cp	edge/matrix	1.56	0.093	0.070	0.060
786	852663135	TE14-01-754.3	0.0001	0.0011	71.44	76	31.95	generous	cp	edge/matrix	1.82	0.086	0.070	0.047
787	852967035	TE14-01-754.3	0.0003	0.0015	109.95	88	32.11	generous	cp	edge/matrix	1.51	0.092	0.073	0.061
788	854738761	TE14-01-754.3	0.0004	0.0027	74.88	105	30.22	generous	cp	edge/matrix	1.72	0.124	0.083	0.072
789	855415057	TE14-01-754.3	0.0004	0.0030	36.46	81	31.86	generous	cp	inclusion	1.70	0.126	0.097	0.074
790	856497733	TE14-01-754.3	0.0001	0.0011	136.90	77	29.95	generous	cp	edge/matrix	1.22	0.068	0.068	0.056
791	857719346	TE14-01-754.3	0.0013	0.0046	1.39	158	27.98	generous	cp	edge/matrix	1.69	0.148	0.093	0.088
792	860058882	TE14-01-754.3	0.0002	0.0015	27.44	88	29.14	generous	cp	edge/matrix	1.50	0.087	0.082	0.058
793	861689966	TE14-01-754.3	0.0002	0.0018	14.73	81	30.00	generous	cp	edge/matrix	2.92	0.136	0.085	0.047
794	862893465	TE14-01-754.3	0.0002	0.0017	22.90	92	31.97	generous	cp	edge/matrix	1.56	0.091	0.084	0.058
795	864515748	TE14-01-754.3	0.0003	0.0020	1.74	96	29.94	generous	cp	edge/matrix	2.29	0.124	0.089	0.054
796	867436833	TE14-01-754.3	0.0002	0.0015	28.87	84	28.36	generous	cp	edge/matrix	2.92	0.137	0.063	0.047
797	867594634	TE14-01-754.3	0.0002	0.0017	0.01	76	30.50	generous	cp	edge/matrix	1.81	0.111	0.078	0.061
798	868266282	TE14-01-754.3	0.0004	0.0023	1.11	103	28.53	generous	cp	edge/matrix	2.24	0.135	0.077	0.060
799	869124627	TE14-01-754.3	0.0002	0.0011	0.28	78	28.05	generous	cp	edge/matrix	1.22	0.068	0.068	0.056
800	870581631	TE14-01-754.3	0.0002	0.0014	0.02	78	27.40	generous	cp	edge/matrix	1.65	0.089	0.073	0.054
801	871351622	TE14-01-754.3	0.0002	0.0017	0.01	75	29.79	generous	cp	edge/matrix	1.55	0.097	0.072	0.062
802	872095096	TE14-01-754.3	0.0002	0.0017	0.01	85	30.38	generous	cp	edge/matrix	2.74	0.132	0.079	0.048
803	874349777	TE14-01-754.3	0.0004	0.0023	12.42	100	30.37	generous	cp	edge/matrix	2.57	0.154	0.075	0.060
804	875092772	TE14-01-754.3	0.0007	0.0056	0.01	104	37.05	generous	cp	edge/matrix	1.57	0.142	0.124	0.090
805	878026037	TE14-01-754.3	0.0017	0.0059	0.12	174	27.92	generous	cp	edge/matrix	1.21	0.128	0.110	0.106
806	879014655	TE14-01-754.3	0.0004	0.0024	4.54	107	30.46	generous	cp	edge/matrix	1.83	0.123	0.086	0.067
807	880281528	TE14-01-754.3	0.0008	0.0037	0.31	124	29.72	generous	cp	edge/matrix	2.71	0.173	0.094	0.064
808	880301614	TE14-01-754.3	0.0003	0.0024	0.28	75	30.64	generous	cp	edge/matrix	2.16	0.127	0.094	0.059
809	880332402	TE14-01-754.3	0.0003	0.0020	1.80	79	29.82	generous	cp	edge/matrix	1.86	0.106	0.094	0.057
810	880338845	TE14-01-754.3	0.0005	0.0030	0.27	82	30.37	generous	cp	edge/matrix	1.87	0.119	0.114	0.064
811	881284697	TE14-01-754.3	0.0002	0.0014	14.59	84	34.27	generous	cp	edge/matrix	1.78	0.095	0.067	0.054
812	882583934	TE14-01-754.3	0.0011	0.0046	0.73	153	27.56	generous	cp	edge/matrix	1.65	0.141	0.098	0.085
813	885607346	TE14-01-754.3	0.0013	0.0061	3.39	153	31.77	generous	cp	edge/matrix	1.61	0.149	0.118	0.092

814	890070422	TE14-01-754.3	0.0002	0.0014	0.00	94	27.00	generous	cp	edge/matrix	1.46	0.090	0.063	0.061
815	890113134	TE14-01-754.3	0.0002	0.0014	0.00	92	30.00	generous	cp	edge/matrix	2.06	0.096	0.084	0.046
816	890114288	TE14-01-754.3	0.0010	0.0058	1.25	138	34.16	generous	cp	edge/matrix	1.84	0.153	0.125	0.083
817	890843160	TE14-01-754.3	0.0001	0.0012	20.17	77	29.58	generous	cp	edge/matrix	1.38	0.086	0.062	0.062
818	892297573	TE14-01-754.3	0.0002	0.0012	1.06	85	27.48	generous	cp	edge/matrix	1.56	0.086	0.071	0.055
819	893097606	TE14-01-754.3	0.0003	0.0026	0.16	81	33.08	generous	cp	edge/matrix	2.59	0.154	0.096	0.059
820	894473758	TE14-01-754.3	0.0002	0.0009	6.02	86	30.60	generous	cp	edge/matrix	1.56	0.075	0.062	0.048
821	896674951	TE14-01-754.3	0.0004	0.0029	0.01	82	30.08	generous	cp	edge/matrix	2.69	0.151	0.108	0.056
822	897383541	TE14-01-754.3	0.0008	0.0047	16.21	111	31.14	generous	cp	edge/matrix	2.37	0.182	0.096	0.077
823	899844719	TE14-01-754.3	0.0003	0.0021	0.01	94	27.17	generous	cp	edge/matrix	2.05	0.126	0.080	0.062
824	900596272	TE14-01-754.3	0.0002	0.0015	0.00	83	28.66	generous	cp	edge/matrix	2.31	0.110	0.081	0.047
825	902655866	TE14-01-754.3	0.0002	0.0014	1.60	79	29.15	generous	cp	edge/matrix	1.91	0.102	0.078	0.054
826	905084646	TE14-01-754.3	0.0013	0.0079	0.03	117	29.19	generous	cp	edge/matrix	2.75	0.209	0.143	0.076
827	905118478	TE14-01-754.3	0.0012	0.0049	0.02	140	25.96	generous	cp	edge/matrix	1.75	0.143	0.112	0.082
828	905705691	TE14-01-754.3	0.0001	0.0012	20.65	77	28.88	generous	cp	edge/matrix	1.62	0.088	0.068	0.054
829	905849122	TE14-01-754.3	0.0008	0.0069	0.64	98	32.47	generous	cp	edge/matrix	2.83	0.242	0.113	0.086
830	907961984	TE14-01-754.3	0.0004	0.0021	0.11	96	29.89	generous	cp	edge/matrix	1.67	0.115	0.076	0.069
831	909605301	TE14-01-754.3	0.0002	0.0015	0.62	92	34.82	generous	cp	edge/matrix	1.59	0.097	0.064	0.061
832	911856747	TE14-01-754.3	0.0001	0.0009	0.04	78	31.40	generous	cp	edge/matrix	1.56	0.075	0.062	0.048
833	912601018	TE14-01-754.3	0.0005	0.0026	0.23	112	30.08	generous	cp	edge/matrix	1.56	0.121	0.082	0.077
834	914035294	TE14-01-754.3	0.0003	0.0014	5.54	109	26.28	generous	cp	edge/matrix	1.40	0.086	0.071	0.061
835	914127497	TE14-01-754.3	0.0012	0.0049	0.03	179	29.91	generous	cp	edge/matrix	1.36	0.123	0.115	0.090
836	916325760	TE14-01-754.3	0.0001	0.0011	0.00	77	28.83	generous	cp	edge/matrix	1.85	0.095	0.068	0.051
837	916378132	TE14-01-754.3	0.0007	0.0041	0.04	121	30.88	generous	cp	edge/matrix	1.96	0.158	0.089	0.080
838	918621549	TE14-01-754.3	0.0002	0.0020	0.01	84	30.58	generous	cp	edge/matrix	2.33	0.131	0.078	0.056
839	919882118	TE14-01-754.3	0.0001	0.0014	1.44	75	33.19	generous	cp	edge/matrix	2.08	0.100	0.074	0.048
840	920564928	TE14-01-754.3	0.0005	0.0024	0.50	118	28.97	generous	cp	edge/matrix	1.95	0.121	0.085	0.062
841	923372112	TE14-01-754.3	0.0003	0.0037	4.63	77	40.18	generous	cp	edge/matrix	1.53	0.135	0.098	0.088
842	927736538	TE14-01-754.3	0.0002	0.0015	0.73	76	27.29	generous	cp	edge/matrix	1.98	0.114	0.065	0.058
843	928195062	TE14-01-754.3	0.0003	0.0021	1.73	97	34.71	generous	cp	edge/matrix	1.44	0.094	0.090	0.065
844	928616049	TE14-01-754.3	0.0002	0.0020	0.20	85	30.16	generous	cp	edge/matrix	1.44	0.091	0.090	0.063
845	928820362	TE14-01-754.3	0.0009	0.0069	3.70	90	33.38	generous	cp	edge/matrix	3.14	0.254	0.136	0.081
846	929129653	TE14-01-754.3	0.0011	0.0052	0.31	140	30.17	generous	cp	edge/matrix	1.19	0.119	0.110	0.100
847	929755647	TE14-01-754.3	0.0004	0.0024	1.46	83	26.43	generous	cp	edge/matrix	2.80	0.166	0.080	0.059
848	930628747	TE14-01-754.3	0.0003	0.0027	0.02	84	31.20	generous	cp	edge/matrix	1.74	0.118	0.100	0.068
849	931042680	TE14-01-754.3	0.0002	0.0014	0.54	77	30.58	generous	cp	edge/matrix	1.46	0.090	0.063	0.061
850	931320611	TE14-01-754.3	0.0008	0.0040	18.42	156	27.94	generous	cp	edge/matrix	1.46	0.119	0.112	0.081
851	931388337	TE14-01-754.3	0.0002	0.0015	0.01	95	29.56	generous	cp	edge/matrix	1.82	0.102	0.077	0.056
852	932103510	TE14-01-754.3	0.0004	0.0026	0.36	119	33.03	generous	cp	edge/matrix	1.64	0.106	0.094	0.065
853	932131065	TE14-01-754.3	0.0003	0.0024	0.16	84	30.69	generous	cp	edge/matrix	2.07	0.134	0.086	0.065
854	932710892	TE14-01-754.3	0.0004	0.0023	0.22	104	24.22	generous	cp	edge/matrix	1.71	0.110	0.081	0.064
855	932857541	TE14-01-754.3	0.0002	0.0017	1.06	84	30.97	generous	cp	edge/matrix	2.03	0.118	0.068	0.058
856	933448732	TE14-01-754.3	0.0002	0.0009	2.95	88	32.80	generous	cp	edge/matrix	1.56	0.075	0.062	0.048

857	933603399	TE14-01-754.3	0.0002	0.0014	2.49	76	32.42	generous	cp	edge/matrix	1.46	0.090	0.063	0.061
858	934378469	TE14-01-754.3	0.0003	0.0023	0.06	84	34.45	generous	cp	edge/matrix	1.99	0.132	0.083	0.066
859	934992429	TE14-01-754.3	0.0002	0.0018	3.97	79	27.77	generous	cp	edge/matrix	2.07	0.110	0.082	0.053
860	935753698	TE14-01-754.3	0.0006	0.0034	1.48	116	30.57	generous	cp	edge/matrix	1.96	0.129	0.114	0.066
861	936642771	TE14-01-754.3	0.0003	0.0017	0.02	123	28.31	generous	cp	edge/matrix	1.57	0.094	0.078	0.060
862	937206476	TE14-01-754.3	0.0002	0.0018	0.30	83	34.06	generous	cp	edge/matrix	1.54	0.093	0.087	0.060
863	937381472	TE14-01-754.3	0.0006	0.0041	0.07	84	31.73	generous	cp	edge/matrix	2.00	0.160	0.140	0.080
864	937945091	TE14-01-754.3	0.0003	0.0027	0.47	77	34.40	generous	cp	edge/matrix	2.40	0.157	0.071	0.065
865	938137095	TE14-01-754.3	0.0001	0.0014	1.30	78	32.00	generous	cp	edge/matrix	1.90	0.104	0.076	0.054
866	940174849	TE14-01-754.3	0.0003	0.0020	7.50	86	29.60	generous	cp	edge/matrix	2.15	0.126	0.075	0.059
867	940776520	TE14-01-754.3	0.0003	0.0018	0.01	98	30.94	generous	cp	edge/matrix	1.64	0.109	0.071	0.066
868	941152161	TE14-01-754.3	0.0003	0.0020	0.02	100	28.44	generous	cp	edge/matrix	1.73	0.103	0.085	0.060
869	941531318	TE14-01-754.3	0.0005	0.0029	0.41	130	29.74	generous	cp	edge/matrix	1.59	0.113	0.091	0.072
870	941881071	TE14-01-754.3	0.0019	0.0076	0.14	193	28.86	generous	cp	edge/matrix	2.30	0.207	0.123	0.090
871	943389106	TE14-01-754.3	0.0004	0.0030	0.06	97	36.27	generous	cp	edge/matrix	2.21	0.141	0.098	0.064
872	945460772	TE14-01-754.3	0.0003	0.0021	0.01	102	27.81	generous	cp	edge/matrix	1.27	0.093	0.080	0.074
873	945539279	TE14-01-754.3	0.0010	0.0041	0.49	163	33.29	generous	cp	edge/matrix	1.51	0.124	0.103	0.082
874	946072265	TE14-01-754.3	0.0003	0.0029	0.45	78	30.50	generous	cp	edge/matrix	1.68	0.124	0.087	0.074
875	946956615	TE14-01-754.3	0.0003	0.0018	0.01	95	32.28	generous	cp	edge/matrix	1.45	0.093	0.080	0.064
876	947623182	TE14-01-754.3	0.0002	0.0014	0.00	88	27.65	generous	cp	edge/matrix	1.46	0.090	0.063	0.061
877	947704943	TE14-01-754.3	0.0002	0.0014	0.02	90	30.12	generous	cp	edge/matrix	1.73	0.097	0.067	0.056
878	947717152	TE14-01-754.3	0.0005	0.0027	0.38	99	30.90	generous	cp	edge/matrix	1.73	0.126	0.085	0.073
879	949054205	TE14-01-754.3	0.0003	0.0020	0.30	87	31.84	generous	cp	edge/matrix	1.47	0.094	0.085	0.064
880	949313580	TE14-01-754.3	0.0002	0.0015	1.71	92	30.46	generous	cp	edge/matrix	1.70	0.097	0.074	0.057
881	949813874	TE14-01-754.3	0.0024	0.0123	0.25	164	31.89	generous	cp	edge/matrix	2.79	0.272	0.164	0.097
882	950561383	TE14-01-754.3	0.0001	0.0011	0.14	83	31.45	generous	cp	edge/matrix	1.73	0.082	0.077	0.047
883	950915964	TE14-01-754.3	0.0002	0.0014	0.10	90	30.14	generous	cp	edge/matrix	2.45	0.114	0.072	0.047
884	951466272	TE14-01-754.3	0.0008	0.0052	15.86	135	30.83	generous	cp	edge/matrix	2.70	0.216	0.096	0.080
885	952453870	TE14-01-754.3	0.0011	0.0058	0.18	127	30.38	generous	cp	edge/matrix	2.63	0.206	0.117	0.079
886	952858217	TE14-01-754.3	0.0005	0.0026	0.07	111	29.66	generous	cp	edge/matrix	1.67	0.112	0.100	0.067
887	954273931	TE14-01-754.3	0.0003	0.0020	0.88	97	34.91	generous	cp	edge/matrix	1.47	0.094	0.085	0.064
888	955158302	TE14-01-754.3	0.0004	0.0026	2.16	96	31.12	generous	cp	edge/matrix	2.19	0.133	0.099	0.061
889	955815067	TE14-01-754.3	0.0002	0.0012	0.43	95	26.25	generous	cp	edge/matrix	1.38	0.086	0.062	0.062
890	956117018	TE14-01-754.3	0.0003	0.0018	0.42	104	30.59	generous	cp	edge/matrix	1.50	0.096	0.085	0.064
891	956671129	TE14-01-754.3	0.0007	0.0035	0.44	141	29.44	generous	cp	edge/matrix	1.58	0.127	0.091	0.081
892	956735072	TE14-01-754.3	0.0001	0.0009	0.39	81	31.45	generous	cp	edge/matrix	1.70	0.084	0.061	0.049
893	958238189	TE14-01-754.3	0.0004	0.0021	0.05	117	29.11	generous	cp	edge/matrix	1.66	0.103	0.086	0.062
894	958390411	TE14-01-754.3	0.0001	0.0009	0.14	79	31.65	generous	cp	edge/matrix	1.56	0.075	0.062	0.048
895	959155624	TE14-01-754.3	0.0004	0.0020	0.08	120	26.71	generous	cp	edge/matrix	1.44	0.091	0.090	0.063
896	959688693	TE14-01-754.3	0.0006	0.0029	0.14	115	28.72	generous	cp	edge/matrix	2.22	0.131	0.103	0.059
897	959731011	TE14-01-754.3	0.0004	0.0030	0.63	80	31.72	generous	cp	edge/matrix	2.87	0.156	0.107	0.054
898	959898284	TE14-01-754.3	0.0002	0.0014	0.42	103	31.76	generous	cp	edge/matrix	1.31	0.081	0.075	0.062
899	962850320	TE14-01-754.3	0.0003	0.0017	0.79	110	27.46	generous	cp	edge/matrix	1.34	0.092	0.073	0.069

900	964212617	TE14-01-754.3	0.0006	0.0034	0.10	106	28.48	generous	cp	edge/matrix	1.68	0.127	0.100	0.075
901	964837973	TE14-01-754.3	0.0005	0.0024	2.66	130	28.21	generous	cp	edge/matrix	1.65	0.108	0.087	0.066
902	965005687	TE14-01-754.3	0.0004	0.0027	6.87	98	30.75	generous	cp	edge/matrix	2.52	0.151	0.097	0.060
903	965090551	TE14-01-754.3	0.0002	0.0012	0.00	108	27.22	generous	cp	edge/matrix	1.56	0.086	0.071	0.055
904	965309833	TE14-01-754.3	0.0004	0.0021	0.00	123	26.68	generous	cp	edge/matrix	1.60	0.102	0.082	0.064
905	965714940	TE14-01-754.3	0.0002	0.0015	0.00	78	29.43	generous	cp	edge/matrix	1.59	0.097	0.064	0.061
906	965773216	TE14-01-754.3	0.0001	0.0011	0.00	78	29.36	generous	cp	edge/matrix	1.95	0.091	0.062	0.047
907	967318510	TE14-01-754.3	0.0003	0.0020	0.00	110	32.14	generous	cp	edge/matrix	1.39	0.094	0.082	0.068
908	968301602	TE14-01-754.3	0.0004	0.0029	0.00	91	30.43	generous	cp	edge/matrix	2.71	0.168	0.080	0.062
909	968314450	TE14-01-754.3	0.0004	0.0021	0.00	116	28.56	generous	cp	edge/matrix	1.69	0.113	0.083	0.067
910	968323423	TE14-01-754.3	0.0005	0.0023	0.00	126	24.56	generous	cp	edge/matrix	1.54	0.101	0.089	0.065
911	968777844	TE14-01-754.3	0.0005	0.0027	0.00	97	30.98	generous	cp	edge/matrix	2.28	0.140	0.085	0.061
912	968870088	TE14-01-754.3	0.0001	0.0009	0.00	82	30.85	generous	cp	edge/matrix	1.56	0.075	0.062	0.048
913	969509175	TE14-01-754.3	0.0003	0.0018	0.00	103	30.23	generous	cp	edge/matrix	1.54	0.093	0.086	0.061
914	970797007	TE14-01-754.3	0.0004	0.0030	0.00	105	30.86	generous	cp	edge/matrix	2.11	0.151	0.079	0.072
915	973039591	TE14-01-754.3	0.0005	0.0037	0.00	89	30.48	generous	cp	edge/matrix	2.02	0.134	0.112	0.066
916	973051717	TE14-01-754.3	0.0004	0.0027	0.00	101	29.66	generous	cp	edge/matrix	1.54	0.119	0.083	0.078
917	973192681	TE14-01-754.3	0.0003	0.0017	0.00	109	25.48	generous	cp	edge/matrix	1.55	0.097	0.072	0.062
918	974020176	TE14-01-754.3	0.0005	0.0023	0.00	115	25.69	generous	cp	edge/matrix	1.79	0.112	0.084	0.063
919	976116491	TE14-01-754.3	0.0001	0.0009	0.00	75	30.60	generous	cp	edge/matrix	1.56	0.075	0.062	0.048
920	976121880	TE14-01-754.3	0.0007	0.0041	0.00	105	29.47	generous	cp	edge/matrix	2.78	0.194	0.090	0.070
921	977804776	TE14-01-754.3	0.0003	0.0020	0.00	92	29.28	generous	cp	edge/matrix	1.47	0.094	0.085	0.064
922	977817708	TE14-01-754.3	0.0002	0.0020	0.00	88	32.91	generous	cp	edge/matrix	2.08	0.125	0.079	0.060
923	978298875	TE14-01-754.3	0.0001	0.0009	0.00	77	33.39	generous	cp	edge/matrix	1.22	0.069	0.069	0.056
924	978556342	TE14-01-754.3	0.0003	0.0024	0.00	92	35.05	generous	cp	edge/matrix	1.99	0.116	0.106	0.058
925	978809613	TE14-01-754.3	0.0002	0.0012	0.00	81	29.92	generous	cp	edge/matrix	1.59	0.086	0.066	0.055
926	979375168	TE14-01-754.3	0.0015	0.0056	0.00	164	27.10	generous	cp	edge/matrix	3.03	0.221	0.096	0.073
927	979580660	TE14-01-754.3	0.0002	0.0011	0.00	112	30.33	generous	cp	edge/matrix	1.00	0.067	0.067	0.067
928	980985937	TE14-01-754.3	0.0009	0.0052	0.00	130	33.76	generous	cp	edge/matrix	1.53	0.140	0.113	0.091
929	980986738	TE14-01-754.3	0.0008	0.0047	0.00	125	31.49	generous	cp	edge/matrix	1.45	0.128	0.113	0.088
930	980989169	TE14-01-754.3	0.0004	0.0029	0.00	120	34.08	generous	cp	edge/matrix	1.78	0.118	0.092	0.066
931	981734279	TE14-01-754.3	0.0003	0.0020	0.00	75	34.47	generous	cp	edge/matrix	1.60	0.106	0.070	0.066
932	982491510	TE14-01-754.3	0.0001	0.0009	0.00	81	36.17	generous	cp	edge/matrix	1.22	0.069	0.069	0.056
933	983554129	TE14-01-754.3	0.0011	0.0062	0.00	111	29.18	generous	cp	edge/matrix	2.19	0.170	0.138	0.078
934	983955748	TE14-01-754.3	0.0002	0.0020	0.00	91	33.83	generous	cp	edge/matrix	1.72	0.108	0.093	0.063
935	984292758	TE14-01-754.3	0.0003	0.0024	0.00	80	34.26	generous	cp	edge/matrix	1.78	0.112	0.095	0.063
936	984746201	TE14-01-754.3	0.0002	0.0014	0.00	84	34.00	generous	cp	edge/matrix	1.46	0.090	0.063	0.061
937	985123092	TE14-01-754.3	0.0002	0.0012	0.00	93	31.00	generous	cp	edge/matrix	1.31	0.082	0.070	0.062
938	985161748	TE14-01-754.3	0.0001	0.0014	0.00	76	35.08	generous	cp	edge/matrix	1.71	0.093	0.078	0.054
939	985266911	TE14-01-754.3	0.0005	0.0040	0.00	89	33.13	generous	cp	edge/matrix	2.15	0.155	0.118	0.072
940	985478291	TE14-01-754.3	0.0004	0.0023	0.00	106	28.85	generous	cp	edge/matrix	1.36	0.100	0.084	0.074
941	985796693	TE14-01-754.3	0.0003	0.0023	0.00	97	30.46	generous	cp	edge/matrix	1.83	0.114	0.083	0.062
942	985996122	TE14-01-754.3	0.0004	0.0023	0.00	121	26.76	generous	cp	edge/matrix	1.44	0.107	0.074	0.074

943	986145709	TE14-01-754.3	0.0004	0.0029	0.00	99	30.15	generous	cp	edge/matrix	1.66	0.124	0.086	0.075
944	986234761	TE14-01-754.3	0.0003	0.0020	0.00	102	33.52	generous	cp	edge/matrix	1.26	0.092	0.078	0.073
945	986622686	TE14-01-754.3	0.0001	0.0011	0.00	80	34.36	generous	cp	edge/matrix	1.22	0.068	0.068	0.056
946	986651804	TE14-01-754.3	0.0003	0.0024	0.00	84	31.90	generous	cp	edge/matrix	2.50	0.126	0.119	0.050
947	986796086	TE14-01-754.3	0.0003	0.0015	0.00	86	31.68	generous	cp	edge/matrix	1.70	0.102	0.062	0.060
948	987387444	TE14-01-754.3	0.0002	0.0012	0.00	81	25.13	generous	cp	edge/matrix	1.38	0.086	0.062	0.062
949	987728959	TE14-01-754.3	0.0003	0.0023	0.00	107	30.78	generous	cp	edge/matrix	1.69	0.118	0.075	0.070
950	987738696	TE14-01-754.3	0.0003	0.0023	0.00	108	34.38	generous	cp	edge/matrix	1.48	0.100	0.088	0.067
951	988067582	TE14-01-754.3	0.0005	0.0032	0.00	115	28.63	generous	cp	edge/matrix	1.34	0.111	0.090	0.083
952	988395448	TE14-01-754.3	0.0002	0.0014	0.00	89	25.54	generous	cp	edge/matrix	1.46	0.090	0.063	0.061
953	989067136	TE14-01-754.3	0.0002	0.0020	0.00	75	33.76	generous	cp	edge/matrix	2.53	0.122	0.094	0.048
954	989234492	TE14-01-754.3	0.0001	0.0009	0.00	89	30.70	generous	cp	edge/matrix	1.56	0.075	0.062	0.048
955	989773041	TE14-01-754.3	0.0002	0.0017	0.00	82	33.13	generous	cp	edge/matrix	2.01	0.119	0.072	0.059
956	990522989	TE14-01-754.3	0.0001	0.0009	0.00	78	35.05	generous	cp	edge/matrix	2.05	0.097	0.058	0.047
957	991960451	TE14-01-754.3	0.0005	0.0032	0.00	91	30.95	generous	cp	edge/matrix	1.62	0.120	0.105	0.074
958	992673584	TE14-01-754.3	0.0003	0.0018	0.00	95	28.27	generous	cp	edge/matrix	1.52	0.098	0.072	0.064
959	994808943	TE14-01-754.3	0.0001	0.0011	0.00	86	29.78	generous	cp	edge/matrix	1.92	0.097	0.057	0.051
960	994935134	TE14-01-754.3	0.0002	0.0017	0.00	82	25.79	generous	cp	edge/matrix	1.65	0.099	0.072	0.060
961	995196785	TE14-01-754.3	0.0002	0.0011	0.00	99	31.78	generous	cp	edge/matrix	1.80	0.088	0.068	0.049
962	995666477	TE14-01-754.3	0.0002	0.0012	0.00	75	33.04	generous	cp	edge/matrix	1.69	0.090	0.065	0.053
963	996380329	TE14-01-754.3	0.0003	0.0015	0.00	94	31.39	generous	cp	edge/matrix	1.53	0.093	0.079	0.061
964	996423693	TE14-01-754.3	0.0006	0.0049	0.00	81	27.61	generous	cp	edge/matrix	3.77	0.221	0.110	0.059
965	998277486	TE14-01-754.3	0.0002	0.0011	0.00	77	25.82	generous	cp	edge/matrix	1.22	0.068	0.068	0.056
966	998667056	TE14-01-754.3	0.0043	0.0262	0.00	92	29.70	generous	cp	edge/matrix	3.16	0.345	0.294	0.109
967	999101019	TE14-01-754.3	0.0003	0.0024	0.00	82	31.18	generous	cp	edge/matrix	1.98	0.122	0.108	0.062
968	999473629	TE14-01-754.3	0.0004	0.0034	0.00	80	32.31	generous	cp	edge/matrix	2.03	0.152	0.086	0.075
969	1E+09	TE14-01-754.3	0.0011	0.0056	0.00	137	31.98	generous	cp	edge/matrix	2.21	0.174	0.112	0.078
970	1E+09	TE14-01-754.3	0.0004	0.0032	0.00	79	30.13	generous	cp	edge/matrix	2.35	0.150	0.089	0.064
971	1.001E+09	TE14-01-754.3	0.0001	0.0011	0.00	84	35.35	generous	cp	edge/matrix	1.79	0.097	0.059	0.054
972	1.001E+09	TE14-01-754.3	0.0012	0.0079	0.00	108	30.88	generous	cp	edge/matrix	2.79	0.244	0.128	0.087
973	1.003E+09	TE14-01-754.3	0.0003	0.0020	0.00	93	28.61	generous	cp	edge/matrix	1.62	0.103	0.077	0.063
974	1.004E+09	TE14-01-754.3	0.0007	0.0046	0.00	98	28.21	generous	cp	edge/matrix	2.36	0.165	0.121	0.070
975	1.005E+09	TE14-01-754.3	0.0011	0.0085	0.00	99	31.66	generous	cp	edge/matrix	1.47	0.176	0.160	0.119
976	1.005E+09	TE14-01-754.3	0.0002	0.0017	0.00	80	27.57	generous	cp	edge/matrix	1.94	0.119	0.068	0.061
977	1.01E+09	TE14-01-754.3	0.0001	0.0009	0.00	79	29.75	generous	cp	edge/matrix	1.23	0.069	0.062	0.056
978	1.011E+09	TE14-01-754.3	0.0006	0.0047	0.00	87	34.29	generous	cp	edge/matrix	1.45	0.135	0.114	0.093
979	1.011E+09	TE14-01-754.3	0.0004	0.0029	0.00	92	28.84	generous	cp	edge/matrix	1.61	0.115	0.104	0.071
980	1.012E+09	TE14-01-754.3	0.0021	0.0067	0.00	208	27.65	generous	cp	edge/matrix	1.58	0.156	0.114	0.099
981	1.012E+09	TE14-01-754.3	0.0008	0.0046	0.00	118	29.45	generous	cp	edge/matrix	2.15	0.149	0.133	0.069
982	1.015E+09	TE14-01-754.3	0.0001	0.0011	0.00	81	34.55	generous	cp	edge/matrix	1.48	0.082	0.065	0.055
983	1.016E+09	TE14-01-754.3	0.0008	0.0055	0.00	82	29.36	generous	cp	edge/matrix	5.67	0.302	0.126	0.054
984	1.017E+09	TE14-01-754.3	0.0002	0.0014	0.00	100	31.46	generous	cp	edge/matrix	1.50	0.090	0.065	0.060
985	1.018E+09	TE14-01-754.3	0.0003	0.0018	0.00	102	26.42	generous	cp	edge/matrix	1.47	0.092	0.086	0.063

986	1.018E+09	TE14-01-754.3	0.0003	0.0015	0.00	110	31.00	generous	cp	edge/matrix	1.38	0.090	0.081	0.066
987	1.019E+09	TE14-01-754.3	0.0003	0.0021	0.00	77	30.13	generous	cp	edge/matrix	2.48	0.140	0.081	0.057
988	1.02E+09	TE14-01-754.3	0.0001	0.0009	0.00	78	29.60	generous	cp	edge/matrix	1.56	0.075	0.062	0.048
989	1.021E+09	TE14-01-754.3	0.0003	0.0024	0.00	93	32.41	generous	cp	edge/matrix	1.76	0.125	0.078	0.071
990	1.021E+09	TE14-01-754.3	0.0002	0.0011	0.00	91	32.09	generous	cp	edge/matrix	1.48	0.082	0.065	0.055
991	1.021E+09	TE14-01-754.3	0.0002	0.0012	0.00	91	34.00	generous	cp	edge/matrix	1.38	0.086	0.062	0.062
992	1.022E+09	TE14-01-754.3	0.0002	0.0017	0.00	95	32.31	generous	cp	edge/matrix	1.55	0.097	0.072	0.062
993	1.023E+09	TE14-01-754.3	0.0002	0.0012	0.00	85	29.04	generous	cp	edge/matrix	1.64	0.090	0.063	0.055
994	1.023E+09	TE14-01-754.3	0.0002	0.0017	0.00	81	31.90	generous	cp	edge/matrix	1.64	0.100	0.067	0.061
995	1.023E+09	TE14-01-754.3	0.0002	0.0021	0.00	83	35.17	generous	cp	edge/matrix	1.77	0.124	0.079	0.070
996	1.025E+09	TE14-01-754.3	0.0003	0.0021	0.00	101	33.76	generous	cp	edge/matrix	2.11	0.122	0.084	0.058
997	1.026E+09	TE14-01-754.3	0.0002	0.0017	0.00	93	31.10	generous	cp	edge/matrix	1.85	0.100	0.082	0.054
998	1.026E+09	TE14-01-754.3	0.0002	0.0014	0.00	79	31.70	generous	cp	edge/matrix	2.34	0.117	0.061	0.050
999	1.027E+09	TE14-01-754.3	0.0004	0.0023	0.00	97	28.97	generous	cp	edge/matrix	1.56	0.105	0.091	0.067
1000	1.027E+09	TE14-01-754.3	0.0002	0.0012	0.00	89	27.54	generous	cp	edge/matrix	1.38	0.086	0.062	0.062
1001	1.027E+09	TE14-01-754.3	0.0004	0.0026	0.00	105	31.65	generous	cp	edge/matrix	1.89	0.121	0.090	0.064
1002	1.028E+09	TE14-01-754.3	0.0002	0.0014	0.00	91	27.52	generous	cp	edge/matrix	1.31	0.081	0.075	0.062
1003	1.03E+09	TE14-01-754.3	0.0002	0.0017	0.00	96	28.24	generous	cp	edge/matrix	1.55	0.090	0.083	0.058
1004	1.03E+09	TE14-01-754.3	0.0002	0.0020	0.00	77	33.06	generous	cp	edge/matrix	1.52	0.111	0.078	0.073
1005	1.031E+09	TE14-01-754.3	0.0006	0.0030	0.00	110	30.76	generous	cp	edge/matrix	1.53	0.119	0.102	0.078
1006	1.032E+09	TE14-01-754.3	0.0002	0.0015	0.00	79	28.66	generous	cp	edge/matrix	1.80	0.107	0.065	0.060
1007	1.032E+09	TE14-01-754.3	0.0002	0.0018	0.00	86	31.83	generous	cp	edge/matrix	2.70	0.131	0.095	0.049
1008	1.033E+09	TE14-01-754.3	0.0002	0.0014	0.00	75	29.85	generous	cp	edge/matrix	1.83	0.102	0.064	0.056
1009	1.033E+09	TE14-01-754.3	0.0005	0.0024	0.00	111	28.14	generous	cp	edge/matrix	2.00	0.137	0.075	0.068
1010	1.033E+09	TE14-01-754.3	0.0003	0.0017	0.00	97	26.38	generous	cp	edge/matrix	1.55	0.097	0.072	0.062
1011	1.034E+09	TE14-01-754.3	0.0002	0.0012	0.00	82	29.88	generous	cp	edge/matrix	1.79	0.095	0.063	0.053
1012	1.034E+09	TE14-01-754.3	0.0002	0.0015	0.00	79	26.32	generous	cp	edge/matrix	1.69	0.102	0.062	0.060
1013	1.034E+09	TE14-01-754.3	0.0002	0.0014	0.00	96	31.31	generous	cp	edge/matrix	1.92	0.100	0.079	0.052
1014	1.035E+09	TE14-01-754.3	0.0007	0.0052	0.00	107	32.27	generous	cp	edge/matrix	2.02	0.169	0.124	0.084
1015	1.035E+09	TE14-01-754.3	0.0002	0.0015	0.00	95	29.33	generous	cp	edge/matrix	1.36	0.091	0.076	0.067
1016	1.037E+09	TE14-01-754.3	0.0005	0.0035	0.00	108	33.30	generous	cp	edge/matrix	2.28	0.158	0.102	0.069
1017	1.038E+09	TE14-01-754.3	0.0017	0.0082	0.00	136	28.27	generous	cp	edge/matrix	1.67	0.167	0.149	0.100
1018	1.038E+09	TE14-01-754.3	0.0003	0.0023	0.00	88	32.49	generous	cp	edge/matrix	2.06	0.131	0.086	0.064
1019	1.038E+09	TE14-01-754.3	0.0002	0.0020	0.00	81	32.50	generous	cp	edge/matrix	2.17	0.124	0.084	0.057
1020	1.039E+09	TE14-01-754.3	0.0005	0.0026	0.00	125	30.55	generous	cp	edge/matrix	1.91	0.124	0.084	0.065
1021	1.039E+09	TE14-01-754.3	0.0002	0.0014	0.00	79	32.46	generous	cp	edge/matrix	1.69	0.088	0.083	0.052
1022	1.04E+09	TE14-01-754.3	0.0005	0.0027	0.00	110	32.26	generous	cp	edge/matrix	2.03	0.138	0.089	0.068
1023	1.042E+09	TE14-01-754.3	0.0006	0.0047	0.00	92	33.49	generous	cp	edge/matrix	3.31	0.213	0.114	0.064
1024	1.042E+09	TE14-01-754.3	0.0003	0.0024	0.00	106	33.54	generous	cp	edge/matrix	1.46	0.104	0.093	0.072
1025	1.044E+09	TE14-01-754.3	0.0004	0.0023	0.00	119	28.24	generous	cp	edge/matrix	1.36	0.098	0.085	0.072
1026	1.045E+09	TE14-01-754.3	0.0003	0.0015	0.00	106	29.04	generous	cp	edge/matrix	2.09	0.113	0.066	0.054
1027	1.046E+09	TE14-01-754.3	0.0002	0.0011	0.00	79	27.68	generous	cp	edge/matrix	1.22	0.068	0.068	0.056
1028	1.047E+09	TE14-01-754.3	0.0003	0.0018	0.00	76	33.39	generous	cp	edge/matrix	1.54	0.097	0.083	0.063

1029	1.047E+09	TE14-01-754.3	0.0002	0.0014	0.00	86	28.92	generous	cp	edge/matrix	1.67	0.090	0.075	0.054
1030	1.047E+09	TE14-01-754.3	0.0053	0.0142	0.00	244	27.81	generous	cp	edge/matrix	1.83	0.223	0.141	0.122
1031	1.048E+09	TE14-01-754.3	0.0005	0.0038	0.00	76	34.66	generous	cp	edge/matrix	2.67	0.156	0.117	0.058
1032	1.05E+09	TE14-01-754.3	0.0004	0.0017	0.00	122	30.21	generous	cp	edge/matrix	1.55	0.097	0.072	0.062
1033	1.05E+09	TE14-01-754.3	0.0002	0.0015	0.00	77	31.23	generous	cp	edge/matrix	1.22	0.079	0.079	0.064
1034	1.054E+09	TE14-01-754.3	0.0003	0.0021	0.00	91	29.03	generous	cp	edge/matrix	2.56	0.134	0.083	0.053
1035	1.057E+09	TE14-01-754.3	0.0003	0.0027	0.00	91	32.19	generous	cp	edge/matrix	2.58	0.160	0.096	0.062
1036	1.059E+09	TE14-01-754.3	0.0001	0.0011	0.00	75	31.68	generous	cp	edge/matrix	1.22	0.068	0.068	0.056
1037	1.062E+09	TE14-01-754.3	0.0002	0.0015	0.00	76	27.96	generous	cp	edge/matrix	1.59	0.097	0.064	0.061
1038	1.062E+09	TE14-01-754.3	0.0003	0.0021	0.00	95	33.03	generous	cp	edge/matrix	2.24	0.138	0.069	0.062
1039	1.063E+09	TE14-01-754.3	0.0013	0.0053	0.00	169	28.12	generous	cp	edge/matrix	1.43	0.134	0.116	0.094
1040	1.066E+09	TE14-01-754.3	0.0002	0.0012	0.00	90	26.79	generous	cp	edge/matrix	1.58	0.086	0.066	0.055
1041	1.068E+09	TE14-01-754.3	0.0002	0.0017	0.00	75	30.80	generous	cp	edge/matrix	1.78	0.108	0.069	0.061
1042	1.069E+09	TE14-01-754.3	0.0008	0.0052	0.00	120	31.75	generous	cp	edge/matrix	1.93	0.169	0.106	0.088
1043	1.072E+09	TE14-01-754.3	0.0002	0.0015	0.00	93	29.19	generous	cp	edge/matrix	1.56	0.093	0.070	0.060
1044	1.073E+09	TE14-01-754.3	0.0009	0.0043	0.00	115	27.98	generous	cp	edge/matrix	2.82	0.196	0.112	0.069
1045	1.101E+09	TE14-01-754.3	0.0002	0.0011	0.00	91	27.82	generous	cp	edge/matrix	1.48	0.082	0.065	0.055
1046	1.101E+09	TE14-01-754.3	0.0005	0.0032	0.00	101	31.76	generous	cp	edge/matrix	2.00	0.153	0.079	0.076
1047	1.107E+09	TE14-01-754.3	0.0003	0.0021	0.00	93	34.97	generous	cp	edge/matrix	1.41	0.092	0.092	0.065
1048	1.116E+09	TE14-01-754.3	0.0002	0.0018	0.00	91	34.84	generous	cp	edge/matrix	1.47	0.101	0.075	0.068
1049	11798719	GRS14-OP1	0.0013	0.0053	150.98	146	31.19	generous	bn	edge	2.03	0.179	0.097	0.088
1050	31919096	GRS14-OP1	0.0001	0.0007	73.94	109	35.40	generous	bn	inclusion	1.37	0.067	0.060	0.049
1051	48852356	GRS14-OP1	0.0002	0.0011	68.46	106	34.07	generous	bn	edge	1.59	0.087	0.058	0.055
1052	58193949	GRS14-OP1	0.0235	0.1284	130.83	178	36.78	generous	bn	edge	2.33	0.655	0.384	0.282
1053	59845033	GRS14-OP1	0.0062	0.0300	83.53	154	34.35	generous	bn	edge	2.30	0.392	0.282	0.168
1054	61507610	GRS14-OP1	0.0007	0.0051	0.61	114	37.07	generous	bn	edge	1.97	0.188	0.120	0.095
1055	70118780	GRS14-OP1	0.0006	0.0023	153.35	175	29.28	generous	bn	edge	1.46	0.102	0.088	0.070
1056	70861587	GRS14-OP1	0.0001	0.0007	404.69	104	32.40	generous	bn	edge	1.70	0.075	0.055	0.044
1057	88551110	GRS14-OP1	0.0002	0.0014	123.45	99	35.56	generous	bn	edge	2.39	0.107	0.097	0.045
1058	90216866	GRS14-OP1	0.0004	0.0027	118.18	102	33.83	generous	bn	edge	1.76	0.133	0.087	0.075
1059	93775861	GRS14-OP1	0.0014	0.0070	306.26	121	32.60	generous	bn	edge	3.66	0.284	0.091	0.078
1060	107638639	GRS14-OP1	0.0002	0.0011	1.13	112	34.93	generous	bn	edge	1.65	0.084	0.073	0.051
1061	129201630	GRS14-OP1	0.0087	0.0394	78.71	216	34.80	generous	bn	edge	2.90	0.489	0.291	0.159
1062	132542084	GRS14-OP1	0.0005	0.0023	24.20	124	34.50	generous	bn	edge	1.38	0.103	0.079	0.075
1063	132800335	GRS14-OP1	0.0213	0.1146	260.64	187	35.51	generous	bn	edge	3.19	1.039	0.399	0.324
1064	134181065	GRS14-OP1	0.0084	0.0421	1.39	172	35.46	generous	bn	edge	4.02	0.585	0.255	0.158
1065	134455265	GRS14-OP1	0.0007	0.0052	4.56	105	37.35	generous	bn	edge	2.59	0.204	0.114	0.079
1066	134509745	GRS14-OP1	0.0007	0.0030	40.74	151	31.71	generous	bn	edge	1.50	0.112	0.099	0.075
1067	138839453	GRS14-OP1	0.0004	0.0030	3.35	101	34.37	generous	bn	edge	3.05	0.202	0.069	0.066
1068	140495652	GRS14-OP1	0.0006	0.0052	19.44	108	37.46	generous	bn	edge	1.79	0.152	0.135	0.085
1069	167969588	GRS14-OP1	0.0004	0.0028	0.09	105	35.30	generous	bn	edge	2.40	0.166	0.079	0.069
1070	167975319	GRS14-OP1	0.0005	0.0034	15.95	113	36.85	generous	bn	edge	1.44	0.141	0.103	0.098
1071	182006998	GRS14-OP1	0.0036	0.0187	65.75	192	37.35	generous	bn	edge	1.91	0.290	0.188	0.152

1072	186960283	GRS14-OP1	0.0008	0.0058	2.08	116	35.16	generous	bn	edge	1.94	0.166	0.128	0.086
1073	187954649	GRS14-OP1	0.0008	0.0048	57.07	101	34.71	generous	bn	edge	3.04	0.211	0.119	0.069
1074	192016833	GRS14-OP1	0.0002	0.0010	0.01	100	28.88	generous	bn	edge	1.46	0.081	0.057	0.055
1075	251653524	GRS14-OP1	0.0003	0.0011	17.40	144	33.85	generous	bn	edge	1.55	0.084	0.063	0.054
1076	129201630	GRS14-OP1	0.0018	0.0072	2206.34	216	46.51	strict	bn	edge	1.87	0.192	0.121	0.103

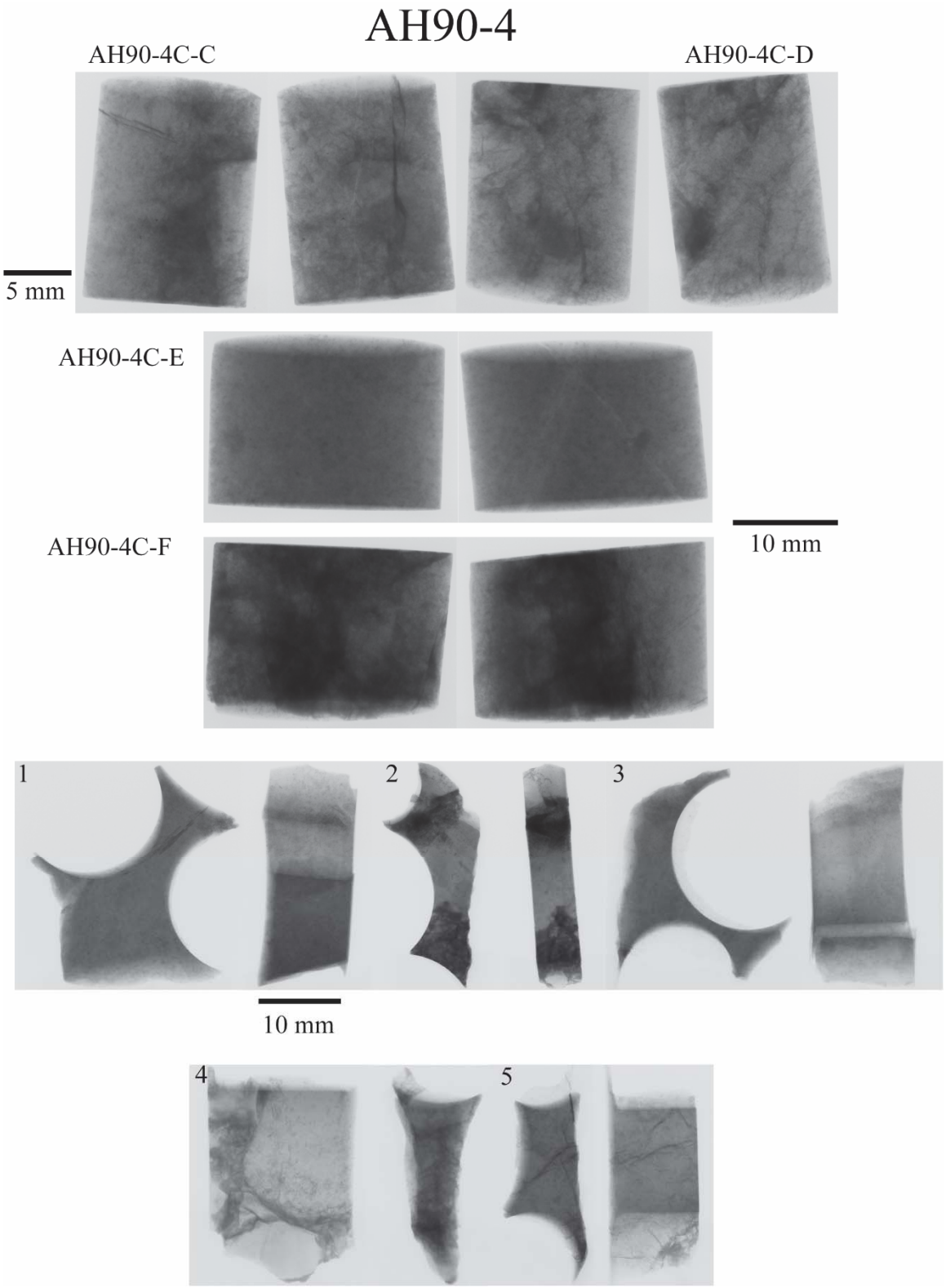
AH90-4
AH90-4C-C
AH90-4C-D
5 mm
AH90-4C-E
AH90-4C-F
10 mm
1
2
3
10 mm
4
5

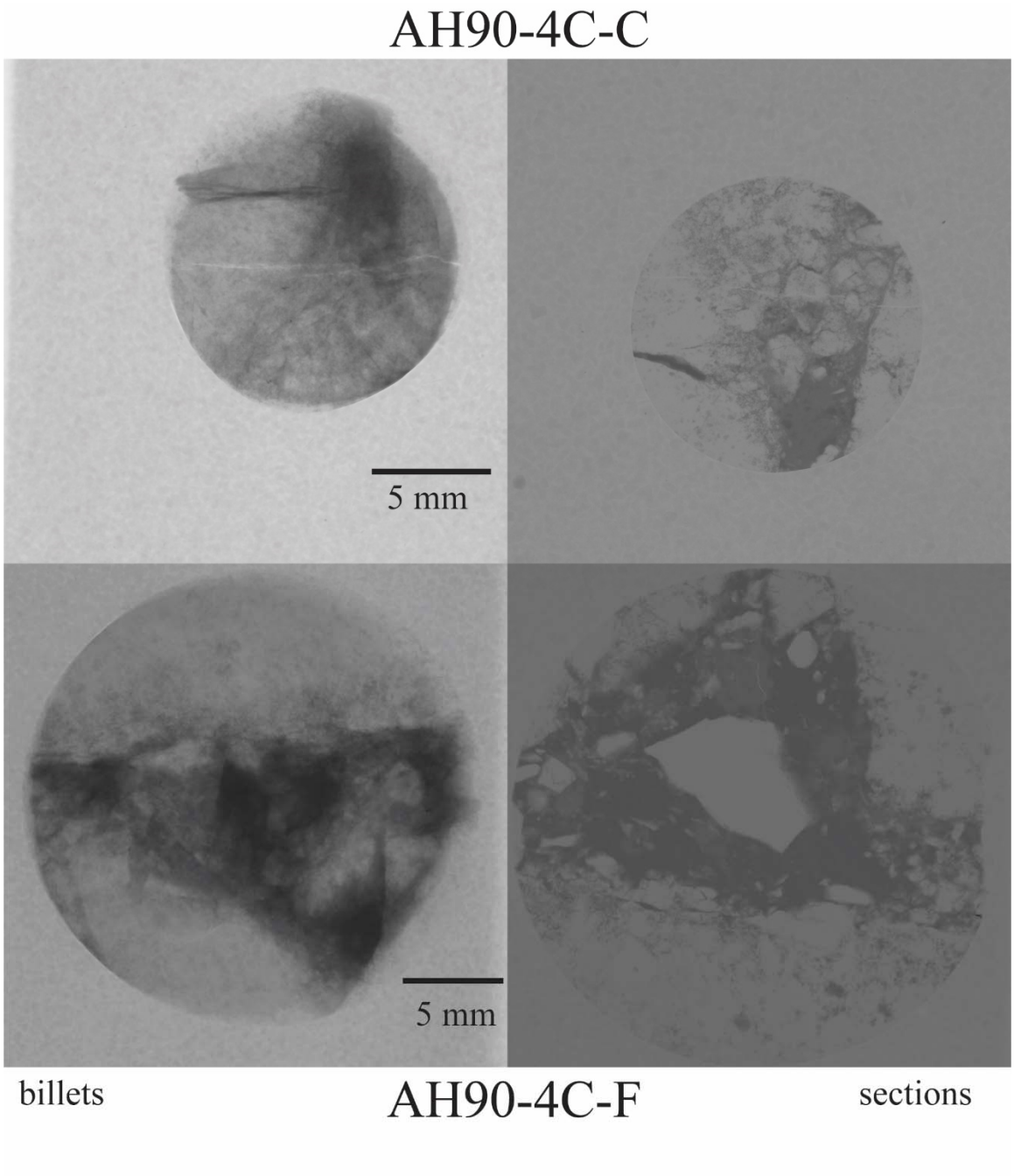
AH90-4C-C
5 mm
5 mm
billets
AH90-4C-F
sections

GRS37-170-645.9

GRS37-170-645.9

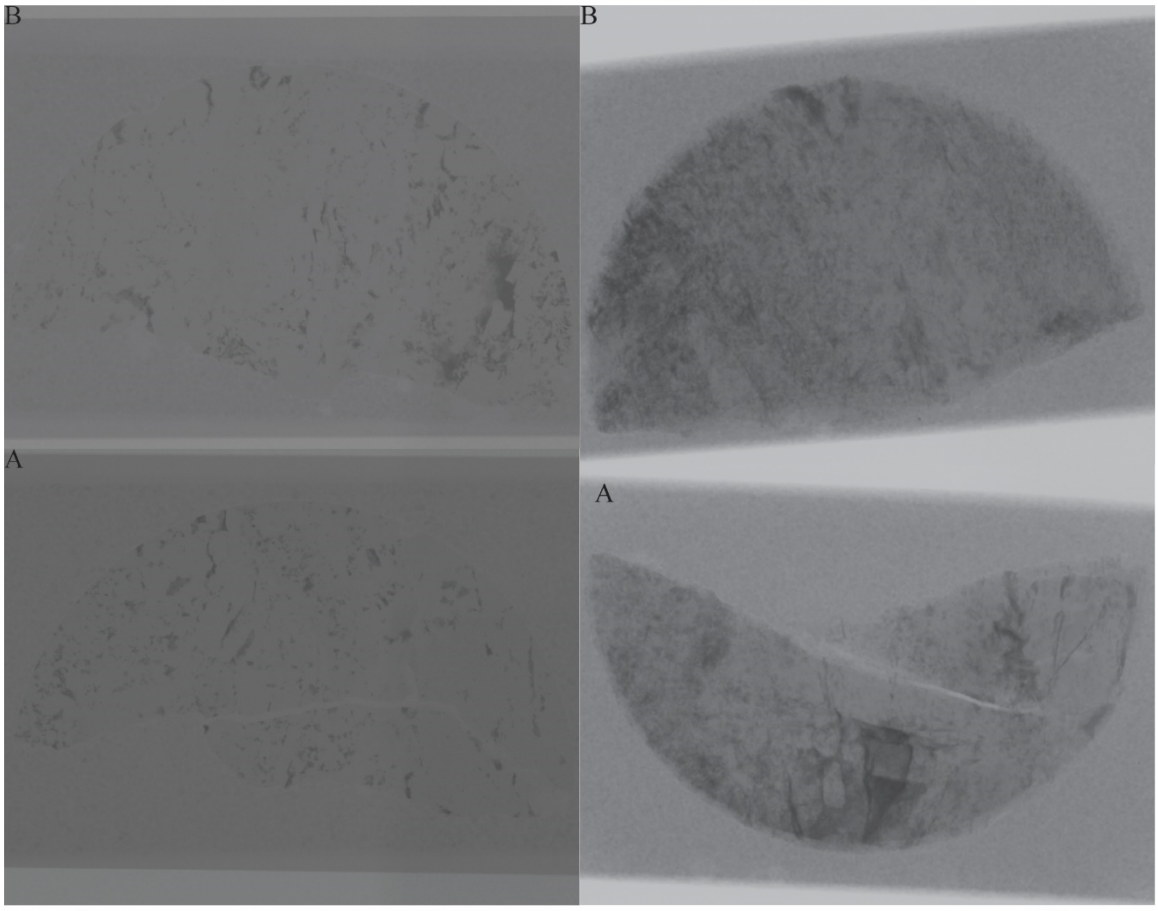

GRS37-170-714.2

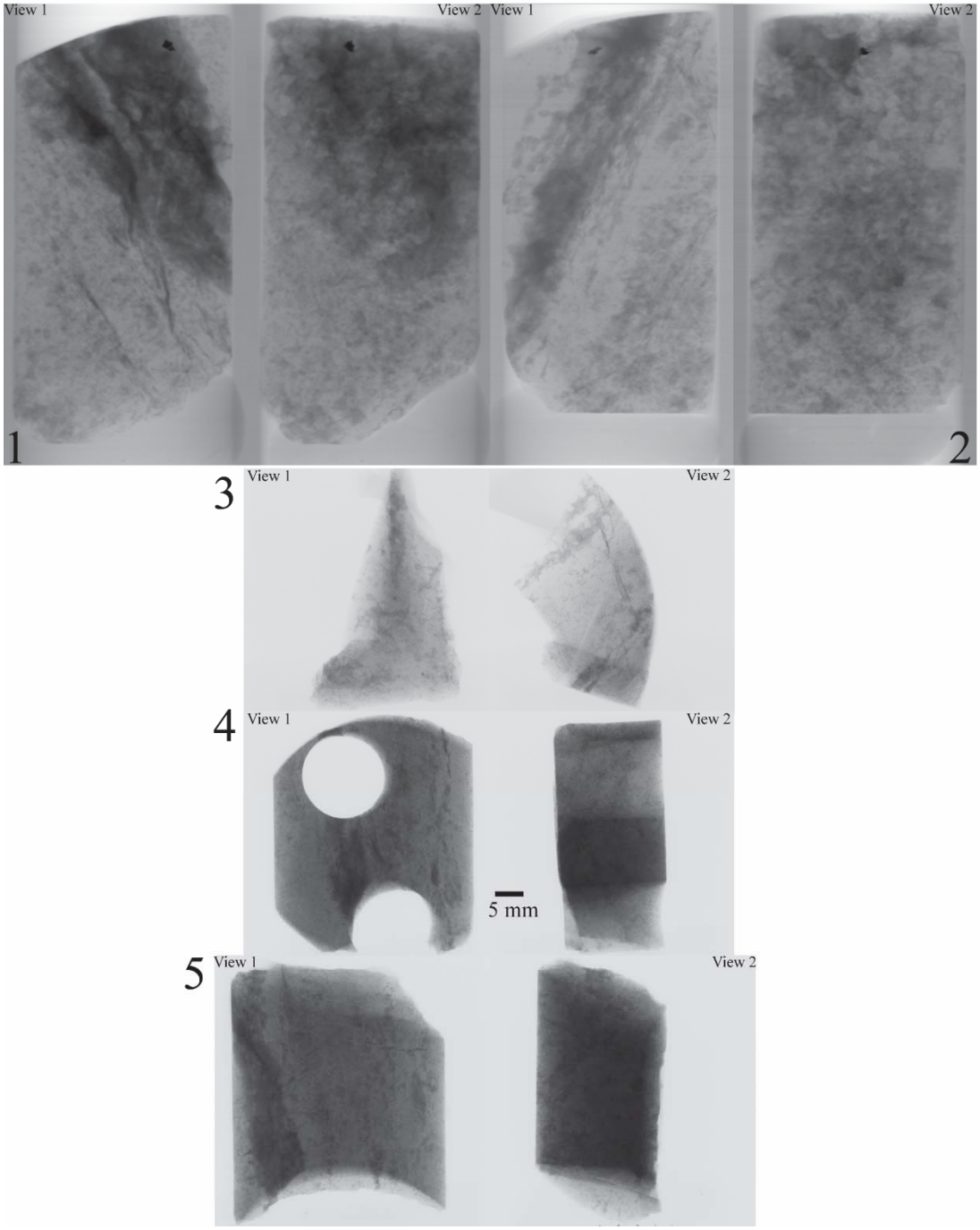

GRS37-170-742.2

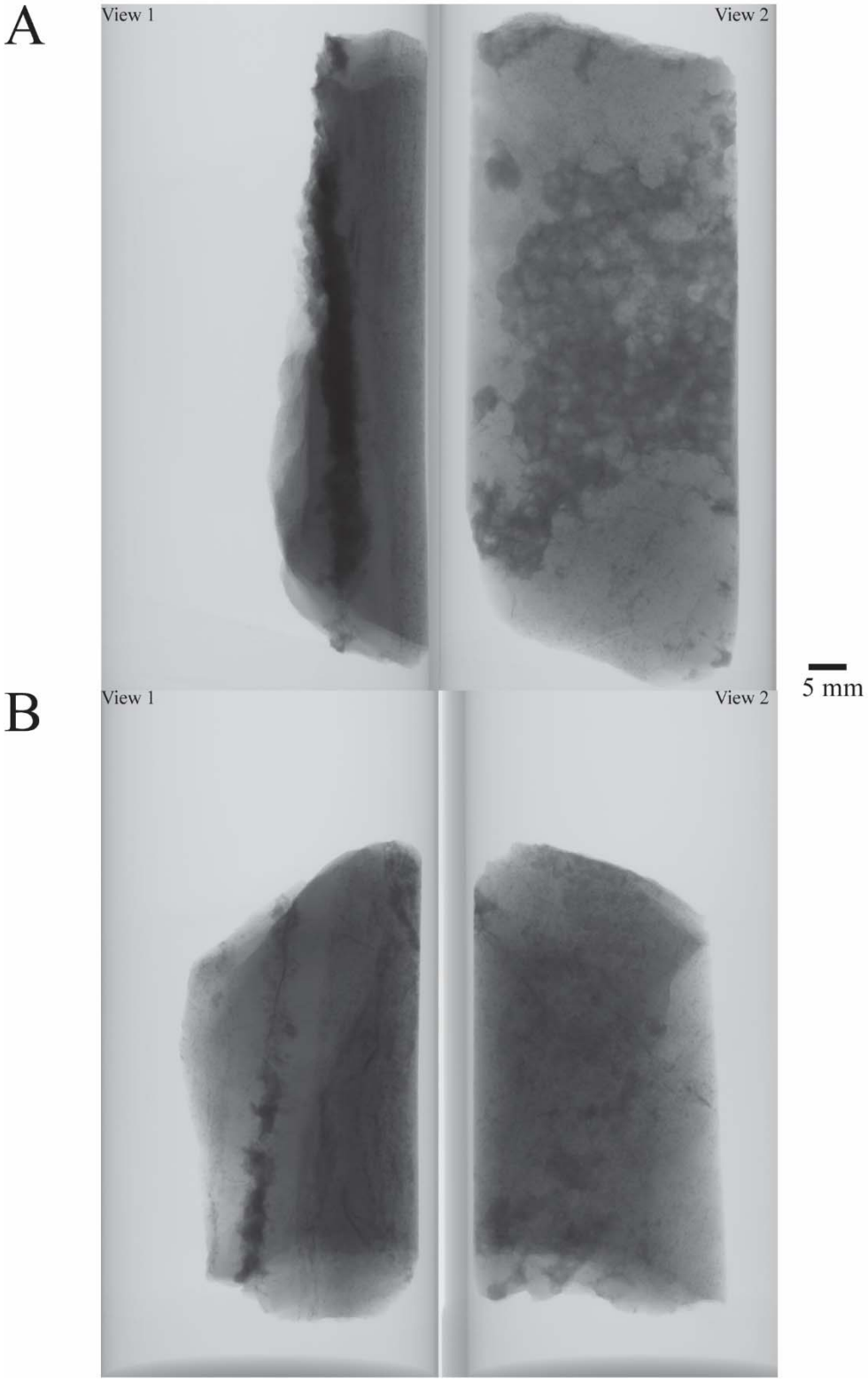

GRS37-170-742.2

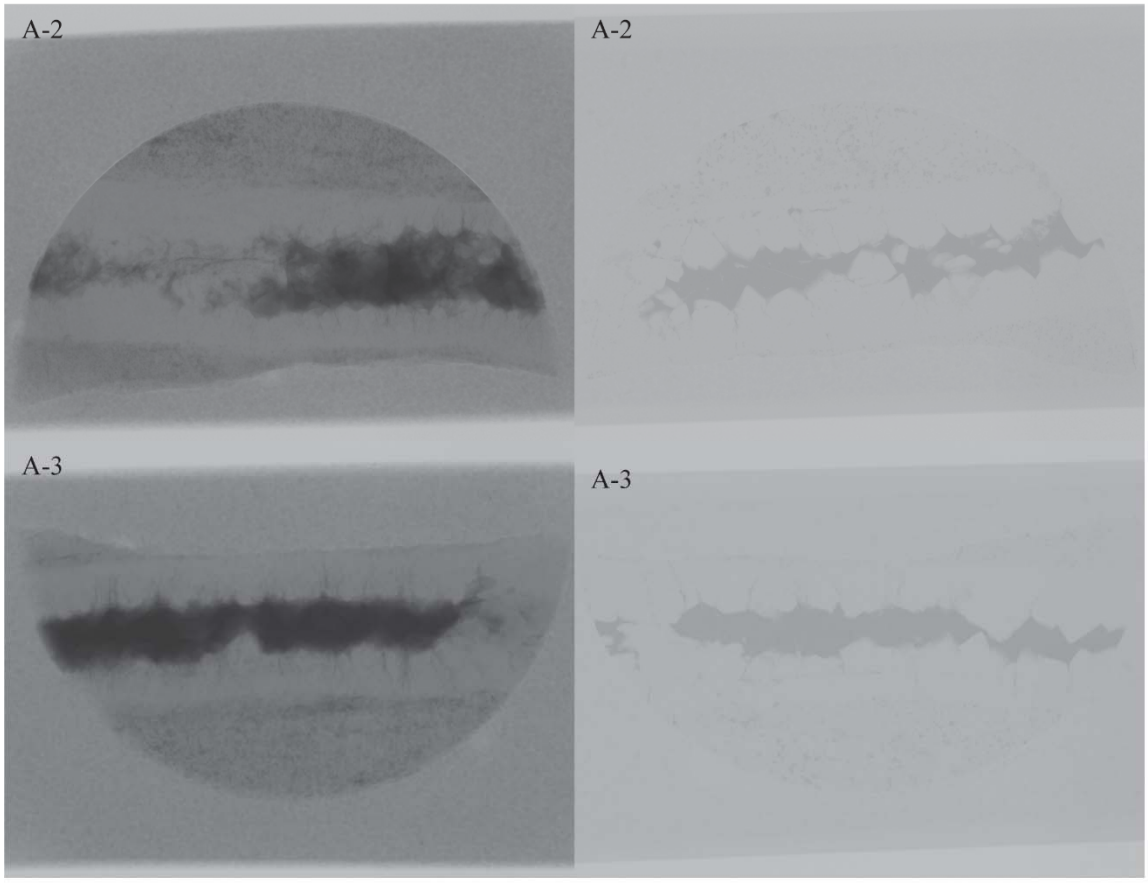

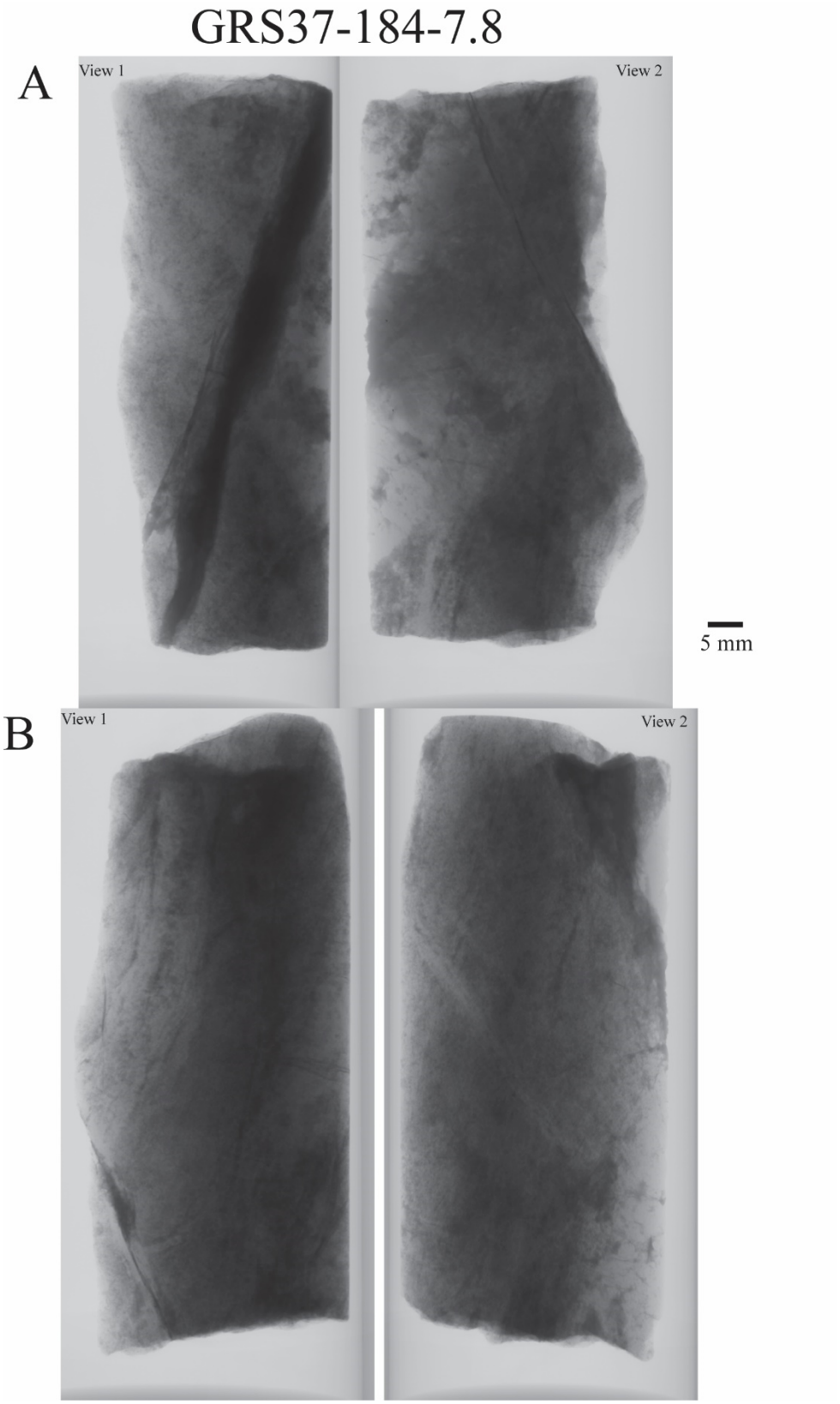
GRS37-184-7.8
A
View 1
View 2
5 mm
B
View 1
View 2

GRS37-184-7.8A+B

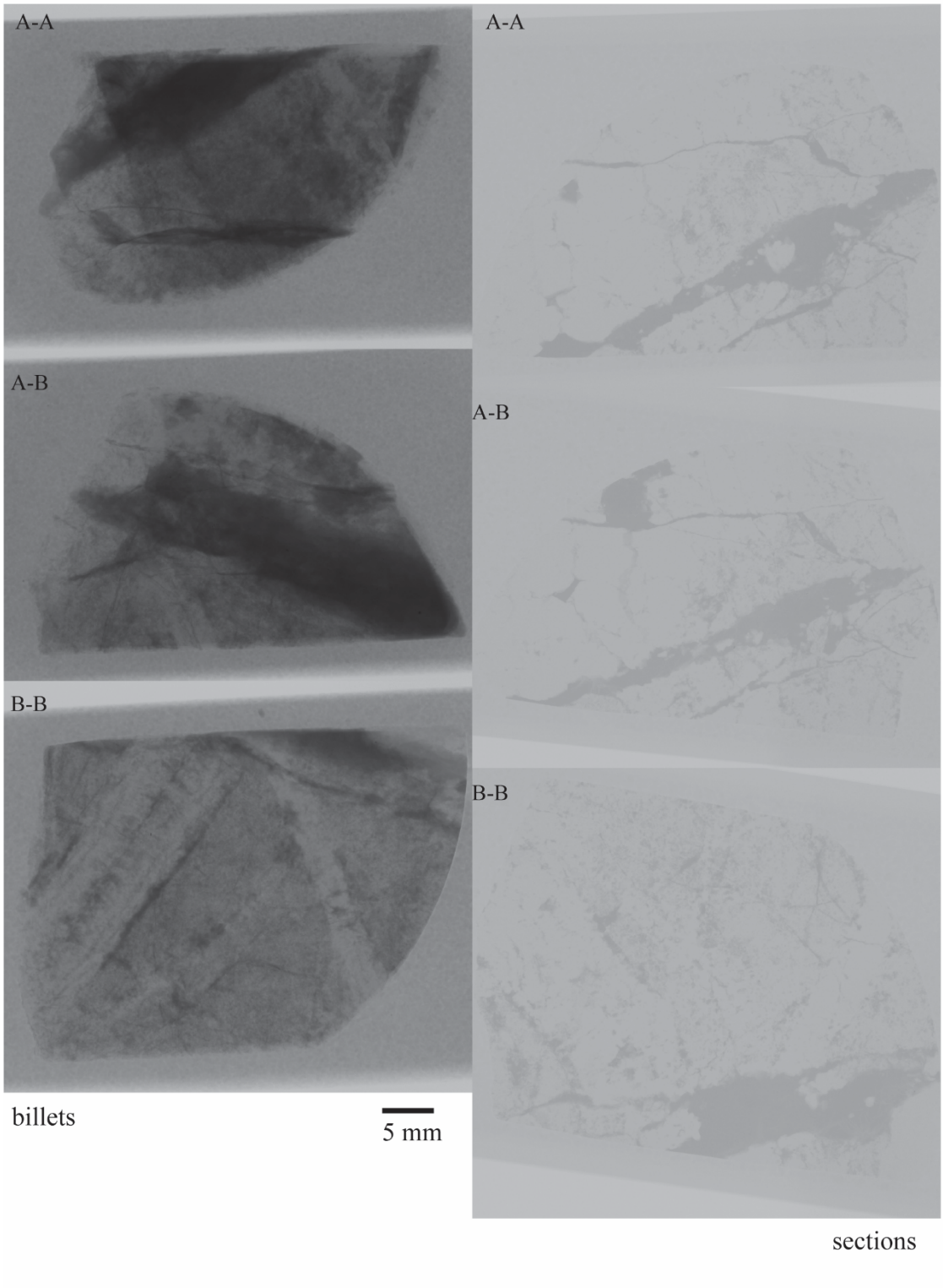

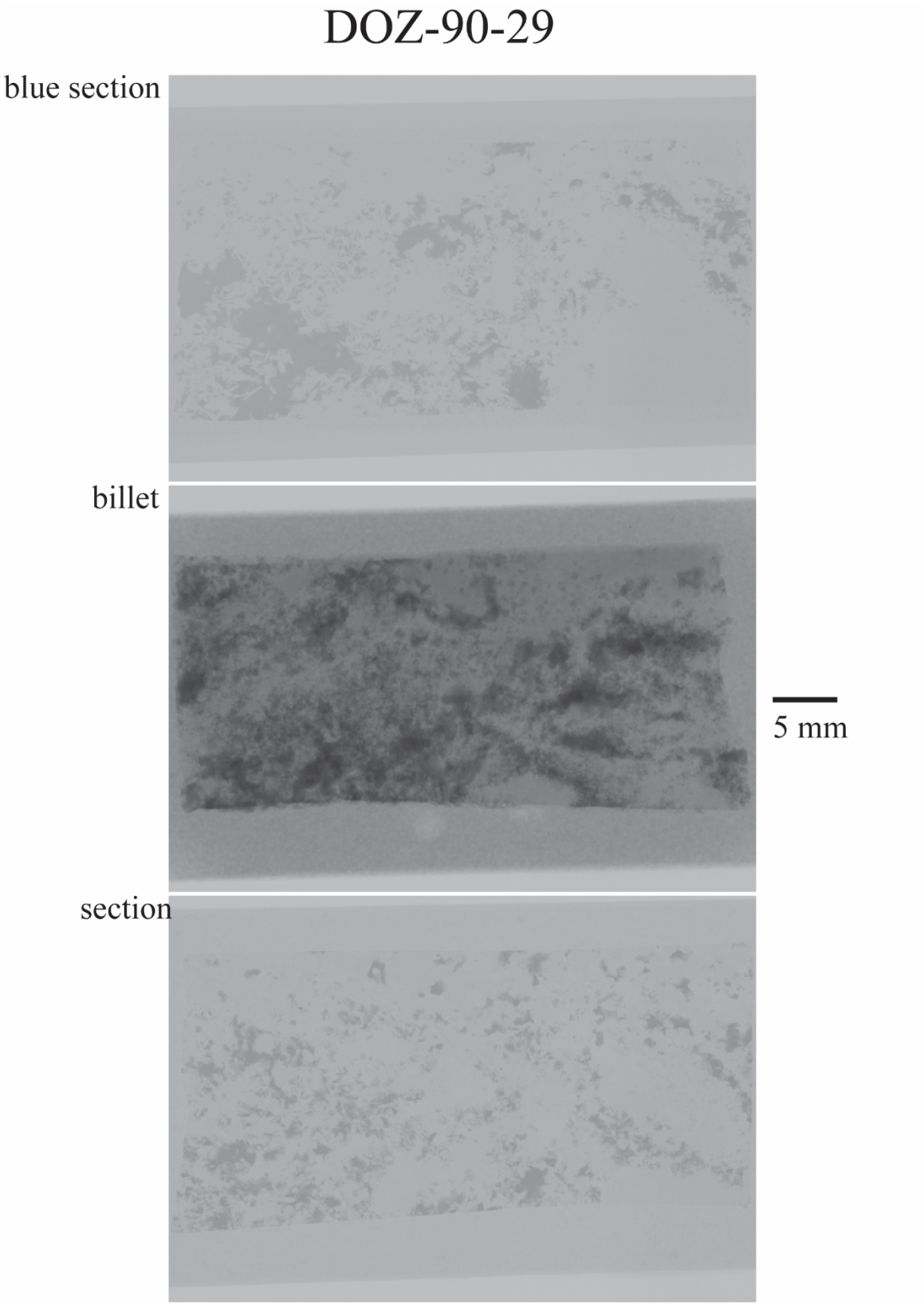
DOZ-90-29
blue section
billet
section
5 mm

TE14-01-754.3

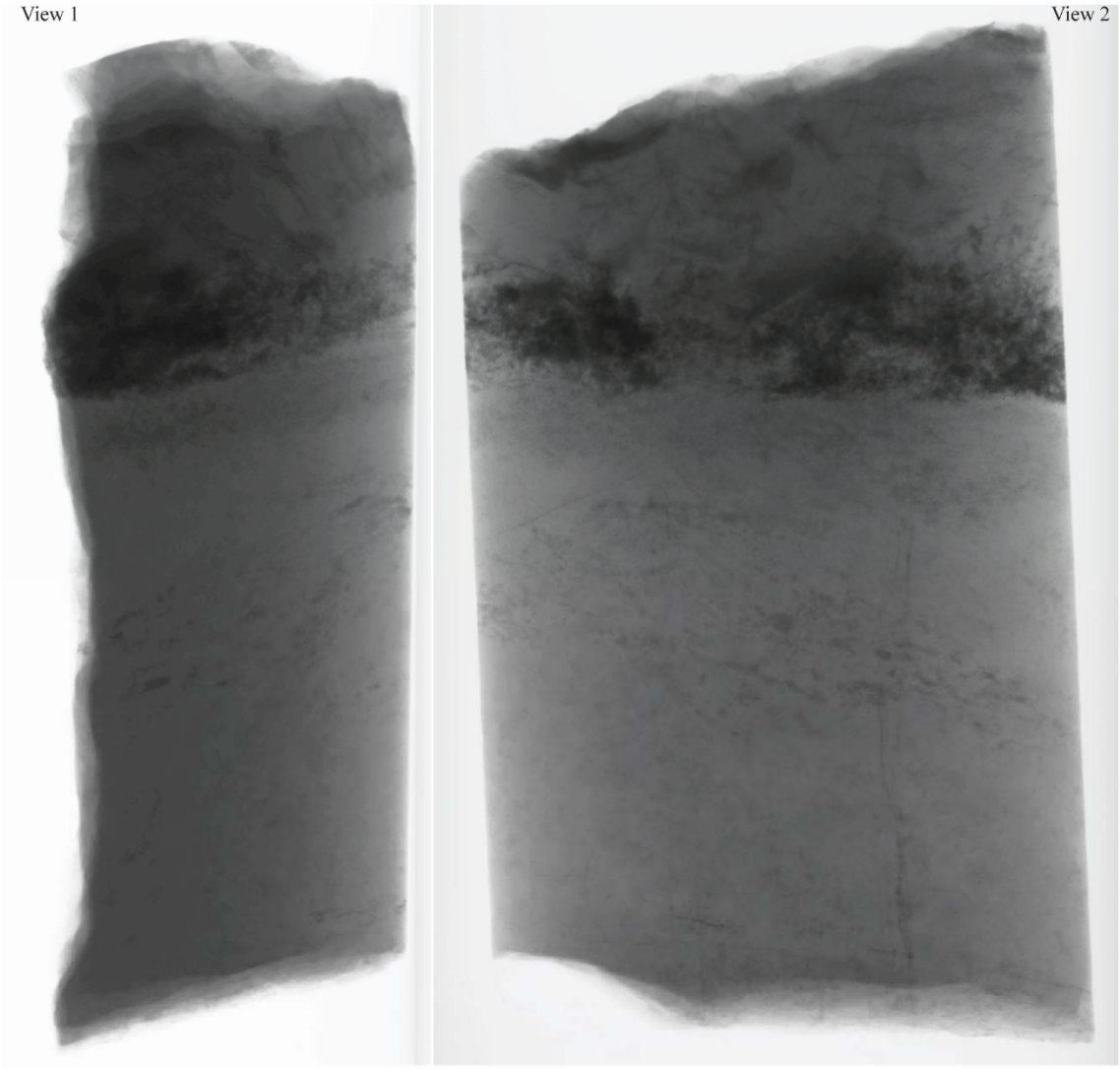

TE14-01-754.3

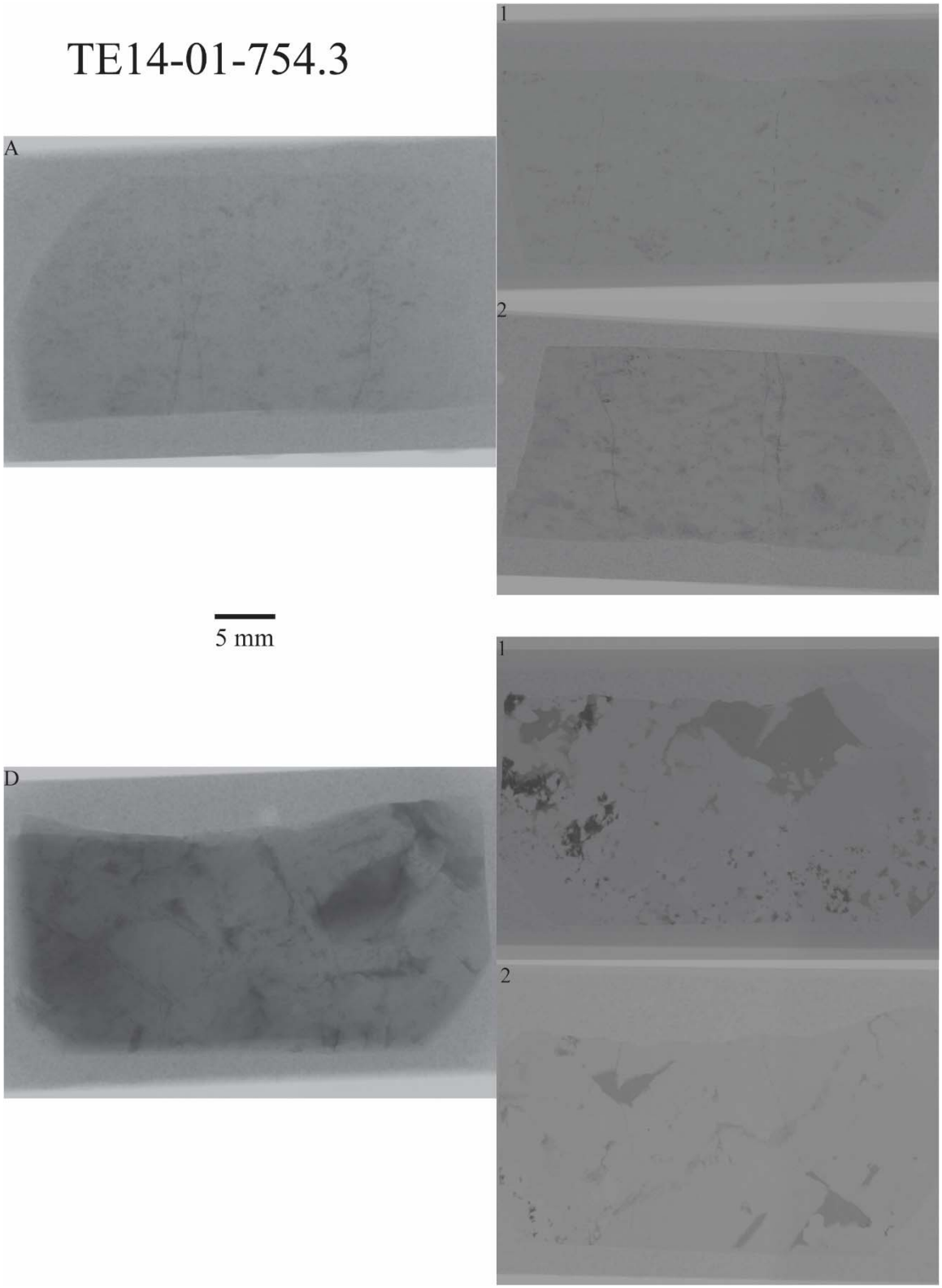

TE01-16-566

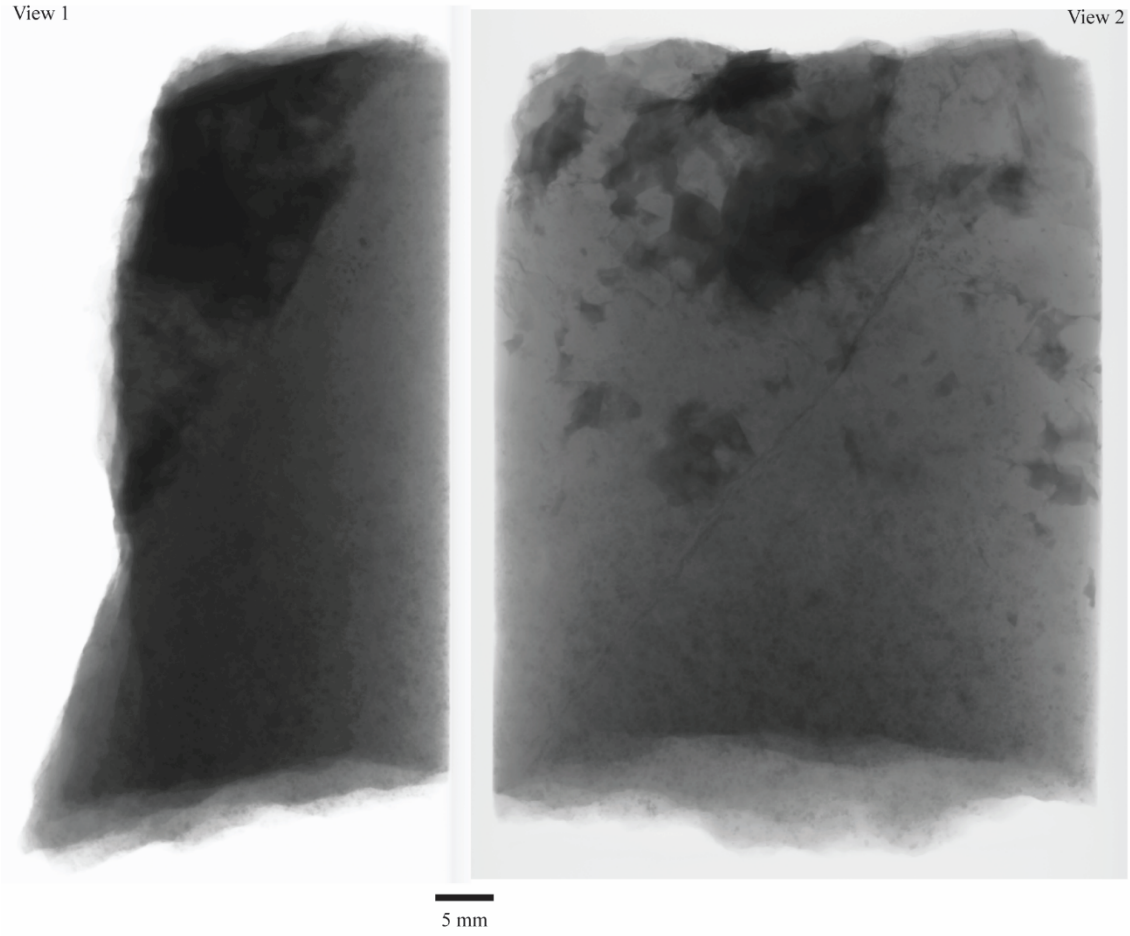

TE01-16-566

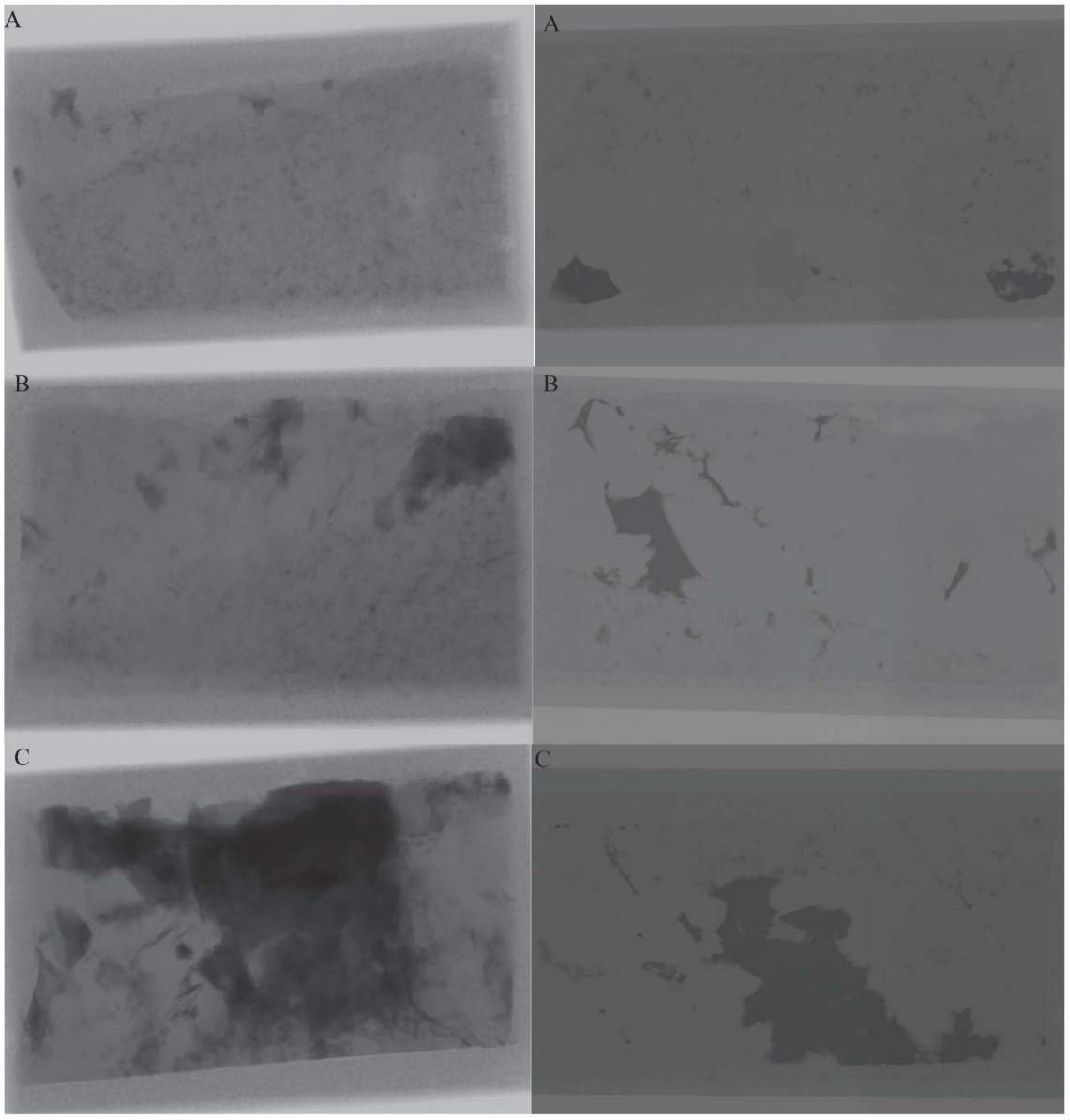

Appendix C: LA-ICP-MS Geochemical Data

				Mn				Ni			
Analysis #	**Sample**	**Mineral**	**Type**	ppm	2σ std error	LOD	Signal/ Noise	ppm	2σ std error	LOD	Signal/ Noise
Spot #4	AH90-4C-F	cp	vein	0.44	0.06	0.12	3.70	0.03	0.03	0.05	0.59
Spot #5	AH90-4C-F	cp	vein	0.55	0.06	0.13	4.22	<mdl	1.00	0.06	
Spot #6	AH90-4C-F	cp	vein	0.46	0.05	0.13	3.52	<mdl	1.00	0.05	
Spot #7	AH90-4C-F	bn	vein	0.54	0.06	0.10	5.37	<mdl	1.00	0.04	
Spot #8	AH90-4C-F	bn	vein	0.28	0.04	0.09	3.01	<mdl	1.00	0.04	
Spot #9	AH90-4C-F	bn	vein	0.44	0.05	0.10	4.60	<mdl	1.00	0.03	
Spot #10	AH90-4C-F	bn	vein	0.38	0.05	0.11	3.45	<mdl	1.00	0.06	
Spot #11	AH90-4C-F	cp	vein	0.76	0.08	0.13	5.81	0.06	0.04	0.03	1.97
Spot #12	AH90-4C-F	cp	vein	0.61	0.09	0.13	4.72	<mdl	1.00	0.04	
Spot #13	AH90-4C-F	bn	vein	0.34	0.04	0.09	3.68	<mdl	1.00	0.06	
Grid #4-01	AH90-4C-F	bn	vein	<mdl	0.07	0.17		<mdl	0.08	0.27	
Grid #4-02	AH90-4C-F	bn	vein	<mdl	0.08	0.17		<mdl	0.09	0.28	
Grid #4-03	AH90-4C-F	bn	vein	<mdl	0.09	0.17		<mdl	0.09	0.27	
Grid #4-04	AH90-4C-F	bn	vein	<mdl	0.06	0.17		<mdl	0.08	0.24	
Grid #4-05	AH90-4C-F	bn	vein	<mdl	0.08	0.18		<mdl	0.09	0.26	
Grid #4-06	AH90-4C-F	bn	vein	<mdl	0.07	0.18		0.30	0.09	0.23	1.28
Grid #5-01	AH90-4C-F	cp	vein	<mdl	0.11	0.21		0.35	0.13	0.29	1.21
Grid #5-02	AH90-4C-F	cp	vein	<mdl	0.10	0.22		0.40	0.13	0.39	1.03
Grid #5-03	AH90-4C-F	cp	vein	1.44	0.15	0.22	6.55	0.46	0.15	0.33	1.39
Grid #5-04	AH90-4C-F	cp	vein	0.81	0.19	0.22	3.68	0.32	0.13	0.28	1.14
Grid #5-05	AH90-4C-F	cp	vein	<mdl	0.11	0.25		<mdl	0.13	0.38	
Grid #5-06	AH90-4C-F	cp	vein	0.29	0.12	0.25	1.16	<mdl	0.12	0.37	
Grid #6-01	AH90-4C-F	cp	vein	<mdl	0.13	0.24		0.39	0.14	0.34	1.15
Grid #6-02	AH90-4C-F	cp	vein	0.93	0.31	0.21	4.43	0.43	0.14	0.30	1.43
Grid #6-03	AH90-4C-F	cp	vein	0.29	0.10	0.18	1.59	0.39	0.13	0.29	1.34
Grid #6-04	AH90-4C-F	cp	vein	<mdl	0.10	0.20		<mdl	0.12	0.33	
Grid #6-05	AH90-4C-F	cp	vein	0.32	0.11	0.24	1.33	0.42	0.14	0.36	1.17
Grid #6-06	AH90-4C-F	cp	vein	0.37	0.12	0.25	1.48	<mdl	0.13	0.38	
Grid #7-01	AH90-4C-F	bn	vein	<mdl	0.10	0.16		<mdl	0.12	0.33	
Grid #7-02	AH90-4C-F	bn	vein	<mdl	0.09	0.19		<mdl	0.09	0.31	
Grid #7-03	AH90-4C-F	bn	vein	<mdl	0.10	0.20		<mdl	0.10	0.30	
Grid #7-04	AH90-4C-F	bn	vein	<mdl	0.09	0.22		<mdl	0.10	0.27	
Grid #7-05	AH90-4C-F	bn	vein	<mdl	0.08	0.22		0.28	0.11	0.24	1.17
Grid #7-06	AH90-4C-F	bn	vein	<mdl	0.09	0.24		<mdl	0.10	0.30	
Spot #8	AH90-4C-F	bn	matrix	<mdl	0.09	0.20		0.30	0.10	0.27	1.11
Spot #9	AH90-4C-F	bn	matrix	<mdl	0.08	0.18		<mdl	0.09	0.24	
Grid #35	AH90-4C-C	cp	vein	1.63	0.11	0.16	10.19	<mdl	1.00	0.07	
_1	AH90-4C-C	cp	vein	1.50	0.11	0.15	10.00	0.10	0.06	0.07	1.42
_2	AH90-4C-C	cp	vein	0.62	0.07	0.17	3.63	<mdl	1.00	0.06	
_4	AH90-4C-C	cp	vein	1.99	0.27	0.15	13.27	<mdl	1.00	0.08	
_5	AH90-4C-C	cp	vein	0.32	0.05	0.15	2.11	<mdl	1.00	0.08	
_6	AH90-4C-C	cp	vein	0.51	0.10	0.14	3.64	<mdl	1.00	0.11	
Spot #36	AH90-4C-C	bn	vein	0.48	0.08	0.12	4.02	0.18	0.07	0.07	2.63
Spot #37	AH90-4C-C	bn	vein	0.42	0.05	0.11	3.80	0.40	0.11	0.03	13.33
Spot #38	AH90-4C-C	bn	vein	0.39	0.05	0.14	2.76	0.21	0.08	0.05	4.57

Grid #23-01	GRS37-184-7.8A-B	cp	vein	1.25	0.13	0.23	5.43	<mdl	0.11	0.38	
Grid #23-02	GRS37-184-7.8A-B	cp	vein	3.34	0.51	0.22	15.18	<mdl	0.13	0.37	
Grid #23-03	GRS37-184-7.8A-B	cp	vein	0.63	0.18	0.25	2.52	<mdl	0.12	0.38	
Grid #23-04	GRS37-184-7.8A-B	cp	vein	1.40	0.18	0.26	5.38	<mdl	0.12	0.31	
Grid #23-05	GRS37-184-7.8A-B	cp	vein	2.99	0.25	0.24	12.46	0.36	0.13	0.28	1.29
Grid #23-06	GRS37-184-7.8A-B	cp	vein	1.94	0.24	0.26	7.46	0.33	0.13	0.31	1.06
Grid #24-01	GRS37-184-7.8A-B	cp	vein	0.93	0.21	0.26	3.58	<mdl	0.12	0.27	
Grid #24-02	GRS37-184-7.8A-B	cp	vein	0.82	0.18	0.28	2.93	0.38	0.15	0.34	1.12
Grid #24-03	GRS37-184-7.8A-B	cp	vein	0.51	0.16	0.32	1.59	0.57	0.20	0.31	1.84
Grid #24-04	GRS37-184-7.8A-B	cp	vein	<mdl	0.13	0.26		<mdl	0.14	0.39	
Grid #24-05	GRS37-184-7.8A-B	cp	vein	<mdl	0.12	0.30		<mdl	0.15	0.40	
Grid #24-06	GRS37-184-7.8A-B	cp	vein	<mdl	0.11	0.28		<mdl	0.15	0.40	
Spot #25	GRS37-184-7.8A-B	cp	matrix	<mdl	0.14	0.25		<mdl	0.11	0.33	
Spot #26	GRS37-184-7.8A-B	bn	matrix	<mdl	0.08	0.17		0.39	0.12	0.21	1.86
Grid #27-01	GRS37-184-7.8A-B	cp	vein	5.83	0.33	0.26	22.42	<mdl	0.13	0.29	
Grid #27-02	GRS37-184-7.8A-B	cp	vein	4.26	0.27	0.24	17.75	0.38	0.14	0.33	1.15
Grid #27-03	GRS37-184-7.8A-B	cp	vein	5.57	0.38	0.25	22.28	<mdl	0.13	0.38	
Grid #27-04	GRS37-184-7.8A-B	cp	vein	5.81	0.34	0.23	25.26	<mdl	0.12	0.37	
Grid #27-05	GRS37-184-7.8A-B	cp	vein	4.88	0.27	0.22	22.18	<mdl	0.12	0.34	
Grid #27-06	GRS37-184-7.8A-B	cp	vein	5.04	0.26	0.23	21.91	0.35	0.13	0.33	1.06
Grid #48-01	GRS37-170-714.2	cp	vein	0.40	0.13	0.27	1.48	0.28	0.12	0.23	1.22
Grid #48-02	GRS37-170-714.2	cp	vein	0.95	0.11	0.19	5.00	0.30	0.11	0.22	1.36
Grid #48-03	GRS37-170-714.2	cp	vein	0.62	0.13	0.26	2.38	0.30	0.12	0.22	1.36
Grid #48-04	GRS37-170-714.2	cp	vein	<mdl	0.10	0.22		<mdl	0.09	0.24	
Grid #48-05	GRS37-170-714.2	cp	vein	1.04	0.14	0.18	5.78	<mdl	0.10	0.25	
Grid #48-06	GRS37-170-714.2	cp	vein	1.00	0.13	0.22	4.55	0.31	0.12	0.22	1.41
Grid #49-01	GRS37-170-714.2	cp	matrix	0.87	0.14	0.24	3.63	0.46	0.16	0.29	1.59
Grid #49-02	GRS37-170-714.2	cp	matrix	0.51	0.13	0.24	2.13	0.30	0.12	0.28	1.07
Grid #49-03	GRS37-170-714.2	cp	matrix	0.55	0.14	0.24	2.29	<mdl	0.09	0.29	
Grid #49-04	GRS37-170-714.2	cp	matrix	0.72	0.15	0.30	2.40	0.38	0.15	0.28	1.36
Grid #49-05	GRS37-170-714.2	cp	matrix	0.81	0.15	0.24	3.38	<mdl	0.13	0.45	
Grid #49-06	GRS37-170-714.2	cp	matrix	0.46	0.13	0.29	1.59	<mdl	0.13	0.35	
Grid #50-01	GRS37-170-714.2	cp	vein	<mdl	0.08	0.24		<mdl	0.09	0.28	
Grid #50-02	GRS37-170-714.2	cp	vein	<mdl	0.10	0.25		<mdl	0.10	0.29	

Grid #50-03	GRS37-170-714.2	cp	vein	<mdl	0.09	0.21		<mdl	0.11	0.24	
Grid #50-04	GRS37-170-714.2	cp	vein	1.12	0.14	0.24	4.67	<mdl	0.11	0.27	
Grid #50-05	GRS37-170-714.2	cp	vein	1.42	0.15	0.24	5.92	<mdl	0.10	0.29	
Grid #50-06	GRS37-170-714.2	cp	vein	0.25	0.10	0.23	1.09	<mdl	0.12	0.28	
Grid #28-01	GRS37-170-742.2A-2	cp	vein	0.41	0.13	0.27	1.52	<mdl	0.13	0.37	
Grid #28-02	GRS37-170-742.2A-2	cp	vein	0.39	0.13	0.28	1.39	<mdl	0.09	0.39	
Grid #28-03	GRS37-170-742.2A-2	cp	vein	0.35	0.13	0.26	1.35	<mdl	0.11	0.38	
Grid #28-04	GRS37-170-742.2A-2	cp	vein	<mdl	0.12	0.32		0.45	0.16	0.41	1.10
Grid #28-05	GRS37-170-742.2A-2	cp	vein	0.48	0.17	0.30	1.60	0.40	0.16	0.35	1.14
Grid #28-06	GRS37-170-742.2A-2	cp	vein	1.18	0.46	0.27	4.37	0.41	0.15	0.30	1.37
Grid #29-01	GRS37-170-742.2A-2	cp	vein	<mdl	0.13	0.25		<mdl	0.11	0.30	
Grid #29-02	GRS37-170-742.2A-2	cp	vein	0.38	0.11	0.25	1.52	<mdl	0.11	0.29	
Grid #29-03	GRS37-170-742.2A-2	cp	vein	20.50	6.40	0.25	82.00	0.34	0.13	0.23	1.48
Grid #29-04	GRS37-170-742.2A-2	cp	vein	0.76	0.33	0.30	2.53	<mdl	0.11	0.37	
Grid #29-05	GRS37-170-742.2A-2	cp	vein	0.87	0.13	0.26	3.35	<mdl	0.12	0.44	
Grid #29-06	GRS37-170-742.2A-2	cp	vein	1.05	0.20	0.25	4.20	0.31	0.13	0.30	1.03
Spot #30	GRS37-170-742.2A-2	bn	matrix	<mdl	0.09	0.18		0.24	0.11	0.23	1.04
Spot #31	GRS37-170-742.2A-2	cp	matrix	0.35	0.14	0.23	1.52	<mdl	0.13	0.28	
Spot #33	GRS37-170-742.2A-2	cp	matrix	0.37	0.15	0.29	1.28	0.50	0.18	0.37	1.35
Grid #34-01	GRS37-170-742.2A-2	cp	vein	2.24	0.18	0.31	7.23	<mdl	0.14	0.33	
Grid #34-02	GRS37-170-742.2A-2	cp	vein	1.46	0.19	0.31	4.71	0.40	0.16	0.33	1.21
Grid #34-03	GRS37-170-742.2A-2	cp	vein	2.81	0.21	0.29	9.69	<mdl	0.15	0.45	
Grid #34-04	GRS37-170-742.2A-2	cp	vein	1.62	0.30	0.30	5.40	0.60	0.21	0.37	1.62
Grid #34-05	GRS37-170-742.2A-2	cp	vein	3.00	0.31	0.28	10.71	0.36	0.16	0.35	1.03
Grid #34-06	GRS37-170-742.2A-2	cp	vein	3.03	0.28	0.36	8.42	<mdl	0.16	0.42	
Grid #35-01	GRS37-170-742.2A-2	cp	vein	1.50	0.24	0.27	5.56	0.34	0.14	0.32	1.06
Grid #35-02	GRS37-170-742.2A-2	cp	vein	1.30	0.22	0.28	4.64	<mdl	0.14	0.33	
Grid #35-03	GRS37-170-742.2A-2	cp	vein	0.57	0.13	0.22	2.59	<mdl	0.11	0.36	
Grid #35-04	GRS37-170-742.2A-2	cp	vein	1.09	0.18	0.31	3.52	<mdl	0.11	0.31	
Grid #35-05	GRS37-170-742.2A-2	cp	vein	<mdl	0.12	0.27		0.33	0.14	0.32	1.03
Grid #35-06	GRS37-170-742.2A-2	cp	vein	<mdl	0.15	0.28		<mdl	0.15	0.37	
Spot #36	GRS37-170-742.2A-2	cp	vein	<mdl	0.10	0.19		<mdl	0.10	0.28	
Spot #37	GRS37-170-742.2A-2	cp	vein	<mdl	0.09	0.20		<mdl	0.10	0.25	
Spot #39	GRS37-170-742.2A-2	cp	vein	481.00	25.00	0.30	1603.33	6.04	0.59	0.42	14.38

Grid #42	GRS37-170-742.2A-2	cp	vein	1.70	0.10	0.14	12.13	<mdl	1.00	0.09
_13	GRS37-170-742.2A-2	cp	vein	1.35	0.10	0.14	9.65	<mdl	1.00	0.09
_14	GRS37-170-742.2A-2	cp	vein	1.23	0.11	0.15	8.20	<mdl	1.00	0.07
_15	GRS37-170-742.2A-2	cp	vein	1.68	0.12	0.13	12.92	<mdl	0.01	0.06
_16	GRS37-170-742.2A-2	cp	vein	1.60	0.15	0.14	11.43	<mdl	1.00	0.06
_17	GRS37-170-742.2A-2	cp	vein	1.25	0.11	0.15	8.33	<mdl	1.00	0.04
Grid #43	GRS37-170-742.2A-2	cp	vein	0.63	0.08	0.17	3.69	<mdl	1.00	0.09
_18	GRS37-170-742.2A-2	cp	vein	0.57	0.10	0.17	3.36	<mdl	1.00	0.09
_19	GRS37-170-742.2A-2	cp	vein	1.32	0.38	0.12	11.00	<mdl	1.00	0.10
_20	GRS37-170-742.2A-2	cp	vein	0.68	0.08	0.14	4.86	<mdl	1.00	0.10
_21	GRS37-170-742.2A-2	cp	vein	0.75	0.09	0.15	4.99	<mdl	1.00	
_22	GRS37-170-742.2A-2	cp	vein	0.77	0.09	0.14	5.50	<mdl	1.00	0.04
Spot #45	GRS37-170-742.2A-2	cp	vein	0.43	0.07	0.15	2.85	<mdl	1.00	0.09
Spot #46	GRS37-170-742.2A-2	cp	vein	0.42	0.08	0.13	3.24	<mdl	1.00	0.06
Spot #47	GRS37-170-742.2A-2	cp	vein	0.33	0.06	0.11	2.95	<mdl	1.00	0.07
Spot #49	GRS37-170-742.2A-2	cp	vein	0.23	0.07	0.13	1.78	<mdl	1.00	0.04
Spot #50	GRS37-170-742.2A-2	cp	vein	1.05	0.23	0.14	7.50	<mdl	1.00	0.04
Line #39	GRS37-170-742.2A-2	cp	vein	0.49	0.08	0.22	2.21	<mdl	1.00	
_27	GRS37-170-742.2A-2	cp	vein	0.38	0.07	0.14	2.72	<mdl	1.00	0.04
_28	GRS37-170-742.2A-2	cp	vein	0.32	0.06	0.11	2.89	<mdl	1.00	0.07
_29	GRS37-170-742.2A-2	cp	vein	0.38	0.07	0.12	3.18	<mdl	1.00	0.08
_30	GRS37-170-742.2A-2	cp	vein	0.28	0.06	0.15	1.85	<mdl	1.00	0.08
Line #40	GRS37-170-742.2A-2	cp	vein	0.27	0.05	0.12	2.25	<mdl	1.00	0.08
_31	GRS37-170-742.2A-2	cp	vein	0.22	0.06	0.12	1.83	<mdl	1.00	0.08
_32	GRS37-170-742.2A-2	cp	vein	0.66	0.17	0.16	4.13	<mdl	1.00	0.08
_33	GRS37-170-742.2A-2	cp	vein	0.44	0.07	0.14	3.16	<mdl	1.00	0.11
Line #41	GRS37-170-742.2A-2	cp	vein	0.35	0.06	0.13	2.67	<mdl	1.00	0.05
_34	GRS37-170-742.2A-2	cp	vein	0.43	0.06	0.14	3.08	<mdl	1.00	0.05
_35	GRS37-170-742.2A-2	cp	vein	0.96	0.16	0.14	6.86	<mdl	1.00	0.08
_36	GRS37-170-742.2A-2	cp	vein	1.15	0.09	0.14	8.19	<mdl	1.00	0.06
_37	GRS37-170-742.2A-2	cp	vein	1.26	0.09	0.15	8.42	<mdl	1.00	0.12
Line #44	GRS37-170-742.2A-2	cp	vein	0.69	0.08	0.15	4.59	<mdl	1.00	0.07
_38	GRS37-170-742.2A-2	cp	vein	0.40	0.06	0.14	2.86	<mdl	1.00	0.06
_39	GRS37-170-742.2A-2	cp	vein	0.38	0.06	0.10	3.78	<mdl	1.00	

_40	GRS37-170-742.2A-2	cp	vein	0.38	0.06	0.13	2.92	<mdl	1.00	0.04	
_41	GRS37-170-742.2A-2	cp	vein	0.34	0.05	0.16	2.11	<mdl	1.00	0.07	
Line #48	GRS37-170-742.2A-2	cp	vein	0.56	0.11	0.12	4.67	<mdl	1.00	0.11	
_42	GRS37-170-742.2A-2	cp	vein	0.39	0.06	0.14	2.76	<mdl	1.00	0.12	
_43	GRS37-170-742.2A-2	cp	vein	0.78	0.07	0.13	5.97	<mdl	1.00	0.11	
_44	GRS37-170-742.2A-2	cp	vein	0.58	0.06	0.14	4.15	<mdl	1.00		
_45	GRS37-170-742.2A-2	cp	vein	0.85	0.08	0.14	6.04	<mdl	1.00		
Line #53	GRS37-170-742.2A-2	cp	vein	0.52	0.07	0.14	3.71	<mdl	1.00	0.05	
_46	GRS37-170-742.2A-2	cp	vein	0.36	0.06	0.16	2.25	<mdl	1.00	0.05	
_47	GRS37-170-742.2A-2	cp	vein	0.34	0.07	0.15	2.24	0.08	0.06	0.08	1.04
_48	GRS37-170-742.2A-2	cp	vein	0.47	0.08	0.15	3.12	0.21	0.10	0.05	4.67
_49	GRS37-170-742.2A-2	cp	vein	0.68	0.08	0.12	5.67	<mdl	1.00	0.05	
Line #54	GRS37-170-742.2A-3	cp	vein	0.33	0.06	0.15	2.19	<mdl	1.00		
_50	GRS37-170-742.2A-3	cp	vein	0.32	0.07	0.14	2.31	<mdl	1.00	0.08	
_51	GRS37-170-742.2A-3	cp	vein	0.41	0.07	0.13	3.12	<mdl	1.00	0.10	
_52	GRS37-170-742.2A-3	cp	vein	0.42	0.07	0.15	2.79	<mdl	1.00		
_53	GRS37-170-742.2A-3	cp	vein	0.68	0.12	0.16	4.25	<mdl	1.00	0.08	
_54	GRS37-170-742.2A-3	cp	vein	0.42	0.07	0.14	3.01	<mdl	1.00	0.07	
_55	GRS37-170-742.2A-3	cp	vein	0.27	0.07	0.15	1.79	<mdl	1.00	0.08	
Line #55	GRS37-170-742.2A-3	cp	vein	0.30	0.06	0.15	2.01	<mdl	1.00	0.12	
_56	GRS37-170-742.2A-3	cp	vein	0.42	0.07	0.15	2.83	<mdl	1.00	0.12	
_57	GRS37-170-742.2A-3	cp	vein	0.45	0.05	0.13	3.45	<mdl	1.00	0.06	
_58	GRS37-170-742.2A-3	cp	vein	2.08	0.40	0.17	12.24	<mdl	0.07	0.14	
_59	GRS37-170-742.2A-3	cp	vein	0.34	0.06	0.15	2.25	<mdl	1.00	0.05	
Line #56	GRS37-170-742.2A-3	cp	vein	0.50	0.08	0.19	2.64	<mdl	1.00	0.08	
_60	GRS37-170-742.2A-3	cp	vein	0.44	0.07	0.18	2.42	<mdl	1.00	0.08	
_61	GRS37-170-742.2A-3	cp	vein	1.28	0.22	0.15	8.53	<mdl	1.00	0.12	
_62	GRS37-170-742.2A-3	cp	vein	0.84	0.09	0.15	5.61	<mdl	1.00		
_63	GRS37-170-742.2A-3	cp	vein	1.02	0.15	0.15	6.80	<mdl	1.00		
_64	GRS37-170-742.2A-3	cp	vein	0.78	0.07	0.15	5.18	<mdl	1.00	0.12	
Line #57	GRS37-170-742.2A-3	cp	vein	0.57	0.07	0.15	3.81	<mdl	1.00	0.07	
_65	GRS37-170-742.2A-3	cp	vein	0.85	0.10	0.15	5.67	<mdl	1.00	0.07	
_66	GRS37-170-742.2A-3	cp	vein	0.90	0.12	0.16	5.63	<mdl	1.00	0.05	
_67	GRS37-170-742.2A-3	cp	vein	0.73	0.09	0.16	4.53	<mdl	1.00	0.09	

_68	GRS37-170-742.2A-3	cp	vein	0.82	0.09	0.16	5.11	<mdl	1.00	0.08	
_69	GRS37-170-742.2A-3	cp	vein	<mdl	0.09	210.00		<mdl	1.00	0.06	
_70	GRS37-170-742.2A-3	cp	vein	0.76	0.08	0.14	5.42	<mdl	1.00	0.05	
_71	GRS37-170-742.2A-3	cp	vein	1.81	0.15	0.15	12.07	<mdl	1.00	0.05	
_72	GRS37-170-742.2A-3	cp	vein	1.24	0.17	0.16	7.75	<mdl	1.00	0.10	
_73	GRS37-170-742.2A-3	cp	vein	1.66	0.88	0.15	11.07	<mdl	0.04	0.13	
_74	GRS37-170-742.2A-3	cp	vein	1.92	0.13	0.17	11.29	<mdl	1.00	0.08	
_75	GRS37-170-742.2A-3	cp	vein	2.20	0.16	0.16	13.75	<mdl	1.00	0.08	
_76	GRS37-170-742.2A-3	cp	vein	1.65	0.14	0.17	9.71	0.09	0.06	0.08	1.11
_77	GRS37-170-742.2A-3	cp	vein	1.40	0.13	0.19	7.37	<mdl	0.02	0.14	
_78	GRS37-170-742.2A-3	cp	vein	1.25	0.13	0.17	7.35	<mdl	1.00	0.07	
_79	GRS37-170-742.2A-3	cp	vein	1.40	0.14	0.17	8.24	<mdl	1.00	0.08	
_80	GRS37-170-742.2A-3	cp	vein	7.30	2.10	0.16	45.63	<mdl	1.00		
_81	GRS37-170-742.2A-3	cp	vein	0.28	0.07	0.15	1.85	<mdl	1.00	0.06	
_82	GRS37-170-742.2A-3	cp	vein	0.27	0.06	0.16	1.70	<mdl	1.00		
_83	GRS37-170-742.2A-3	cp	vein	0.45	0.08	0.16	2.81	<mdl	1.00	0.08	
_84	GRS37-170-742.2A-3	cp	vein	1.30	0.35	0.15	8.67	<mdl	1.00	0.11	
_85	GRS37-170-742.2A-3	cp	vein	0.83	0.09	0.16	5.19	<mdl	1.00	0.06	
_86	GRS37-170-742.2A-3	cp	vein	0.96	0.11	0.16	6.00	<mdl	1.00	0.08	
_87	GRS37-170-742.2A-3	cp	vein	1.05	0.11	0.15	7.00	<mdl	1.00	0.05	
_88	GRS37-170-742.2A-3	cp	vein	1.42	0.14	0.17	8.35	<mdl	1.00	0.06	
_89	GRS37-170-742.2A-3	cp	vein	1.56	0.10	0.17	9.18	<mdl	1.00	0.08	
_90	GRS37-170-742.2A-3	cp	vein	1.68	0.13	0.15	11.20	<mdl	0.04	0.06	
_91	GRS37-170-742.2A-3	cp	vein	1.38	0.13	0.18	7.67	<mdl	1.00	0.16	
_92	GRS37-170-742.2A-3	cp	vein	1.43	0.12	0.13	11.00	<mdl	1.00	0.09	
_93	GRS37-170-742.2A-3	cp	vein	1.56	0.15	0.17	9.18	<mdl	1.00		
_94	GRS37-170-742.2A-3	cp	vein	0.75	0.08	0.19	3.96	<mdl	1.00	0.17	
_95	GRS37-170-742.2A-3	cp	vein	1.89	0.15	0.16	11.81	<mdl	1.00	0.10	
_96	GRS37-170-742.2A-3	cp	vein	1.61	0.11	0.17	9.47	<mdl	1.00	0.05	
_97	GRS37-170-742.2A-3	cp	vein	1.32	0.10	0.17	7.74	<mdl	1.00	0.09	
_98	GRS37-170-742.2A-3	cp	vein	1.19	0.11	0.15	7.93	<mdl	0.05	0.07	
_99	GRS37-170-742.2A-3	cp	vein	0.77	0.09	0.17	4.55	<mdl	1.00	0.14	
_100	GRS37-170-742.2A-3	cp	vein	1.01	0.09	0.16	6.31	<mdl	1.00	0.05	
_101	GRS37-170-742.2A-3	cp	vein	1.05	0.10	0.17	6.18	<mdl	1.00		

_102	GRS37-170-742.2A-3	cp	vein	0.94	0.09	0.16	5.90	<mdl	1.00	0.09	
_103	GRS37-170-742.2A-3	cp	vein	0.71	0.08	0.15	4.74	<mdl	1.00	0.11	
_104	GRS37-170-742.2A-3	cp	vein	1.02	0.11	0.17	6.00	<mdl	1.00	0.09	
_105	GRS37-170-742.2A-3	cp	vein	1.43	0.18	0.18	7.94	<mdl	1.00	0.08	
_106	GRS37-170-742.2A-3	cp	vein	1.08	0.12	0.17	6.35	<mdl	0.04	0.07	
_107	GRS37-170-742.2A-3	cp	vein	0.76	0.08	0.16	4.74	<mdl	1.00	0.12	
_108	GRS37-170-742.2A-3	cp	vein	0.72	0.08	0.12	5.99	<mdl	1.00	0.10	
_109	GRS37-170-742.2A-3	cp	vein	0.96	0.10	0.16	6.00	<mdl	1.00	0.11	
_110	GRS37-170-742.2A-3	cp	vein	1.00	0.10	0.15	6.67	<mdl	1.00	0.13	
_111	GRS37-170-742.2A-3	cp	vein	1.28	0.15	0.16	8.00	<mdl	1.00	0.07	
_112	GRS37-170-742.2A-3	cp	vein	0.97	0.13	0.13	7.46	<mdl	1.00	0.07	
_113	GRS37-170-742.2A-3	cp	vein	0.63	0.07	0.16	3.94	<mdl	1.00	0.06	
Grid #10-01	DOZ-90-29	bn	vein/matrix	2.39	0.86	0.17	14.06	1.20	0.26	0.21	5.71
Grid #10-02	DOZ-90-29	bn	vein/matrix	<mdl	0.08	0.18		1.82	0.38	0.21	8.67
Grid #10-03	DOZ-90-29	bn	vein/matrix	<mdl	0.08	0.19		0.93	0.16	0.22	4.23
Grid #10-04	DOZ-90-29	bn	vein/matrix	0.25	0.10	0.17	1.47	0.88	0.25	0.23	3.83
Grid #10-05	DOZ-90-29	bn	vein/matrix	<mdl	0.07	0.20		0.98	0.21	0.26	3.77
Grid #10-06	DOZ-90-29	bn	vein/matrix	<mdl	0.07	0.22		0.48	0.13	0.22	2.18
Grid #13-01	DOZ-90-29	bn	vein/matrix	<mdl	0.09	0.16		0.36	0.11	0.20	1.80
Grid #13-02	DOZ-90-29	bn	vein/matrix	<mdl	0.06	0.18		0.41	0.16	0.25	1.64
Grid #13-03	DOZ-90-29	bn	vein/matrix	<mdl	0.09	0.20		0.35	0.12	0.30	1.17
Grid #13-04	DOZ-90-29	bn	vein/matrix	<mdl	0.07	0.19		0.42	0.12	0.23	1.83
Grid #13-05	DOZ-90-29	bn	vein/matrix	<mdl	0.07	0.19		0.81	0.22	0.25	3.24
Grid #13-06	DOZ-90-29	bn	vein/matrix	<mdl	0.08	0.18		0.49	0.16	0.26	1.88
Grid #14-01	DOZ-90-29	bn	vein/matrix	<mdl	0.09	0.21		<mdl	0.10	0.27	
Grid #14-02	DOZ-90-29	bn	vein/matrix	<mdl	0.08	0.21		2.37	0.74	0.27	8.78
Grid #14-03	DOZ-90-29	bn	vein/matrix	<mdl	0.11	0.19		<mdl	0.12	0.28	
Grid #14-04	DOZ-90-29	bn	vein/matrix	<mdl	0.08	0.21		<mdl	0.10	0.34	
Grid #14-05	DOZ-90-29	bn	vein/matrix	<mdl	0.09	0.21		0.35	0.14	0.27	1.30
Grid #14-06	DOZ-90-29	bn	vein/matrix	<mdl	0.09	0.20		<mdl	0.09	0.26	
Grid #18-01	TE14-01-754.3	cp	vein	3.14	0.30	0.27	11.63	<mdl	0.13	0.36	
Grid #18-02	TE14-01-754.3	cp	vein	2.79	0.24	0.27	10.33	<mdl	0.12	0.36	
Grid #18-03	TE14-01-754.3	cp	vein	2.75	0.27	0.26	10.58	<mdl	0.13	0.41	
Grid #18-04	TE14-01-754.3	cp	vein	3.39	0.30	0.22	15.41	<mdl	0.12	0.37	
Grid #18-05	TE14-01-754.3	cp	vein	3.39	0.31	0.25	13.56	<mdl	0.12	0.35	
Grid #18-06	TE14-01-754.3	cp	vein	2.35	0.32	0.24	9.79	<mdl	0.13	0.46	
Grid #19-01	TE14-01-754.3	cp	vein	2.32	0.26	0.21	11.05	<mdl	0.11	0.39	
Grid #19-02	TE14-01-754.3	cp	vein	2.22	0.17	0.21	10.57	<mdl	0.12	0.40	
Grid #19-03	TE14-01-754.3	cp	vein	2.81	0.29	0.23	12.22	0.35	0.13	0.29	1.21
Grid #19-04	TE14-01-754.3	cp	vein	2.04	0.21	0.25	8.16	<mdl	0.11	0.32	

Grid #19-05	TE14-01-754.3	cp	vein	3.00	0.25	0.23	13.04	0.37	0.12	0.32	1.16
Grid #19-06	TE14-01-754.3	cp	vein	2.77	0.24	0.22	12.59	<mdl	0.11	0.28	
Grid #20-01	TE14-01-754.3	cp	vein	<mdl	0.13	0.23		<mdl	0.12	0.44	
Grid #20-02	TE14-01-754.3	cp	vein	<mdl	0.11	0.27		<mdl	0.14	0.52	
Grid #20-03	TE14-01-754.3	cp	vein	<mdl	0.09	0.27		<mdl	0.11	0.29	
Grid #20-04	TE14-01-754.3	cp	vein	0.79	0.18	0.26	3.04	0.39	0.14	0.35	1.11
Grid #20-05	TE14-01-754.3	cp	vein	<mdl	0.10	0.24		<mdl	0.11	0.41	
Grid #20-06	TE14-01-754.3	cp	vein	0.30	0.14	0.29	1.03	0.35	0.13	0.34	1.03
Grid #21-01	TE14-01-754.3	cp	vein	3.58	0.32	0.25	14.32	0.39	0.14	0.31	1.26
Grid #21-02	TE14-01-754.3	cp	vein	5.42	0.66	0.24	22.58	<mdl	0.11	0.30	
Grid #21-03	TE14-01-754.3	cp	vein	5.07	0.54	0.26	19.50	0.39	0.14	0.36	1.08
Grid #21-04	TE14-01-754.3	cp	vein	4.98	0.59	0.22	22.64	<mdl	0.12	0.30	
Grid #21-05	TE14-01-754.3	cp	vein	3.86	0.39	0.28	13.79	<mdl	0.12	0.30	
Grid #21-06	TE14-01-754.3	cp	vein	3.37	0.25	0.21	16.05	<mdl	0.13	0.42	
Grid #22-01	TE14-01-754.3	cp	vein	<mdl	0.11	33.00		<mdl	0.12	0.29	
Grid #22-02	TE14-01-754.3	cp	vein	<mdl	0.13	0.28		0.50	0.16	0.35	1.43
Grid #22-03	TE14-01-754.3	cp	vein	<mdl	0.11	0.31		0.37	0.16	0.36	1.03
Grid #22-04	TE14-01-754.3	cp	vein	0.33	0.12	0.22	1.50	<mdl	0.06	0.28	
Grid #22-05	TE14-01-754.3	cp	vein	<mdl	0.12	0.24		<mdl	0.10	0.37	
Grid #22-06	TE14-01-754.3	cp	vein	<mdl	0.11	0.27		<mdl	0.13	0.33	
Spot #40	TE14-01-754.3	cp	matrix	328.00	10.00	0.35	937.14	4.76	0.69	0.44	10.82
Spot #41	TE14-01-754.3	cp	matrix	56.00	3.80	0.09	651.16	82.30	5.00	0.11	748.18
Spot #42	TE14-01-754.3	cp	matrix	82.80	9.40	0.32	258.75	3.03	0.54	0.33	9.18
Spot #43	TE14-01-754.3	cp	matrix	176.00	16.00	0.10	1795.92	84.70	5.50	0.08	1008.33
Spot #44	TE14-01-754.3	cp	matrix	2700.00	1100.00	0.15	18000.00	27.30	3.80	0.20	136.50
Spot #45	TE14-01-754.3	cp	matrix	319.00	14.00	0.16	1993.75	32.50	1.90	0.14	232.14
Spot #46	TE14-01-754.3	cp	matrix	303.00	15.00	0.18	1683.33	43.00	2.10	0.21	204.76
Spot #47	TE14-01-754.3	cp	matrix	483.00	18.00	0.14	3450.00	34.80	2.00	0.20	174.00
Spot #17	TE01-16-566C	cp	vein	1.00	0.09	0.15	6.67	<mdl	1.00	0.08	
Spot #18	TE01-16-566C	cp	vein	0.39	0.06	0.15	2.62	<mdl	1.00	0.07	
Spot #19	TE01-16-566C	cp	vein	0.35	0.07	0.14	2.51	<mdl	1.00	0.04	
Spot #20	TE01-16-566C	cp	vein	0.37	0.07	0.14	2.67	<mdl	1.00	0.04	
Spot #21	TE01-16-566C	cp	vein	2.27	0.71	0.16	14.19	0.10	0.07	0.06	1.66
Spot #22	TE01-16-566C	cp	vein	2.81	0.24	0.16	17.56	0.08	0.06	0.06	1.42

Spot #23	TE01-16-566C	cp	vein	0.33	0.06	0.15	2.17	<mdl	1.00	0.04
Spot #24	TE01-16-566C	cp	vein	0.38	0.07	0.14	2.68	<mdl	1.00	0.04
Spot #25	TE01-16-566C	cp	vein	0.42	0.06	0.14	2.99	<mdl	1.00	0.04
Grid #14	TE01-16-566C	cp	vein	11.41	0.44	0.18	63.39	<mdl	1.00	0.32
_1	TE01-16-566C	cp	vein	10.45	0.40	0.14	74.64	<mdl	1.00	0.07
_2	TE01-16-566C	cp	vein	11.05	0.38	0.15	73.67	<mdl	1.00	
_4	TE01-16-566C	cp	vein	13.42	0.39	0.15	89.47	<mdl	1.00	
_5	TE01-16-566C	cp	vein	14.48	0.54	0.15	96.53	<mdl	1.00	0.07
_6	TE01-16-566C	cp	vein	13.02	0.48	0.15	86.80	<mdl	1.00	0.07
Grid #15	TE01-16-566C	cp	vein	0.48	0.07	0.16	2.99	<mdl	1.00	0.07
_7	TE01-16-566C	cp	vein	0.42	0.06	0.16	2.61	<mdl	1.00	0.07
_8	TE01-16-566C	cp	vein	0.45	0.07	0.14	3.24	<mdl	1.00	0.08
_9	TE01-16-566C	cp	vein	0.41	0.07	0.16	2.59	<mdl	1.00	0.06
_10	TE01-16-566C	cp	vein	0.41	0.07	0.15	2.75	<mdl	1.00	0.10
_11	TE01-16-566C	cp	vein	0.40	0.07	0.15	2.67	<mdl	1.00	0.05
Grid #16	TE01-16-566C	cp	vein	0.31	0.06	0.14	2.23	<mdl	1.00	0.06
_12	TE01-16-566C	cp	vein	0.33	0.07	0.14	2.39	<mdl	0.02	0.06
_13	TE01-16-566C	cp	vein	0.37	0.05	0.14	2.65	<mdl	1.00	0.07
_14	TE01-16-566C	cp	vein	0.36	0.06	0.13	2.73	<mdl	1.00	0.04
_15	TE01-16-566C	cp	vein	0.36	0.05	0.12	2.97	<mdl	1.00	0.05
_16	TE01-16-566C	cp	vein	0.39	0.06	0.21	1.84	<mdl	1.00	0.12
Spot #28	TE01-16-566A	cp	vein	0.54	0.08	0.16	3.40	<mdl	1.00	0.03
Spot #29	TE01-16-566A	cp	vein	0.43	0.07	0.14	3.09	<mdl	1.00	0.06
Spot #30	TE01-16-566A	cp	vein	0.64	0.14	0.16	4.00	<mdl	1.00	0.06
Spot #31	TE01-16-566A	cp	vein	0.87	0.13	0.11	7.91	<mdl	1.00	
Spot #32	TE01-16-566A	cp	vein	0.39	0.07	0.14	2.76	<mdl	1.00	0.11
Spot #33	TE01-16-566A	cp	vein	0.57	0.08	0.13	4.36	<mdl	1.00	0.10
Spot #34	TE01-16-566A	cp	vein	0.33	0.06	0.13	2.53	<mdl	1.00	0.05
Grid #26	TE01-16-566A	cp	vein	12.86	0.58	0.23	55.91	<mdl	1.00	0.13
_17	TE01-16-566A	cp	vein	11.06	0.45	0.16	69.13	<mdl	1.00	0.13
_18	TE01-16-566A	cp	vein	13.63	0.51	0.15	90.87	<mdl	1.00	0.05
_19	TE01-16-566A	cp	vein	14.32	0.70	0.14	102.29	<mdl	1.00	0.16
_20	TE01-16-566A	cp	vein	15.13	0.59	0.13	116.38	<mdl	1.00	0.06
_21	TE01-16-566A	cp	vein	13.52	0.57	0.24	56.33	<mdl	1.00	0.12

Grid #27	TE01-16-566A	cp	vein	13.19	0.47	0.23	57.35	<mdl	1.00	0.12
_22	TE01-16-566A	cp	vein	11.55	0.48	0.15	77.00	<mdl	1.00	0.05
_23	TE01-16-566A	cp	vein	8.45	0.35	0.15	56.33	<mdl	1.00	0.08
_24	TE01-16-566A	cp	vein	8.51	0.37	0.14	60.79	<mdl	1.00	0.08
_25	TE01-16-566A	cp	vein	4.15	0.19	0.15	27.67	<mdl	1.00	0.07
_26	TE01-16-566A	cp	vein	4.62	0.22	0.24	19.25	<mdl	1.00	

	Zn				As				Se			
Analysis #	ppm	2σ std error	LOD	Signal/ Noise	ppm	2σ std error	LOD	Signal/ Noise	ppm	2σ std error	LOD	Signal/ Noise
Spot #4	32.30	1.90	0.15	215.33	0.66	0.20	0.55	1.20	451.00	24.00	2.10	214.76
Spot #5	25.10	1.70	0.17	147.65	1.12	0.26	0.61	1.84	357.00	20.00	2.30	155.22
Spot #6	26.00	2.10	0.18	144.44	0.82	0.17	0.56	1.46	228.00	11.00	1.80	126.67
Spot #7	4.85	0.48	0.14	34.64	0.60	0.15	0.44	1.36	393.00	19.00	1.40	280.71
Spot #8	1.98	0.28	0.13	15.23	0.48	0.16	0.38	1.26	405.00	23.00	1.20	337.50
Spot #9	1.31	0.22	0.13	10.08	0.57	0.15	0.37	1.54	319.00	15.00	1.10	290.00
Spot #10	1.98	0.27	0.54	3.67	0.75	0.20	0.43	1.74	391.00	13.00	1.20	325.83
Spot #11	171.00	35.00	0.18	950.00	1.07	0.29	0.50	2.14	356.00	18.00	1.70	209.41
Spot #12	242.00	31.00	0.13	1861.54	0.72	0.20	0.53	1.36	265.00	14.00	1.20	220.83
Spot #13	1.55	0.23	0.16	9.69	0.81	0.18	0.43	1.88	618.00	27.00	1.00	618.00
Grid #4-01	70.90	3.80	0.52	136.35	<mdl	0.24	0.61		367.00	19.00	4.10	89.51
Grid #4-02	82.70	6.20	0.53	156.04	<mdl	0.21	0.62		340.00	18.00	4.20	80.95
Grid #4-03	83.50	6.60	0.52	160.58	<mdl	0.20	0.60		349.00	20.00	3.30	105.76
Grid #4-04	72.20	6.40	0.46	156.96	<mdl	0.25	0.45		336.00	15.00	4.10	81.95
Grid #4-05	86.00	8.40	0.48	179.17	<mdl	0.20	0.58		352.00	21.00	2.70	130.37
Grid #4-06	81.80	4.80	0.47	174.04	<mdl	0.21	0.48		335.00	17.00	2.00	167.50
Grid #5-01	35.20	4.60	0.63	55.87	<mdl	0.28	0.70		295.00	17.00	4.80	61.46
Grid #5-02	307.00	50.00	0.63	487.30	<mdl	0.36	0.65		205.00	15.00	3.90	52.56
Grid #5-03	506.00	66.00	0.67	755.22	<mdl	0.33	0.73		372.00	22.00	5.00	74.40
Grid #5-04	260.00	53.00	0.96	270.83	<mdl	0.31	0.79		239.00	16.00	4.30	55.58
Grid #5-05	174.80	7.70	0.73	239.45	<mdl	0.36	0.92		416.00	23.00	5.00	83.20
Grid #5-06	327.00	52.00	0.71	460.56	<mdl	0.33	0.81		392.00	24.00	3.90	100.51
Grid #6-01	140.00	19.00	0.73	191.78	<mdl	0.39	0.76		346.00	19.00	3.70	93.51
Grid #6-02	113.00	20.00	0.66	171.21	<mdl	0.29	0.80		322.00	19.00	4.20	76.67
Grid #6-03	484.00	72.00	0.68	711.76	<mdl	0.26	0.70		397.00	18.00	3.70	107.30
Grid #6-04	204.00	41.00	0.67	304.48	<mdl	0.27	0.69		417.00	22.00	4.60	90.65
Grid #6-05	303.00	48.00	0.91	332.97	<mdl	0.32	0.62		401.00	21.00	4.30	93.26
Grid #6-06	393.00	79.00	0.75	524.00	<mdl	0.38	0.75		401.00	24.00	3.90	102.82
Grid #7-01	2.46	0.49	0.63	3.90	<mdl	0.26	0.57		347.00	18.00	2.50	138.80
Grid #7-02	1.90	0.41	0.74	2.57	<mdl	0.29	0.68		357.00	18.00	2.40	148.75
Grid #7-03	76.50	5.00	0.80	95.63	<mdl	0.27	0.73		360.00	17.00	3.30	109.09
Grid #7-04	111.00	15.00	0.58	191.38	<mdl	0.28	0.65		355.00	16.00	2.40	147.92
Grid #7-05	82.70	7.30	0.66	125.30	<mdl	0.24	0.61		353.00	18.00	3.30	106.97
Grid #7-06	82.50	5.20	0.63	130.95	<mdl	0.27	0.58		355.00	19.00	2.50	142.00
Spot #8	5.03	0.64	0.53	9.49	<mdl	0.24	0.69		323.00	14.00	3.10	104.19
Spot #9	85.00	4.50	0.48	177.08	<mdl	0.21	0.62		325.00	15.00	2.80	116.07

Grid #35	350.00	78.00	0.24	1458.33	0.71	0.25	0.57	1.25	508.00	20.00	1.60	317.50
_1	375.00	52.00	0.22	1704.55	0.90	0.24	0.52	1.73	504.00	24.00	1.40	360.00
_2	520.00	140.00	0.18	2888.89	0.89	0.28	0.58	1.53	234.00	12.00	1.50	156.00
_4	450.00	110.00	0.20	2250.00	0.81	0.26	0.66	1.23	292.00	12.00	1.70	171.76
_5	136.00	36.00	0.20	680.00	0.87	0.29	0.65	1.34	473.00	20.00	1.70	278.24
_6	350.00	85.00	0.22	1590.91	0.85	0.25	0.58	1.47	430.00	17.00	1.90	226.32
Spot #36	136.00	24.00	0.15	906.67	0.72	0.24	0.40	1.80	452.00	19.00	1.10	410.91
Spot #37	92.60	4.30	0.13	712.31	0.50	0.20	0.40	1.25	445.00	14.00	1.20	370.83
Spot #38	74.80	3.50	0.19	393.68	0.52	0.20	0.41	1.27	432.00	15.00	1.20	360.00
Grid #23-01	37.10	3.20	0.75	49.47	1.23	0.29	0.61	2.02	259.00	16.00	3.90	66.41
Grid #23-02	10700.00	2400.00	0.73	14657.53	0.65	0.24	0.59	1.10	259.00	19.00	3.70	70.00
Grid #23-03	14.80	1.30	0.79	18.73	1.12	0.28	0.71	1.58	249.00	19.00	4.10	60.73
Grid #23-04	18.10	1.70	0.83	21.81	<mdl	0.24	0.80		210.00	14.00	4.10	51.22
Grid #23-05	44.00	5.00	0.78	56.41	0.89	0.25	0.73	1.22	226.00	16.00	2.90	77.93
Grid #23-06	40.90	5.00	0.86	47.56	0.71	0.23	0.64	1.11	246.00	16.00	3.50	70.29
Grid #24-01	29.50	6.30	0.73	40.41	0.72	0.26	0.60	1.20	210.00	15.00	3.90	53.85
Grid #24-02	44.30	8.80	0.91	48.68	0.90	0.30	0.81	1.11	378.00	28.00	4.50	84.00
Grid #24-03	41.00	3.90	0.89	46.07	1.18	0.31	0.89	1.33	376.00	26.00	3.70	101.62
Grid #24-04	25.00	2.10	0.89	28.09	1.43	0.36	0.76	1.88	257.00	17.00	4.10	62.68
Grid #24-05	64.90	8.70	0.84	77.26	1.08	0.32	0.74	1.46	246.00	17.00	3.80	64.74
Grid #24-06	22.20	1.80	0.87	25.52	<mdl	0.23	0.77		262.00	17.00	3.60	72.78
Spot #25	59.60	3.20	0.66	90.30	0.91	0.25	0.77	1.18	239.00	16.00	3.20	74.69
Spot #26	19.70	1.80	0.52	37.88	0.59	0.17	0.45	1.31	557.00	22.00	3.20	174.06
Grid #27-01	222.00	10.00	0.74	300.00	1.00	0.32	0.61	1.64	242.00	14.00	4.10	59.02
Grid #27-02	187.60	8.50	0.86	218.14	0.97	0.29	0.73	1.33	224.00	15.00	4.70	47.66
Grid #27-03	204.90	9.50	0.69	296.96	<mdl	0.22	0.80		244.00	15.00	4.20	58.10
Grid #27-04	298.00	22.00	0.70	425.71	1.08	0.32	0.75	1.44	232.00	13.00	2.90	80.00
Grid #27-05	314.00	44.00	0.86	365.12	0.78	0.23	0.62	1.26	232.00	17.00	4.80	48.33
Grid #27-06	337.00	39.00	0.79	426.58	1.00	0.25	0.76	1.32	247.00	17.00	4.80	51.46
Grid #48-01	460.00	170.00	0.48	958.33	0.92	0.25	0.55	1.67	277.00	20.00	4.30	64.42
Grid #48-02	96.20	4.90	0.41	234.63	<mdl	0.18	0.64		285.00	16.00	3.50	81.43
Grid #48-03	21.30	1.60	0.36	59.17	0.65	0.20	0.53	1.23	234.00	15.00	2.40	97.50
Grid #48-04	12.60	1.30	0.52	24.23	0.70	0.21	0.52	1.35	274.00	14.00	3.00	91.33
Grid #48-05	179.00	22.00	0.53	337.74	0.55	0.18	0.48	1.15	269.00	17.00	2.80	96.07
Grid #48-06	111.90	4.90	0.53	211.13	<mdl	0.18	0.50		279.00	16.00	1.40	199.29

Grid #49-01	187.20	8.40	0.71	263.66	0.83	0.28	0.71	1.17	389.00	21.00	4.70	82.77
Grid #49-02	140.10	6.70	0.69	203.04	0.76	0.23	0.69	1.10	363.00	25.00	4.60	78.91
Grid #49-03	144.30	6.20	0.85	169.76	1.15	0.31	0.72	1.60	392.00	23.00	3.40	115.29
Grid #49-04	176.80	9.20	0.64	276.25	0.68	0.22	0.62	1.10	394.00	25.00	4.20	93.81
Grid #49-05	173.00	7.70	0.51	339.22	<mdl	0.23	0.68		393.00	23.00	3.30	119.09
Grid #49-06	150.50	8.20	0.69	218.12	0.73	0.25	0.56	1.30	373.00	24.00	3.00	124.33
Grid #50-01	75.00	14.00	0.66	113.64	<mdl	0.19	0.61		279.00	14.00	2.50	111.60
Grid #50-02	22.70	1.70	0.70	32.43	<mdl	0.19	0.64		298.00	16.00	2.60	114.62
Grid #50-03	41.00	5.40	0.62	66.13	0.75	0.26	0.69	1.09	286.00	17.00	2.10	136.19
Grid #50-04	118.10	5.80	0.59	200.17	0.76	0.23	0.56	1.36	302.00	16.00	3.70	81.62
Grid #50-05	167.00	21.00	0.53	315.09	0.61	0.21	0.53	1.15	315.00	18.00	3.30	95.45
Grid #50-06	19.60	1.70	0.57	34.39	0.67	0.20	0.50	1.34	282.00	15.00	4.80	58.75
Grid #28-01	153.00	17.00	0.91	168.13	0.76	0.36	0.70	1.09	596.00	43.00	5.40	110.37
Grid #28-02	154.10	9.20	0.94	163.94	1.20	0.33	0.72	1.67	610.00	42.00	5.60	108.93
Grid #28-03	139.00	11.00	0.77	180.52	0.89	0.27	0.69	1.29	661.00	48.00	6.30	104.92
Grid #28-04	173.00	11.00	0.82	210.98	0.90	0.27	0.82	1.10	644.00	45.00	3.30	195.15
Grid #28-05	251.00	66.00	0.89	282.02	1.39	0.39	0.76	1.83	656.00	54.00	5.50	119.27
Grid #28-06	114.00	54.00	0.80	142.50	1.29	0.36	0.79	1.63	620.00	36.00	4.70	131.91
Grid #29-01	107.00	22.00	0.74	144.59	<mdl	0.30	0.87		613.00	31.00	3.60	170.28
Grid #29-02	50.40	3.60	0.72	70.00	1.09	0.28	0.84	1.30	643.00	34.00	3.50	183.71
Grid #29-03	1620.00	370.00	0.75	2160.00	<mdl	0.24	0.85		577.00	33.00	3.50	164.86
Grid #29-04	49.80	5.10	0.89	55.96	0.93	0.25	0.79	1.18	632.00	31.00	4.40	143.64
Grid #29-05	182.00	28.00	0.88	206.82	<mdl	0.22	0.63		584.00	29.00	4.30	135.81
Grid #29-06	167.00	16.00	0.81	206.17	0.89	0.27	0.70	1.27	596.00	27.00	4.10	145.37
Spot #30	151.00	34.00	0.46	328.26	0.70	0.20	0.46	1.52	711.00	40.00	2.40	296.25
Spot #31	15.90	1.70	0.61	26.07	0.97	0.31	0.63	1.54	387.00	40.00	2.70	143.33
Spot #33	90.70	5.40	0.96	94.48	1.36	0.36	0.66	2.06	670.00	46.00	4.40	152.27
Grid #34-01	270.00	30.00	0.70	385.71	<mdl	0.25	0.91		621.00	43.00	6.30	98.57
Grid #34-02	160.00	11.00	0.70	228.57	<mdl	0.25	0.91		593.00	33.00	6.30	94.13
Grid #34-03	232.00	21.00	0.87	266.67	1.23	0.32	0.88	1.40	642.00	45.00	5.10	125.88
Grid #34-04	171.00	12.00	0.85	201.18	1.25	0.32	0.84	1.49	659.00	37.00	3.60	183.06

Grid #34-05	269.00	26.00	0.86	312.79	1.45	0.36	0.80	1.81	654.00	39.00	6.60	99.09
Grid #34-06	206.00	24.00	0.92	223.91	<mdl	0.30	0.87		649.00	45.00	5.70	113.86
Grid #35-01	159.50	8.80	0.47	339.36	0.74	0.23	0.71		574.00	28.00	3.20	179.38
Grid #35-02	244.00	39.00	0.48	508.33	<mdl	0.21	0.74		611.00	29.00	3.30	185.15
Grid #35-03	168.90	8.00	0.67	252.09	0.91	0.28	0.71	1.28	588.00	26.00	3.00	196.00
Grid #35-04	181.00	12.00	0.77	235.06	1.03	0.28	0.90	1.14	607.00	25.00	4.40	137.95
Grid #35-05	34.00	2.80	0.71	47.89	1.11	0.32	0.84	1.32	646.00	26.00	4.30	150.23
Grid #35-06	75.10	5.00	0.87	86.32	1.19	0.36	0.85	1.40	544.00	25.00	3.80	143.16
Spot #36	14.10	1.10	0.48	29.38	<mdl	0.27	0.94		877.00	43.00	2.70	324.81
Spot #37	27.90	2.10	0.65	42.92	0.68	0.26	0.50	1.36	861.00	45.00	2.80	307.50
Spot #39	404.00	23.00	0.88	459.09	0.95	0.30	0.92	1.03	303.00	21.00	4.90	61.84
Grid #42	250.00	130.00	0.27	925.93	0.73	0.22	0.57	1.28	589.00	26.00	1.70	346.47
_13	129.00	20.00	0.28	460.71	0.99	0.27	0.59	1.68	615.00	30.00	1.80	341.67
_14	57.10	3.10	0.26	219.62	0.79	0.27	0.64	1.23	604.00	31.00	71.00	8.51
_15	80.90	7.10	0.21	385.24	0.80	0.22	0.52	1.54	563.00	27.00	1.50	375.33
_16	125.00	18.00	0.22	568.18	0.74	0.26	0.57	1.30	594.00	32.00	1.70	349.41
_17	96.00	11.00	0.17	564.71	0.87	0.23	0.62	1.40	597.00	35.00	1.60	373.13
Grid #43	141.40	6.80	0.22	642.73	0.76	0.27	0.54	1.41	600.00	23.00	1.60	375.00
_18	65.50	3.80	0.23	284.78	0.76	0.29	0.55	1.38	549.00	23.00	1.60	343.13
_19	96.00	20.00	0.16	600.00	0.63	0.27	0.61	1.03	577.00	20.00	1.50	384.67
_20	242.00	34.00	0.15	1613.33	<mdl	0.28	0.64		633.00	21.00	1.70	372.35
_21	153.40	8.40	0.26	590.00	0.92	0.26	0.67	1.37	593.00	23.00	1.80	329.44
_22	114.00	23.00	0.26	438.46	0.70	0.24	0.54	1.30	472.00	17.00	1.50	314.67
Spot #45	30.30	1.60	0.18	168.33	0.86	0.26	0.47	1.83	773.00	27.00	1.70	454.71
Spot #46	37.00	18.00	0.19	194.74	<mdl	0.22	0.65		606.00	21.00	1.50	404.00
Spot #47	39.90	3.70	0.16	249.38	0.63	0.23	0.56	1.13	643.00	18.00	1.50	428.67
Spot #49	26.80	1.30	0.14	191.43	0.59	0.21	0.52	1.13	947.00	31.00	1.50	631.33
Spot #50	138.20	6.40	0.14	987.14	0.90	0.28	0.54	1.67	569.00	21.00	1.60	355.63
Line #39	71.00	17.00	0.30	236.67	<mdl	0.20	0.77		431.00	15.00	2.40	179.58
_27	58.90	4.90	0.17	346.47	<mdl	0.21	0.49		511.00	21.00	1.90	268.95
_28	77.00	16.00	0.24	320.83	<mdl	0.20	0.44		518.00	22.00	1.30	398.46
_29	148.00	34.00	0.22	672.73	<mdl	0.20	0.49		532.00	21.00	1.80	295.56
_30	47.80	4.70	0.21	227.62	<mdl	0.22	0.50		568.00	23.00	1.50	378.67
Line #40	60.20	8.60	0.22	273.64	<mdl	0.18	0.52		699.00	30.00	2.00	349.50
_31	29.30	1.70	0.22	133.18	<mdl	0.18	0.52		613.00	28.00	2.00	306.50
_32	35.40	8.30	0.21	168.57	<mdl	0.24	0.47		549.00	24.00	2.20	249.55
_33	19.80	1.40	0.18	110.00	<mdl	0.17	0.46		627.00	27.00	1.10	570.00
Line #41	37.50	5.20	0.28	133.93	<mdl	0.21	0.51		688.00	24.00	1.30	529.23
_34	58.00	10.00	0.29	200.00	<mdl	0.22	0.52		598.00	23.00	1.30	460.00
_35	35.90	4.10	0.27	132.96	<mdl	0.18	0.54		552.00	21.00	1.70	324.71
_36	74.10	4.40	0.29	255.52	<mdl	0.19	0.41		543.00	21.00	1.40	387.86
_37	68.40	3.40	0.23	297.39	<mdl	0.21	0.52		553.00	20.00	1.30	425.38
Line #44	104.00	43.00	0.27	385.19	<mdl	0.20	0.54		515.00	22.00	1.70	302.94
_38	47.40	3.50	0.26	182.31	<mdl	0.18	0.50		515.00	20.00	1.60	321.88
_39	72.70	7.60	0.20	363.50	<mdl	0.18	0.48		542.00	25.00	1.00	542.00
_40	101.00	17.00	0.16	631.25	<mdl	0.16	0.47		519.00	21.00	1.50	346.00

_41	73.40	7.70	0.19	386.32	<mdl	0.21	0.58	515.00	19.00	1.60	321.88
Line #48	14.30	1.00	0.26	55.00	<mdl	0.20	0.42	734.00	31.00	1.10	667.27
_42	17.79	0.98	0.29	61.34	<mdl	0.21	0.47	930.00	45.00	1.30	715.38
_43	21.90	1.50	0.23	95.22	<mdl	0.21	0.61	702.00	32.00	1.40	501.43
_44	60.20	8.00	0.21	286.67	<mdl	0.21	0.46	348.00	18.00	1.70	204.71
_45	181.00	14.00	0.27	670.37	<mdl	0.18	0.53	567.00	25.00	1.50	378.00
Line #53	58.60	3.60	0.25	234.40	<mdl	0.21	0.45	593.00	20.00	1.40	423.57
_46	62.30	3.40	0.27	230.74	<mdl	0.22	0.49	680.00	27.00	1.50	453.33
_47	86.00	15.00	0.26	330.77	<mdl	0.26	0.58	714.00	30.00	1.50	476.00
_48	88.70	4.10	0.20	443.50	<mdl	0.19	0.47	545.00	23.00	1.80	302.78
_49	119.90	4.40	0.23	521.30	<mdl	0.22	0.54	520.00	23.00	1.30	400.00
Line #54	91.00	22.00	0.26	350.00	<mdl	0.19	0.48	639.00	28.00	1.10	580.91
_50	110.00	26.00	0.26	423.08	<mdl	0.22	0.58	580.00	22.00	2.10	276.19
_51	137.00	43.00	0.45	304.44	<mdl	0.21	0.58	551.00	25.00	1.50	367.33
_52	167.00	31.00	0.30	556.67	<mdl	0.21	0.55	384.00	17.00	1.70	225.88
_53	500.00	120.00	0.31	1612.90	<mdl	0.22	0.67	451.00	21.00	1.60	281.88
_54	208.00	46.00	0.28	742.86	<mdl	0.21	0.55	514.00	24.00	1.60	321.25
_55	64.40	8.90	0.26	247.69	<mdl	0.20	0.53	510.00	25.00	1.50	340.00
Line #55	54.50	7.10	0.26	209.62	<mdl	0.21	0.56	570.00	31.00	1.80	316.67
_56	65.40	7.00	0.26	251.54	<mdl	0.20	0.56	603.00	36.00	1.80	335.00
_57	160.00	29.00	0.24	666.67	<mdl	0.22	0.51	623.00	34.00	1.60	389.38
_58	140.00	20.00	0.28	500.00	<mdl	0.23	0.50	707.00	34.00	1.20	589.17
_59	91.60	8.80	0.24	381.67	<mdl	0.22	0.54	671.00	39.00	1.60	419.38
Line #56	35.80	1.80	0.28	127.86	<mdl	0.22	0.49	680.00	22.00	1.50	453.33
_60	61.10	5.00	0.27	226.30	<mdl	0.22	0.46	464.00	20.00	1.40	331.43
_61	38.70	2.90	0.30	129.00	<mdl	0.21	0.56	524.00	22.00	8.60	60.93
_62	76.90	4.60	0.25	307.60	<mdl	0.22	0.53	503.00	23.00	1.80	279.44
_63	43.40	3.40	0.30	144.67	<mdl	0.22	0.57	554.00	25.00	1.70	325.88
_64	59.60	2.90	0.31	192.26	<mdl	0.22	0.51	501.00	22.00	1.90	263.68
Line #57	60.70	2.70	0.35	173.43	<mdl	0.22	0.54	543.00	19.00	1.90	285.79
_65	65.50	4.60	0.34	192.65	<mdl	0.20	0.53	558.00	19.00	1.80	310.00
_66	88.00	8.60	0.21	419.05	<mdl	0.17	0.50	548.00	24.00	1.40	391.43
_67	95.60	9.60	0.21	455.24	<mdl	0.21	0.50	556.00	16.00	1.50	370.67
_68	330.00	140.00	0.31	1064.52	<mdl	0.20	0.54	559.00	23.00	2.20	254.09
_69	58.40	7.10	0.32	182.50	<mdl	0.24	0.44	532.00	21.00	1.60	332.50
_70	55.30	3.40	0.28	197.50	<mdl	0.18	0.54	558.00	18.00	1.30	429.23
_71	107.10	7.10	0.25	428.40	<mdl	0.20	0.63	564.00	19.00	1.60	352.50
_72	129.00	21.00	0.22	586.36	<mdl	0.19	0.51	563.00	21.00	2.00	281.50
_73	112.50	9.10	0.26	432.69	<mdl	0.20	0.56	548.00	20.00	1.80	304.44
_74	129.00	14.00	0.25	516.00	<mdl	0.17	0.54	548.00	20.00	2.20	249.09
_75	116.00	11.00	0.35	331.43	<mdl	0.20	0.53	575.00	24.00	1.40	410.71
_76	700.00	230.00	0.33	2121.21	<mdl	0.20	0.65	560.00	22.00	1.80	311.11
_77	210.00	42.00	0.28	750.00	<mdl	0.20	0.58	544.00	22.00	1.60	340.00
_78	133.00	12.00	0.18	738.89	<mdl	0.22	0.51	546.00	21.00	1.60	341.25
_79	80.80	4.40	0.25	323.20	<mdl	0.18	0.51	523.00	23.00	1.60	326.88
_80	62900.00	2700.00	0.30	209666.67	<mdl	0.23	0.68	528.00	21.00	1.70	310.59
_81	53.50	5.50	0.44	121.59	<mdl	0.20	0.50	520.00	21.00	1.10	472.73
_82	85.00	16.00	0.31	274.19	<mdl	0.16	0.51	458.00	19.00	1.80	254.44
_83	180.00	36.00	0.32	562.50	<mdl	0.22	0.56	565.00	22.00	2.00	282.50
_84	68.90	6.40	0.34	202.65	<mdl	0.22	0.63	529.00	20.00	2.00	264.50
_85	178.00	29.00	0.38	468.42	<mdl	0.21	0.58	537.00	20.00	1.80	298.33
_86	118.60	4.70	0.28	423.57	<mdl	0.19	0.50	506.00	17.00	1.10	460.00

_87	133.00	6.90	0.26	511.54	<mdl	0.24	0.46		546.00	19.00	1.90	287.37
_88	99.20	3.90	0.40	248.00	<mdl	0.22	0.53		545.00	22.00	1.40	389.29
_89	118.30	4.60	0.29	407.93	<mdl	0.22	0.56		549.00	19.00	1.50	366.00
_90	118.30	8.50	0.29	407.93	<mdl	0.23	0.51		540.00	22.00	1.60	337.50
_91	151.00	33.00	0.26	580.77	<mdl	0.18	0.53		549.00	22.00	1.40	392.14
_92	112.70	4.00	0.33	341.52	<mdl	0.19	0.50		546.00	19.00	1.30	420.00
_93	139.00	19.00	0.32	434.38	<mdl	0.23	0.44		540.00	21.00	1.30	415.38
_94	69.30	4.20	0.27	256.67	<mdl	0.19	0.53		537.00	24.00	1.50	358.00
_95	193.00	21.00	0.29	665.52	<mdl	0.17	0.45		558.00	26.00	2.10	265.71
_96	182.00	14.00	0.30	606.67	<mdl	0.20	0.47		531.00	21.00	1.70	312.35
_97	169.00	14.00	0.29	582.76	<mdl	0.22	0.51		551.00	20.00	1.60	344.38
_98	147.00	18.00	0.21	700.00	<mdl	0.21	0.45		545.00	20.00	1.70	320.59
_99	132.00	13.00	0.34	388.24	<mdl	0.18	0.50		520.00	21.00	1.70	305.88
_100	162.00	17.00	0.28	578.57	<mdl	0.20	0.49		526.00	21.00	1.50	350.67
_101	181.00	23.00	0.31	583.87	<mdl	0.19	0.45		544.00	22.00	2.20	247.27
_102	151.00	19.00	0.33	457.58	<mdl	0.19	0.53		538.00	22.00	1.70	316.47
_103	117.00	13.00	0.27	433.33	<mdl	0.19	0.50		523.00	25.00	1.90	275.26
_104	197.00	23.00	0.31	635.48	<mdl	0.19	0.55		517.00	20.00	1.80	287.22
_105	99.20	6.60	0.28	354.29	<mdl	0.23	0.49		588.00	22.00	1.50	392.00
_106	158.00	28.00	0.26	607.69	<mdl	0.19	0.54		537.00	21.00	1.90	282.63
_107	126.00	12.00	0.20	630.00	<mdl	0.17	0.48		533.00	23.00	1.80	296.11
_108	147.00	12.00	0.14	1050.00	<mdl	0.17	0.49		532.00	20.00	1.60	332.50
_109	212.00	17.00	0.28	757.14	<mdl	0.20	0.44		527.00	19.00	1.80	292.78
_110	150.30	8.60	0.26	578.08	<mdl	0.19	0.47		538.00	23.00	1.80	298.89
_111	172.00	13.00	0.34	505.88	<mdl	0.16	0.54		530.00	21.00	1.60	331.25
_112	132.00	9.20	0.23	573.91	<mdl	0.21	0.44		544.00	23.00	1.10	494.55
_113	106.80	6.20	0.39	273.85	<mdl	0.21	0.41		548.00	19.00	2.20	249.09
Grid #10-01	5.65	0.90	0.55	10.27	<mdl	0.25	0.56		443.00	22.00	3.30	134.24
Grid #10-02	2.10	0.41	0.56	3.75	<mdl	0.22	0.57		445.00	14.00	3.40	130.88
Grid #10-03	1.54	0.33	0.62	2.48	<mdl	0.25	0.55		457.00	20.00	2.40	190.42
Grid #10-04	2.17	0.43	0.54	4.02	<mdl	0.21	0.51		422.00	16.00	3.50	120.57
Grid #10-05	1.58	0.33	0.63	2.51	<mdl	0.24	0.60		450.00	18.00	3.40	132.35
Grid #10-06	1.70	0.34	0.70	2.43	<mdl	0.28	0.67		437.00	21.00	2.40	182.08
Grid #13-01	1.62	0.37	0.68	2.38	0.74	0.23	0.51	1.45	407.00	21.00	2.60	156.54
Grid #13-02	1.54	0.37	0.79	1.95	0.79	0.28	0.77	1.03	399.00	15.00	3.30	120.91
Grid #13-03	1.76	0.34	0.69	2.55	0.97	0.26	0.59	1.64	423.00	17.00	3.40	124.41
Grid #13-04	1.64	0.31	0.64	2.56	0.84	0.21	0.50	1.68	405.00	15.00	3.40	119.12
Grid #13-05	1.79	0.38	0.76	2.36	0.95	0.26	0.72	1.32	401.00	20.00	2.80	143.21
Grid #13-06	1.64	0.35	0.67	2.45	0.92	0.25	0.60	1.53	408.00	21.00	3.00	136.00
Grid #14-01	45.00	12.00	1.10	40.91	0.82	0.23	0.67	1.22	628.00	29.00	4.50	139.56
Grid #14-02	10.10	3.20	1.10	9.18	0.89	0.22	0.67	1.33	628.00	27.00	4.50	139.56

Grid #14-03	99.00	24.00	0.77	128.57	1.26	0.27	0.57	2.21	615.00	27.00	3.00	205.00
Grid #14-04	1.54	0.35	0.78	1.97	0.90	0.24	0.65	1.38	740.00	40.00	3.70	200.00
Grid #14-05	276.00	56.00	0.68	405.88	<mdl	0.26	0.65		649.00	23.00	3.40	190.88
Grid #14-06	16.10	4.80	0.76	21.18	0.66	0.26	0.61	1.08	640.00	31.00	4.00	160.00
Grid #18-01	1060.00	240.00	0.86	1232.56	1.13	0.28	0.80	1.41	928.00	33.00	3.60	257.78
Grid #18-02	1210.00	260.00	0.85	1423.53	<mdl	0.24	0.79		914.00	31.00	3.50	261.14
Grid #18-03	650.00	150.00	0.79	822.78	1.40	0.32	0.85	1.65	980.00	35.00	4.50	217.78
Grid #18-04	1450.00	270.00	1.00	1450.00	1.12	0.27	0.68	1.65	900.00	36.00	3.20	281.25
Grid #18-05	1800.00	260.00	0.85	2117.65	0.76	0.23	0.75	1.01	880.00	32.00	2.80	314.29
Grid #18-06	750.00	260.00	0.85	882.35	1.54	0.34	0.71	2.17	955.00	41.00	3.40	280.88
Grid #19-01	1240.00	260.00	0.92	1347.83	0.62	0.20	0.57	1.09	898.00	40.00	4.70	191.06
Grid #19-02	396.00	83.00	0.79	501.27	0.93	0.26	0.65	1.43	942.00	43.00	3.50	269.14
Grid #19-03	1190.00	300.00	0.66	1803.03	0.97	0.27	0.66	1.47	988.00	32.00	4.20	235.24
Grid #19-04	370.00	64.00	0.72	513.89	1.09	0.29	0.66	1.65	776.00	35.00	2.80	277.14
Grid #19-05	1180.00	190.00	0.84	1404.76	1.30	0.30	0.71	1.83	593.00	28.00	2.90	204.48
Grid #19-06	1080.00	200.00	1.00	1080.00	0.80	0.23	0.76	1.05	856.00	41.00	2.90	295.17
Grid #20-01	3900.00	1000.00	0.90	4333.33	<mdl	0.29	0.73		466.00	24.00	4.60	101.30
Grid #20-02	205.00	16.00	1.00	205.00	1.89	0.48	0.85	2.22	678.00	36.00	5.40	125.56
Grid #20-03	510.00	190.00	0.85	600.00	1.40	0.32	0.92	1.52	552.00	26.00	4.50	122.67
Grid #20-04	2990.00	860.00	1.00	2990.00	1.29	0.31	0.74	1.74	538.00	22.00	3.30	163.03
Grid #20-05	1450.00	810.00	0.84	1726.19	1.59	0.37	0.84	1.89	398.00	24.00	3.70	107.57
Grid #20-06	3500.00	1300.00	0.81	4320.99	1.49	0.36	0.80	1.86	505.00	30.00	3.00	168.33
Grid #21-01	1040.00	230.00	0.86	1209.30	1.03	0.29	0.74	1.39	925.00	41.00	3.00	308.33
Grid #21-02	1340.00	350.00	0.83	1614.46	1.35	0.31	0.72	1.88	769.00	37.00	2.90	265.17
Grid #21-03	2470.00	510.00	0.84	2940.48	<mdl	0.30	0.68		800.00	37.00	4.00	200.00
Grid #21-04	2300.00	500.00	0.73	3150.68	0.85	0.29	0.74	1.15	796.00	34.00	4.30	185.12
Grid #21-05	1030.00	320.00	0.71	1450.70	1.15	0.31	0.76	1.51	848.00	40.00	3.60	235.56
Grid #21-06	350.00	100.00	0.77	454.55	0.86	0.26	0.64	1.34	820.00	30.00	3.90	210.26
Grid #22-01	2610.00	470.00	0.85	3070.59	1.00	0.25	0.67	1.49	791.00	43.00	2.90	272.76
Grid #22-02	3060.00	660.00	0.97	3154.64	1.42	0.35	0.72	1.97	763.00	45.00	3.10	246.13

Grid #22-03	233.00	26.00	1.30	179.23	2.12	0.46	0.82	2.59	706.00	37.00	4.90	144.08
Grid #22-04	3550.00	470.00	0.87	4080.46	1.21	0.29	0.68	1.78	749.00	40.00	4.50	166.44
Grid #22-05	1030.00	430.00	0.85	1211.76	1.49	0.34	0.73	2.04	650.00	25.00	4.00	162.50
Grid #22-06	444.00	85.00	0.89	498.88	1.06	0.36	0.86	1.23	879.00	45.00	3.60	244.17
Spot #40	201.00	6.00	0.98	205.10	1.64	0.42	0.84	1.95	173.00	14.00	6.40	27.03
Spot #41	35.50	6.50	0.24	147.92	24.90	1.30	0.20	124.50	236.00	11.00	1.50	157.33
Spot #42	58.80	7.10	0.82	71.71	1.75	0.39	0.79	2.22	191.00	14.00	5.00	38.20
Spot #43	7.74	0.95	0.16	48.38	24.50	1.40	0.29	84.48	192.40	9.00	1.30	148.00
Spot #44	390.00	120.00	0.37	1054.05	7.60	2.00	0.37	20.54	154.00	16.00	2.60	59.23
Spot #45	88.70	6.30	0.33	268.79	<mdl	0.14	0.45		<mdl	0.64	2.40	
Spot #46	65.50	4.00	0.35	187.14	0.70	0.17	0.38	1.84	2.70	1.20	2.00	1.35
Spot #47	59.60	2.90	0.35	170.29	<mdl	0.14	0.44		<mdl	0.68	2.40	
Spot #17	25.70	1.30	0.22	116.82	0.74	0.24	0.59	1.25	302.00	14.00	58.00	5.21
Spot #18	6.46	0.67	0.21	30.76	0.66	0.23	0.56	1.18	202.00	10.00	55.00	3.67
Spot #19	7.31	0.51	0.22	33.23	0.58	0.23	0.54	1.07	241.00	10.00	1.20	200.83
Spot #20	13.48	0.96	0.22	61.27	3.70	1.10	0.55	6.73	279.50	9.80	1.20	232.92
Spot #21	20.60	2.00	0.19	108.42	26.00	7.70	0.63	41.27	293.00	21.00	1.30	225.38
Spot #22	4.68	0.60	0.18	26.00	20.90	2.60	0.61	34.26	107.90	8.00	1.30	83.00
Spot #23	7.06	0.69	0.20	35.30	0.81	0.31	0.53	1.53	96.90	7.50	1.60	60.56
Spot #24	6.34	0.67	0.26	24.38	<mdl	0.24	0.55		103.00	9.30	1.10	93.64
Spot #25	6.05	0.54	0.27	22.41	0.73	0.24	0.57	1.28	70.00	5.50	1.10	63.64
Grid #14	687.00	79.00	0.38	1807.89	<mdl	0.27	0.95		255.00	12.00	3.60	70.83
_1	799.00	81.00	0.53	1507.55	0.61	0.27	0.54	1.13	231.70	9.60	2.00	115.85
_2	830.00	120.00	0.30	2766.67	<mdl	0.24	0.61		245.00	11.00	2.70	90.74
_4	900.00	120.00	0.29	3103.45	<mdl	0.23	0.58		263.00	11.00	2.60	101.15
_5	1800.00	320.00	0.28	6428.57	<mdl	0.22	0.62		256.00	11.00	2.70	94.81
_6	1030.00	150.00	0.20	5150.00	<mdl	0.22	0.65		241.00	11.00	1.80	133.89
Grid #15	1880.00	610.00	0.21	8952.38	<mdl	0.25	0.67		153.60	9.60	1.90	80.84
_7	790.00	240.00	0.20	3950.00	<mdl	0.20	0.67		128.30	8.90	1.90	67.53
_8	640.00	120.00	0.28	2285.71	<mdl	0.21	0.54		142.00	9.10	1.60	88.75
_9	1080.00	300.00	0.24	4500.00	<mdl	0.23	0.60		182.90	8.90	2.10	87.10
_10	1370.00	350.00	0.25	5480.00	<mdl	0.22	0.51		162.00	8.30	2.20	73.64
_11	2360.00	630.00	0.26	9076.92	<mdl	0.19	0.56		194.00	13.00	1.90	102.11
Grid #16	567.00	79.00	0.22	2577.27	<mdl	0.21	0.60		120.70	7.60	1.80	67.06
_12	479.00	52.00	0.22	2177.27	<mdl	0.22	0.59		127.10	8.10	1.80	70.61
_13	305.00	95.00	0.28	1089.29	<mdl	0.19	0.49		211.00	12.00	1.70	124.12
_14	455.00	77.00	0.22	2068.18	<mdl	0.23	0.48		163.30	9.90	1.20	136.08
_15	435.00	77.00	0.24	1812.50	<mdl	0.19	0.66		143.60	9.40	1.70	84.47
_16	483.00	88.00	0.44	1097.73	<mdl	0.22	0.88		154.00	13.00	1.80	85.56
Spot #28	14.40	1.40	0.30	48.00	0.65	0.25	0.61	1.07	279.00	12.00	1.40	199.29
Spot #29	20.20	2.00	0.20	101.00	0.99	0.31	0.63	1.57	213.50	9.80	1.30	164.23
Spot #30	7.82	0.58	0.23	34.00	0.80	0.32	0.70	1.14	210.00	12.00	1.40	150.00
Spot #31	21.60	1.40	0.24	90.00	0.96	0.25	0.44	2.18	285.00	10.00	0.96	296.88
Spot #32	9.16	0.73	0.18	50.89	0.73	0.21	0.50	1.46	234.00	13.00	1.50	156.00
Spot #33	13.70	1.20	0.17	80.59	0.54	0.21	0.46	1.17	254.00	14.00	1.40	181.43
Spot #34	14.00	1.10	0.16	87.50	<mdl	0.22	0.56		258.00	16.00	1.40	184.29
Grid #26	860.00	110.00	0.48	1791.67	<mdl	0.19	0.96		240.00	11.00	2.00	120.00
_17	884.00	97.00	0.19	4652.63	<mdl	0.21	0.55		240.00	10.00	1.50	160.00
_18	990.00	170.00	0.28	3535.71	<mdl	0.19	0.52		241.00	12.00	1.40	172.14

_19	760.00	120.00	0.24	3166.67	<mdl	0.22	0.53		226.00	10.00	1.30	173.85
_20	750.00	100.00	0.21	3571.43	<mdl	0.21	0.58		238.00	12.00	1.60	148.75
_21	920.00	200.00	0.28	3285.71	<mdl	0.20	0.72		228.00	12.00	1.80	126.67
Grid #27	1057.00	84.00	0.28	3775.00	<mdl	0.19	0.71		322.00	15.00	1.80	178.89
_22	943.00	74.00	0.27	3492.59	<mdl	0.22	0.55		309.00	18.00	1.50	206.00
_23	699.00	46.00	0.23	3039.13	<mdl	0.21	0.47		322.00	18.00	1.50	214.67
_24	784.00	47.00	0.20	3920.00	<mdl	0.22	0.48		333.00	17.00	1.80	185.00
_25	563.00	50.00	0.19	2963.16	<mdl	0.19	0.53		308.00	13.00	1.80	171.11
_26	634.00	64.00	0.33	1921.21	<mdl	0.23	0.83		322.00	23.00	2.60	123.85

	Mo				Ag				In			
Analysis #	ppm	2σ std error	LOD	Signal/ Noise	ppm	2σ std error	LOD	Signal/ Noise	ppm	2σ std error	LOD	Signal/ Noise
Spot #4	<mdl	1.00	0.01		1.77	0.29	0.02	104.12	3.76	0.20	0.01	268.57
Spot #5	<mdl	1.00	0.01		5.43	0.45	0.02	285.79	4.24	0.22	0.02	282.67
Spot #6	<mdl	1.00	0.01		2.43	0.19	0.02	162.00	3.99	0.17	0.01	332.50
Spot #7	0.01	0.01	0.01	1.29	258.00	11.00	0.01	21500.00	0.54	0.04	0.01	56.67
Spot #8	0.03	0.02	0.01	3.30	261.00	12.00	0.04	6365.85	0.73	0.05	0.01	66.00
Spot #9	<mdl	0.01	0.09		256.00	10.00	0.01	18285.71	0.38	0.03	0.01	40.00
Spot #10	<mdl	1.00	0.01		251.80	7.10	0.02	11445.45	0.98	0.05	0.01	89.09
Spot #11	<mdl	0.01	0.02		70.80	7.80	0.06	1141.94	4.28	0.19	0.02	251.76
Spot #12	<mdl	1.00	0.01		1.31	0.16	0.02	77.06	4.22	0.20	0.01	383.64
Spot #13	<mdl	1.00	0.02		255.00	11.00	0.01	21250.00	0.26	0.03	0.01	21.75
Grid #4-01	<mdl	1.00	0.06		247.40	9.80	0.04	6185.00	1.00	0.09	0.04	25.67
Grid #4-02	<mdl	1.00	0.06		245.30	9.20	0.04	5982.93	1.08	0.09	0.04	27.74
Grid #4-03	<mdl	0.01	0.04		244.40	8.70	0.04	5683.72	1.10	0.07	0.04	30.50
Grid #4-04	<mdl	0.02	0.04		235.20	8.50	0.05	5113.04	1.02	0.07	0.03	32.77
Grid #4-05	<mdl	1.00	0.05		244.30	9.10	0.02	10621.74	1.02	0.07	0.03	35.24
Grid #4-06	<mdl	0.01	0.02		246.80	9.00	0.03	9140.74	1.05	0.07	0.04	29.28
Grid #5-01	<mdl	1.00	0.04		3.63	0.51	0.04	82.50	4.18	0.21	0.04	99.52
Grid #5-02	<mdl	1.00	0.06		1.80	0.17	0.05	33.33	4.24	0.20	0.04	100.95
Grid #5-03	<mdl	1.00	0.10		7.52	0.70	0.03	300.80	4.69	0.22	0.05	99.79
Grid #5-04	<mdl	1.00	0.04		1.18	0.17	0.03	47.20	4.63	0.24	0.04	107.67
Grid #5-05	<mdl	1.00	0.06		2.56	0.45	0.05	56.89	4.87	0.25	0.05	99.39
Grid #5-06	<mdl	1.00	0.06		2.00	0.33	0.04	51.28	4.67	0.24	0.04	116.75
Grid #6-01	0.11	0.06	0.04	2.75	0.63	0.11	0.05	12.60	4.55	0.34	0.05	98.91
Grid #6-02	<mdl	1.00	0.06		0.67	0.13	0.04	18.61	4.82	0.29	0.04	120.50
Grid #6-03	<mdl	1.00	0.05		0.75	0.12	0.06	13.64	4.29	0.19	0.04	115.95
Grid #6-04	<mdl	1.00	0.05		0.70	0.14	0.04	15.91	4.66	0.25	0.04	116.50
Grid #6-05	<mdl	1.00	0.06		0.86	0.15	0.06	14.83	4.67	0.27	0.05	101.52
Grid #6-06	<mdl	1.00	0.05		0.82	0.13	0.05	16.08	4.97	0.26	0.04	121.22
Grid #7-01	<mdl	1.00	0.05		242.00	8.10	0.03	7333.33	0.75	0.08	0.04	20.32
Grid #7-02	<mdl	1.00	0.04		236.30	7.80	0.04	5907.50	1.00	0.07	0.04	27.00
Grid #7-03	<mdl	1.00	0.06		241.40	7.90	0.03	8046.67	1.27	0.09	0.05	27.61
Grid #7-04	<mdl	1.00	0.04		251.20	8.20	0.05	5233.33	1.34	0.09	0.03	39.44
Grid #7-05	<mdl	1.00	0.05		239.40	8.50	0.06	4127.59	1.23	0.11	0.04	30.00
Grid #7-06	<mdl	1.00	0.05		239.90	5.70	0.05	4798.00	1.27	0.09	0.04	31.63
Spot #8	<mdl	1.00	0.04		225.60	7.80	0.04	5246.51	0.12	0.02	0.04	3.21

Spot #9	<mdl	1.00	0.04		283.00	11.00	0.04	7447.37	0.51	0.05	0.04	14.60
Grid #35	<mdl	1.00	0.02		4.85	0.38	0.04	115.48	4.52	0.20	0.02	282.50
_1	<mdl	1.00	0.01		4.01	0.30	0.04	105.53	4.23	0.16	0.02	282.00
_2	<mdl	1.00	0.05		3.79	0.24	0.04	105.28	4.59	0.20	0.01	353.08
_4	<mdl	1.00	0.02		4.31	0.30	0.02	179.58	4.43	0.18	0.01	340.77
_5	<mdl	1.00	0.02		5.05	0.35	0.02	210.42	4.20	0.21	0.01	323.08
_6	<mdl	1.00	0.05		17.40	2.30	0.02	828.57	4.52	0.19	0.01	322.86
Spot #36	<mdl	0.01	0.02		463.00	19.00	0.02	21045.45	0.65	0.06	0.01	66.43
Spot #37	<mdl	1.00	0.02		472.00	12.00	0.05	9254.90	0.64	0.04	0.01	58.55
Spot #38	<mdl	1.00	0.01		420.00	11.00	0.03	15000.00	0.50	0.04	0.01	41.42
Grid #23-01	<mdl	0.03	0.08		1.16	0.20	0.08	13.81	6.15	0.31	0.06	109.82
Grid #23-02	<mdl	1.00	0.08		2.12	0.25	0.08	26.17	7.01	0.44	0.05	129.81
Grid #23-03	<mdl	0.02	0.06		2.15	0.29	0.07	33.08	6.28	0.36	0.06	101.29
Grid #23-04	<mdl	1.00	0.09		2.13	0.24	0.06	37.37	6.04	0.36	0.06	102.37
Grid #23-05	<mdl	0.02	0.06		1.29	0.18	0.05	25.29	6.10	0.35	0.04	138.64
Grid #23-06	<mdl	0.03	0.06		1.85	0.23	0.07	27.61	5.92	0.33	0.04	134.55
Grid #24-01	<mdl	1.00	0.05		3.04	0.36	0.07	46.06	6.13	0.30	0.05	127.71
Grid #24-02	<mdl	1.00	0.08		3.57	0.48	0.07	48.24	6.46	0.37	0.07	90.99
Grid #24-03	<mdl	1.00	0.06		1.59	0.31	0.09	18.28	5.70	0.30	0.06	101.79
Grid #24-04	<mdl	1.00	0.10		0.17	0.06	0.07	2.46	6.08	0.35	0.08	76.96
Grid #24-05	<mdl	1.00	0.07		0.14	0.06	0.07	2.18	6.02	0.26	0.06	95.56
Grid #24-06	<mdl	1.00	0.07		0.96	0.18	0.06	16.00	5.91	0.31	0.05	111.51
Spot #25	<mdl	1.00	0.03		0.77	0.14	0.04	18.33	5.93	0.26	0.06	100.51
Spot #26	<mdl	1.00	0.04		425.00	16.00	0.05	8673.47	0.33	0.05	0.03	11.45
Grid #27-01	<mdl	0.01	0.07		0.91	0.17	0.07	12.30	5.81	0.26	0.06	103.75
Grid #27-02	<mdl	1.00	0.07		0.63	0.13	0.05	11.67	5.95	0.27	0.05	114.42
Grid #27-03	0.10	0.05	0.07	1.49	1.06	0.17	0.06	17.38	5.57	0.27	0.05	118.51
Grid #27-04	<mdl	0.03	0.07		0.40	0.09	0.07	6.00	5.79	0.25	0.05	107.22
Grid #27-05	<mdl	0.01	0.05		1.20	0.20	0.05	23.08	5.45	0.26	0.04	129.76
Grid #27-06	<mdl	0.03	0.06		0.77	0.15	0.08	9.51	5.79	0.22	0.05	115.80
Grid #48-01	<mdl	1.00	0.08		8.12	0.66	0.04	203.00	3.41	0.25	0.05	69.59
Grid #48-02	<mdl	1.00	0.02		3.80	0.37	0.07	58.46	3.05	0.18	0.04	76.25
Grid #48-03	<mdl	1.00	0.04		5.45	0.38	0.04	126.74	3.11	0.16	0.03	91.47
Grid #48-04	<mdl	0.02	0.05		6.18	0.44	0.06	112.36	3.31	0.16	0.04	76.98
Grid #48-05	<mdl	1.00	0.05		4.77	0.40	0.04	108.41	3.19	0.16	0.03	93.82

Grid #48-06	<mdl	0.01	0.06		4.47	0.37	0.05	87.65	3.30	0.15	0.04	78.57
Grid #49-01	<mdl	0.01	0.08		3.25	0.30	0.07	46.43	3.24	0.17	0.05	72.00
Grid #49-02	<mdl	1.00	0.07		7.70	1.60	0.07	113.24	3.19	0.18	0.04	72.50
Grid #49-03	<mdl	1.00	0.06		3.97	0.32	0.04	96.83	3.36	0.19	0.05	68.57
Grid #49-04	<mdl	1.00	0.10		4.26	0.42	0.04	99.07	3.27	0.17	0.07	48.81
Grid #49-05	<mdl	1.00	0.03		5.71	0.43	0.06	89.22	3.29	0.23	0.05	64.51
Grid #49-06	<mdl	1.00	0.06		4.58	0.40	0.06	76.33	3.19	0.20	0.05	61.35
Grid #50-01	<mdl	1.00	0.05		2.96	0.29	0.05	58.04	3.20	0.15	0.05	68.09
Grid #50-02	<mdl	1.00	0.06		3.17	0.32	0.05	58.70	3.46	0.14	0.05	70.61
Grid #50-03	<mdl	1.00	0.05		2.44	0.20			3.28	0.16	0.05	61.89
Grid #50-04	0.14	0.05	0.06	2.40	5.99	0.38	0.04	136.14	3.29	0.18	0.05	68.54
Grid #50-05	<mdl	0.03	0.08		8.72	0.56	0.06	140.65	3.44	0.17	0.04	80.00
Grid #50-06	2.30	0.37	0.07	31.08	2.27	0.20	0.04	56.75	3.21	0.16	0.05	62.94
Grid #28-01	<mdl	1.00	0.06		5.12	0.52	0.07	76.42	3.39	0.20	0.04	96.86
Grid #28-02	0.17	0.08	0.06	2.80	1.93	0.28	0.07	27.57	3.28	0.23	0.04	91.11
Grid #28-03	<mdl	1.00	0.06		21.40	5.20	0.07	289.19	3.67	0.32	0.05	74.90
Grid #28-04	<mdl	0.02	0.06		3.30	0.46	0.06	57.89	3.73	0.32	0.06	65.44
Grid #28-05	<mdl	1.00	0.09		3.83	0.52	0.07	53.94	3.50	0.32	0.06	63.64
Grid #28-06	<mdl	1.00	0.04		5.57	0.78	0.06	89.84	3.34	0.22	0.05	66.80
Grid #29-01	<mdl	1.00	0.04		1.24	0.16	0.07	17.97	3.16	0.18	0.05	59.62
Grid #29-02	<mdl	1.00	0.04		4.79	0.34	0.07	72.58	3.32	0.18	0.05	65.10
Grid #29-03	<mdl	1.00	0.08		3.91	0.35	0.05	73.77	3.26	0.19	0.05	65.20
Grid #29-04	<mdl	0.03	0.05		1.49	0.22	0.07	20.14	3.20	0.19	0.05	66.67
Grid #29-05	<mdl	0.02	0.05		2.06	0.24	0.04	52.82	3.19	0.16	0.06	50.63
Grid #29-06	<mdl	0.01	0.05		1.74	0.20	0.05	35.51	3.29	0.17	0.06	58.75
Spot #30	<mdl	1.00	0.05		311.00	17.00	0.04	7232.56	0.64	0.08	0.04	18.14
Spot #31	<mdl	1.00	0.07		2.21	0.31	0.04	55.25	2.38	0.24	0.04	59.50
Spot #33	<mdl	1.00	0.08		1.05	0.18	0.04	25.61	2.69	0.20	0.06	44.10
Grid #34-01	<mdl	1.00	0.05		2.96	0.34	0.05	58.04	3.10	0.22	0.05	57.41
Grid #34-02	<mdl	1.00	0.05		2.52	0.28	0.05	49.41	3.06	0.23	0.05	56.67
Grid #34-03	<mdl	1.00	0.09		3.18	0.34	0.06	49.69	3.50	0.23	0.07	50.72

Grid #34-04	<mdl	1.00	0.08		2.81	0.38	0.12	23.42	3.49	0.23	0.06	61.23
Grid #34-05	<mdl	1.00	0.09		2.75	0.33	0.05	50.93	3.44	0.22	0.04	80.00
Grid #34-06	<mdl	1.00	0.07		2.87	0.36	0.08	34.17	3.07	0.20	0.07	41.49
Grid #35-01	<mdl	0.03	0.08		2.79	0.23	0.06	46.50	3.36	0.19	0.06	61.09
Grid #35-02	<mdl	1.00	0.08		2.11	0.23	0.06	34.03	3.34	0.19	0.06	58.60
Grid #35-03	<mdl	1.00	0.04		1.75	0.20	0.06	30.70	3.00	0.17	0.04	68.18
Grid #35-04	<mdl	0.02	0.05		2.01	0.22	0.07	30.45	3.20	0.18	0.06	57.14
Grid #35-05	<mdl	1.00	0.08		4.33	0.33	0.04	108.25	3.25	0.19	0.05	72.22
Grid #35-06	<mdl	1.00	0.07		0.64	0.13	0.06	10.49	3.21	0.15	0.06	50.95
Spot #36	<mdl	1.00	0.05		0.55	0.10	0.04	13.41	2.54	0.18	0.05	56.44
Spot #37	<mdl	1.00	0.08		0.63	0.11	0.04	16.15	2.61	0.14	0.04	74.57
Spot #39	<mdl	0.03	0.09		0.87	0.18	0.05	18.51	2.33	0.17	0.05	44.81
Grid #42	0.06	0.03	0.02	2.68	6.72	0.44	0.03	224.00	3.02	0.15	0.01	328.26
_13	0.08	0.04	0.02	3.30	5.06	0.38	0.03	163.23	3.12	0.18	0.01	328.42
_14	<mdl	0.03	2.60		<mdl	0.29	11.00		2.96	0.19	0.01	227.69
_15	0.03	0.02	0.03	1.04	3.87	0.33	0.02	184.29	3.03	0.15	0.01	303.00
_16	0.37	0.08	0.03	13.29	4.92	0.34	0.02	223.64	3.13	0.16	0.01	284.55
_17	0.05	0.03	0.03	1.93	3.29	0.31	0.04	88.92	3.03	0.17	0.01	233.08
Grid #43	<mdl	1.00	0.02		5.26	0.32			3.00	0.13	0.02	187.50
_18	<mdl	1.00	0.02		6.46	0.99			3.04	0.15	0.02	178.82
_19	<mdl	1.00	0.02		8.43	0.78	0.04	221.84	3.05	0.13	0.02	169.44
_20	<mdl	0.01	0.02		5.17	0.41	0.02	235.00	3.29	0.12	0.01	274.17
_21	<mdl	1.00	0.02		6.58	0.57	0.06	117.50	3.17	0.14	0.02	211.33
_22	0.97	0.23	0.03	35.93	4.11	0.32	0.04	100.24	3.22	0.11	0.01	268.33
Spot #45	<mdl	1.00	0.04		2.47	0.17	0.02	123.50	3.12	0.15	0.01	283.64
Spot #46	<mdl	1.00	0.03		2.95	0.49	0.03	105.36	3.12	0.13	0.02	208.00
Spot #47	<mdl	1.00	0.03		0.87	0.12	0.03	33.46	2.99	0.11	0.01	415.28
Spot #49	<mdl	1.00	0.02		2.28	0.18			3.04	0.12	0.01	253.33
Spot #50	<mdl	1.00	0.02		4.55	0.53			3.15	0.14	0.01	242.31
Line #39	<mdl	1.00			1.11	0.11	0.03	41.11	3.17	0.15	0.02	186.47
_27	<mdl	1.00	0.03		0.92	0.10	0.02	41.64	3.13	0.13	0.01	343.96
_28	0.04	0.03	0.02	1.70	0.81	0.10	0.02	42.63	3.16	0.14	0.01	243.08
_29	0.45	0.12	0.02	28.13	1.05	0.11	0.02	58.33	3.38	0.16	0.01	307.27
_30	0.04	0.02			0.96	0.11	0.02	50.53	3.28	0.18	0.01	298.18
Line #40	<mdl	1.00			0.76	0.08	0.03	26.24	3.19	0.15	0.01	245.38
_31	<mdl	1.00			0.86	0.10	0.03	29.48	3.08	0.17	0.01	236.92
_32	<mdl	1.00			7.20	1.30	0.01	514.29	3.12	0.16	0.01	222.86
_33	<mdl	1.00	0.02		1.87	0.17	0.02	85.00	3.04	0.17	0.01	515.25
Line #41	<mdl	1.00	0.02		0.98	0.10			3.04	0.14	0.01	233.85
_34	<mdl	1.00	0.02		1.16	0.12			3.18	0.15	0.01	244.62
_35	0.07	0.04	0.02	4.56	5.55	0.43	0.02	308.33	2.91	0.14	0.01	207.86
_36	<mdl	1.00			1.65	0.18	0.02	68.75	3.09	0.15	0.01	257.50
_37	<mdl	1.00	0.03		2.15	0.14	0.01	153.57	3.17	0.15	55.00	0.06
Line #44	<mdl	1.00	0.03		274.00	43.00	0.01	21076.92	3.01	0.15	0.01	231.54
_38	<mdl	1.00	0.03		0.99	0.14	0.01	76.15	3.15	0.13	0.01	262.50
_39	<mdl	1.00	0.02		0.93	0.12	0.01	71.54	3.05	0.13	0.01	305.00

_40	<mdl	1.00	0.02		1.25	0.12	0.01	96.15	3.22	0.17	0.01	292.73
_41	<mdl	1.00	0.04		1.31	0.14	0.03	43.67	3.03	0.14	0.01	309.18
Line #48	<mdl	1.00	0.02		7.72	0.97	0.03	285.93	2.89	0.14	0.02	192.67
_42	<mdl	1.00	0.02		2.91	0.24	0.03	93.87	3.26	0.19	0.02	203.75
_43	<mdl	1.00	0.03		73.00	27.00	0.02	3173.91	3.11	0.19	0.01	361.63
_44	<mdl	0.01	0.02		2.27	0.16	0.01	174.62	3.15	0.17	0.01	286.36
_45	<mdl	1.00			3.58	0.26	0.02	238.67	3.06	0.16	0.01	218.57
Line #53	<mdl	1.00	0.03		72.30	4.60	0.02	3615.00	3.01	0.15	0.01	215.00
_46	<mdl	1.00	0.04		105.40	5.50	0.02	5019.05	2.97	0.14	0.02	198.00
_47	<mdl	1.00			103.50	7.00			3.36	0.17	0.02	210.00
_48	0.11	0.04	0.02	4.74	7.46	0.68	0.02	414.44	3.08	0.14	0.01	308.00
_49	0.04	0.03	0.02	1.46	4.34	0.49	0.02	228.42	3.09	0.15	0.01	280.91
Line #54	<mdl	0.01	0.02		1.66	0.15	0.03	50.30	2.99	0.15	0.01	249.17
_50	<mdl	1.00			1.59	0.15	0.02	93.53	3.13	0.16	0.01	240.77
_51	<mdl	1.00	0.04		1.36	0.14	0.03	46.90	2.97	0.17	0.01	212.14
_52	<mdl	1.00	0.03		1.08	0.13	0.03	31.76	3.17	0.18	0.02	198.13
_53	<mdl	1.00	0.02		1.18	0.12	0.04	31.05	2.99	0.16	0.02	199.33
_54	<mdl	1.00	0.04		1.15	0.13			3.12	0.17	0.02	208.00
_55	<mdl	1.00	0.03		1.78	0.18	0.02	80.91	2.99	0.15	0.01	213.57
Line #55	<mdl	1.00	0.03		1.83	0.19	0.03	57.19	3.18	0.14	0.01	481.82
_56	<mdl	1.00	0.03		1.45	0.16	0.03	45.31	3.11	0.18	0.01	471.21
_57	<mdl	1.00			1.25	0.13	0.03	43.10	3.22	0.18	0.02	189.41
_58	<mdl	1.00			10.10	2.00	0.03	336.67	3.20	0.18	0.01	246.15
_59	<mdl	1.00	0.02		1.66	0.17	0.01	118.57	3.15	0.18	0.01	414.47
Line #56	<mdl	1.00	0.03		2.82	0.21	0.02	165.88	3.18	0.15	0.01	227.14
_60	<mdl	1.00	0.03		1.46	0.15	0.02	91.25	3.22	0.17	0.01	247.69
_61	<mdl	1.00	0.03		5.18	0.35	0.02	235.45	3.21	0.15	0.01	321.00
_62	<mdl	1.00	0.06		3.82	0.28	0.02	238.75	3.09	0.16	0.01	237.69
_63	<mdl	1.00	0.03		5.75	0.63			3.18	0.16	0.02	176.67
_64	<mdl	1.00			3.47	0.26	0.02	157.73	3.29	0.13	0.01	299.09
Line #57	0.05	0.04	0.02	2.50	4.14	0.34	0.02	276.00	2.91	0.14	0.02	194.00
_65	<mdl	1.00	0.02		3.09	0.22	0.02	206.00	3.14	0.13	0.01	224.29
_66	0.17	0.07	0.02	9.39	3.12	0.25	0.02	156.00	3.07	0.14	0.01	219.29
_67	0.10	0.04	0.04	2.80	2.23	0.17	0.02	111.50	2.98	0.13	0.01	248.33
_68	0.35	0.09			7.46	0.48			2.97	0.14	0.01	401.35
_69	0.56	0.15	22.00	0.03	6.88	0.69	0.03	245.71	3.03	0.15	0.02	189.38
_70	<mdl	1.00	0.03		3.43	0.30	0.02	228.67	2.98	0.14	0.02	186.25
_71	<mdl	1.00	0.03		2.18	0.19	0.02	145.33	3.10	0.17	0.01	281.82
_72	<mdl	1.00			2.30	0.17			3.07	0.15	0.01	255.83
_73	<mdl	0.01	0.03		2.43	0.25	0.02	121.50	3.04	0.13	0.02	178.82
_74	<mdl	1.00	0.05		2.50	0.18	0.04	58.14	3.14	0.13	0.01	224.29
_75	<mdl	0.02	0.04		2.22	0.19	0.02	96.52	3.24	0.14	0.02	162.00
_76	<mdl	0.01	0.03		2.92	0.27	0.02	121.67	3.06	0.16	0.02	191.25
_77	<mdl	1.00	0.03		2.62	0.21	0.02	119.09	3.10	0.12	0.02	193.75
_78	<mdl	1.00	0.04		1.47	0.16	0.02	98.00	3.17	0.16	0.01	243.85
_79	<mdl	1.00	0.02		1.52	0.15	0.02	66.09	3.19	0.17	0.01	265.83
_80	<mdl	1.00			5.47	0.37	0.03	160.88	4.00	0.17	0.01	493.83
_81	0.07	0.04	0.03	2.48	0.73	0.10	0.03	26.21	3.02	0.14	0.01	215.71
_82	0.27	0.07	0.03	10.15	0.44	0.07	0.02	27.44	3.02	0.15	0.01	232.31
_83	<mdl	1.00	0.04		0.72	0.10	0.02	42.53	3.08	0.13	0.02	205.33
_84	0.66	0.15			3.13	0.22	0.03	111.79	3.14	0.13	0.01	241.54
_85	<mdl	1.00	0.02		1.96	0.16			3.13	0.14	0.01	284.55

_86	<mdl	1.00	0.03		2.24	0.17	0.02	131.76	3.04	0.13	0.01	276.36
_87	<mdl	1.00	0.04		2.00	0.16	0.03	76.92	3.17	0.14	0.01	326.80
_88	<mdl	1.00	0.05		2.07	0.15	0.02	94.09	3.19	0.14	0.01	227.86
_89	<mdl	0.01	0.03		2.34	0.17	0.02	146.25	3.19	0.15	0.01	419.74
_90	<mdl	1.00	0.03		3.53	0.26	0.02	220.63	3.09	0.14	0.02	206.00
_91	<mdl	0.02	0.03		2.60	0.19	0.03	86.67	3.14	0.17	0.01	261.67
_92	<mdl	1.00	0.04		2.12	0.18	0.02	132.50	3.08	0.13	0.01	256.67
_93	<mdl	1.00	0.04		2.57	0.23	0.03	102.80	3.03	0.13	0.01	233.08
_94	<mdl	1.00	0.04		4.05	0.27	0.02	202.50	3.01	0.14	0.01	273.64
_95	0.17	0.30	0.05	3.54	2.82	0.30	0.02	128.18	3.15	0.15	0.01	242.31
_96	<mdl	1.00	0.02		1.99	0.18	0.02	132.67	3.08	0.14	0.01	256.67
_97	<mdl	1.00	0.06		1.87	0.15	0.02	124.67	3.06	0.16	0.02	191.25
_98	<mdl	1.00	0.03		2.59	0.20	0.03	99.62	3.02	0.14	0.02	188.75
_99	<mdl	1.00	0.02		1.65	0.18	0.02	78.57	3.06	0.14	0.01	255.00
_100	<mdl	1.00	0.02		1.65	0.15	0.02	110.00	3.05	0.14	0.01	217.86
_101	<mdl	1.00	0.05		1.84	0.20	0.02	83.64	3.07	0.14	0.01	236.15
_102	<mdl	1.00	0.03		1.69	0.18	0.02	84.50	3.01	0.15	0.01	250.83
_103	<mdl	1.00	0.03		1.84	0.17	0.02	87.62	3.08	0.15	0.01	236.92
_104	<mdl	1.00	0.03		1.35	0.14	0.03	50.00	3.09	0.14	0.01	309.00
_105	0.07	0.04	0.03	2.52	2.55	0.23			3.17	0.13	0.02	176.11
_106	0.01	0.01			1.79	0.16	0.02	85.24	3.09	0.15	0.01	237.69
_107	<mdl	1.00	0.02		2.18	0.21	0.02	90.83	3.07	0.15	0.01	279.09
_108	<mdl	1.00	0.02		1.76	0.16	0.02	73.33	3.01	0.15	0.01	273.64
_109	<mdl	1.00	0.02		1.93	0.17	0.01	137.86	3.14	0.13	0.01	241.54
_110	<mdl	1.00			1.96	0.23	0.02	122.50	3.15	0.13	0.01	242.31
_111	<mdl	1.00	0.02		1.91	0.19	0.03	76.40	3.00	0.13	0.02	176.47
_112	0.20	0.06	0.03	7.50	2.03	0.22	0.03	81.20	3.09	0.15	0.01	220.71
_113	<mdl	1.00	0.05		2.53	0.17	0.02	115.00	3.07	0.14	0.01	255.83
Grid #10-01	<mdl	1.00	0.03		143.00	28.00	0.04	3763.16	0.27	0.03	0.04	7.30
Grid #10-02	<mdl	1.00	0.04		145.00	27.00	0.04	3717.95	0.27	0.04	0.04	7.08
Grid #10-03	<mdl	0.01	0.03		97.00	10.00	0.06	1701.75	0.26	0.04	0.04	6.92
Grid #10-04	<mdl	0.01	0.04		84.40	8.80	0.06	1507.14	0.26	0.03	0.04	6.12
Grid #10-05	<mdl	1.00	0.05		123.00	8.70	0.03	4241.38	0.18	0.03	0.03	5.21
Grid #10-06	<mdl	1.00	0.05		157.00	16.00	0.04	4025.64	0.24	0.04	0.03	6.91
Grid #13-01	<mdl	0.01	0.03		89.00	13.00	0.04	2282.05	0.22	0.03	0.04	6.31
Grid #13-02	<mdl	0.01	0.05		185.00	27.00	0.05	3490.57	0.21	0.03	0.03	6.24
Grid #13-03	<mdl	1.00	0.05		100.00	12.00	0.03	2941.18	0.23	0.04	0.04	5.83
Grid #13-04	<mdl	1.00	0.06		118.00	12.00	0.06	2107.14	0.18	0.03	0.04	4.19
Grid #13-05	<mdl	1.00	0.05		116.00	16.00	0.05	2274.51	0.23	0.03	0.04	5.90
Grid #13-06	<mdl	1.00	0.05		194.00	23.00	0.41	473.17	0.22	0.04	0.05	4.67
Grid #14-01	<mdl	1.00	0.06		51.30	9.70	0.05	1091.49	0.30	0.05	0.05	6.59
Grid #14-02	<mdl	1.00	0.06		600.00	100.00	0.05	12765.96	0.18	0.03	0.05	3.91

Grid #14-03	<mdl	1.00	0.06	163.00	28.00	0.03	5620.69	0.29	0.05	0.04	7.23
Grid #14-04	<mdl	1.00	0.02	129.30	6.40	0.04	3494.59	0.28	0.04	0.05	5.98
Grid #14-05	<mdl	1.00	0.06	130.00	10.00	0.03	3823.53	0.42	0.06	0.05	8.15
Grid #14-06	<mdl	1.00	0.07	76.00	4.60	0.03	2620.69	0.23	0.04	0.04	5.92
Grid #18-01	<mdl	1.00	0.04	0.53	0.10	0.04	12.93	2.64	0.13	0.05	51.76
Grid #18-02	<mdl	1.00	0.04	0.49	0.11	0.04	12.25	2.87	0.16	0.05	57.40
Grid #18-03	<mdl	1.00	0.08	0.50	0.10	0.04	13.16	2.83	0.13	0.05	60.21
Grid #18-04	<mdl	1.00	0.08	0.50	0.10	0.09	5.87	2.82	0.15	0.05	54.23
Grid #18-05	<mdl	1.00	0.08	0.46	0.09	0.04	10.43	2.71	0.13	0.05	58.91
Grid #18-06	<mdl	1.00	0.11	8.80	2.30	0.03	303.45	2.82	0.14	0.05	53.21
Grid #19-01	<mdl	1.00	0.05	0.52	0.10	0.04	14.03	2.63	0.15	0.04	67.44
Grid #19-02	<mdl	1.00	0.08	0.43	0.10	0.08	5.44	2.87	0.14	0.05	54.15
Grid #19-03	<mdl	0.01	0.07	0.53	0.11	0.07	7.26	3.04	0.15	0.05	63.33
Grid #19-04	<mdl	1.00	0.05	0.45	0.10	0.04	10.27	2.82	0.17	0.05	55.29
Grid #19-05	<mdl	1.00	0.06	1.60	0.23	0.05	30.19	2.81	0.16	0.04	75.95
Grid #19-06	<mdl	1.00	0.07	0.72	0.16	0.06	12.63	2.73	0.17	0.04	73.78
Grid #20-01	<mdl	1.00	0.08	8.51	0.48	0.04	197.91	3.84	0.22	0.06	66.21
Grid #20-02	<mdl	1.00	0.09	8.50	0.54	0.05	166.67	4.05	0.26	0.07	60.45
Grid #20-03	<mdl	1.00	0.04	8.55	0.73	0.06	144.92	3.72	0.15	0.06	66.43
Grid #20-04	<mdl	0.03	0.09	9.45	0.74	0.05	185.29	3.59	0.18	0.06	62.98
Grid #20-05	<mdl	1.00	0.07	7.26	0.49	0.17	42.71	3.77	0.20	0.06	66.14
Grid #20-06	<mdl	1.00	0.08	11.90	1.30	0.06	212.50	4.05	0.19	0.06	68.64
Grid #21-01	<mdl	1.00	0.08	0.40	0.08	0.06	6.93	2.85	0.16	0.05	52.78
Grid #21-02	<mdl	1.00	0.08	10.70	2.40	0.06	194.55	2.68	0.14	0.05	51.54
Grid #21-03	<mdl	1.00	0.07	0.46	0.10	0.08	5.61	2.79	0.15	0.05	52.64
Grid #21-04	<mdl	1.00	0.06	1.10	0.15	0.04	26.19	2.43	0.15	0.04	63.95
Grid #21-05	<mdl	1.00	0.06	0.52	0.10	0.05	10.67	2.57	0.15	0.04	59.77
Grid #21-06	<mdl	1.00	0.07	0.43	0.09	0.04	9.98	2.54	0.16	0.05	49.80
Grid #22-01	<mdl	1.00	0.05	4.60	2.40	0.05	97.87	2.97	0.18	0.05	63.19
Grid #22-02	<mdl	1.00	0.07	2.18	0.39	0.05	43.60	3.10	0.20	0.05	67.39

Grid #22-03	<mdl	0.02	0.10		2.63	0.28	0.07	38.12	3.04	0.20	0.06	48.25
Grid #22-04	<mdl	1.00	0.06		2.31	0.90	0.05	44.42	3.02	0.18	0.06	49.51
Grid #22-05	<mdl	1.00	0.08		2.04	0.24	0.06	34.58	2.83	0.18	0.06	45.65
Grid #22-06	<mdl	1.00	0.05		1.35	0.34	0.06	23.28	3.12	0.18	0.06	51.15
Spot #40	<mdl	1.00	0.08		39.60	2.60	0.07	582.35	6.99	0.31	0.08	87.38
Spot #41	<mdl	0.01	0.02		5.60	0.82	0.02	350.00	0.15	0.04	0.02	7.84
Spot #42	0.11	0.05	0.09	1.23	13.23	0.85	0.06	210.00	4.36	0.26	0.05	80.74
Spot #43	0.06	0.03	0.01	6.13	12.20	2.20	0.02	762.50	0.05	0.01	0.02	3.00
Spot #44	0.13	0.08	0.05	2.31	68.10	8.70	0.04	1891.67	0.39	0.16	0.03	13.93
Spot #45	0.56	0.10	0.04	13.02	<mdl	1.00	0.03		<mdl	0.01	0.03	
Spot #46	0.67	0.09	0.05	13.18	<mdl	1.00	0.05		<mdl	0.01	0.03	
Spot #47	1.23	0.15	0.05	27.33	<mdl	1.00	0.05		0.04	0.01	0.03	1.31
Spot #17	<mdl	1.00	0.03		72.40	3.90	0.02	3810.53	3.10	0.14	0.02	182.35
Spot #18	<mdl	1.00	0.03		33.60	1.80	0.02	1866.67	3.74	0.16	0.02	233.75
Spot #19	<mdl	1.00	0.02		109.80	4.20	0.02	6100.00	3.50	0.15	0.02	233.33
Spot #20	<mdl	1.00	0.03		57.70	2.30	0.02	3205.56	3.62	0.16	0.02	241.33
Spot #21	0.71	0.30	0.02	41.76	58.50	4.30	0.02	2437.50	3.96	0.26	0.02	232.94
Spot #22	0.36	0.09	0.02	22.31	21.60	2.00	0.02	939.13	0.65	0.06	0.02	40.38
Spot #23	<mdl	0.01	0.03		17.80	1.40	0.02	936.84	3.24	0.18	0.02	216.00
Spot #24	<mdl	0.02	0.03		8.60	0.65	0.03	330.77	3.30	0.20	0.01	330.00
Spot #25	<mdl	1.00	0.03		7.23	0.46	0.03	278.08	3.03	0.18	0.01	303.00
Grid #14	<mdl	1.00	0.05		45.60	2.70	0.04	1169.23	1.68	0.10	0.01	129.31
_1	<mdl	1.00	0.02		34.30	2.00	0.02	1715.00	1.74	0.08	0.01	173.90
_2	<mdl	1.00	0.04		39.30	2.90	0.02	1871.43	1.77	0.11	0.02	118.00
_4	<mdl	1.00	0.04		49.40	2.90	0.02	2470.00	1.83	0.10	0.02	122.00
_5	<mdl	1.00	0.03		45.80	2.40			1.84	0.10	0.01	230.00
_6	<mdl	1.00	0.04		47.60	3.60	0.02	3173.33	1.87	0.10	0.01	143.92
Grid #15	<mdl	1.00	0.02		17.65	0.94	0.02	882.50	2.60	0.14	0.01	185.71
_7	<mdl	0.01	0.02		4.64	0.39	0.02	232.00	2.52	0.15	0.01	180.00
_8	<mdl	1.00	0.02		12.39	0.78	0.02	652.11	2.19	0.13	0.01	353.23
_9	<mdl	1.00	0.02		38.00	1.90	0.02	2111.11	2.01	0.11	0.01	182.73
_10	<mdl	1.00			22.30	1.10	0.03	825.93	2.02	0.10	0.01	183.64
_11	<mdl	1.00	0.02		15.30	1.00	0.03	546.43	2.02	0.13	0.01	183.64
Grid #16	<mdl	1.00	0.04		7.29	0.46	0.02	331.36	3.03	0.16	0.01	332.97
_12	<mdl	1.00	0.04		3.55	0.27	0.02	161.36	2.78	0.16	0.01	305.49
_13	<mdl	1.00	0.02		14.02	0.90	0.02	584.17	3.62	0.19	0.01	517.14
_14	<mdl	1.00	0.03		5.02	0.32	0.02	228.18	3.51	0.15	0.01	319.09
_15	<mdl	1.00	0.02		8.62	0.57			6.67	0.33	0.01	606.36
_16	<mdl	1.00	0.04		11.10	0.79	0.03	326.47	7.01	0.47	0.03	280.40
Spot #28	<mdl	1.00	0.04		21.70	2.10	0.02	1033.33	2.53	0.13	0.02	168.67
Spot #29	<mdl	1.00	0.02		6.09	0.36	0.01	553.64	1.76	0.10	0.02	117.27
Spot #30	<mdl	1.00	0.02		7.68	0.38	0.01	590.77	2.47	0.13	0.02	145.29
Spot #31	0.39	0.07	0.02	16.74	53.30	5.20	0.02	3135.29	2.93	0.13	0.01	244.17
Spot #32	<mdl	1.00	0.03		43.50	2.10	0.03	1740.00	2.77	0.14	0.01	213.08
Spot #33	<mdl	0.01	0.03		40.60	3.40	0.02	1765.22	2.84	0.16	0.01	236.67
Spot #34	<mdl	1.00	0.02		44.50	2.80	0.03	1780.00	2.55	0.15	0.01	212.50
Grid #26	<mdl	1.00	0.05		66.50	5.10	0.04	1797.30	1.95	0.10	0.03	72.22
_17	<mdl	1.00	0.03		61.70	5.30	0.03	2468.00	1.93	0.10	0.01	160.83
_18	<mdl	1.00			63.90	4.80	0.01	4564.29	1.88	0.11	0.01	237.97

_19	<mdl	1.00	0.05	86.00	8.00	0.02	4777.78	1.93	0.10	0.01	205.32
_20	<mdl	1.00	0.03	66.50	4.70	0.02	3166.67	2.05	0.11	0.01	170.83
_21	<mdl	1.00	0.03	69.10	5.70	0.03	2657.69	1.91	0.10	0.02	119.19
Grid #27	<mdl	1.00	0.03	90.10	5.50	0.03	3604.00	2.01	0.12	0.02	125.63
_22	<mdl	1.00		66.00	5.40	0.02	3473.68	1.95	0.13	0.02	121.88
_23	<mdl	1.00	0.02	65.90	3.90			2.12	0.12	0.01	192.73
_24	<mdl	1.00	0.03	74.40	4.40	0.03	2861.54	1.98	0.11	0.01	165.00
_25	<mdl	1.00	0.02	88.90	5.30	0.02	3704.17	2.39	0.11	0.01	217.27
_26	<mdl	1.00		74.50	5.70	0.03	2483.33	2.12	0.14	0.02	111.58

	Sn				**Sb**				**Te**			
Analysis #	ppm	2σ std error	LOD	Signal/ Noise	ppm	2σ std error	LOD	Signal/ Noise	ppm	2σ std error	LOD	Signal/ Noise
Spot #4	6.00	0.38	0.09	66.67	<mdl	0.03	0.06		7.60	1.90	1.60	4.75
Spot #5	8.38	0.51	0.10	84.65	<mdl	0.03	0.07		1.96	0.71	1.80	1.09
Spot #6	9.62	0.50	0.10	98.16	0.12	0.04	0.06	1.80	3.27	0.91	1.70	1.92
Spot #7	6.86	0.48	0.08	90.26	<mdl	0.02	0.05		20.50	1.40	1.30	15.77
Spot #8	5.65	0.33	0.06	100.89	0.05	0.02	0.05	1.13	20.30	1.50	1.30	15.62
Spot #9	<mdl	0.33	21.00		<mdl	0.02	14.00		16.10	1.40	1.30	12.38
Spot #10	6.85	0.29	0.07	95.14	0.12	0.03	0.05	2.59	19.70	1.40	1.50	13.13
Spot #11	11.72	0.42	0.12	97.67	0.07	0.03	0.06	1.05	4.53	0.94	1.80	2.52
Spot #12	11.45	0.63	0.08	137.95	<mdl	0.03	0.06		2.84	0.77	1.60	1.78
Spot #13	7.12	0.46	0.06	114.84	<mdl	0.03	0.05		19.40	1.40	1.30	14.92
Grid #4-01	6.32	0.38	0.15	42.13	0.22	0.04	0.05	4.35	20.30	2.50	1.90	10.68
Grid #4-02	7.09	0.57	0.15	47.27	0.22	0.04	0.05	4.27	18.40	2.10	2.00	9.20
Grid #4-03	6.85	0.51	0.16	42.81	0.20	0.05	0.05	4.19	20.60	2.30	2.50	8.24
Grid #4-04	6.67	0.53	0.16	41.69	0.20	0.04	0.07	3.04	20.40	2.10	1.80	11.33
Grid #4-05	6.38	0.48	0.17	37.53	0.20	0.04	0.06	3.62	17.30	2.30	2.40	7.21
Grid #4-06	6.66	0.52	0.17	39.18	0.22	0.04	0.06	3.62	19.70	2.00	2.10	9.38
Grid #5-01	12.41	0.75	0.17	73.00	0.16	0.05	0.06	2.66	5.20	1.20	2.70	1.93
Grid #5-02	12.96	0.62	0.24	54.00	0.10	0.03	0.07	1.41	5.10	1.30	3.10	1.65
Grid #5-03	14.85	0.85	0.21	70.71	0.08	0.03	0.07	1.21	6.30	1.50	3.40	1.85
Grid #5-04	14.18	0.76	0.25	56.72	<mdl	0.02	0.09		5.10	1.20	2.90	1.76
Grid #5-05	15.03	0.91	0.28	53.68	<mdl	0.03	0.10		<mdl	1.40	3.40	
Grid #5-06	14.53	0.84	0.25	58.12	0.12	0.04	0.08	1.55	4.90	1.40	3.40	1.44
Grid #6-01	13.72	0.77	0.33	41.58	<mdl	0.03	0.08		5.50	1.20	4.00	1.38
Grid #6-02	13.00	0.71	0.27	48.15	<mdl	0.03	0.07		5.90	1.40	3.30	1.79
Grid #6-03	12.83	0.68	0.26	49.35	<mdl	0.03	0.09		3.40	1.30	3.10	1.10
Grid #6-04	11.72	0.72	0.27	43.41	0.09	0.03	0.09	1.05	<mdl	1.20	3.10	
Grid #6-05	13.70	0.81	0.33	41.52	0.10	0.04	0.06	1.48	5.00	1.70	3.50	1.43
Grid #6-06	16.12	0.91	0.25	64.48	0.19	0.06	0.06	2.98	4.60	1.20	2.80	1.64
Grid #7-01	7.88	0.56	0.21	37.52	0.17	0.04	0.06	2.67	20.20	2.70	2.80	7.21
Grid #7-02	7.40	0.37	0.21	35.24	0.17	0.04	0.06	2.73	19.40	2.50	2.20	8.82
Grid #7-03	7.27	0.58	0.21	34.62	0.37	0.10	0.07	5.36	17.80	2.30	2.50	7.12
Grid #7-04	7.58	0.59	0.22	34.45	0.14	0.04	0.06	2.28	18.60	2.80	2.60	7.15
Grid #7-05	7.20	0.56	0.22	32.73	0.17	0.04	0.07	2.52	19.20	2.80	3.20	6.00
Grid #7-06	7.19	0.63	0.27	26.63	0.25	0.05	0.08	3.25	16.30	2.60	2.60	6.27
Spot #8	1.35	0.23	0.19	7.11	<mdl	0.02	0.06		19.10	2.70	2.70	7.07

Spot #9	5.15	0.50	0.17	30.29	0.07	0.02	0.06	1.29	20.90	2.00	2.50	8.36
Grid #35	15.82	0.70	0.11	143.82	<mdl	0.03	0.06		3.40	1.00	2.30	1.48
_1	16.29	0.68	0.10	162.90	<mdl	0.03	0.06		6.50	1.20	2.10	3.10
_2	15.81	0.71	0.10	158.10	<mdl	0.03	0.06		4.10	1.00	2.30	1.78
_4	15.73	0.88	0.13	121.00	<mdl	0.03	0.07		5.50	1.20	2.10	2.62
_5	13.91	0.61	0.12	115.92	<mdl	0.03	0.07		3.60	1.10	2.10	1.71
_6	14.66	0.68	0.14	104.71	<mdl	0.03	0.07		2.91	0.87	2.40	1.21
Spot #36	8.41	0.65	0.09	97.79	<mdl	0.03	0.05		41.50	3.30	2.00	20.75
Spot #37	10.23	0.71	0.07	148.26	0.09	0.03	0.04	2.28	53.40	3.80	1.60	33.38
Spot #38	9.18	0.70	0.08	111.95	0.10	0.03	0.05	2.08	50.80	3.50	1.60	31.75
Grid #23-01	35.10	1.50	0.28	125.36	0.16	0.05	0.09	1.75	<mdl	2.20	4.10	
Grid #23-02	36.70	1.80	0.28	131.07	0.19	0.05	0.09	2.14	8.50	2.20	4.00	2.13
Grid #23-03	32.90	1.80	0.23	143.04	0.23	0.06	0.13	1.78	20.10	5.10	4.10	4.90
Grid #23-04	33.20	1.60	0.27	122.96	0.25	0.05	0.09	2.88	5.90	1.70	5.40	1.09
Grid #23-05	31.10	1.50	0.26	119.62	0.13	0.04	0.08	1.58	6.30	2.20	4.10	1.54
Grid #23-06	34.00	1.60	0.33	103.03	0.17	0.05	0.08	2.01	10.70	2.40	3.60	2.97
Grid #24-01	34.80	1.40	0.23	151.30	0.27	0.06	0.07	4.00	9.60	1.70	3.10	3.10
Grid #24-02	43.10	2.10	0.31	139.03	0.22	0.06	0.10	2.19	11.00	2.20	4.20	2.62
Grid #24-03	37.10	1.70	0.29	127.93	0.11	0.04	0.10	1.11	42.00	13.00	4.00	10.50
Grid #24-04	36.70	1.80	0.26	141.15	0.10	0.04	0.10	1.02	5.40	1.90	4.00	1.35
Grid #24-05	37.00	1.50	0.28	132.14	<mdl	0.03	0.10		<mdl	1.90	4.50	
Grid #24-06	35.70	1.80	0.35	102.00	<mdl	0.04	0.10		<mdl	1.90	3.70	
Spot #25	36.20	1.40	0.29	124.83	0.10	0.03	0.08	1.25	8.10	2.20	3.80	2.13
Spot #26	15.90	1.20	0.19	83.68	0.05	0.02	0.04	1.31	109.00	15.00	1.80	60.56
Grid #27-01	40.10	1.60	0.27	148.52	0.08	0.03	0.07	1.20	10.70	2.70	3.60	2.97
Grid #27-02	39.50	1.70	0.32	123.44	0.09	0.04	0.07	1.24	4.00	2.40	3.90	1.03
Grid #27-03	39.10	1.60	0.27	144.81	0.11	0.03	0.08	1.29	7.70	2.20	3.20	2.41
Grid #27-04	39.70	1.60	0.26	152.69	0.09	0.03	0.09	1.08	17.90	3.30	3.90	4.59
Grid #27-05	37.60	1.60	0.25	150.40	0.12	0.03	0.08	1.53	17.90	3.30	3.60	4.97
Grid #27-06	38.30	1.60	0.28	136.79	<mdl	0.03	0.08		12.30	2.80	3.70	3.32
Grid #48-01	19.05	0.83	0.28	68.04	0.54	0.08	0.09	6.02	5.20	1.30	3.50	1.49
Grid #48-02	16.74	0.77	0.21	79.71	0.19	0.05	0.05	3.92	6.60	1.40	2.70	2.44
Grid #48-03	16.48	0.82	0.18	91.56	0.26	0.06	0.08	3.40	4.10	1.40	3.10	1.32
Grid #48-04	15.88	0.88	0.23	69.04	0.31	0.06	0.06	5.33	4.00	1.40	3.40	1.18
Grid #48-05	16.74	0.83	0.21	79.71	<mdl	0.04	0.15		17.50	2.80	3.40	5.15
Grid #48-06	17.40	0.80	0.25	69.60	0.09	0.03	0.03	2.68	9.30	2.00	2.40	3.88
Grid #49-01	12.13	0.74	0.28	43.32	0.16	0.05	0.09	1.77	7.30	1.90	3.80	1.92
Grid #49-02	5.72	0.51	0.27	21.19	0.26	0.05	0.09	2.87	6.50	1.80	3.70	1.76
Grid #49-03	10.90	0.61	0.35	31.14	0.24	0.06	0.07	3.58	7.40	1.90	4.70	1.57
Grid #49-04	12.87	0.76	0.28	45.96	0.21	0.06	0.09	2.32	8.20	2.00	4.00	2.05
Grid #49-05	10.02	0.66	0.30	33.40	0.30	0.07	0.12	2.51	7.40	1.70	3.30	2.24
Grid #49-06	12.31	0.83	0.31	39.71	0.26	0.06	0.07	3.61	8.30	2.30	3.40	2.44
Grid #50-01	18.83	0.77	0.26	72.42	0.10	0.03	0.06	1.58	5.00	1.50	3.60	1.39
Grid #50-02	17.56	0.81	0.27	65.04	0.32	0.06	0.07	4.89	8.60	1.70	3.80	2.26
Grid #50-03	18.83	0.75	0.23	81.87	0.12	0.03	0.07	1.57	5.80	1.40	3.00	1.93
Grid #50-04	20.10	0.88	0.25	80.40	0.17	0.04	0.08	2.13	19.50	2.90	2.40	8.13
Grid #50-05	20.31	0.79	0.25	81.24	0.19	0.05	0.07	2.81	24.20	4.80	3.80	6.37
Grid #50-06	17.91	0.81	0.29	61.76	0.17	0.05	0.07	2.31	3.50	1.40	3.20	1.09
Grid #28-01	48.20	3.00	0.30	160.67	0.55	0.08	0.08	7.08	8.50	1.50	2.60	3.27
Grid #28-02	51.40	3.20	0.30	171.33	0.26	0.07	0.08	3.17	7.20	2.00	2.60	2.77
Grid #28-03	57.30	3.30	0.36	159.17	0.53	0.07	0.09	5.65	11.30	2.40	3.50	3.23

Grid #28-04	52.30	3.50	0.30	174.33	0.22	0.06	0.09	2.38	7.80	1.80	3.80	2.05
Grid #28-05	51.40	3.90	0.30	171.33	0.33	0.07	0.10	3.33	<mdl	1.70	92.00	
Grid #28-06	47.50	2.20	0.32	148.44	0.57	0.10	0.08	7.31	5.70	1.80	3.80	1.50
Grid #29-01	42.60	1.70	0.29	146.90	<mdl	0.03	0.10		8.70	2.20	4.00	2.18
Grid #29-02	43.90	2.00	0.28	156.79	0.32	0.06	0.10	3.40	9.80	1.80	3.90	2.51
Grid #29-03	43.10	2.10	0.29	148.62	0.25	0.06	0.08	3.15	10.20	2.00	2.50	4.08
Grid #29-04	44.60	2.10	0.35	127.43	0.22	0.05	0.10	2.24	8.10	2.30	4.10	1.98
Grid #29-05	44.30	1.80	0.33	134.24	0.12	0.04	0.08	1.46	9.50	3.20	3.40	2.79
Grid #29-06	44.00	1.70	0.40	110.00	0.14	0.04	0.08	1.77	9.70	3.80	3.30	2.94
Spot #30	79.00	4.80	0.19	415.79	0.54	0.07	0.06	8.93	154.30	8.10	2.30	67.09
Spot #31	8.98	0.85	0.30	29.93	0.16	0.05	0.08	1.95	7.60	2.00	3.70	2.05
Spot #33	6.73	0.65	0.39	17.26	0.70	0.10	0.09	7.78	5.00	2.00	4.70	1.06
Grid #34-01	43.00	2.40	0.33	130.30	0.21	0.05	0.09	2.38	19.00	3.20	4.00	4.75
Grid #34-02	41.80	2.10	0.32	130.63	0.10	0.04	0.09	1.10	17.90	3.20	4.00	4.48
Grid #34-03	44.60	2.70	0.39	114.36	0.22	0.05	0.12	1.84	22.40	3.80	4.50	4.98
Grid #34-04	46.60	2.50	0.36	129.44	0.20	0.05	0.12	1.70	23.00	4.10	4.30	5.35
Grid #34-05	48.10	2.60	0.38	126.58	0.20	0.06	0.08	2.40	19.70	3.30	3.40	5.79
Grid #34-06	43.80	2.70	0.39	112.31	0.22	0.06	0.10	2.33	23.40	4.30	3.90	6.00
Grid #35-01	44.50	2.10	0.30	148.33	0.11	0.03	0.08	1.43	18.10	3.80	4.10	4.41
Grid #35-02	46.20	1.60	0.31	149.03	0.15	0.04	0.08	1.80	9.50	2.00	4.20	2.26
Grid #35-03	46.10	1.60	0.22	209.55	0.14	0.04	0.05	2.55	<mdl	1.90	3.60	
Grid #35-04	47.30	1.70	0.26	181.92	0.11	0.04	0.09	1.33	9.50	2.30	4.10	2.32
Grid #35-05	46.70	1.50	0.35	133.43	0.25	0.06	0.10	2.62	11.50	1.90	3.10	3.71
Grid #35-06	49.10	2.10	0.36	136.39	<mdl	0.03	0.10		7.10	2.10	3.90	1.82
Spot #36	10.50	0.61	0.24	43.75	0.14	0.04	0.07	2.17	<mdl	1.50	2.90	
Spot #37	11.29	0.56	0.18	62.72	0.15	0.04	0.06	2.33	4.10	1.30	3.10	1.32
Spot #39	7.88	0.73	0.37	21.30	0.19	0.06	0.09	2.02	8.20	2.60	4.00	2.05
Grid #42	54.10	2.20	0.09	594.51	0.33	0.04	0.06	5.53	18.60	2.00	2.20	8.45
_13	54.50	2.20	0.09	586.02	0.27	0.04	0.06	4.37	10.00	1.20	2.30	4.35
_14	53.60	2.40	0.13	412.31	0.16	0.05	0.06	2.73	6.10	1.20	2.40	2.54
_15	52.40	2.00	0.12	436.67	<mdl	0.03	0.05		15.00	2.00	2.10	7.14
_16	53.10	2.00	0.13	408.46	0.11	0.04	0.06	1.95	13.60	2.60	2.30	5.91
_17	54.60	2.00	0.11	496.36	0.15	0.04	0.05	2.85	8.90	1.30	2.20	4.05
Grid #43	42.10	1.30	0.11	382.73	0.22	0.05	0.06	3.64	6.30	1.20	2.20	2.86
_18	42.10	1.70	0.11	382.73	0.54	0.07	0.06	8.68	7.50	1.30	2.30	3.26
_19	41.10	1.30	0.10	415.15	0.42	0.07	0.06	6.93	7.60	1.40	2.60	2.92
_20	44.80	1.30	0.15	298.67	0.18	0.05	0.06	3.08	18.00	2.80	2.50	7.20
_21	45.40	1.50	0.13	349.23	0.17	0.05	0.06	2.76	8.00	1.20	2.10	3.81
_22	42.60	1.30	0.11	387.27	0.28	0.05	0.07	4.01	7.90	1.30	2.50	3.16
Spot #45	40.70	1.30	0.11	370.00	0.07	0.04	0.05	1.28	6.60	1.30	2.50	2.64
Spot #46	42.20	1.40	0.12	351.67	0.07	0.03	0.06	1.10	6.10	1.40	2.30	2.65
Spot #47	41.50	1.40	0.12	345.83	<mdl	0.03	0.06		5.90	1.30	2.40	2.46
Spot #49	40.80	1.40	0.13	313.85	0.11	0.04	0.06	1.79	6.30	1.00	2.30	2.74
Spot #50	39.20	1.30	0.14	280.00	0.12	0.04	0.07	1.88	4.60	1.20	2.40	1.92
Line #39	47.60	1.40	0.20	238.00	0.08	0.02	0.05	1.42	6.00	1.00	2.50	2.40
_27	48.50	1.70	0.14	346.43	0.09	0.02	0.05	1.63	6.70	1.20	1.80	3.72
_28	50.80	2.30	0.13	390.77	0.07	0.02	0.06	1.26	6.20	1.10	2.00	3.10
_29	51.30	2.20	0.14	366.43	0.08	0.02	0.04	2.05	5.50	1.20	2.30	2.39
_30	55.70	2.20	0.14	397.86	0.09	0.02	0.05	1.98	7.00	1.20	2.10	3.33
Line #40	45.80	1.70	0.10	462.63	0.10	0.02	0.05	2.00	5.08	0.95	1.90	2.67
_31	43.30	1.90	0.10	437.37	0.13	0.03	0.05	2.73	4.84	0.89	1.90	2.55
_32	39.10	1.80	0.11	355.45	0.96	0.10	0.05	20.87	6.30	1.30	2.00	3.15

_33	37.70	1.50	9.80	3.85	0.31	0.04	0.04	6.98	6.80	1.50	2.00	3.40
Line #41	47.70	1.90	0.17	280.59	0.10	0.02	0.06	1.68	5.80	1.10	2.20	2.64
_34	50.20	2.10	0.18	278.89	0.11	0.03	0.06	1.84	6.20	1.00	2.30	2.70
_35	49.80	2.00	0.15	332.00	0.40	0.05	0.05	8.06	6.10	1.10	2.50	2.44
_36	49.90	1.70	0.10	499.00	0.12	0.02	0.05	2.52	6.10	1.10	2.20	2.77
_37	49.30	1.60	0.11	448.18	0.13	0.03	0.05	2.58	5.40	1.10	2.50	2.16
Line #44	39.90	1.60	0.14	285.00	0.59	0.07	0.06	10.26	6.26	0.96	2.50	2.50
_38	39.70	1.70	0.13	305.38	0.07	0.02	0.05	1.36	5.70	1.20	2.30	2.48
_39	39.50	1.70	0.13	303.85	0.08	0.02	0.06	1.50	6.30	1.00	2.40	2.63
_40	38.30	1.70	0.14	273.57	0.07	0.02	0.06	1.24	5.60	1.10	2.30	2.43
_41	39.00	1.40	0.14	278.57	0.07	0.02	0.05	1.34	5.80	1.10	2.30	2.52
Line #48	38.10	1.70	0.09	409.68	1.02	0.11	0.05	22.17	7.60	1.70	2.20	3.45
_42	39.90	1.90	0.10	399.00	0.38	0.05	0.05	7.37	11.90	3.20	2.40	4.96
_43	41.60	1.90	0.17	244.71	0.24	0.04	0.05	4.35	8.60	1.40	2.10	4.10
_44	39.60	1.90	0.13	304.62	0.11	0.02	0.06	1.98	6.20	1.20	2.10	2.95
_45	42.30	1.90	0.15	282.00	0.16	0.03	0.06	2.82	7.90	1.50	2.30	3.43
Line #53	43.80	1.70	0.15	292.00	0.55	0.07	0.06	8.70	29.50	4.20	2.20	13.41
_46	47.90	2.10	0.16	299.38	0.59	0.07	0.07	8.48	54.60	6.30	2.40	22.75
_47	56.50	2.70	0.13	434.62	0.96	0.10	0.05	18.02	57.00	5.80	2.40	23.75
_48	37.50	1.50	0.15	250.00	0.28	0.04	0.05	5.63	50.00	14.00	2.00	25.00
_49	40.40	1.70	0.13	310.77	0.17	0.03	0.05	3.46	8.10	1.30	2.30	3.52
Line #54	39.00	1.60	0.12	325.00	0.09	0.02	0.05	1.85	7.80	1.40	3.00	2.60
_50	40.30	1.60	0.18	223.89	0.07	0.02	0.05	1.39	8.90	1.40	3.00	2.97
_51	42.30	1.70	0.14	302.14	0.08	0.02	0.05	1.59	9.30	1.50	3.20	2.91
_52	40.20	1.60	0.15	268.00	0.06	0.02	0.06	1.02	8.70	1.40	2.70	3.22
_53	39.00	1.50	0.15	260.00	0.10	0.02	0.06	1.56	9.20	1.40	2.60	3.54
_54	39.90	1.70	0.13	306.92	0.08	0.02	0.06	1.30	9.30	1.30	2.30	4.04
_55	41.20	1.60	0.14	294.29	0.13	0.03	0.05	2.53	8.20	1.50	2.50	3.28
Line #55	40.20	1.60	0.14	287.14	0.10	0.02	0.05	1.96	8.90	1.50	2.90	3.07
_56	39.90	1.80	0.14	285.00	0.11	0.03	0.05	2.18	7.60	1.30	2.90	2.62
_57	40.40	1.70	0.13	310.77	<mdl	0.02	0.06		6.50	1.30	2.50	2.60
_58	41.60	1.90	0.20	208.00	0.09	0.02	0.07	1.32	13.90	6.70	2.60	5.35
_59	41.40	2.00	0.15	276.00	0.07	0.02	0.05	1.46	6.50	1.30	2.40	2.71
Line #56	44.00	1.40	0.16	275.00	0.08	0.02	0.07	1.12	5.70	1.40	3.00	1.90
_60	44.60	1.60	0.15	297.33	0.11	0.03	0.07	1.51	5.80	1.20	2.90	2.00
_61	43.20	1.50	0.16	270.00	0.37	0.05	0.06	5.83	6.30	1.30	2.60	2.42
_62	43.00	1.50	0.15	286.67	0.41	0.05	0.07	6.00	5.90	1.20	2.80	2.11
_63	43.30	1.70	0.16	270.63	0.67	0.09	0.06	12.13	5.50	1.30	2.70	2.04
_64	42.80	1.90	0.17	251.76	0.35	0.05	0.05	6.54	5.70	1.10	2.00	2.85
Line #57	36.70	1.20	0.15	244.67	0.61	0.07	0.06	9.68	6.70	1.20	2.40	2.79
_65	42.40	1.60	0.15	282.67	0.69	0.08	0.06	11.06	5.50	1.20	2.40	2.29
_66	41.80	1.50	0.13	321.54	0.45	0.06	0.06	7.39	5.90	1.20	2.40	2.46
_67	41.30	1.40	0.13	317.69	0.14	0.03	0.05	3.16	4.30	1.00	2.70	1.59
_68	44.20	1.60	0.17	260.00	0.82	0.09	0.05	16.14	7.90	1.30	2.50	3.16
_69	41.20	1.20	0.15	274.67	0.48	0.06	0.05	9.66	5.70	1.30	2.50	2.28
_70	43.90	1.30	0.16	274.38	0.43	0.06	0.04	9.95	6.10	1.30	2.10	2.90
_71	46.70	1.80	0.16	291.88	0.23	0.03	0.06	4.05	6.00	1.40	2.80	2.14
_72	42.70	1.40	0.17	251.18	0.16	0.03	0.06	2.77	7.20	1.30	2.50	2.88
_73	41.70	1.40	0.17	245.29	0.13	0.03	0.05	2.48	11.60	1.80	2.30	5.04
_74	42.00	1.50	0.14	300.00	0.24	0.04	0.06	4.40	12.90	1.80	3.00	4.30
_75	43.90	1.70	0.18	243.89	0.22	0.04	0.06	3.52	9.70	1.80	2.50	3.88
_76	43.30	1.50	0.18	240.56	0.29	0.04	0.06	4.74	11.90	2.30	2.70	4.41

_77	41.30	1.30	0.14	295.00	0.17	0.04	0.06	2.92	19.50	3.50	2.20	8.86
_78	41.00	1.50	0.16	256.25	0.11	0.03	0.06	1.96	11.20	2.20	2.40	4.67
_79	43.50	1.70	0.22	197.73	0.15	0.03	0.05	2.77	6.10	1.30	2.40	2.54
_80	44.90	1.50	0.17	264.12	0.37	0.05	0.05	7.77	7.40	1.40	2.70	2.74
_81	42.10	1.60	0.16	263.13	<mdl	0.02	0.08		6.40	1.10	2.60	2.46
_82	44.50	1.30	0.15	296.67	0.08	0.02	0.05	1.63	6.80	1.40	2.50	2.72
_83	42.90	1.30	0.14	306.43	0.12	0.03	0.08	1.40	7.30	1.40	2.40	3.04
_84	42.70	1.50	0.20	213.50	0.25	0.04	0.06	4.03	7.20	1.10	2.70	2.67
_85	43.20	1.50	0.15	288.00	<mdl	0.03	21.00		11.60	1.70	2.70	4.30
_86	41.70	1.30	0.20	208.50	0.19	0.03	0.06	3.26	11.80	2.20	2.90	4.07
_87	41.80	1.40	0.14	298.57	0.16	0.03	0.05	2.91	8.90	1.40	2.60	3.42
_88	43.40	1.50	0.16	271.25	0.15	0.03	0.06	2.63	7.60	1.40	2.90	2.62
_89	43.70	1.60	0.17	257.06	0.25	0.04	0.06	4.49	6.70	1.60	2.70	2.48
_90	43.70	1.50	0.14	312.14	0.31	0.05	0.05	6.41	9.30	1.90	2.60	3.58
_91	42.20	1.50	0.17	248.24	0.21	0.04	0.06	3.74	6.20	1.30	2.60	2.38
_92	41.10	1.50	0.16	256.88	0.18	0.04	0.06	3.03	8.30	1.50	2.20	3.77
_93	42.70	1.70	0.15	284.67	0.19	0.04	0.05	4.04	7.10	1.50	2.20	3.23
_94	41.30	1.50	0.15	275.33	0.22	0.04	0.07	3.36	7.60	1.40	2.90	2.62
_95	41.80	1.40	0.17	245.88	0.19	0.04	0.06	3.30	14.60	1.80	2.60	5.62
_96	41.40	1.30	0.15	276.00	0.16	0.04	0.05	3.26	16.80	1.80	2.40	7.00
_97	38.70	1.30	0.16	241.88	0.15	0.03	0.06	2.59	15.10	1.90	2.30	6.57
_98	38.50	1.40	0.13	296.15	0.15	0.03	0.05	3.15	11.60	4.40	2.60	4.46
_99	37.40	1.10	0.13	287.69	0.12	0.03	0.05	2.46	8.40	1.70	2.30	3.65
_100	37.90	1.40	0.21	180.48	0.11	0.03	0.06	1.86	14.60	1.90	3.00	4.87
_101	36.70	1.40	0.16	229.38	0.12	0.03	0.06	2.05	13.90	2.30	2.70	5.15
_102	39.30	1.50	0.13	302.31	0.11	0.03	0.05	2.04	10.40	1.90	2.50	4.16
_103	38.30	1.30	0.14	273.57	0.15	0.03	0.05	3.24	9.00	1.60	2.60	3.46
_104	40.30	1.40	0.17	237.06	0.11	0.03	0.06	1.91	11.60	1.80	2.90	4.00
_105	42.80	1.70	0.19	225.26	0.37	0.06	0.05	7.04	6.10	1.40	2.70	2.26
_106	44.50	1.50	0.15	296.67	0.34	0.04	0.05	6.35	5.60	1.20	2.50	2.24
_107	41.60	1.70	0.15	277.33	0.12	0.03	0.06	1.91	8.50	1.70	2.50	3.40
_108	42.20	1.70	0.14	301.43	0.13	0.03	0.04	3.28	9.80	2.20	2.40	4.08
_109	44.00	1.60	0.15	293.33	0.15	0.03	0.05	2.86	12.50	2.20	2.60	4.81
_110	43.70	1.80	0.18	242.78	0.14	0.03	0.06	2.20	14.80	2.60	2.50	5.92
_111	45.40	1.40	0.14	324.29	0.14	0.03	0.06	2.37	13.80	2.00	2.70	5.11
_112	43.80	1.70	0.14	312.86	0.14	0.03	0.06	2.60	7.60	1.50	3.00	2.53
_113	43.20	1.70	0.15	288.00	0.27	0.04	0.05	5.78	4.80	1.20	2.40	2.00
Grid #10-01	1.76	0.20	0.17	10.35	0.19	0.07	0.05	3.70	139.00	18.00	2.20	63.18
Grid #10-02	2.01	0.24	0.17	11.82	0.17	0.06	0.05	3.25	157.00	21.00	2.20	71.36
Grid #10-03	2.35	0.20	0.20	11.75	0.13	0.04	0.07	2.02	102.00	10.00	2.70	37.78
Grid #10-04	1.91	0.23	0.20	9.55	0.07	0.02	0.06	1.10	87.20	9.70	2.60	33.54
Grid #10-05	1.92	0.20	0.20	9.60	<mdl	0.03	0.07		121.50	9.50	2.50	48.60
Grid #10-06	1.89	0.21	0.23	8.22	0.07	0.02	0.05	1.33	129.00	12.00	2.30	56.09
Grid #13-01	2.46	0.28	0.24	10.25	0.10	0.03	0.05	1.76	93.00	12.00	2.20	42.27
Grid #13-02	2.14	0.22	0.23	9.30	<mdl	0.03	0.08		142.00	19.00	2.60	54.62
Grid #13-03	2.31	0.26	0.21	11.00	0.07	0.02	0.06	1.21	97.00	12.00	2.60	37.31
Grid #13-04	1.76	0.19	0.21	8.38	0.06	0.02	0.05	1.14	125.00	12.00	2.20	56.82
Grid #13-05	1.95	0.24	0.24	8.13	0.07	0.03	0.06	1.09	121.00	17.00	2.80	43.21
Grid #13-06	1.61	0.22	0.18	8.94	0.06	0.02	0.05	1.34	154.00	19.00	2.80	55.00
Grid #14-01	0.66	0.14	0.27	2.44	0.10	0.03	0.06	1.48	54.20	6.60	2.80	19.36
Grid #14-02	0.68	0.15	0.27	2.52	0.10	0.03	0.06	1.50	366.00	73.00	2.80	130.71
Grid #14-03	0.86	0.15	0.25	3.44	0.09	0.03	0.07	1.35	91.00	13.00	2.70	33.70

Grid #14-04	2.09	0.24	0.17	12.29	0.11	0.03	0.08	1.47	146.90	9.10	3.10	47.39
Grid #14-05	1.23	0.16	0.30	4.10	0.08	0.03	0.07	1.19	120.00	11.00	3.40	35.29
Grid #14-06	1.07	0.17	0.21	5.10	0.08	0.03	0.05	1.60	78.40	7.40	2.20	35.64
Grid #18-01	28.40	1.10	0.28	101.43	0.09	0.03	0.07	1.30	<mdl	1.60	3.20	
Grid #18-02	29.00	1.20	0.27	107.41	0.10	0.03	0.07	1.53	<mdl	1.50	3.10	
Grid #18-03	30.20	1.20	0.27	111.85	<mdl	0.03	0.08		<mdl	1.50	3.60	
Grid #18-04	28.90	1.30	0.29	99.66	<mdl	0.03	0.08		<mdl	1.50	3.50	
Grid #18-05	31.50	1.30	0.31	101.61	0.13	0.04	0.06	2.23	3.60	1.40	4.60	0.78
Grid #18-06	31.30	1.10	0.35	89.43	0.39	0.07	0.08	5.12	750.00	160.00	3.50	214.29
Grid #19-01	33.80	1.70	0.31	109.03	0.08	0.03	0.07	1.04	6.30	1.60	2.80	2.25
Grid #19-02	33.40	1.50	0.29	115.17	<mdl	0.03	0.09		6.60	1.70	2.60	2.54
Grid #19-03	33.70	1.60	0.29	116.21	<mdl	0.03	0.08		10.30	2.90	3.50	2.94
Grid #19-04	35.80	1.50	0.24	149.17	0.08	0.03	0.06	1.38	9.40	1.90	3.40	2.76
Grid #19-05	35.10	1.60	0.25	140.40	0.20	0.04	0.06	3.38	4.50	1.40	2.50	1.80
Grid #19-06	32.90	1.40	0.29	113.45	<mdl	0.03	0.10		15.60	4.20	3.10	5.03
Grid #20-01	22.80	1.10	0.32	71.25	0.19	0.05	0.10	1.87	<mdl	1.80	3.80	
Grid #20-02	23.60	1.40	0.37	63.78	0.63	0.10	0.12	5.27	5.00	2.40	4.40	1.14
Grid #20-03	22.20	1.10	0.31	71.61	0.97	0.12	0.10	9.90	6.60	1.70	4.50	1.47
Grid #20-04	20.90	1.10	0.26	80.38	0.26	0.06	0.09	2.81	6.50	1.40	4.10	1.59
Grid #20-05	19.20	1.10	0.31	61.94	0.36	0.07	0.08	4.73	5.60	1.50	4.50	1.24
Grid #20-06	20.50	1.20	0.35	58.57	1.06	0.12	0.09	11.78	10.10	2.30	3.50	2.89
Grid #21-01	30.90	1.50	0.27	114.44	<mdl	0.03	0.07		3.20	1.40	3.40	0.94
Grid #21-02	30.20	1.20	0.26	116.15	0.38	0.06	0.07	5.60	<mdl	1.30	3.30	
Grid #21-03	30.60	1.40	0.29	105.52	<mdl	0.03	0.07		3.60	1.60	3.40	1.06
Grid #21-04	28.20	1.10	0.26	108.46	0.11	0.03	0.07	1.46	9.20	1.90	2.60	3.54
Grid #21-05	28.70	1.40	0.24	119.58	0.13	0.04	0.07	1.76	5.20	1.40	3.50	1.49
Grid #21-06	30.40	1.50	0.25	121.60	<mdl	0.03	0.08		5.90	1.70	3.10	1.90
Grid #22-01	28.90	1.70	0.24	120.42	0.11	0.04	0.06	1.73	3.90	3.20	3.60	1.08
Grid #22-02	29.90	1.70	0.28	106.79	0.21	0.05	0.09	2.39	1.60	2.00	4.20	0.38
Grid #22-03	32.10	1.50	0.35	91.71	0.47	0.09	0.10	4.78	6.30	1.90	3.80	1.66
Grid #22-04	30.20	1.30	0.28	107.86	0.19	0.05	0.09	2.22	7.10	1.80	3.30	2.15
Grid #22-05	28.10	1.50	0.31	90.65	0.52	0.09	0.07	7.19	5.70	1.50	3.90	1.46
Grid #22-06	33.70	1.90	0.40	84.25	0.11	0.04	0.07	1.49	10.20	2.20	3.10	3.29
Spot #40	10.95	0.74	0.39	28.08	0.31	0.07	0.11	2.77	13.70	2.90	5.00	2.74
Spot #41	0.47	0.08	0.10	4.96	0.09	0.02	0.03	3.37	160.20	7.80	1.20	133.50
Spot #42	5.53	0.85	0.32	17.28	0.26	0.06	0.09	2.78	7.40	1.70	3.80	1.95
Spot #43	0.21	0.05	0.10	2.09	0.11	0.02	0.03	3.77	241.00	24.00	1.10	219.09
Spot #44	30.00	14.00	0.18	166.67	0.52	0.22	0.05	10.20	32.60	4.50	5.00	6.52
Spot #45	0.94	0.13	0.17	5.53	0.05	0.02	0.05	1.04	<mdl	0.85	2.20	
Spot #46	1.25	0.16	0.19	6.58	0.09	0.03	0.05	1.81	2.50	1.20	2.20	1.14
Spot #47	1.29	0.15	0.12	10.75	<mdl	0.02	0.05		4.35	0.91	2.40	1.81
Spot #17	16.27	0.57	0.09	174.95	<mdl	0.02	0.07		22.50	2.70	2.40	9.38
Spot #18	16.74	0.66	0.09	190.23	<mdl	0.03	0.07		8.20	1.40	2.30	3.57
Spot #19	19.39	0.68	0.09	220.34	<mdl	0.03	0.06		9.70	1.40	2.30	4.22
Spot #20	14.27	0.57	0.09	158.56	<mdl	0.03	0.06		6.50	1.00	2.40	2.71
Spot #21	14.30	1.10	0.12	119.17	0.07	0.06	0.07	1.03	8.40	1.50	2.90	2.90
Spot #22	0.42	0.08	0.12	3.48	0.19	0.06	0.06	3.03	5.30	1.40	2.70	1.96
Spot #23	18.70	1.00	0.10	188.89	<mdl	0.03	0.07		13.60	1.80	2.10	6.48
Spot #24	17.28	0.96	0.10	172.80	<mdl	0.03	0.08		6.00	1.30	2.20	2.73
Spot #25	14.78	0.72	0.11	134.36	<mdl	0.03	0.08		5.30	1.10	2.30	2.30
Grid #14	32.90	1.30	0.19	173.16	<mdl	0.04	0.09		24.10	2.30	3.30	7.30

_1	32.70	1.10	0.15	218.00	<mdl	0.03	0.07		23.90	2.30	3.10	7.71
_2	32.70	1.40	0.15	218.00	0.08	0.03	0.07	1.22	22.10	2.70	3.00	7.37
_4	32.06	0.96	0.14	229.00	0.12	0.03	0.06	1.97	23.80	2.50	2.90	8.21
_5	30.30	1.20	0.12	252.50	0.13	0.03	0.07	1.86	23.40	2.00	2.70	8.67
_6	30.93	0.99	0.15	206.20	0.13	0.03	0.07	2.05	21.00	2.20	2.60	8.08
Grid #15	23.70	1.00	0.15	158.00	0.12	0.03	0.07	1.78	7.30	1.00	2.30	3.17
_7	52.00	2.20	0.15	346.67	0.10	0.03	0.07	1.49	5.30	1.20	2.30	2.30
_8	31.30	1.40	0.10	326.04	0.10	0.02	0.07	1.49	6.70	1.10	2.30	2.91
_9	16.51	0.65	0.12	137.58	0.10	0.02	0.05	1.81	8.60	1.40	2.40	3.58
_10	16.64	0.71	0.25	66.56	0.09	0.02	0.06	1.60	10.50	1.10	2.50	4.20
_11	18.80	1.00	0.14	134.29	0.11	0.03	0.07	1.62	7.70	1.40	2.60	2.96
Grid #16	35.40	1.50	0.12	295.00	0.10	0.02	0.06	1.48	6.90	1.00	2.40	2.88
_12	25.00	1.10	0.12	208.33	0.11	0.03	0.06	1.67	4.40	1.20	2.40	1.83
_13	6.98	0.36	0.13	53.69	0.09	0.02	0.06	1.49	4.15	0.91	2.40	1.73
_14	12.31	0.60	0.15	82.07	0.07	0.02	0.05	1.27	5.00	1.10	2.50	2.00
_15	27.90	1.40	0.13	214.62	<mdl	0.02	0.06		3.70	1.10	2.10	1.76
_16	36.30	2.10	0.23	157.83	<mdl	0.02	0.10		5.80	1.20	3.90	1.49
Spot #28	13.17	0.56	0.12	109.75	<mdl	0.02	0.06		10.00	1.70	2.50	4.00
Spot #29	5.89	0.38	0.11	53.55	<mdl	0.04	0.07		4.40	1.20	2.50	1.76
Spot #30	11.39	0.58	0.13	87.62	<mdl	0.04	0.08		5.00	1.20	2.80	1.79
Spot #31	16.85	0.70	0.08	210.63	0.11	0.04	0.05	2.23	11.90	1.90	1.80	6.61
Spot #32	12.49	0.66	0.09	134.30	<mdl	0.03	0.06		3.17	0.93	2.10	1.51
Spot #33	13.28	0.55	0.09	156.24	<mdl	0.02	0.05		5.20	1.00	1.90	2.74
Spot #34	12.54	0.65	0.10	125.40	<mdl	0.03	0.05		4.26	0.92	2.10	2.03
Grid #26	34.80	1.30	0.25	139.20	0.11	0.03	0.11	1.04	20.70	2.60	4.20	4.93
_17	35.70	1.50	0.16	223.13	0.10	0.03	0.06	1.75	22.30	2.90	2.70	8.26
_18	35.90	1.50	0.13	276.15	0.11	0.03	0.04	2.87	21.70	2.60	2.70	8.04
_19	34.80	1.50	0.12	290.00	0.12	0.03	0.06	1.92	23.00	3.20	2.50	9.20
_20	35.60	1.30	0.12	296.67	0.11	0.02	0.05	2.15	20.40	2.10	2.50	8.16
_21	36.20	1.50	0.15	241.33	0.10	0.02	0.07	1.37	19.80	2.60	3.00	6.60
Grid #27	36.10	1.40	0.15	240.67	0.15	0.03	0.07	2.12	24.50	2.80	3.00	8.17
_22	37.00	1.90	0.13	284.62	0.15	0.03	0.05	2.98	18.70	2.20	2.40	7.79
_23	34.30	1.40	0.14	245.00	0.13	0.03	0.05	2.36	20.60	2.10	2.40	8.58
_24	33.90	1.50	0.13	260.77	0.16	0.03	0.05	2.87	23.30	2.40	2.00	11.65
_25	30.39	0.99	0.13	233.77	0.14	0.03	0.05	2.84	21.20	2.80	2.40	8.83
_26	32.20	1.40	0.21	153.33	0.14	0.03	0.06	2.49	16.70	2.00	2.70	6.19

	Au				Pb				Bi			
Analysis #	ppm	2σ std error	LOD	Signal/ Noise	ppm	2σ std error	LOD	Signal/ Noise	ppm	2σ std error	LOD	Signal/ Noise
Spot #4	0.08	0.04	0.01	10.00	<mdl	0.06	5.60		<mdl	0.01	50.00	
Spot #5	0.03	0.01	0.01	3.48	<mdl	0.09	6.20		<mdl	0.01	55.00	
Spot #6	0.02	0.01	0.01	2.20	3.95	0.25	0.02	179.55	0.07	0.02	0.02	4.12
Spot #7	<mdl	0.00	0.01		81.90	9.50	0.02	4817.65	402.00	18.00	0.01	30923.08
Spot #8	<mdl	1.00	0.01		89.70	6.70	0.02	5606.25	398.00	20.00	0.02	23411.76
Spot #9	<mdl	0.01	0.04		14.90	1.40	0.01	1619.57	364.00	14.00	0.91	400.00
Spot #10	<mdl	1.00	0.01		176.50	6.50	0.04	4525.64	405.00	11.00	0.04	10384.62
Spot #11	0.60	0.11	0.01	92.31	21.30	2.10	0.02	1065.00	24.90	3.00	0.02	1131.82
Spot #12	0.03	0.01			3.31	0.26	0.02	206.88	0.11	0.02	0.05	2.24

Spot #13	<mdl	0.00	0.01		69.30	2.60	0.02	4331.25	395.00	15.00	0.01	35909.09
Grid #4-01	<mdl	1.00	0.02		34.30	2.60	0.01	2858.33	415.00	18.00	0.02	27666.67
Grid #4-02	<mdl	1.00	0.02		33.30	1.50	0.01	2775.00	413.00	16.00	0.02	27533.33
Grid #4-03	<mdl	0.01	0.02		29.90	2.60	0.02	1495.00	423.00	18.00	0.02	18391.30
Grid #4-04	<mdl	1.00	0.03		34.20	2.00	0.02	2280.00	421.00	15.00	0.03	16192.31
Grid #4-05	<mdl	1.00	0.05		29.40	1.70	0.03	1176.00	418.00	13.00	0.01	29857.14
Grid #4-06	<mdl	1.00	0.03		27.90	1.90	0.03	900.00	421.00	15.00	0.03	16840.00
Grid #5-01	0.04	0.02	0.03	1.16	4.88	0.67	0.02	221.82	5.93	0.82	0.02	247.08
Grid #5-02	0.01	0.01			4.32	0.30	0.04	113.68	0.13	0.03	0.02	6.24
Grid #5-03	<mdl	1.00	0.03		46.50	1.60	0.03	1550.00	0.20	0.05	0.02	10.58
Grid #5-04	<mdl	1.00	0.03		6.50	1.50	0.03	260.00	0.08	0.03	0.04	1.93
Grid #5-05	<mdl	1.00	0.04		7.71	0.40			0.10	0.03	0.03	3.41
Grid #5-06	<mdl	0.01	0.04		17.90	0.96	0.06	319.64	0.21	0.04	0.02	12.41
Grid #6-01	<mdl	1.00	0.03		4.10	1.10	0.03	146.43	0.04	0.02	0.03	1.54
Grid #6-02	<mdl	1.00	0.05		2.78	0.80	0.04	79.43	0.08	0.03	0.03	2.33
Grid #6-03	<mdl	1.00	0.04		4.70	0.29	0.03	142.42	0.08	0.03	0.02	3.67
Grid #6-04	<mdl	1.00	0.04		3.50	0.24	0.02	159.09	0.04	0.02	0.01	3.07
Grid #6-05	<mdl	1.00	0.02		4.65	0.34	0.05	93.00	0.05	0.02	0.02	2.67
Grid #6-06	<mdl	1.00	0.03		6.41	0.40	0.03	200.31	0.14	0.05	0.03	4.15
Grid #7-01	<mdl	1.00	0.03		57.60	3.80	0.01	4114.29	466.00	16.00	0.02	24526.32
Grid #7-02	<mdl	1.00	0.02		43.80	1.60	0.04	1152.63	464.00	14.00	0.02	25777.78
Grid #7-03	0.06	0.03	0.03	2.48	107.00	23.00	0.04	2972.22	476.00	13.00	0.02	25052.63
Grid #7-04	<mdl	1.00	0.02		17.95	0.55	0.03	718.00	455.00	12.00	0.02	19782.61
Grid #7-05	<mdl	1.00	0.02		27.60	1.40	0.02	1150.00	460.00	15.00	0.04	13142.86
Grid #7-06	<mdl	1.00	0.03		21.10	1.00	0.04	479.55	455.00	14.00	0.02	28437.50
Spot #8	0.33	0.34	0.02	22.00	59.60	4.40	0.02	2709.09	443.00	16.00	0.02	23315.79
Spot #9	<mdl	1.00	0.01		46.50	4.10	0.02	2447.37	438.00	15.00	0.02	25764.71
Grid #35	<mdl	0.01	0.02		47.10	2.00	0.01	4281.82	0.19	0.03	0.01	15.83
_1	0.06	0.02	0.02	3.53	42.30	1.80	0.01	4316.33	0.21	0.03	0.01	18.64
_2	0.02	0.01	0.01	1.89	0.53	0.09	0.01	48.09	0.04	0.01	0.01	3.15
_4	<mdl	0.01	0.02		17.40	1.10	0.01	2023.26	0.14	0.03	0.02	9.27
_5	0.06	0.02	0.02	4.20	0.27	0.05	0.01	31.51	0.05	0.02	0.01	3.43
_6	0.13	0.03	0.01	9.14	1.93	0.21	0.01	148.46	0.08	0.02	0.02	4.22
Spot #36	8.80	4.10	0.02	488.89	194.00	50.00	0.01	24250.00	398.00	12.00	0.01	41030.93
Spot #37	0.31	0.04	0.02	20.80	64.70	1.80	0.01	4621.43	391.10	8.60	0.01	39110.00
Spot #38	0.22	0.05	0.01	21.50	63.30	2.00	0.01	6330.00	389.50	9.80	0.01	35409.09
Grid #23-01	0.05	0.03	0.04	1.39	897.00	34.00	0.03	29900.00	1.42	0.14	0.03	47.33
Grid #23-02	0.25	0.07	0.04	7.11	818.00	43.00	0.03	28206.90	2.14	0.16	0.03	73.79
Grid #23-03	0.42	0.13	0.03	13.13	160.00	46.00	0.03	5925.93	2.22	0.18	0.04	61.67
Grid #23-04	0.10	0.04	0.02	4.59	711.00	51.00	0.03	27346.15	2.54	0.19	0.03	97.69
Grid #23-05	0.07	0.04	0.03	2.23	895.00	39.00	0.05	19042.55	1.56	0.13	0.03	45.88
Grid #23-06	0.17	0.06	0.02	7.04	925.00	48.00	0.03	27205.88	2.14	0.17	0.01	164.62
Grid #24-01	0.14	0.05	0.04	3.50	16.90	1.30	0.04	456.76	2.86	0.25	0.02	190.67
Grid #24-02	<mdl	1.00	0.05		14.50	2.00	0.04	362.50	1.84	0.16	0.02	122.67
Grid #24-03	1.50	0.55	0.03	57.69	40.40	6.60	0.04	939.53	1.48	0.13	0.02	61.67

Grid #24-04	<mdl	1.00	0.07		1.34	0.15	0.04	31.90	0.29	0.05	0.03	10.56
Grid #24-05	<mdl	1.00	0.04		1.80	0.35			0.17	0.04	0.03	6.58
Grid #24-06	0.07	0.04	0.04	1.52	239.10	9.90	0.04	6462.16	1.78	0.15		
Spot #25	0.03	0.02			827.00	28.00	0.03	27566.67	0.68	0.09	0.02	31.09
Spot #26	42.30	4.10	0.02	2226.32	4.17	0.27	0.04	112.70	1464.00	47.00	0.01	112615.38
Grid #27-01	0.16	0.07	0.05	3.02	186.20	6.10			0.79	0.11	0.04	18.81
Grid #27-02	0.05	0.03	0.05	1.07	210.40	6.10	0.03	6375.76	0.44	0.06	0.04	12.25
Grid #27-03	0.06	0.03	0.03	1.70	199.40	8.20	0.03	5864.71	1.04	0.12	0.03	34.67
Grid #27-04	0.11	0.06	0.04	2.87	212.30	7.50	0.02	11173.68	0.34	0.06	0.02	19.76
Grid #27-05	0.25	0.08	0.03	7.81	158.70	5.10	0.04	3870.73	0.68	0.08	0.04	19.43
Grid #27-06	0.23	0.08	0.04	6.63	216.50	7.30	0.06	3608.33	0.85	0.08	0.02	44.74
Grid #48-01	0.08	0.04	0.02	3.46	68.60	4.10	0.04	1715.00	0.08	0.03	0.01	6.23
Grid #48-02	0.06	0.03	0.04	1.30	289.70	9.80	0.04	7242.50	0.05	0.02	0.02	2.83
Grid #48-03	<mdl	0.02	0.04		61.40	3.40	0.04	1754.29	0.05	0.02	0.02	3.38
Grid #48-04	<mdl	0.01	0.03		9.46	0.77	0.02	430.00	0.04	0.02	0.01	2.50
Grid #48-05	0.48	0.12	0.03	14.55	382.00	11.00	0.02	17363.64	0.01	0.01		
Grid #48-06	0.20	0.06	0.05	3.70	422.00	15.00	0.04	10047.62	<mdl	0.01	0.02	
Grid #49-01	<mdl	1.00	0.03		208.20	7.20	0.04	5078.05	0.10	0.03	0.03	3.28
Grid #49-02	<mdl	0.01	0.02		144.70	7.50	0.04	3710.26	0.56	0.16	0.03	20.00
Grid #49-03	<mdl	0.01	0.03		395.00	16.00	0.05	8777.78	0.10	0.03	0.03	3.69
Grid #49-04	<mdl	0.02	0.04		204.20	8.10	0.03	6806.67	0.15	0.04	0.02	6.35
Grid #49-05	<mdl	1.00	0.04		145.40	7.70	0.02	7270.00	0.21	0.04	0.02	11.39
Grid #49-06	0.06	0.03	0.02	2.70	400.00	21.00	0.03	14814.81	0.08	0.03	0.02	4.88
Grid #50-01	0.03	0.02			2.13	0.34	0.03	81.92	0.02	0.01	0.02	1.38
Grid #50-02	<mdl	1.00			10.60	1.40	0.03	392.59	0.05	0.02	0.02	3.06
Grid #50-03	0.05	0.03	0.03	1.52	2.64	0.24	0.03	77.65	<mdl	1.00	0.02	
Grid #50-04	0.44	0.10	0.04	11.95	611.00	15.00	0.04	15275.00	<mdl	0.01	0.02	
Grid #50-05	0.46	0.11			709.00	20.00	0.11	6445.45	0.05	0.02	0.02	2.09
Grid #50-06	<mdl	0.01	0.02		13.20	1.60	0.04	330.00	0.03	0.02	0.01	2.08
Grid #28-01	<mdl	1.00	0.03		245.00	24.00	0.03	7903.23	0.89	0.11	0.02	55.63
Grid #28-02	<mdl	1.00	0.03		221.00	16.00	0.03	6906.25	0.34	0.06	0.02	19.71

Grid #28-03	<mdl	1.00	0.06		275.00	22.00	0.04	6547.62	2.57	0.44	0.03	77.88
Grid #28-04	<mdl	1.00	0.04		286.00	18.00	0.05	5836.73	0.26	0.05	0.02	11.77
Grid #28-05	<mdl	1.00	0.04		511.00	48.00	0.02	24333.33	0.48	0.08		
Grid #28-06	<mdl	1.00	0.05		178.00	26.00	0.03	6357.14	0.94	0.14	0.03	28.48
Grid #29-01	<mdl	1.00	0.04		66.00	45.00	0.03	2357.14	0.03	0.02	0.03	1.32
Grid #29-02	<mdl	1.00	0.04		116.30	7.20	0.03	4307.41	0.52	0.07	0.02	21.50
Grid #29-03	<mdl	1.00	0.03		1500.00	540.00	0.04	40540.54	0.43	0.06		
Grid #29-04	<mdl	1.00			27.00	10.00	0.07	375.00	0.17	0.04	0.01	12.00
Grid #29-05	0.24	0.09	0.05	4.63	504.00	25.00	0.05	10500.00	0.22	0.04	0.03	8.76
Grid #29-06	0.10	0.06	0.03	2.82	554.00	37.00	0.03	16294.12	0.19	0.05	0.01	14.85
Spot #30	2.54	0.30	0.02	127.00	102.30	9.10	0.05	2223.91	1246.00	75.00	0.02	83066.67
Spot #31	<mdl	1.00	0.04		2.51	0.34	0.08	32.60	0.07	0.03	0.05	1.51
Spot #33	<mdl	1.00	0.03		52.30	4.20	0.05	1162.22	0.43	0.06	0.03	12.71
Grid #34-01	0.53	0.13	0.04	12.33	418.00	22.00	0.04	11611.11	0.55	0.08	0.03	21.19
Grid #34-02	0.27	0.08	0.04	6.33	401.00	23.00	0.04	11138.89	0.39	0.06	0.03	14.88
Grid #34-03	0.35	0.10	0.04	9.21	409.00	18.00	0.05	8180.00	0.64	0.10	0.03	22.07
Grid #34-04	0.41	0.17	0.08	4.94	481.00	26.00	0.05	9250.00	0.37	0.07	0.03	14.23
Grid #34-05	0.36	0.11	7.30	0.05	402.00	20.00	0.04	10578.95	0.59	0.09	0.03	17.32
Grid #34-06	0.40	0.10	0.04	9.76	502.00	30.00	0.03	14764.71	0.64	0.09	0.02	29.27
Grid #35-01	0.32	0.12	0.05	6.15	375.00	21.00	0.03	11363.64	0.24	0.05	0.02	10.00
Grid #35-02	0.00	0.01	0.05	0.07	325.00	14.00	0.03	9558.82	0.38	0.07	0.03	15.20
Grid #35-03	0.04	0.03	0.04	1.03	219.00	12.00	0.04	6083.33	0.27	0.05	0.01	22.58
Grid #35-04	0.08	0.04	0.02	3.39	335.00	11.00	0.03	10151.52	0.25	0.05	0.02	11.67
Grid #35-05	<mdl	1.00	0.04		290.00	130.00	0.04	7250.00	0.74	0.09		
Grid #35-06	<mdl	1.00	0.05		27.10	3.00	0.02	1231.82	<mdl	0.01	0.03	
Spot #36	<mdl	1.00	0.04		2.41	0.22	0.04	56.05	0.08	0.03	0.02	4.61
Spot #37	<mdl	1.00	0.04		1.23	0.16	0.02	53.48	0.04	0.02	0.01	4.20
Spot #39	0.05	0.03	0.02	2.04	2.30	0.24	0.90	2.56	0.23	0.06	0.05	4.98
Grid #42	0.43	0.07	0.02	22.68	435.00	17.00	0.02	22894.74	0.36	0.04	0.02	22.56
_13	0.08	0.03	0.02	3.85	452.00	36.00	0.02	23789.47	0.30	0.04	0.02	17.76
_14	<mdl	1.00	0.01		471.00	28.00	0.02	20478.26	0.34	0.05	0.02	21.38
_15	0.33	0.07	0.01	35.05	473.00	31.00	0.02	31533.33	0.11	0.02	0.01	11.65
_16	0.38	0.09	0.01	38.00	489.00	36.00	0.02	30562.50	0.20	0.03	0.01	17.73
_17	0.07	0.03	0.01	7.47	460.00	24.00	0.03	16428.57	0.25	0.03	0.01	21.17
Grid #43	<mdl	1.00	0.01		266.00	9.30	0.02	13300.00	0.34	0.04	0.01	24.14
_18	<mdl	1.00	0.01		158.30	7.80	0.02	7915.00	0.90	0.08	0.01	64.00

_19	0.02	0.01	0.01	2.10	320.00	120.00	0.03	12307.69	0.89	0.07	0.01	119.20
_20	0.38	0.10			285.20	9.40	0.02	16776.47	0.30	0.03	0.01	32.64
_21	<mdl	1.00	0.01		315.00	11.00	0.02	18529.41	0.30	0.04	0.01	53.21
_22	<mdl	1.00	0.01		170.00	12.00	0.02	11333.33	0.60	0.05	0.02	37.44
Spot #45	0.05	0.04	0.01	3.77	0.80	0.07	0.01	66.50	0.08	0.02	0.01	5.86
Spot #46	<mdl	1.00	0.02		9.60	2.60	0.01	960.00	0.31	0.09	0.01	28.27
Spot #47	<mdl	1.00	0.01		1.19	0.16	0.01	108.18	0.11	0.02	0.01	12.27
Spot #49	<mdl	1.00	0.02		6.62	0.39	0.02	348.42	0.50	0.05	0.01	41.67
Spot #50	2.69	0.88	0.02	158.24	204.70	6.40	0.02	10235.00	0.66	0.09	0.01	55.17
Line #39	<mdl	1.00			1.70	0.82	0.02	70.83	0.04	0.01	0.01	3.36
_27	<mdl	1.00	0.01		0.61	0.14	0.01	55.45	0.02	0.01	0.01	2.28
_28	<mdl	1.00	0.01		2.49	0.50			0.03	0.01	0.01	2.15
_29	<mdl	1.00	0.01		7.70	1.40	0.01	550.00	0.04	0.01	0.01	7.88
_30	<mdl	1.00			44.00	15.00			0.04	0.02	0.02	2.73
Line #40	<mdl	1.00	0.02		0.89	0.12	0.01	63.57	0.06	0.02	0.01	7.13
_31	<mdl	1.00	0.02		0.62	0.06	0.01	44.00	0.05	0.01	0.01	5.80
_32	10.90	5.10			19.40	2.00	0.01	1616.67	1.27	0.12	0.02	70.56
_33	0.06	0.07	0.01	6.67	4.84	0.62	0.01	605.00	0.42	0.06	0.01	30.14
Line #41	<mdl	1.00	0.01		1.91	0.78			0.04	0.01	0.01	4.16
_34	<mdl	1.00	0.01		1.99	0.49			0.05	0.01	0.01	5.44
_35	<mdl	1.00	0.01		79.80	6.60	0.02	4987.50	1.05	0.08	0.01	118.43
_36	<mdl	1.00	0.02		470.00	27.00	0.01	36153.85	0.12	0.03	0.01	12.84
_37	<mdl	1.00	0.03		481.00	24.00	0.02	20041.67	0.21	0.03	0.01	18.82
Line #44	3770.00	700.00	0.03	134642.86	116.40	7.80	0.02	6847.06	1.68	0.13	0.01	224.00
_38	1.71	0.60	0.03	65.77	9.40	5.60	0.02	626.67	0.02	0.01	0.01	3.39
_39	2.40	0.63	0.01	244.90	1.95	0.22	0.02	121.88	0.02	0.01	0.01	2.53
_40	1.02	0.31	0.01	72.86	12.10	9.60	0.01	1512.50	0.03	0.01	0.01	3.99
_41	0.26	0.09	0.02	13.53	2.66	0.21	0.01	241.82	0.02	0.01	0.01	1.93
Line #48	0.13	0.07	0.01	9.85	20.60	2.10	0.02	1084.21	1.36	0.12	0.01	104.62
_42	0.21	0.08	0.02	13.87	9.37	0.70	0.02	446.19	0.62	0.06	0.01	44.14
_43	650.00	320.00	0.02	38235.29	12.61	0.98	0.02	700.56	0.89	0.08	0.01	98.67
_44	0.13	0.07	0.02	6.89	48.10	7.60	0.02	3206.67	0.10	0.02	0.01	20.60
_45	0.13	0.06	0.02	6.63	350.00	19.00	0.01	36842.11	0.23	0.03	0.02	15.00
Line #53	2.55	0.46			134.00	12.00	0.02	8933.33	151.50	6.90	0.02	8416.67
_46	4.70	0.72			132.00	18.00	0.02	8250.00	197.00	7.20	0.02	9850.00
_47	3.57	0.51	0.02	223.13	284.00	79.00	0.01	20285.71	281.00	22.00	0.01	45322.58
_48	1.79	0.90			235.00	17.00	0.87	270.11	14.90	1.50	0.01	1490.00
_49	0.33	0.10	0.01	33.30	345.00	15.00	0.02	23000.00	9.30	1.30	0.01	1223.68
Line #54	0.03	0.02	0.02	1.24	0.92	0.09	0.01	91.70	0.04	0.01	0.01	2.93
_50	0.05	0.02	0.02	2.94	0.93	0.09	0.02	61.67	0.03	0.01	0.02	1.63
_51	0.02	0.02	0.01	1.85	1.12	0.13	0.02	53.33	0.03	0.01	0.01	4.63
_52	0.04	0.02	0.02	1.80	1.64	0.11	0.01	117.14	0.02	0.01		
_53	0.03	0.02	0.02	1.89	50.00	25.00	0.01	4545.45	0.04	0.02	0.01	4.42
_54	<mdl	0.00	0.01		5.80	1.70	0.03	193.33	0.04	0.01	0.01	2.64
_55	<mdl	1.00	0.02		2.46	0.41	0.02	144.71	0.05	0.01	0.01	5.17
Line #55	<mdl	0.01	0.02		1.15	0.20			0.05	0.02	0.01	5.15
_56	0.03	0.02	0.02	1.33	13.10	3.30			0.03	0.01	0.01	3.51
_57	0.04	0.02	0.01	2.57	0.90	0.10	0.02	56.44	0.03	0.01	0.01	3.48
_58	0.33	0.11	0.01	30.00	128.00	51.00			3.17	0.68	0.01	372.94
_59	<mdl	1.00			1.26	0.22	0.02	70.00	0.06	0.02	0.01	4.07
Line #56	<mdl	1.00			4.75	0.45	0.02	263.89	0.11	0.02	0.01	8.23
_60	<mdl	1.00			4.68	0.61	0.02	275.29	0.05	0.02	0.01	4.50

_61	<mdl	1.00	0.01		39.30	6.90	0.01	2807.14	0.81	0.08	0.01	128.25
_62	<mdl	1.00	0.01		243.00	11.00	0.01	17357.14	0.67	0.06	0.01	51.69
_63	<mdl	1.00	0.01		127.70	8.60	0.02	7511.76	2.08	0.36	0.01	173.33
_64	<mdl	1.00			249.00	11.00	0.02	15562.50	0.58	0.05	0.01	57.90
Line #57	<mdl	1.00			111.50	5.10	0.02	6968.75	0.63	0.06	0.01	52.58
_65	<mdl	1.00			130.20	8.10	0.02	8137.50	0.52	0.05	0.01	47.27
_66	<mdl	1.00	0.02		297.00	19.00	0.01	22846.15	0.46	0.05	0.01	79.82
_67	<mdl	1.00	0.02		288.00	18.00	0.02	19200.00	0.26	0.03		
_68	0.03	0.02	0.02	1.13	101.10	5.90	0.02	5947.06	1.46	0.10	0.01	162.22
_69	0.00	0.01			97.70	7.60	0.01	6978.57	1.27	0.10		
_70	<mdl	1.00	0.01		213.20	9.70	0.02	11844.44	0.91	0.09	0.01	70.31
_71	<mdl	1.00	0.01		373.00	18.00	0.01	28692.31	0.44	0.05	0.01	33.69
_72	0.05	0.02	0.02	2.24	430.00	28.00	0.03	17200.00	0.31	0.03	0.01	38.88
_73	0.19	0.05			347.00	12.00	0.02	14458.33	0.29	0.03	0.01	35.56
_74	0.22	0.05	0.01	18.25	399.00	19.00	0.04	10500.00	0.39	0.04	0.01	59.09
_75	0.14	0.05			430.00	19.00	0.01	30714.29	0.41	0.04	0.01	44.78
_76	0.24	0.10	0.02	10.68	385.00	16.00	0.03	11323.53	0.47	0.05	0.01	69.12
_77	0.54	0.14	0.01	45.00	375.00	17.00	0.16	2343.75	0.33	0.04	0.01	37.70
_78	0.25	0.06	0.02	15.31	414.00	19.00	0.03	16560.00	0.16	0.03	0.01	27.00
_79	<mdl	1.00	0.01		397.00	20.00	0.03	14178.57	0.28	0.03	0.01	20.14
_80	<mdl	1.00	0.01		840.00	260.00	0.02	35000.00	1.54	0.11	0.01	220.00
_81	<mdl	1.00	0.02		3.34	0.70	0.04	85.64	0.06	0.02	0.01	5.09
_82	<mdl	1.00	0.01		6.40	2.70	0.02	304.76	0.03	0.01	0.01	2.21
_83	<mdl	1.00	0.02		7.40	2.20	0.03	255.17	0.12	0.02	0.01	9.23
_84	0.05	0.02			102.80	5.80	0.02	5140.00	1.10	0.08	0.01	120.77
_85	0.19	0.05	0.01	15.67	245.50	8.10	0.01	17535.71	0.27	0.04	0.02	15.76
_86	0.30	0.07	0.01	22.77	279.30	8.90	0.02	15516.67	0.27	0.04	0.01	24.45
_87	0.13	0.04	0.02	5.95	277.80	9.20	0.03	9260.00	0.21	0.04	0.01	34.67
_88	0.01	0.01	0.02	0.71	316.00	11.00	0.03	11703.70	0.30	0.04	0.01	27.36
_89	0.03	0.03	0.01	2.58	306.00	12.00	0.03	11769.23	0.34	0.04	0.01	31.00
_90	0.14	0.07			357.00	21.00	0.02	21000.00	0.51	0.05	0.01	46.36
_91	<mdl	1.00	0.02		348.00	19.00	0.03	10235.29	0.38	0.04	0.01	31.33
_92	0.07	0.04	0.02	4.19	315.00	15.00	0.02	15000.00	0.29	0.04	0.01	20.71
_93	0.04	0.02			287.00	11.00	0.02	15944.44	0.28	0.04	0.01	20.21
_94	<mdl	1.00	0.03		145.20	5.80	0.03	5377.78	0.66	0.07	0.01	60.00
_95	0.30	0.07	0.02	17.59	333.00	12.00	0.02	15136.36	0.38	0.04	0.01	42.11
_96	0.34	0.07	0.02	21.00	271.00	10.00	0.35	774.29	0.47	0.04	0.01	80.00
_97	0.26	0.06	0.02	16.06	259.80	8.30	0.02	10825.00	0.35	0.04	0.01	34.90
_98	0.19	0.09	0.01	17.45	320.00	17.00	0.03	12307.69	0.31	0.04	0.01	23.77
_99	0.10	0.06	0.01	9.45	313.00	21.00	0.02	14904.76	0.23	0.03	0.01	17.46
_100	0.23	0.06	0.01	21.27	303.00	14.00	0.01	23307.69	0.22	0.03	0.01	18.25
_101	0.21	0.05	0.03	8.15	268.00	14.00	0.03	10307.69	0.24	0.03	0.02	13.88
_102	0.15	0.04	0.02	9.93	302.00	16.00	0.02	16777.78	0.18	0.03	0.01	13.62
_103	0.05	0.02	0.01	4.45	254.00	16.00	0.02	12095.24	0.36	0.04	0.01	36.00
_104	0.18	0.05	0.02	10.59	360.00	18.00	0.03	11250.00	0.24	0.04	0.01	39.03
_105	<mdl	1.00			445.00	24.00	0.02	29666.67	0.44	0.06	0.01	46.49
_106	0.01	0.01			387.00	22.00	0.03	12900.00	0.29	0.03	0.01	49.66
_107	0.17	0.06			376.00	14.00	0.04	9400.00	0.27	0.04	0.01	27.53
_108	0.14	0.05	0.01	12.73	318.00	11.00	0.02	13826.09	0.25	0.03	0.01	25.98
_109	0.19	0.05	0.01	17.36	328.00	14.00	0.02	14260.87	0.28	0.04	0.01	23.58
_110	0.38	0.12			317.00	13.00	0.03	12680.00	0.37	0.04	0.01	41.80
_111	0.28	0.08	0.01	25.73	349.00	21.00	0.04	9971.43	0.29	0.04	0.01	48.98

_112	0.13	0.04	0.03	4.89	450.00	32.00	0.03	18000.00	0.24	0.04	0.02	15.25
_113	0.05	0.02	0.03	1.88	388.00	19.00	0.03	11757.58	0.44	0.05	0.01	69.84
Grid #10-01	<mdl	1.00	0.02		1450.00	280.00	0.17	8529.41	114.00	3.70		
Grid #10-02	<mdl	1.00	0.02		368.00	55.00	0.17	2164.71	119.30	2.80		
Grid #10-03	<mdl	1.00	0.03		2250.00	300.00	0.04	60810.81	127.30	3.70	0.02	7488.24
Grid #10-04	<mdl	1.00	0.02		554.00	92.00	0.06	8935.48	116.20	3.60	0.03	4303.70
Grid #10-05	<mdl	1.00			1660.00	140.00	0.11	15090.91	118.60	3.60	0.02	7412.50
Grid #10-06	<mdl	1.00	0.02		207.00	22.00	0.05	3905.66	121.50	3.60	0.03	4860.00
Grid #13-01	<mdl	1.00	0.04		1430.00	440.00	0.03	52962.96	128.10	4.30	0.02	7535.29
Grid #13-02	<mdl	1.00	0.05		362.00	73.00	0.03	11312.50	124.70	3.60	0.03	4796.15
Grid #13-03	<mdl	1.00	0.04		490.00	200.00	0.03	14848.48	126.30	3.30	0.02	6647.37
Grid #13-04	<mdl	1.00	0.04		47.90	5.60	0.04	1228.21	125.30	3.70	0.03	4640.74
Grid #13-05	<mdl	1.00	0.03		187.00	39.00	0.03	7480.00	121.40	3.60	0.02	6389.47
Grid #13-06	<mdl	1.00	0.02		610.00	130.00	0.20	3050.00	120.10	3.80	0.01	13054.35
Grid #14-01	<mdl	1.00	0.03		434.00	27.00	0.02	28933.33	112.20	4.80	0.02	5905.26
Grid #14-02	0.03	0.02	0.03	1.19	373.00	46.00	0.02	24866.67	116.70	3.70	0.02	6142.11
Grid #14-03	<mdl	1.00	0.04		482.00	27.00	0.06	8169.49	124.00	4.20	0.01	13333.33
Grid #14-04	0.09	0.04	0.04	2.57	1890.00	190.00	0.03	57272.73	131.40	5.00	0.02	8212.50
Grid #14-05	<mdl	1.00	0.04		764.00	57.00	0.03	26344.83	123.80	5.00	0.02	5895.24
Grid #14-06	<mdl	1.00	0.02		510.00	47.00	0.03	15937.50	122.80	6.20	0.09	1444.71
Grid #18-01	<mdl	1.00	0.05		19.20	2.40	0.03	662.07	2.34	0.28		
Grid #18-02	<mdl	1.00	0.05		22.20	1.70	0.03	792.86	2.37	0.70		
Grid #18-03	<mdl	1.00	0.02		23.70	2.50	0.03	877.78	3.53	0.83	0.02	207.65
Grid #18-04	<mdl	1.00	0.04		28.20	2.00	0.03	1044.44	2.69	0.23	0.02	128.10
Grid #18-05	<mdl	1.00	0.02		13.50	1.30	0.04	306.82	1.86	0.17	0.10	19.38
Grid #18-06	0.12	0.07	0.05	2.30	28.30	4.40	0.04	808.57	970.00	280.00	0.02	53888.89
Grid #19-01	<mdl	1.00	0.02		8.29	0.54	0.03	243.82	4.90	1.00	0.02	257.89
Grid #19-02	<mdl	1.00	0.03		19.30	1.80	0.02	1072.22	3.11	0.66	0.03	124.40
Grid #19-03	<mdl	1.00	0.04		19.50	1.20	0.03	672.41	9.50	2.90	0.02	431.82
Grid #19-04	<mdl	1.00	0.03		8.47	0.62	0.02	470.56	3.90	1.50	0.02	243.75
Grid #19-05	<mdl	1.00			14.50	2.80	0.03	537.04	6.10	0.41	0.03	196.77

Grid #19-06	<mdl	1.00	0.04		19.80	1.20	0.04	550.00	15.90	4.90		
Grid #20-01	<mdl	1.00	0.04		1.15	0.14	0.02	52.27	1.21	0.12	0.02	50.42
Grid #20-02	<mdl	1.00	0.05		6.06	0.80	0.03	242.40	4.86	0.36	0.03	173.57
Grid #20-03	<mdl	1.00	0.06		42.00	14.00	0.05	913.04	5.11	0.52	0.01	393.08
Grid #20-04	<mdl	1.00	0.03		375.00	52.00	0.04	9146.34	1.53	0.14	0.03	54.64
Grid #20-05	<mdl	1.00	0.03		6.90	1.60	0.03	215.63	4.06	0.29	0.02	203.00
Grid #20-06	<mdl	1.00	0.06		610.00	270.00	0.03	21785.71	13.20	3.20	0.02	733.33
Grid #21-01	<mdl	1.00	0.04		6.26	0.43	0.04	145.58	2.22	0.31	0.03	74.00
Grid #21-02	<mdl	0.01	0.04		20.30	1.20	0.04	495.12	24.30	1.30	0.03	837.93
Grid #21-03	<mdl	1.00	0.04		7.90	0.46	0.02	415.79	1.83	0.16	0.02	87.14
Grid #21-04	<mdl	1.00	0.04		8.45	0.63	0.04	192.05	6.05	0.56	0.03	201.67
Grid #21-05	<mdl	1.00	0.02		5.68	0.35	0.04	135.24	4.10	0.27	0.01	372.73
Grid #21-06	<mdl	1.00	0.02		5.73	0.30	0.04	163.71	3.24	0.30	0.03	129.60
Grid #22-01	0.05	0.04	0.04	1.13	6.40	2.70	0.03	220.69	3.80	1.10	0.03	135.71
Grid #22-02	<mdl	1.00	0.04		5.64	0.70	0.05	125.33	2.94	0.35	0.03	101.38
Grid #22-03	<mdl	1.00	0.04		11.50	3.70	0.02	522.73	9.93	0.59	0.03	320.32
Grid #22-04	0.03	0.03	0.02	1.23	4.50	1.20	0.03	173.08	2.45	0.86	0.02	144.12
Grid #22-05	<mdl	1.00	0.03		5.11	0.41	0.02	268.95	7.03	0.46	0.01	585.83
Grid #22-06	<mdl	0.01	0.03		5.04	0.70			1.08	0.15	0.03	41.54
Spot #40	0.53	0.15	0.05	10.60	14.90	1.40	0.04	354.76	25.40	1.10		
Spot #41	0.25	0.03	0.01	21.00	80.00	6.20	0.01	8000.00	73.40	3.40		
Spot #42	0.06	0.03	0.04	1.53	23.40	3.00	0.05	520.00	19.90	1.00	0.03	621.88
Spot #43	0.55	0.09	0.01	42.23	1100.00	260.00	0.01	120879.12	469.00	61.00	0.01	80862.07
Spot #44	1.43	0.27	0.03	47.67	107.00	19.00	0.02	5350.00	127.00	20.00	0.01	9769.23
Spot #45	<mdl	1.00	0.02		<mdl	1.00	0.03		<mdl	1.00	0.02	
Spot #46	<mdl	1.00	0.03		0.60	0.17	0.03	24.00	<mdl	0.01	0.01	
Spot #47	<mdl	1.00	0.03		0.16	0.04	0.03	5.82	<mdl	1.00	0.01	
Spot #17	0.07	0.02	0.02	3.94	69.00	2.40	0.03	2555.56	5.07	0.17	0.02	241.43
Spot #18	<mdl	1.00	0.02		28.10	1.30	0.03	1124.00	2.58	0.11	0.02	129.00
Spot #19	0.03	0.02	0.01	3.94	86.80	3.70	0.02	5105.88	1.63	0.09	0.02	90.78
Spot #20	<mdl	1.00	0.01		109.50	3.70	0.02	6441.18	4.03	0.18	0.02	212.11
Spot #21	0.76	0.37	0.01	54.29	98.90	5.10	0.21	470.95	13.40	2.30	0.02	705.26
Spot #22	<mdl	0.01	0.01		1.47	0.19	0.21	7.00	14.80	1.60	0.02	822.22
Spot #23	<mdl	1.00	0.01		7.62	0.46	0.02	476.25	1.40	0.11	0.02	73.68
Spot #24	<mdl	1.00	0.01		3.16	0.22	0.01	405.13	1.09	0.10	0.02	57.37
Spot #25	<mdl	1.00	0.01		4.43	0.28	0.01	553.75	0.67	0.06	0.02	35.26
Grid #14_1	0.37	0.06			7.81	0.39	0.02	433.89	7.74	0.75	0.02	322.50
	0.21	0.04	0.03	7.61	4.34	0.23	0.01	333.85	8.57	0.36	0.01	714.17

_2	0.18	0.04			6.92	0.31	0.02	329.52	9.84	0.36	0.01	984.00
_4	0.42	0.07			11.00	0.53	0.02	550.00	8.74	0.61	0.01	891.84
_5	0.34	0.06	0.02	18.94	21.64	0.87	0.02	983.64	6.91	0.29	0.01	493.57
_6	0.25	0.05	0.02	16.93	18.20	0.62	0.02	1137.50	11.52	0.56	0.01	1047.27
Grid #15	<mdl	0.01	0.02		0.20	0.04	0.01	16.42	0.71	0.07	0.02	41.59
_7	<mdl	1.00	0.02		0.07	0.02	0.01	5.75	0.40	0.05	0.02	23.76
_8	0.01	0.01			0.26	0.05	0.01	30.96	0.49	0.05	0.01	35.21
_9	0.07	0.02	0.01	6.97	0.54	0.06	0.01	65.61	0.67	0.06	0.01	91.51
_10	0.02	0.01	0.01	1.50	0.39	0.06	0.01	32.83	0.56	0.05	0.01	105.66
_11	<mdl	1.00	0.01		0.75	0.08	0.02	37.40	0.97	0.12	0.01	119.75
Grid #16	<mdl	1.00	0.02		0.10	0.02	0.01	6.86	0.35	0.04	0.02	18.63
_12	<mdl	1.00	0.02		0.09	0.02	0.01	6.69	0.29	0.04	0.02	16.11
_13	<mdl	1.00			0.35	0.05			1.04	0.09	0.01	122.24
_14	<mdl	1.00	0.02		0.22	0.03	0.01	20.27	0.62	0.06	0.01	56.09
_15	<mdl	1.00	0.01		0.11	0.03	0.01	13.78	0.27	0.04	0.01	27.30
_16	0.00	0.00			0.16	0.03	0.02	7.71	0.36	0.05	0.01	25.64
Spot #28	<mdl	1.00	0.01		30.10	3.70	0.02	1505.00	1.34	0.10	0.02	83.75
Spot #29	<mdl	1.00	0.02		11.70	0.53	0.02	731.25	8.04	0.39	0.02	536.00
Spot #30	<mdl	1.00	0.02		9.24	0.49	0.02	513.33	2.38	0.14	0.02	140.00
Spot #31	0.13	0.04	0.01	15.90	58.80	2.10	0.01	5880.00	13.00	3.10	0.01	1083.33
Spot #32	<mdl	1.00			24.24	0.98	0.01	2203.64	7.52	0.52	0.02	470.00
Spot #33	0.01	0.01			45.70	2.30	0.01	4570.00	4.32	0.30	0.01	308.57
Spot #34	0.06	0.02	0.01	5.17	22.00	1.10	0.01	1692.31	1.80	0.14	0.02	120.00
Grid #26	0.14	0.03			8.79	0.44	0.02	382.17	20.00	1.40	0.02	1333.33
_17	0.14	0.04			2.18	0.13	0.01	167.69	20.30	1.20	0.02	1353.33
_18	0.22	0.04			2.05	0.14	0.01	170.83	16.20	1.10	0.01	2050.63
_19	0.20	0.03	0.02	11.59	5.93	0.38	0.02	370.63	18.50	1.60	0.01	2078.65
_20	0.19	0.04	0.01	14.54	6.03	0.32	0.01	548.18	21.20	1.60	0.01	1630.77
_21	0.26	0.05	0.02	13.53	1.93	0.13			18.90	1.50	0.02	1111.76
Grid #27	0.35	0.05	0.02	18.37	14.89	0.70			22.00	1.20	0.02	1294.12
_22	0.26	0.05	0.01	25.60	15.72	0.70	0.01	1310.00	16.15	0.89	0.01	1345.83
_23	0.18	0.04			48.00	1.90	0.01	5647.06	16.63	0.80	0.01	1187.86
_24	0.23	0.04	0.01	22.60	67.10	2.40			19.00	0.83	0.01	2065.22
_25	0.19	0.04	0.02	12.33	81.40	2.70			22.30	1.10	0.01	2858.97
_26	0.16	0.04			70.30	3.40	0.03	2703.85	22.20	1.30	0.01	1850.00

References

Arif, J. & Baker, T., 2004. Gold Paragenesis and chemistry at Batu Hijau, Indonesia: implications for gold-rich porphyry copper deposits. *Mineralium Deposita,* Volume 39, pp. 523-535.

Audétat, A., Günther, D. & Heinrich, C. A., 1998. Formation of a magmatic-hydrothermal ore deposit: Insights with LA-ICP-MS analysis of fluid inclusions. *Science,* Volume 279, pp. 2091-2094.

Aurenhammer, F., 1991. Voronoi diagrams- a survey of fundamental geometric data structure. *ACM Computing Surveys,* Volume 23, pp. 345-405.

Baline, L. M., 2007. *Hydrothermal fluids and Cu-Au mineralization of the Deep Grasberg porphyry deposit, Papua, Indonesia,* Austin, TX: University of Texas at Austin. Master's thesis.

Boyle, R. W., 1979. *Geological Survey Bulletin 280: The geochemistry of gold and its deposits.* 1 ed. Ottawa, CA: Geological Survey of Canada: Energy, Mines, and Resources Canada.

Carew, M. J., Mark, G., Oliver, N. H. S. & Pearson, N., 2006. Trace element geochemistry of magnetite and pyrite in Fe-oxide (±Cu-Au) mineralised systems: Insights into the geochemistry of ore-forming fluids. *Geochimica et Cosmochimica Acta,* Volume 70, p. A83.

Carlson, W. D., 1991. Competetive diffusion-controlled growth of porphyroblasts. *Mineralogical Magazine,* Volume 55, pp. 317-339.

Carlson, W. D. & Denison, C., 1992. Mechanisms of porphyroblast crystallization: results from High-Resolution Computed X-ray Tomography. *Science,* Volume 257, pp. 1236-1239.

Cline, J. S., 2001. Timing of gold and arsenic sulfide mineral deposition at the Getchell Carlin-Type gold deposit, north-central Nevada. *Economic Geology,* Volume 96, pp. 75-89.

Cloos, M., 2001. Bubbling magma chambers, cupolas, and porphyry copper deposits. *International Geology Review,* 43(4), pp. 285-311.

Cloos, M. et al., 2005. Collisional delamination in New Guinea: The geotectonics of subducting slab breakoff. *Geological Society of America, Special Paper,* Volume 400, pp. 1-50.

Cooke, D. R., Hollings, P. & Walshe, J. L., 2005. Giant porphyry deposits: characteristics, distribution, and tectonic controls. *Economic Geology,* Volume 100, pp. 801-818.

Cook, N. J. & Chryssoulis, S. L., 1990. Concentrations of "invisible gold" in the common sulfides. *Journal of the Mineralogical Association of Canada,* Volume 28, pp. 1-16.

Cook, N. J., Ciobanu, C. L., Danyushevsky, L. V. & Gilbert, S., 2011. Minor and trace elements in bornite and associated Cu-(Fe)-sulfides: A LA-ICP-MS study. *Geochimica et Cosmochimica Acta,* Volume 75, pp. 6473-6496.

Cook, N. J. et al., 2016. Trace element analysis of minerals in magmatic-hydrothermal ores by Laser Ablation Inductively-Coupled-Plasma Mass Spectrometry: approaches and opportunities. *Minerals,* Volume 6, pp. 1-34.

Danyushevsky, L. et al., 2011. Routine quantitative multi-elements analysis of sulphide minerals by laser ablation ICP-MS: Standard development and consideration of matrix effects. *Geochemistry: Exploration, Environment, Analysis,* Volume 11, pp. 51-60.

Deditius, A. P. et al., 2011. Trace metal nanoparticles in pyrite. *Ore Geology Reviews,* Volume 42, pp. 32-46.

Dozy, J. J., 1939. Geological results of the Carstensz expedition, 1936. *Leidsche Geologische Mededelingen,* Volume 11, pp. 68-131.

Einaudi, M. T. & Burt, D. M., 1982. A special issue devoted to skarn deposits: Introduction- terminalogy, classification, and composition of skarn deposits. *Economic Geology,* Volume 77, pp. 745-754.

FCX, 2015. *Annual Report,* Phoenix, AZ: Freeport McMoRan Copper & Gold Inc.

FEI, 2016. *Amira-Avizo.* Hillsboro(Oregon): FEI Visualization Sciences Group.

Fraley, K. J. & Frank, M. R., 2014. Gold solubilities in bornite, intermediate solid solution, and pyrrhotite at 500° to 700° and 100 MPa. Volume 109, pp. 407-418.

Frank, M. R. et al., 2011. Gold and copper partitioning in magmatic hydrothermal systems at 800°C and 100 MPa. *Geochimica et Cosmochimica Acta,* Volume 75, pp. 2470-2482.

Gibbins, S. L., 2006. *The magmatic and hydrothermal evolution of the Ertsberg intrusion in the Gunung Bijih (Ertsberg) mining district, West Papua, Indonesia,* Tucson, AZ: University of Arizona.PhD dissertation.

Graham, D. J. & Midgley, N. G., 2000. Graphical representations of particle shape using triangular diagrams; an excel spreadsheet method. *Earth Surface Processes and Landforms,* Volume 25, pp. 1473-1477.

Guillong, M. et al., 2005. Preliminary characterization of new glass reference materials (GSA-1G, GSC-1G, GSD-1G, and GSE-1G) by Laser Ablation-Inductively Coupled

Plasma-Mass Spetrometry using 193 nm, 213 nm, and 266 nm wavelengths. *Geostandards and Geoanalytical Research,* Volume 29, pp. 315-331.

Günther, D., Audétat, A., Frischknecht, R. & and Heinrich, C. A., 1998. Quantitative analysis of major, minor, and trace elements in fluid inclusions using laser ablation-inductively coupled plasma-mass spectrometry (LA-ICP-MS). *Journal of Analytical Atomic Spectroscopy,* Volume 13, pp. 263-270.

Halter, W. E., Heinrich, C. A. & Pettke, T., 2005. Magma evolution and the formation of porphyry Cu-Au ore fluids: evidence from silicate and sulfide melt inclusions. *Mineralium Deposita,* Volume 39, pp. 845-863.

Heinrich, C. A. et al., 2003. Quantitative multi-element analysis of minerals, fluid and melt inclusions by laser-ablation inductively-coupled-plasma mass-spectrometry. *Geochimica et Cosmochimica Acta,* Volume 67, pp. 3473-3496.

Jochum, K. P. et al., 2005. Chemical characterisation of the USGS reference glasses GSA-1G, GSC-1G, GSD-1G, GSE-1G, BCR-2G, BHVO-2G, and BIR-1G using EMPA, ID-TIMS, ID-ICP-MS, LA-ICP-MS. *Geostandards and Geoanalytical Research,* Volume 29, pp. 285-302.

John, D. A. et al., 2010. *Porphyry Copper Deposit Model chap. B of Mineral deposit models for resource assessment,* Reston, VA: U.S. Geological Survey Scientific Investigations Report 2010-5070-B.

Johnson, K. M., Hammarstrom, J. M., Zientek, M. L. & Dicken, C. L., 2014. *Global mineral resource assessment: estimate of undiscovered copper resources of the world, 2013,* Reston, VA: U.S. Geological Survery.

Kesler, S. E., 2004. Gold in sulphide minerals and ore deposits. *The Gangue: G.A.C.-Mineral Deposits Division,* Volume 83, pp. 3-8.

Kesler, S. E., Chryssoulis, S. L. & Simon, G., 2002. Gold in porphyry copper deposits: its abundance and fate. Volume 21, pp. 103-124.

Ketcham, R. A., 2005. Computational methods for quantitative analysis of three-dimensional features in geological specimens. *Geosphere,* Volume 1, pp. 32-41.

Ketcham, R. A. & Carlson, W. D., 2001. Acquisition, optimization and interpretation of X-ray computed tomographic imagery: applications to the geosciences. *Computational Geoscience,* Volume 27, pp. 381-400.

Kyle, J., 2017. *Personal Communication.* Austin, TX: s.n.

Kyle, J. H., Breuer, P. L., Bunney, K. G. & Pleysier, R., 2012. Review of trace toxic elements (PB, Cd, Hg, As, Sb, Bi, Se, Te) and their deportment in gold processing: Part II: Deportment in gold ore processing by cyanidation. *Hydrometallurgy,* Volume 111-112, pp. 10-21.

Kyle, J. H. et al., 2011. Review of trace toxic elements (Pb, Cd, Hg, As, Sb, Bi, Se, Te) and their deportment in gold processing. Part I: Mineralogy, acqueous chemistry and toxicity. *Hydrometallurgy,* Volume 107, pp. 91-100.

Kyle, J. R. & Ketcham, R. A., 2003. In-situ distribution of gold in ores using high resolution X-ray computed tomography. *Economic Geology,* Volume 98, pp. 1697-1701.

Kyle, J. R. & Ketcham, R. A., 2015. Application of high resolution X-ray computed tomography to mineral deposit origin, evaluation, and processing. *Ore Geology Reviews,* Volume 65, pp. 821-839.

Kyle, J. R., Mote, A. S. & Ketcham, R. A., 2008. High resolution X-ray computed tomography studies of Grasberg porphyry Cu-Au ores, Papua, Indonesia. *Mineralium Deposita,* Volume 43, pp. 519-532.

Ledvina, M. D., 2017. *Fluid inclusion constraints on the hydrothermal processes responsible for Cu-Au mineralization in the Ertsberg-East Skarn System, Papua, Indonesia,* Austin, TX: University of Texas at Austin. Master's thesis.

Leys, C. A., Cloos, M., New, B. T. E. & MacDonald, G. D., 2012. Copper-Gold ± Molybdenum Deposits of The Ertsberg-Grasberg District, Papua, Indonesia. *Society of Economic Geologists Special Publication,* Volume 16, pp. 215-235.

Lindgren, P. et al., 2015. The paradox between low shock-stage and evidence for compaction in CM carbonaceous chondrites explained by multiple low-intensity impacts. *Geochimica et Cosmochimica Acta,* Volume 148, pp. 159-178.

MacDonald, G. D. & Arnold, L. C., 1994. Geological and geochemical zoning of the Grasberg Igneous Complex, Irian Jaya, Indonesia. *Journal of Geochemical Exploration,* Volume 50, pp. 143-178.

Max Planck Institute, n.d. *Geologic and Environmental Reference Materials.* [Online] Available at: http://georem.mpch-mainz.gwdg.de/sample_query.asp

McDowell, F. W., McMahon, T. P., Warren, P. Q. & Cloos, M., 1996. Pliocene Cu-Au bearing igneous intrusions of the Gunung Bijih (Ertsberg) District, Irian Jaya, Indonesia: K-Ar Geochronology. *Journal of Geology,* Volume 104, pp. 327-340.

McMahon, T., 1994b. Pliocene intrusions in the Gunung Bijih (Ertsberg) mining district, Irian Jaya, Indonesia: petrography and mineral chemistry. *International Geology Review,* Volume 36, pp. 820-849.

McMahon, T. P., 1994a. *Pliocene intrusions in the Ertsberg (Gunung Bijih) mining district, Irian Jaya, Indonesia: Petrography, geochemistry, and tectonic setting,* Austin, TX: University of Texas at Austin. PhD dissertation.

McMahon, T. P., 1999. The Ertsberg intrusion and the Grasberg complex: Contrasting styles of magmatic evolution and Cu-Au mineralization in the Gunung Bijih (Ertsberg) mining district, Irian Jaya, Indonesia. *Buletin Geologi,* Volume 31, pp. 123-132.

Meinert, L. D., 1992. Skarns and skarn deposits. *Geoscience Canada,* Volume 19, pp. 145-162.

Meinert, L. D., Dipple, G. M. & Nicolescu, S., 2005. World skarn deposits. *Economic Geology,* Volume 100, p. 299.

Mertig, H. J., Rubin, J. N. & Kyle, J. R., 1994. Skarn Cu-Au orebodies of the Gunung Bijih (Ertsberg) Districy, Irian Jaya, Indonesia. *Journal of Geochemical Exploration,* Volume 50, pp. 179-202.

Mote, A. S., 2004. *A kinematic investigation in the Cripple Creek District, central Colorado: Implications regarding the structural controls influencing the location and distribution of gold ore zones,* Austin, TX: University of Texas at Austin. Master's thesis.

Mote, A. S. et al., 2005. *High resolution X-ray computed tomography investigations of high-grade gold ore zones in the Cripple Creek District, Colorado.* Reno, Nevada, Proceedings of the Geological Society of Nevada Symposium: Window to the World, pp. 1169-1175.

Norman, M., Robinson, P. & Clark, D., 2003. Major- and trace-element analysis of sulfide ores by Laser-Ablation ICP-MS, Solution ICP-MS, and XRF: new data on international reference materials. *The Canadian Mineralogist,* Volume 41, pp. 293-305.

Ostwald, W., 1896. *Lehrbuch der Allgemeinen Chemie.* 2 ed. Leipzig, Germany: V. von Wilhem Engelmann.

Paton, C. et al., 2011. Iolite: Freeware for the visualization and processing of mass spectrometric data. *Journal of Analytical Atomic Spectrometry,* Volume 26, pp. 2508-2518.

Prendergast, K., Clarke, G. W., Pearson, N. J. & Harris, K., 2005. Genesis of pyrite-Au-As-Zn-Bi-Te zones associated with Cu-Au Skarns: evidence from the Big Gossan and Wanagon Gold deposits, Ertsberg District, Papua, Indonesia. *Economic Geology,* Volume 100, pp. 1021-1050.

Quarles van Ufford, A. I., 1996. *Stratigraphy, structural geology, and tectonics of a young foreare-continent collision, western Central Range, Irian Jaya (western new Guinea), Indonesia,* Austin, TX: University of Texas at Austin. PhD dissertation.

Quarles van Ufford, A. I. & Cloos, M., 2005. Cenozoic tectonics of New Guinea. *AAPG Bulletin,* Volume 89, pp. 119-140.

Rasband, W. S., 1997-2016. *ImageJ.* Bethesda(MD): NIH.

Rees, C. E., 1978. Sulfur isotope measurements using SO2 and SF6. *Geochimica et Cosmochimica Acta,* Volume 42, pp. 383-389.

Reich, M. et al., 2005. Solubility of gold in arsenian pyrite. *Geochimica et Cosmochimica Acta,* Volume 69, pp. 2781-2796.

Reich, M., Palacios, C., Barra, F. & Chryssoulis, S., 2013. "Invisible" silver in chalcopyrite and bornite from the Mantos Blancos Cu deposit, northern Chile. *European Journal of Mineralogy,* Volume 25, pp. 453-460.

Reich, M. et al., 2006. Thermal behavior of metal nanoparticles in geologic materials. *Geology,* Volume 34, pp. 1033-1036.

Reyes, F. et al., 2017. Calibrated X-ray micro-tomography for mineral ore quantification. *Minerals Engineering,* Volume 110, pp. 122-130.

Robert, F., Poulsen, K. H. & Dubé, B., 1997. *Gold deposits and their geological classification.* Toronto, Ontario, CN, Prospectors and Developers Association of Canada, pp. 209-220.

Rubin, J. N., 1996. *Skarn formation and ore deposition at the Gunung Bijih Timur (Ertsberg East) complex, Irian Jaya, Indonesia,* Austin, TX: University of Texas at Austin. PhD dissertation.

Rubin, J. N. & Kyle, J. R., 1997. Precious metal mineralogy in porphyry-, skarn-, and replacement-type ore deposits of the Ertsberg (Gunung Bijih) District, Irian Jaya, Indonesia. *Economic Geology,* Volume 92, pp. 535-550.

Sapiie, B. & Cloos, M., 2004. Strike-slip faulting in the core of the Central Range of west New Guinea: Ertsberg Mining District, Indonesia. *GSA Bulletin,* Volume 116, pp. 277-293.

Sillitoe, R. H., 2010. Porphyry copper systems. *Economic Geology,* Volume 105, pp. 3-41.

Simon, G., Kesler, S. E. & Essene, E. J., 2000. Gold in porphyry copper deposits: experimental determination of the distribution of gold in the Cu-Fe-S system at 400° to 700° C. *Economic Geology,* Volume 95, pp. 259-270.

Sneed, E. D. & Folk, R. L., 1958. Pebbles in the Lower Colorado River, Texas a study in particle morphogenesis. *Journal of Geology,* Volume 66, pp. 114-150.

Stefanova, V., Volkov, A. V., Serafimovski, T. & Sidorov, A. A., 2015. Native gold of the Borovik Ore Field, Republic of Macedonia (FYROM). *Geology of Ore Deposits,* Volume 57, pp. 133-137.

Sylvester, P. J. C. L. J. et al., 2005. Synthesis and evaluation of a fused pyrrhotite standard reference material for platinum group element and gold analysis by laser ablation-ICPMS. *10th International Platinum Symposium: Oulu, Geological Survey of Finland, Extended Abstracts,* Volume 10, pp. 16-20.

Tomkins, A. G. & Mavrogenes, J. A., 2001. Redistribution of gold within Arsenopyrite and Lollingite during pro-and retrograde metamorphism: Application to timing of mineralization. *Economic Geology,* Volume 96, pp. 525-534.

UTCT, 2016a. *About CT: Acquisition of CT Data.* [Online]
Available at: http://www.ctlab.geo.utexas.edu/about-ct/acquisition-of-ct-data/
[Accessed 3 5 2017].

UTCT, 2016b. *About CT: Artifacts and Partial Volume Effects.* [Online]
Available at: http://www.ctlab.geo.utexas.edu/about-ct/artifacts-and-partial-volume-effects/
[Accessed 26 6 2017].

Van Nort, S. D. et al., 1991. Geology and mineralization of the Grasberg porphyry copper-gold deposit, Irian Jaya, Indonesia. *Mining Engineering,* Volume 43, pp. 300-303.

Wafforn, S., 2017. *Geo- and Thermochronology of the Ertsberg-Grasberg Cu-Au Mining District, west New Guinea, Indonesia,* Austin, TX: University of Texas at Austin. PhD dissertation.

Watling, R. J. & Herbert, H. K., 1994. Gold fingerprinting by laser ablation inductively coupled plasma mass spectrometry. *Spectrochimica Acta,* Volume 49B, pp. 205-219.

Watling, R. J., Herbert, H. K. & Abell, I. D., 1995. The application of laser ablation-inductively coupled plasma-mass spectrometry (LA-ICP-MS) to the analysis of selected sulphide minerals. *Chemical Geology,* Volume 124, pp. 67-81.

Wilson, F. K., 1981. *Conquest of Copper Mountain.* New York: Atheneum Press.

Zhu, Y., An, F. & Tan, J., 2011. Geochemistry of hydrothermal gold deposits: a review. *Geoscience Frontiers,* Volume 2, pp. 367-374.